GENERAL ANALYSIS OF PILE FOUNDATIONS AND APPLICATION TO DEFECTIVE PILES

KENNETH J. XU

2000

This thesis has been accepted for the award of the degree in the Faculty of Engineering

GENERAL ANALYSIS OF PILE FOUNDATIONS AND APPLICATON TO DEFECTIVE PILES

BY

KENNETH J. XU, B.SC., M.E.

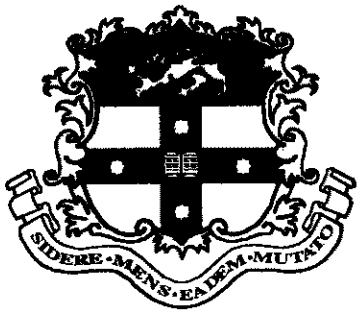

Thesis Submitted for the Degree of

Doctor of Philosophy

The University of Sydney

January 2000

Synopsis

This thesis falls naturally into four main topics to form a broad study of a general analysis of pile foundations and its application to defective piles.

Firstly, a general rigorous 3-D elastic numerical analysis for "global" pile foundations (which include multiple pile groups) is developed using the boundary element method. It considers all 6 load/displacement components for each of the piles with arbitrary dimensions, and also incorporates full coupling effects. Via hierarchical structures, twelve non-zero sub-matrices in a global matrix are derived for the basic influence factors. The analysis is implemented via a computer program, GEPAN.

Secondly, via a number of theoretical-derived expressions for "free field" soil movements/stresses being incorporated into the pile-soil governing equations, a unified 3-D coupled boundary element approach is presented to analyze the response of pile foundations subjected to "passive" loadings. It is shown that the method is capable of giving realistic estimates of passive pile behaviour under a variety of situations, including soil shrink/swelling; soil surface surcharge loading; tunnelling; soil movements arising from driving piles; cavity formation in soil; excavation; and retaining wall construction.

Thirdly, via applying GEPAN, the behaviour of pile foundations containing defects in some or all of the piles is analyzed. An extensive parametric study of the load-deformation behaviour within a single pile, a two-pile group and a pile group containing pile defects is performed under general loadings (axial, lateral, moment and torsional). Model testing of defective piles shows that the general analysis can serve as a "benchmark" for more approximate analyses of defective pile behaviour.

Finally, the further development of non-linear analysis for pile foundations is presented. A comprehensive study on simulating the shearing behaviour of frictional materials is carried out. A set of two unified explicit equations and two basic parameters, describing the distortional and volumetric behaviours, are presented independently. The model

developed has potential for future application in the analysis of piles and pile groups, making allowance for real soil behaviour.

Preface

The candidate carried out the work described in this thesis during the period 1997-2000. All of the work was conducted in the Department of Civil Engineering , The University of Sydney. The candidate was supervised by Professor H. G. Poulos, Professor of Civil Engineering (Soil Mechanics) in the Department of Civil Engineering and Senior Principal of Coffey Geosciences Pty. Ltd.. In accordance with the By-Laws of the University of Sydney, a candidate for the degree of Doctor of Philosophy is required to indicate the sections of the thesis that are original. Although many references have been used during the course of this research program, any information or ideas derived from these sources has been acknowledged in the text. In accordance with the above mentioned By-Laws the author claims originality for the following work:

1) the theory of general 3-D elastic analysis of piles and pile groups in Chapter 3;
2) the theory of general 3-D elastic analysis of piles subjected to "passive" loading in Chapter 4;
3) the theory for the study of pile behaviour induced by a soil cut in Chapter 5;
4) analysis of the behaviour of single piles containing defects in Chapter 6;
5) interaction analysis of sound and defective piles in Chapter 7;
6) analysis of the behaviour of pile groups containing defective piles in Chapter 8;
7) model testing for defective piles in Chapter 9;
8) method of non-linear analysis of pile foundations in Chapter 10;
9) the theory of simulating the shearing behaviour of frictional materials Chapter 11;
10) development of the soft ware GEPAN (GEneral Pile ANalysis).

During the period of the Author's candidature, the following papers were prepared by Author, in cooperation with Professor H.G. Poulos, Professor J.P. Carter, Professor C.S. Desai, Doctor M.D. Liu, Doctor D. Airey and PhD Candidate N. Loganathan, and are presented in support of his candidature:

Xu, K. J. and Poulos, H. G. (2000)
Measured and Predicted Axial Response of Piles Containing Structural Defects
Submitted for publication to Gotechnical Engineering Journal

Xu, K. J. and Poulos, H. G. (2000)
Behaviour of Pile Group Containing Defects
Accepted by 15th International Conference on Soil Mechanics and Geotechnical Engineering (ICSMGE), Istanbul 2001

Xu, K. J., and Poulos, H. G. (2000)
Interaction Analysis of Sound and Defective Piles
Accepted by 10th International Conference on the International Association for Computer Methods and Advances in Geomechanics, Tucson, Arizona, USA

Xu, K. J., and Poulos, H. G. (1999)
General Elastic Analysis of Piles and Pile Groups,
International Journal for Numerical and Analytical Methods in Geomechanics, (in press)

Xu, K. J. and Poulos, H. G. (1999)
General 3-D Elastic Analysis of Piles Subjected to "Passive" Loadings,
Submitted for publication to Computers and Geotechnics

Xu, K. J. and Poulos, H. G. (1999)
Theoretical Study of Pile Behaviour Induced by a Soil Cut
Accepted by GeoEng2000, Melbourne, ISSMGE

Xu, K. J. and Poulos, H. G. (1999)
Principles of Program GEPAN for general pile elastic analysis
Department of Civil Engineering, Sydney University, Research Report No. R782

Liu, M.D, J. P. Carter, Desai, C. S. and Xu, K. J (1999)
Analysis of the Compression of Structured Soils Using the Disturbed State Concept
International Journal for Numerical and Analytical Methods in Geomechanics, (in press)

Liu, M.D, Carter, J. P., Airey D. and Xu, K. J (1999)
Quantifying the Influence of Cementation on Sand Behaviour
Pre-failure Deformation Characteristics of Geomaterials, Jamiolkowski *et al* (*ed*), pp.475-481.

Loganathan, N. Poulos, H. G. and Xu, K. J (1999)
Ground Deformations and Pile-Ground Responses Due to Tunneling,
Submitted for publication to Soils and Foundations

Xu, K. J., Liu, M. D., Carter, J. P. and Poulos, H. G. (1998)
Simulating the Shearing Behaviour of Frictional Materials
In preparation for submission to Geotechnique

Xu, K. J., Liu, M. D., Carter, J. P. and Poulos, H. G. (1997)
Explicit Stress-Strain Equations for Geo-Materials
Department of Civil Engineering, Sydney University, Research Report No. R751

Acknowledgments

The work described in this thesis was made possible by the award of an Australian Research Scholarship to the author.

I am indebted to many people for their assistance during the course of this work. I gratefully acknowledge the value of many discussions with my fellow research students and the academic staff in the Department of Civil Engineering at the University of Sydney. In particular the assistance of Dr. T. S. Hull, Mr. R. Barker and Mr. K. Barry in connection with the experimental work is greatly appreciated.

I wish to thank my colleagues, in particular, Dr. M.D Liu, and N. Loganathan for their constructive criticisms and helpful suggestions.

To Professor J. P. Carter, for his invaluable assistance and support during my candidature, I am deeply indebted.

For his constant support, enthusiasm for my work and guidance throughout a long and eventful course of study, I give many thanks to Professor H. G. Poulos.

Finally, I wish to express my love and gratitude to my wife, Lora, for her understanding, encouragement, support and exceptional patience given to me during my candidature.

Contents

A List of Symbols in Chapters 1 to 10

$\emptyset$	zero sub-matrix
A	area of pile
a	maximum horizontal soil movement at soil cut
AD	summation matrix
A_d	area of defect
$A_{i,j}$	area of element j of pile i
b	distance of pile and soil-cut surface
$b_{i,j}$	displacements at element j of pile i due to unit tip displacements at pile i
c	spacing (c/c) between two pile groups
c_v	coefficient of consolidation
D	pile diameter
D_1	intact diameter of defective pile
D_2	necked diameter of defective pile
d_d	diameter of defect
$d_{i,i,l}$	characteristic displacement in direction l at element i ($d_{p,i,l} - d_{u,i,l}$)
$d_{i,j}$	displacements at element j of pile j due to unit head loads on pile i
$d_{i,l}$	displacement in direction l at element i
$d_{u,i,l}$	displacement at $p_{l,i} = p_{u,l,i}$ before the peck stress $p_{p,l,i}$ (the corresponding displacement $d_{p,i,l}$) reached, in direction l at element i
$D_{x,i,j}$	distance in X-direction between load on cap i and the centre of the head of pile j
$D_{y,i,j}$	distance in Y-direction between load on cap i and the centre of the head of pile j
e	void ratio
E_b	base Young's modulus
$E_{b,d}$	base Young's modulus at defect
$E_{o,i,l}$	initial tangent Young's modulus of soil, in direction l, at element i
E_p	pile Young's modulus
$E_{p,c,i}$	pile Young's modulus in compression, at element i
$E_{p,d}$	pile Young's modulus at defect

$E_{p,i}$ pile elastic Young's modulus, at element i

$E_{p,t,i}$ pile Young's modulus in tension, at element i

E_s soil Young's modulus

$E_{s,i,l}$ tangent Young's modulus of soil, in direction l, at element i

f_b limiting end bearing resistance on pile-soil interface

$f_{c,i,l}$ limiting pile-soil stress in direction l, at element i, for compression loading

FE pile compression matrix

f_s limiting skin friction on pile-soil interface

$f_{t,i,l}$ limiting pile-soil stress in direction l, at element i, for tensile loading

$G_{p,s,i}$ pile shear modulus at element i

H depth of soil-cut

$h_{i,j}$ loads on pile cap i due to unit head loads on pile j

IF soil behaviour matrix

$I_{i,j}$ displacements at soil element i due to unit stresses on soil element j

I_p moment of inertia of pile section

$I_{\theta H}$ influence factor on rotation θ due to horizontal loading H

$I_{\theta M}$ influence factor on rotation θ due to moment loading M

$I_{\rho M}$ influence factor on lateral displacement ρ due to moment loading M

$J_{i,j}$ displacements at pile element i due to unit stresses on pile element j

K pile-soil stiffness factor

K_R lateral pile-soil flexibility factor

K_T torsional pile-soil stiffness factor

L pile length

L_1 intact length of defective pile

L_2 necked length of defective pile

L_d length of defect

L_i length of pile i

M moment loading

m total number of elements

M_r resultant pile head moment

$ncap$ total number of pile caps

ncpil(i) total number of the piles under cap *i*

ncpsum total number of piles of pile-groups

necs(i) total number of shaft and discontinuous elements of the piles under pile cap *i*

nect(i) total number of elements of the piles under pile cap *i*

neps(i) total number of shaft and discontinuous elements of pile *i*

nept(i) total number of elements of pile *i*

nipsum total number of individual piles

npils total number of piles

ntot total number of elements

$o_{i,j}$ head displacements on pile *i* due to unit stresses on element *j* of pile *i*

P vertical loading

p_i head displacements of pile *i* due to unit tip displacements of pile *i*

$p_{i,l}$ interaction stress in direction *l*, at element *i*

$p_{tot,i,l}$ total pile-soil stress in direction *l*, at element *i*, at the previous load step

$p_{u,i,l}$ limiting value of interaction stress in direction *l*, at element *i*.

$q_{i,j}$ head displacements of pile *j* due to unit displacements of cap *i*

R_c ratio of post-yield modulus to elastic Young's modulus in compression

R_{fb} hyperbolic parameter for base elements for non-linear response

R_{fs} hyperbolic parameter for shaft elements for non-linear response

$R_{G,H\rho}$ group reduction factor on horizontal displacement due to horizontal loading

$R_{G,V}$ group reduction factor on vertical displacement due to vertical loading

r_i head displacements of pile *i* due to unit head loads on pile *i*

$R_{i,j}$ distance between load on cap *i* and the centre of the head of pile *j*

$R_{i,l}$ hyperbolic factor in direction *l*, for element *i*

$R_{KG,H,\theta}$ horizontal group (cap) stiffness reduction factor on cap rotation θ due to centrally horizontal cap loading *H*

$R_{KG,H,\rho}$ horizontal group (cap) stiffness reduction factor on horizontal cap displacement ρ due to centrally horizontal cap loading *H*

$R_{KG,N}$ vertical group (cap) stiffness reduction factor on vertical cap displacement due to centrally vertical cap loading

R_{ks} pile (head) stiffness reduction factor

R_{KS} pile (head) stiffness reduction factor

$R_{KS,H,\theta}$ R_{KS} on rotation θ due to horizonal loading H

$R_{KS,H,\rho}$ R_{KS} on lateral displacement ρ due to horizontal loading H

$R_{KS,M,\theta}$ R_{KS} on rotation θ due to moment loading M

$R_{KS,M,\rho}$ R_{KS} on lateral displacement ρ due to moment loading M

$R_{KS,N}$ R_{KS} on axial displacement s due to axial loading P

$R_{KS,T}$ R_{KS} on twist ω due to torsional loading T

R_s ratio of post-yield share modulus to elastic shear modulus

R_t ratio of post-yield modulus to elastic Young's modulus in tension

s spacing (c/c) between two piles and pile groups respectively

$s_{i,j}$ head loads on pile i due to unit stresses on element j of pile i

T torsional loading

u_b bottom horizontal displacement at cut

u_c central horizontal displacement at cut

u_t top horizontal displacement at cut

v_i head load on pile i due to unit loads on pile i.

W coefficient matrix of slip-friction

X distance of pile and soil-cut surface

X_e vector of pile-soil stresses

$X_{i,j}$ force arm in X-direction of element j at pile i

X_s vector of slips in cylindrical coordinate system

$Y_{i,j}$ force arm in Y-direction of element j at pile i

Y_s vector of constants

Z coefficient matrix of slip

z vertical position along pile

z_d depth of defect

$Z_{i,j}$ force arm in Z-direction of element j at pile i.

ΔP increment of applied load on pile head

Δp vector of incremental pile-soil intersection stresses

Δp_i interaction stress increments on element i

$\Delta p_{i,l}$ increment pile-soil stress in direction l, at element i.

ΔS_e vector of incremental "free-field" soil movement

$\Delta\rho_b$ incremental displacement of pile tip

$\Phi_{i,j}$ angle of $R_{i,j}$ line in horizontal plane with respect to X axis

α_{dd} cross interaction factor of two identical damaged piles

α_{di} cross interaction factor of the damaged pile on the intact pile

α_g group interaction factor

$\alpha_{g,\rho H}$ lateral group interaction factor

α_{id} cross interaction factor of the intact pile on the damaged pile

α_{ii} cross interaction factor of two identical intact piles

α_{ij} axial interaction factor of pile i on pile j

$\alpha_{\phi,ij}$ torsional interaction factor of pile i on pile j

$\alpha_{\theta H}$ lateral interaction factor

$\alpha_{\omega F,ij}$ lateral (moment) interaction factor of head movement ω of pile i due to pile head load F on pile j

ν_p Poisson's ratio of pile

ν_s Poisson's ratio of soil

θ_y pile head rotation

ρ_x pile head horizontal displacement

ρ_z pile head vertical displacement

σ'_v effective vertical stress of soil

BIFM Basic Influence Factor Matrix

DAMPA Damaged Pile Analysis (software, by Poulos)

DAMPIG Damaged Pile Groups Analysis (software, by Poulos)

DEFPIG Deformation Analysis of Pile Group (software, by Poulos)

GEPAN General Pile analysis (software, by Xu and Poulos)

PGROUP Program of Pile Group Analysis (software, by Banerjee *et al*)

PIES Axial Response of Pile in Expansive Soils (software, by Poulos)

PIGLET Analysis and Design of Pile Groups (software, by Randolph)

Chapter 1

Introduction

1.1 General Introduction

The response of a pile foundation can be defined in terms of six load/deformation components related to a convenient reference system (three forces and three moments; three deflections and three rotations). At present, the general load-movement analyses of pile foundations (excepting finite element analyses) are usually carried out by combining the results of three simplified types of analysis, *i.e.*, axial, lateral, torsional. Three separate models for pile response, each model simplified to a one-dimensional problem without introducing coupling effects, allow any load case to be analysed. However, pile-soil interaction is a three-dimensional problem, and each of the load-components has deformation-coupling effects.

Furthermore, owing to the limitations of computer technology at the time of their development, most analyses involve a number of simplifications and idealizations, such as: 1. pile to pile interaction (rather than pile element to pile element interaction) is considered; 2. full cylindrical and/or annular elements (rather than smaller elements) are used; 3. pile cross sections are taken as uniform; and 4. a single group is taken as a global system. All the effects mentioned may be important if the behaviour of pile foundations is to be modelled accurately. Because of rapid developments in computer technology, the use of accurate algorithms can now take precedence over earlier concerns about computer speed and capacity.

The elastic continuum model of soil is widely used in pile foundation analysis, within which predictions of response are logically based upon measurable parameters that are basic (fundamental) soil properties. In contrast, empirical approaches employ parameters that are undetermined functions of the soil properties, the pile properties and the form of loading, while taking no account of interaction. The elastic-based theory provides a simple-but-effective model that takes account of the interaction throughout the soil mass.

Problems involving passive pile loadings (*i.e.*, loads induced in the piles by the action of soil moving past the piles vertically and/or horizontally) have been the subject of much recent research. Examples include consolidating, swelling, and shrinking of clay; tunnelling, excavation, cavity development, excavation and retaining wall construction. However, most of the researchers consider a single pile and de-coupled loadings in two dimensions, and the external soil movements are often derived empirically with little theoretical background.

It is a common experience to encounter defects in various types of piles, such as necking, honeycombing and base softening. There are many methods, especially low/high strain dynamic methods, which can be used to identify such defects. However, there is very little information on the load-deformation behaviour of pile groups containing defective piles, and in particular, the interaction between two individual piles which may contain defects, and the stiffness reduction of groups containing defective piles. It is desirable to develop general defective pile analyses which will serve as a "benchmark" for more approximate analyses which have been proposed relatively recently. However, before these analyses are applied to practical problems, the accuracy of the predicted behaviour needs to be established. This can best be achieved by carrying out model pile tests under controlled conditions.

A critical aspect in the general non-linear analysis of pile foundations is to model the shearing behaviour at the pile-soil interface. However, it is very difficult to obtain good predictions of the shearing strength without making allowance for the volume changes that occur in the soil. On the other hand, the key problem in the boundary element method applied to pile foundations is to set up some explicit equations for the load-deformation behaviour in soils. Thus, it is very important to set up a set of unified explicit equations describing the distortional and volumetric behaviours of soil, if the boundary element method is to be applied for general non-linear analysis of pile foundations.

1.2 Research Objectives

In this thesis, a general analysis of pile foundations will be developed that can be used to investigate the load-deformation behaviour of active piles and passive piles, as well as to improve the general understanding of the behaviour of pile groups containing defective piles. In order to achieve the general research objectives, the principal specific objectives of this research study are:

1. via elastic continuum based boundary element analysis, to develop a theory of general rigorous 3-D elastic analysis of piles and pile groups
2. to develop a theoretical methodology for passive pile loadings and to investigate the corresponding "passive" behaviour
3. to improve the understand of the fundamental aspects of the behviour of pile groups containing defective piles
4. to implement the above analysis, and develop a software program which can serve as a "benchmark" for general analysis of pile foundation
5. to improve the understanding of distortional and volumetric behaviour of frictional materials for further future development of general non-linear analysis of pile foundations.

1.3 Thesis Outline

The thesis consists of twelve chapters, with the main theoretical, experimental and field comparison work being presented in the ten central chapters.

In order to establish the context of the present investigation, studies relating to the theoretical and engineering backgrounds of general active and/or passive pile analysis, together with the defective piles and corresponding testing methods, will be reviewed in Chapter 2.

Via 3-D boundary element analysis, a general rigorous elastic analysis (implemented by a program called GEPAN) of pile foundations considering all six coupled load/deformation components will be developed in Chapter 3.

In Chapter 4, a general 3-D elastic analysis of piles subjected to "passive" loadings is presented. The analysis is employed to examine pile response when subjected to some typical passive loadings, such as soil shrink/swelling, soil surface surcharge loading, tunnelling, soil movements arising from driving piles, and cavity formation in soil.

In Chapter 5, general explicit equations are derived firstly for cut-induced soil movements. These equations are then incorporated into the program of GEPAN, and an analytical methodology will be set up to study pile behaviour induced by a soil-cut, such as an excavation or retaining wall construction near the piles.

Chapter 6, presents analyses via the program GEPAN for the response of single piles with three typical defects (necking, honey-combing and soft-base). For each type of defect, typical relationships for pile stiffness reduction have been developed under general pile loadings (axial, lateral, moment and torsional).

In Chapter 7, based on introducing accurate definitions of interaction factors, the interaction between two piles containing defects is analyzed, and some simple-but-important relationships between interaction factors of defective pile are developed.

The load-displacement performance of groups containing defective piles is assessed in Chapter 8. An attempt is made to relate the type of defects, pile spacing, pile stiffness/flexibility factors, to the behaviour of group, as represented by the group stiffness reduction factors, load redistribution, and "off-line" movements.

In Chapter 9 a series of model tests performed by the author are described. It describes the results of tests on model piles containing structural "defects", and driven into clay. The static load-settlement behaviour of the defective piles, is investigated for various values of the length and diameter of the defects. Comparisons are also presented between the theoretical and measured reductions of pile head stiffness due to the defects.

Chapter 10 presents the further development of non-linear analysis for pile foundations. Various models for a 3-D non-linear analysis of a pile-soil system have been set up for incorporation into GEPAN.

In Chapter 11, a comprehensive study on simulating the shearing behaviour of frictional materials is described. The model developed may be applied as a tool to unify the shearing behaviour at the pile-soil interface in pile foundation analysis using boundary element approaches. A set of two explicit equations, describing the relationship among the shear stress ratio and the distortional strain and volumetric strain, are formulated independently. Two basic parameters of frictional materials to describe distortional and volumetric behaviours respectively are presented. Because the material in this chapter differs in nature from the remainder of the thesis, a separate reference list is provided.

Chapter 12 summarizes the main conclusions derived from the study and suggests avenues for future research into the general behaviour of pile foundation systems.

Chapter 2

Literature Review

2.1 Introduction

In this chapter a review is made of general analyses of pile foundations, "passive piles", and the behaviour of piles containing defects.

Section 2.2 reviews the theoretical background of some elementary solutions for boundary element method. In the elementary solutions, two kinds of problems (force-displacement, displacement-displacement) are involved. The next section briefly introduces currently widely-used programs for general pile analysis, such as PIES, DEFPIG, PIGLET and PGROUP. Section 2.4 deals with the analysis of piles subjected to "passive" loadings, that is, to loadings induced by soil movements. Such problems include consolidation of clay; swelling or shrinking of an expansive clay; tunnelling; excavation; embankment loading, and installation of adjacent piles. Section 2.5 reviews knowledge in relation to defective piles, including defect types, causes, and preventive measures for defects; and then model testing and numerical analysis of defective piles. Following this is a section reviewing methods of pile testing (low/high strain test, static test), with emphasis being placed on the identification of defects from such tests.

A summary of the major findings of the literature survey is then made with indications of the areas that will be investigated in this thesis.

2.2 Elementary Solutions for Boundary Element Method Applied to Pile Foundations

2.2.1 Force-Displacement (F-D) Problems

Force-Displacement (F-D) problems are defined as problems in which the boundary conditions are only in terms of stresses (or forces) and only the strain (displacement) field is required. This kind of problem is often used in pile analysis via the boundary element method.

The indirect formulation of the boundary element method involves the selection of an elementary singular solution of the governing differential equation of the problem. For three-dimensional problems the elementary solution may be chosen to be, for example (Mindlin,1936, Poulos and Davis, 1974, Banerjee *et al*,1976):

1. Kelvin's solution for a point load within an infinite solid
2. Mindlin's solution for a point load within a semi-infinite solid
3. Boussinesq's and Cerutti's solutions for a point load acting on the surface of a half space.

As set out by Banerjee *et al* (1976), the three components of displacements $u_i(A)$ at a point A due to the three components of the forces $P_j(B)$ acting at B can be expressed as:

$$u_i(A) = P_j(B)K_{ij}(A,B) \quad \text{.....(2.1)}$$

where $K_{ij}(A,B)$ is a function of the positions of A and B with respect to a Cartesian co-ordinate system. If the fictitious traction vectors $\varphi_j(B)$ are distributed over the surface S the displacements due to the total effects of these fictitious tractions can be expressed as:

$$u_i(A) = \int_S \varphi_j(B)K_{ij}(A,B)dS \quad \text{.....(2.2)}$$

2.2.2 Displacement-Displacement (D-D) Problems

A displacement-displacement (D-D) problem occurs when the boundary conditions are only in terms of strains (or displacements) and only strains (or displacements) are required. This type of problems often met in analysing the response of piles subjected to "passive" loadings caused by soil movements.

Sagaseta (1987) presented closed form solutions for obtaining the strain field in an initially isotropic and homogeneous incompressible soil due to near-surface ground loss. This problem fits into a category of cases in which the imposed boundary conditions are only or mainly in terms of displacements (strain-controlled problems). In these cases there is a possibility of eliminating the stresses and obtaining the strains by using only the incompressibility condition. The presence of the top free surface is considered by means of a virtual image technique using appropriate results for the elastic half-space. The results are simple, especially for the movements of the soil surface. The application to some typical problems, such as soft ground tunnelling and pile driving or extraction, shows that the calculated movements agree well with the experimental observations and compare favourably with commonly used numerical methods (Sagaseta, 1987, Chow and Teh, 1990, Loganathan *et al*, 1999a, 1999b).

2.3 General Pile Analysis

2.3.1 Methods of General Pile Analysis

In general, a pile group may be subjected to simultaneous axial load, lateral load, moment, and possibly, torsional load. Various numerical approaches have been employed to estimate the pile group response to such loadings, and these may be broadly classified into the following categories:

1. Methods based on the theory of subgrade reaction, including equivalent bent (frame) analyses that reduce the pile group to a structural system but take some account of the effect of the soil by determining equivalent free-standing lengths of the piles (Hrennikoff, 1950; Kocsis, 1968; Nair *et al*, 1969).

2. Hybrid analyses that combine load transfer analyses for single pile response and elastic theory to estimate pile-soil-pile interaction (Focht *et al*, 1973; O'Neill *et al*, 1977; Chow, 1986).

3. Elastic-based analyses that use elastic theory for both single pile response and pile-soil-pile interaction (Poulos, 1979, 1989a; Randolph,1980, 1989; Banerjee *et al*, 1976).

4. Finite element methods that include a number of ways to analyze pile group deformations (Ottaviani, 1975; Desai, 1974; Pressley *et al*, 1986).

2.3.2 General Elastic Continuum Based Pile Analysis

Computer programs for the analysis of pile groups vary in the type of approach used and in the sophistication of treatment of different aspects of group behaviour. Some elastic continuum-based analyses are widely applied to pile foundations, and are reviewed below.

2.3.2.1 PIES

This program, developed by Poulos (1989b), computes the axial movement and load distribution within a single pile, or a pile within a group, subjected to axial load and/or externally-imposed soil movements (heave or consolidation), such as are developed in an expansive soil by changes in moisture conditions.

The program uses a simplified boundary element formulation, and the soil can be represented either by a continuum or a series of springs. In each case, non-linear response of the interface can be incorporated by

1. assuming an elastic-plastic or hyperbolic relationship between soil stiffness and stress level, and
2. allowing for the effects of pile-soil slip and end-bearing failure by specifying limiting values of shaft resistance and end-bearing resistance.

Three types of elements are used: cylindrical shaft elements, annular base elements and annular discontinuity elements at locations where the pile diameter changes abruptly. The behaviour of each element is considered at a node which is located at the centre of that

element and along a common vertical plane through the pile axis. Governing equations in PIES are expressed as follows:

The compatibility at pile-soil interface in non-failure state:

$$[IF - AD \cdot FE]\{\Delta p\} - \Delta\rho_b\{1\} = -\{\Delta S_e\} \quad \text{.....(2.3)}$$

where

$\Delta\rho_b$ = incremental displacement of pile tip

$\{1\}$ = vector whose elements are unity

$[AD]$ = summation matrix

$[FE]$ = pile compression matrix

$\{\Delta p\}$ = vector of incremental pile-soil intersection stresses

$[IF]$ = soil behaviour matrix

$\{\Delta S_e\}$ =vector of incremental "free-field" soil movement

In addition, for vertical equilibrium of a pile:

$$\sum_{i=1}^{m} A_i \Delta p_i = \Delta P \quad \text{.....(2.4)}$$

where

A_i = surface area of element i

Δp_i = interaction stress increments on element i

m = total number of elements

ΔP = increment of applied load on pile head.

Matrices of pile displacement, $[AD]$ and $[FE]$, can be determined from the structural principles. The soil behaviour matrix, $[IF]$, is determined from integration of the equations from the theory of Mindlin (1936), as described by Poulos and Davis (1968).

Equations 2.3 and 2.4 may be solved for the unknown interaction stress increments Δp and base incremental displacement $\Delta\rho_b$, from which the incremental pile deflections may be calculated from structural principles.

2.3.2.2 DEFPIG

DEFPIG, developed by Poulos (1979,1990a), is a FORTRAN computer program for determining the deformation and load distribution within a group of piles subjected to vertical, horizontal and moment loading. The program considers a group of identical elastic piles having axial and lateral stiffness that are constant with depth. The piles are supported by a linear elastic medium, but the program allows for the possibility of slippage between the piles and the soil under axial loading and for the development of yield of the soil adjacent to the pile due to lateral loading. The stress distribution is computed from Mindlin's solutions for an isotropic homogeneous linear elastic medium, but nonhomogeneity of the soil along the pile length can be approximately taken into account. The piles are assumed to be attached to a rigid pile cap, so that all undergo equal lateral defection and rotation, or alternatively, the piles can be subjected to specified loads or deflections. Raking or battered piled may be present in the group, but only battered in the direction of the lateral loading. Load-deformation relationships to failure may be obtained if desired. Any consistent set of units may be used.

The first stage in the program is the evaluation of two-pile interaction factors. The interaction factors of axial and/or lateral loading can be input for various dimensionless center-to-center spacings, computed by the program, or calculated by some approximate expressions.

The program then evaluates the matrices of interaction factors for the specified group by interpolation of the computed or input interaction factors. The limiting pile-soil stresses for both axial and lateral loadings are then input for each axial and lateral element. A check is made to determine whether any of the computed axial pile loads exceed the ultimate value.

The program combines the following five analyses:

1. settlement of single axially loaded pile (Mattes and Poulos, 1969)
2. settlement of a group of piles, using superposition of two-pile interaction factors (Poulos and Mattes, 1971)
3. lateral response of a single pile (Poulos 1971a)
4. lateral response of a pile group, using superposition of two-pile interaction factors (Poulos, 1971b)
5. analysis of a group of piles containing batter piles and subjected to lateral and vertical load and moment (Poulos and Madhav, 1971).

2.3.2.3 PIGLET

The computer program, PIGLET, developed by Randolph (1980, 1989), analyses the load deformation response of a pile group under general loading conditions. The program is based on a number of approximate, but compact, solutions for the response of single piles to axial, torsional and lateral loading, with due allowance made for the effects of interaction between piles in the group. In these solutions, the soil is modelled as a linear elastic material, with a stiffness which varies linearly with depth.

Based on the technique of treating load transferred from the pile shaft separately from that at the pile base, an approximate closed form solution for single axially loaded piles has been described in detail for floating piles by Randolph and Wroth (1978a), and extended to end-bearing piles by Randolph and Wroth (1978b). Similar to the axially loaded pile analysis, an analytical solution for the torsional response of piles has been presented by Randolph (1981a). The solution of laterally loaded piles was developed by Randolph (1981b) by curve fitting the results of finite element analyses of laterally loaded piles embedded in elastic "soil".

2.3.2.4 PGROUP

A more complete boundary element analysis, PGROUP, developed by Banerjee *et at* (1976), can analyse for raked pile groups subjected to vertical loads, horizontal loads and moments is described. In the analysis, the equations for pile compressibility and pile flexibility are discretized by a differential method and soil behaviour is assumed to be elastic and is represented via a boundary element discretization scheme.

2.3.2.5 Comparisons of Program PGROUP, DEFPIG and PIGLET

The three programs, PGROUP, DEFPIG and PIGLET, have been compared by Poulos and Randolph (1983). All three of these programs are based on elastic continuum analysis, although DEFPIG can also be extended into the non-linear range be specifying limiting values of skin friction and lateral pressure. A brief survey of the capabilities of the three programs is given in Table 2.1 (Randolph, 1992).

2.4 Behaviour of Piles Subjected to "Passive" Loading

The consideration of passive loadings is important because they can lead to overstress and damage of piles and hence to the development of defects in the piles. There are several circumstances in which piles are subjected to loading by the movement of the surrounding soil past the pile. Such circumstances are termed "passive" loadings and some of these are described below.

2.4.1 General Externally-Imposed Soil Movements

Poulos (1994a) describes the analysis of piles subjected to externally-imposed soil movements and demonstrates the importance of considering the pile-soil interaction if a proper understanding of the pile behaviour is to be developed. For piles subjected to axial soil movements, it has been shown that significant additional forces can be developed in

the pile by the soil movements, and that applied axial loading in the direction of the soil movement can lead to substantial increases in pile displacement. For piles subjected to lateral soil movements, additional moments and shears are developed in the piles, and these may be large enough to cause structural failure. In the case of a pile within an unstable slope, several mechanisms of failure are possible. The initial mechanism depends largely on the extent of embedment of the pile, the distribution with depth of the soil movement, the relative flexibility of the pile, and yield moment of the pile section.

2.4.2 Negative Friction and Expansive Soil

Poulos (1990b) points out that negative friction itself due to vertical soil movements will not cause geotechnical failure of the pile, but may cause excessive movement of the pile if the working load is too large, and may result in large axial forces in the piles due to "downdrag". Tests have been carried out by Challa *et al* (1991) on model piles in an expansive clay. It is found that swelling of the soil may induce substantial tensile forces in the pile. The pile head movement increases as the soil heave increases, but tends to approach a constant value if the piles are founded in a stable sound layer below the swelling clay. Teh *et al* (1995) describes the numerical analysis of the downdrag forces in end-bearing pile groups. Parametric studies indicated that interior piles of a larger pile group experience relatively small downdrag forces, especially when the pile spacing is small. Jeong *et al* (1998) point out the major parameters very much influencing the interaction factors are the group spacing, the total number of piles, and the relative position of the piles within the group.

2.4.3 Lateral Soil Movement

Chen and Poulos (1997) present a theoretical procedure for analyzing the lateral response of vertical piles subjected to lateral soil movements. The lateral pile response is computed via a simplified boundary-element analysis, using a specified free-field soil movement profile. For practical convenience, some elastic solutions have been generated using a boundary element program and are presented in chart form, as shown in Fig. 2.1. These

design charts tend to give an upper-bound estimation of the maximum pile bending moment and pile head defection, although a close estimation may be obtained for small soil movements.

2.4.4 Excavation

There have been reports of severe damage to piled foundations due to an excavation operations (*e.g.* Finno *et al,* 1991; Chu, 1994), and thus it is important to develop a better understanding of the problem so that appropriate measures can be taken to minimize any potential damage. Poulos and Chen (1996, 1997) analyse the pile response adjacent to an excavation. In their study, a two-stage analysis involving the finite element method and the boundary element method is used to study pile response due to excavation-induced lateral soil movements, focusing on both unsupported and braced excavations in clay layers. Maximum pile bending moment and deflection are presented in chart form which may readily be used in practice. Key factors influencing the response of a single pile are found to include excavation depth, excavation support conditions, soil properties, and pile properties. For the unsupported excavations, as the pile head condition has been found to have major effects on the pile response and the existence of restraint at the pile can greatly increase the maximum bending moment induced in the pile, proper account should therefore be taken of the pile head condition when using the presented charts for piles whose head condition are not free from rotation and deflection.

2.4.5 Tunnelling

Chen *et al* (1999) describe a method for analyzing the behaviour of piles influenced by tunnelling operations. The method involves the estimation of soil movements caused by a tunnel construction, using both an empirical formula and an analytical formula, and the

computation of lateral and axial pile responses, via a boundary element analysis. The analysis results show that tunnelling adjacent to a pile can cause significant bending moment, lateral deflection, axial force and vertical settlement in the pile. Explicit expressions for tunnelling-induced ground movements presented by Loganathan and Poulos (1998) have been incorporated into a general pile analysis developed by Xu and Poulos (1999a), and Loganathan *et al* (1999a, 1999b) have evaluated the response of single piles and pile groups to tunnelling. They have considered the effects of various factors such as tunnel geometry, ground loss ratio, pile diameter and ratio of pile length to tunnel depth. A 2×2 pile group has been analysed for varying pile lengths and lateral distance from the tunnel. The behaviour of a pile in the group has been compared with the behaviour of an identical single pile, as shown in Fig. 2.2. The study shows that a single pile analysis can predict adequately the tunneling-induced bending moment, lateral deformation and settlement for a pile in a pile group, at an identical distance from the tunnel. However, the tunnelling-induced axial down-drag force estimated for single pile is about 20% higher than for a pile in a pile group, in that study (Loganathan *et al*, 1999b).

2.4.6 Piles near Embankments

The analysis and design of piles through embankments has been considered by a number of researchers, such as Poulos (1996), Poulos (1994b), Goh *et al* (1997), Low *et al* (1994), Hewlett *et al* (1988). Goh *et al* (1997) described a simplified numerical procedure based on the finite-element method for analyzing the response of single piles to lateral soil movements. The flexural bending of the pile is modeled by beam elements. The complex phenomenon of the pile-soil interaction is modeled by hyperbolic soil springs, as shown in Fig. 2.3(1). The method gives results for pile displacements and bending moments that compare well with the analytical solution by Poulos (1973) as shown in Fig. 2.3(2). Based on parametric studies, empirical design solutions for pile foundation systems at the base of a sloped embankment are presented.

2.4.7 Effects of Pile Driving

When a pile is driven into soil, horizontal and vertical movements (especially ground surface heave adjacent the pile) are developed in the soil surrounding the pile. Poulos (1994c) studied the installation effect due to pile driving, via applying the expression for radial soil displacement proposed by Carter *et al* (1979) from cavity expansion theory. It has been demonstrated that the soil movements caused by the driving of piles can generate significant axial and lateral forces and movement in already-installed piles. When driving end-bearing piles, downward soil movements occur at early stages of penetration, but as final penetration is approached, soil heave occurs around the pile. Fig. 2.4 shows that the forces in the adjacent pile are primarily compressive in the early stages, but become completely tensile at final penetration. The existence of restraint at the pile head may lead to bending moments that are two or more times the value for an unrestrained pile head, as shown in Fig. 2.5.

Using the source-sink technique developed by Sagaseta (1987), Chow and The (1990) also analysed the effects of movements caused by pile-driving on nearby piles. The ground surface heave, induced by the pile-driving, increases with pile diameter and the penetration depth of the pile. The rate of increase in surface heave is slow when the pile penetrates beyond a certain depth. Beyond this depth, the major soil movement is near the pile toe, where the soil deforms downwards as well as outwards. The pile heave increases with increasing length-to-diameter ratio, *L/d*, for piles in stiff clay, but in very soft clay the reverse may occur due to the complex interaction behaviour.

2.5 Defective Piles

2.5.1 Reports of Problems in Pile Construction

For structures being founded in poor subsoil conditions and for heavy loads, concrete piles are extensively used. It is a common experience to come across defects in these piles. Foundation engineers all over the world are being confronted with many pile foundation failures and in some of these cases, the reasons for such failures could be

identified, as seen given from the following typical case records reviewed by Rao *et al* (1992) and described below.

Hobbs (1957) reported a case of failure of a cast in situ pile which developed necking during installation. This occurred as a result of artesian ground water conditions prevailing. Peck (1965) described a case of a building which suffered large differential settlements because of large scale discontinuities in the piling concrete, and these gaps were found to be filled with peaty soil. An interesting case of failure of large diameter bored piles has been reported by Bobrowski *et al* (1970). A five storeyed office building in Canada was founded on large diameter bored piles and at the time of the completion of the construction, there was found to be a large differential settlement of nearly 250 mm. This was found to be a result of discontinuities in the piles, and the structure had to be demolished and rebuilt.

Baker and Khan (1971) reported a case of failure where the concrete was poured in water accumulated to a depth of nearly 600 *mm* in the bottom of the bore hole. Subsequent coring operations indicated that a layer of sand and gravel accumulated at the bottom due to improper cleaning of the bore hole, and washing out of cement. Hearne *et al* (1981) reported the failure of a drilled shaft foundation that was supporting a bridge pier and was found to have settled by about 100 *mm*, even though the full load had not been applied to the structure. This excessive settlement was attributed to the defective end bearing of the drilled shafts.

Leonards (1982) reported an investigation of an oil tank foundation failure at Fawley, England. There were many gaps and discontinuities found in these piles. Olson *et al* (1985) reported a case of a five storey building which failed during the construction phase, mainly because of the presence of discontinuities/voids in the founding pier shafts.

2.5.2 Types, Causes and Preventative Measures of Pile Defects

Broms (1995) points out that a large number of factors can contribute to the damage to driven piles such as excessive height of fall of the hammer, eccentricity of the driving force, initial lack of straightness of the piles, stones or boulders in the soil, or steeply sloping bedding planes and overdriving.

Baker and Khan (1971) listed various types of conditions that can lead to faulty piles including excess water at cold joints resulting in weak concrete; improper placement of concrete; development of voids in the shaft due to arching; and side or surface cave-in of soil resulting in contaminated concrete. The last two conditions are illustrated in Fig. 2.6.

Thorburn *et al* (1977) found that a principal cause of defects in bored piles is associated with the removal of temporary casings. Of these defects, the most important is the occurrence of overbreak cavities which can undermine the structural integrity of piles. "Overbreak" is the term describing the removal of the soil material by physical or chemical forces, sometimes resulting in cavitation and discontinuity. Removal of the material can be caused by boring ahead of the casing in unstable soil or the release of ground water as shown in Fig. 2.7. The ultimate result may be a contamination of the concrete, a reduction in cross-sectional area of the shaft and the exposure of the reinforcement to corrosion. Although such defects may not affect the pile performance in the short term, long term behaviour may be impaired, particularly when the pile is subjected to bending. The direct causes of pile defects and problems associated with groundwater, together with preventive measures, are listed in Table 2.2.

2.5.3 Classification of Basic Types of Pile Defects

Based on the experience gained through the reported cases of failures of defective piles, Rao *et al* (1992) summarized the defects into three types, *i.e.*, improper end bearing, discontinuity and necking.

Poulos (1997) divided broadly the defective piles into two categories, *i.e.*, structural defects and geotechnical defects, as shown in Fig. 2.8. Structural defects generally are related to construction, and result in the size, strength and/or stiffness of the pile being less than assumed in design (for example, "necking"). Geotechnical defects arise from either a mis-assessment of the in-situ conditions during design, or else from construction-related problems, such as a soft base.

Based on the two classifications and considering the typical pile defects presented by Thorburn *et al* (1977), in general, Rao's classification is adopted in this thesis. However, for the purposes of clear description, the terminology of the basic types of defective piles to be considered as follows:

1. necking
2. honey-combing
3. soft base.

Fig. 2.9 shows an idealized diagram of these types of pile defects, which are used subsequently in this thesis for numerical analysis.

2.5.4 Testing of Model Defective Piles

Rao *et al* (1992) carried out a testing programme on model pies embedded in silty clay in a test tank. Concrete piles of 100 *mm* dia and 1050 *mm* length with a central duct accommodating electrical strain gauges have been used. The defects introduced into the test piles were: improper end bearing (with air gap provided at the pile tip), and discontinuities in the form of bands of highly compressible material and necking in the pile. Standard load tests were conducted on these piles, and in all these cases, typical load settlement curves and load distribution with depth were established. The results revealed that in the case of piles with improper end bearing, the capacity was drastically reduced. In the case of piles with poor end bearing, the load on pile top could be maintained indicating that load is balanced largely by skin friction, however, the ultimate capacity was greatly reduced. Excessive settlement can also result from defects in the piles, but in the case of a pile with a discontinuity, the capacity of the pile may not be as low as

obtained in the case of pile with improper end bearing. It was found that in bored piles in which necking was present, the resulting failure was mainly due to the structural collapse of the pile.

2.5.5 Numerical Analysis for Defective Piles

A theoretical non-linear defective pile analysis, via a simplified boundary element method, was developed by Poulos (1997). The analysis has been implemented via the program DAMPA (DAMaged Pile Analysis) and DAMPIG (DAMaged Pile Groups). Furthermore, through introducing a pile (head) stiffness reduction factor, R_{ks} (ratio of stiffness of defective pile to stiffness of intact pile), he performed a parametric study on the behaviour of piles and pile groups containing structural and geotechnical defects.

For single piles, the presence of defects leads to a reduction in pile head stiffness, and the possibility of reduced load capacity. If failure of the pile occurs because of a structural defect, there is a sudden and dramatic increase in settlement. With geotechnical defects, the apparent loss of load capacity is characterised by a more gradual increase in settlement with increasing load. The effects of load level on stiffness reduction due to structural defect and geotechical defect are shown in Fig. 2.10.

For each type of defect, typical relationships have been developed, for a single pile, between the reduction in stiffness. the extent of the defect, and the applied load level. These relationships have then been used to examine the behaviour of a typical six-pile group containing defective piles. The ability of the group to redistribute the pile loads from defective to intact piles results in a less severe reduction in axial stiffness than is the case for a single defective pile. However, the presence of defective piles will generally lead to the development of lateral deflection and rotation of the group, and induces additional bending moments in the piles, even under purely applied loading, as shown in Fig. 2.11.

2.6 Pile Testing

There are a number of methods used for testing the integrity and capacity of piles, ranging from simple excavation and exploratory coring, static testing, to more sophisticated methods as low-strain integrity testing, and high-strain dynamic pile testing (for example Davis *et al*, 1991; Rausche *et al*, 1992; Likins *et al*, 1993; Turner, 1997; Middendorp *et al*, 1988; Kido *et al*, 1988). The latter three methods are described in the sections below.

2.6.1 Low-Strain Integrity Testing

There are various types of low-strain tests, including sonic tests, frequency response tests, and echo tests. Fleming *et al* (1992) summarized the principles, advantages and disadvantages of these low-strain tests. The measurements can be analyzed either directly in the time domain or converted to the frequency domain. The main low-strain methods used in Australia at present are the sonic method (in the time domain) and the frequency response method (in the frequency domain) (AS 2159). The principles of the two methods are briefly described below.

Sonic method

A hammer blow struck at the top of a pile produces a stress wave which can be detected by a surface mounted accelerometer at the pile head. When the pile is struck, the adjacent accelerometer picks up the wave which has traveled to the base of the pile (or a discontinuity) and has been reflected back, and the principle of stress wave propagation for a necked pile, for example, is shown in Fig. 2.12. The time taken between the hammer blow and the wave to travel down, then up the pile shaft will be: $\Delta t = 2L/c$, where L = pile length, c = pile wave speed. The wave speed "c" for say concrete is dependent upon concrete properties as follows: $c = (E/\rho)^{1/2}$, where E = pile Young's Modulus and ρ =

density of pile. Discontinuities and changes in pile cross-section produce reflections, which change the shape of the signal. The signal then can be interpreted according to its shape. Major defects, together with an indication of the depth at which they occur, can usually be detected. The arrangement of a typical site-testing layout for the sonic method is illustrated in Fig. 2.13.

Frequency response method

In the vibration test, an electrodynamic vibrator is placed on the prepared pile head, and the pile is subjected to a continuous vibration over a broad frequency band. The response of the pile is monitored via a velocity transducer. Resonance peaks are produced, which may be used to deduce the effective length of the pile and to reveal apparent defects. The idealized response curve from a vibration test is shown in Fig. 2.14, where the distance between resonance peaks at higher frequencies is related to the effective pile length, l, by the expression: $\Delta f = V_c/2l$, where V_c is the velocity of longitudinal wave propagation in concrete. Hence l may be estimated. A value for the cross-sectional area of the pile, A_c, may be obtained from the mean mechanical admittance of the pile head, N, over the higher frequency range, from the relationship: $N = 1/\rho_c V_c A_c$, where ρ_c is the average density of the pile concrete. The arrangement of typical test equipment of the method is shown in Fig. 2.15.

2.6.2 High-Strain Integrity Testing

Wave Equation Analysis

The propagation of driving energy along a pile, allowing for interaction with the surrounding soil, may be analyzed with sufficient accuracy using "one-dimensional elastic wave equation". Historically, the equation has been implemented using finite difference or finite element techniques, with the pile being modeled as a discrete assembly of mass points interconnected by springs. This model, originating in the work of Smith (1960), forms the basis of a range of computer programs for studying pile drivability.

Signal Matching Method

Signal matching provides the most reliable means of predicting the performance of a pile tested by dynamic methods. The pile and the soil data are modelled according to the best estimates made by the operator performing the analysis, and a calculation is made using wave equation methods. The calculated signals are displayed on the computer screen along with the measured signals. The operator then performs a number of iterations, varying the input data until a satisfactory match between the measured and calculated signal is obtained. Once a satisfactory match is obtained, a plausible model of the pile-soil system is deemed to be established, and from this, the mobilized static loading can be predicted. The main software used to perform the signal matching process is CAPWAP which is one of the most widely utilized programs for such analyses, originating from the work of Goble and his workers (Goble and Rausche, 1979).

2.6.3 Static Load Testing

Static load testing is used to evaluate pile performance at preliminary or later stages of work, or to proof-test nominated piles as work proceeds. The test load is applied to the pile by jacking against a reaction system. The reaction system may comprise ground or rock anchors, kentledge or reaction piles. The details are to be found in AS-2159, Fleming *et al* (1992) and Tomlinson (1987). In the analysis of defective piles, static load testing is often performed on instrumented piles and model piles to evaluate the static load-displacement behaviour of the piles containing defects (such as, Rao, 1996).

2.7 Summary and Discussion

This chapter introduces briefly some theoretical and engineering background of boundary element analysis applied to pile foundations, and then discusses defective piles and pile testing.

The principles and features of current widely-used programs of general pile analysis are reviewed. All reviewed analyses are based on elastic continuum theory, however they are de-coupled and based on a number of simplifications. It is clear that investigators have paid some attention to the analysis of the behaviour of piles subjected to "passive" loadings. The considerations have been mainly on single piles, and the principles empirically are quite different for specific "passive" loadings. For most of these, design methods are derived empirically with little theoretical background. A unified and more accurate passive pile analysis should therefore be set up, which can be linked to the normal "active" loading analysis. It is a common experience to come across defects in piles, and by knowing the soil characteristics and installation conditions, it is possible to identify and classify the pile defects. However, relatively few investigators have reported the behaviour of piles and groups containing defective piles. The mechanisms of behaviour of defective piles deserve to be investigated thoroughly and the corresponding theories need to be evaluated by controlled pile testing. The development and application of theoretical analysis applied to the study of defective piles will be a key aspect of the work to be described in this thesis.

Table 2.1 Comparisons of the Program, PGROUP, DEFPIG, PIGLET (Randolph, 1992)

Program	Analytical Approach	Capabilities	Feathers
PGROUP	Elastic boundary element analysis	1. Linear variation of soil modulus with depth 2. Horizontal loading in one direction 3. Pile raked in plane of vert. & horiz. Loading 4. Pile cap contact modelled	Rigorous analysis, but accuracy limited by level of discretisation of piles, particularly when considering lateral response. Requires considerable computer resources and relatively slow and labour intensive to run
DEFPIG	Boundary element analysis of single piles with interaction factors for pile groups	1. Any variation of soil modulus 2. Yilding and slip allowed for by limiting stress 3. Horizontal loading in one direction 4. Piles raked in plane of vert. And horiz. Loading 5. Pile cap contact modelled	Versatile program, with main limitation being the approximate treatment of variations in modulus with depth. Microcomputer version available, but relatively slow and non-interactive.
PIGLET	Elastic closed form solutions (single piles), interaction factors for group	1. Linear variation of soil modulus with depth 2. Separate modulus for axial and lateral loading 3. Horiz. Loading in any direction, torsional loading 4. Piles raked in any direction	Fast and simple program but limited to linear response, extensively checked against more rigorous analysis. Microcomputer based, with fully interactive data input/editing. Standard version can analysis groups of up to 100 piles (version also available for 300 piles)

Table 2.2 Types and Causes and Preventive Measures of Piles Defects (Thorburn *et al*, 1977)

Types of Defect	Cause of Defect	Preventative Measure
Hollow on the surface of pile shaft with associated small bulbous projection some short distance beneath hollow	Overbreak in unstable strata	1. Advancing temporary casing ahead of auger by vibratory or rotary method 2. Drilling techniques using bentonite in suspension 3. Use of permanent casing
Discontinuity in pile shaft with associated large bulbous projection some short distance beneath cavity	Overbreak in unstable strata	1. Advancing temporary casing ahead of auger by vibratory or rotary method 2. Drilling techniques using bentonite in suspension 3. Use of permanent casing
Coarse-grained soil or debris embedded in concrete near top of pile	Overbreak in coarse gravel or made ground near ground-surface producing sudden loss of concrete when casing is completely extracted	1. Advancing temporary casing ahead of auger by vibratory or rotary method 2. Drilling techniques using bentonite in suspension 3. Use of permanent casing
Horizontal fractures in pile shaft or unseating of pile bases from bearing strata (pile uplift) or lateral displacement of piles	Soil displacement as experienced with driven piles	Pre-boring or multiliner techniques
Soil or rock debris at bases of piles	Dislogement of small blocks of soil or rock material from sides of bore, sometimes caused by delay in concreting the shaft	1. Concrete shaft with minimum delay 2. Temporary casing 3. Drilling techniques using bentonite in suspension
Debris embedded in pile shafts	Carelessness or lack of short length of temporary casing at top of pile bore	Provision of short length of temporary casing which projects above ground surface
Hollow on the surface of pile shaft with associated small bulbous projection some short distance beneath hollow	Use of double temporary casings and extraction of outer casing before inner casing resulting in local cavitation	Extraction of inner casing before outer casing
Local reductions in diameter of shafts of bored or driven cast-in-situ piles (necking) with associated bulbs at greater depths	Insufficient head of concrete within steel liner during extraction	Adequate head of concrete within liner

Table 2.2 Types and Causes and Preventive Measures of Piles Defects (Continued) (Thorburn *et al*, 1977)

Types of Defect	Cause of Defect	Preventative Measure
Discontinuities in pile shaft, mainly soil inclusions	Low workability concrete or premature setting of concrete or excessive period of time between mixing concrete and extraction of casing or liner	1. Use of high workability concrete mixes 2. Care should be taken in hot weather 3. Proper planning of supplies of ready-mix concrete and/or use of retarders
Hollow on surface of piles shaft with associated small bulbous projection some short distance beneath hollow	Rupture of very soft peat layers	Provision of permanent liner
Distortion of shafts of driven cast-in-place piles	Lateral movements of steel liner during extraction	Adequate ground restraint to minimise plant movement. Provision of adequate granular working platform
Containment of concrete within cage with resultant lack of cover to reinforcement or lack of concrete in under-reamed bases	Excessive quantity of reinforcement in cage	Use of a few heavy steel sections rather than a large number of closely spaced reinforcing rods
Collapse of reinforcement cage	Inadequate design or construction of cage	Proper design of cage, which should also be sufficiently rigid to be capable to withstanding normal site handling
Poorly consolidated concrete which is occasionally absent outside the reinforcement cage	Low workability concrete	Use of high workability concrete mixes
Discontinuities on pile shaft, often complete separation of concrete	Low workability concrete	Use of high workability concrete mixes
Dilution of water cement paste and formation of soft whitish cement paste	Penetration of groundwater into body of pile because of incorrect mix design	Proper design of concrete mix
Excessive bleeding of water from the exposed surface at top of pile	High water-cement ratio concrete mix	Proper design of concrete mix
Weak and partially segregated concrete at pile base	Significant accumulation of groundwater at base of bore prior to placing first batch of concrete	Use of tremie

Table 2.2 Types and Causes and Preventive Measures of Piles Defects (Continued) (Thorburn *et al*, 1977)

Types of Defect	Cause of Defect	Preventative Measure
Inclusions of clay lumps within pile shaft	Clay lumps adhering to temporary casing which are subsequently displaced by the viscous concrete and incorporated in the body of the pile	Use of clean casing
Occasional segregation of concrete in pile shaft	Concrete impinging on reinforcement cage during placing	Use of short length of trunking
Segregation of concrete with dilution of water cement paste and formation of soft whitish cement paste; sometimes layers of sand and gravel are found within body of pile	Uncontrolled activation of trip mechanisms in concrete placers used to place concrete in waterfilled bores	Use of tremie
Segregation of concrete with dilution of water cement paste and formation of soft whitish cement paste; sometimes layers of sand and gravel are found within body of pile	Raising of tremie above surface of concrete either accidentally or in an attempt to re-start placing after interruption of free flow of concrete	Proper use of tremie
Inclusion of soil and debris in pile shaft near top of pile	"Topping up" operations. Additional concrete discharged on top of previous lift after casing or liner is removed	No "Topping up" after removal of casing or liner
Discontinuities in pile shaft	Low workability concrete in lower portion of pile shaft because of lack of continuity in placing concrete	Proper planning of supplies of ready-mix concrete and/or the use of retarders
Soil inclusions in shafts of driven piles	Lower edged of steel liner withdrawn above upper surface of batch of concrete being driven from liner by internal drop hammer	Proper technique of extraction of steel liner
Serious discontinuities in pile shaft	Aggregate interlock and raising of concrete with casing during extraction from used of poker vibrator	Proper design of concrete mic to ensure self-compaction. Prohibit use of poker vibrator
Segregation of concrete with dilution of water-cement paste and formation of soft whitish cement paste. Sometimes layers of sand and gravel are found within body of pile	Significant ground-water flow through relatively permeable strata	Use of permanent casing
Disintegration of concrete	Chemical attack	Proper site investigation and guidance by C & CA

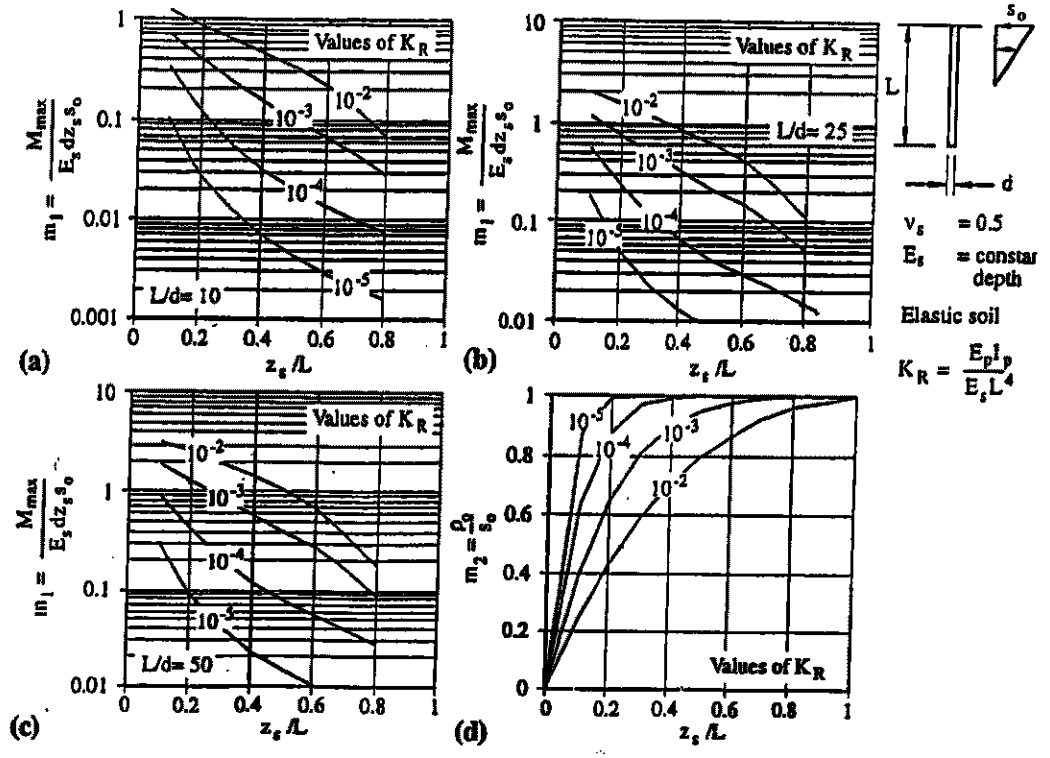

(a) In uniform soil

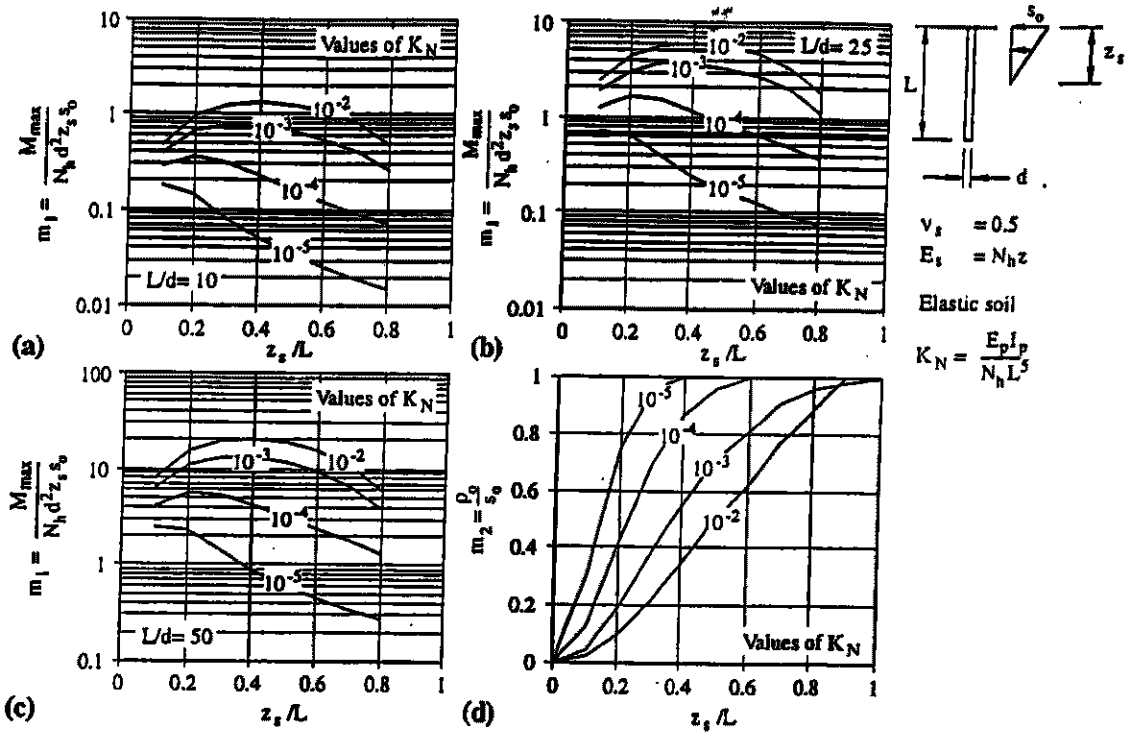

(b) In Gibson soil

Fig. 2.1 Elastic solution for unrestrained free-head pile (Linear soil movement profile) (After Chen and Poulos, 1997)

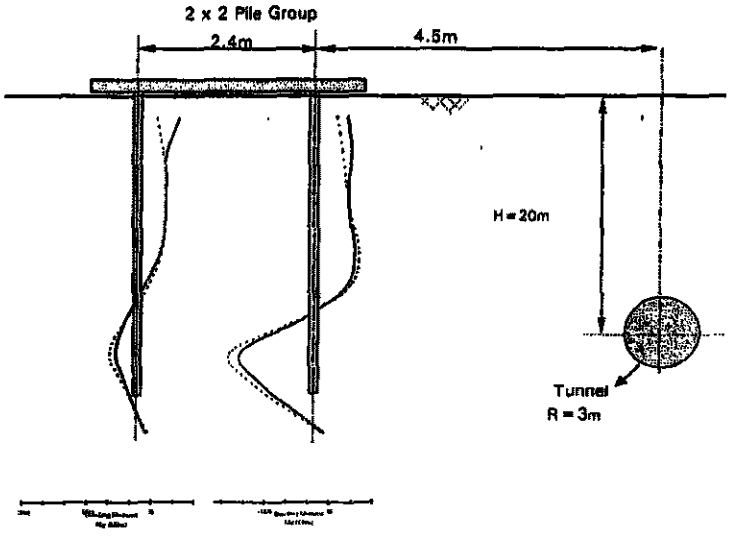

(a) Comparison of the induced bending moment on a pile in a group and a single pile

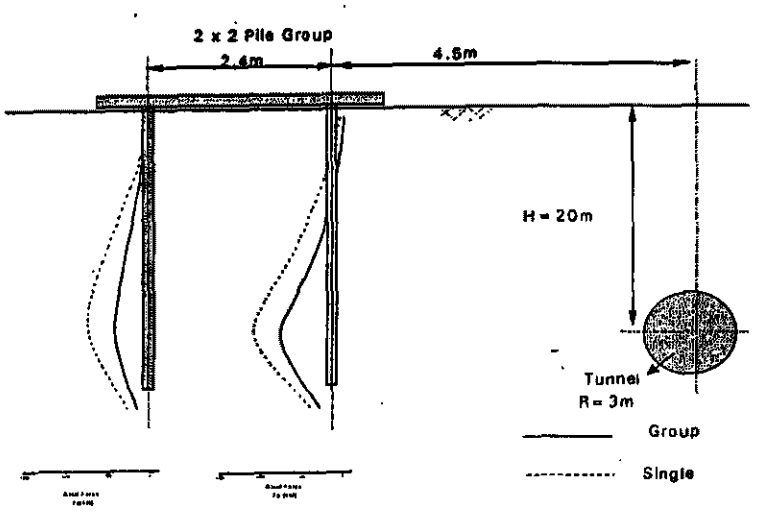

(b) Comparison of the induced axial forces on a pile in a group and a single pile

Fig. 2.2 Pile-ground response due to tunnlling
(After Loganathan et al, 1999b)

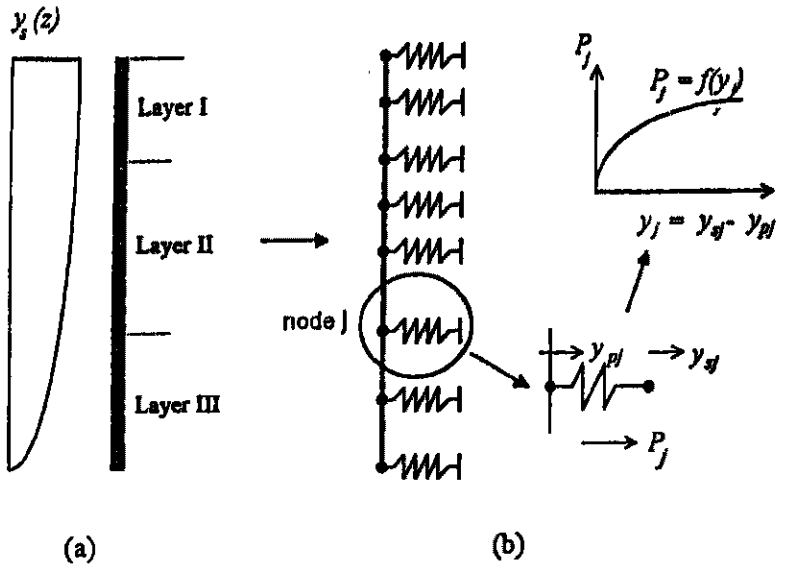

1. (a) Pile in layered soil undergoing lateral movement; (b) Discretization of problem

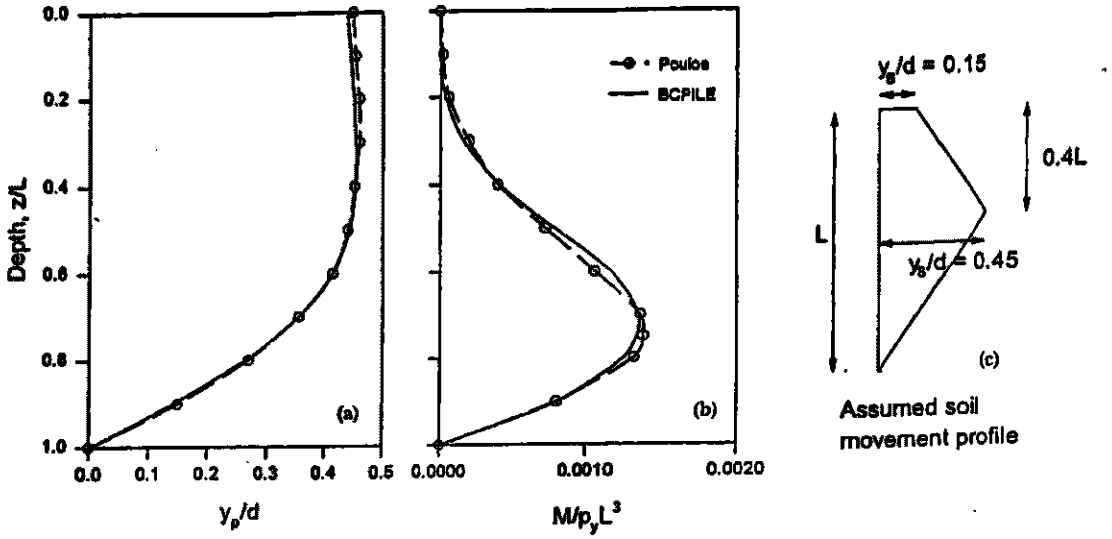

2. Lateral pile displacement and bending moment due to trapezoidal soil deformation profile

Fig. 2.3 Pile subjected to embankment induced lateral soil movements (After Goh *et al*, 1997)

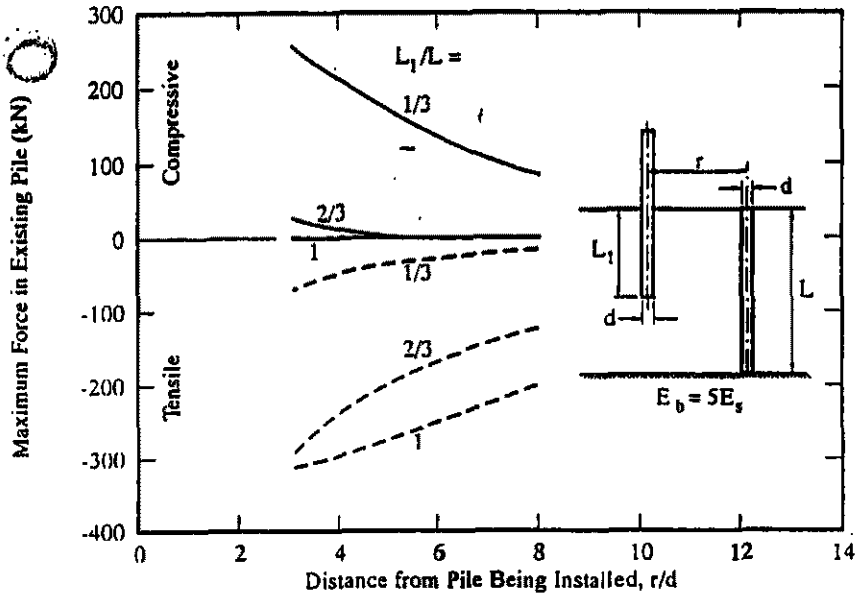

Fig. 2.4 Maximum compressive and tensile forces induced in existing pile due to adjacent end-bearing pile (After Poulos, 1994)

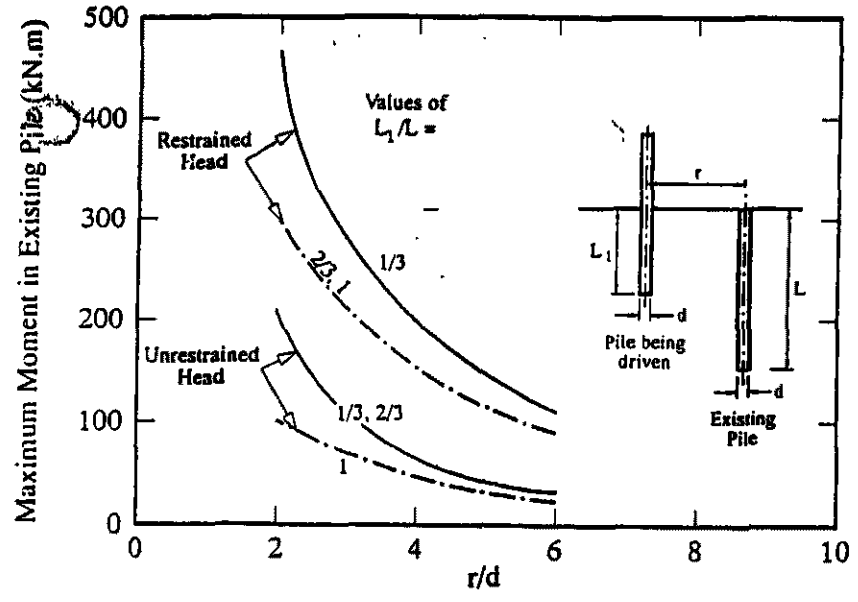

Fig. 2.5 Influence of pile spacing on maximum moment in pile due to driving of adjacent pile (After Poulos, 1994)

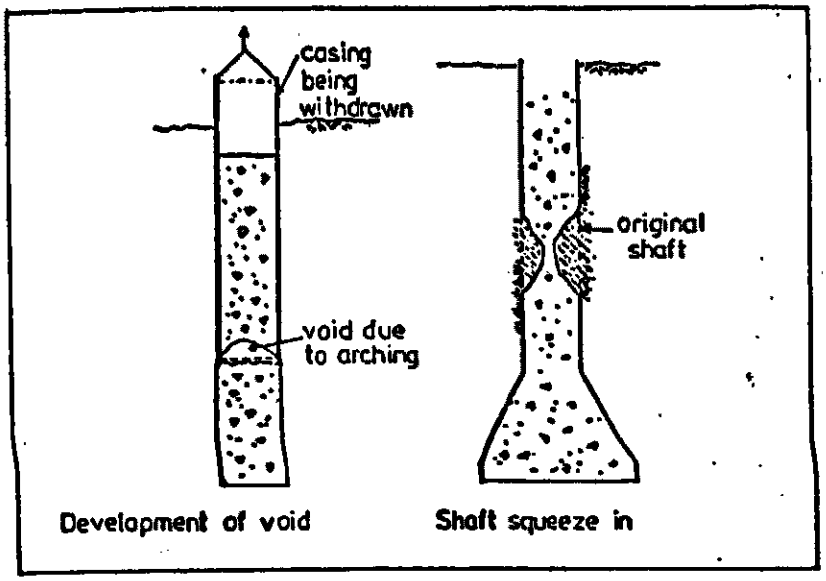

Fig. 2.6 Formation of defects in bored pile construction
(After Baker and Khan, 1971)

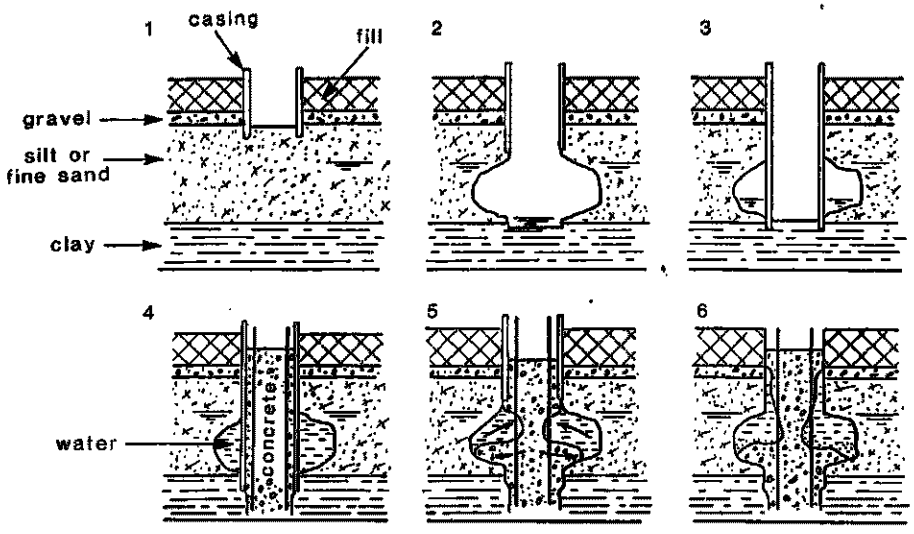

Fig. 2.7 Schematic presentation of formation of water-filled cavities
(After Thorburn *et al*, 1977)

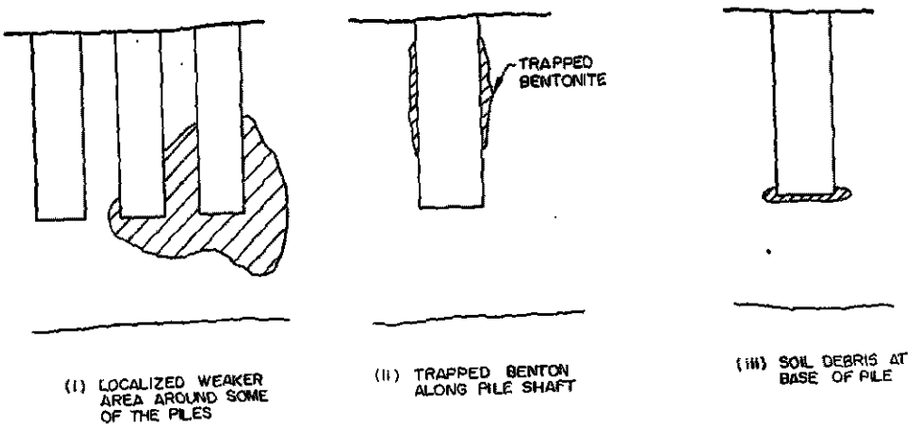

a) TYPICAL GEOTECHNICAL DEFECTS

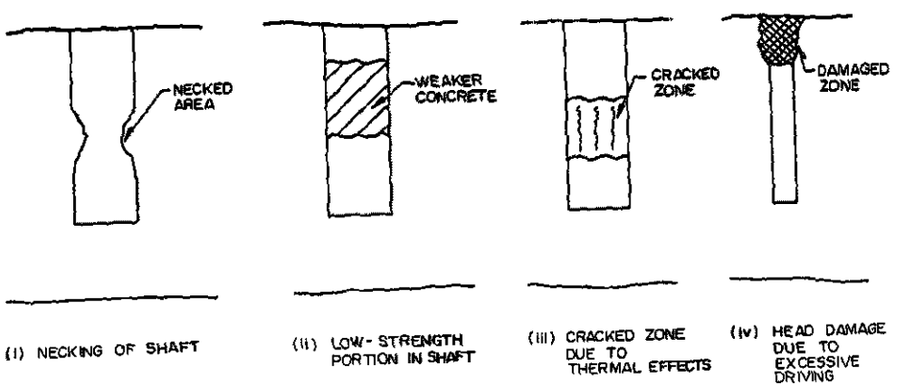

b) TYPICAL STRUCTURAL DEFECTS

Fig. 2.8 Example of geotechnical and structural defects in piles (After Poulos, 1997)

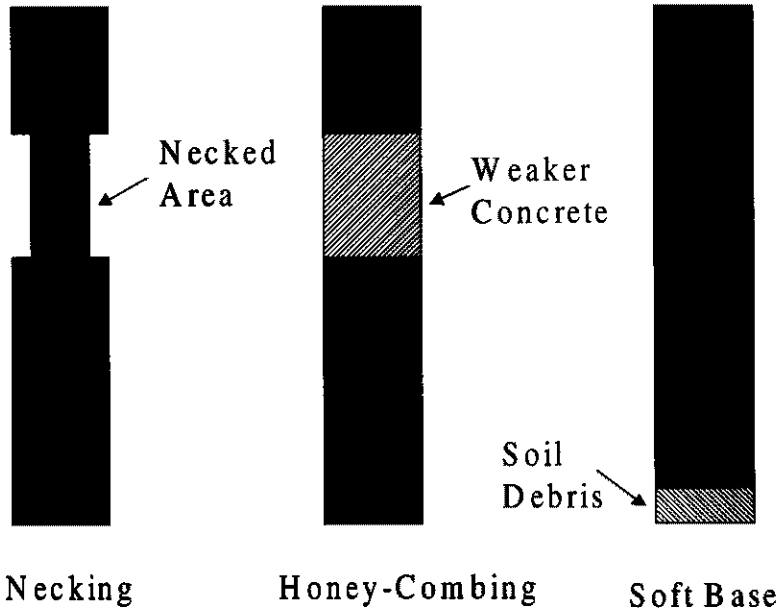

Fig. 2.9 Basic types of defective piles for numerical analysis

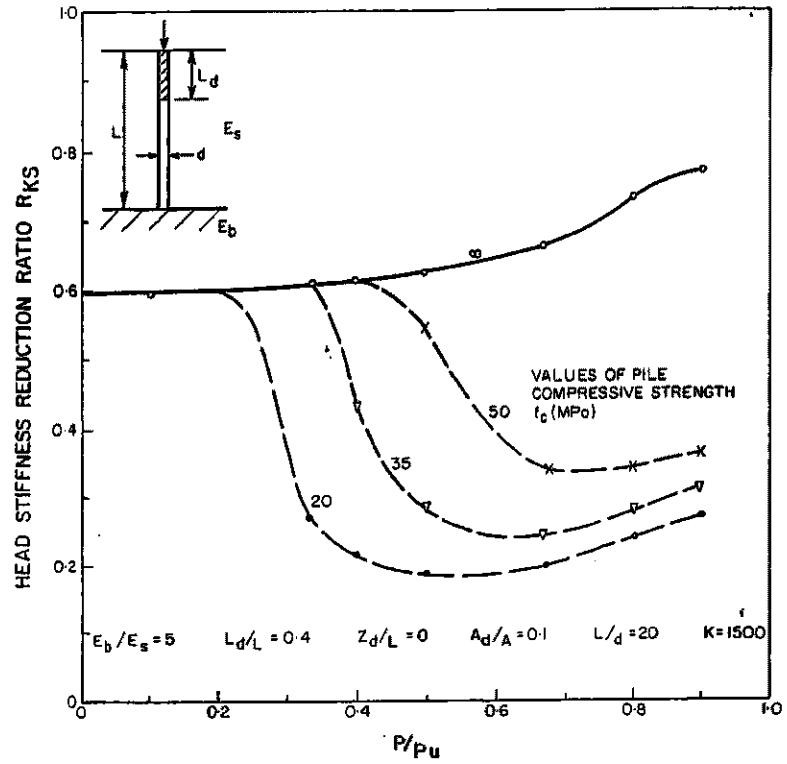

(a) Due to structural defect

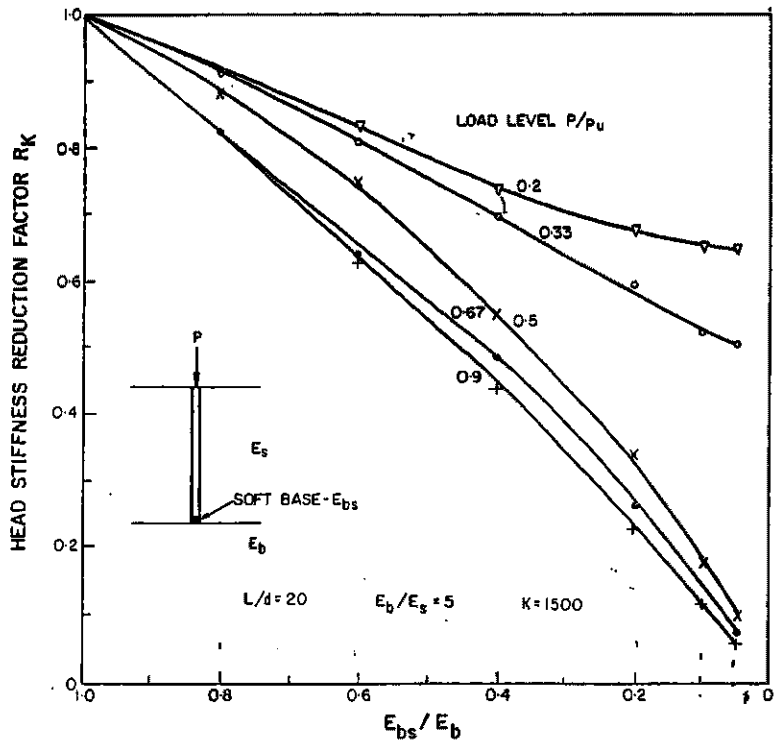

(b) Due to geotechnical defect

Fig. 2.10 Effect of load level on stiffness reduction due to pile defects (After Poulos, 1997)

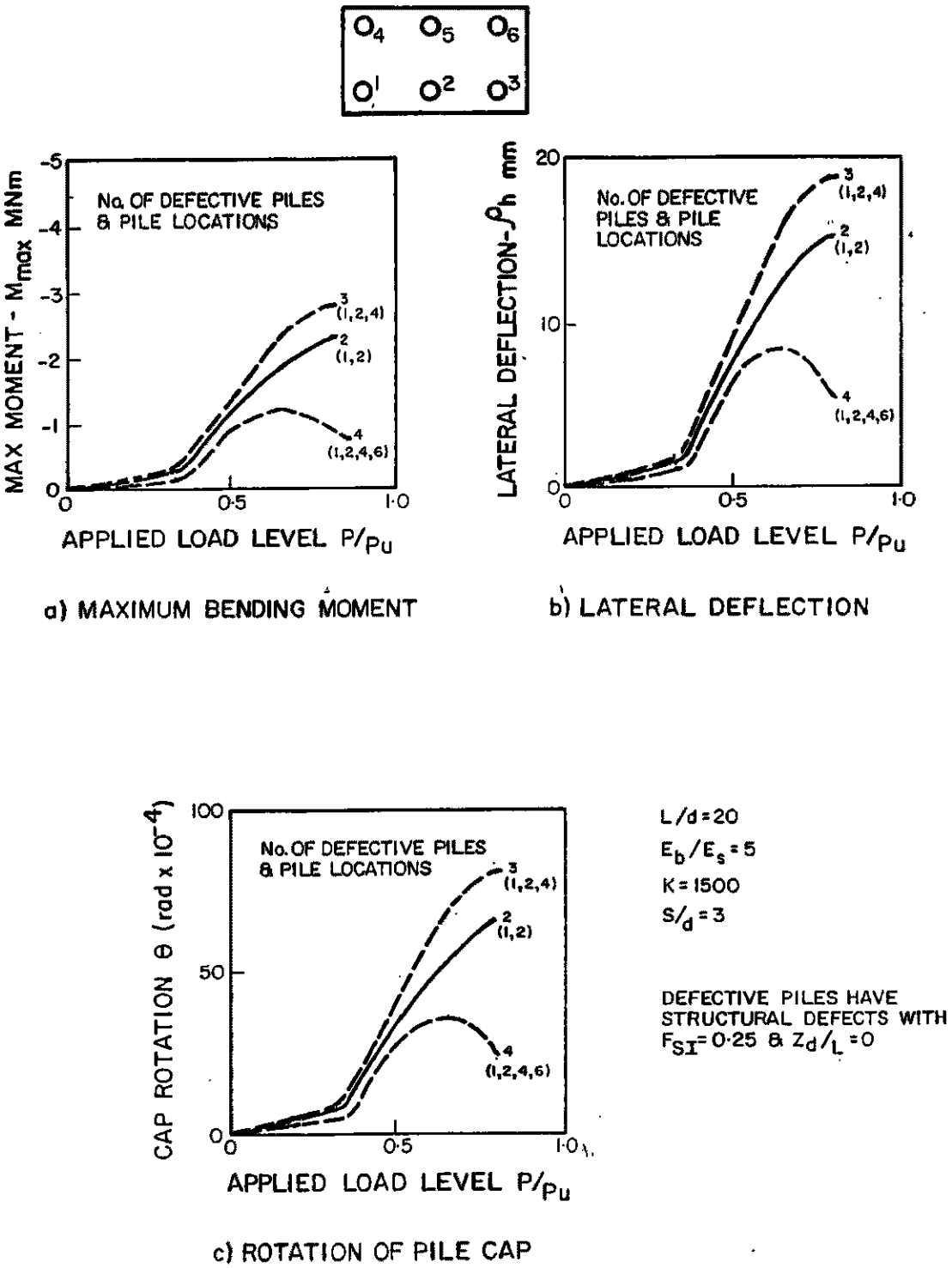

Fig. 2.11 Effect of proportion of structurally defective piles on lateral response of group under axial loading (After Poulos, 1997)

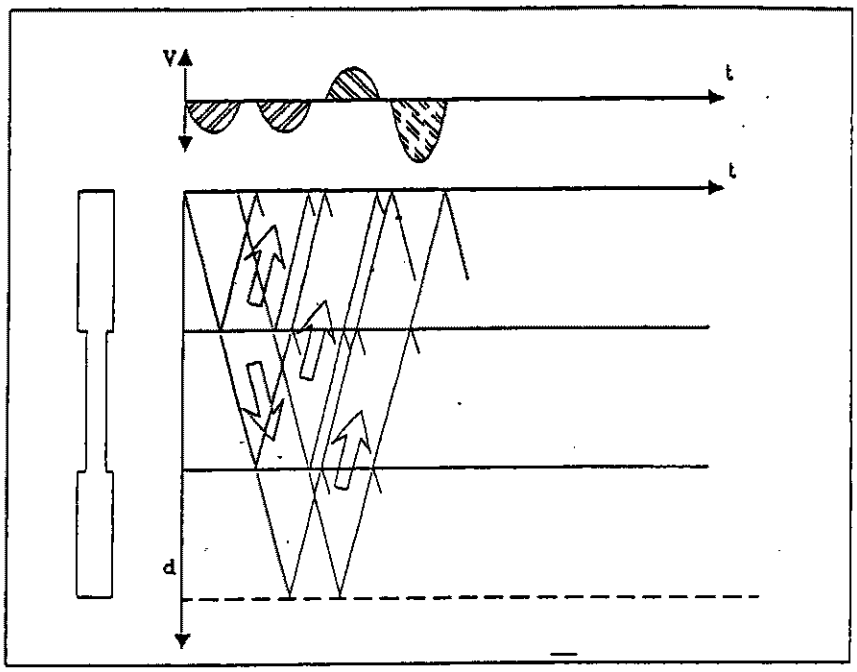

Fig. 2.12 Stress wave propagation for necked pile

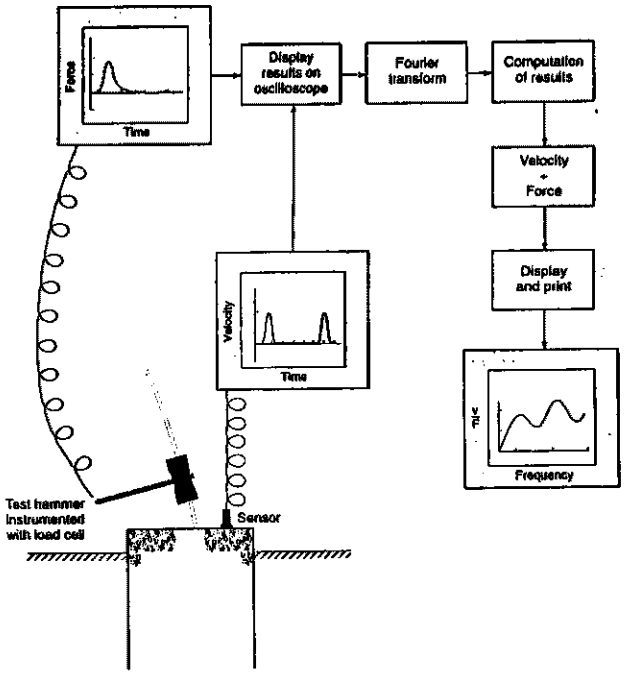

Fig. 2.13 Elements of a typical sonic method test (after Stain, 1982)

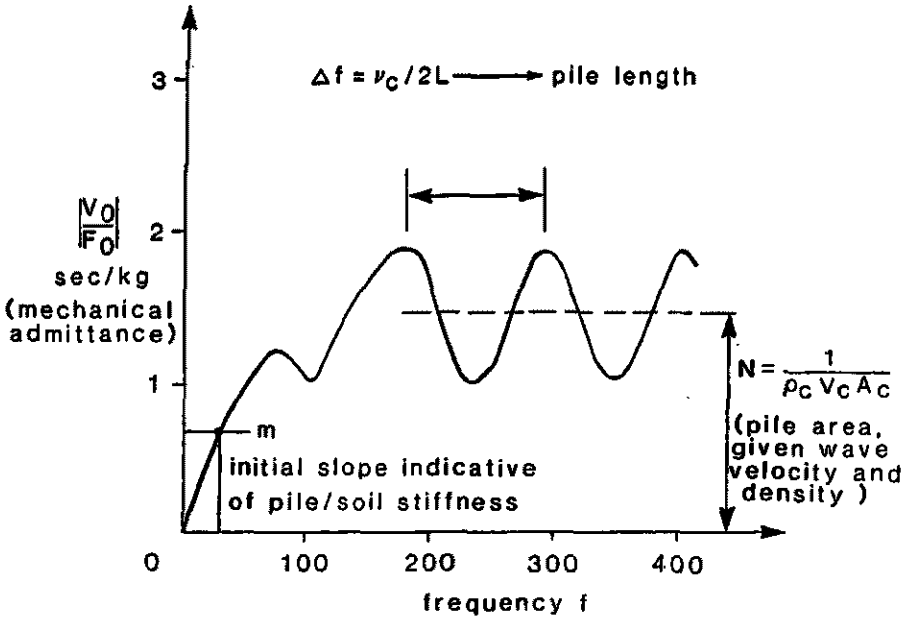

Fig. 2.14 Idealized response curve form a vibration test

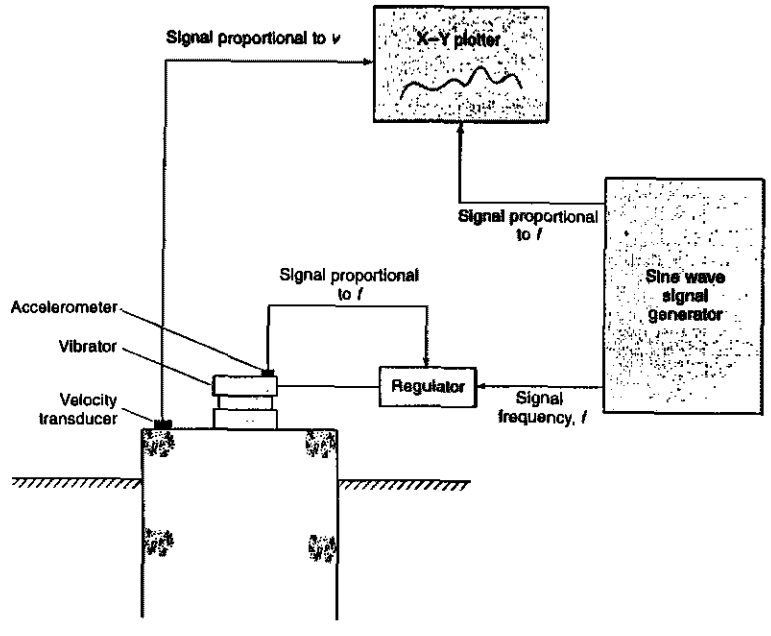

Fig. 2.15 Elements of frequency response method test (after Turner, 1997)

Chapter 3

General Elastic Analysis of Piles and Pile Groups

3.1 Introduction

Computer programs for the analysis of pile groups vary in the type of approach used and in the sophistication of treatment of different aspects of group behavior. As reviewed in Chapter 2, three programs which have been used for pile group analysis are PGROUP (Banerjee *et al*, 1976), DEFPIG (Poulos, 1990a) and PIGLET (Randolph, 1989), and these have been compared by Poulos and Randolph (1983). All three programs are based on an elastic continuum analysis, although DEFPIG can also be extended into the non-linear range by specifying limiting values of skin friction and lateral pressure along the piles.

Although these programs have been used widely, they all involve a number of simplifications and idealizations, owing to the limitations of computer technology at the time of their development.

For these and other similar programs (excepting finite element analyses), there are simplifications and limitations with respect to at least six aspects:

(1) *Interaction*. Pile to pile interaction is widely considered, but a more accurate method requires consideration of pile *element* to pile *element* interaction.

(2) *Elements*. Full cylindrical and/or annual elements are usually used, but the stress distribution on an element is generally not uniform around the pile circumference for cases of general loading.

(3) *Load-deformation coupling*. Normally the axial, lateral and torsional responses of the piles are treated separately, *i.e.* de-coupled. However pile-soil interaction is a three-dimensional problem, and each of the load-components has deformation-coupling effects, *e.g.* vertical loading induces lateral movements as well as vertical movements.

(4) *Pile cross-section*. Normally the pile cross sections are taken as uniform. However, for some cases, such as piles with defects, the cross-sections of at least some of the piles are not uniform.

(5) *Loadings*. Loadings applied to pile groups are usually applied directly to the piles ("on-pile" loading), but sometimes loadings are induced by ground movements ("off-pile" loadings), such as those arising from loading caused by adjacent structures, or from nearby tunnel construction or excavations.

(6) *Global pile foundation*. Rather than a single group, multiple individual piles and/or pile groups may exist simultaneously in many engineering projects.

All the effects mentioned above may be important if the behavior of pile foundations is to be modelled accurately. Because of rapid developments in computer technology, the use of accurate algorithms can now take precedence over earlier concerns about computer speed and capacity. This chapter describes the development of a computer program that eliminates the above limitations and is therefore more general as a tool for the elastic analysis of the behavior of piles and pile groups. The accuracy of the program is tested via comparisons with existing solutions. Some aspects of pile behaviour which cannot be computed by conventional approaches are also described.

3.2 Basic Principles

3.2.1 Introduction

Using the principles of three-dimensional boundary element method, the "analysis platform" is set up for a half space with a global foundation system, as illustrated in Fig. 3.1. The analysis considers the overall foundation performance of multiple single piles and pile groups and can incorporate the effects of such factors as defective piles, soil movements, general pile loadings *etc.* at the same time.

In the governing equation, a global matrix is derived, which is composed of several sub-matrices. Through the introduction of the concept of hierarchical structures and basic influence factor matrices, a set of sub-matrices is developed both for the presentation of the analysis and for computer program implementation. The development of the global matrix is described below.

3.2.2 Assumptions and Terminologies

The following assumptions are employed for the analysis:

1. The soil is assumed to be an ideal homogeneous isotropic elastic weightless half-space, having elastic parameters E_s and ν_s that are not influenced by the presence of the piles. However, it is possible to consider, in an approximate manner, the soil mass as a non-homogeneous continuum.

2. Piles are assumed to be circular in cross-section and made of a homogeneous isotropic elastic material with two unchangeable elastic parameters E_p and ν_p. The piles are vertical and perfectly rough. Where the diameter of a pile changes abruptly, no account is taken of local stress concentrations.

3. The deformation of the piles and soil mass are elastic and the superposition principle is valid.

4. Two kinds of elements are considered at the soil-pile interface, soil elements and pile elements. These boundary elements are meshed in partly cylindrical or annular surfaces. The distributions of the stress components on the boundary elements at the pile-soil interface are assumed to be uniform over each element.

5. To simplify the compatibility and equilibrium equations for pile heads and caps, the load and displacement components at the top of each pile are assumed to be uniform and equal to the average value.

6. The pile caps above each pile group are assumed to be rigid and not in contact with the soil surface.

7. There is no slip and gap at the pile-soil interface, *i.e.* the soil element and the pile element are in contact at the soil-pile interface.

8. Pile head and element displacements due to pile tip displacements are calculated assuming rigid body movements and ignoring the pile flexibility.

The term "stress" above and below is used for the load over the area of pile-soil element whose shape is either plane (at the pile base elements) or cylindrical (at the pile side elements). A diagrammatic illustration of elements and stresses on a pile is given in Fig. 3.2. Each element has three stress components (p_x, p_y, p_z) acting on it in the Cartesian coordinate system. It should be noted that the elements in fact are subjected to shear tractions, τ_{rz} and $\tau_{r\theta}$, and a normal traction τ_{rr} in a polar coordinate system. However using the Cartesian coordinate system it is easier to set up compatibility and equilibrium equations in the pile group analysis. The computed stresses in the X, Y, Z directions are translated into the real tractions by coordinate transformation.

For "structural analysis", each pile is treated as a one-dimensional beam-column which is able to compress or extend axially, bend in the X-Z and Y-Z planes and twist in the X-Y plane. Effects of Poisson's ratio of piles are involved in torsional behaviour since the shear modulus of the piles is determined by E_p and ν_p. Although the piles are treated as one-dimensional beam-columns, three basic deformations are considered simultaneously *i.e.* the axial, bending and torsional deformations of piles are produced by the three components of stresses (p_x, p_y, p_z) on the elements. For example, p_z results in axial and bending deformations while p_x and p_y produce bending and torsional deformations.

In developing this method, stresses, loads and displacements in Cartesian coordinates are assumed to obey the right hand "screw" rule. In numbering piles, priority is given to piles within pile groups and then to individual piles.

3.2.3 Global Equation

The general equations contain the following four kinds of independent equations:

1. *Compatibility equations at the pile-soil interfaces*. The relative displacements at any pile-soil element are zero for elastic response.

2. *Equilibrium equations for pile heads and caps*. The loads on the pile caps are balanced by the head loads on piles in the corresponding group.

3. *Compatibility equations for pile heads and caps*. The pile cap displacements are compatible with the head displacements of the grouped piles as shown in Fig. 3.3. The

pile head displacements have contributions from pile-soil stresses, tip displacements of piles in the group, and head loads of the grouped piles.

4. *Equilibrium equations for piles.* Tractions or stresses on the pile-soil interfaces (including tip loads) are balanced by the head loads on the piles, which are generally unknown for grouped piles but are generally known for individual piles.

.2.3.1 Global Equation

A global equation can be set up based on the four kinds of equations, as shown in Eq. 3.1:

$$\begin{pmatrix} A & B & \emptyset & D \\ \emptyset & \emptyset & G & H \\ O & P & Q & R \\ S & \emptyset & \emptyset & V \end{pmatrix} \begin{pmatrix} X_e \\ X_b \\ X_c \\ X_t \end{pmatrix} = \begin{pmatrix} Y_q \\ Y_c \\ \emptyset \\ Y_p \end{pmatrix} \quad \text{..... (3.1)}$$

where

$\emptyset$ = zero sub-matrix

A = sub-matrix describing pile and soil behaviour at all elements

= $SIF + PIF$

SIF = sub-matrix of displacements due to stresses at soil elements

PIF = sub-matrix of displacements due to stresses at pile elements

B = sub-matrix of pile element displacements due to pile tip displacements

D = sub-matrix of pile element displacements due to pile head loads

G = sub-matrix of pile cap loads due to pile cap displacements by cap-tie-cap beam forces (to allow for pile caps jointed by tie beams)

H = sub-matrix of pile cap loads due to pile head loads

O = sub-matrix of pile head displacements due to pile element stresses

P = sub-matrix of pile head displacements due to pile tip displacements

Q = sub-matrix of pile head displacements due to pile cap displacements

R = sub-matrix of pile head displacements due to pile head loads

S = sub-matrix of pile head loads due to pile element stresses

V = sub-matrix of pile head loads due to pile head loads

Y_q = vector of element stress offsets

= $Y_{q,t} + Y_{q,e}$

$Y_{q,t}$ = vector of pile element displacements due to head loads on individual piles

Y_{qe} = vector of pile element displacements due to external soil displacements/stresses/forces

Y_c = vector of loads on pile caps

Y_p = vector of pile head loads on individual piles

X_e = vector of pile-soil stresses

X_b = vector of pile tip displacements

X_c = vector of pile cap displacements

X_t = vector of pile head forces at the pile cap.

The global foundation is assumed to contain *ncap* pile groups with any configuration, *npils* non-identical piles which have *nipsum* individual piles and *ncpsum* piles in pile groups, and *ntot* elements of any size which may include partly cylindrical elements on shafts and partly ring elements on both bases and discontinuities. Then, a coupled global matrix with

[*3*ntot+6*npils+6*ncap+6*ncpsum*] dimensions is set up, and the following unknowns can be solved:

1. *3*ntot* pile-soil element stresses $\{X_e\}$
2. *6*npils* pile tip displacements $\{X_b\}$
3. *6*ncap* pile cap displacements $\{X_c\}$
4. *6*ncpsum* pile head loads for grouped piles $\{X_t\}$.

After the pile-soil stresses $\{X_e\}$ and pile tip displacements $\{X_b\}$ are computed from Eq. 3.1, the head displacements of individual piles $\{X_i\}$ can be determined from the following equation:

$$\{X_i\}=[O]\{X_e\}+[P]\{X_b\}+[R]\{Y_p\} \quad \text{.....(3.2)}$$

As a special case, if only individual piles exist, Equation 3.1 can be reduced to a much simplified form, as shown in Equation 3.3:

$$\begin{pmatrix} A & B \\ S & \emptyset \end{pmatrix}\begin{pmatrix} X_e \\ X_b \end{pmatrix}=\begin{pmatrix} Y_q \\ Y_p \end{pmatrix} \quad \text{.....(3.3)}$$

3.2.3.2 Sub-Matrix Classifications and Known Vectors

In the global matrix, there are twelve non-zero sub-matrices, *i.e. SIF, PIF, B, D, G, H, O, P, Q, R, S, V.* These sub-matrices can be classified into four categories according to the method of their derivation:

1. The sub-matrix *SIF* for displacements and stresses on soil elements, is obtained by integration of Mindlin's equations (Mindlin, 1936). The detailed integral equations of 3-D displacements on soil elements are derived in Appendix B.
2. The sub-matrices *PIF, D, G, O, R* relating displacements due to stresses or loads on a pile, are determined via the principles of structural analysis.

3. The sub-matrices B, P, Q relating displacements among heads, tips and elements on piles, are derived via the rigid body movements of the piles.

4. The sub-matrices H, S, V relating pile head loads, loads on the pile caps, or stresses on piles, are established by force equilibrium.

The detailed expressions for the various sub-matrices are set out in Appendix A.

There are four types of known vectors, *i.e.* $Y_{q,t}$, $Y_{q,e}$, Y_c , Y_p . The vector of element displacements due to pile head loads $Y_{q,t}$ is determined by structural analysis. Both vectors of pile cap loads Y_c and individual pile head loads Y_p have six components. Element displacements due to external soil displacements/stresses/forces are incorporated into the vector $Y_{q,e}$, which will be described in detail later in the chapter.

3.2.4 Numerical Analysis of the Sub-Matrices in the Global Matrix

3.2.4.1 Basic Influence Factor Matrix (BIFM)

The term "influence factor" is used here to define the response of one mechanical parameter (such as load/stress/displacement) caused by imposing another unit mechanical parameter. The concept of influence factors was introduced into pile foundation analysis by Poulos *et al* (1980) for de-coupled cases. However, it is difficult to set up a general 3-D fully coupled pile analysis if single uncoupled influence factors are considered, since the influence factors are coupled and are tensors rather than scalar values. For any two soil elements i and j, for example, there are nine stress-displacement influence factors $I_{i,j,k,l}$ in a general 3-D fully coupled problem, for example, $I_{i,j,k,l}$ = soil displacement in k direction at element i due to a unit stress in l direction on element j (l, k = 1,2,3). The matrix which contains all components of the influence factors is called here the basic influence factor matrix (BIFM). The above influence factors $I_{i,j,k,l}$, for example, are composed of a 3×3 basic influence factor matrix (BIFM) of stress-displacement response. It is found that an efficient way to set up the sub-matrices in the global matrix is to consider the basic influence factor matrices (BIFM's) as "basic elements" in sub-matrices, *i.e.* instead of single influence factors, the sub-matrices are formed by assembling the individual basic influence factor matrices (BIFM's). This important concept simplifies the setting up of the general 3-D fully coupled pile analysis. Corresponding to the sub-matrices, there are twelve BIFM's which

are defined in Appendix A. The BIFM's which make up the sub-matrices are set out in Appendix A as well.

3.2.4.2 Hierarchical Structure of Sub-Matrices in the Global Matrix

Because of the full coupling of the six stress/displacement components with element-element interaction, expressing these sub-matrices in the global matrix in full is cumbersome. However, it is found that every sub-matrix has a hierarchical structure, *i.e.* a sub-matrix can be divided (or "layered") into some smaller sub-matrices. The "innermost layer" of a sub-matrix is composed of several basic influence factor matrices (BIFM's), and the outline of the hierarchical structure is as follows:

$$A=\underbrace{\begin{pmatrix} a_{1,1} & \cdots & a_{1,n1} \\ \cdots & \cdots & \cdots \\ \cdots & a_{i1,j1} & \cdots \\ a_{m1,1} & \cdots & a_{m1,n1} \end{pmatrix}}_{Sub-Matrices} \Rightarrow a_{i1,j1}=\underbrace{\begin{pmatrix} b_1 & & \\ & \cdots & \\ & & b_{i2} \\ & & & b_{m2} \end{pmatrix}}_{Hierarchical\ Matrices} \Rightarrow b_{i2}=\begin{pmatrix} c_1 \\ \cdots \\ c_{i3} \\ c_{m3} \end{pmatrix}$$

The global matrix A outlined above is assembled from sub-matrices $a_{i1,j1}$ ($i1$=1,$m1$; $j1$=1,$n1$). The sub-matrix $a_{i1,j1}$ is formed from diagonally arranged matrices b_{i2} ($i2$=1,$m2$) where the matrix b_{i2} is obtained from basic influence factor matrices c_{i3} ($i3$=1,$m3$) which are arranged vertically.

Each of these BIFM's has clear physical meaning and can be evaluated easily via short computer subroutines. The sub-matrices in the global matrix can be conveniently built up by calling the corresponding subroutines. The hierarchical structures of the sub-matrices are presented in more detail in Appendix A.

3.2.4.3 Soil Element Movements

The soil movements in this paper are evaluated via soil influence factors through the integration of Mindlin's equations (Mindlin, 1936) (displacement in l direction at point i due to a unit force in k direction at point j in half space, l,k=1,2,3) on a soil element area. It should be emphasized that there are nine soil influence factors which form a BIFM, because the loads and deformations are fully coupled in three dimensions.

It is found that most of the computer running time is consumed in generating the first type of sub-matrix, which involves numerical integration of Mindlin's equations. It is obvious that the result is increasingly insensitive to the number of integration points as the distance between two elements is increased. Therefore, the "changeable integration point" method has been introduced here, and involves the use of adjustable integration points, with less integration points being used as the distance between two elements becomes greater.

3.2.4.4 Pile Element Movements

The deformations due to axial and horizontal forces, moments and torsion in pile elements are coupled, and the diameter of any element may be arbitrary. Calculation of the second kind of sub-matrix is therefore more complicated than the de-coupled model presented by Poulos (1989b). Considering the advantages of do-loop functions in computation, the expressions for load-deformation characteristics of pile elements are derived via a nested recursion form which makes the computer program shorter and easier than in previous methods. Suppose a pile is divided into a number of cylindrical elements, then, as an example, the nested recursion form for rotation of pile element i is as follows:

$$\theta_{z,i} = \theta_{z,i-1} + \frac{T_i (L_i / 2)}{G_i J_i} \qquad \text{..... (3.4)}$$

where $\theta_{z,i}$ and $\theta_{z,i-1}$ are the rotations of pile elements i and i-1 respectively, T_i, L_i, G_i, J_i are torsion, length, shear modulus and polar moment of inertia respectively of element i of the pile.

Derivations of the pile behaviour equations are relatively cumbersome. In de-coupled situations, Poulos (1989b) derived pile displacement equations that are expressed by a product of a summation matrix *AD* and a pile compression matrix *FE*. However, following this concept in the full-coupled situation will be very complicated. The method proposed in this paper uses "adding operations" instead of "multiplier operations", *i.e.* pile displacement behaviour is decomposed and expressed by two sub-matrices (sub-matrix of displacements due to stresses at pile elements *PIF*, and sub-matrix of pile element displacements due to pile head loads *D* for pile groups) and a vector (the vector of pile element displacements due to pile head loads $Y_{q,t}$ for individual piles).

The matrices and vector are relatively simple to express and may be derived from the principles of structural analyses.

The detailed equations of nested recursion in the pile influence factors are set out in Appendix C.

3.2.5 Non-Homogeneous Soil

In the elastic continuum theory, the soil stiffness is directly related to the Young's modulus of the soil. If a non-homogeneous soil mass is considered, the following approximation is used by Poulos (1979,1989b) to evaluate the stress-displacement influence factors of soil elements by Mindlin's equation when the soil variation between adjacent elements is not large or a soil layer is not overlain by a much stiffer layer:

$$E_{s,i,j} = 0.5(E_{s,i} + E_{s,j}) \quad \text{.....(3.5)}$$

where $E_{s,i}$ and $E_{s,j}$ are the values of the Young's modulus of the soil at elements i and j respectively.

As shown in Appendix A, the element (influence factor) of BIFM of soil element $I_{i,j}$ in the sub-matrix SIF is $I_{i,j,k,l}$ (soil displacement in k direction at element i due to a unit stress in l direction on element j, k, l = 1,2,3). It is convenient if $I_{i,j,k,l}$ can be expressed as the value of the influence factor for a unit value of Young's modulus, $IF_{i,j,k,l}$, divided by the average soil Young's modulus, $E_{s,i,j}$, *i.e.*

$$I_{i,j,k,l} = \frac{IF_{i,j,k,l}}{E_{s,i,j}} \quad \text{.....(3.6)}$$

The solution for the displacement within a uniform semi-infinite soil mass caused by a pile can also be used to estimate the displacement of a pile founded within a layer of a system of m layers of different soils which lie below the pile tip (Poulos *et al*, 1980). The displacement of the pile is given approximately as:

$$I_{i,j,k,l} = \sum_{n=1}^{m-1} \frac{IF_{i,j,k,l,n} - IF_{i,j,k,l,n+1}}{E_{s,i,j,n}} + \frac{IF_{i,j,k,l,m}}{E_{s,i,j,m}} \quad \text{.....(3.7)}$$

where

$IF_{i,j,k,l,n} = IF_{i,j,k,l}$ (in Eq. 3.6 with following defined j) for layer n

$E_{s,i,j,n} = E_{s,i,j}$ (in Eq. 3.5 with following defined j) for layer n

j = represents the soil element, if n=1; or refers to the pile axis at the level of the top of layer n, if n>1.

3.3 Computer Program GEPAN

To implement the above analysis, a FORTRAN computer program called GEPAN (General Pile Analysis) has been developed.

After reading the source soil and pile data, GEPAN automatically generates a group of unified geometry and control parameters. The movements of pile and soil of shaft, base and discontinuity elements can be calculated via appropriate subroutines. Each sub-matrix in the global matrix is assembled by combining the relevant BIFM's, which are formed by relatively simple subroutines. Discontinuity elements (annular elements at diameter changes within a pile) can be automatically generated and labeled. The main chart flow for program GEPAN is shown in Fig. 3.4.

The cylindrical or annular boundary elements are transformed into rectangular elements by mathematical transforms. Then the simple rectangular integration method, where the rectangular elements are divided into $J \times J$ smaller rectangles, is used for integration of Mindlin's equation. GEPAN automatically eliminates the singularity of the integration for the displacements of an element from loads of the element itself via appropriate mathematical processes.

Because the proposed analysis considers element-element interaction within a global foundation system, the global matrix in GEPAN can be very large. GEPAN uses dynamic memory storage technology for more rational and effective use of the computer memory. A matrix with changeable dimensions is allocated only when needed and de-allocated as soon as it is no longer needed.

3.4 Evaluation of Analysis

Comparisons have been made between the results of the program GEPAN and the widely used pile analysis programs DEFPIG (Poulos, 1990a) and PIGLET (Randolph, 1989), as well as with other published solutions. In these comparisons, results obtained author using these programs are labeled with the program names, while results from published papers are indicated by the appropriate source and reference number. In pile parametric studies, two important parameters which describe the behaviour under axial and lateral loadings respectively are the pile stiffness factor K and the pile-flexibility factor K_R, where K is defined as ratio of the Young's moduli of pile and soil (E_p/E_s) and K_R is a dimensionless measure of the flexibility of the pile relative to the soil ($E_pI_p/E_s/L^4$) (Poulos *et al*, 1980). Some of these comparisons are presented below.

3.4.1 Single Pile

Figs. 3.5 and 3.6 compare various solutions for the top settlement S and distribution of shear stress p along the shaft respectively for a single pile under an axial load. The comparisons for a single pile with horizontal loading and moment among results via using GEPAN, DEFPIG, PIGLET and the finite element analyses from Hull (1987) are shown in Fig. 3.7 and 3.8, where $I_{\rho M}$ is defined as the influence factor for displacement caused by moment for constant E_s, and $I_{\theta M}$, $I_{\theta H}$ are the influence factors for rotation caused by moment and horizontal load respectively for constant E_s ($I_{\rho M}$ = $I_{\theta M}$ from the reciprocal theorem) (Poulos *et al*, 1980). A further comparison, for the rotation of a single pile subjected to torsion, is shown in Fig. 3.9. Although the principles of the programs GEPAN, DEFPIG and PIGLET are quite different, the results agree well in most cases. It should be noted that the solutions from PIGLET for a very compressible axially loaded pile, and for a rigid laterally loaded pile, tend to be inaccurate because of the inherent assumptions involved in that analysis (Randolph, 1989).

3.4.2 Pile Group

Figs. 3.10 and 3.11 show group reduction factors (group reduction factor = ratio of group stiffness to the sum of the stiffness of individual piles (Poulos *et al*, 1980)) for a 2^2 and a 3^2 pile group, for vertical and horizontal loading respectively. Fig. 3.12 compares the load distribution, expressed in terms of the ratio of pile head load P and average pile head load P_{av}, in a 3^2 pile

group subjected to a vertical load. The agreement is generally good, although GEPAN gives lower values of the group reduction factors than DEFPIG or PIGLET for horizontal loading. For a 3^2 pile group subjected to torsion, Fig. 3.13 shows the load distribution, expressed as the ratio of pile head torsion load T and average pile head torsion load T_{av}, by GEPAN and PIGLET. GEPAN considers torsional interaction whereas PIGLET ignores torsional interaction (Randolph, 1989) and therefore does not distinguish between the various piles. Fig. 3.14 illustrates a practical problem presented by Poulos and Davis (1980). Four methods are compared in Table 3.1 in which ρ_{v3}, ρ_h and θ are the vertical head displacement of pile no.3, the horizontal head displacement of the piles, and the head rotation of the piles respectively. Good agreement is observed among the three analyses which consider pile-soil-pile interaction, whereas the equivalent-bent method (which represents the pile group as a structural frame) gives rather different results.

Table 3.1 Comparison methods of the general analysis on a pile group

Quantity	Equivalent-Bent Analysis (Poulos *et al*, 1980)	Elastic Continuum Analysis (Poulos *et al*, 1980)	PIGLET	GEPAN
V_1 (kN)	67.2	50.5	55.7	54.0
V_2 (kN)	200	163.4	155	156.0
V_3 (kN)	332.8	386.1	389.3	390.0
H_1 (kN)	66.8	75.9	80.4	73.7
H_2 (kN)	66.7	48.2	39.3	50.9
H_3 (kN)	66.6	75.9	80.4	75.4
M_1 (kNm)	-6.2	-39.6	-42.0	-38.5
M_2 (kNm)	-6.2	-23.5	-16.3	-26.1
M_3 (kNm)	-6.2	-39.6	-42.0	-38.6
ρ_{v3} (mm)	17.5	14.8	9.9	10.8
ρ_h (mm)	8.9	11.8	11.4	10.5
θ (rad)	0.00581	0.00248	0.00242	0.00241

3.4.3 Piles Embedded in Nonhomogeneous Soils

Fig. 3.15 compares the head settlements of end-bearing piles with different base Young's moduli E_b using programs GEPAN and PIES (Poulos, 1989b). The latter analyses the axial movement of piles by consideration of the interaction of annular ring-elements at the pile-soil interface. There is a good agreement between the solutions. Fig. 3.16 compares the computed head settlements of a floating-pile embedded in an underlying rigid base below the soil layer. Solutions from GEPAN, PIES and DEFPIG all agree well. The settlement interaction between two piles in which the soil profile is layered is illustrated for two cases in Fig. 3.17, using Eq. 3.7 for the non-homogeneous soil profile. The agreement between settlement interaction factors from the present approach, and from the solution of Mylonakis *et al* (1998), is again good (the settlement interaction factor is the ratio of the additional settlement caused by an adjacent pile to the settlement of an isolated pile under an equal load).

3.4.4 Numerical Efficiency of GEPAN

It is found that, for a typical pile length, when the pile is divided into 20 or more elements vertically and 4 or more circumferentially, the numerical results from GEPAN become almost independent of the number of elements.

The technique of changeable integration points in GEPAN results in substantial savings in computer time, without sacrificing accuracy, as shown in Fig. 3.18 and Table 3.2. For vertical loading with a symmetrical configuration of piles, three cases are given in Fig. 3.18(a). In case I, 9×9 integration points are used, regardless of the distance between two elements. For cases II and III, changeable integration points are used. The integration point depends on the distance between two elements over pile diameter X/d, with a smaller of number of integration points being taken as the distance between two elements increases. In case II, for example, 9×9 points are used if X/d=0, 8×8 if X/d=2, ..., down to 2×2 if $X/d \geq 8$. It is seen that, in case II, GEPAN saves about 75% computer running time as compared with the time for case I, while the relative error is only about 0.05%. It is shown that, considering the both of accuracy and running-time, the much efficiency integration pattern is case II among these three cases.

Table 3.2 Comparison of unchangeable and changeable integration points

Number of Piles	Case I		Case II		Case III	
	$S_{z,1}$ (mm)	Time, t_1	$S_{z,2}$ (mm)	Time, t_2	$S_{z,3}$ (mm)	Time, t_3
1	4.7123	19"	4.7098	4"	4.6394	2"
4	2.7977	5'01"	2.7969	1'18"	2.7763	56"
9	2.1169	36'43"	2.1164	17'22"	2.1042	15'59"
L=20m, d=1m, s=3m, E_p=30000MPa, E_s=20MPa, v_p=0.3, v_s=0.5 $S_{z,i}$ = top vertical movement of piles for case i, t_i computer running time for case i Computer: CP, Pentium 200, 160Mb RAM						

3.5 Some Applications

The GEPAN analysis appears to have potential application to a variety of pile analysis problems. Three simple applications are described below to illustrate the utility of the analysis.

3.5.1 Off-Line Effects of Piles

"Off-line" response exists between piles. For example, two piles with vertical loads may also experience some horizontal movement. Since GEPAN is a fully coupled load-deformation program, it can, as a matter of course, describe the off-line effects. Fig. 3.19 shows an example of the horizontal pile head movements due to vertical load on a group of two piles. It is found that the off-line horizontal movements are significant for axially loaded piles that are highly compressible and closely-spaced. It should also be noted that the horizontal off-line movement in case II (anti-symmetrical) is larger than one in case I (symmetrical). As a further example, for two horizontally loaded piles, Fig. 3.20 shows the torsional twist at the pile head due to the horizontal loads. When the angle β (between the direction of loading and the piles) is about 45°, the off-line twist reaches a maximum value.

3.5.2 Difference between "Positive" and "Negative" Interaction Factors

The concept of interaction factors is widely applied to pile foundation problems (Poulos *et al*, 1980; Mylonakis *et al*, 1998; Cheung *et al*, 1988; Lee, 1993) to compute group effects on deformations. The interaction factor α, which is defined as the ratio of additional settlement caused by adjacent pile and settlement of pile under its own load (Poulos *et al*, 1980), is generally determined for two piles with loads in the same direction (symmetrical). If two loads are opposite (anti-symmetrical) this interaction factor α is generally assumed to have the same magnitude but to be opposite in sign. However, the magnitude of the "positive" and "negative" influence factors are, in fact, different, as can be discovered indirectly from some two-dimensional analyses (Poulos *et al*, 1980; Mylonakis *et al*, 1998). The GEPAN analysis reveals that the interaction factor in the anti-symmetrical case is larger, especially when the two piles are closely-spaced, Figs. 3.21 and 3.22 show this for the interaction factors $\alpha_{\rho H}$ and $\alpha_{\theta H}$ which apply for a free-head pile subjected to horizontal load only (Poulos *et al*, 1980). This phenomenon is mainly attributed to the effects of the different off-line responses, as already discussed in relation to Fig. 3.19.

3.5.3 Interaction between Two Pile Groups

GEPAN can analyse the interaction behaviour of multiple groups of piles. Group interaction factors can be defined in a similar manner to the interaction factors for individual piles. For example, the group interaction factors α_g ($\alpha_{g,\rho H}$) can be defined as the ratio of additional vertical (horizontal) movement caused by an adjacent pile group over vertical (horizontal) movement of pile group under its own vertical (horizontal) load. Figs. 3.23 and 3.24 show group interaction factors for two 2^2 groups, for the fixed head condition, for vertical and horizontal loadings respectively. As can be seen, the interaction factors between the two groups have a similar trend to those for two individual piles.

3.5.4 Other Potential Applications

The method presented herein has the potential to analyse complex pile foundation problems and is capable of being developed to consider more general pile foundation analyses such as the following:

(1). *Ground-pile interaction problems.* In practical engineering problems, ground movements, such as those from soil shrinkage/expansion, tunneling, excavation, embankment and installation of adjacent piles, may affect the pile behaviour. If the directly-imposed "free-field" ground displacements or stresses are known, the complex ground-pile interaction problems may be assessed by employing the equations of ground movements. The applications of the ground-pile interaction problems are to be presented in Chapters 4 and 5.

(2). ***Behaviour of pile groups containing defective piles.*** At present, most available computer programs to have no capability for analysing the effects of defective piles. The program GEPAN may be used to examine the effects of various defects and numbers of defective piles on a pile group because each pile in the group can be specified as having different properties and /or geometry. Chapters 6 to 9 will describe this application in detail.

(3). Load-transfer analysis. A general load-transfer analysis may be carried out by representing the sub-matrix *SIF* by the "*t-z*" and "*p-y*" concepts. In this case, only diagonal elements are considered in the matrix *SIF*. The principle is presented in Chapter 10.

(4). *Non-linear and elastoplastic analysis.* A general non-linear and elastoplastic analysis for piles and pile groups may be developed by modifying the matrices *SIF* and *PIF*. The further development is presented in Chapter 10.

(5). *Pile foundation-structure analysis.* Since multiple pile-groups can be analysed by this analysis, it can be extended further to consider a pile foundation-structure interaction if the global matrix is expanded into a "global pile foundation-structure matrix" by assembling the pile foundation matrix presented in this paper and the structure matrix developed via, for example, a conventional direct stiffness method.

3.6 Conclusions

This chapter presents a general three dimensional load-deformation analysis for pile foundations using the boundary element method.

For a "global" foundation which includes multiple pile groups and the effects of soil movements, the analysis uses the concepts of hierarchical structures and a basic influence factor matrix (BIFM), to derive the sub-matrices for the global matrix. The analysis is implemented via a computer program, GEPAN.

Through extensive comparisons, it is shown that, for direct loading effects, the three different pile analyses, PIGLET, DEFPIG and GEPAN generally agree well, although each of these approaches has a different basis.

However, the present analysis is more general and allows proper considerations of "true" three dimensional situations, as it considers all 6 load components and 6 displacement components for each of the piles, and also incorporates full coupling effects. Arbitrary dimensions of piles and general 3-D soil movements can be analyzed, enabling problems involving both direct loading and ground movements to be analyzed. GEPAN exhibits a high numerical accuracy and the method of changeable integration points enables significant savings to be made in computation times.

The present analysis reveals some subtle phenomena, which conventional analysis cannot, such as off-line effects of piles, different interaction factors for compression and uplift loadings, interaction among pile groups, and interaction within groups subjected to torsion. It is also capable of being extended to cover more complex ground-pile interaction problems, such as those involving ground movements and defects within some of the piles in a group.

Appendix A Hierarchical Structures and BIFM's

In the governing equation the global matrix has twelve non-zero sub-matrices which are hierarchical and assembled by several basic influence factor matrices (BIFM's). The hierarchical structures of and the BIFM's of the sub-matrices are introduced below.

A1 Sub-Matrix *SIF*

$$SIF = \begin{pmatrix} I_{1,1} & I_{1,2} & I_{1,j} & I_{1,ntot} \\ I_{2,1} & I_{2,2} & \cdots & \cdots \\ I_{i,1} & \cdots & I_{i,j} & \cdots \\ I_{ntot,1} & \cdots & \cdots & I_{ntot,ntot} \end{pmatrix}_{3*ntot \times 3*ntot}$$

$I_{i,j}$ is the 3×3 BIFM of displacements at soil element i due to unit loads on soil element j which is expressed as follows:

$$I_{i,j} = \begin{pmatrix} I_{i,j,1,1} & I_{i,j,1,2} & I_{i,j,1,3} \\ I_{i,j,2,1} & I_{i,j,2,2} & I_{i,j,2,3} \\ I_{i,j,3,1} & I_{i,j,3,2} & I_{i,j,3,3} \end{pmatrix}_{3\times 3}$$

$I_{i,j,k,l}$ = soil displacement in direction k at element i due to a unit load in direction l on element j.

The soil influence factor $I_{i,j,k,l}$ is carried out by integration of Mindlin's equations. The details are shown in Appendix B.

A2 Sub-Matrix *PIF*

$$PIF = \begin{pmatrix} J_1 & & & \\ & J_2 & & \\ & & J_i & \\ & & & J_{npils} \end{pmatrix}_{3*ntot \times 3*ntot} \qquad J_i = \begin{pmatrix} J_{1,1} & \cdots & J_{1,neps(i)} & \varnothing \\ \cdots & J_{i,j} & \cdots & \cdots \\ J_{neps(i),1} & \cdots & J_{neps(i),neps(i)} & \varnothing \\ \varnothing & \cdots & \varnothing & \varnothing \end{pmatrix}_{nept(i)\times nept(i)}$$

where

nept(i) = total number of elements of pile *i*

neps(i) = total number of shaft and discontinuous elements of pile *i*.

$J_{i,j}$ = the 3×3 BIFM of displacements at pile element *i* due to unit loads on pile element *j* which is expressed as follows:

$$J_{i,j} = \begin{pmatrix} J_{i,j,1,1} & J_{i,j,1,2} & J_{i,j,1,3} \\ J_{i,j,2,1} & J_{i,j,2,2} & J_{i,j,2,3} \\ J_{i,j,3,1} & J_{i,j,3,2} & J_{i,j,3,3} \end{pmatrix}_{3\times3}$$

$J_{i,j,k,l}$ = displacement in direction *k* at pile element *i* due to a unit load in direction *l* at pile element *j*, the expressions of which are derived in nested recursion form from the principles of structural analysis. The more details are shown in Appendix C.

A3 Sub-Matrix *B*

$$B = \begin{pmatrix} b_1 & & & & \\ & b_2 & & & \\ & & \cdots & & \\ & & & b_i & \\ & & & & b_{npils} \end{pmatrix}_{3*ntot\times6*npil} \qquad b_i = \begin{pmatrix} b_{i,1} \\ b_{i,2} \\ \cdots \\ b_{i,j} \\ b_{i,nept(i)} \end{pmatrix}_{3*nept(i)\times6}$$

$b_{i,j}$ is the 3×6 BIFM of displacements at element *j* of pile *i* due to unit tip displacements on pile *i*, which can be expressed as shown:

$$b_{i,j} = \begin{pmatrix} -1 & 0 & 0 & -H_{i,j} & 0 & r_{i,j}\sin\theta_{i,j} \\ 0 & -1 & 0 & 0 & H_{i,j} & -r_{i,j}\cos\theta_{i,j} \\ 0 & 0 & -1 & 0 & 0 & 0 \end{pmatrix}_{3\times6}$$

$b_{i,j,k,l}$ = displacement in direction *k* at element *j* of pile *i* due to a unit tip displacement in component *l* at pile *i*

$H_{i,j}$ = vertical distance between element *j* and tip of pile *i*

$r_{i,j}$ = distance of Z axis to element j of pile i

$\theta_{i,j}$ = angle of element j around Z axis based on X axis.

These geometrical parameters of elements are shown schematically in Fig.A3.1.

A4 Sub-Matrix *D*

$$D = \begin{pmatrix} d_1 & & & \\ & d_2 & & \\ & & d_i & \\ & & & d_{ncpsum} \\ \emptyset & \emptyset & \cdots & \emptyset \end{pmatrix}_{3*ntot\times 6*ncpsum} \qquad d_i = \begin{pmatrix} d_{i,1} \\ d_{i,2} \\ d_{i,j} \\ d_{i,neps(i)} \\ \emptyset \end{pmatrix}_{3*nept(i)\times 6}$$

$d_{i,j}$ is the 3×6 BIFM of displacements at element j of pile i due to unit head loads on pile i, which can be developed from the principles of structural analysis in a similar way to the basic influence factor matrix $J_{i,j}$, *i.e.*

$$d_{i,j} = \begin{pmatrix} d_{i,j,1,1} & d_{i,j,1,2} & \cdots & \cdots & \cdots & d_{i,j,1,6} \\ d_{i,j,2,1} & \cdots & \cdots & \cdots & \cdots & d_{i,j,2,6} \\ d_{i,j,3,1} & \cdots & \cdots & \cdots & \cdots & d_{i,j,3,6} \end{pmatrix}_{3\times 6}$$

$d_{i,j,k,l}$ = displacement in direction k at element j of pile i due to a unit head load in component l on pile i.

A5 Sub-Matrix *G*

It is assumed that a tie beams have rectangular cross-sections and their ends are joined at the loading centers of caps as show Fig.A3.2.

$$G = \begin{pmatrix} g_{1,1} & g_{1,2} & \cdots & g_{1,ncap} \\ g_{2,1} & \cdots & \cdots & \cdots \\ \cdots & \cdots & g_{i,j} & \cdots \\ g_{ncap,1} & \cdots & \cdots & g_{ncap,ncap} \end{pmatrix}_{6*ncap\times 6*ncap}$$

$g_{i,j}$ is a 6×6 BIFM of loads of cap i due to displacements of cap j which is expanded as $g_{i,j,k,l}$ = load in component k of cap i due to a unit displacement in component l of cap j. It can be derived from the principles of structural analysis for tie-beams and the deformation geometry of the pile caps.

$g_{i,j}$ is expressed as follows:

$$g_{i,j} = \begin{cases} \emptyset & \text{If cap } i \text{ and cap } j \text{ are independent} \\ TU_{ij}T^T & \text{If cap } i \text{ and cap } j \text{ are jointed by a tie beam, and } i = j \\ TU_{ij}T^T & \text{If cap } i \text{ and cap } j \text{ are jointed by a tie beam, and } i \neq j \end{cases}$$

Where

$$U_{jj} = \begin{pmatrix} a & 0 & 0 & 0 & 0 & 0 \\ 0 & 12b & 0 & -6lb & 0 & 0 \\ 0 & 0 & -12lc & 0 & 6lc & 0 \\ 0 & -6lb & 0 & 0 & 4l^2b & 0 \\ 0 & 0 & -6lc & 0 & 0 & 4l^2c \\ 0 & 0 & 0 & 0 & 0 & d \end{pmatrix}$$

$$U_{ij} = \begin{pmatrix} -a & 0 & 0 & 0 & 0 & 0 \\ 0 & -12b & 0 & 6lb & 0 & 0 \\ 0 & 0 & -12lc & 0 & 6lc & 0 \\ 0 & -6lb & 0 & 0 & 2l^2b & 0 \\ 0 & 0 & -6lc & 0 & 0 & 2l^2c \\ 0 & 0 & 0 & 0 & 0 & -d \end{pmatrix}$$

$$T = \begin{pmatrix} \cos\beta & -\sin\beta & 0 & 0 & 0 & 0 \\ \sin\beta & \cos\beta & 0 & 0 & 0 & 0 \\ 0 & 0 & 1 & 0 & 0 & 0 \\ 0 & 0 & 0 & \cos\beta & -\sin\beta & 0 \\ 0 & 0 & 0 & \sin\beta & \cos\beta & 0 \\ 0 & 0 & 0 & 0 & 0 & 1 \end{pmatrix}$$

$$T^T = \begin{pmatrix} \cos\beta & \sin\beta & 0 & 0 & 0 & 0 \\ -\sin\beta & \cos\beta & 0 & 0 & 0 & 0 \\ 0 & 0 & 1 & 0 & 0 & 0 \\ 0 & 0 & 0 & \cos\beta & \sin\beta & 0 \\ 0 & 0 & 0 & -\sin\beta & \cos\beta & 0 \\ 0 & 0 & 0 & 0 & 0 & 1 \end{pmatrix}$$

$$a = \frac{E_b A_b}{L_b} \quad b = \frac{E_b I_{z,b}}{L_b^2} \quad c = \frac{E_b I_{y,b}}{L_b^3} \quad d = \frac{k_1 E_b h_b w_b^3}{2(1+\nu_b) L_b}$$

E_b = Young's modulus of tie beam

A_b = cross-section of tie beam

L_b = length of tie beam

ν_b= Poisson's ratio of tie beam

E_b = Young's modulus of tie beam

$I_{y,b}$ = moment of inertia along Y axis of tie beam

$I_{z,b}$ = moment of inertia along Z axis of tie beam

h_b = height of cross section of tie beam

w_b = width of cross section of tie beam

β = angle of tie beam in global coordinate system

k_1 = a torque constant for rectangular beam defined by Timoshenko (1970).

Above geometric parameters are shown in Fig.A3.2.

A6 Sub-Matrix *H*

$$H=\begin{pmatrix} h_1 & & & \\ & h_2 & & \\ & & h_i & \\ & & & h_{ncap} \end{pmatrix}_{6*ncap\times 6*ncpsum} \qquad h_i=\begin{pmatrix} h_{i,1} & h_{i,2} & h_{i,j} & h_{i,ncpil(i)} \end{pmatrix}_{6\times 6*ncpil(i)}$$

where

ncpil(i) = total number of the piles under pile cap *i*.

$h_{i,j}$ = the basic influence factor matrix for loads on cap i due to unit head loads on pile j, which can be determined by the general equilibrium relations. The elements of $h_{i,j}$ are $h_{i,j,k,l}$ = head load (component k) on cap i due to a unit head load (component l) on pile j.

$$h_{i,j}=\begin{pmatrix} 1 & 0 & 0 & 0 & 0 & 0 \\ 0 & 1 & 0 & 0 & 0 & 0 \\ 0 & 0 & 1 & 0 & 0 & 0 \\ 0 & 0 & D_{y,i,j} & 1 & 0 & 0 \\ 0 & 0 & -D_{x,i,j} & 0 & 1 & 0 \\ -D_{y,i,j} & D_{x,i,j} & 0 & 0 & 0 & 1 \end{pmatrix}_{6\times 6}$$

where

$D_{x,i,j}$ = distance in X-direction between loading centre on cap i and the centre of the head of pile j

$D_{y,i,j}$ = distance in Y-direction between loading centre on cap i and the centre of the head of pile j.

These geometric parameters are shown in Fig.A3.3.

A7 Sub-Matrix *O*

$$O=\begin{pmatrix} o_1 & & & \emptyset \\ & o_2 & & \emptyset \\ & & o_i & \cdots \\ & & & o_{ncap} \quad \emptyset \end{pmatrix}_{6*ncpsum\times 3*ntot} \qquad o_i=\begin{pmatrix} o_{i,1} & o_{i,2} & o_{i,j} & o_{i,necs(i)} & \emptyset \end{pmatrix}_{6\times nect(i)}$$

where

nect(i) = total number of elements of the piles under pile cap *i*

necs(i) = total number of shaft and discontinuous elements of the piles under pile cap *i*.

$o_{i,j}$ = the 6×3 BIFM for the head displacements on pile *i* due to unit loads on element *j* of pile *i*, which can be derived in nested recursion form from the principles of structural analysis.

$$o_{i,j} = \begin{pmatrix} o_{i,j,1,1} & o_{i,j,1,2} & o_{i,j,1,3} \\ o_{i,j,2,1} & \cdots & \cdots \\ \cdots & \cdots & \cdots \\ \cdots & \cdots & \cdots \\ \cdots & \cdots & \cdots \\ o_{i,j,6,1} & \cdots & o_{i,j,6,3} \end{pmatrix}_{6\times 3}$$

$o_{i,j,k,l}$ = the head displacement (component *k*) of pile *i* due to a unit load (direction *l*) on element *j* of pile *i*.

A8 Sub-Matrix *P*

$$P = \begin{pmatrix} p_1 & & & & & \\ & p_2 & & & & \\ & & p_i & & & \\ & & & p_{ncpsum} & & \\ & & & & \emptyset & \end{pmatrix}_{6*ncpsum\times 6*npils}$$

p_i is the 6×6 BIFM of the head displacements on pile *i* due to the unit tip displacements of pile *i*, the elements are $p_{i,k,l}$ = the head displacement (component *k*) of pile *i* due to a unit tip displacement (component *l*) of pile *i* and are expressed as follows:

$$p_i = \begin{pmatrix} 1 & 0 & 0 & 0 & -L_i & 0 \\ 0 & 1 & 0 & L_i & 0 & 0 \\ 0 & 0 & 1 & 0 & 0 & 0 \\ 0 & 0 & 0 & 1 & 0 & 0 \\ 0 & 0 & 0 & 0 & 1 & 0 \\ 0 & 0 & 0 & 0 & 0 & 1 \end{pmatrix}_{6\times6}$$

e

L_i = length of pile i.

A9 Sub-Matrix Q

$$Q = \begin{pmatrix} q_1 & & & & \\ & q_2 & & & \\ & & q_i & & \\ & & & q_{ncap} & \end{pmatrix}_{6*ncpsum\times 6*ncap} \qquad q_i = \begin{pmatrix} q_{i,1} \\ q_{i,2} \\ q_{i,j} \\ q_{i,ncpil(i)} \end{pmatrix}_{6*ncpil(i)\times 6}$$

$q_{i,j}$ is the 6×6 BIFM for the head displacements on pile j due to unit displacements of cap i, which can be developed from geometry.

$$q_{i,j} = -\begin{pmatrix} 1 & 0 & 0 & 0 & 0 & -R_{i,j}\sin(\Phi_{i,j}) \\ 0 & 1 & 0 & 0 & 0 & R_{i,j}\cos(\Phi_{i,j}) \\ 0 & 0 & 1 & R_{y,i,j} & -R_{x,i,j} & 0 \\ 0 & 0 & 0 & 1 & 0 & 0 \\ 0 & 0 & 0 & 0 & 1 & 0 \\ 0 & 0 & 0 & 0 & 0 & 1 \end{pmatrix}_{6\times6}$$

$q_{i,j,k,l}$ = the head displacement (component k) of pile j due to a unit cap displacement (component l) of cap i

$R_{i,j}$ = distance between load acting on the centre of cap i and the centre of pile j

$$R_{i,j} = \sqrt{R_{x,i,j}^2 + R_{y,i,j}^2}$$

$\Phi_{i,j}$ = angle of $R_{i,j}$ line in horizontal plane with respect to X axis, *i.e.*

$$\Phi_{i,j} = \tan^{-1}\left(\frac{R_{x,i,j}}{R_{y,i,j}}\right)$$

The geometric relationships between caps and piles are shown in Fig.A3.3.

A10 Sub-Matrix *R*

$$R = \begin{pmatrix} r_1 & & & & \\ & r_2 & & & \\ & & r_i & & \\ & & & r_{ncpsum} & \end{pmatrix}_{6*ncpsum \times 6*ncpsum}$$

r_i is the 6×6 BIFM for the head displacements of pile i due to unit head loads on pile i, which can be developed from the principles of structural analysis.

$$r_i = \begin{pmatrix} r_{i,1,1} & r_{i,1,2} & \cdots & \cdots & \cdots & r_{i,1,6} \\ r_{i,2,1} & r_{i,2,2} & \cdots & \cdots & \cdots & \cdots \\ \cdots & \cdots & \cdots & \cdots & \cdots & \cdots \\ \cdots & \cdots & \cdots & \cdots & \cdots & \cdots \\ \cdots & \cdots & \cdots & \cdots & \cdots & \cdots \\ r_{i,6,1} & \cdots & \cdots & \cdots & \cdots & r_{i,6,6} \end{pmatrix}_{6\times 6}$$

$r_{i,k,l}$ = the head displacement (component k) due to a unit head load (component l) of pile i.

A11 Sub-Matrix *S*

$$S = \begin{pmatrix} s_1 & & & \\ & s_2 & & \\ & & s_i & \\ & & & s_{npils} \end{pmatrix}_{6*npils \times 3*ntot} \qquad s_i = \begin{pmatrix} s_{i,1} & s_{i,2} & s_{i,j} & s_{i,nept(i)} \end{pmatrix}_{6\times 3*nept(i)}$$

$s_{i,j}$ is the 6×3 BIFM for the head loads on pile i due to unit stresses on element j of pile i, which can be developed from the equilibrium equations.

$$s_{i,j} = \begin{pmatrix} A_{i,j} & 0 & 0 \\ 0 & A_{i,j} & 0 \\ 0 & 0 & A_{i,j} \\ 0 & -A_{i,j} * Z_{i,j} & A_{i,j} * Y_{i,j} \\ A_{i,j} * Z_{i,j} & 0 & -A_{i,j} * X_{i,j} \\ -A_{i,j} * Y_{i,j} & A_{i,j} * X_{i,j} & 0 \end{pmatrix}_{6\times 3}$$

$s_{i,j,k,l}$ = the head load (component k) on pile i due to a unit stress on element j (component l) of pile i.

A12 Sub-Matrix *V*

$$V = \begin{pmatrix} v_1 & & & & \\ & v_2 & & & \\ & & v_i & & \\ & & & v_{ncpsum} & \\ \emptyset & \emptyset & \ldots & \emptyset & \end{pmatrix}_{6*npils\times 6*ncpsum}$$

v_i is the 6×6 BIFM for the head loads on pile i due to the unit head loads on pile i.

$$v_i = \begin{pmatrix} 1 & & & & & \\ & 1 & & & & \\ & & 1 & & & \\ & & & 1 & & \\ & & & & 1 & \\ & & & & & 1 \end{pmatrix}_{6\times 6}$$

$v_{i,k,l}$ = the head load (component k) of pile i due to unit head load (component l) of pile i.

Appendix B Integral Expressions in Soil influence factors

B1 Notations

i = element i where displacements to be calculated

D = depth of element j

θ = radial-angle of element j

r = radius of element j

θ_1, θ_2 = radial-angle boundary of partly cylindrical/annual element j

D_1, D_2 = depth boundary of partly cylindrical element j

r_1, r_2 = radius boundary of partly annual element j

x_i, y_i, z_i = centre coordinators of element i

ν = Poison's ratio of soil

$$\theta_i = \tan^{-1}(\frac{y_i}{x_i})$$

$$r_i = \sqrt{x_i^2 + y_i^2}$$

$$x = x_i - r\cos\theta$$

$$y = y_i - r\sin\theta$$

$$R_1^2 = r^2 + r_i^2 - 2rr_i\cos(\theta - \theta_i) + (z_i - D)^2$$

$$R_2^2 = r^2 + r_i^2 - 2rr_i\cos(\theta - \theta_i) + (z_i + D)^2$$

Unit loads acting on elements are shown in Fig. A3.4.

Above geometric parameters are shown in Fig. A3.5 and A3.6.

2 Integral Expression in Soil Influence Factor

$I_{a,bc}$= displacement c at element i due to uniform force on the a element j in direction b

Where $c = u, v, w$ displacement

$b = x, y, z$ direction

$a = s, b$ (s = shaft, b = base)

$$I_{s,bc} = fn(x_i, y_i, z_i, D_1, D_2, \theta_1, \theta_2, r)$$

$$I_{b,bc} = fn(x_i, y_i, z_i, r_1, r_2, \theta_1, \theta_2, D)$$

B2.1 Integral Expressions in Soil Influence Factors of Shaft Element

$$I_{s,zu} = \int_{D_1}^{D_2}\int_{\theta_1}^{\theta_2} \frac{(x_i - r\cos\theta)}{16\pi(1-\nu)G}\left[\frac{z_i - D}{R_1^3} + \frac{(3-4\nu)(z_i - D)}{R_2^3} - \frac{4(1-\nu)(1-2\nu)}{R_2(R_2 + z_i + D)} + \frac{6z_i D(z_i + D)}{R_2^5}\right] r\,d\theta\,dD$$

$$I_{s,zv} = \int_{D_1}^{D_2}\int_{\theta_1}^{\theta_2} \frac{(y_i - r\sin\theta)}{16\pi(1-\nu)G}\left[\frac{z_i - D}{R_1^3} + \frac{(3-4\nu)(z_i - D)}{R_2^3} - \frac{4(1-\nu)(1-2\nu)}{R_2(R_2 + z_i + D)} + \frac{6z_i D(z_i + D)}{R_2^5}\right] r\,d\theta\,dD$$

$$I_{s,zw} = \int_{D_1}^{D_2}\int_{\theta_1}^{\theta_2} \frac{1}{16\pi(1-\nu)G}\left[\frac{3-4\nu}{R_1} + \frac{(z_i - D)^2}{R_1^3} + \frac{1 + 4(1-\nu)(1-2\nu)}{R_2}\right.$$
$$\left. + \frac{(3-4\nu)(z_i + D)^2 - 2z_i D}{R_2^3} + \frac{6z_i D(z_i + D)^2}{R_2^5}\right] r\,d\theta\,dD$$

$$I_{s,xu} = \int_{D_1}^{D_2}\int_{\theta_1}^{\theta_2} \frac{1}{16\pi(1-\nu)G}\left[\frac{3-4\nu}{R_1} + \frac{(x_i - r\cos\theta)^2}{R_1^3} - \frac{1}{R_2} + \frac{(3-4\nu)(x_i - r\cos\theta)^2}{R_2^3}\right.$$
$$\left. + \frac{2z_i D}{R_2^3}\left(1 - \frac{3(x_i - r\cos\theta)^2}{R_2^2}\right) + \frac{4(1-\nu)(1-2\nu)}{R_2 + z_i + D}\left(1 - \frac{(x_i - r\cos\theta)^2}{R_2(R_2 + z_i + D)}\right)\right] r\,d\theta\,dD$$

$$I_{s,xv}=\int_{D_1}^{D_2}\int_{\theta_1}^{\theta_2}\frac{(x_i-r\cos\theta)(y_i-r\sin\theta)}{16\pi(1-\nu)G}\left[\frac{1}{R_1^3}+\frac{3-4\nu}{R_2^3}-\frac{6z_iD}{R_2^5}-\frac{4(1-\nu)(1-2\nu)}{R_2(R_2+z_i+D)^2}\right]rd\theta dD$$

$$I_{s,xw}=\int_{D_1}^{D_2}\int_{\theta_1}^{\theta_2}\frac{(x_i-r\cos\theta)}{16\pi(1-\nu)G}\left[\frac{z_i-D}{R_1^3}+\frac{(3-4\nu)(z_i-D)}{R_2^3}-\frac{6z_iD(z_i+D)}{R_2^5}+\frac{4(1-\nu)(1-2\nu)}{R_2(R_2+z_i+D)^2}\right]rd\theta dD$$

$$I_{s,yu}=\int_{D_1}^{D_2}\int_{\theta_1}^{\theta_2}\frac{(x_i-r\cos\theta)(y_i-r\sin\theta)}{16\pi(1-\nu)G}\left[\frac{1}{R_1^3}+\frac{3-4\nu}{R_2^3}-\frac{6z_iD}{R_2^5}-\frac{4(1-\nu)(1-2\nu)}{R_2(R_2+z_i+D)^2}\right]rd\theta dD$$

$$I_{s,yv}=\int_{D_1}^{D_2}\int_{\theta_1}^{\theta_2}\frac{1}{16\pi(1-\nu)G}\left[\frac{3-4\nu}{R_1}+\frac{(y_i-r\sin\theta)^2}{R_1^3}-\frac{1}{R_2}+\frac{(3-4\nu)(y_i-r\sin\theta)^2}{R_2^3}\right.$$
$$\left.+\frac{2z_iD}{R_2^3}\left(1-\frac{3(y_i-r\sin\theta)^2}{R_2^2}\right)+\frac{4(1-\nu)(1-2\nu)}{R_2+z_i+D}\left(1-\frac{(y_i-r\sin\theta)^2}{R_2(R_2+z_i+D)}\right)\right]rd\theta dD$$

$$I_{s,yw}=\int_{D_1}^{D_2}\int_{\theta_1}^{\theta_2}\frac{(y_i-r\sin\theta)}{16\pi(1-\nu)G}\left[\frac{z_i-D}{R_1^3}+\frac{(3-4\nu)(z_i-D)}{R_2^3}-\frac{6z_iD(z_i+D)}{R_2^5}+\frac{4(1-\nu)(1-2\nu)}{R_2(R_2+z_i+D)^2}\right]rd\theta dD$$

B2.2 Integral Expressions in Soil Influence Factors of Base/Discontinuity Element

$$I_{b,zu}=\int_{r_1}^{r_2}\int_{\theta_1}^{\theta_2}\frac{(x_i-r\cos\theta)}{16\pi(1-\nu)G}\left[\frac{z_i-D}{R_1^3}+\frac{(3-4\nu)(z_i-D)}{R_2^3}-\frac{4(1-\nu)(1-2\nu)}{R_2(R_2+z_i+D)}+\frac{6z_iD(z_i+D)}{R_2^5}\right]rd\theta dr$$

$$I_{b,zv}=\int_{r_1}^{r_2}\int_{\theta_1}^{\theta_2}\frac{(y_i-r\sin\theta)}{16\pi(1-\nu)G}\left[\frac{z_i-D}{R_1^3}+\frac{(3-4\nu)(z_i-D)}{R_2^3}-\frac{4(1-\nu)(1-2\nu)}{R_2(R_2+z_i+D)}+\frac{6z_iD(z_i+D)}{R_2^5}\right]rd\theta dr$$

$$I_{b,zw}=\int_{r_1}^{r_2}\int_{\theta_1}^{\theta_2}\frac{1}{16\pi(1-\nu)G}\left[\frac{3-4\nu}{R_1}+\frac{(z_i-D)^2}{R_1^3}+\frac{1+4(1-\nu)(1-2\nu)}{R_2}\right.$$
$$\left.+\frac{(3-4\nu)(z_i+D)^2-2z_iD}{R_2^3}+\frac{6z_iD(z_i+D)^2}{R_2^5}\right]rd\theta dr$$

$$I_{b,xu}=\int_{r_1}^{r_2}\int_{\theta_1}^{\theta_2}\frac{1}{16\pi(1-\nu)G}\left[\frac{3-4\nu}{R_1}+\frac{(x_i-r\cos\theta)^2}{R_1^{\,3}}-\frac{1}{R_2}+\frac{(3-4\nu)(x_i-r\cos\theta)^2}{R_2^{\,3}}\right.$$

$$\left.+\frac{2z_iD}{R_2^{\,3}}\left(1-\frac{3(x_i-r\cos\theta)^2}{R_2^{\,2}}\right)+\frac{4(1-\nu)(1-2\nu)}{R_2+z_i+D}\left(1-\frac{(x_i-r\cos\theta)^2}{R_2(R_2+z_i+D)}\right)\right]rd\theta dr$$

$$I_{b,xv}=\int_{r_1}^{r_2}\int_{\theta_1}^{\theta_2}\frac{(x_i-r\cos\theta)(y_i-r\sin\theta)}{16\pi(1-\nu)G}\left[\frac{1}{R_1^{\,3}}+\frac{3-4\nu}{R_2^{\,3}}-\frac{6z_iD}{R_2^{\,5}}-\frac{4(1-\nu)(1-2\nu)}{R_2(R_2+z_i+D)^2}\right]rd\theta dr$$

$$I_{b,xw}=\int_{r_1}^{r_2}\int_{\theta_1}^{\theta_2}\frac{(x_i-r\cos\theta)}{16\pi(1-\nu)G}\left[\frac{z_i-D}{R_1^{\,3}}+\frac{(3-4\nu)(z_i-D)}{R_2^{\,3}}-\frac{6z_iD(z_i+D)}{R_2^{\,5}}+\frac{4(1-\nu)(1-2\nu)}{R_2(R_2+z_i+D)^2}\right]rd\theta dr$$

$$I_{b,yu}=\int_{r_1}^{r_2}\int_{\theta_1}^{\theta_2}\frac{(x_i-r\cos\theta)(y_i-r\sin\theta)}{16\pi(1-\nu)G}\left[\frac{1}{R_1^{\,3}}+\frac{3-4\nu}{R_2^{\,3}}-\frac{6z_iD}{R_2^{\,5}}-\frac{4(1-\nu)(1-2\nu)}{R_2(R_2+z_i+D)^2}\right]rd\theta dr$$

$$I_{b,yv}=\int_{r_1}^{r_2}\int_{\theta_1}^{\theta_2}\frac{1}{16\pi(1-\nu)G}\left[\frac{3-4\nu}{R_1}+\frac{(y_i-r\sin\theta)^2}{R_1^{\,3}}-\frac{1}{R_2}+\frac{(3-4\nu)(y_i-r\sin\theta)^2}{R_2^{\,3}}\right.$$

$$\left.+\frac{2z_iD}{R_2^{\,3}}\left(1-\frac{3(y_i-r\sin\theta)^2}{R_2^{\,2}}\right)+\frac{4(1-\nu)(1-2\nu)}{R_2+z_i+D}\left(1-\frac{(y_i-r\sin\theta)^2}{R_2(R_2+z_i+D)}\right)\right]rd\theta dr$$

$$I_{b,yw}=\int_{r_1}^{r_2}\int_{\theta_1}^{\theta_2}\frac{(y_i-r\sin\theta)}{16\pi(1-\nu)G}\left[\frac{z_i-D}{R_1^{\,3}}+\frac{(3-4\nu)(z_i-D)}{R_2^{\,3}}-\frac{6z_iD(z_i+D)}{R_2^{\,5}}+\frac{4(1-\nu)(1-2\nu)}{R_2(R_2+z_i+D)^2}\right]rd\theta dr$$

Appendix C Nested Recursions in Pile Influence Factors

C1 Notation

i = pile element to be loaded

j = pile element which displacements are to be analysed

k = pile segment containing pile element j

k-1 = lower previous segment of k

c = centre

t = top

x, y, z = direction x, y, z

L = length of segment

P = force at element centre

M = moment/torque at element centre

U, V, W = displacement in x, y, z respectively

θ = rotation

X,Y,Z = local coordinators of element centre (X= 0, Y= 0 at pile axis)

A = area of element

E = Young's modulus of pile element

G = Shear modulus of pile element

I = inertial moment of pile element section

$J_{i,j,k,l}$ = displacement in direction k at pile element i due to a unit load in direction l at pile element j

$$R_j = \sqrt{X_j^2 + Y_j^2}$$

$$\alpha_j = tan^{-1}\left(\frac{Y_j}{X_j}\right)$$

Above geometric parameters are shown in Fig. A3.7.

C2 Loads at segment *k* due to loads at element *i*

$Px_k = 1.0 * A_i$ $\quad Py_k = 1.0 * A_i$ $\quad Pz_k = 1.0 * A_i$

$My_{x,c,k} = (Z_k - Z_i)Px_i$ $\quad My_{x,t,k} = (Z_k - Z_i - L_k/2)Px_i$ $\quad Mz_{x,k} = Px_i Y_i$

$Mx_{y,c,k} = (Z_k - Z_i)Py_i$ $\quad Mx_{y,t,k} = (Z_k - Z_i - L_k/2)Py_i$ $\quad Mz_{y,k} = Py_i X_i$

$Mx_{z,k} = Pz_i Y_i$ $\quad My_{z,k} = Pz_i X_i$

C3 Nested recursions of displacements at segment *k*

C3.1 Displacements at segment *k* by an uniform load in *x*-direction on element *i*

$$\theta y_{c,k} = \theta y_{t,k-1} + \frac{Px_k (L_k/2)^2}{2E_k I_k} + \frac{My_{x,c,k}(L_k/2)}{E_k I_k}$$

$$U_{c,x,k} = U_{t,x,k-1} + \theta y_{t,k-1}(L_k/2) + \frac{Px_k (L_k/2)^3}{3E_k I_k} + \frac{My_{x,c,k}(L_k/2)^2}{2E_k I_k}$$

$$\theta z_{c,k} = \theta z_{t,k-1} + \frac{Mz_{x,k}(L_k/2)}{G_k J_k}$$

$$\theta y_{t,k} = \theta y_{t,k-1} + \frac{Px_k L_k^{\,2}}{2E_k I_k} + \frac{Mx_{y,c,k} L_k}{E_k I_k}$$

$$U_{t,x,k} = U_{t,x,k-1} + \theta y_{t,k-1} L_k + \frac{Px_k L_k^{\,3}}{3E_k I_k} + \frac{Mx_{y,c,k} L_k^{\,2}}{2E_k I_k}$$

$$\theta z_{t,k} = \theta z_{t,k-1} + \frac{Mz_{x,k} L_k}{G_k J_k}$$

C3.2 Displacements at segment *k* by an uniform load in *y*-direction on element *i*

$$\theta x_{c,k} = \theta x_{t,k-1} + \frac{Py_k (L_k/2)^2}{2E_k I_k} + \frac{Mx_{y,c,k}(L_k/2)}{E_k I_k}$$

$$V_{c,y,k} = V_{t,y,k-1} + \theta x_{t,k-1}(L_k/2) + \frac{Py_k(L_k/2)^3}{3E_kI_k} + \frac{My_{y,c,k}(L_k/2)^2}{2E_kI_k}$$

$$\theta z_{c,k} = \theta z_{t,k-1} + \frac{Mz_{y,k}(L_k/2)}{G_kJ_k}$$

$$\theta y_{t,k} = \theta y_{t,k-1} + \frac{Py_kL_k^2}{2E_kI_k} + \frac{Mx_{y,c,k}L_k}{E_kI_k}$$

$$V_{t,x,k} = V_{t,x,k-1} + \theta y_{,t,k-1}L_k + \frac{Py_kL_k^3}{3E_kI_k} + \frac{Mx_{y,c,k}L_k^2}{2E_kI_k}$$

$$\theta x_{z,c,k} = \theta x_{z,t,k-1} + \frac{Mx_{z,k}(L_k/2)}{G_kJ_k}$$

3.3 Displacements at segment k by an uniform load in z-direction on element i

$$\theta x_{z,c,k} = \theta x_{z,t,k-1} + \frac{Mx_{z,k}(L_k/2)}{E_kI_k}$$

$$\theta y_{z,c,k} = \theta y_{z,t,k-1} + \frac{My_{z,k}(L_k/2)}{E_kI_k}$$

$$U_{c,z,k} = U_{t,z,k-1} + \theta y_{z,t,k-1} + \frac{My_{z,k}(L_k/2)^2}{2E_kI_k}$$

$$V_{c,z,k} = V_{t,z,k-1} + \theta x_{z,t,k-1} + \frac{Mx_{z,k}(L_k/2)^2}{2E_kI_k}$$

$$W_{c,z,k} = W_{c,z,k-1} + \frac{Pz_k(L_k/2)}{E_kA_k}$$

$$\theta x_{z,t,k} = \theta x_{z,t,k-1} + \frac{Mx_{z,k}L_k}{E_kI_k}$$

$$\theta y_{z,t,k} = \theta y_{z,t,k-1} + \frac{My_{z,k}L_k}{G_kJ_k}$$

$$U_{t,z,k} = U_{t,z,k-1} + \theta y_{z,t,k-1} + \frac{My_{z,k}L_k^2}{2E_kI_k}$$

$$V_{t,z,k} = V_{t,z,k-1} + \theta x_{z,t,k-1} + \frac{Mx_{z,k} L_k^{\,2}}{2E_k I_k}$$

$$W_{t,z,k} = W_{t,z,k-1} + \frac{Pz_k L_k}{E_k A_k}$$

C.4 Displacement at element *j* due to unit loads at element *i*

$$J_{i,j,x,y} = \begin{cases} U_{c,x,k} - R_j[\cos(\theta_{z,c,k} + \alpha_j) - \cos(\theta_{z,c,k})] & Z_j < Z_i \\ U_{c,x,k} - R_j[\cos(\theta_{z,c,k} + \alpha_j) - \cos(\theta_{z,c,k})] + \theta_{y,c,k}(Z_j - Z_i) & Z_j \geq Z_i \end{cases}$$

$$J_{i,j,x,y} = -R_j[\sin(\theta_{z,c,k} + \alpha_j) - \sin(\theta_{z,c,k})]$$

$$J_{i,j,x,z} = \theta_{y,c,k} X_j$$

$$J_{i,j,y,x} = R_j[\cos(\theta_{z,c,k} + \alpha_j) - \cos(\theta_{z,c,k})]$$

$$J_{i,j,y,y} = \begin{cases} V_{c,y,k} + R_j[\sin(\theta_{z,c,k} + \alpha_j) - \sin(\theta_{z,c,k})] & Z_j < Z_i \\ V_{c,y,k} + R_j[\sin(\theta_{z,c,k} + \alpha_j) - \sin(\theta_{z,c,k})] + \theta_{x,c,k}(Z_j - Z_i) & Z_j \geq Z_i \end{cases}$$

$$J_{i,j,y,z} = \theta_{x,c,k} Y_j$$

$$J_{i,j,z,x} = \begin{cases} U_{c,z,k} & Z_j < Z_i \\ U_{c,z,k} + \theta_{y,c,k}(Z_j - Z_i) & Z_j \geq Z_i \end{cases}$$

$$J_{i,j,z,y} = \begin{cases} V_{c,z,k} & Z_j < Z_i \\ V_{c,z,k} + \theta_{x,c,k}(Z_j - Z_i) & Z_j \geq Z_i \end{cases}$$

$$J_{i,j,z,z} = W_{c,z,k} + \theta_{x,c,k}(Z_j - Z_i) + \theta_{y,c,k}(Z_j - Z_i)$$

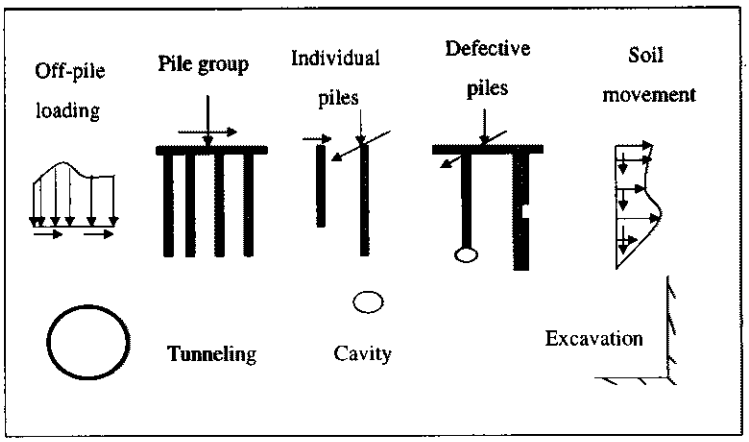

Fig. 3.1 Schematic global foundation system

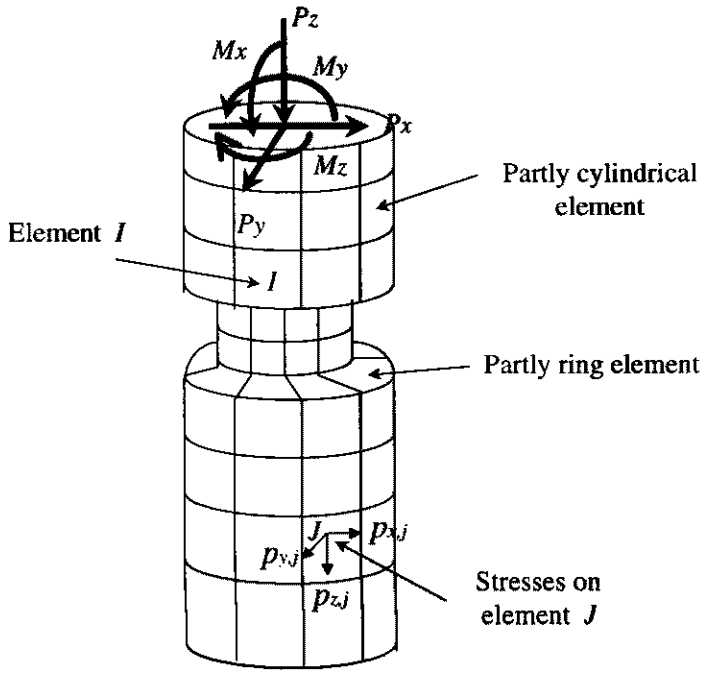

Fig. 3.2 Elements and stresses of a pile

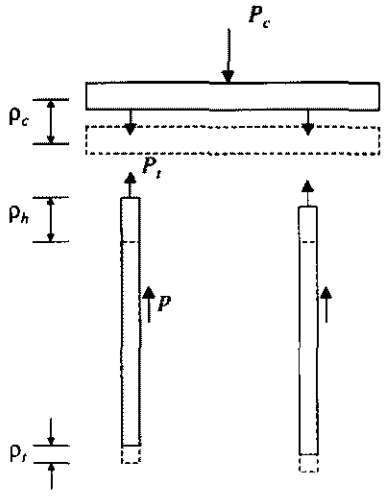

P_c = cap load

P_t = head load of the grouped pile

p = pile-soil traction on element

ρ_c = cap displacement

ρ_h = total pile head displacement

ρ_t = pile tip displacement

$\rho_{h,elmt}$ = pile head displacement by p

$\rho_{h,head}$ = pile head displacement by P_t

$\rho_{h,tip}$ = pile head displacement by ρ_t

Compatibility of pile head and cap:

$$\rho_c=\rho_h=\Sigma\rho_{h,elmt}+\rho_{h,head}+\rho_{h,tip}$$

Fig. 3.3 Schematic compatibility of pile head and cap

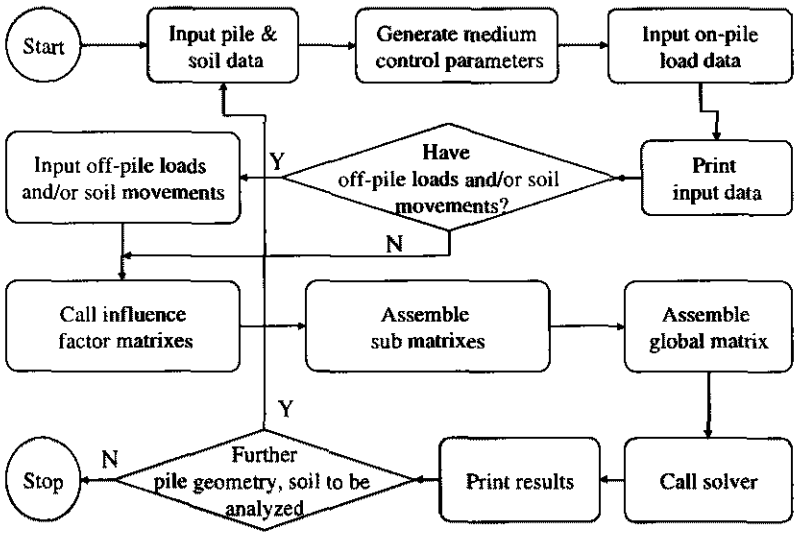

Fig. 3.4 Flow Chart for program GEPAN

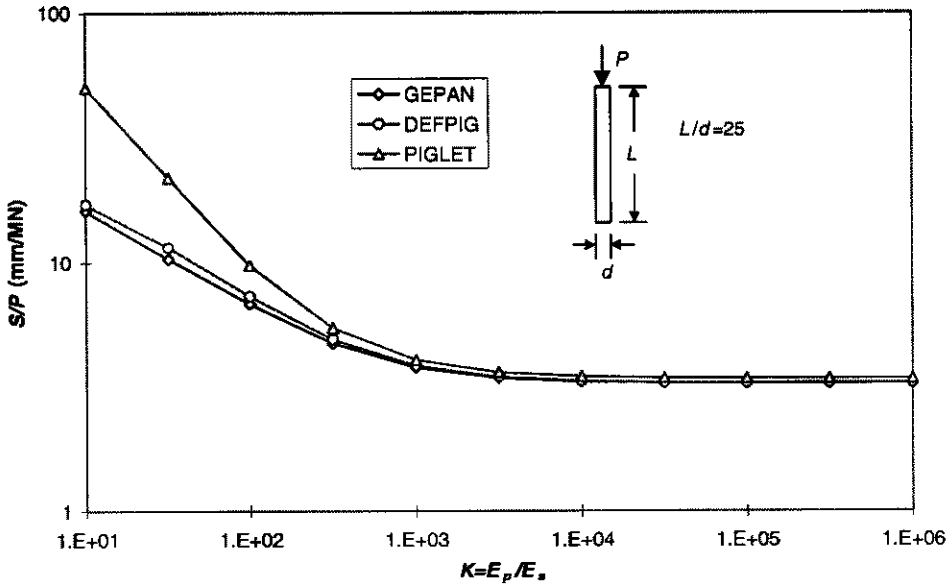

Fig. 3.5 Comparison of the top settlements S of axially loaded single pile

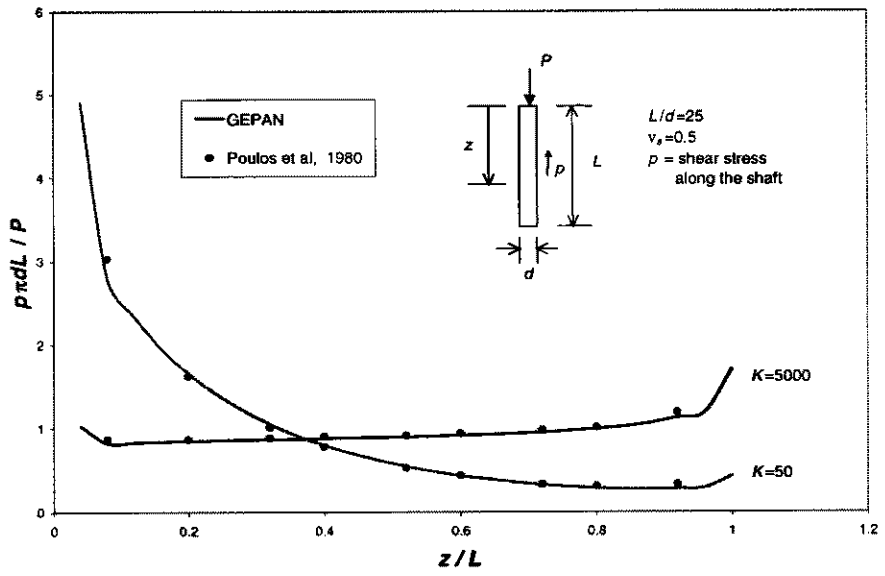

Fig. 3.6 Comparison of axial load distribution along single pile

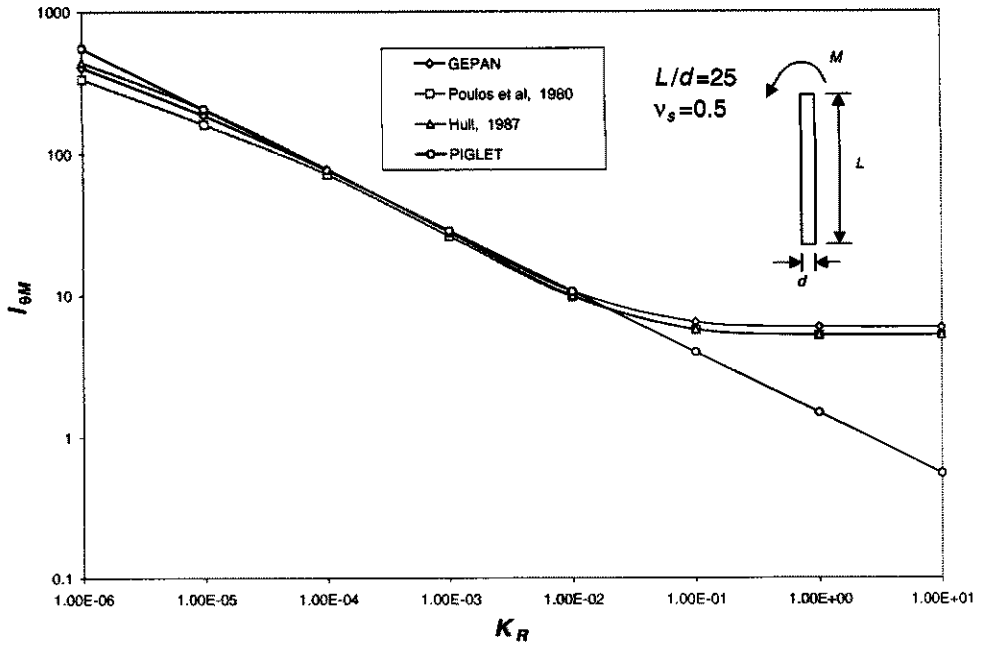

Fig. 3.7 Comparison of the influence factor $I_{\theta M}$ of horizontally loaded single pile

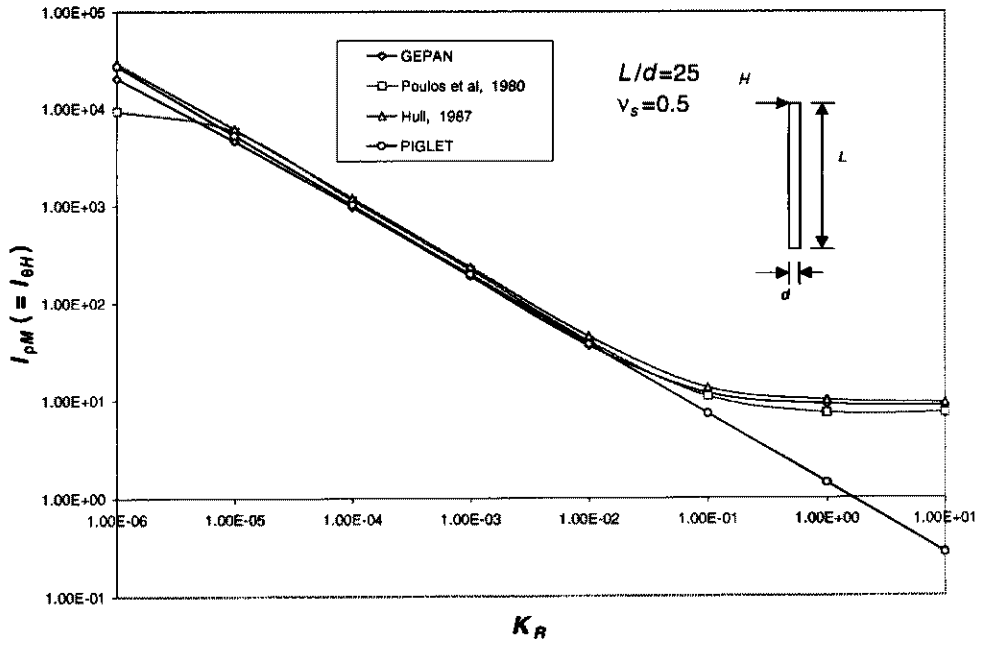

Fig. 3.8 Comparison of the influence factor $I_{\rho M}$ of horizontally loaded single pile

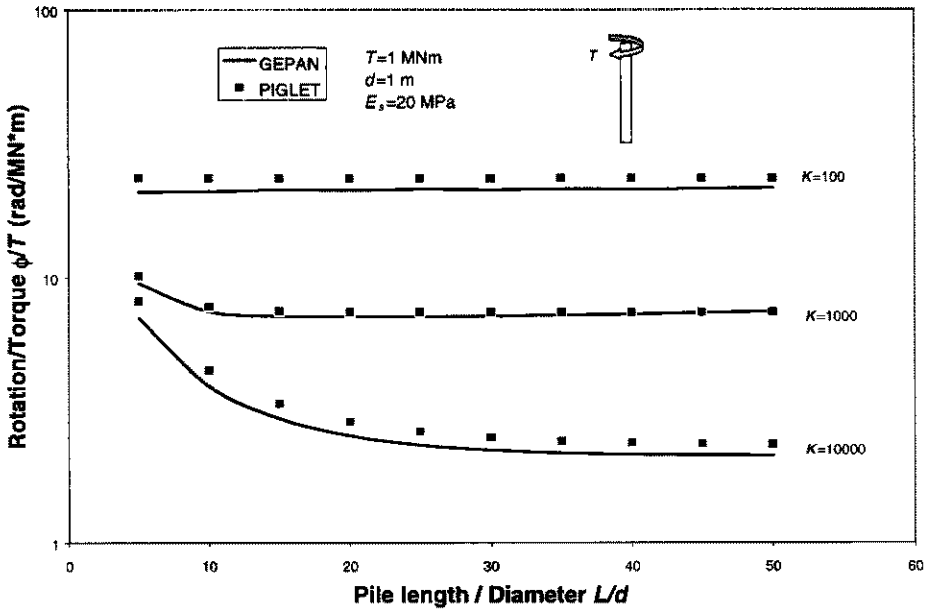

Fig. 3.9 Comparison of the top rotation of torsionally loaded single pile

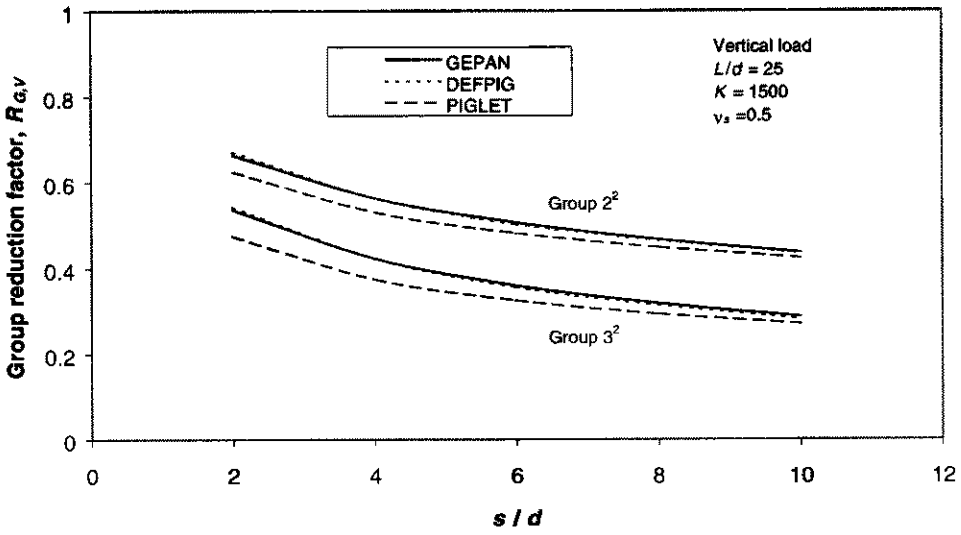

Fig. 3.10 Comparison of the reduction factors of vertically loaded pile-groups

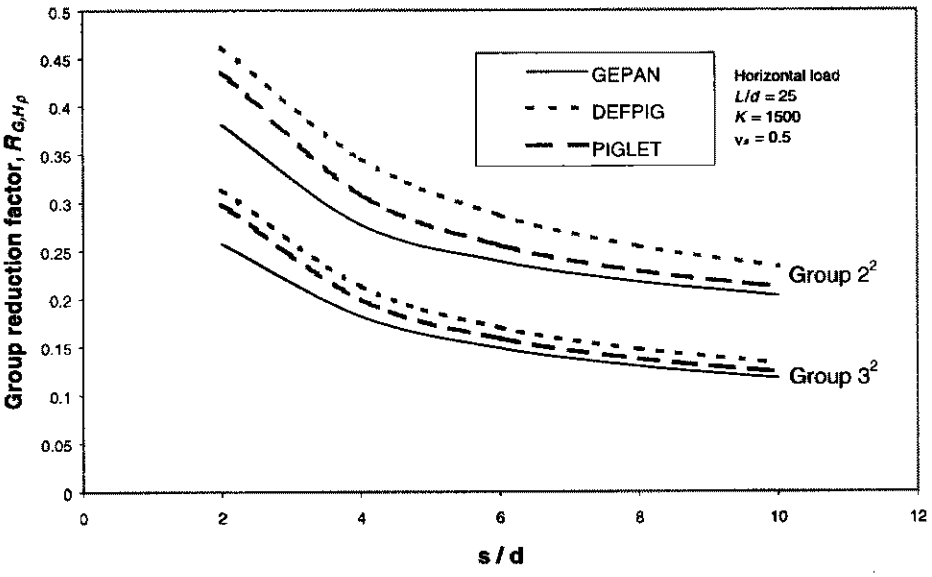

Fig. 3.11 Comparison of the reduction factors of horizontally loaded pile-groups

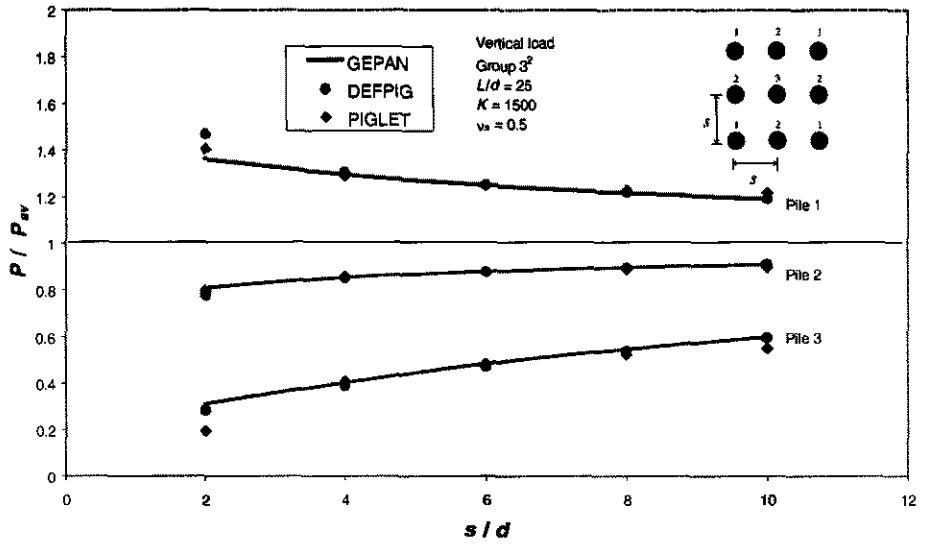

Fig. 3.12 Comparison of the load distributions of vertically loaded in 3^2 group

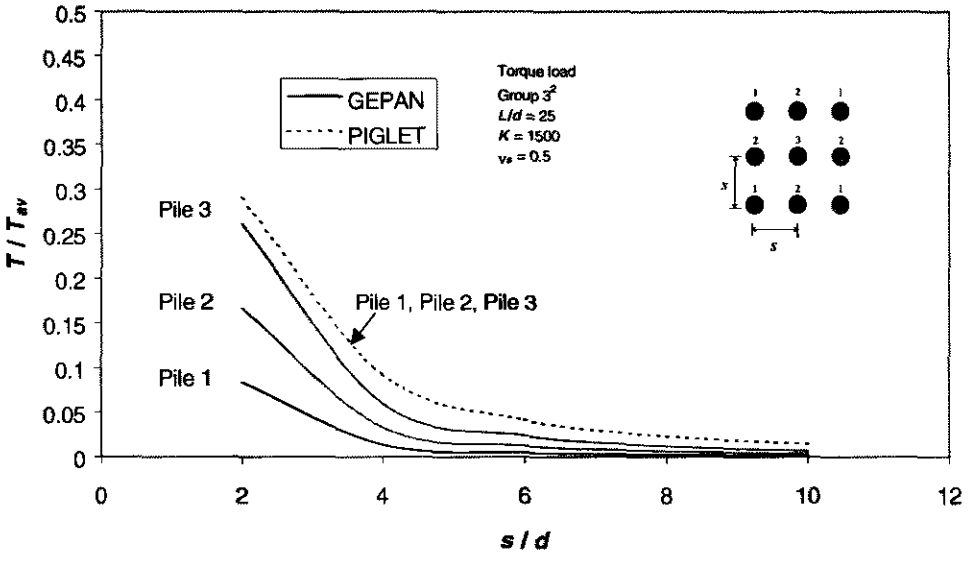

Fig. 3.13 Comparison of the load distributions of torsion loading of 3^2 group

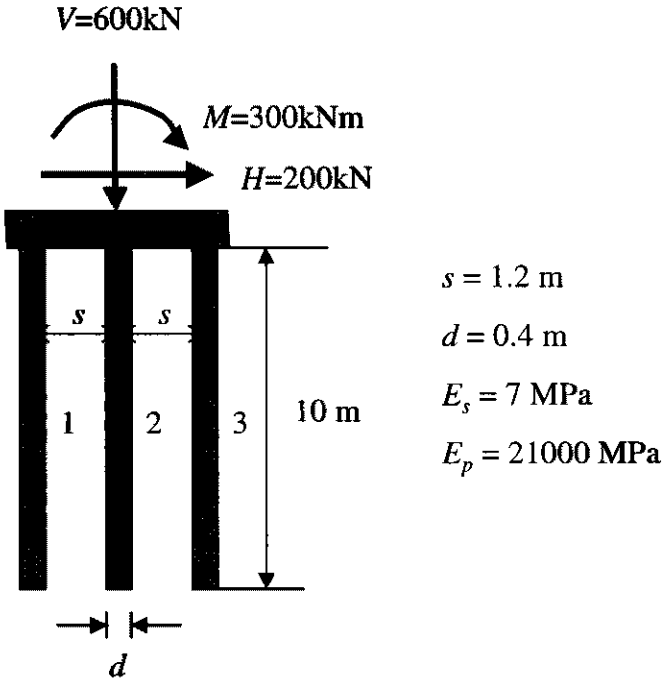

Fig. 3.14 Pile groups considered in comparison of methods

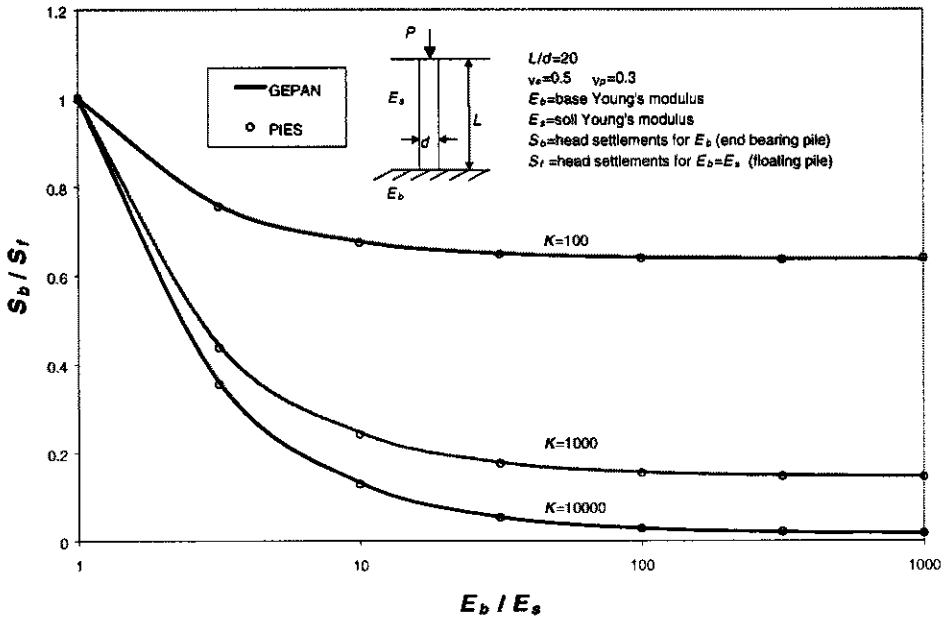

Fig. 3.15 Head settlements of an end-bearing pile

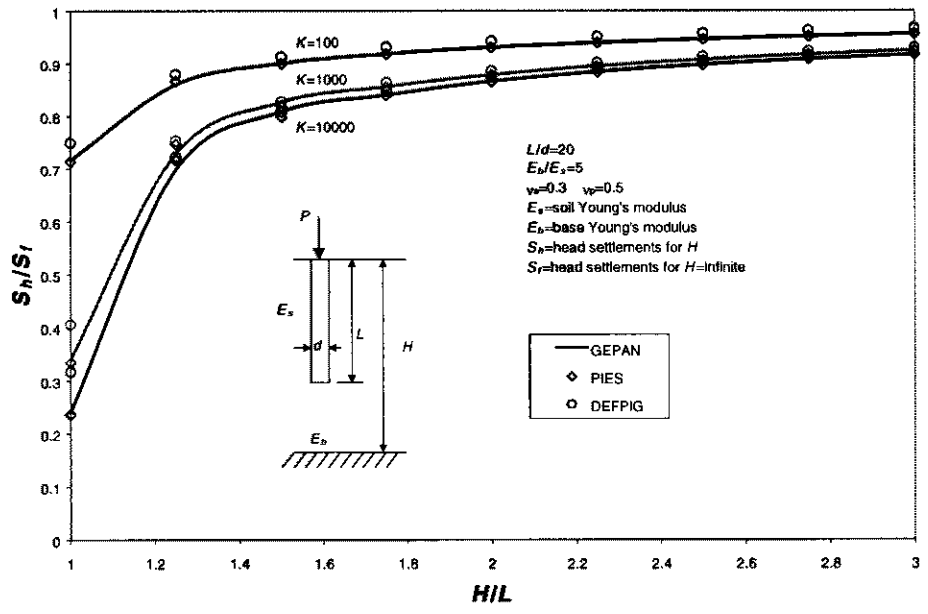

Fig. 3.16 Head settlements of a floating-pile embedded an underlying rigid base

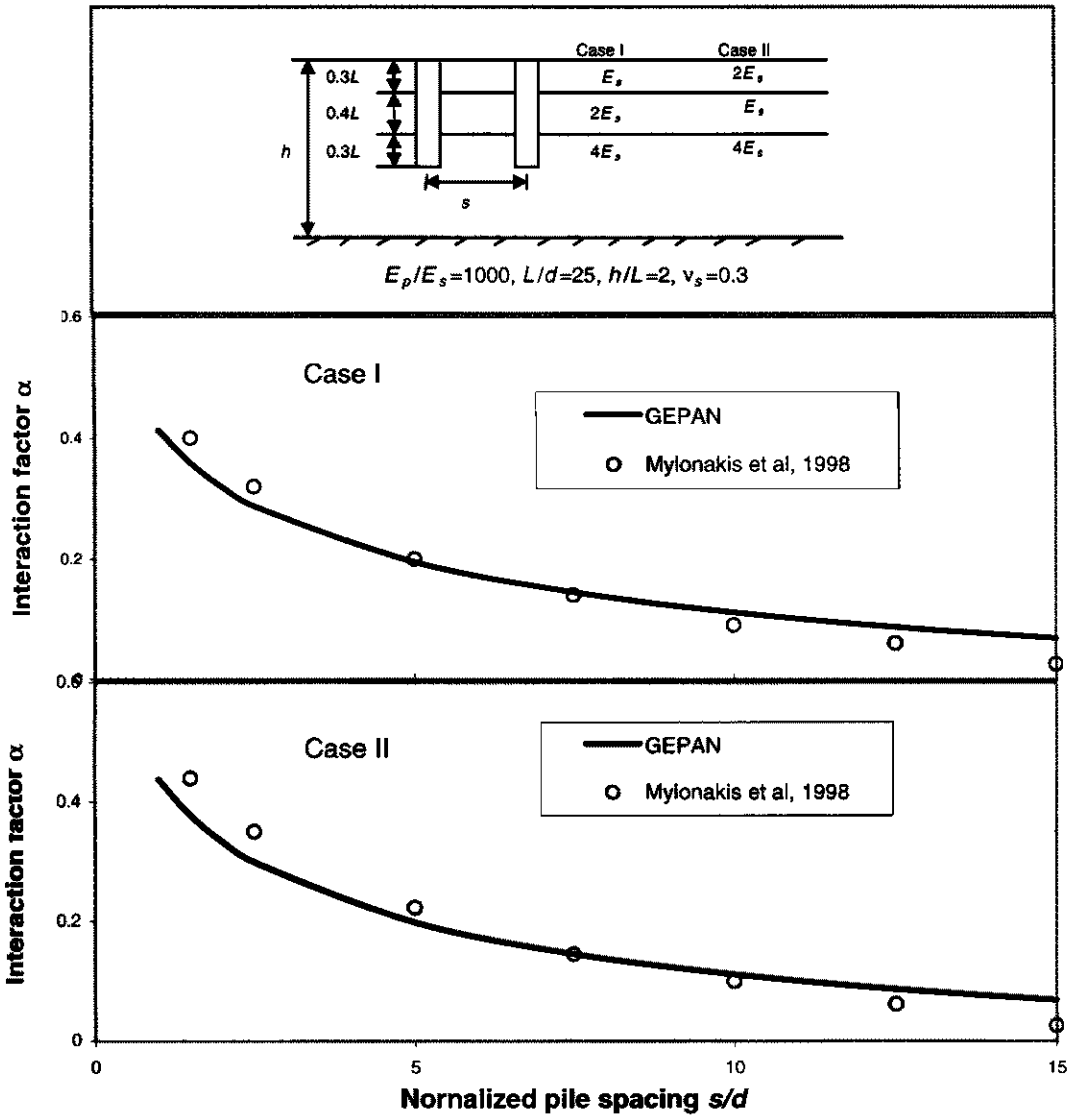

Fig. 3.17 Interaction factors for pile groups embedded in layered soils

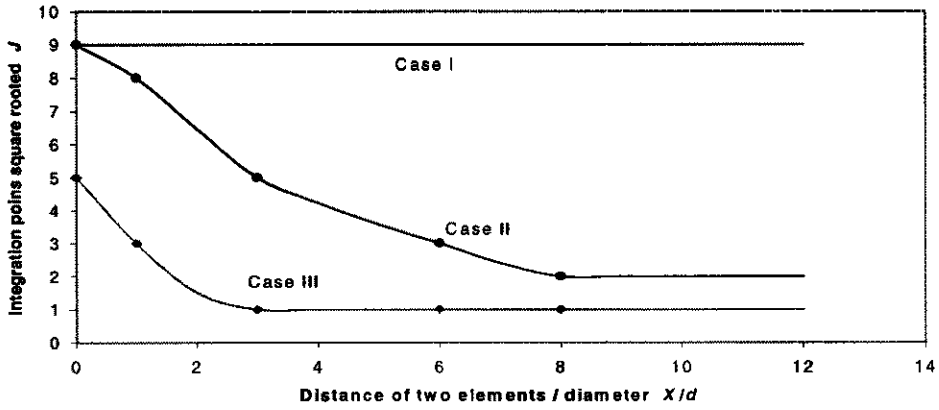

(a) Three cases of integration point cures

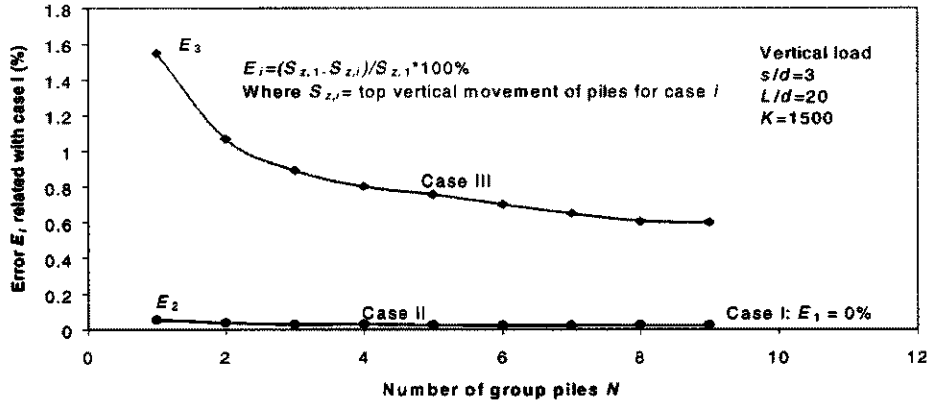

(b) Relative errors of cases II and III compared with case I

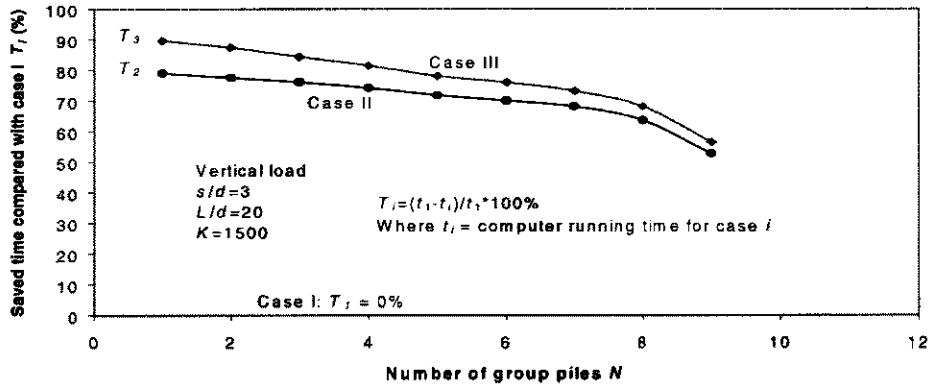

(c) Saved computer time for cases II and III compared with case I

Fig. 3.18 Numerical efficiency on dynamic integration point methods

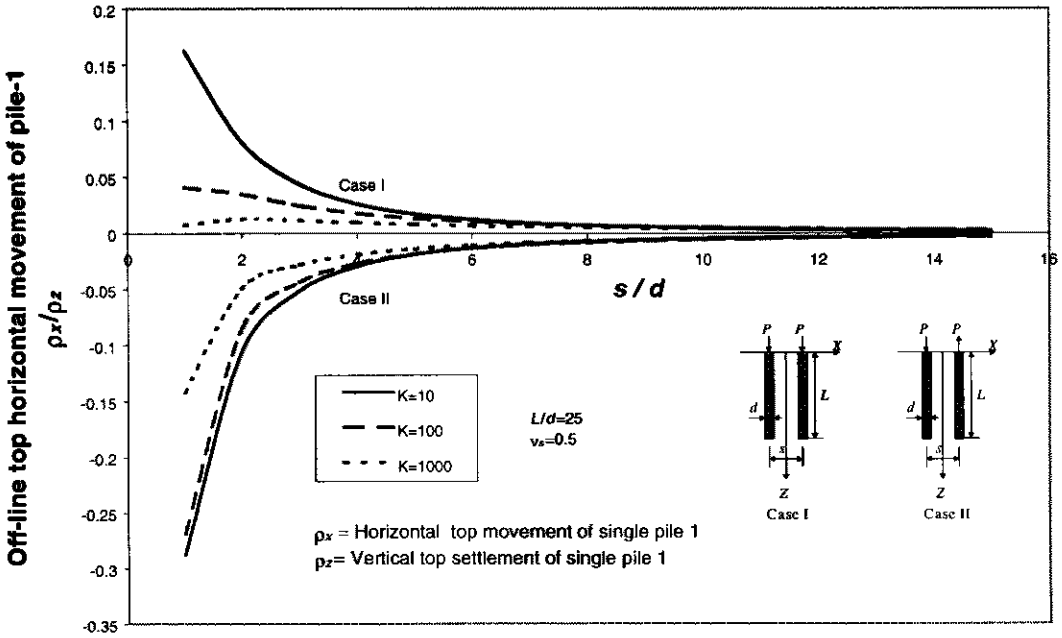

Fig. 3.19 Off-line effects of vertically loaded piles

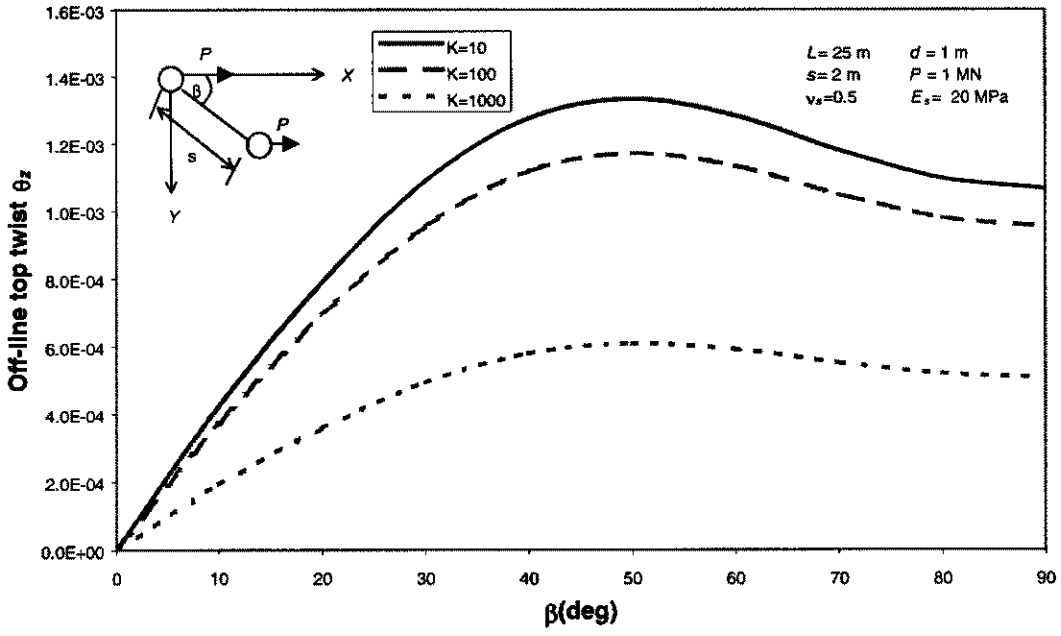

Fig. 3.20 Off-line effects of horizontal loaded piles

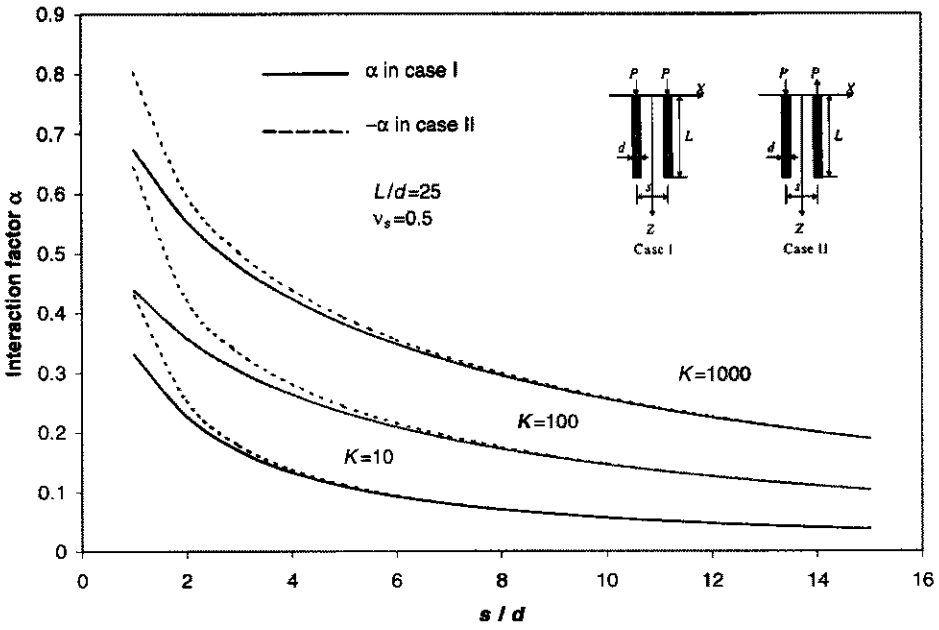

Fig. 3.21 Positive and negative interaction factors of vertical loaded piles

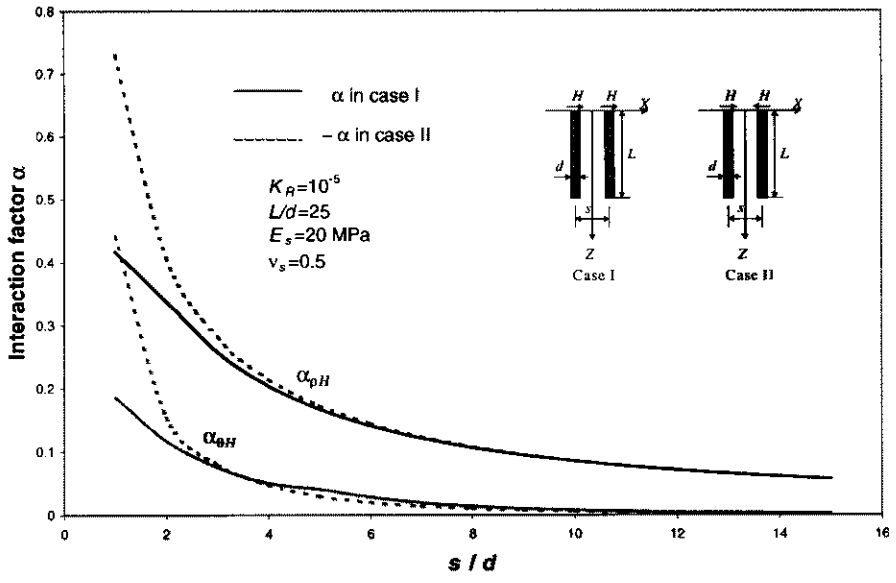

Fig. 3.22 Positive and negative interaction factors of horizontal loaded piles

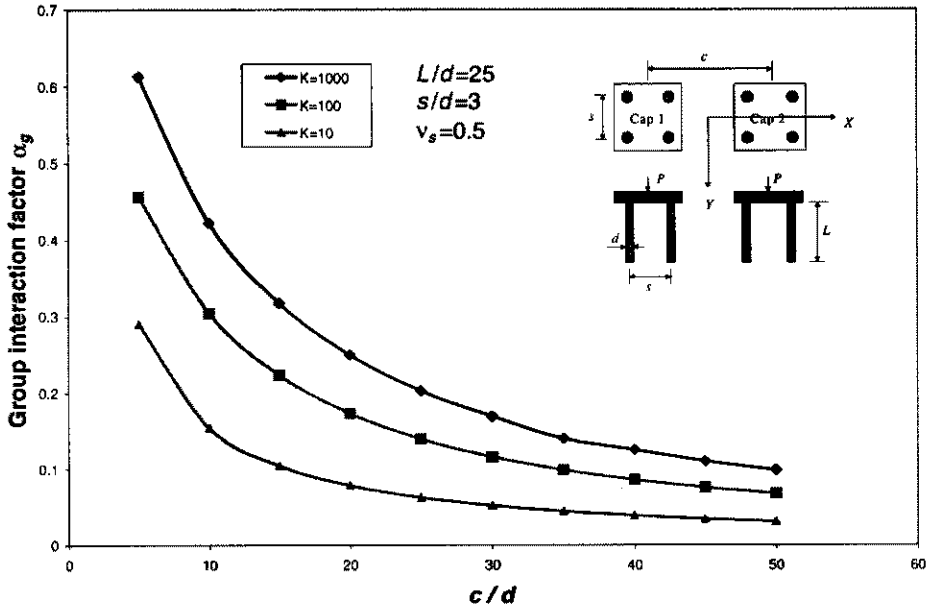

Fig. 3.23 Group interaction factor α_g of two 2^2 vertical loaded groups

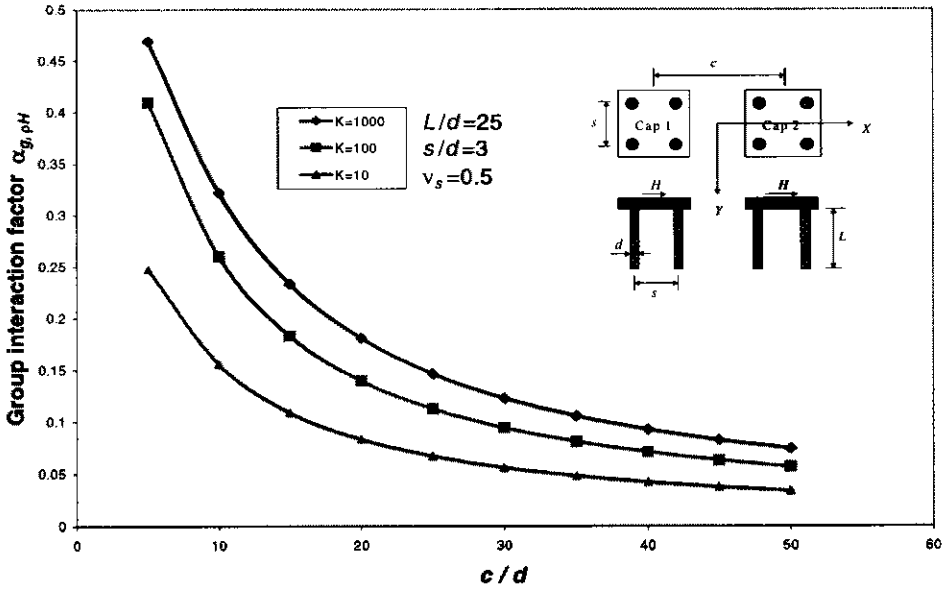

Fig. 3.24 Group interaction factor $\alpha_{g,\rho H}$ of two 2^2 horizontal loaded groups

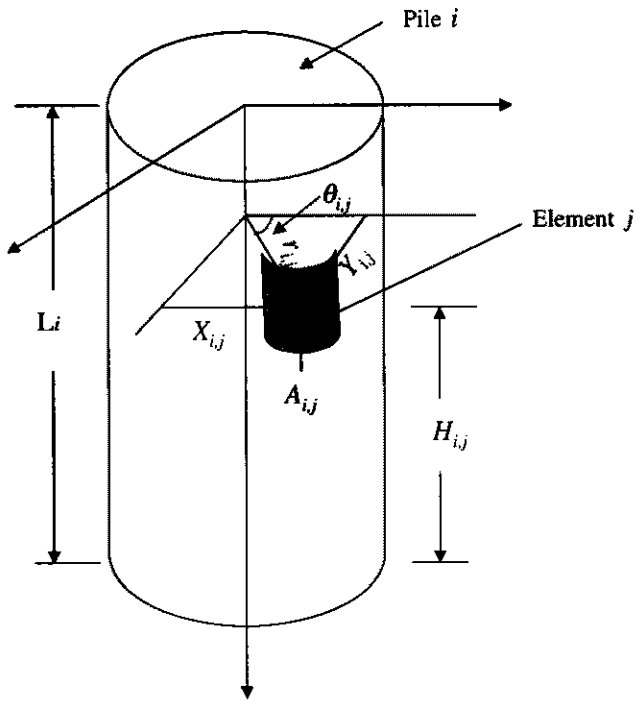

Fig. A3.1 Geometry parameters of element on a pile

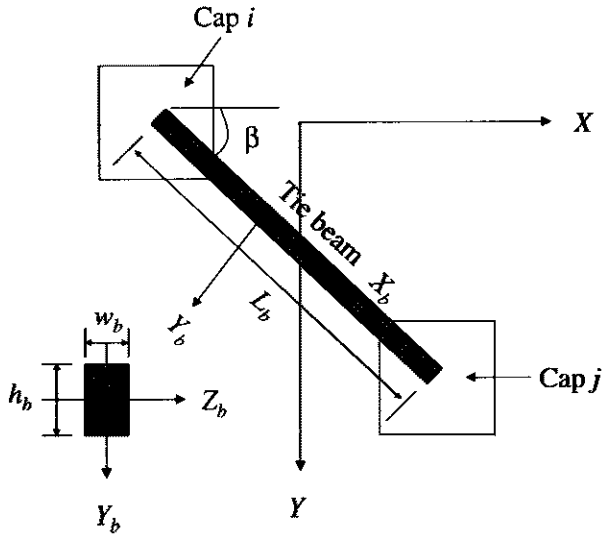

Fig.A3.2 Geometric relations of caps and tie pile

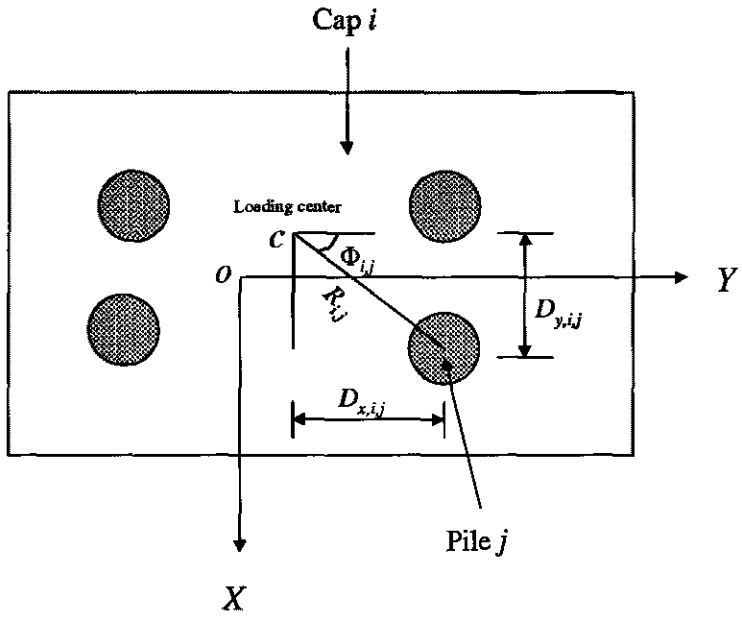

Fig. A3.3 Geometric relations of cap and pile

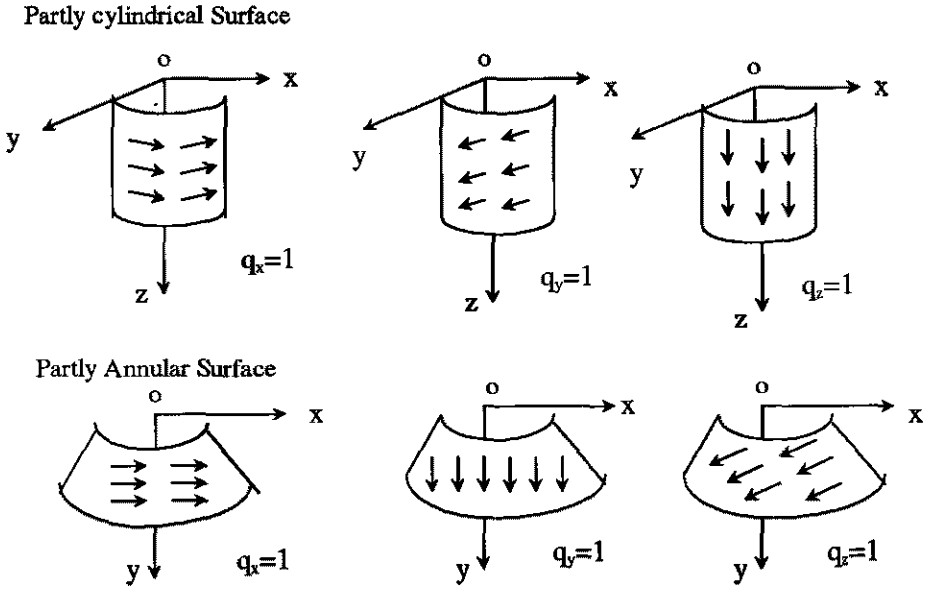

Fig. A3.4 Loads acting on shaft/annular element

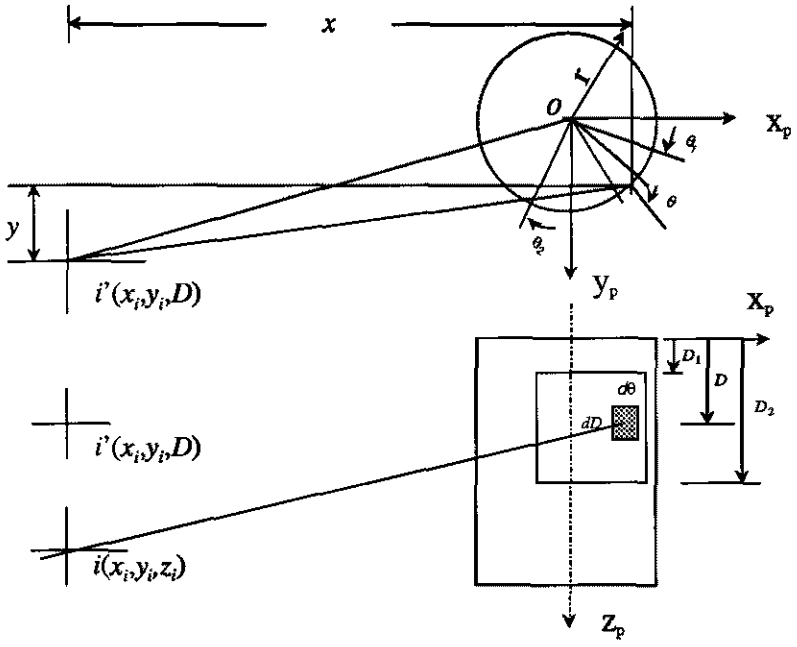

Fig. A.3.5 Geometry for integration along shaft element

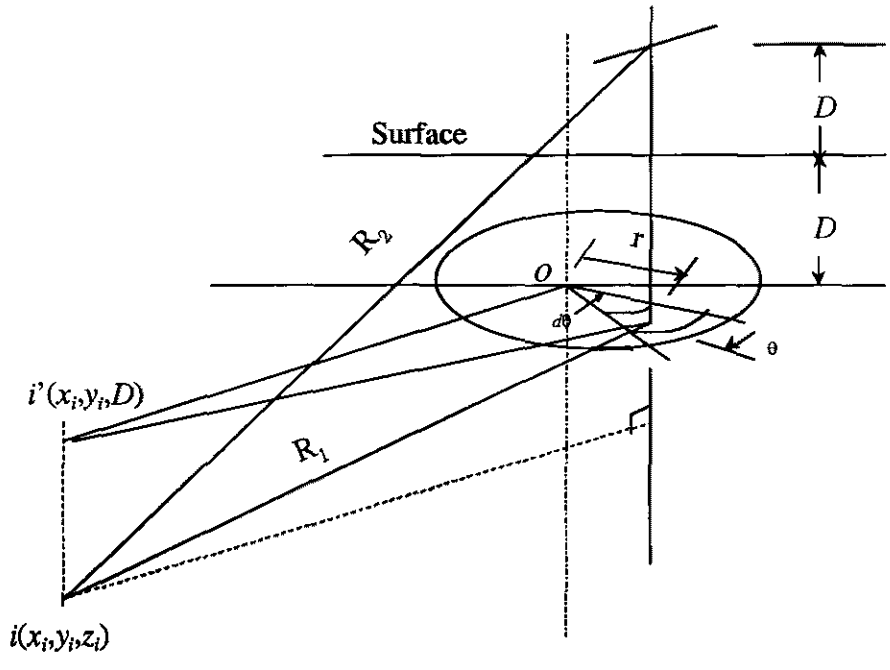

Fig. A3.6 Geometry for integration over annular element

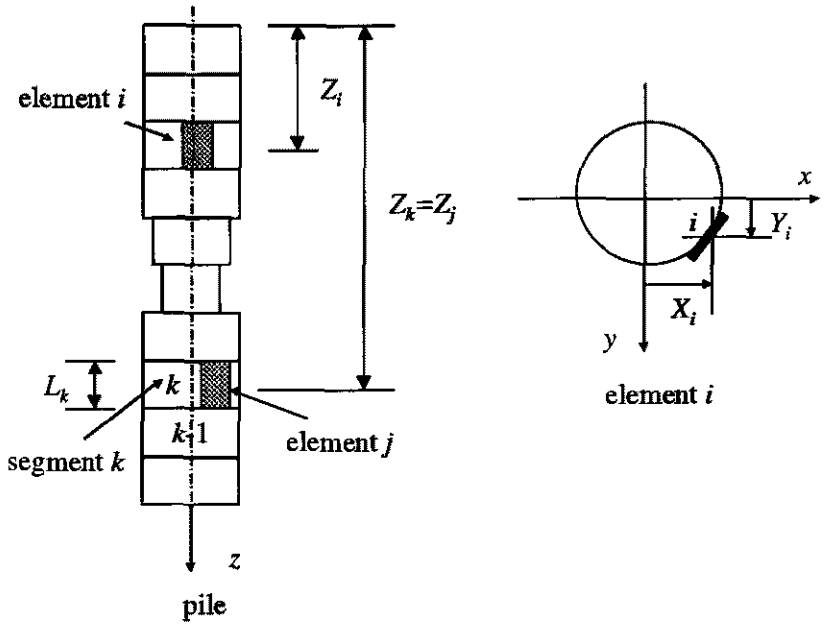

Fig. A3.7 Geometry for nested recursions of pile influence factors

Chapter 4

General 3-D Elastic Analysis of Piles Subjected to "Passive" Loadings

4.1 Introduction

The majority of piles are designed to support "active" loadings, that is, loads which are applied directly to the pile head by a structure. However, there are many cases in which the piles have to withstand "passive" loadings, *i.e.* loads induced in the piles by the action of soil moving past the piles vertically and/or horizontally. Examples include consolidation of clay; swelling or shrinking of an expansive clay; tunnelling; excavation; cavity development; slope movement, and installation of piles. These externally-imposed soil movements will induce additional forces and stresses into pile foundations, and it is important to be able to assess these forces and stresses and their effect on the performance and integrity of the pile foundation.

As reviewed in Chapter 2, problems involving passive pile loadings have been the subject of much recent research. However, most of the above research considers a single pile and de-coupled loadings in two dimensions, while the external soil movements are often derived empirically with little theoretical background.

The boundary element method provides a convenient means of analyzing the load-deformation behavior of piles or pile groups, and of incorporating the influence of soil movements. The soil displacements arise from two sources: the stresses developed at the pile-soil interface by the loading of the pile, and the external (or "free-field") soil movements which are induced from the passive loadings. By imposing displacement compatibility at the pile-soil interface, a series of equations can be obtained. These, together with the equilibrium equations, may be solved to obtain the pile-soil interface stress and the displacement at each point along the pile.

This chapter describes a general 3-D coupled boundary element analysis for piles and pile groups subjected to passive loadings. Using a program called GEPAN, the 3-D pile behaviors caused by a variety of passive loadings, such as soil shrink/swelling, soil surface surcharge, tunnelling, pile installation by driving and cavity formation in soil, are evaluated and characterized. Where possible, the solutions from the GEPAN analysis are

compared with existing published solutions. For each of the cases considered, expressions are also presented for the ground movements, both vertical and lateral.

The modeling of pile-soil interaction is based on a general 3-D coupled pile and pile group analysis which has been developed in Chapter 3. So only modelling of soil movements due to passive loadings is to be described in detail in following section.

4.2 Modelling of Soil Movements due to Passive Loadings

4.2.1 Assumptions

One of the most attractive advantages of the proposed analysis is that externally imposed movements are very easily incorporated into the governing equations if the distributions of these movements are known. These movements are taken to be "free-field" ground movements, *i.e.* independent of the presence of the piles, and it is assumed that the principle of superposition can be applied.

Soil movements are assumed to be independent of time, although in many cases, especially those involving clay soils, the distribution of movement will change with time because of pore pressure dissipation and consequent consolidation of the soil. Thus, it may be necessary to perform a series of analyses, each for a particular time, in order to examine how the pile behaviour varies with time. However, it may often be adequate simply to consider the long-term or drained condition, when consolidation of the soil is complete.

4.2.2 Extra Soil Movements and Stresses on Pile-Soil Interface

4.2.2.1 Directly-Imposed Soil Displacements

Soil displacements arise from two sources: the stresses developed at the pile-soil interface by the loading of the pile, and the external (or "free-field") soil movements which produce the passive pile loadings. By imposing compatibility between the pile and soil displacements at various points along the pile, the ground movements can then be

absorbed into the vector of element stress offset $\{Y_q\}$ in the governing equation 3.1 in Chapter 3 as follows:

$$\{Y_q\}=\{Y_{q,t}\}+\{Y_{q,e}\} \quad \text{.....(4.1)}$$

where $Y_{q,t}$ = vector of pile element displacements due to head loads of individual piles, $Y_{q,e}$ = vector of pile element displacements due to extra soil displacements/stresses/forces.

The effects of external ground movements can be considered in two ways: as directly-imposed displacements based on the known ground movements, or as induced stresses based on the known ground movements. In the first case, the free-field soil movements at the pile-soil interface are indicated by a vector $\{u_{soil}\}$, *i.e.*

$$\{Y_{qe}\}=\{u_{soil}\} \quad \text{.....(4.2)}$$

$$\{u_{soil}\}=\begin{pmatrix} U_1 \\ U_2 \\ \cdots \\ U_{ntot} \end{pmatrix}_{3*ntot\times 1} \qquad U_i=\begin{pmatrix} u_{x,i} \\ u_{y,i} \\ u_{z,i} \end{pmatrix} \quad \text{.....(4.3)}$$

where *ntot* = total soil elements at soil-pile interface, $u_{x,i}$, $u_{y,i}$, $u_{z,i}$ are soil displacements at element i in X, Y and Z directions respectively.

4.2.2.2 Directly-Imposed Soil Stresses

In the second case, the induced stresses are represented by a vector $\{\sigma_{soil}\}$. The corresponding soil movements due to the soil stresses are the product of the soil influence factor matrix $[SIF]$ and the soil stress vector $\{\sigma_{soil}\}$, which is assumed to exhibit an elastic response, *i.e.*

$$\{Y_{qe}\}=[SIF]\{\sigma_{soil}\} \quad \text{.....(4.4)}$$

where *SIF* is a sub-matrix of displacements due to stresses at soil elements, which is expressed:

$$SIF = \begin{pmatrix} I_{1,1} & I_{1,2} & I_{1,j} & I_{1,ntot} \\ I_{2,1} & I_{2,2} & \cdots & \cdots \\ I_{i,1} & \cdots & I_{i,j} & \cdots \\ I_{ntot,1} & \cdots & \cdots & I_{ntot,ntot} \end{pmatrix}_{3*ntot \times 3*ntot} \quad \text{.....(4.5)}$$

where ***ntot*** is total soil elements on soil-pile interface, and $I_{i,j}$ is the 3×3 BIFM of displacements at soil element i due to unit stresses on soil element j which is expressed as follows:

$$I_{i,j} = \begin{pmatrix} I_{i,j,1,1} & I_{i,j,1,2} & I_{i,j,1,3} \\ I_{i,j,2,1} & I_{i,j,2,2} & I_{i,j,2,3} \\ I_{i,j,3,1} & I_{i,j,3,2} & I_{i,j,3,3} \end{pmatrix}_{3\times 3} \quad \text{.....(4.6)}$$

$I_{i,j,k,l}$ = soil displacement in direction k at element i due to a unit stress in direction l on element j.

The soil influence factor $I_{i,j,k,l}$ is evaluated by integration of Mindlin's equations (Mindlin, 1936). It should be emphasized that there are nine such equations, because the loads and deformations are fully coupled in three dimensions.

$$\{\sigma_{soil}\} = \begin{pmatrix} \Sigma_1 \\ \Sigma_2 \\ \Sigma_i \\ \Sigma_{ntot} \end{pmatrix}_{3\times ntot,1} \qquad \Sigma_i = \begin{pmatrix} \sigma_{x,i} \\ \sigma_{y,i} \\ \sigma_{z,i} \end{pmatrix} \quad \text{.....(4.7)}$$

where, $\sigma_{x,i}$, $\sigma_{y,i}$, $\sigma_{z,i}$ are external soil stresses at element i in the x, y and z directions respectively.

4.2.3 Soil Movements and Stresses in Typical Geo-Engineering Problems

4.2.3.1 Indirectly-Imposed Soil Displacements/Stresses

As mentioned above, the general 3-D coupled pile-soil interaction has been modeled in Chapter 3 govern by Eq. 3.1 and the "interface" between the pile-soil model and passive loadings is set up by Eqs. 4.1 to 4.3. The next task is then to develop the expression for the "free field" soil movements and stresses, $\{u_{soil}\}$ and $\{\sigma_{soil}\}$, arising from specific passive loadings.

4.2.3.2 Explicit Expressions for Ground Movements

External vertical soil movements can usually be calculated from conventional settlement analyses, provided that the underlying causes of the settlement can be recognized and quantified. For some special cases of passive loading, there exist well-established equations for free soil movements and/or stresses, which can be applied directly to the pile soil-movement analysis. A comprehensive collection of explicit expressions for conventional external soil movements from the theory of elasticity relevant to soil and rock mechanics was assembled by Poulos and Davis (1974), and may be employed in Eq. 4.2 or Eq. 4.4 to study the pile behaviour induced by these soil movements.

Some of the sources of expressions relevant to passive pile loading are summarized Table 4.1.

Table 4.1. The 3-D Theoretical Expressions of Soil Movement by Passive Pile Loadings

Passive Pile Loadings	Expressions derived by	Equation incorporated
Externally imposed soil movements	Directly input	Eq. 4.2
Externally imposed soil stresses	Mindlin (1936)	Eq. 4.4
Embankment loadings	Scott (1963) Jurgenson (1934) Gray (1936)	Eq. 4.4
Tunnelling	Loganathan *et al* (1998) Verruijt *et al* (1996) Sagaseta (1987)	Eq. 4.2
Cavity Formation	Sagaseta (1987)	Eq. 4.2
Excavation Retaining wall	Sagaseta (1987) Mindlin (1936)	Eq. 4.2
Installation effects of piles	Sagaseta (1987) Carter *et al* (1979)	Eq. 4.2

4.3 Evaluation and Applications

In analyzing the pile response from passive pile loadings, some simple applications are described to illustrate the utility of the analysis, and where possible, comparisons have been made between the results from GEPAN and other published solutions.

The applications considered herein include soil swelling/shrinking, tunnelling, installation effects of pile driving, and soil cavity formation. A number of other sources of passive pile loading, such as embankment construction, and retaining wall movement will be examined in future papers.

4.3.1 Simple Distributions of Soil Movements

4.3.1.1 Vertical Soil Movements

Piles are frequently used to support structures on expansive soils, as they can substantially reduce the amount of movement which the structure may undergo if the soil shrinks or swells, or on consolidating clays which give rise to negative friction. These problems may be considered as passive loading on the piles induced by vertical soil movements. A typical vertical soil movement distribution is presented by Poulos and Davis (1980), which decreases linearly with depth from S_o at the surface to zero at a depth z_s as shown in Fig. 4.1 (except for a change in sign, the performances of piles in swelling or shrinking soil are similar when elastic behaviour is considered). The computed variations of dimensionless pile movement, ρ_{zo}/S_o, with L/d and z_s/L are shown in Fig. 4.2 and are compared with the solution of Poulos and Davis (1980). Fig. 4.3 gives another comparison of dimensionless pile load, $P_{max}/E_s d S_o$, with L/d and z_s/L. It is found the agreement between the present method and the Poulos and Davis solutions is generally good, although the analysis details are rather different. Fig. 4.4 indicates that the vertical pile movement changes very little with depth along the pile considered. Via a numerical curve-fitting process using the program EXCEL, a compact expression for pile settlement due to the vertical soil movement has been derived and is given in Eq. 4.8.

$$\frac{\rho_{zo}}{s_o} = 0.35\left(\frac{z_s}{L}\right)^{0.86}\left(\frac{L}{d}\right)^{0.05} \quad \text{..... (4.8)}$$

As indicated in Fig. 4.2, this approximate expression agrees well with the GEPAN solution.

4.3.1.2 Horizontal Soil Movements

Horizontal soil movements may arise from a variety of sources, including soil slope movement or instability, retaining wall movements, and seismic effects. A simple representation of typical horizontal soil movements is via a linear distribution with depth

(Chen *et al*, 1997) as illustrated in Fig. 4.5. Figs. 4.5 and 4.6 show design charts for dimensionless horizontal pile head movements ρ_{xo}/S_o and dimensionless maximum pile moment $M_{max}/E_s dz_s S_o$ respectively due to the horizontal soil movements. Comparisons are shown between the present approach and results presented by Chen *et al* (1997), and these indicate good agreement. Furthermore, by curve-fitting to the GEPAN results, the design chart for the horizontal pile head movements can be expressed by the following approximate equation:

$$\frac{\rho_{xo}}{s_o} = 1 + (x_1 - 1)\exp\left(-\frac{x_1}{0.064x_2^2 - 0.605x_2 + 1.5}\right) \quad \text{.....(4.9)}$$

where $\quad x_1 = \frac{z_s}{L} \qquad x_2 = -\log K_R$

As shown in Fig. 4.5, this approximate expression closely follows the other two solutions. In order to more clearly understand the mechanism of piles subjected to horizontal soil movement, the pile horizontal and vertical movement distributions with depth are given in Fig. 4.7 and Fig. 4.8 respectively. As expected, Fig. 4.7 shows that the horizontal deflection profile of a pile is more "curved" as the pile flexibility factor K_R decreases. Fig. 4.7 shows that the "fixity point", where zero horizontal pile displacement occurs, becomes lower as K_R and/or z_s/L increase. The distributions of vertical pile movement are plotted in Fig. 4.8. Although small compared with the horizontal pile movements, the vertical pile movement do exist and are induced by the 3-D coupled effect. The solutions of Chen *et al* (1997) can not give these "off-line" pile movements. For piles in unstable soil slopes, Figs. 4.9(a) and 4.9(b) present the computed lateral response of a free-head pile subjected to a constant soil movement profile in a uniform soil. The results of analyses by Madhav *et al* (1997) are also shown, these having been derived via a subgrade reaction analysis. The general characteristics of behaviour are similar, but there are some differences in the details of the pile response.

4.3.2 Soil Surface Loading

When a surcharge is applied to soil near a pile foundation, the pile will undergo some deformation. If the "free field" soil stresses due to the surcharge can be quantified and recognized, the passive piles may be analyzed via Eq. 4.4.

As an example, a horizontal surface loading near four piles is shown in Fig. 4.10. The results of the GEPAN analysis are shown in Fig. 4.11, and indicate that the major pile head movements are horizontal (in both the x and y directions) while minor vertical movements ρ_z and rotations θ_y and θ_z also occur. Piles 1, 4 experience upward vertical head movements while piles 2, 3 move downward. Piles 1 and 4 are "pulled" inside while piles 2 and 3 are "pushed" outside. The head of piles 1 and 2 is twisted clockwise while piles 3 and 4 are twisted anti-clockwise. The above coupled phenomena are as might be expected, but can not be detected via conventional de-coupled pile analysis programs.

4.3.3 Circular Tunnels

Mathematical expressions for tunnelling-induced ground movement have been presented by Loganathan *et al* (1998), Verruijt *et al* (1996) and Sagaseta (1987). These equations have been incorporated into program GEPAN and enable the behaviours of passive piles near a circular tunnel to be characterized. Combining the governing equation 3.1 and the expressions developed by Loganathan *et al* (1998), Loganathan *et al* (1999a, 1999b) have evaluated the response of single piles and pile groups to tunnelling, and have considered the effects of various factors such as tunnel geometry, ground loss ratio, pile diameter and ratio of pile length to tunnel depth. Figure 4.12, for example, shows profiles of bending moment, lateral deflection, axial downdrag force and vertical movement along a pile, corresponding to three average ground loss ratios ε, for a lateral distance x=4.5 m, away from the tunnel centerline. (The relevant parameters are: soil Young's modulus, E_s=24 MPa; pile Young's modulus, E_p=30000 MPa; tunnel radius, R=30 m; the depth of tunnel axis, H=20 m; pile diameter, d=0.5 m and pile length, L_d=25 m) (Loganathan *et al*, 1999a).

As expected, larger forces, moments and deflections are developed as ε increases, thus emphasizing the importance of minimizing ground loss in tunnel construction.

4.3.4 Installation Effect of Driven Piles

When a pile is driven into soil, horizontal and vertical movements are developed in the soil surrounding the pile. Poulos (1994c) studied the installation effect due to pile driving, via applying the expression for radial soil displacement proposed by Carter *et al* (1979) from cavity expansion theory. Using the source-sink technique developed by Sagaseta (1987), Chow and Teh (1990) also analysed the effects of movements caused by pile-driving on nearby piles.

Although both analyses provide successful predictions for some practical cases, they are only suitable for 2-D de-coupled pile problems. Based on the source-sink approach, a 3-D coupled driven pile analysis has been set up in program GEPAN. Firstly, a small cylindrical pile element is taken as a small spherical point sink. The point sink is assumed to cause axially symmetrical deformations. The soil movements at the plane that co-planes with calculation point *i*, and sink point *j*, are determined via applying Sagaseta's equation (1987). These soil movements are then projected onto the *X* and *Y* planes respectively and the vertical and horizontal components of soil movement are obtained. Finally, all the contributions of soil movements from each cylindrical pile elements are considered. It should be noted that this is a quite approximate method because only the installation effect of "additional soil movements" due to pile driving is considered. The other installation effects like sand densification and clay remolding are not discussed here.

Pile heave measurements of driven cast in situ piles in stiff fissured clays at three sites in the UK were reported by Hammond *et al* (1980) and a theoretical simulation was made by Chow and Teh (1990). In the theoretical analysis, the parameters are estimated by Chow and The (1990), which the theoretical upper bound are L=12 *m*, d=0.48 *m*, L/d=25, and E_s=74 MN/m^2; for the lower bound, L=7.5 *m*, d=0.43 *m*, L/d=17, and E_s=48 MN/m^2. The Young's modulus of concrete is assumed to be 30000 MN/m^2 and the soil Poisson's ratio to be 0.5. Fig. 4.13 shows that the measured pile heave *vs.* normalized pile spacing *s/d* is a

good agreement with their results and also from GEPAN which uses the same soil parameters as Chow and Teh (1990). The pile head horizontal movement and rotation, predicted by GEPAN using the computed soil movements, are shown in Fig. 4.14.

The responses to nearby pile driving, of a single pile, a 2×2 pile group and 2×2 individual piles have been studied, and are shown in Fig. 4.15; they are referred to as case 1, case 2, and case 3 respectively. Figs. 4.16 and 4.17 illustrate the computed horizontal and vertical pile head movements, and show that the results for a single pile in case 1, and pile group in case 2, lie between those for the front piles (pile 1 and pile 4) and the rear piles (pile 2 and pile 3) of case 3. When $s/d>10$, the passive behaviour of a single pile and a pile group are very similar. Furthermore, in case 3, the 4 already-installed individual piles are "pushed away and twisted" by driving a pile, as shown in Fig. 4.18(a). These piles have 6 fully-coupled deformation components, *i.e.* vertical and horizontal movements and rotations and twist, as shown in Figs. 4.18(b) and 4.18(c).

4.3.5 Cavity Formation

In limestone, solution cavities can develop, and the development (or shrinking) of cavities will induce ground movements which can affect the behaviour of nearby piles. Sagaseta (1987) presents closed form solutions for the strain field in a soil due to near-surface ground loss/gain. This concept can be applied to the soil movement due to cavity shrinking/swelling in the soil (the characteristics of cavity shrinking or swelling are similar in elastic behaviour, except for a change in sign). The soil is assumed to be isotropic, homogeneous, and incompressible, and the cavity is idealized as spherical. Applying Sagaseta's equation (Sagaseta, 1987), general 3-D expressions of soil movements due to the spherical cavity can be developed. The 3-D expressions of soil movements are incorporated into Eq. 4.2, and then the behaviours of a nearby pile due to the cavities may be analysed by solving the governing equation 3.1.

Fig. 4.19(a) and Fig. 4.20(a) illustrate the case where a cavity is formed under a 2×2 pile group (ratio of length to diameter is 20 and the centre-to-centre spacing is 4 diameters). A

cavity is assumed to exist at a depth b from the tip of the piles, and is assumed initially to have a radius equal to the pile diameter. The cavity is assumed to exhibit a ground "loss or gain" ε, due to shrinking/swelling, of 50%. The location of the cavity varies from "centre" to the "outside" of the piles, along the x-axis shown in Fig. 4.19(a), and to shift from the "center" to the "outside" along a diagonal line, as illustrated in Fig. 4.20(a). It is found that the vertical pile cap movement is larger than the horizontal pile head movement (Figs. 4.19(a) and 4.19(b)). When the dimensionless horizontal distance of the cavity from the centre of the group, a/d (along the x-axis) or e/d (along a diagonal line), is greater than 10, the effects of the depth of cavity are negligible, as shown in Figs. 4.19 and 4.20. Fig. 4.21 schematically shows the positions of a cavity which produces the largest pile cap movements. The largest vertical displacement is induced by cavity "*E*" when the cavity is close to the tip of a pile (*i.e.* b/d=1), or by cavity "*A*" if the dimensionless distance b/d between the cavity and the tip of the pile is about 5. Cavity "*F*" produces the largest horizontal pile cap displacement. The next most critical positions are cavity "*D*" and cavity "*B*" for vertical pile cap displacement, and cavity "*C*" for horizontal soil movement. It should also be noted that cavity "*F*" and cavity "*C*" are near the edge but "outside" the projected area of the pile cap, rather than "inside" (for b/d =1, for example, a/d=3 for cavity "*C*" shown in Fig. 4.19(a), and e/d=3.2 for cavity "*F*" shown in Fig. 4.20(a)). The pile cap movements will decrease greatly with the relative depth when b/d is less than 2, but when b/d is greater than 2 the pile cap movements decrease more slowly as shown in Fig. 4.22. Fig. 4.23 shows that, if the radius of a cavity increases, vertical pile movements increase more significantly than horizontal movements.

4.4 Conclusions

This chapter describes a theoretical analysis of 3-D coupled passive pile behavior. The modelling of pile-soil interaction and the influence of "free field" soil movements is carried out via boundary pile-soil elements. Comparisons have been made between published solutions and those from the theoretical approach based on the 3-D coupled

boundary element analysis implemented via the program GEPAN. It has been found that GEPAN is capable of giving realistic estimates of passive pile behavior under a variety of situations, including vertical and horizontal soil movements, soil surcharges, tunnelling, pile installation and cavity shrinking or swelling. An important feature of GEPAN is its ability to predict "off-line" behaviour of piles, *e.g.* the horizontal movements of piles subjected to vertical ground movements, and the coupled vertical and lateral behaviour of piles subjected to simultaneous vertical and horizontal ground movements. Using these analyses, it is possible to identify situations in which the risk of pile damage is most severe, thus enabling mitigation strategies to be developed.

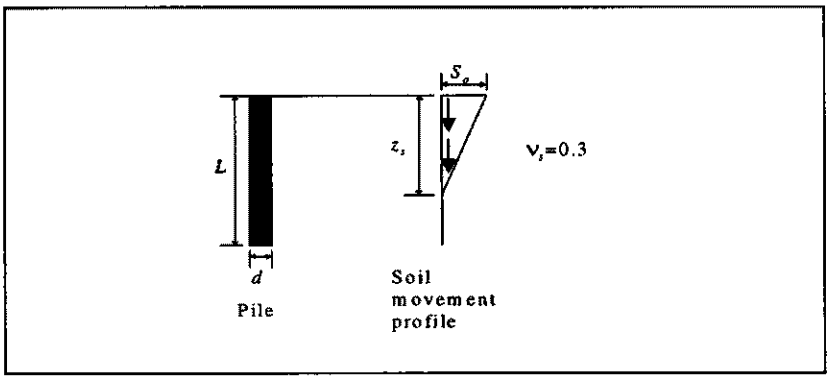

Fig.4. 1 Definiton of a typical vertical soil movement

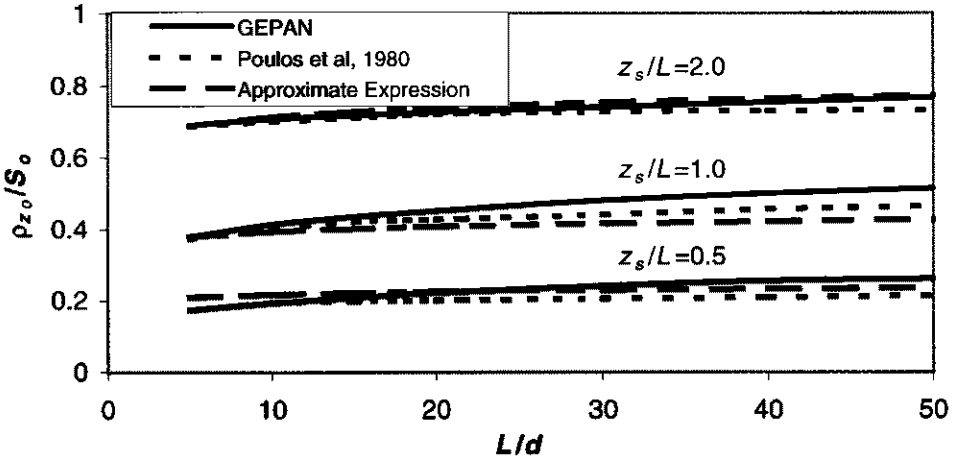

Fig. 4.2 Variation of pile head movement with vertical soil movement

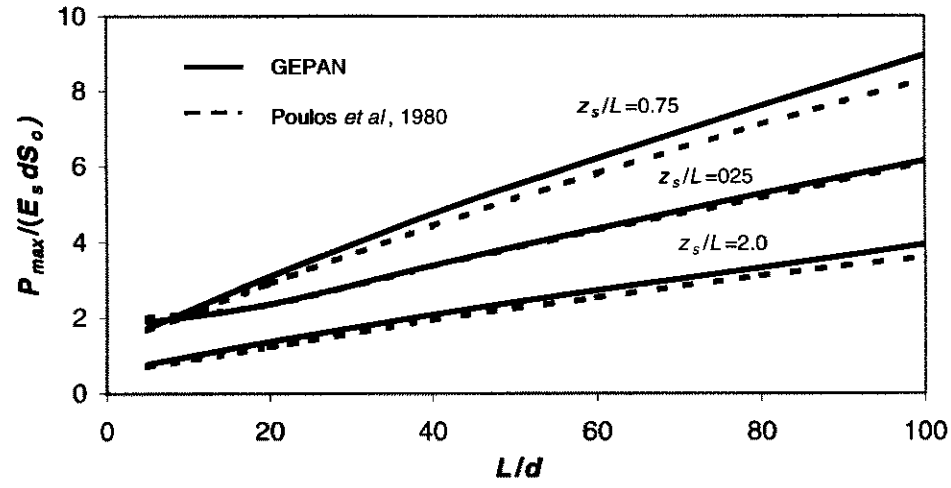

Fig. 4.3 Variation of pile maximum load with vertical soil movement

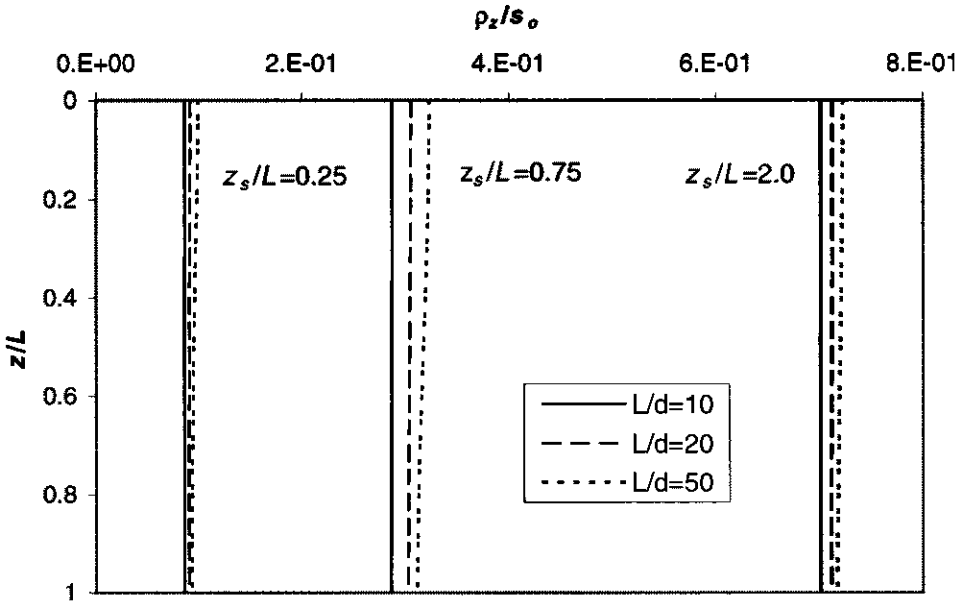

Fig. 4.4 Vertical displacement distribution due to vertical soil movements

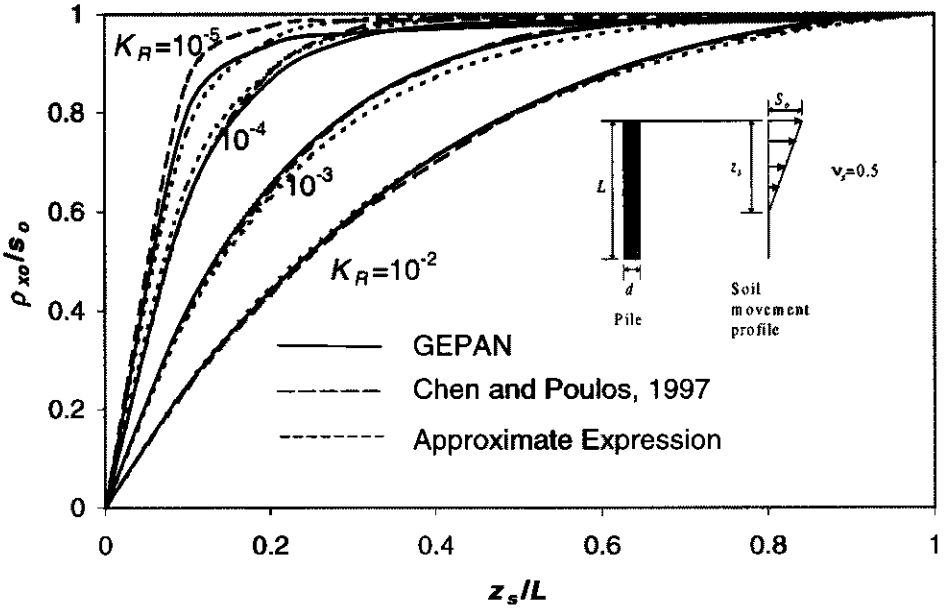

Fig. 4.5 Variation of pile head movement with horizontal soil movement

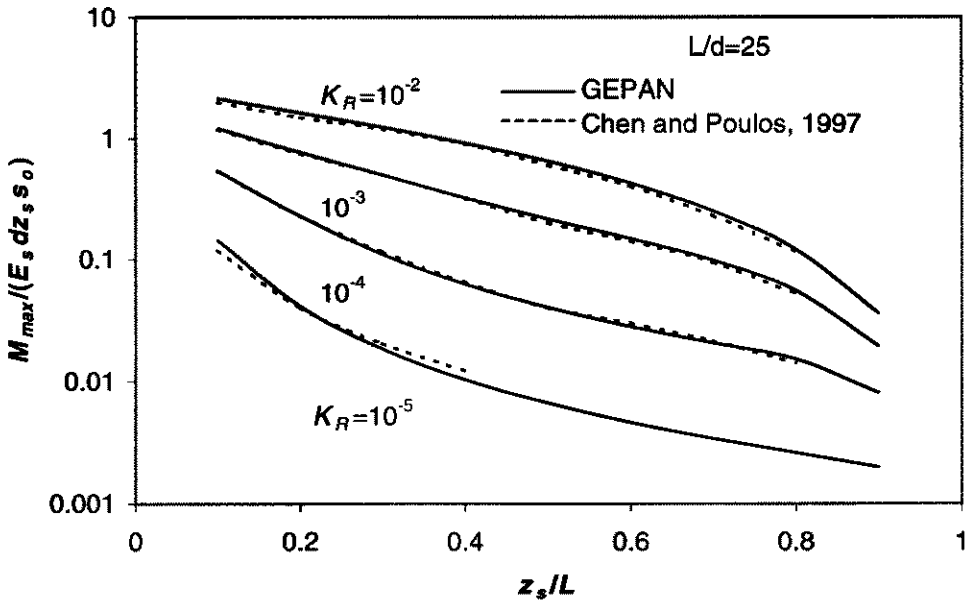

Fig. 4.6 Maximum moment M_{max} in pile due to horizontal soil movement

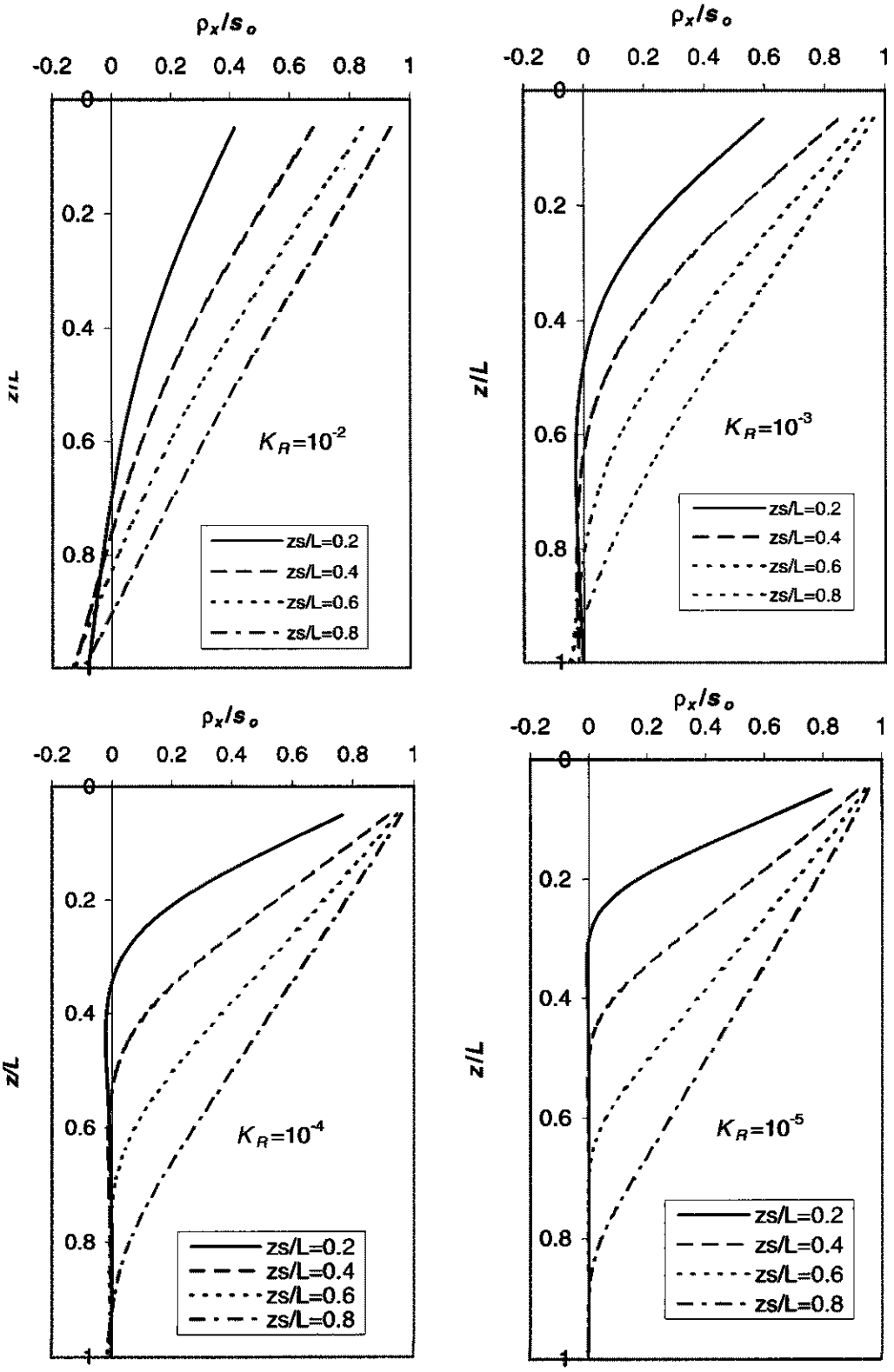

Fig. 4.7 Horizontal displacement distribution along a pile for various K_R values

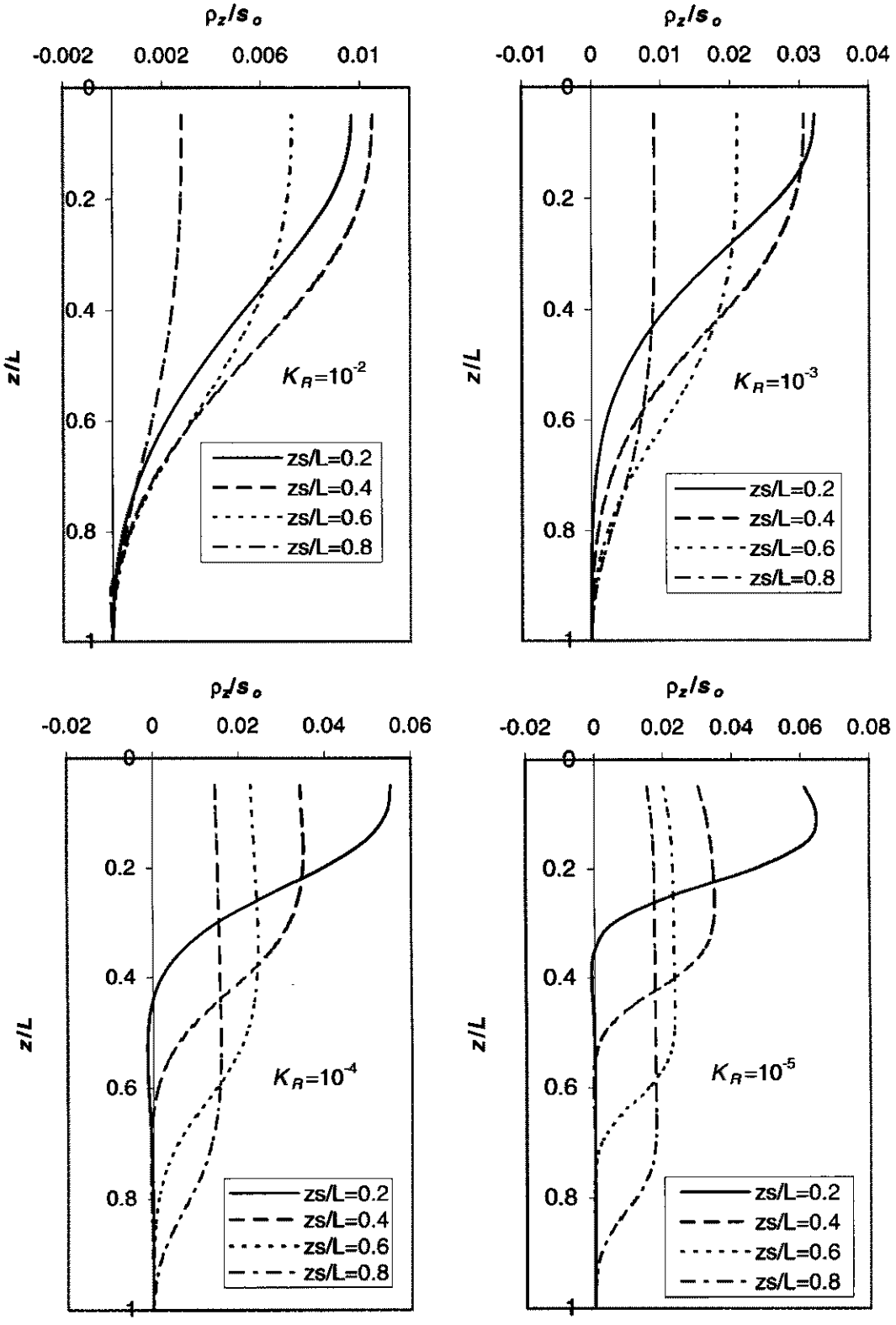

Fig. 4.8 Vertical displacement distribution along a pile for various K_R values

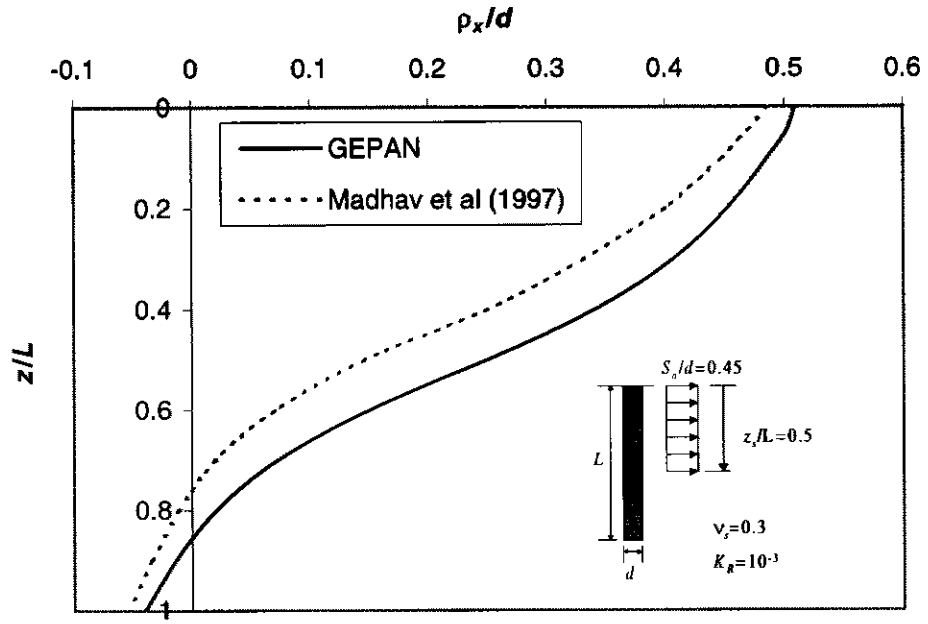

Fig. 4.9(a) Horizontal displacement distribution of a pile due to a horizontal soil movement

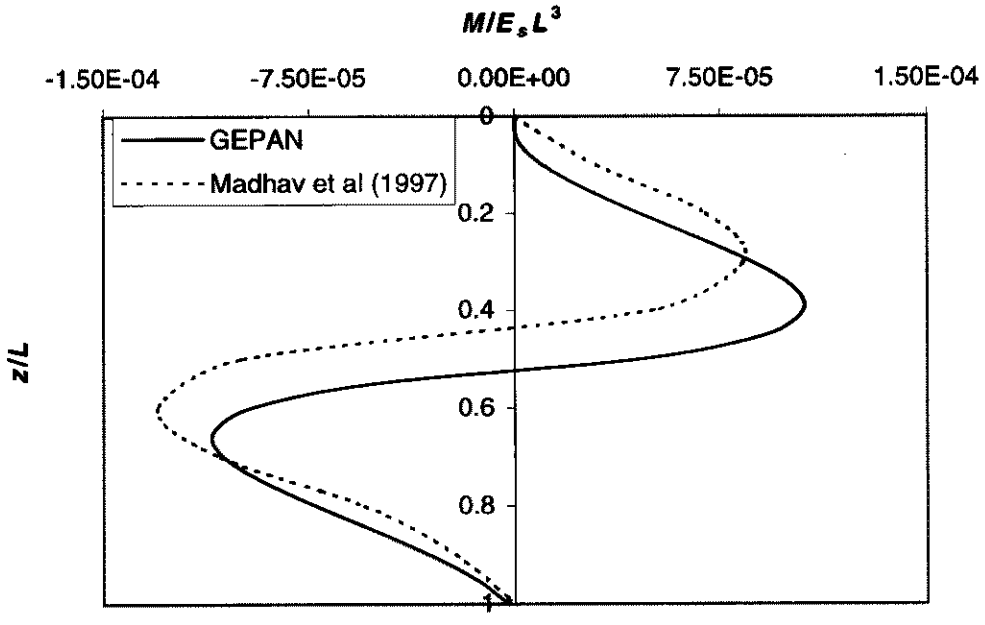

Fig. 4.9(b) Bending momement distribution of a pile due to a horizontal soil movement

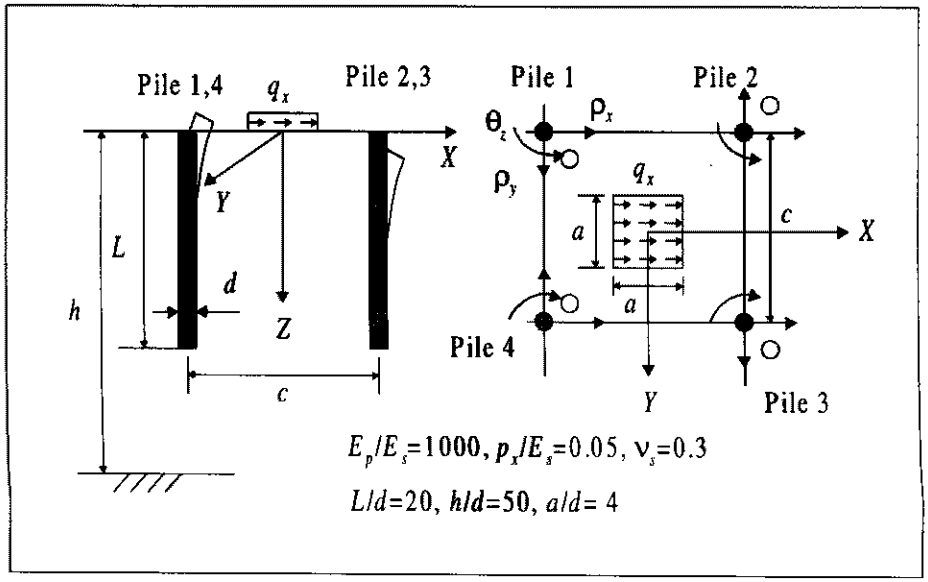

Fig. 4.10 Definition of a problem of piles subjected to soil surcharge

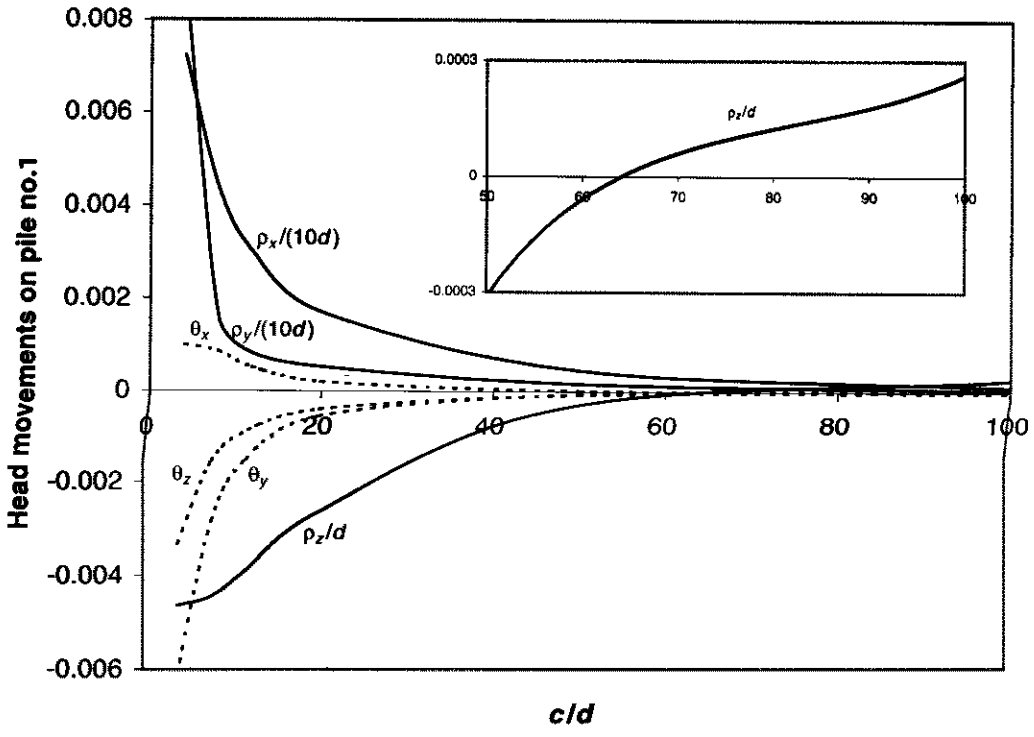

Fig. 4.11 Head movements of pile no.1 defined in Fig. 4.10

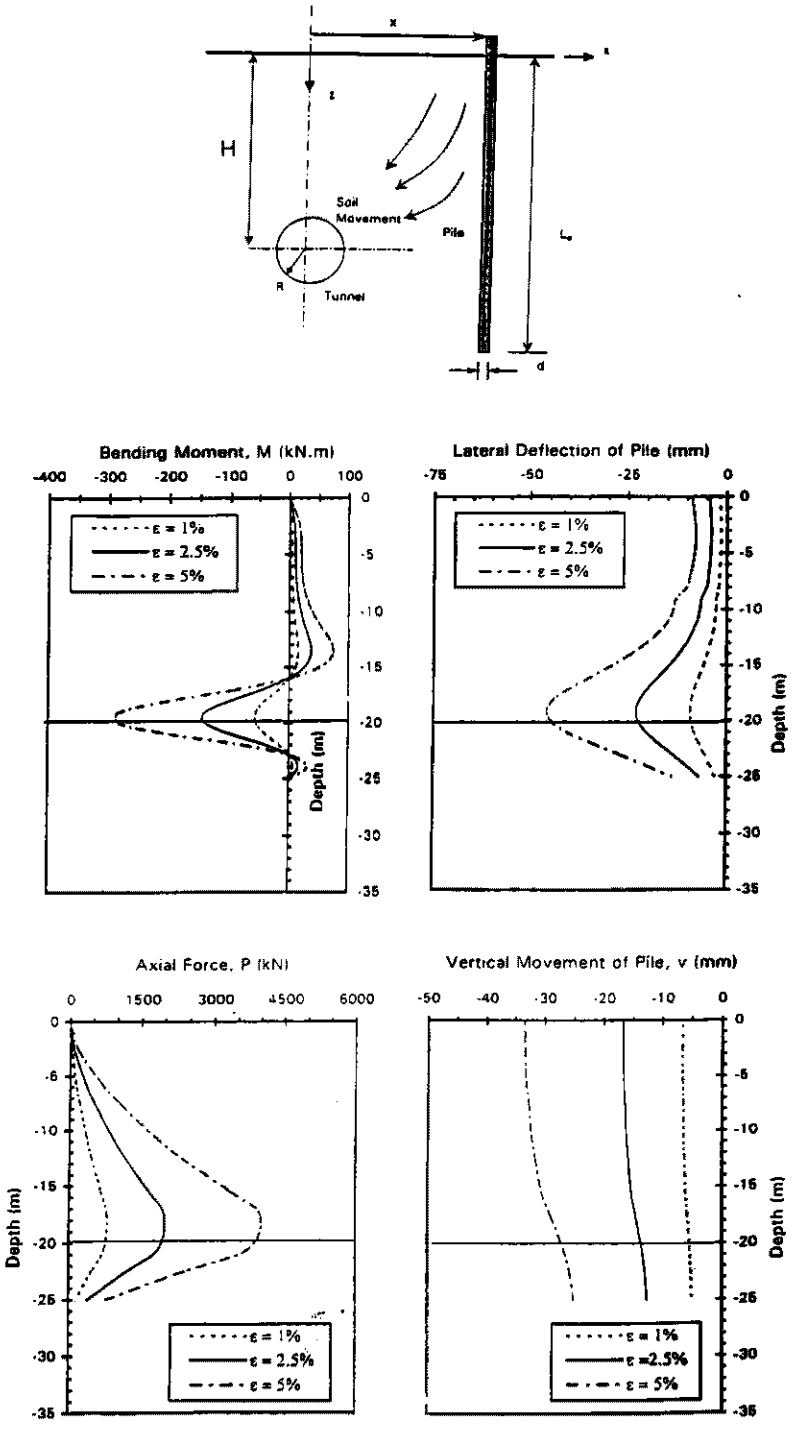

Fig. 4.12 Typical pile response at x=4.5m (Loganathan *et al*, 1999a)

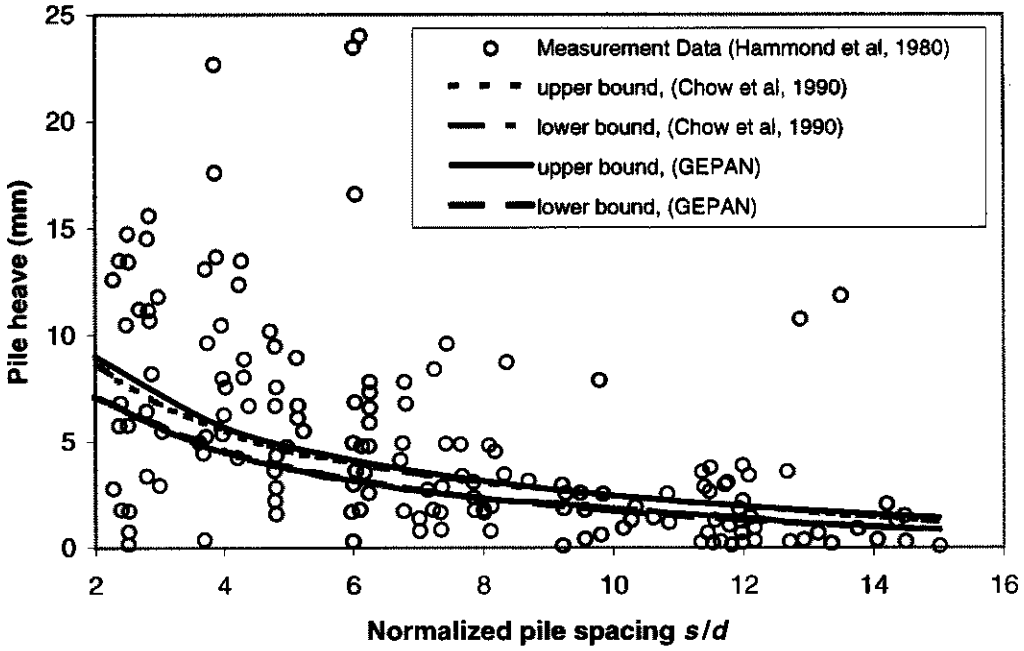

Fig. 4.13 Heave of driven cast in in situ pile in stiff fissured clays

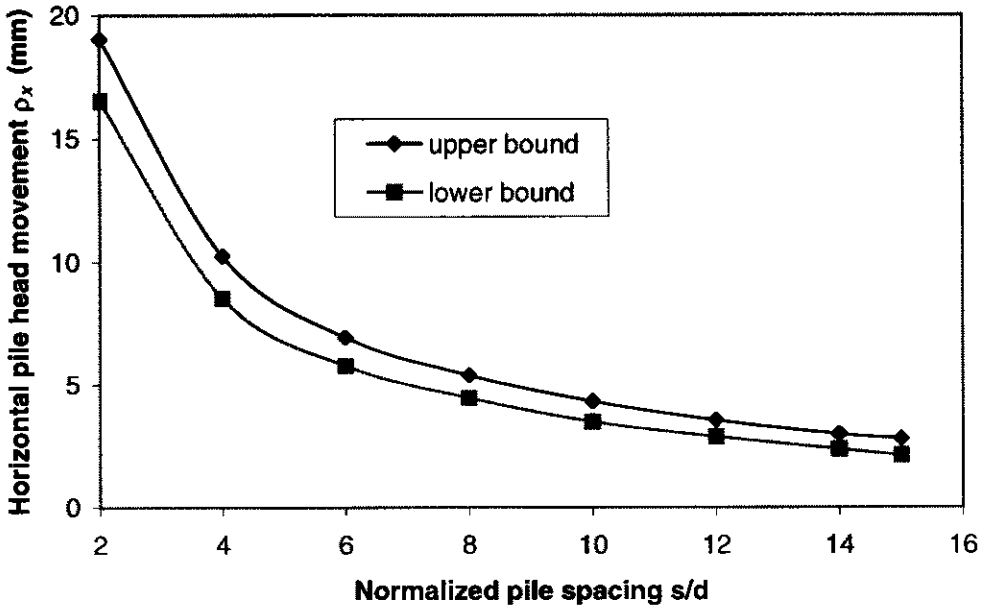

Fig. 4.14(a) Prediction of horizontal pile head movement of driven cast in in situ in pile stiff fissured clays

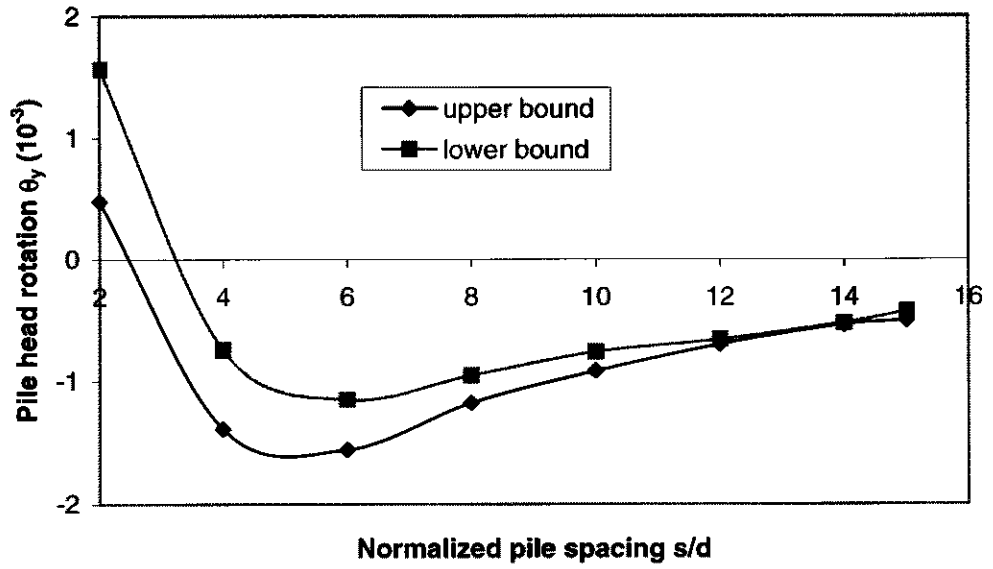

Fig. 14(b) Prediction of pile head rotation of driven cast in in situ pile in stiff fissured clays

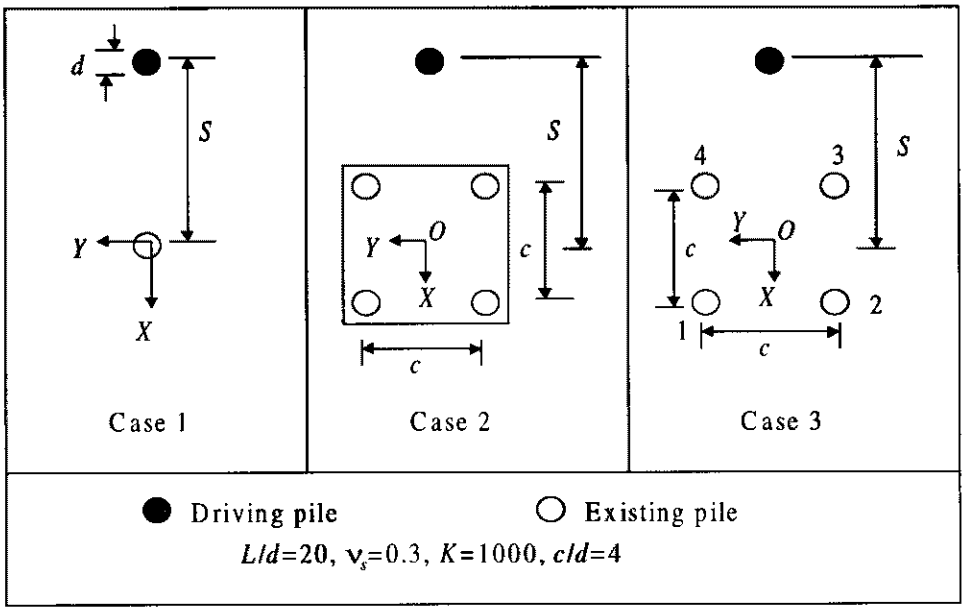

Fig. 4.15 Definition of three cases of installation effect due to a pile driving

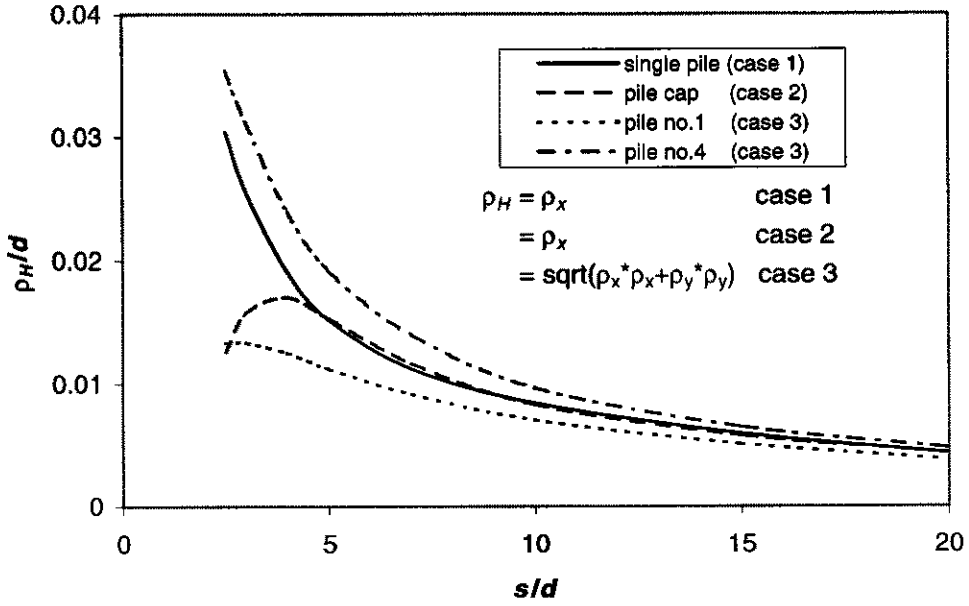

Fig. 4.16 Pile head dispacements of individual piles due to a driven pile

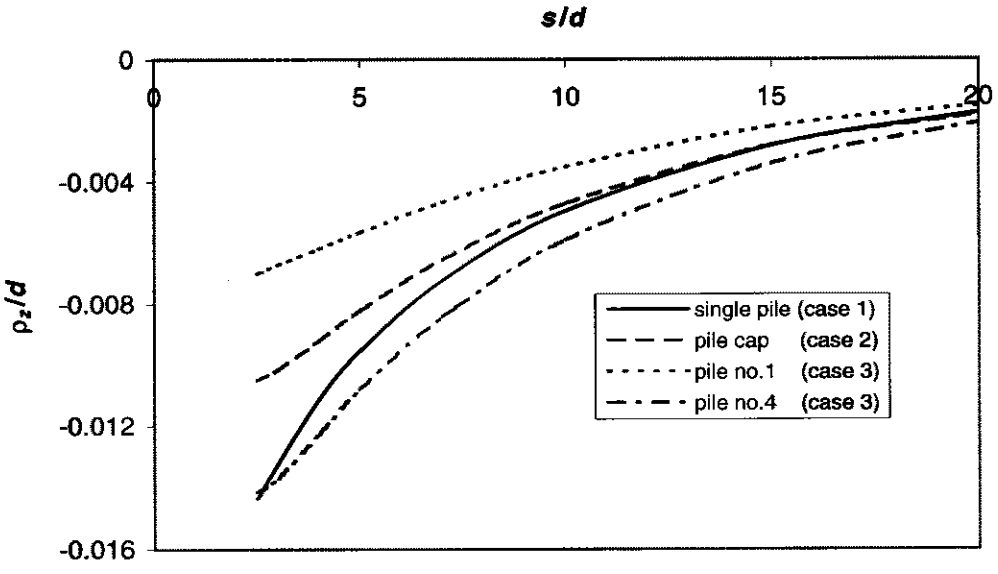

Fig. 4.17 Pile head rotations of individual piles due to a driven pile

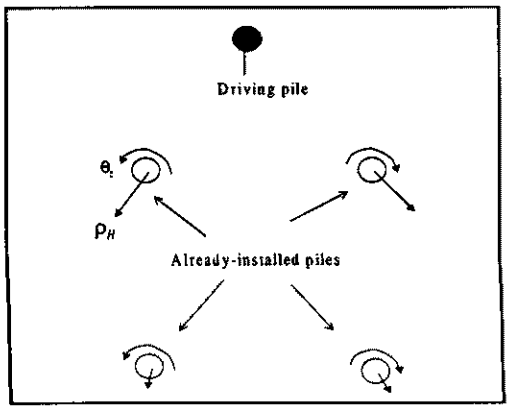

Fig. 4.18(a) Pile head dispacements of individual piles due to a driven pile

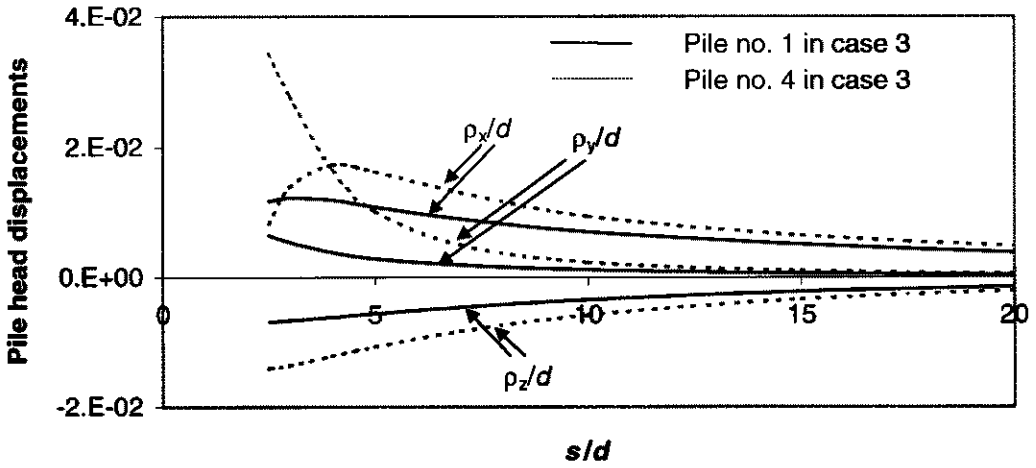

Fig. 4.18(b) Pile head dispacements of individual piles due to a driven pile

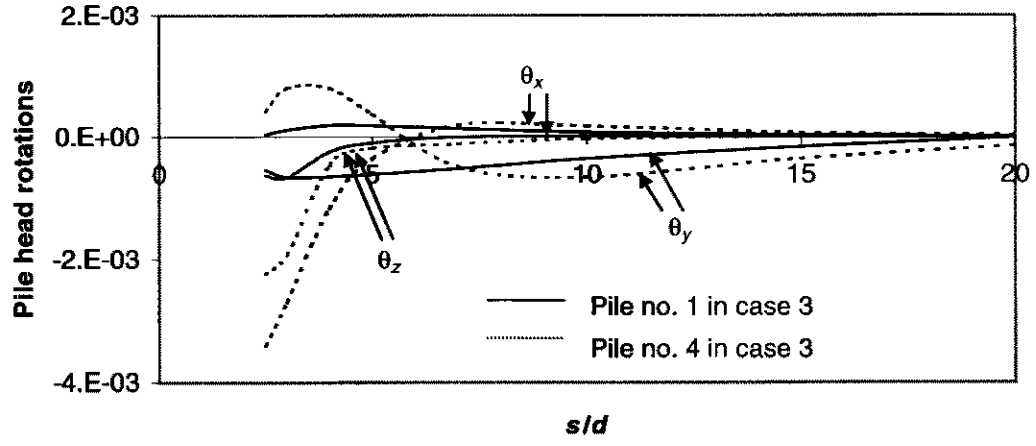

Fig. 4.18(c) Pile head rotations of individual piles due to a driven pile

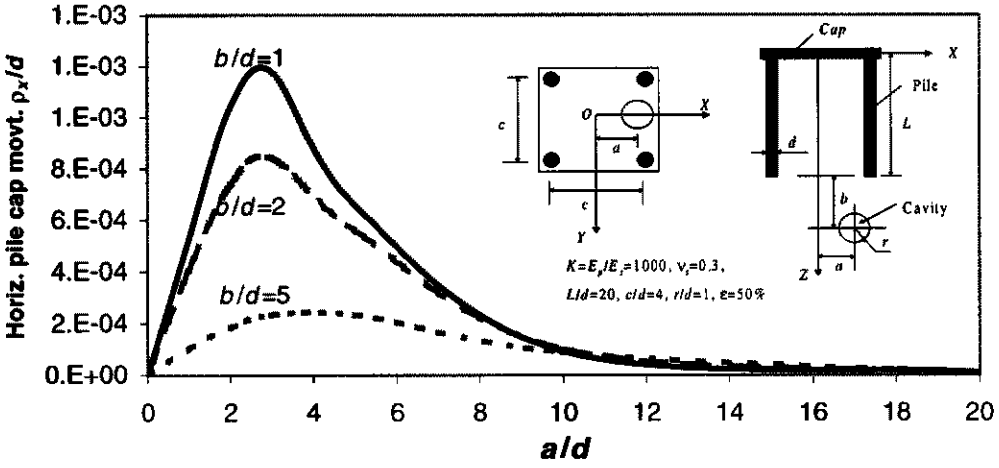

Fig. 4.19(a) Pile cap settlement ρ_x due to a cavity along the centerline

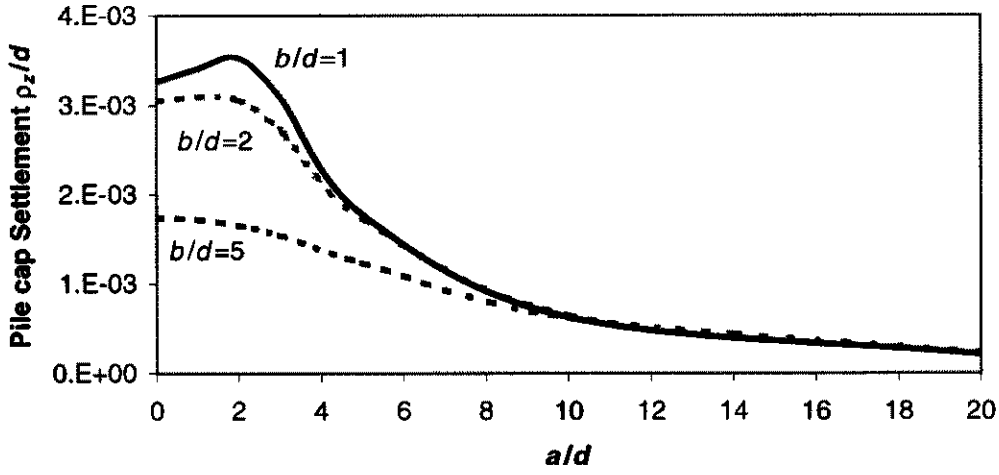

Fig. 4.19(b) Pile cap settlement ρ_z due to a cavity along the centerline

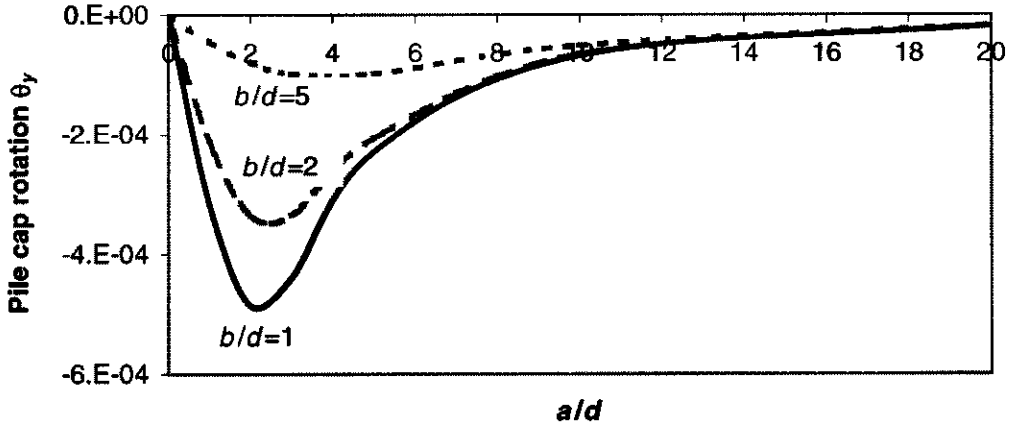

Fig. 4.19(c) Pile cap rotation θ_y due to a cavity along the centerline

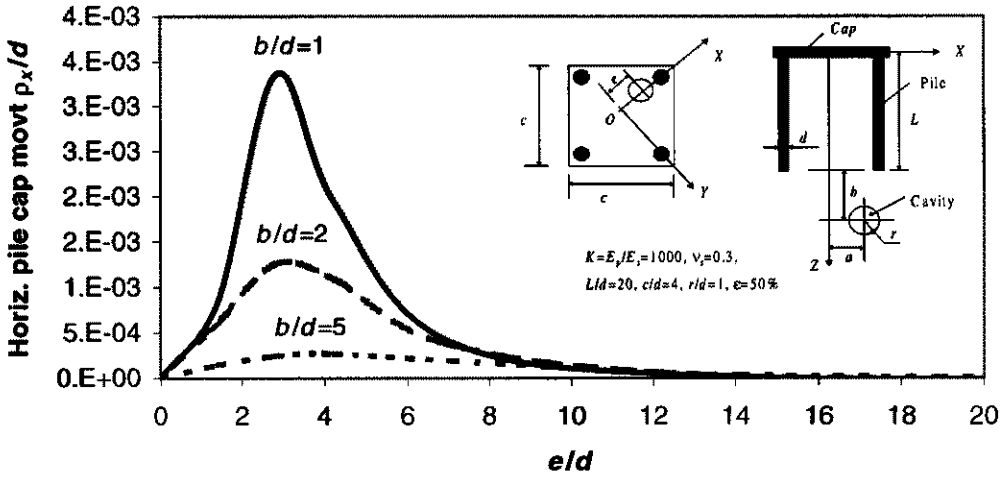

Fig. 4.20(a) Pile cap settlement ρ_x due to a cavity along a diagonal line

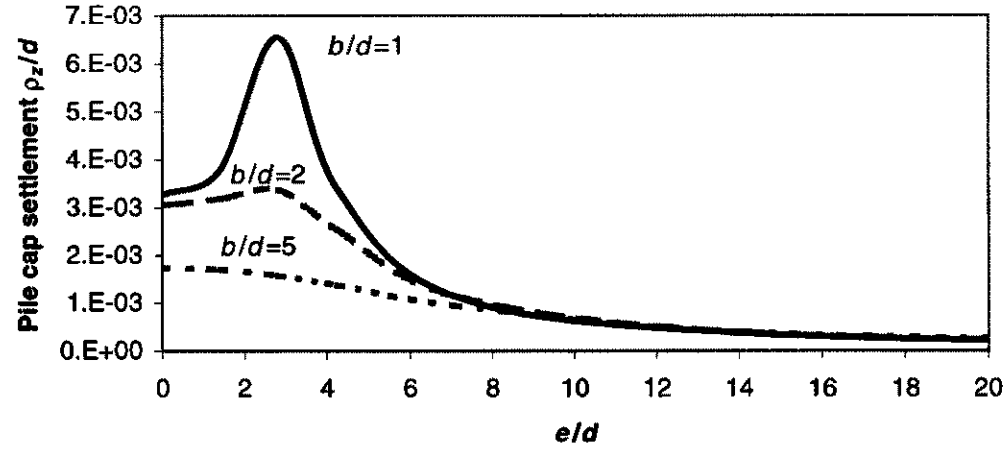

Fig. 4.20(b) Pile cap settlement ρ_z due to a cavity along a diagonal line

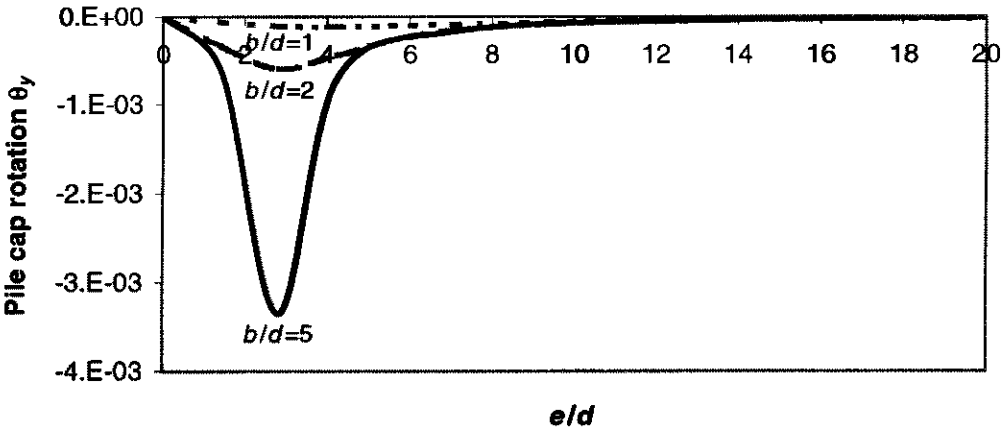

Fig. 4.20(c) Pile cap rotation θ_y due to a cavity along a diagonal line

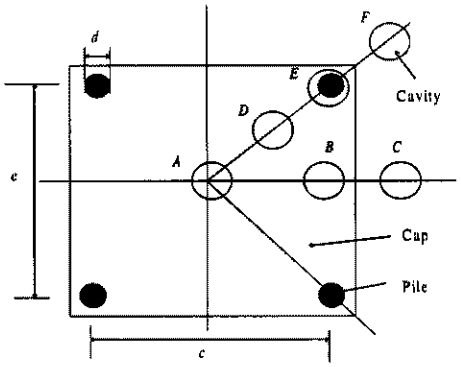

Fig. 4.21 Critical cavity locations under a pile group

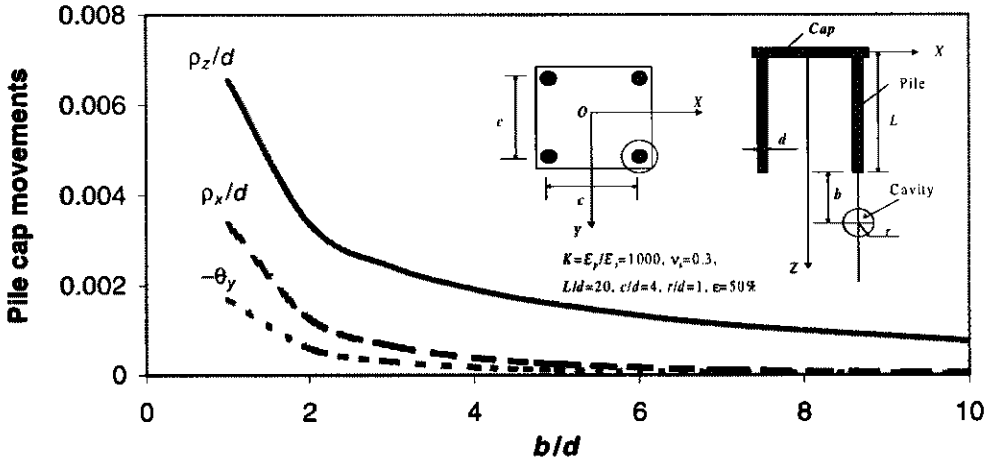

Fig. 4.22 Pile cap movements due to a cavity vs. b/d

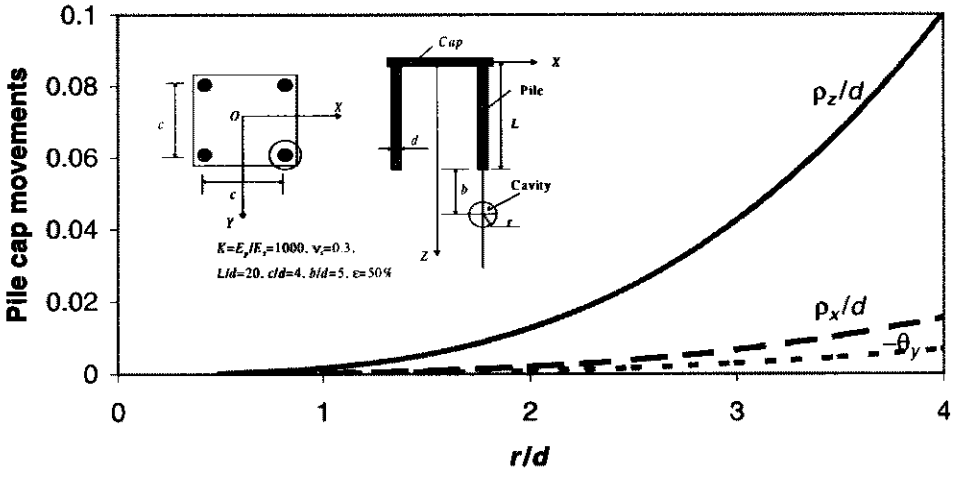

Fig. 4.23 Pile cap movements due to a cavity vs. r/d

Chapter 5

Theoretical Study of Pile Behaviour Induced by a Soil Cut

5.1 Introduction

One of the important sources of "passive loading" is due to cut-induced soil movement, examples of which include excavation and retaining wall construction. With the progress of the soil cut, the surrounding soils will move towards the cut and these movements will induce additional internal forces and deflection in existing nearby piles, which may affect the integrity of surrounding existing piles. There have been reports of severe damage to piled foundations due to soil cuts (*e.g.* Finno and Lawrence, 1991; Chu, 1994), and thus it is important to develop a better understanding of the problem so that appropriate measures can be taken to minimize any potential damage.

As outlined in Chapter 2, the pile response to a soil cut near the piles has been the subject of some research. However, most of the researchers consider a single pile and de-coupled loadings in two dimensions, and the external soil movements are usually derived empirically with little theoretical background. Due to incomplete understanding of the mechanism of the cut-induced behaviour of passive piles, the conventional design of the piles is based on lumped factors of safety and provides no explicit information regarding deflections.

Aside from empirical methods, numerical analyses of piles induced by a soil-cut have used either a "(pile) finite element / (soil) finite element method" (Finno *et al*, 1991; Hara *et al*, 1991) or a "(pile) boundary element/ (soil) finite element method"(Poulos *et al*, 1996, 1997). However, such analyses are time-consuming and involve sophisticated input data pre-processing, such as the generation of finite element meshes.

The main objectives of the present Chapter are to develop a general rigorous methodology using the boundary element method for both soil and pile behaviour, for assessment of the likely impact on adjacent pile foundations of ground movements arising from a soil cut. The effects of various factors on the pile response are also investigated, so that a better understanding of the problem can be achieved.

The analysis involves two stages: the first develops a method of estimating soil-cut-induced ground deformation, and the second examines the effect of such ground deformations on adjacent piles. The general explicit expression of cut-induced "free-field" soil movement is presented using the "source-sink imaging" technique. To analyse pile-soil deformation, the general 3-D boundary element program called GEPAN (in Chapters 3 and 4) is used in this study. Finally, these cut-induced soil movements are incorporated into GEPAN for analyzing pile response.

5.2 Modeling of Pile-Soil Interaction

In modeling of pile-soil interaction, two aspects should be considered, *i.e.* 1). set up a governing equation of pile-soil interaction, 2). incorporate the soil movements induced by a soil cut into the general equation.

The governing equation of pile-soil interaction is based on a general 3-D coupled pile and pile group analysis which has been developed in Chapter 3 (Xu and Poulos, 1999a). The equation involves a global matrix which is composed of several sub-matrices. Through the introduction of the concept of hierarchical structures and basic influence factor matrices, a set of sub-matrices is developed both for the presentation of the analysis and for computer program implementation.

As described in Chapter 4, the externally imposed soil movement induced by a soil cut are very easily incorporated into the governing equation if the distributions of these soil movements are known. These movements are taken to be "free-field" ground movements, *i.e.* independent of the presence of the piles, and the principle of superposition can be applied. The ground movements can then be absorbed into the vector of element stress offsets in the governing equation.

5.3 Modelling of Cut-Induced Soil Movements

5.3.1 Assumptions

The soil-cut is assumed to be sufficiently long that a two dimensional plane strain analysis is applicable. The soil is assumed to be incompressible, which is appropriate for saturated clay under undrained conditions. The soil cut is assumed to be vertical and the wall deflection is taken be parabolic with depth. The parabolic equation can be determined by three known horizontal displacements along the wall, for simplification, the three know horizontal displacements are assumed to be at top, centre and bottom of the wall. The soil is assumed to be elastic in both tension and compression.

In the present study, the soil movements are assumed to be independent of time, although in many cases, especially those involving clay soils, the distribution of movement will change with time because of pore pressure dissipation and consequent consolidation of the soil. Thus, it may be necessary to perform a series of analyses, each for a particular time, in order to examine how the pile behaviour varies with time.

Although a soil cut will cause both vertical and lateral soil movements, the latter component is considered to be more critical for adjacent piles as piles are often not designed to sustain significant lateral loadings.

5.3.2 Source-Sink Imaging Technique

The source-sink imaging technique has been presented by Sagaseta (1987) for the determination of strain fields in incompressible materials due to loss (or gain) of ground near the surface. Theoretical closed-form solutions for soil movement have been obtained taking the incompressibility condition as a basis and using a virtual image technique. The method may be applied in D-D (displacement-displacement) problems (*i.e.* when the displacements are imposed at some points and only the resulting strain field is wanted), in which case the incompressibility equation carries the main part of the information. If the remaining boundary conditions can be reasonably

simplified, the solution obtained is close to the exact solution presented by Sagaseta (1987). This technique has been successfully applied to obtain the soil movements induced by tunnelling (Verruijt and Booker 1996) and pile driving (Sagaseta 1987, Chow and Teh 1990, Xu and Poulos 1999c).

5.3.3 Equations for Cut-Induced Soil Movements

Figure 5.1 shows the problem addressed, of existing piles situated near a vertical soil cut. The wall deflection is imaged via soil loss (or gain) along the wall. First, the horizontal displacement along the wall is divided into n segments, the shape of each small segment being taken as rectangular. Then, each small rectangular area is taken to be a small circle with a radius of $r = (u_h dh/\pi)^{0.5}$ (where dh = the increment of any vertical distance of wall h, u_h = horizontal displacement of the wall at h, see Fig. 5.1), and the small circle becomes a "source-sink". Finally by letting n become infinite, based on the concept of the source-sink technique (Sagaseta, 1987) and the assumptions imposed above, the cut-induced displacements at any point (x,z) are found to be as follows:

$$S_x = \int_0^H \frac{1}{\pi}\left(\alpha h^2 + \beta h + \gamma\right)\left\{-\frac{1}{2}\left(\frac{x}{r_1^2} - \frac{x}{r_2^2}\right) - \frac{x}{r_2^2}\left[1 - 2\frac{z(z+h)}{r_2^2}\right]\right\} dh \quad \text{.....(5.4.1)}$$

$$S_y = 0 \quad \text{..... (5.4.2)}$$

$$S_z = \int_0^H \frac{1}{\pi}\left(\alpha h^2 + \beta h + \gamma\right)\left\{-\frac{1}{2}\left(\frac{z-h}{r_1^2} - \frac{z+h}{r_2^2}\right) + \frac{z}{r_2^2}\left(1 - 2\frac{x^2}{r_2^2}\right)\right\} dh \quad \text{.....(5.4.3)}$$

where

$$r_1 = \left[x^2 + (z-h)^2\right]^{1/2} \qquad r_2 = \left[x^2 + (z+h)^2\right]^{1/2}$$

$$\alpha = -\frac{2}{H^2}(2u_c - u_t - u_b) \qquad \beta = \frac{1}{H}(4u_c - 3u_t - u_b)$$

$$\gamma = u_t$$

H = depth of wall of excavation/retaining wall

u_t = top horizontal displacement of the wall

u_b = bottom horizontal displacement of the wall

u_c = central horizontal displacement of the wall

By using these expressions within the general equations for pile response, the pile performance induced by a soil cut can be analysed once the three horizontal displacements (at the top, bottom and centre of the wall) are estimated. These displacements can be estimated by techniques such as those derived by Clough *et al* (1989).

5.4 Evaluation

Before theories are applied to practical problems, the accuracy of the behaviour predicted by them needs to be established. In this part, some comparisons are presented between the results of the program GEPAN and published field data or theoretical solutions.

Chu (1994) has reported a case where some mortar piles, used to support a large excavation, suffered significant deflections due to the excavation. The piles, 400 *mm* in diameter and 30 *m* in length, were arranged in one row. The average maximum depth of the excavation was about 12.8 *m* and the distance between the piles and excavation face was about 3 *m*. The soil was composed of back fill and soft clay, with an average undrained shear strength c_u of the clay layer of 40 *kPa* within a 20 *m* depth. In the

analysis via GEPAN, the soil Young's modulus was chosen to be 15 *MPa* ($1500c_u$) and the lateral deflection parameters at the excavation wall were assumed as u_t/H=0, u_c/H=6%, u_b/H=0 (*i.e.*, a parabolic distribution). Fig. 5.2 shows the predicted pile deflection profiles together with those measured, and it can be seen that the predicted and the measured profiles agree reasonably well. The predicted bending moment profile from the present study and that predicted by Poulos *et al* (1997) are plotted in Fig. 5.3, although it was not measured in the field. It is found that there are some differences in shape of bending moment profile particularly in the lower part of the pile, where the present analysis assumes zero displacement of the pile tip; however, the general trends from both analysis are fairly similar.

Finno and Lawrence (1991) have described a case where an excavation was carried out inside a framed structure. The structure was supported by groups of capped step-tapered piles that were very close to the excavation face. The single pile, representative of those closest to the excavation face, was 1.5 *m* away from the face. The step-tapered pile was simulated as a uniform pile, having an average diameter of 327 *mm* and a length of 25 *m*. The soil had an average undrained strength c_u of about 50 *kPa*, and in the analysis, soil Young's modulus, E_s, was assumed to be 20 *MPa* ($400c_u$). In this study, the parameters for lateral soil movement at the cut were assumed to be u_t/H=0.8%, u_c/H=0.6%, u_b/H=0.4%, and a trapezoidal distribution was adopted. Fairly good agreement was found between the computed and measured pile deflections, as shown in Fig. 5.4.

Poulos and Chen (1996) analyzed a "standard" problem in which an existing single pile was situated near an unsupported excavation. The main parameters defining the "standard" problem were: pile length, L=22 *m*; pile diameter, d=0.5 *m*; depth of excavation, H=10 *m*; distance from excavation face, X=1.5 *m*; soil Young's modulus E_s=20 *MPa* and pile Young's modulus, E_p=30 *GPa*. For convenience, the depth of excavation may be expressed by the well-known stability factor N_c as $\gamma h/c_u$, where γ = unit weight of soil and wall, h = depth of excavation, c_u = undrained shear strength of soil. For the soil with a stability factor, N_c = 4, the computed lateral soil movement

profiles were computed via a finite element analysis, and 1 *m* away from excavation face and within a depth of 10 *m*, were approximately a trapezoidal distribution with values of u_t=50 *mm* at the top; and u_b=100 *mm* at the bottom of the excavation. The comparison of computed pile deflection response is shown in Fig. 5.5, assuming the lateral soil movement to be trapezoidal at the cut with the corresponding parameters as follows: u_t=120 *mm* at top; u_b=240 *mm* at bottom (the computed lateral soil movement at the cut was not provided, however, it should be larger than the one away from the cut). It is found, except near the pile tip, the results are comparable with these two quite different analyses.

From the foregoing comparisons, it is concluded that the approach adopted in the present paper should be capable of providing reasonable results for the response of a pile near a cut or excavation, provided reasonable estimation can be made of the magnitude and distribution of soil movements.

5.5 Cut-Induced Pile Behaviour

5.5.1 Three Basic Patterns of Soil-Cut Deflection

For practical problems, the shape of the cut movement profiles can be approximately grouped into two types: *i.e.*, parabolic, and linear with depth. In order to simplify and characterize the cut-induced soil movements, the local movements in the vicinity of the cut have been idealized three basic patterns, as indicated in Fig. 5.6. Pattern 1 would represent a braced wall, (Fleming *et al*, 1992; Poulos and Chen, 1997), Pattern 2 a "slope" wall and Pattern 3 an unsupported wall (Poulos and Chen, 1997). The advantages of such as classification are obvious. Firstly, these three patterns are very common in geo-pile engineering; secondly, these are one-parameter patterns, *i.e.*, only the maximum horizontal wall displacement *a* is needed to be quantified, and thirdly, the three basic shapes can be combined into other more complex soil-cut movements (for example, a trapezoidal distribution can be obtained by combining patterns 2 and 3).

In order to investigate the cut-induced pile behaviour systematically, it is convenient to define again a "standard" problem. In the "standard" problem, the definition of the parameters is as follows: L= pile length, d = pile diameter, H = total thickness of soil cut, b = distance of pile and cut, a = maximum horizontal displacement at cut, K = pile-soil stiffness factor (Poulos *et al* 1980), K_R = pile-soil flexibility factor (Poulos and Davis, 1980).

It should be noted that the pile response shown below does not include any deflections or internal forces which may have already existed before the excavation.

5.5.2 A Single Isolated Pile near a Soil-Cut

To illustrate general cut-induced pile behaviour, a case was studied where three cut deflection patterns were involved, and with the parameters K=1000, L/d=20, H/d=10, b/d=4, a/d=0.1. Fig. 5.7 shows the computed deflection and internal force profiles for a single pile, for the three cut-induced horizontal and vertical deflection patterns. The dominant deflection is horizontal, as indicated Fig. 5.7. Computed values of the normalized maximum bending moment corresponding to the cut-induced soil movement are plotted against b/d in Fig. 5.8, and are shown to decrease with increasing b/d, as would be expected.

5.5.3 The influence of Factor L/d, b/L and K_R

Figs. 5.9 shows the influence of the factor L/d on the pile performance, with b/d=4, for the three cut-induced deflection patterns. For the horizontal pile head displacement, the effect of L/d becomes insignificant for $L/d \geq 10$, as seen in Fig. 5.9a. The vertical pile head displacement, (Fig. 5.9b), decreases with increasing L/d, especially in patterns 1 and 2 when $L/d \leq 20$. For pile head rotation, shown in Fig. 5.9c, the effect of L/d is generally only significant for relatively short piles (*i.e.* $L/d \leq 10$). Thus, the factor L/d is important only for vertical head movement and pile head rotation of relatively short piles.

Fig. 5.10a shows that the maximum value of dimensionless horizontal movement, ρ_x/a, occurs at b/d=0, 2.5, 5 for patterns 3, 1, 2 respectively. Fig. 5.10b shows a decrease in pile head settlement as the distance, b, from the cut face increases, and the pile head

settlement tends to zero for $b/d \geq 30$. The pile head rotations in patterns 1 and 2 will change sign if a pile is very close to a cut, as shown in Fig. 5.10c, and they are identical for the three patterns for $b/d \geq 25$.

Fig. 5.11 showd that the pile head movements are affected by the pile flexibility factor, K_R. The horizontal pile head displacement is independent of K_R for flexible piles ($K_R \leq 10^{-4}$), as shown in Fig. 5.11a, while for less-flexible piles it is dependent on the K_R, *i.e.*, it increases for patterns 1 and 2 and decreases for pattern 3, when K_R increases. However, the influence of K_R on pile head settlement is the opposite to the horizontal pile head displacement as shown in Fig. 5.11b, that is, ρ_z/a decreases when K_R increases for flexible piles, while there is little effective for less-flexible piles.

5.5.4 Deflection Profiles of a Single Pile

Figs. 5.12 show normalized pile deflection profiles for various values of b/H and cut deflection patterns. If a pile is located very close to the cut (*e.g.* $b/H \leq 0.5$), the horizontal and vertical pile deflections along the pile depth are significant. If the pile is at a greater distance from the cut (*i.e.* $b/H \geq 1$), the horizontal pile deflection varies linearly with normalized pile depth z/L, while the vertical displacement distribution is almost uniform along the pile depth. The critical position of a pile in a pile-cut system is obviously very close to the edge of the cut, *e.g.* the cases of b/H=0.1 in Figs. 5.12 to 5.14. For the cases b/H=0.1, the maximum horizontal pile displacement is in the upper part of the pile ($z/L \approx 0.3$ in pattern 1, $z/L \approx 0.4$ in pattern 2, and z/L=0 in pattern 3), and the maximum vertical pile displacement is in the middle part of the pile (patterns 1 and 2), or at the pile top in pattern 3. There is an imaginary "hinge" in the lower part of pile, where horizontal pile displacements are convergent. The highest "hinge" occurs in pattern 3 ($z/L \approx 0.6$), while the lowest "hinge" occurs for pattern 2 ($z/L \approx 0.8$), and the middle "hinge" is for pattern 1 ($z/L \approx 0.7$).

5.5.5 Comparison of a Single Pile and a Pile Group

The response, to a nearby soil cut, of an isolated single pile, and a 2×2 pile group are compared in Figs. 5.15, 5.16, and 5.17, with patterns 1, 2, 3 respectively. When b/d>20,

the passive pile head displacements of a single pile and a pile group are very similar. However the group cap rotation is obviously smaller than the single pile head rotation.

5.5.6 Cut-Induced Group Effect

Profiles of pile lateral deflection for the 2×3 pile group shown in Fig. 5.18 are presented in Figs. 5.19 to 5.24. Figs. 5.19 to 5.21 show the response of individual piles of the 2×3 pile group due to a soil cut. If the group is relatively near the cut (*e.g.* b/L=4), the horizontal pile displacement of the "front" pile (pile 1) is significantly higher than the ones of the "rear" pile (pile 3), and the "middle" pile (pile 2). If the group is at a considerable distance from the cut, *e.g.*, $b/L \geq 20$, the horizontal pile displacements of piles 1, 2 and 3 are similar for a given pattern of movement.

5.6 Conclusions

An analytical methodology using the boundary element method has been developed for analysis of passive pile behaviour due to a soil-cut (such as excavation and retaining wall) near the piles. This analysis involves two stages: first, based on source sink imaging technique, general explicit equations are derived for the cut-induced soil movements; second, the general 3-D boundary element method, implemented by the program GEPAN, is employed to examine the effect of such ground deformations on adjacent piles.

For the passive soil movements induced by a vertical soil-cut, only five parameters are involved, *i.e.*, depth of cut, H; lateral movements of cut at top, central and bottom, u_a, u_c, u_b; and the distance of the pile from the cut surface, b. Comparisons with existing solutions and field measurements indicate that the theory is capable of giving realistic estimates of passive pile response induced by a soil-cut, if the parameters are chosen appropriately.

GEPAN has been used to conduct a parametric study of passive pile performance induced by a vertical soil cut, as characterized by three typical deflection patterns. An important feature of GEPAN is its ability to predict "off-line" behavour of passive piles, *e.g.* the vertical movements of piles subjected to horizontal ground movements,

and the coupled vertical and lateral behaviour of piles subjected to situation which cause both vertical and horizontal ground movements. The important conclusions of this study are as follows:

1. The pile length to diameter ratio *L/d* affects mainly the vertical pile head movement and pile head rotation of relatively short piles.
2. If a pile is at some distance from a cut or wall, the passive pile responses are similar, regardless of the cut deflection pattern.
3. The horizontal pile head displacement is almost independent of pile flexibility, K_R, for flexible piles, while the vertical pile head displacement is insensitive to K_R for less-flexible piles.
4. The deflection profiles of a pile are more "curved" in the vicinity of a soil cut. At a considerable distance from the cut, the horizontal pile deflection varies approximately linearly with depth, while the vertical pile deflection is more or less uniform.
5. The passive pile head displacements of a single pile and a pile group are similar except very close to the cut. The group cap rotation is smaller than the single pile head rotation.
6. For a pile group located close to a soil cut, the horizontal pile displacement of the "front" pile is significantly higher than the ones of "rear" pile. At a considerable distance from the cut, the horizontal pile deflections "front" and "rear" piles become identical.

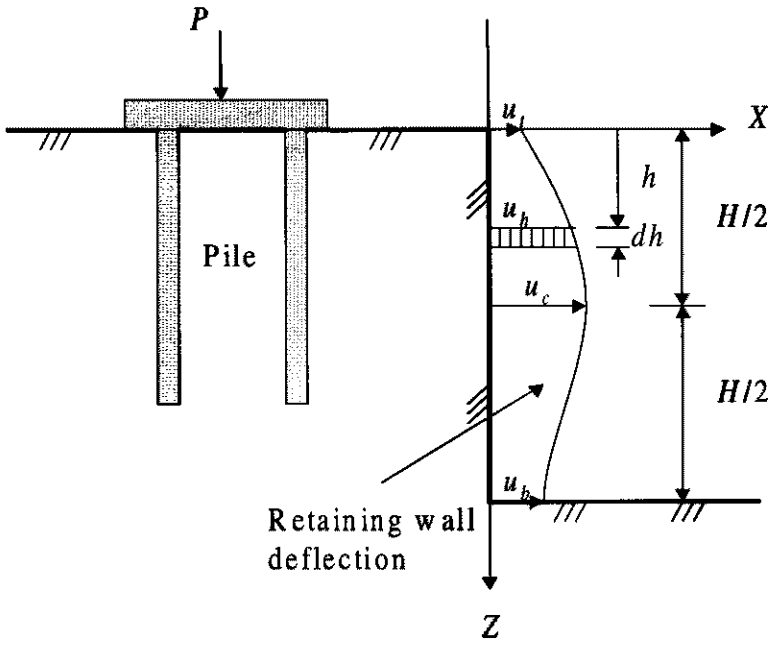

Fig. 5.1 Horizontal deflection along a vertical soil cut

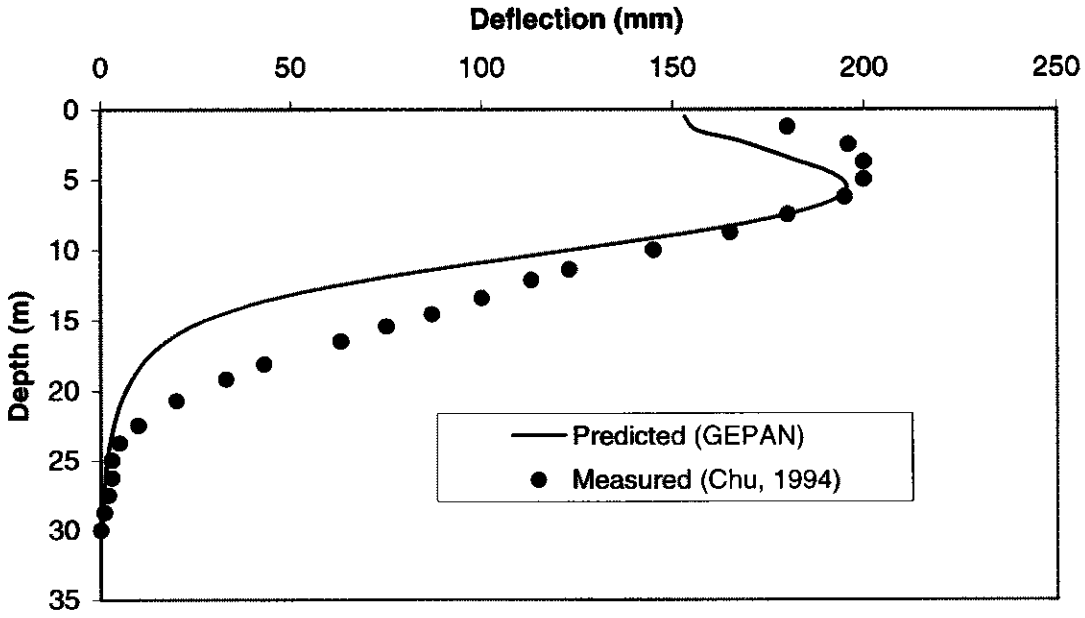

Fig. 5.2 Comparison of Pile Deflection Profile, Case 1

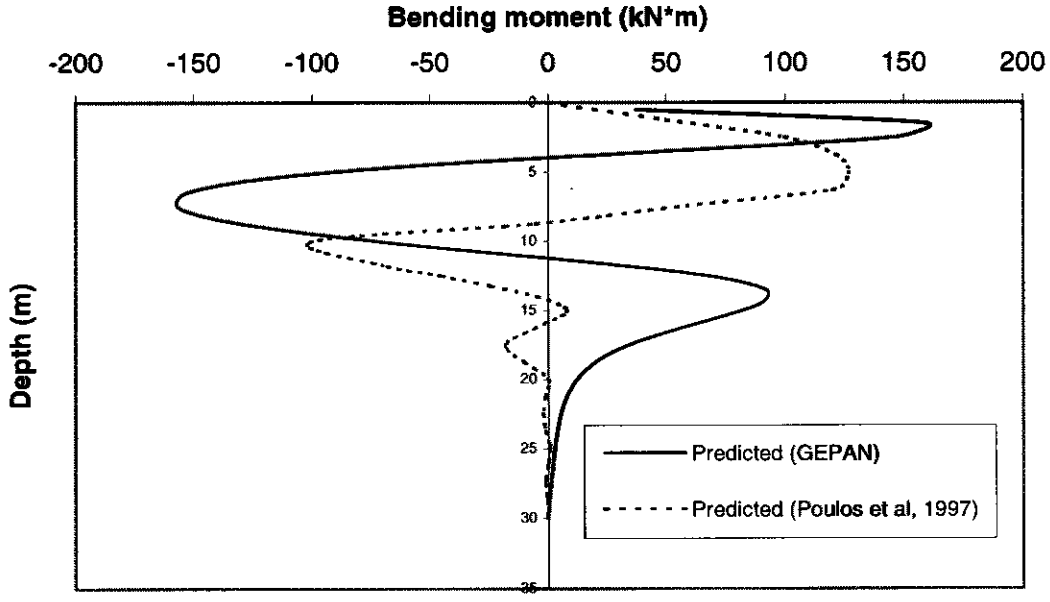

Fig. 5.3 Comparison of Bending Moment Profile, Case 1

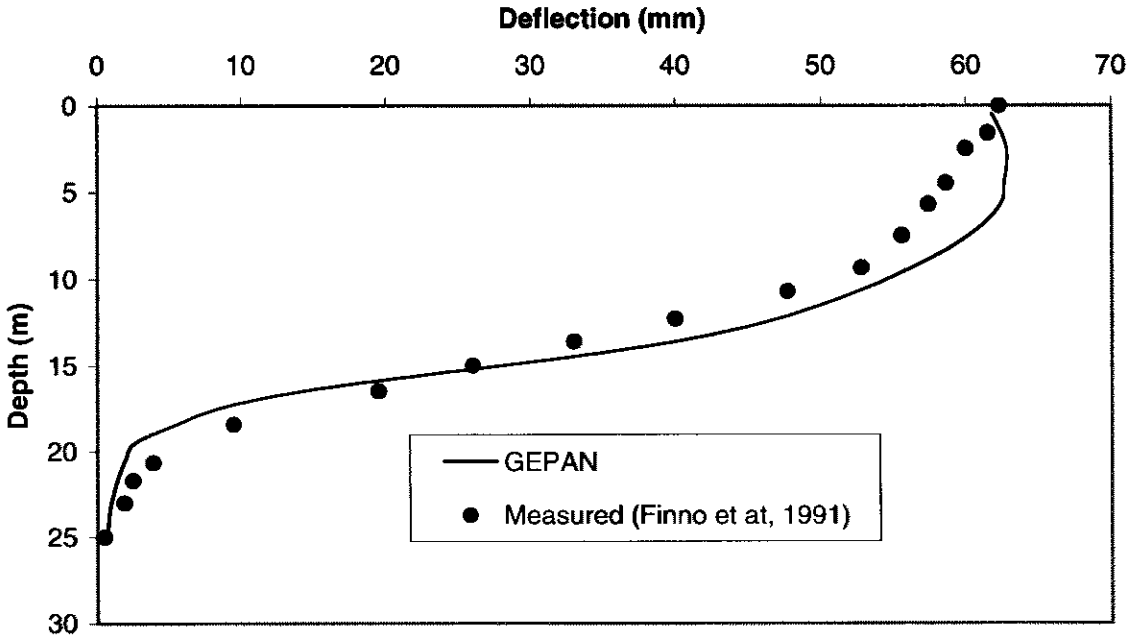

Fig. 5.4 Comparison of Pile Deflection Profile, Case 2

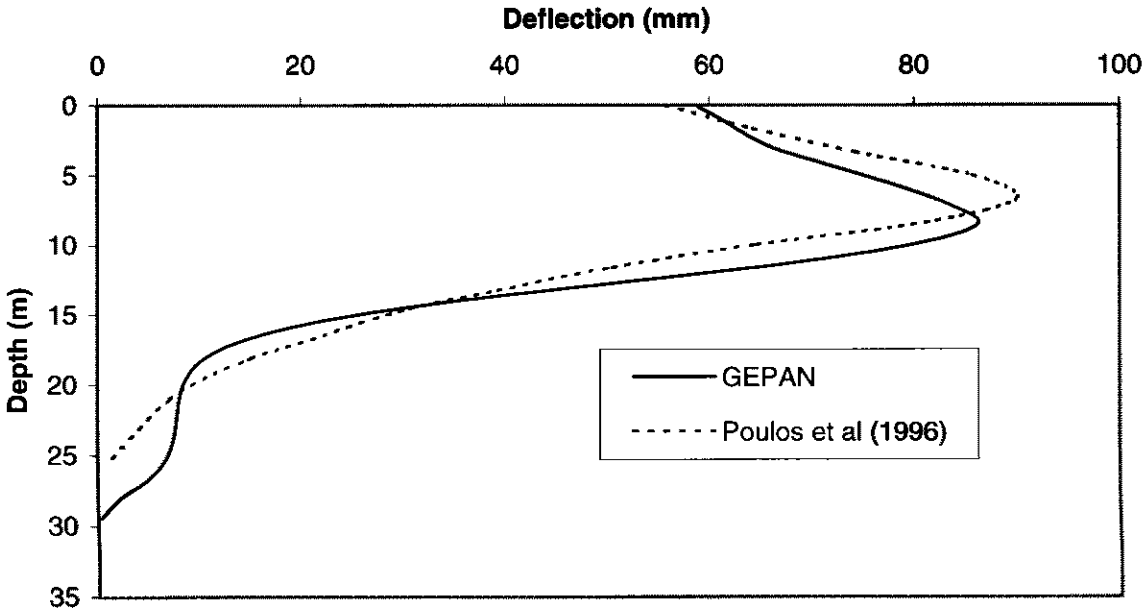

Fig. 5.5 Comparison of Pile Deflection Profile, Case 3

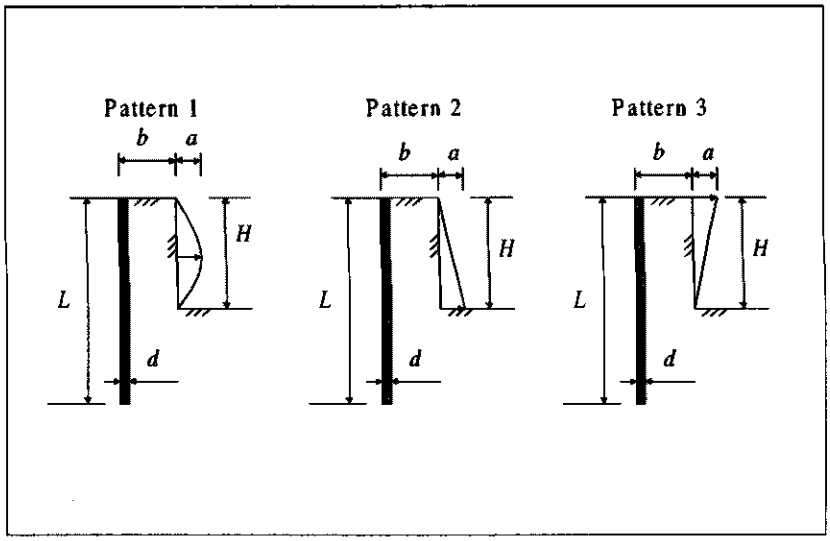

Fig. 5.6 Definition of deformation of a vertical soil cut

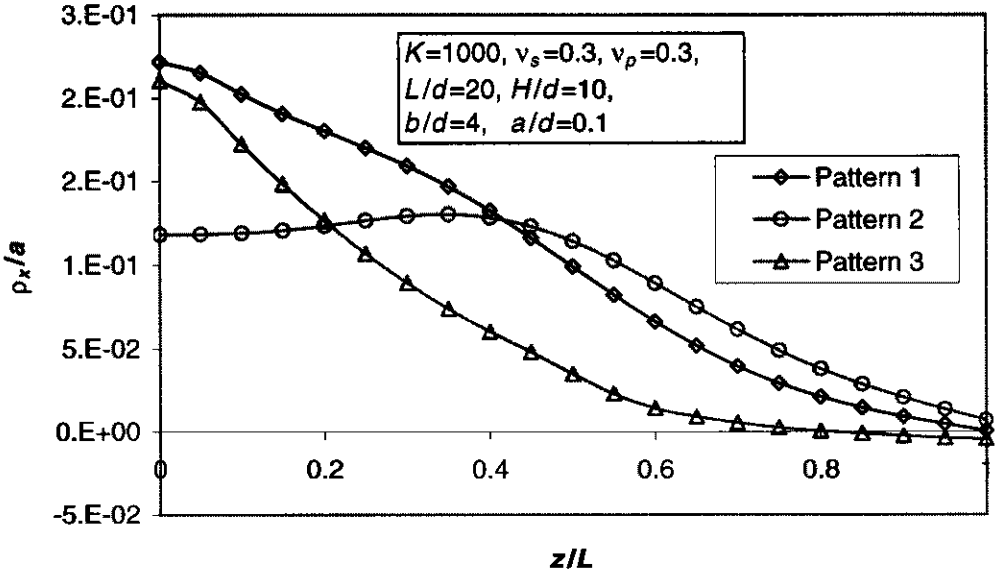

Fig. 5.7a Horizontal movement along pile

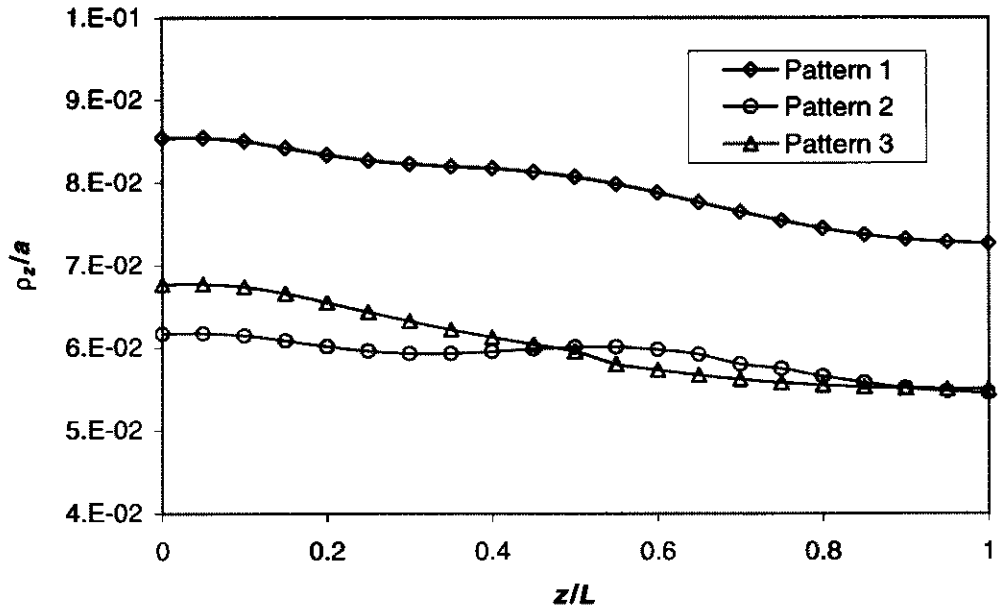

Fig. 5.7b Vertical movement along pile

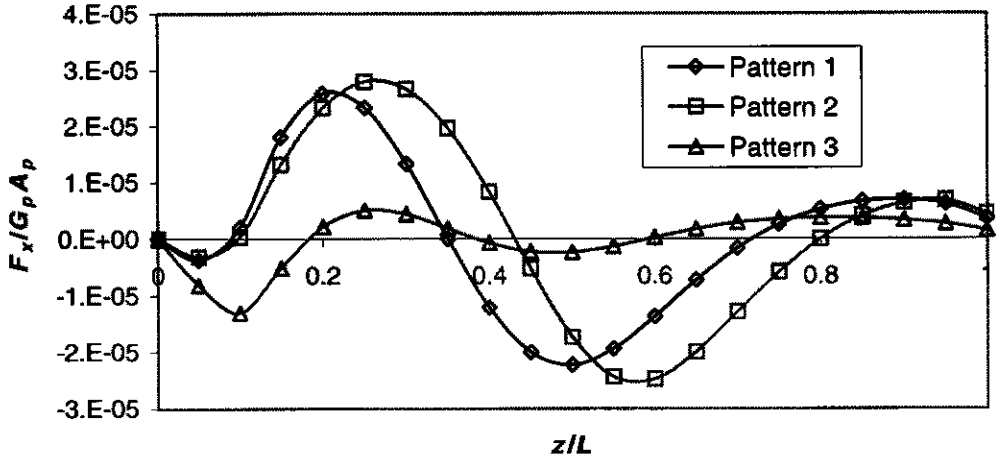

Fig. 5.7c Internal force F_x along pile

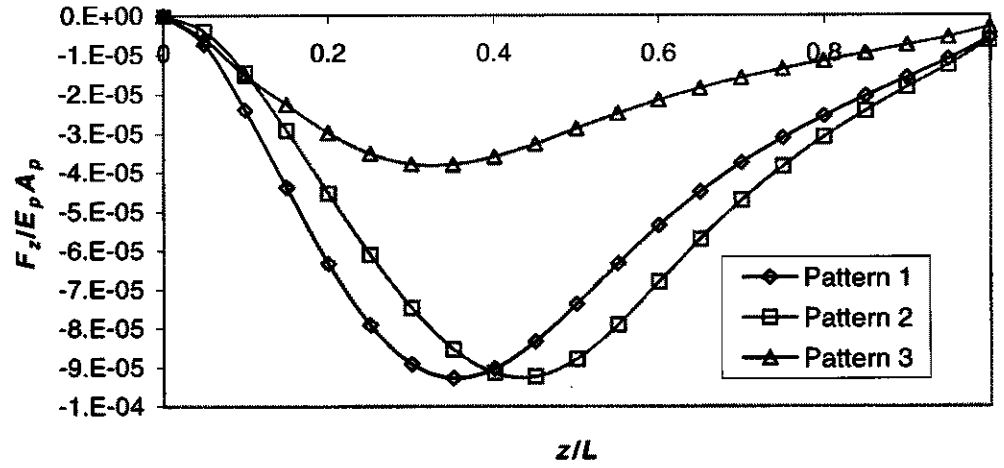

Fig. 5.7d Internal force F_z along pile

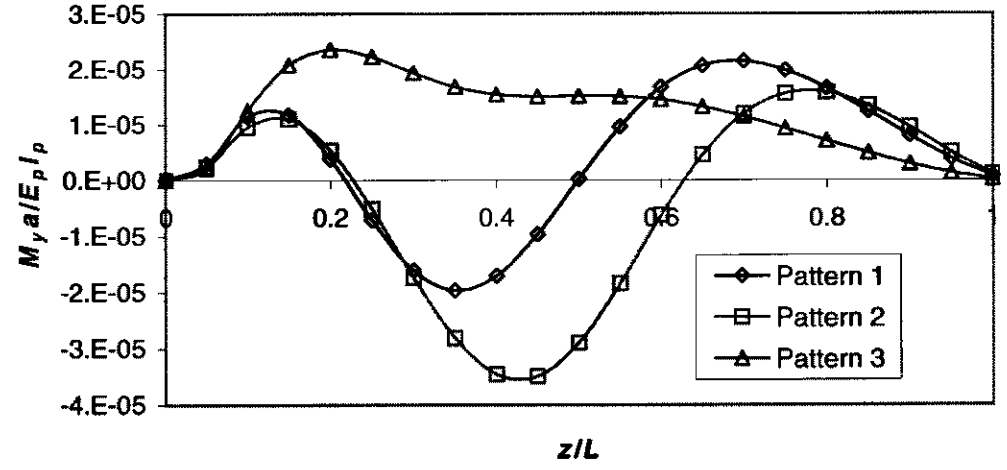

Fig. 5.7e Movement M_y along pile

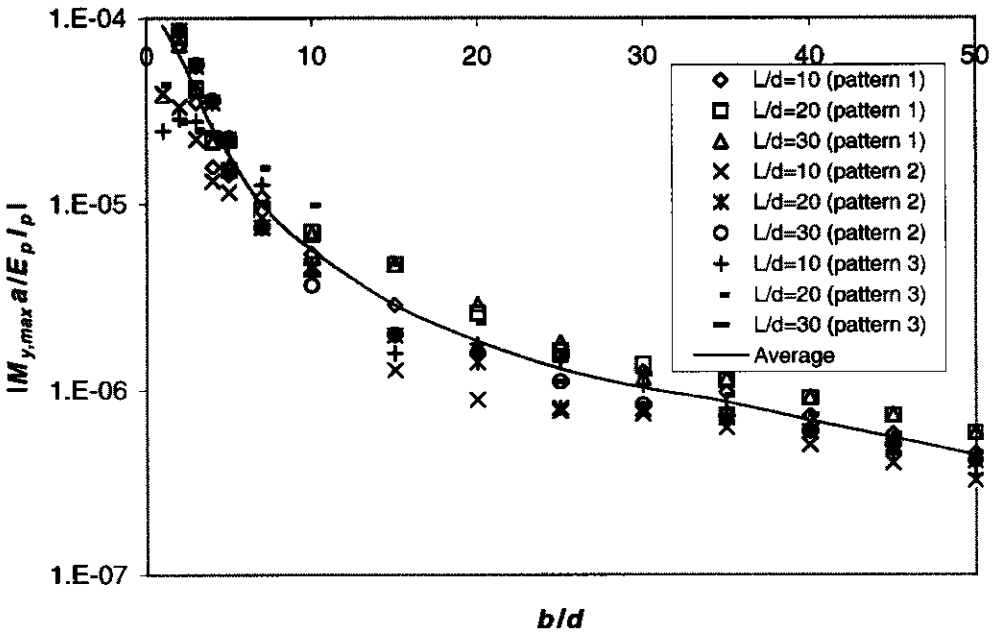

Fig. 5.8 Maximum moment $M_{y,max}$ of a pile due to a soil cut

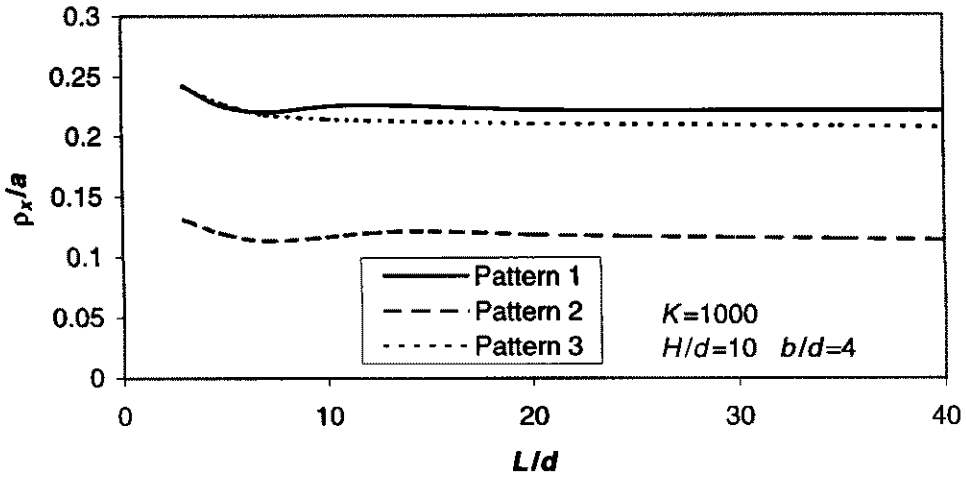

Fig. 5.9a Horizontal pile head movement ρ_x vs. L/d

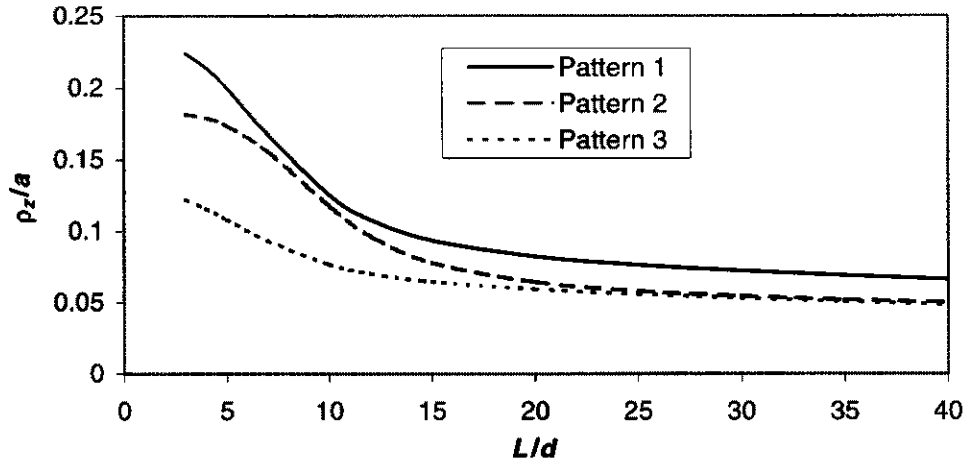

Fig. 5.9b Vertical pile head movement ρ_z vs. L/d

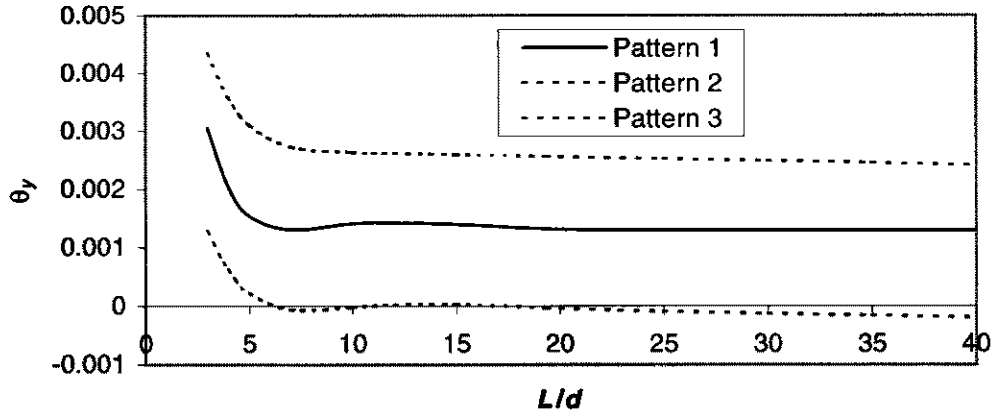

Fig. 5.9c Pile head rotation θ_y vs. L/d

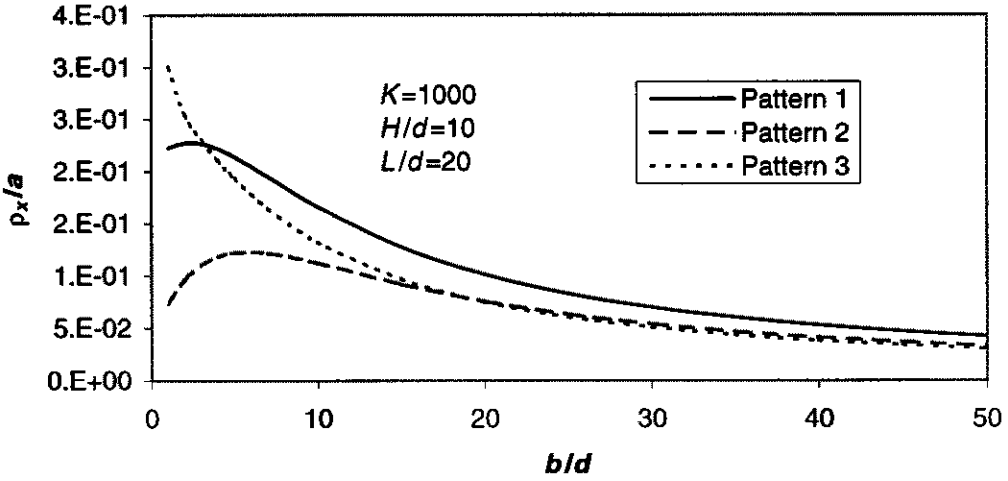

Fig. 5.10a Horizontal pile head movement ρ_x vs. b/d

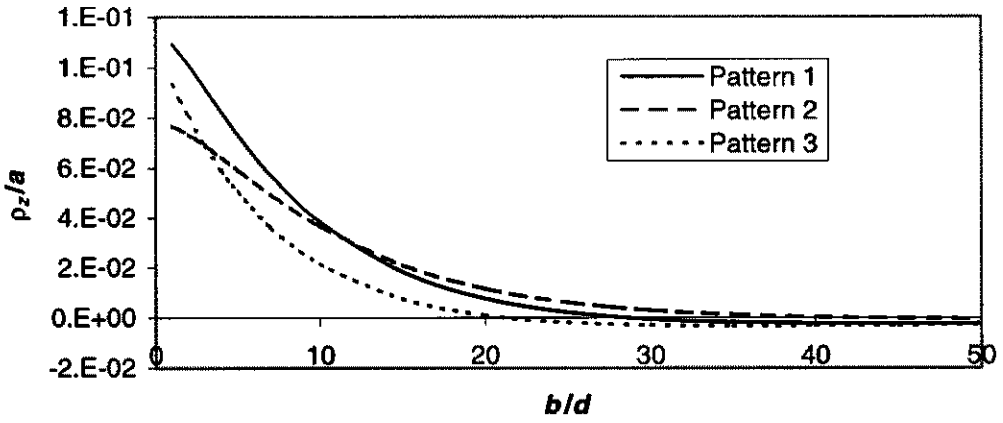

Fig. 5.10b Vertical pile head movement ρ_z vs. b/d

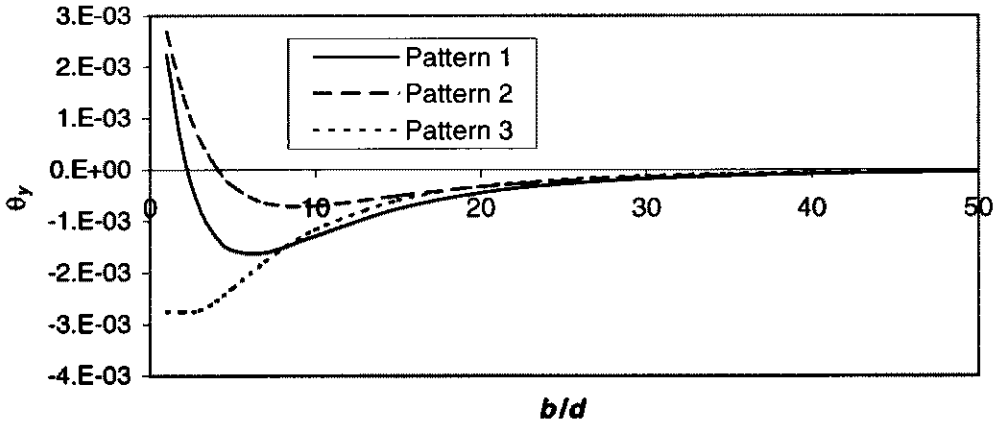

Fig. 5.10c Pile head rotation θ_y vs. b/d

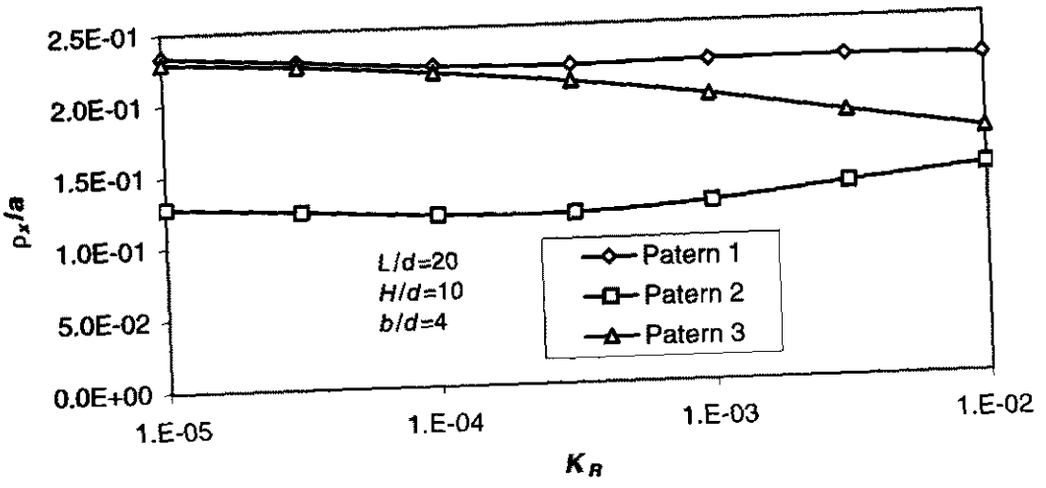

Fig. 5.11a Horizontal pile head horizontal movement ρ_x vs K_R

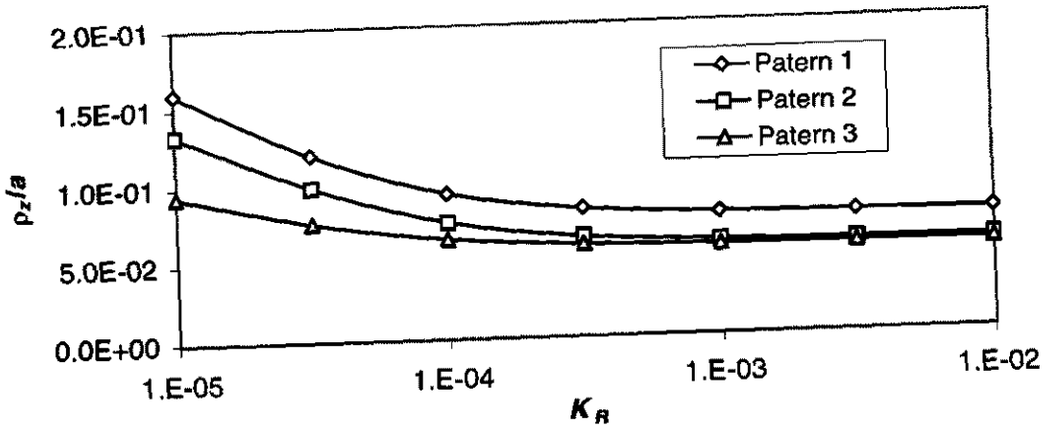

Fig. 5.11b Vertical pile head horizontal movement ρ_z vs K_R

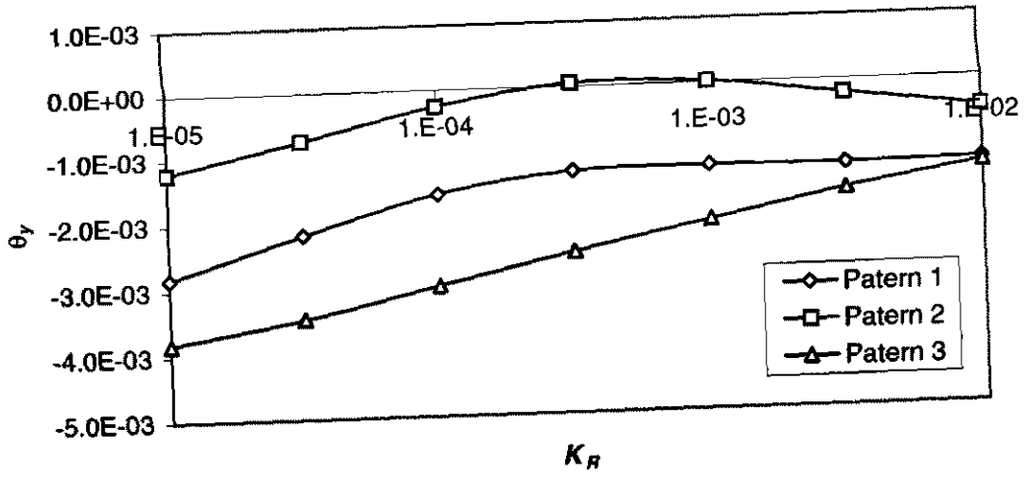

Fig. 5.11c Pile head rotation θ_y vs K_R

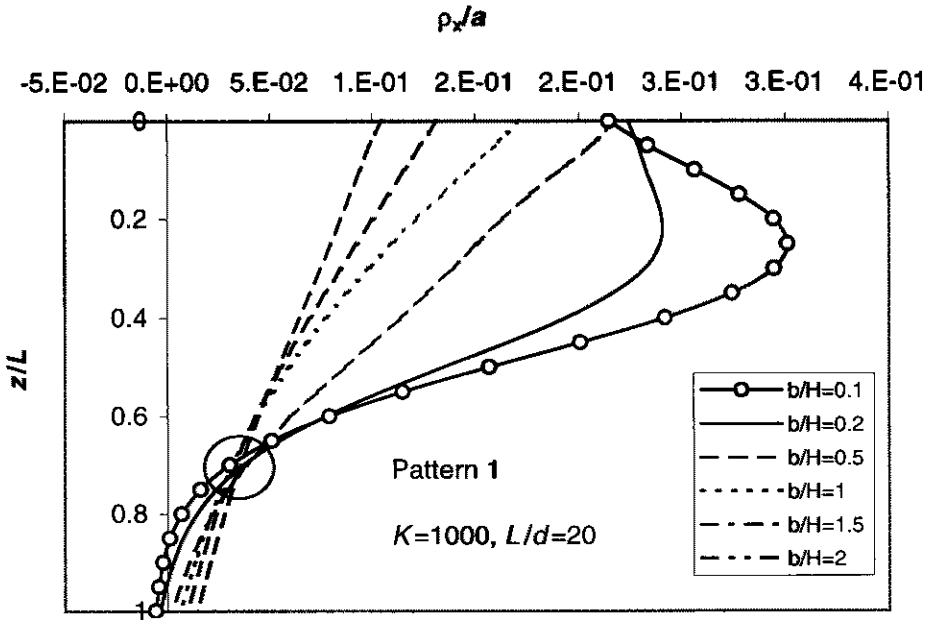

Fig. 5.12a Horizontal pile movements along pile depth in pattern 1

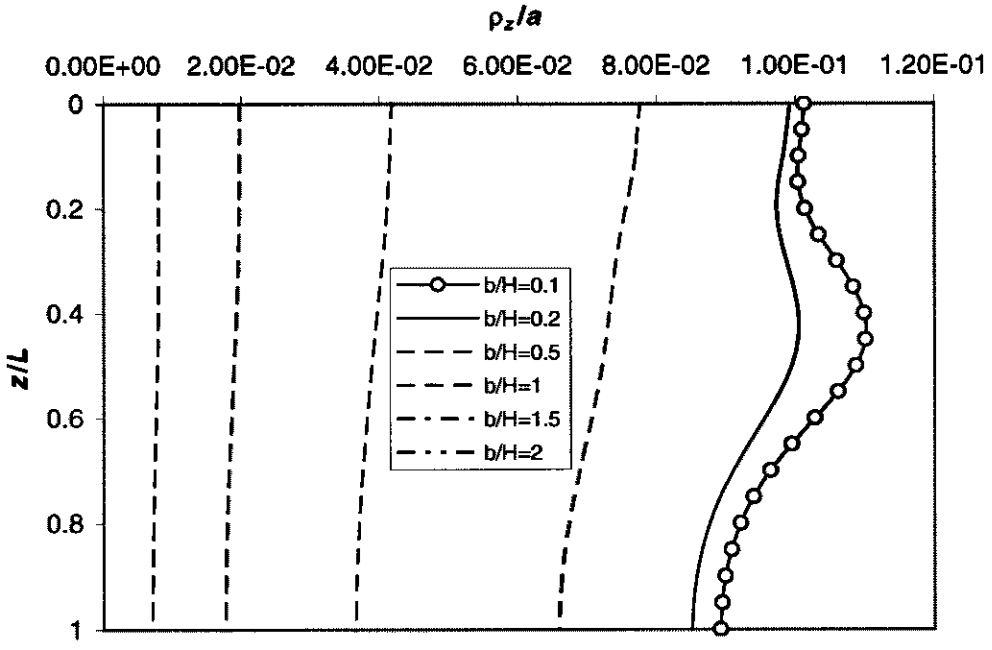

Fig. 5.12b Vertical pile movements along pile depth in pattern 1

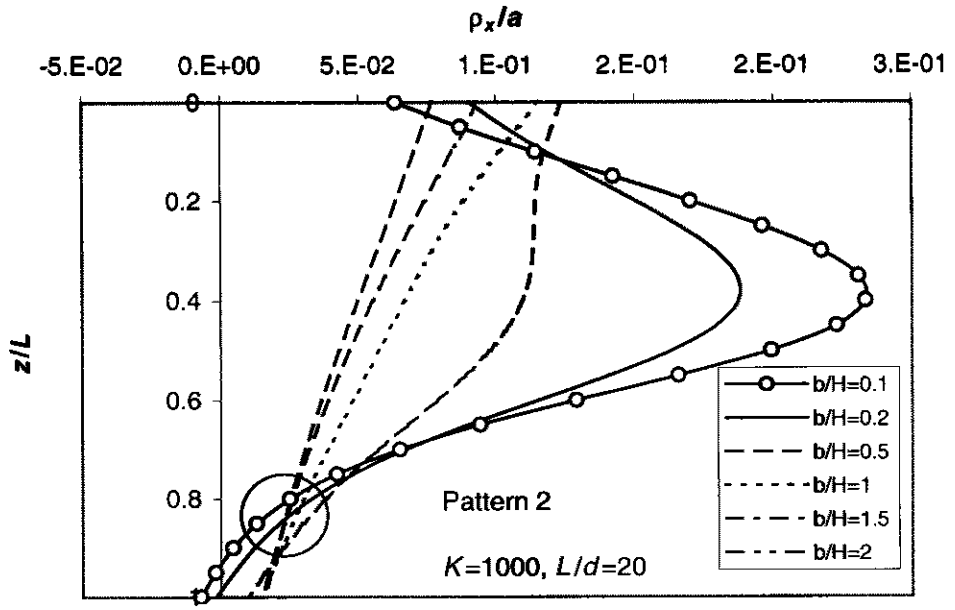

Fig. 5.13a Horizontal pile movements along pile depth in pattern 2

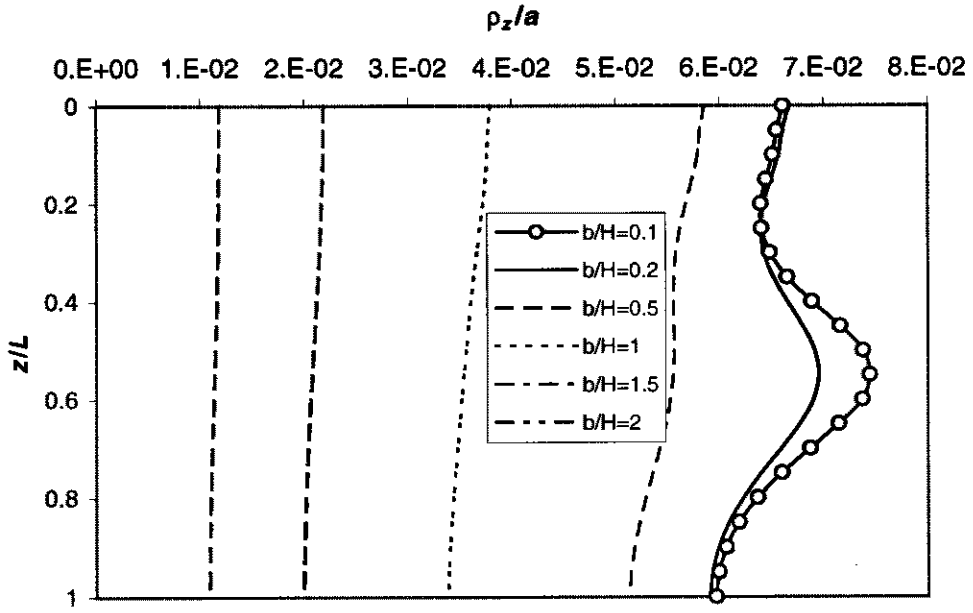

Fig. 5.13b Vertical pile movements along pile depth in pattern 2

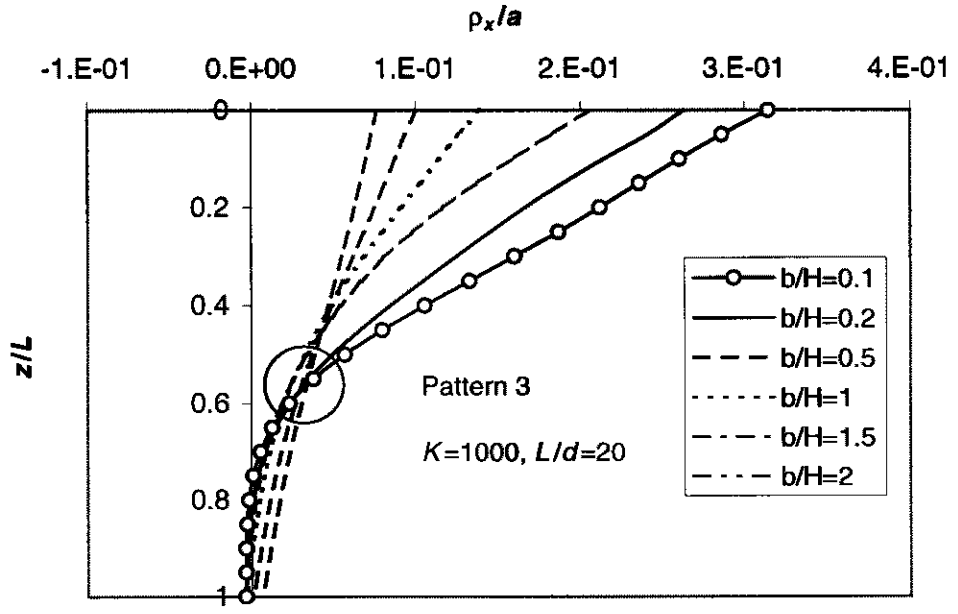

Fig. 5.14a Horizontal pile movements along pile depth in pattern 3

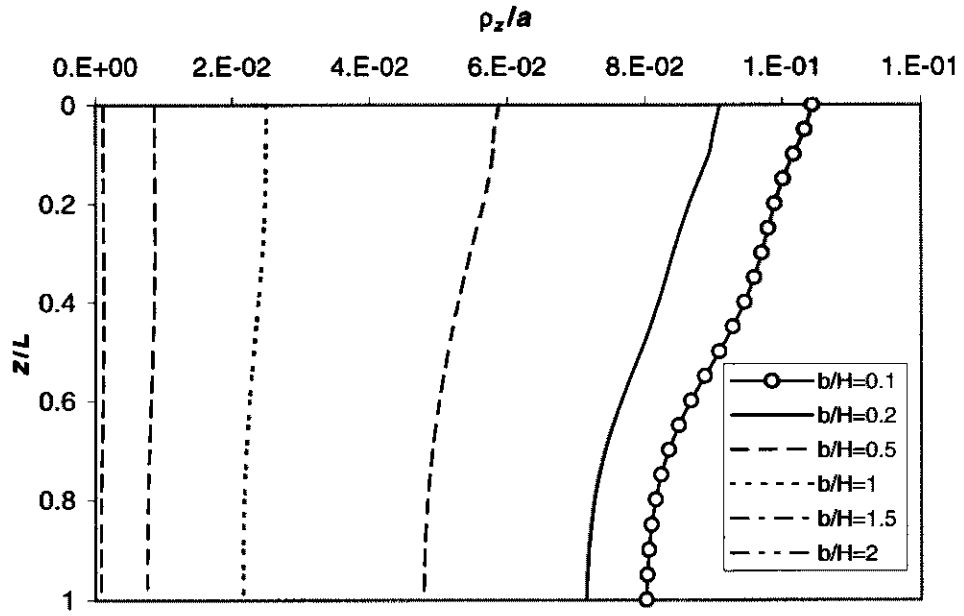

Fig. 5.14b Vertical pile movements along pile depth in pattern 3

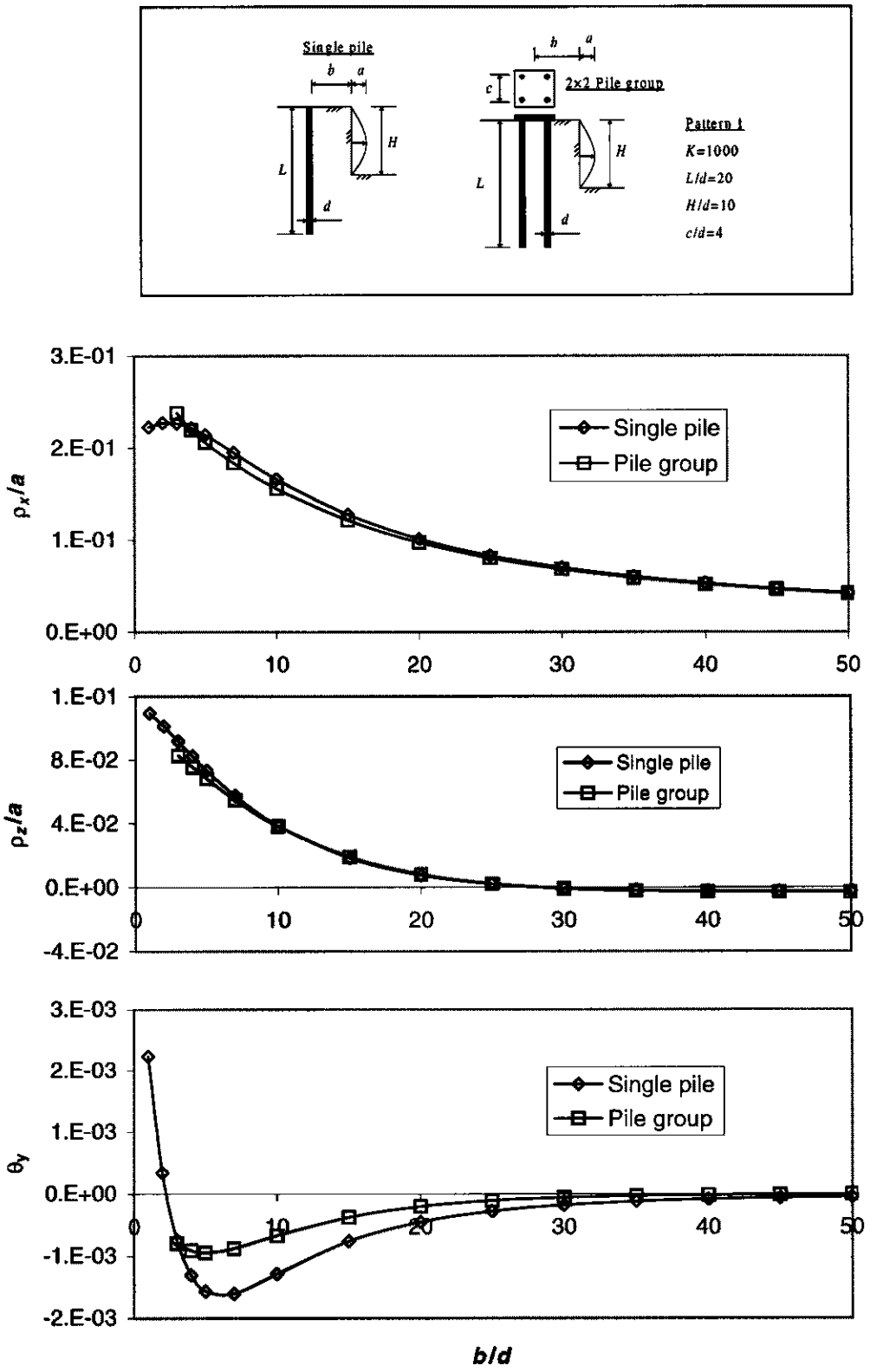

Fig. 5.15 Pile head movements vs. b/H in pattern 1

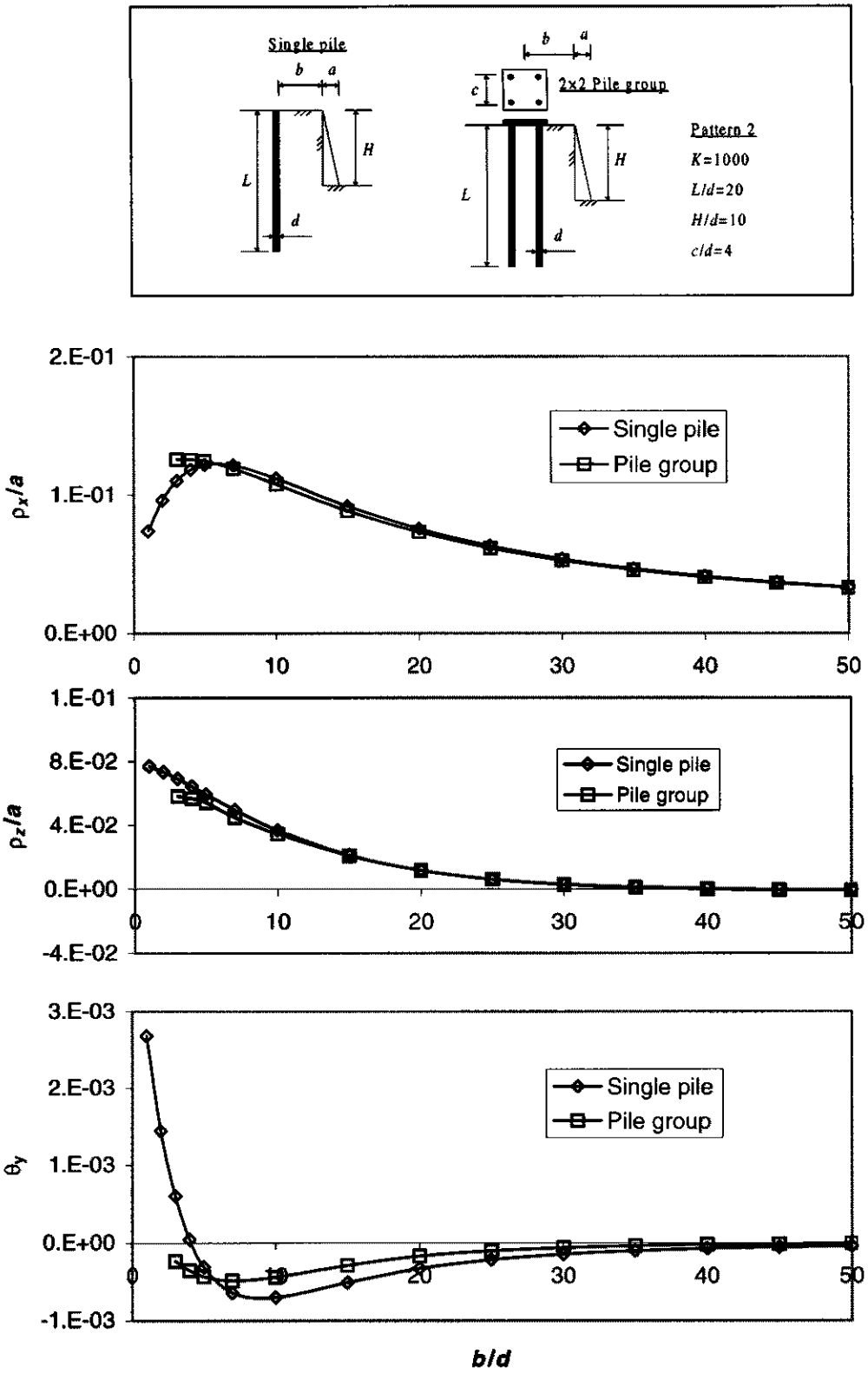

Fig. 5.16 Pile head movements vs. b/H in pattern 2

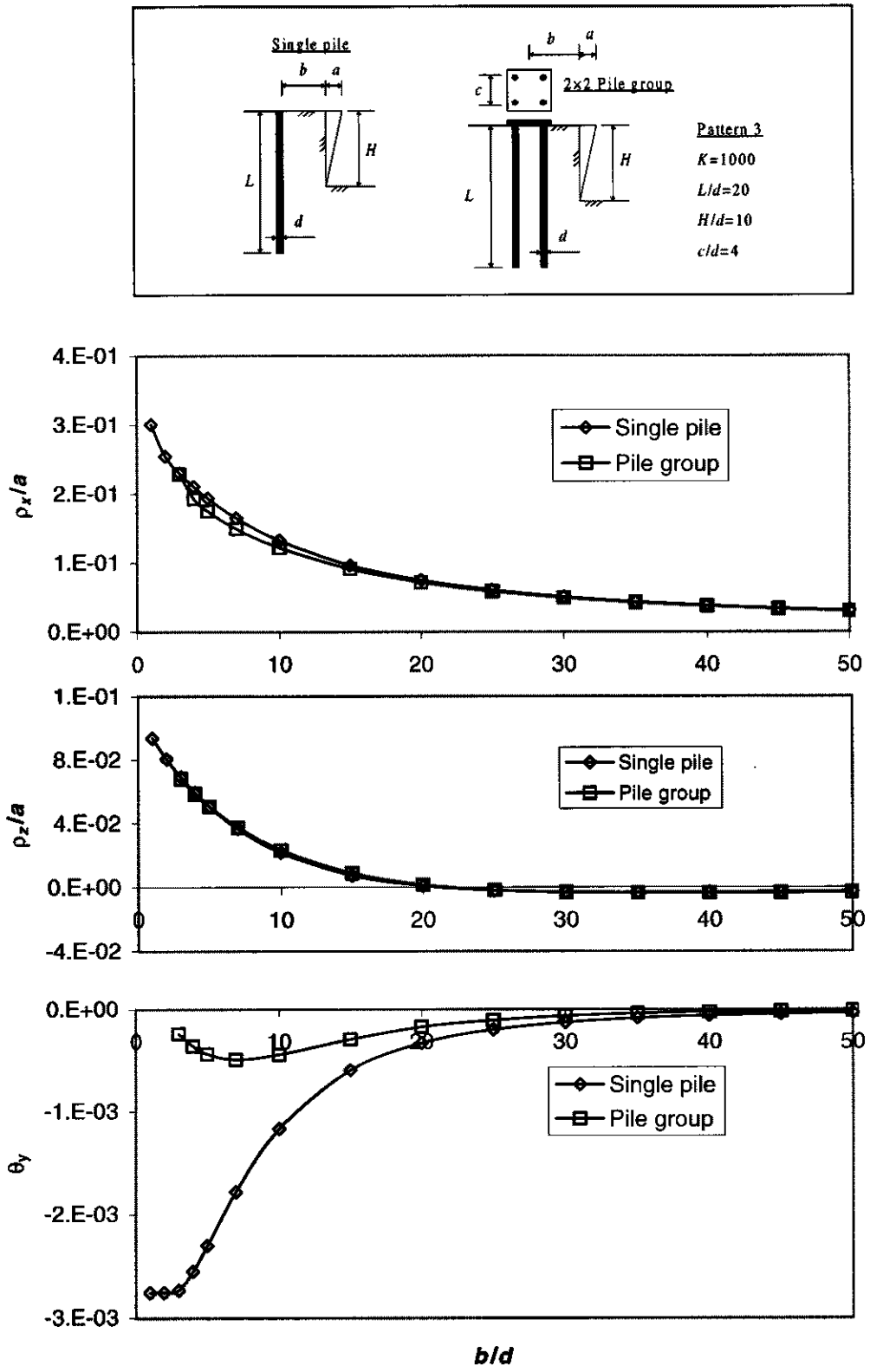

Fig. 5.17 Pile head movements vs. b/H in pattern 3

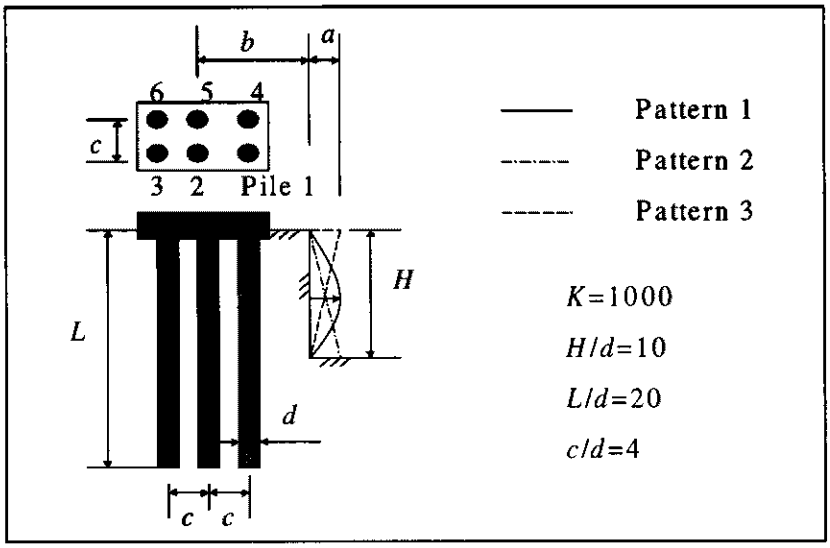

Fig. 5.18 Definition of the problem of a pile group nearby a vertical soil cut

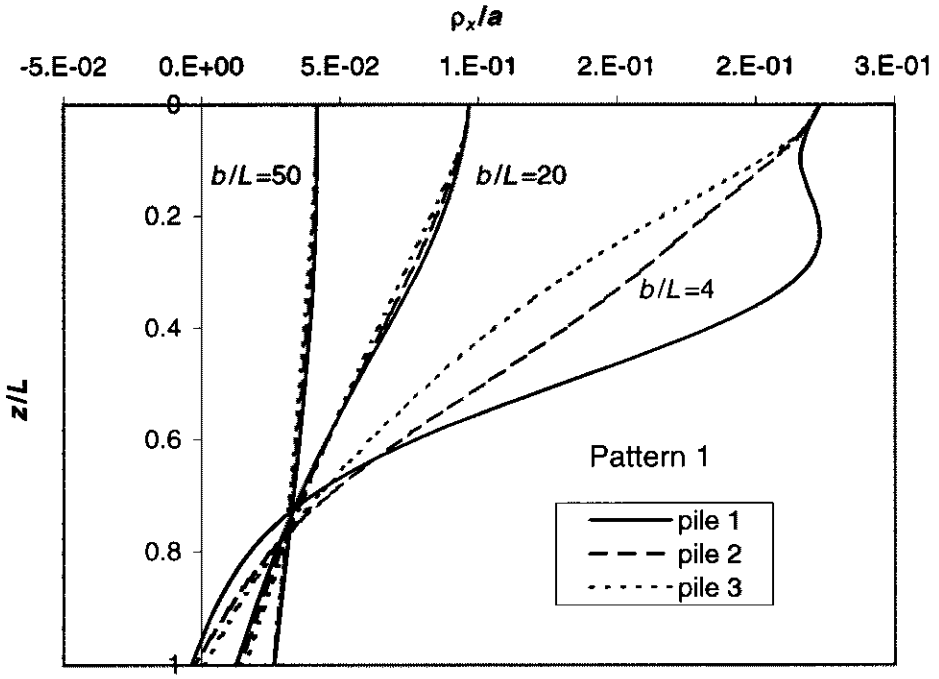

Fig. 5.19 Horizontal pile movements along pile depth in pattern 1

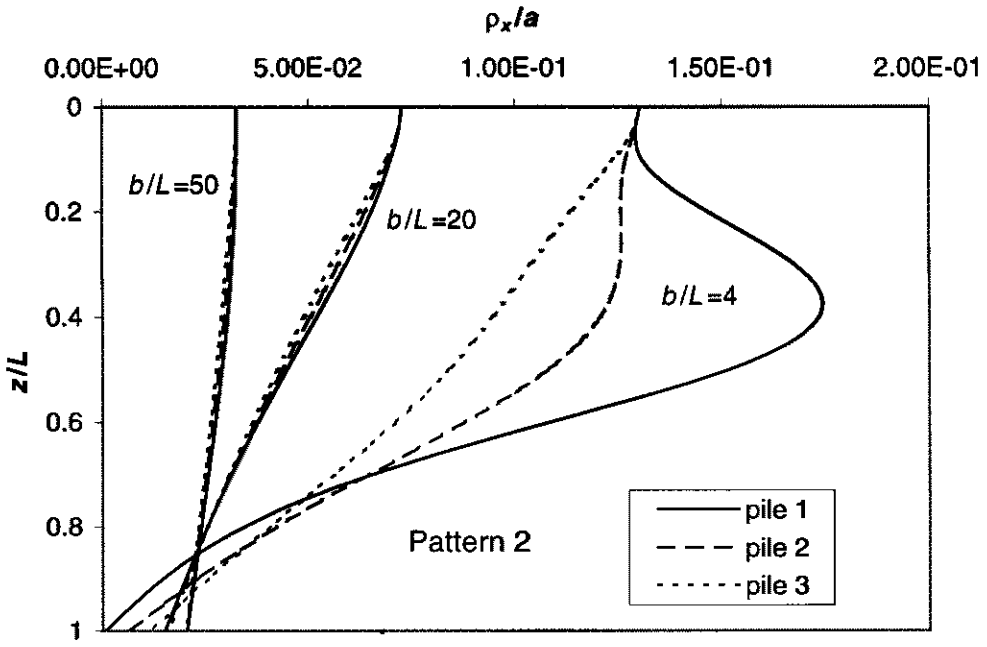

Fig. 5.20 Horizontal pile movements along pile depth in pattern 2

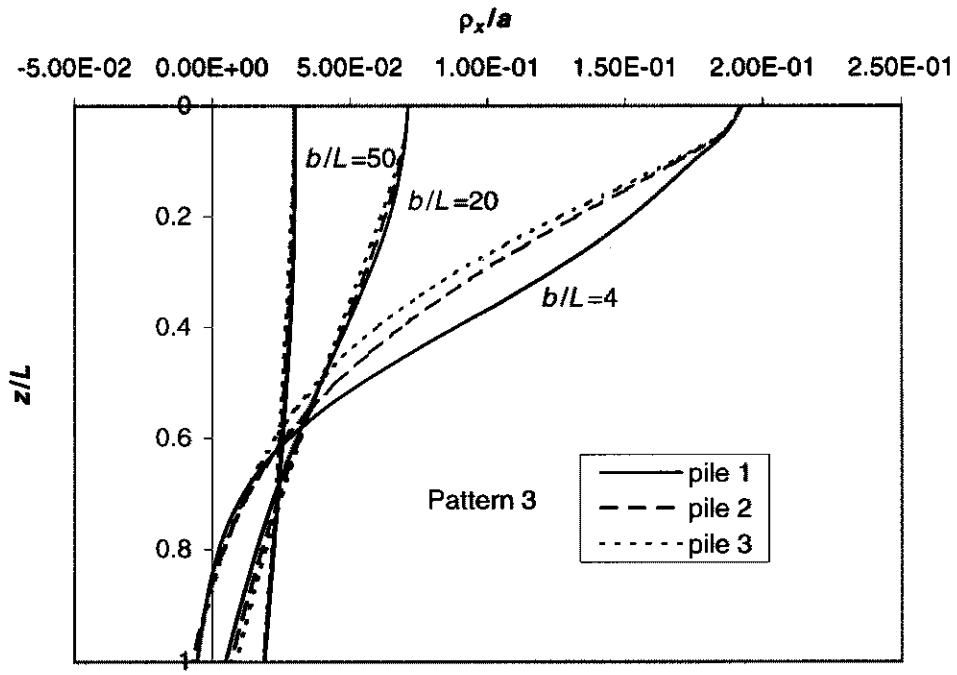

Fig. 5.21 Horizontal pile movements along pile depth in pattern 3

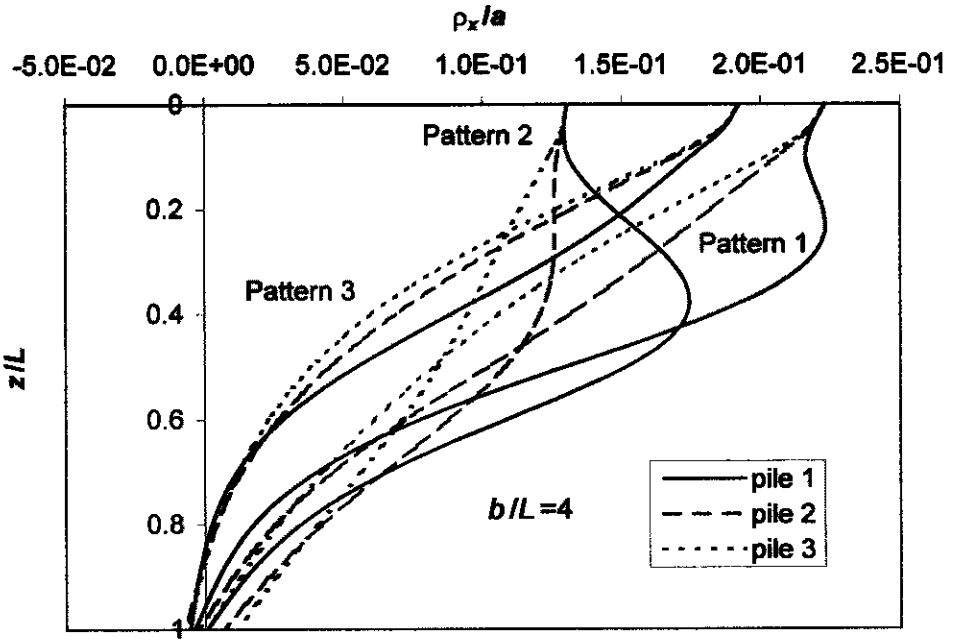

Fig. 5.22 Horizontal pile movements along pile depth with b/d=4

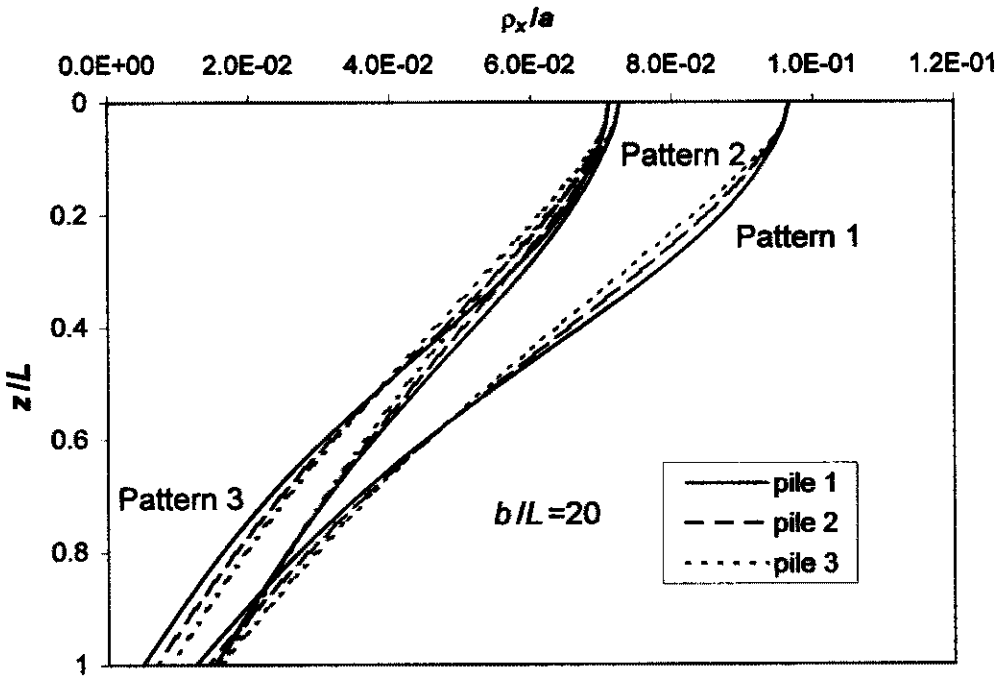

Fig. 5.23 Horizontal pile movements along pile depth with b/d=20

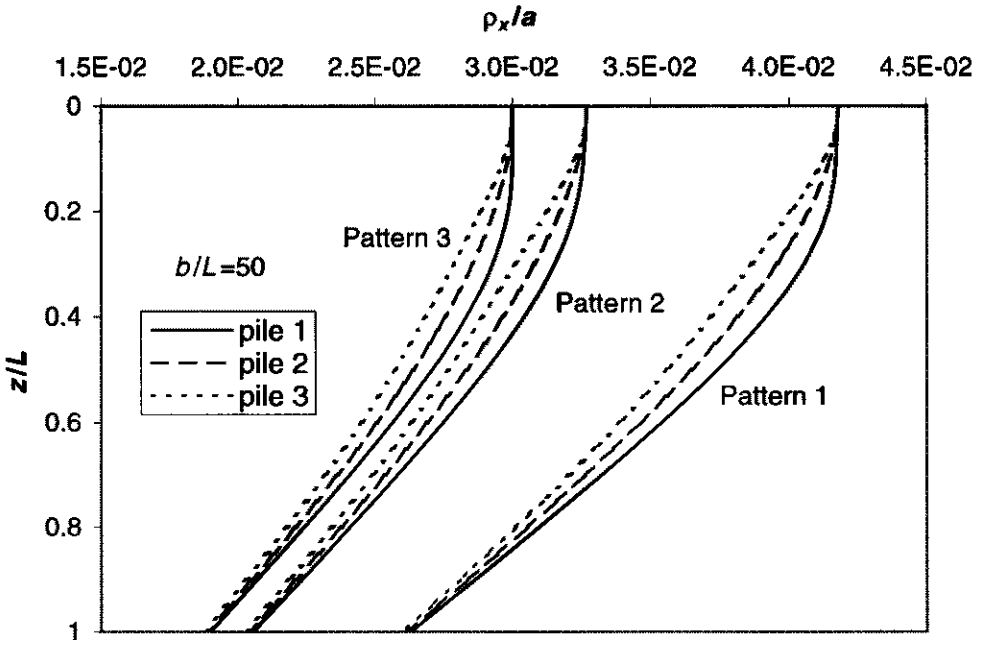

Fig. 5.24 Horizontal pile movements along pile depth with $b/d=50$

Chapter 6

Behaviour of Single Pile Containing Defects

6.1 Introduction

It is a not uncommon experience to encounter defects in various types of piles. The usual types of defects in concrete piles are necking, honey-combing and the presence of a "soft-base". For single piles, the presence of these defects leads to a reduction in pile head stiffness, and the possibility of reduced load capacity. There is a necessity to understand the behaviour of defective piles so as to design effective remedial measures for the foundation system.

Rao *et al* (1992) performed model tests on piles with various types of defects, and found (as would be expected) that significant increases in settlement could occur because of the presence of such defects. A theoretical non-linear defective pile analysis and the corresponding computer program DAMPA, were developed by Poulos (1997) for vertical loading. Furthermore, through the introduction of a pile (head) stiffness reduction factor, R_{ks} (ratio of stiffness of defective pile to stiffness of intact pile), he performed a parametric study on the behaviour of vertically loaded piles containing structural and geotechnical defects. A more general elastic analysis of pile groups containing pile defects has been developed by Xu and Poulos (1999a, 1999c), and has been presented in Chapter 3. This enables lateral and torsional as well as axial behaviour of defective piles to be examined.

The objective of this chapter is to carry out parametric analyses for the response of single piles with the typical defects (necking, honey-combing and soft-base). For each type of defect, typical relationships for pile stiffness reduction factors are developed, for a single pile under general loadings (axial, lateral, moment and torsional), relating the reduction in stiffness to the extent of the defect and the pile-soil stiffness/flexibility factors.

6.2 Pile Defects

6.2.1 Classification of Pile Defects

In this chapter, three kinds of defect are considered: necking, honey-combing and a soft base. As reviewed in Chapter 2, these defects may be among the most common of in pile defects.

6.2.2 Assumptions and Idealizations of Pile Defects

In an elastic analysis, the key parameters of a sound pile are assumed to be: pile Young's modulus E_p, soil Young's modulus, E_s, base Young's modulus E_b, diameter d, cross-sectional area A and length L.

For the convenience in the analysis, the pile defects are represented by simple idealization. Necking is idealized via a reduction in the value of local diameter of a pile. The parameters of necking are the diameter d_d, length L_d, area A_d and depth z_d of the necked zone The "standard" necking in the present solution is characterized by the parameters A_d/A=0.3, L_d/L=0.3, z_d/L=0.2.

Honey-combing is idealized via a reduction in the value of the pile Young's modulus over the defective zone. The honey-combed zone is assumed to have Young's modulus $E_{p,d}$, length L_d and depth z_d. The "standard" honey-combing is represented by the following parameters: $E_{p,d}/E_p$=0.3, L_d/L=0.3, z_s/L=0.2.

"Soft-base" is idealized via a reduced Young's modulus at the pile base $E_{b,d}$, with five percent of the pile length at pile tip being assumed to be "softened". The "standard" soft base is characterized as E_b/E_s=5 and $E_{b,d}/E_b$=0.1.

All assumptions described in Chapter 3 are made in the following elastic defective-pile analysis. The pile is assumed not to fail structurally or geotechnically, *i.e.*, elastic behaviour of both the pile and soil are assumed.

6.3 Definitions

6.3.1 Pile Stiffness/Flexibility Factors

In the parametric study of single piles, the pile stiffness and flexibility factors were defined as follows by Poulos (1980) and Randolph (1981a).

Axial stiffness factor (Poulos, 1980)

$$K = \frac{E_p}{E_s} \qquad \text{..... (6.1)}$$

For a very compressible pile, K=100
For a medium compressible pile, K=1000
For a less compressible pile, K=10000

Lateral flexibility factor (Poulos, 1980)

$$K_R = \frac{E_p I_p}{E_s L^4} \qquad \text{..... (6.2)}$$

For a very flexible pile, $K_R=10^{-5}$
For a medium flexible pile, $K_R=10^{-3}$
For a relatively stiff pile, $K_R=10^{-1}$

Torsional Stiffness factor (Randolph, 1981a)

$$K_T = \frac{G_p}{G_s} \qquad \text{..... (6.3)}$$

For a very "twistable" pile, K_T =100

For a medium "twistable" pile, K_T =1000

For a less "twistable" pile, K_T =10000

6.3.2 Pile Head Stiffness Reduction Factors

To provide a convenient measure of the defective pile performance, Poulos (1997) introduced, the " pile head stiffness reduction factor" R_{KS}, *i.e.*

$$R_{KS} = \frac{\text{stiffness of defective pile}}{\text{stiffness of intact pile}} \qquad \text{.....(6.4)}$$

In order to study the behaviour of a defective pile under general loadings, (e.g. axial, lateral, moment and torsional), the above definition is extended into a general form as follows:

$$R_{KS,A,B} = \frac{\text{Stiffness of defective pile on displacement component A due to loading A}}{\text{Stiffness of intact pile on displacement component B due to loading A}}$$

.....(6.5)

For example

$R_{KS,N,s} = R_{KS,N}$ = pile head stiffness reduction factor, R_{KS}, on axial displacement s due to axial loading P

$R_{KS,H,\rho}$ = R_{KS} on lateral displacement ρ due to horizontal loading H

$R_{KS,H,\theta}$ = R_{KS} on rotation θ due to horizonal loading H

$R_{KS,M,\rho}$ = R_{KS} on lateral displacement ρ due to moment loading M

$R_{KS,M,\theta}$ = R_{KS} on rotation θ due to moment loading M

$R_{KS,T,\omega} = R_{KS,T} = R_{KS}$ on twist ω due to torsional loading T.

6.4 Comparisons

The head settlements, S_z, of a pile containing a neck, are compared via the programs GEPAN and DAMPA (Poulos, 1997). The problem is illustrated in Table 6.1; a pile 20 *m* in length and 1 *m* in diameter, is assumed to contain a neck with z_d/L=0.2 and L_d/L=0.3. The applied load on the pile is 1 *MN*. The number of depth divisions of the pile is 20 for both programs, and the number of circumference divisions of each pile element is 4 for GEPAN and 1 for DAMPA (cylindrical element). As shown in Table 6.1, the relative errors between the two solutions is less than 5%, with the more severe necking resulting in a large relative error.

Fig. 6.1 shows the comparisons for an ending-bearing pile containing a neck, while Fig. 6.2 compares the head settlement of a pile with a honey-comb. It is found that the results from GEPAN and DAMPA are very close although the method of implementation in each program is quite different.

6.5 Pile with a Neck

Fig. 6.3 shows the axial pile stiffness reduction factor, $R_{KS,N}$ computed from GEPAN. $R_{KS,N}$ decreases with increasing ratio of necked area to intact area A_d/A and/or decreasing pile stiffness factor K. The behaviour of an axially-loaded end-bearing pile with a neck is shown in Fig. 6.4. It is found that, for relatively compressible end-bearing piles (such as K=100 to K=1000), the stiffness reduction factor decreases significantly when the ratio of necked and intact area, A_d/A, decreases. Compared with Fig. 6.3 and 6.4, it is demonstrated that, for a relatively stiff pile (such as, K=10000), the difference of the values of the axial reduction factor for a floating pile and an end-bearing pile is small. However, for more compressible piles, the value of the reduction factor for the end-bearing is larger than for the floating pile.

The influence of the position of a neck on the axial stiffness reduction factor are shown in Figs. 6. 5 to 6.6 for floating and end-bearing piles respectively. As z_d/L increases, $R_{KS,N}$ increases. The shallower the neck in the pile, the smaller is the value of the stiffness reduction factor. With varying z_d/L, the values of $R_{KS,N}$ for stiff floating piles are less than for the stiff end-bearing piles, but in contrast to the stiff piles, the values of $R_{KS,N}$ for compressible floating piles are larger than those of the compressible end-bearing piles.

The stiffness reduction for a pile containing a neck, under horizontal loading, is shown in Figs. 6.7 to 6.10. The values of lateral reduction factors, $R_{KS,H\rho}$, $R_{KS,H\theta}$, apparently decrease with increasing A_d/A for the moderately flexible piles (K_R=10^{-3}, 10^{-2}), while they slightly decrease for the more flexible piles (K_R=10^{-4}), as shown in Fig. 6.7 and Fig. 6.9. As a general tendency, the values of lateral reduction factors increase as z_d/L increase, as shown in Figs. 6.8 and 6.10. Furthermore, for the more flexible piles, a shallower "neck" in a pile results in lower values of the lateral stiffness reduction factors. For a "deeper neck" (z_d/L>=0.3) in the more flexible pile, the values of $R_{KS,H\rho}$, $R_{KS,H\theta}$, are approaching 1, since the defect may then be at or below the effective length of the piles. For moderately flexible piles (K_R=10^{-3}, 10^{-2}), the lateral stiffness factors increase approximately-proportionally with the depth of the neck, as shown in Figs. 6.8 and 6.10.

The torsional stiffness reduction for a pile containing a neck, is shown in Figs. 6.11 and 6.12. The torsional stiffness reduction factor, $R_{KS,T}$, decreases with decreasing A_d/A as shown in Fig. 6.11. While $R_{KS,T}$ increases, as z_d/L increases, as shown in Fig. 6.12. The less "twistable" the pile, the less is the torsional stiffness reduction factor. For the more "twistable" piles, the influence of the neck on the torsional stiffness reduction factor becomes negligible for z_d/L>=0.3.

6.6 Pile with a Soft Base

The axial stiffness reduction factors, $R_{KS,N}$, for a pile containing a soft base, with the variation of E_{bs}/E_b, L/d and K, are shown in Figs. 6.13 to 6.14.

Fig. 6.13 shows that the axial reduction factor, $R_{KS,N}$, decreases with decreasing ratio of soft-base Young's modulus and base Young's modulus, $E_{b,s}/E_b$. The stiffness reduction factors for moderate to more compressible piles are less than those of less compressible piles.

$R_{KS,N}$ increases as the ratio of pile length and diameter, L/d, increases as shown in Fig. 6.14. The values of $R_{KS,N}$ with a soft-base in short piles are less than those for larger piles.

The lateral and torsional stiffness reduction factors of a pile containing a soft base are not presented here, because, via similar interaction analyses as above, they are have been proved negligible compared with those under axial loading.

6.7 Pile with a Honey-Comb

The stiffness reduction factors for a pile with a honey-comb are presented in this section.

Figs. 6.15 and 6.16 show that the values of the axial stiffness reduction factor, $R_{KS,N}$, decrease with decreasing $E_{p,d}/E_p$, (a ratio of the pile Young's modulus of honey-combed section to the intact pile Young's modulus). Figs. 6.17 and 6.18 show that the values of $R_{KS,N}$ increase with increasing z_d/L, (the ratio of depth of honey-comb to pile length). With honey-combing, $R_{KS,N}$ for a floating pile is larger than for an end-bearing pile. The stiffness reduction factors for compressible piles containing "shallower" honey-combs are much less than "deeper" honey-combs, while the effect of depth of the defects is not significant for stiff piles.

The lateral (moment) stiffness reduction factors, $R_{KS,H,\rho}$, $R_{KS,H,\theta}$ and $R_{KS,M,\theta}$, for the defective piles for different values of $E_{p,d}/E_p$ are shown in Figs. 6.19, 6.21 and 6.23 respectively. The values of these lateral stiffness reduction factors decrease as $E_{p,d}/E_p$ decreases. For more-flexible piles, the effect of the honey-comb on the lateral stiffness reduction factors can be neglected. The variation of the lateral stiffness reduction factors for the honey-combed piles with varying values of z_d/L, are shown in Figs. 6.20, 6.22 and

6.24. These stiffness reduction factors increase as z_d/L increases. A "shallower" honey-comb results in much lower values of the stiffness reduction factor compared with a "deeper" honey-comb.

The torsional stiffness reduction factors, $R_{SK,T}$, for the defective pile are plotted in Figs. 6.25 and 6.26. It is shown that the value of $R_{SK,T}$ are reduced significantly by severe and/or shallower honey-combs.

6.8 Stress Distribution along Defective Pile

As illustrated above, the characteristics of pile head stiffness reduction of necked and honey-combed piles are similar. However, the corresponding stress distributions in the defective piles are quite different, which is shown by following two examples with "standard" parameters (K=1000, L/d=20, z_d/L=0.2, L_d/L=0.3). Fig. 6.27 shows the pile stress along necked piles. It is found that higher stress will be induced in the severly necked section. The stress increases by about two times in a 40% area necked section. The stress distributions within honey-combed piles are plotted in Fig. 6.28. It is shown that stress decreases only slightly with decreasing local pile Young's modulus in the honey-combed area, $E_{p,d}$. (note: the "honey-combed" section in the thesis is assumed to be solid, in practical cases it may contain voids and in that case, the stress in the section may increase).

6.9 Conclusions

With a numerical analysis via the program GEPAN, this chapter examines the response of single piles with three typical defects (necking, honey-combing and soft-base). For each type of defect, typical relationships have been developed, for a single pile under general loadings (axial, lateral, moment and torsional), for the reduction in stiffness as a function of the extent and position of the defects, and the pile-soil stiffness/flexibility

factors. The main conclusions from the parametric study of defective piles may be summarized as follows:

1) The presence of defects results in reduced stiffness of all components (axial, lateral, moment, torsional) of the pile.
2) Severe and/or shallow defects result in significantly larger reduction in pile stiffness (*i.e.* lower stiffness reduction factor).
3) For less-flexible piles, the stiffness reduction factors on a floating pile and end-bearing pile are little different, however, for the moderate to very flexible piles, the stiffness reduction factor for an end-bearing pile is larger than that for a floating pile.
4) Pile stress in necked section increases significantly.

Table 6.1 Pile Head Settlement ρ_z (mm)

A_d/A	K=100			K=1000			K=10000		
	GEPAN	DAMPA	RE(%)	GEPAN	DAMPA	RE(%)	GEPAN	DAMPA	RE(%)
1	7.6477	7.6728	-0.33	4.3618	4.4084	-1.06	3.9194	3.9682	-1.23
0.9	7.7693	7.7723	-0.04	4.3999	4.4287	-0.65	3.9382	3.9704	-0.81
0.8	7.9073	7.8907	0.21	4.4386	4.4539	-0.34	3.9534	3.9732	-0.50
0.7	8.0728	8.0341	0.48	4.4852	4.4861	-0.02	3.9701	3.9767	-0.17
0.6	8.2749	8.2111	0.78	4.5431	4.5284	0.32	3.9888	3.9815	0.18
0.5	8.5291	8.4356	1.11	4.6186	4.5867	0.70	4.0104	3.9881	0.56
0.4	8.8611	8.7298	1.50	4.7343	4.6722	1.33	4.0371	3.9981	0.98
0.3	9.3313	9.1333	2.17	4.8858	4.8098	1.58	4.0724	4.0145	1.44
0.2	9.9735	9.7244	2.56	5.1778	5.0676	2.17	4.1282	4.0473	2.00
0.1	11.048	10.696	3.29	5.9029	5.7266	3.08	4.2577	4.1435	2.76

Parameters:
P=1MN, L=20m, d=1m
ν_s=0.3, ν_p=0.3
E_s=20MPa
z_d/L=0.2, L_d/L=0.3

Element division:
depth divn. =20 (DAMPA)
depth divn. =20 (GEPAN)
circ. divn. =4 (GEPAN)

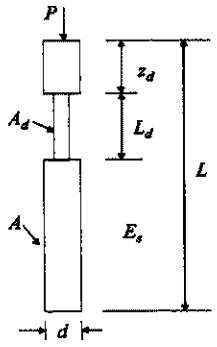

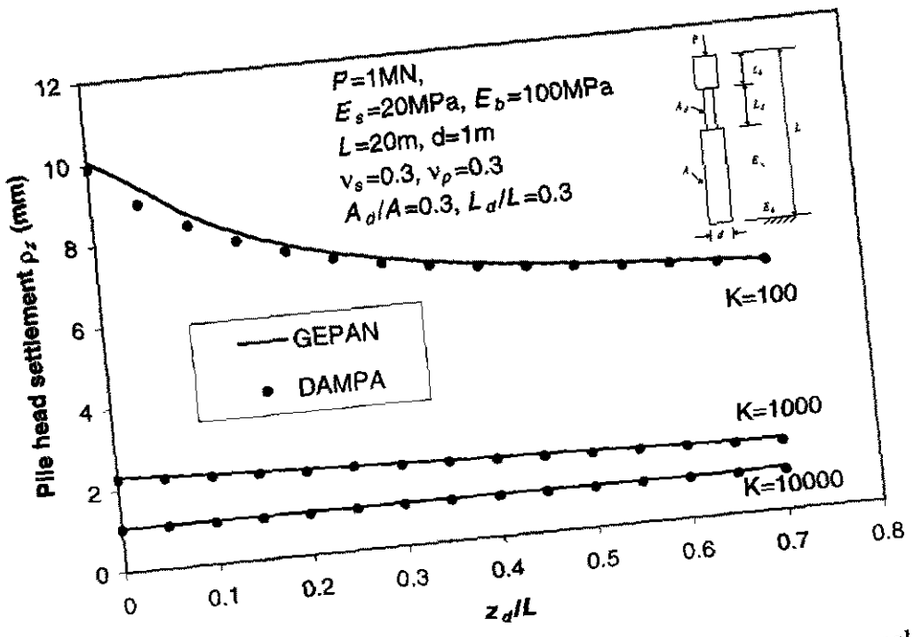

Fig. 6.1 Comparison of settlement of an end-bearing pile containing a neck

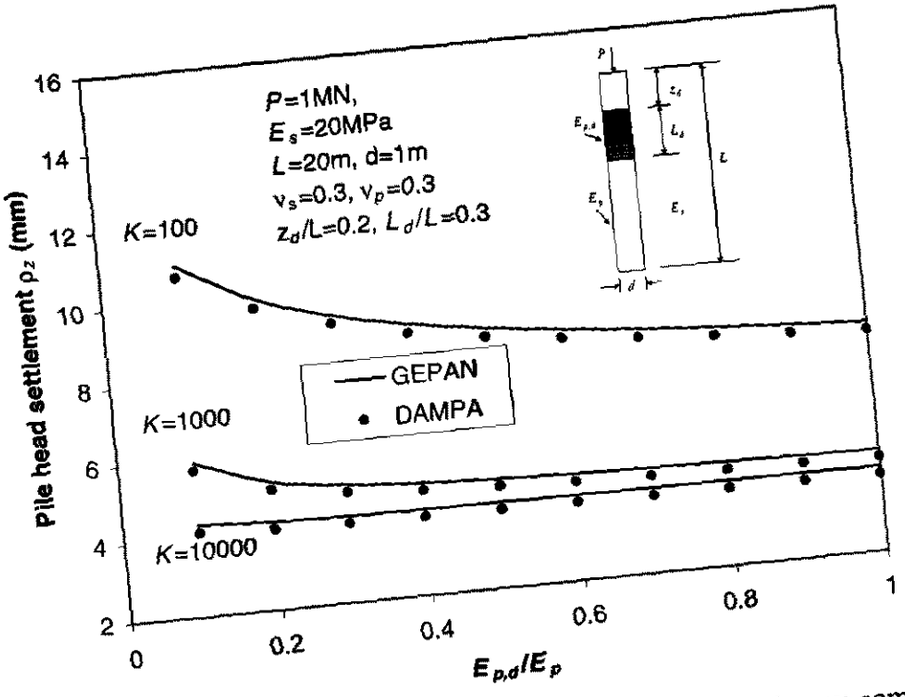

Fig. 6.2 Comparison of settlement of a pile containing a honey-comb

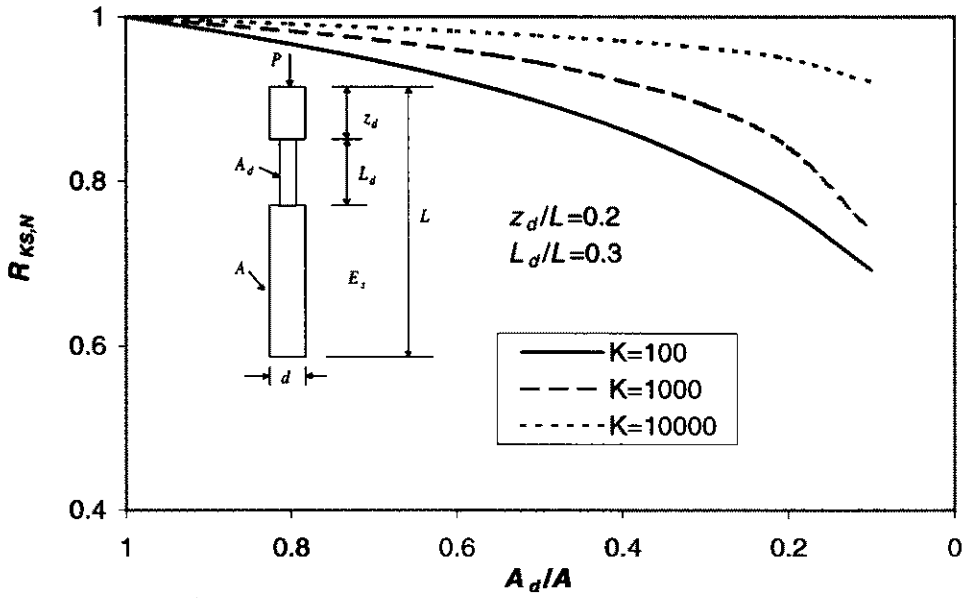

Fig. 6.3 $R_{KS,N}$ vs A_d/A of a pile containing a neck

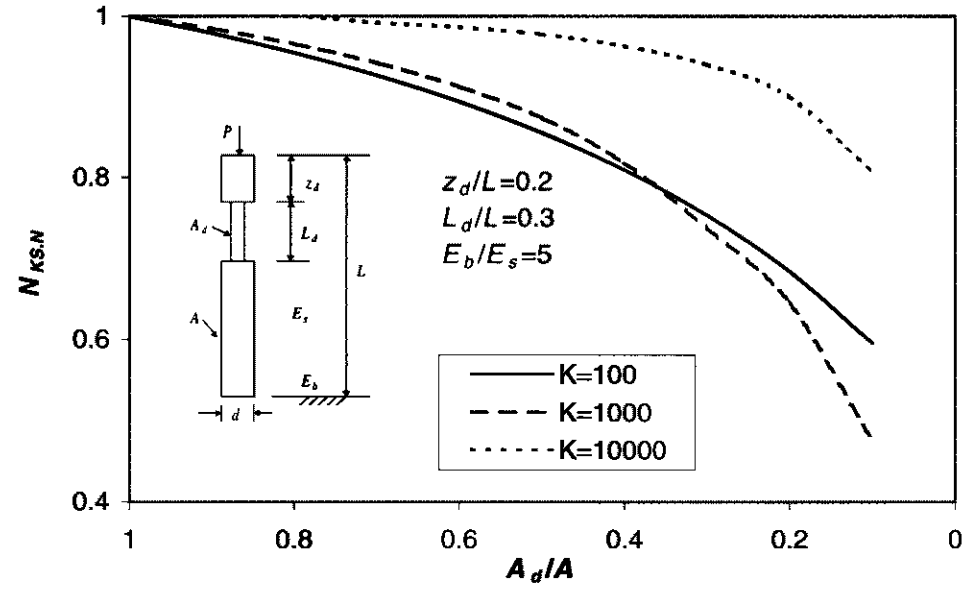

Fig. 6.4 $R_{KS,N}$ vs A_d/A of an end-bearing pile containing a neck

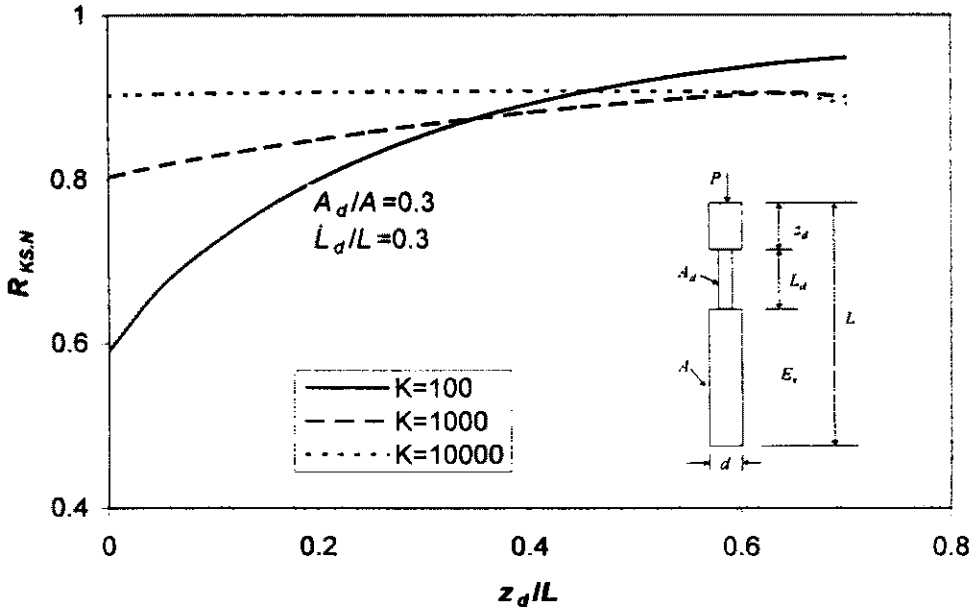

Fig. 6.5 $R_{KS,N}$ vs z_d/L of a pile containing a neck

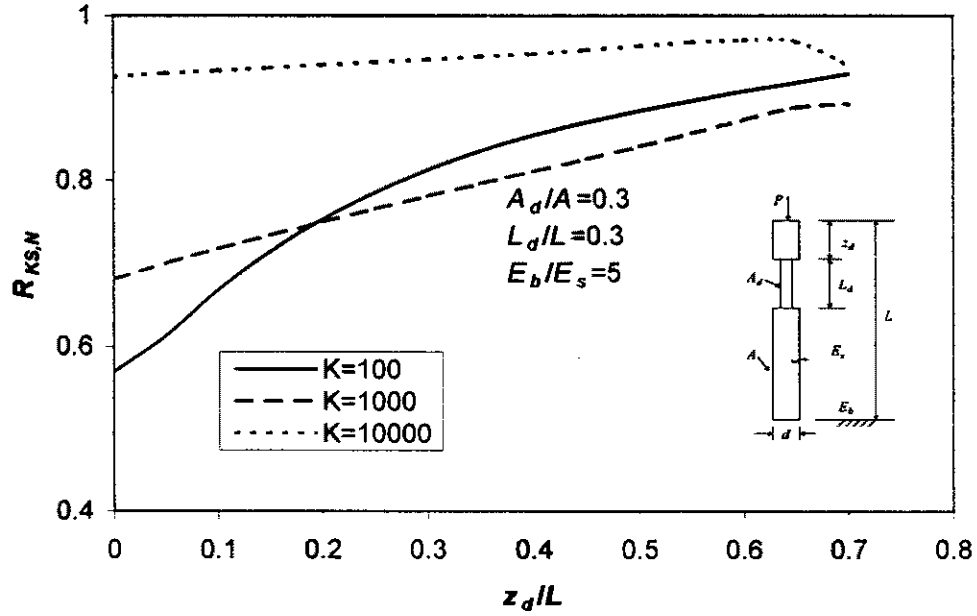

Fig. 6.6 $R_{KS,N}$ vs z_d/L of an end-bearing pile containing a neck

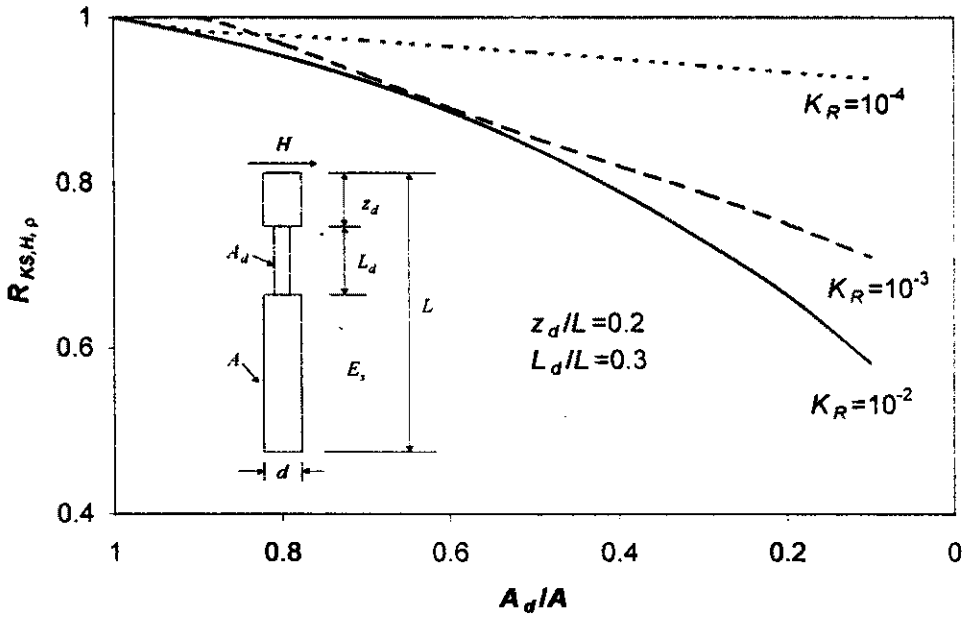

Fig. 6.7 $R_{KS,H,\rho}$ vs A_d/A of a pile containing a neck

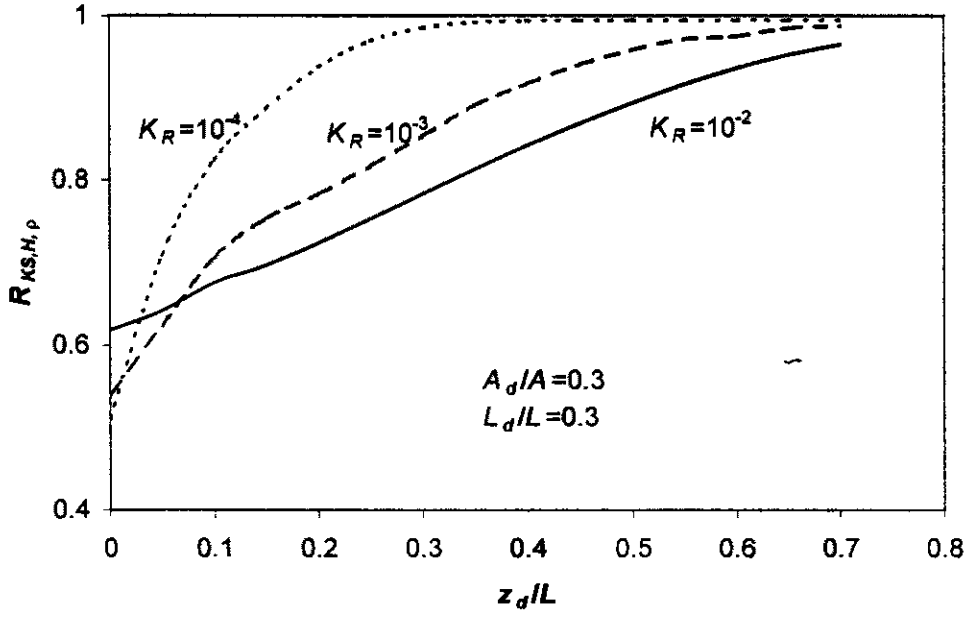

Fig. 6.8 $R_{KS,H,\rho}$ vs z_d/L of a pile containing a neck

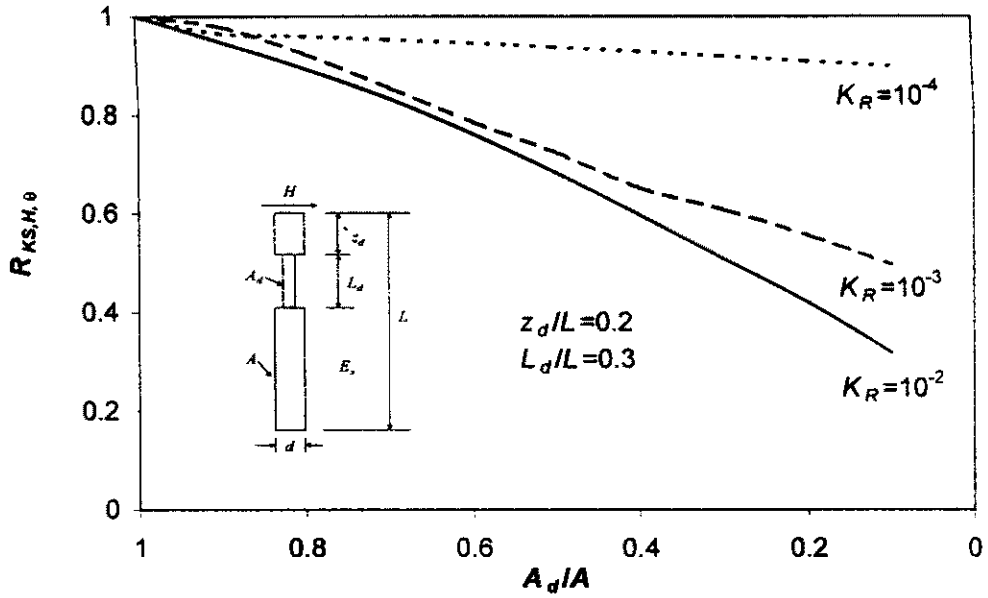

Fig. 6.9 $R_{KS,H,\theta}$ vs A_d/A of a pile containing a neck

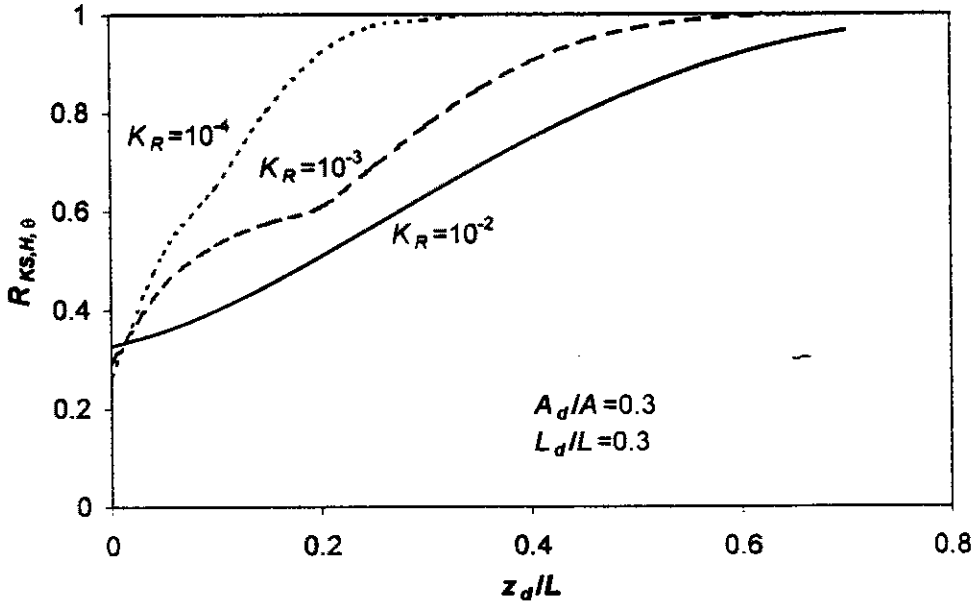

Fig. 6.10 $R_{KS,H,\theta}$ vs z_d/L of a pile containing a neck

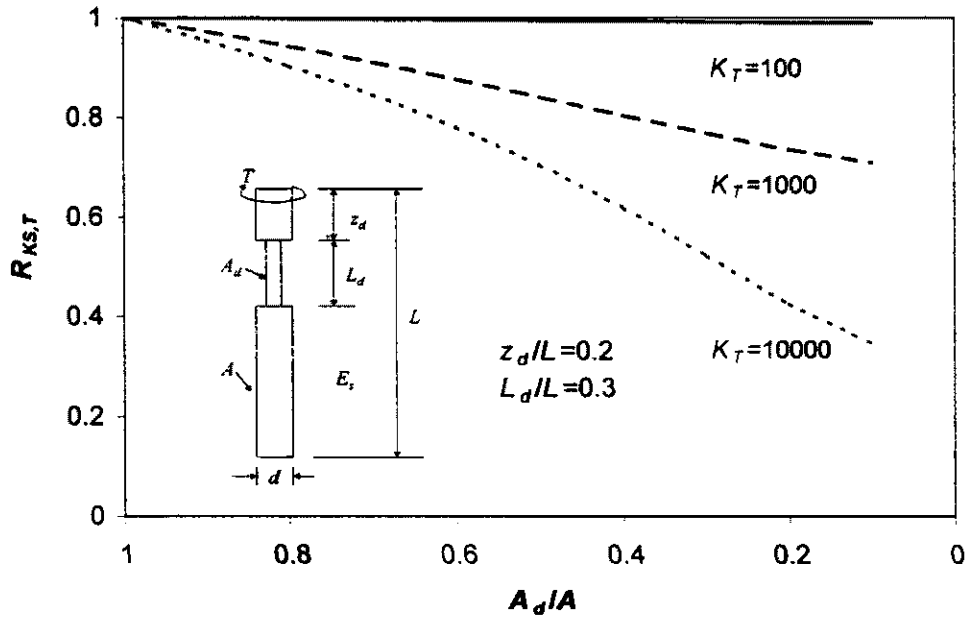

Fig. 6.11 $R_{KS,T}$ vs A_d/A of a pile containing a neck

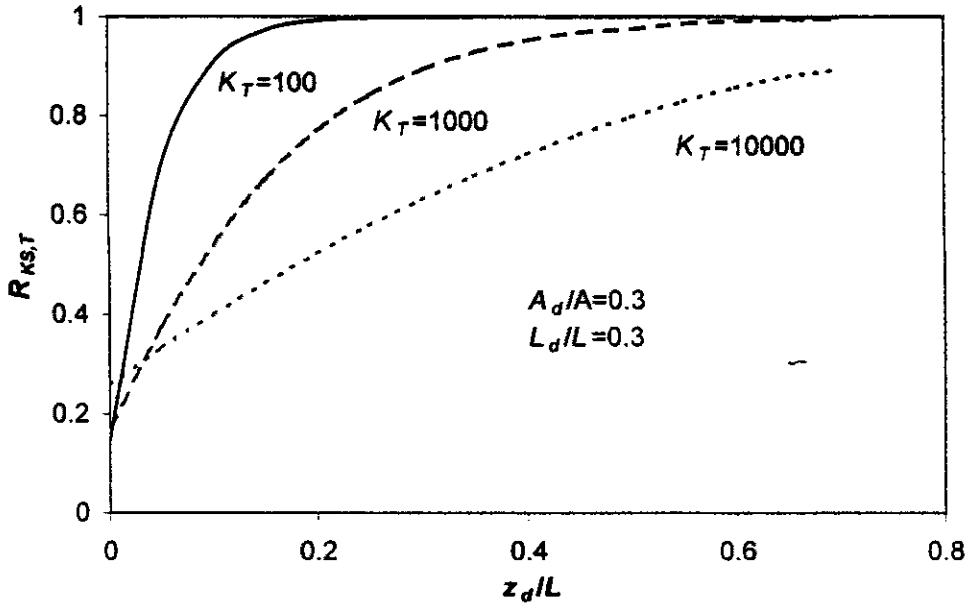

Fig. 6.12 $R_{KS,T}$ vs z_d/L of a pile containing a neck

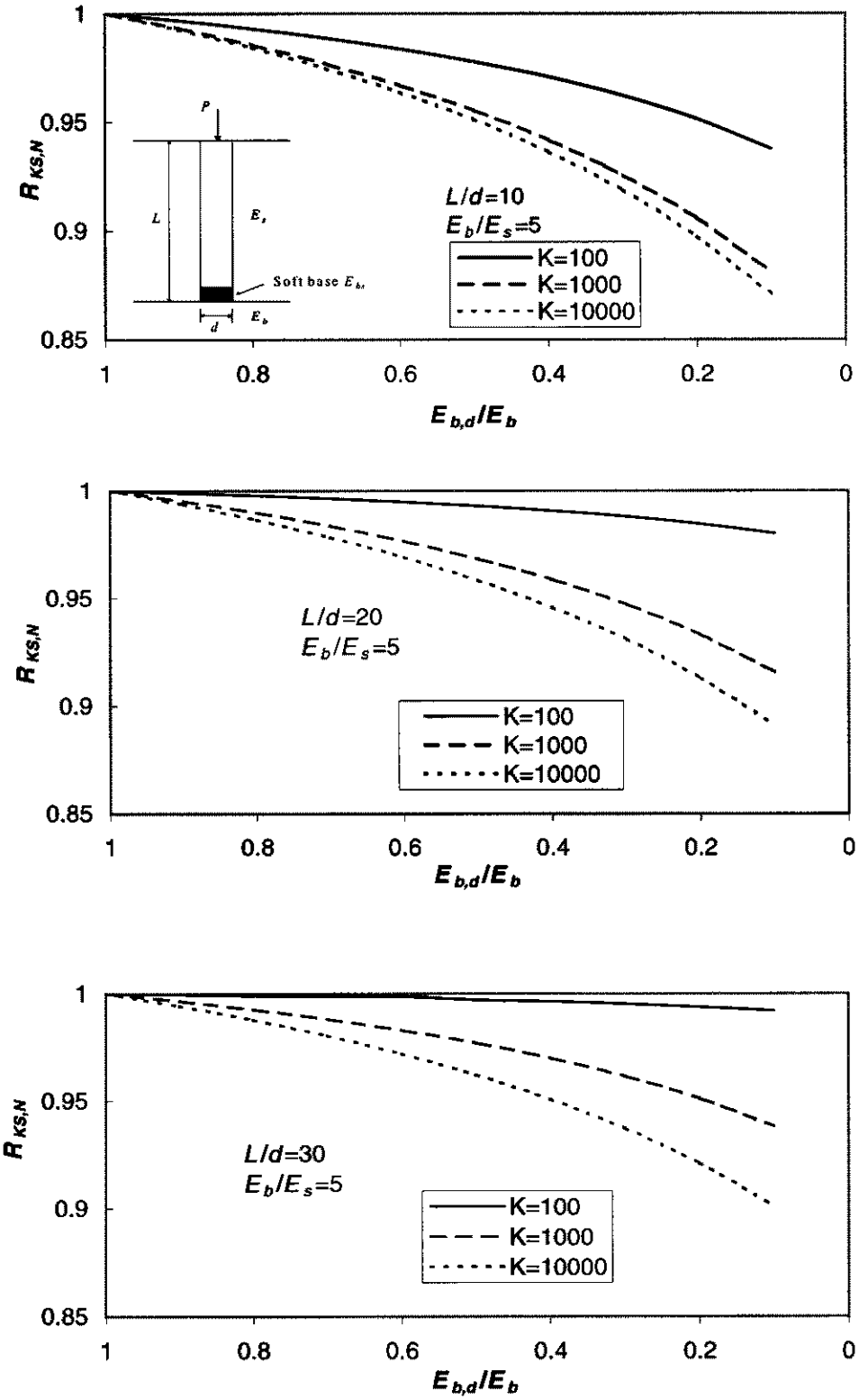

Fig. 6.13 $R_{KS,N}$ vs $E_{b,d}/E_b$ of a pile containging a soft-base

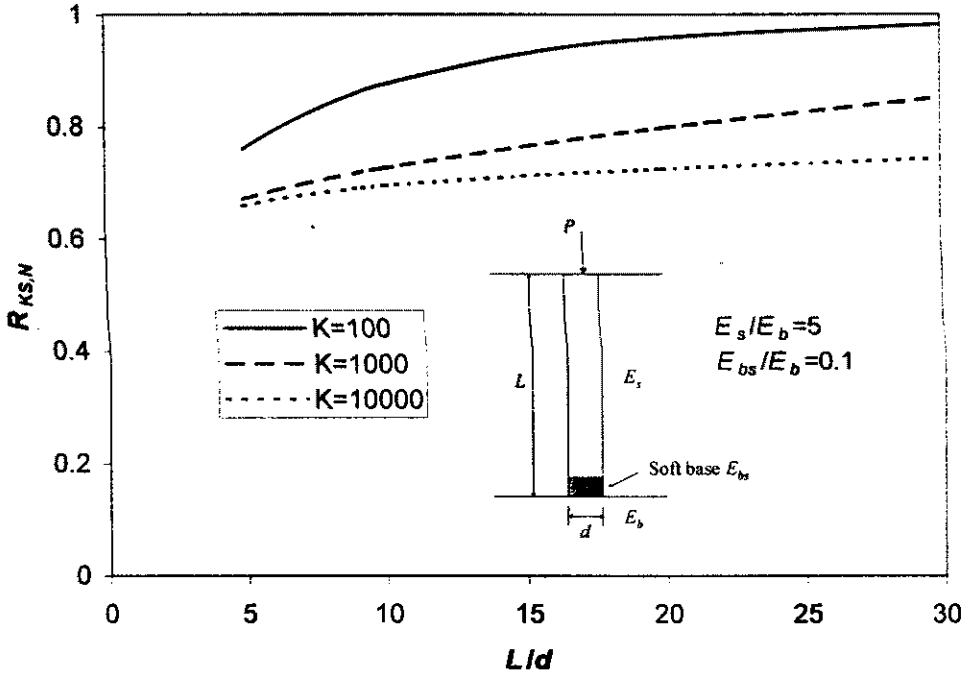

Fig. 6.14 $R_{KS,N}$ vs L/d of a pile containing a soft-base

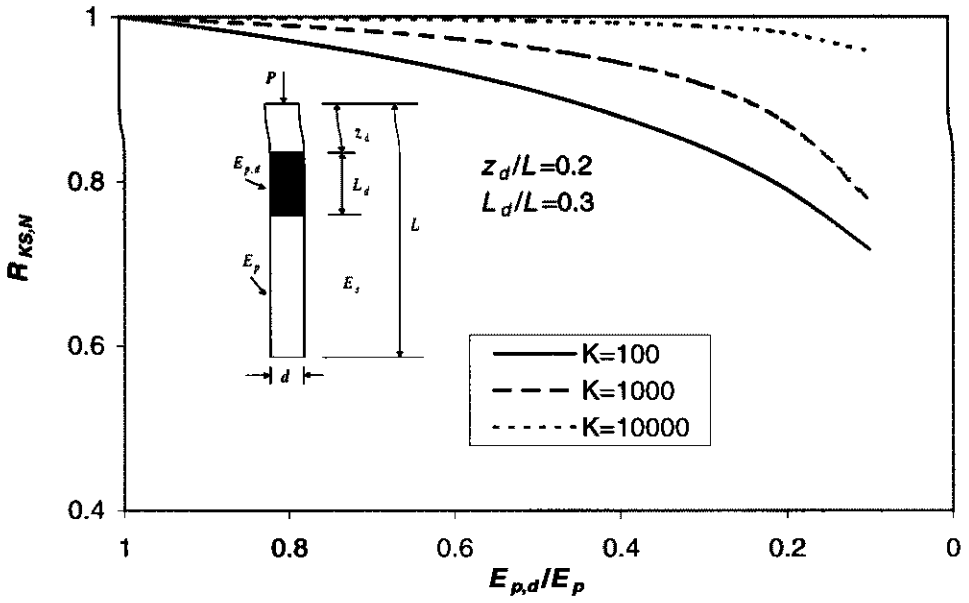

Fig. 6.15 $R_{KS,N}$ vs $E_{p,d}/E_p$ of a pile containing a honey-comb

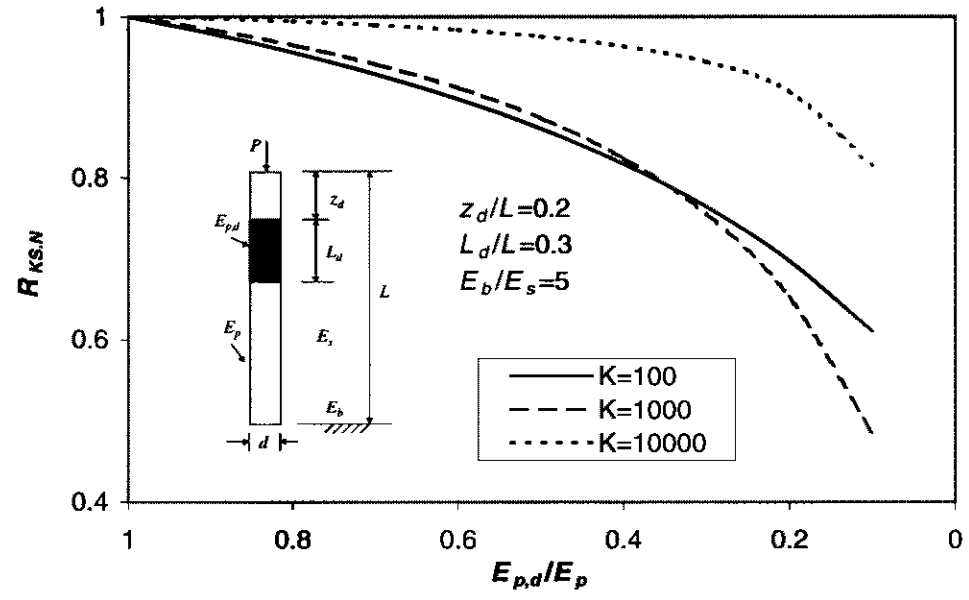

Fig. 6.16 $R_{KS,N}$ vs $E_{p,d}/E_p$ of an end-bearing pile containing a honey-comb

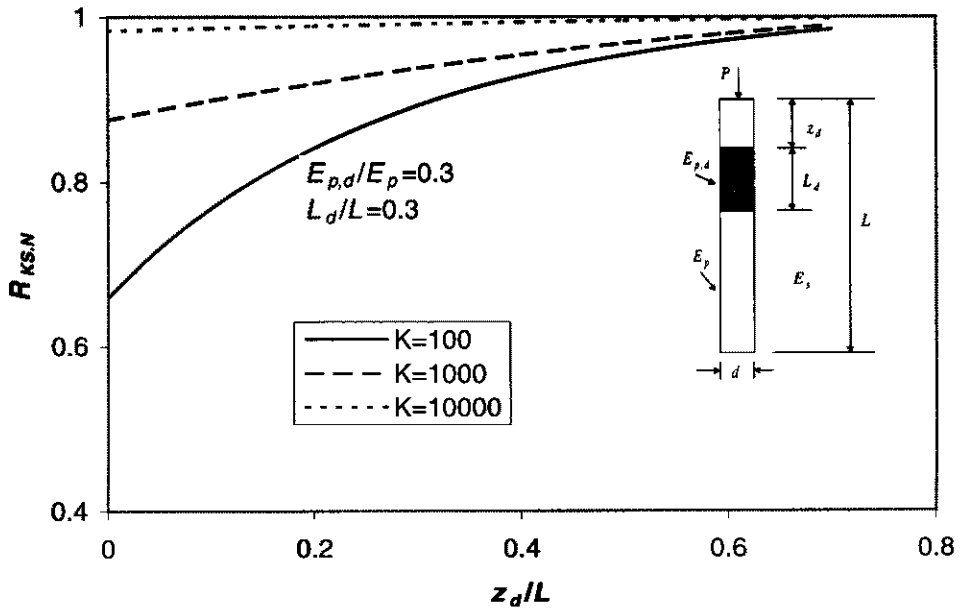

Fig. 6.17 $R_{KS,N}$ vs z_d/L of a pile containing a honey-comb

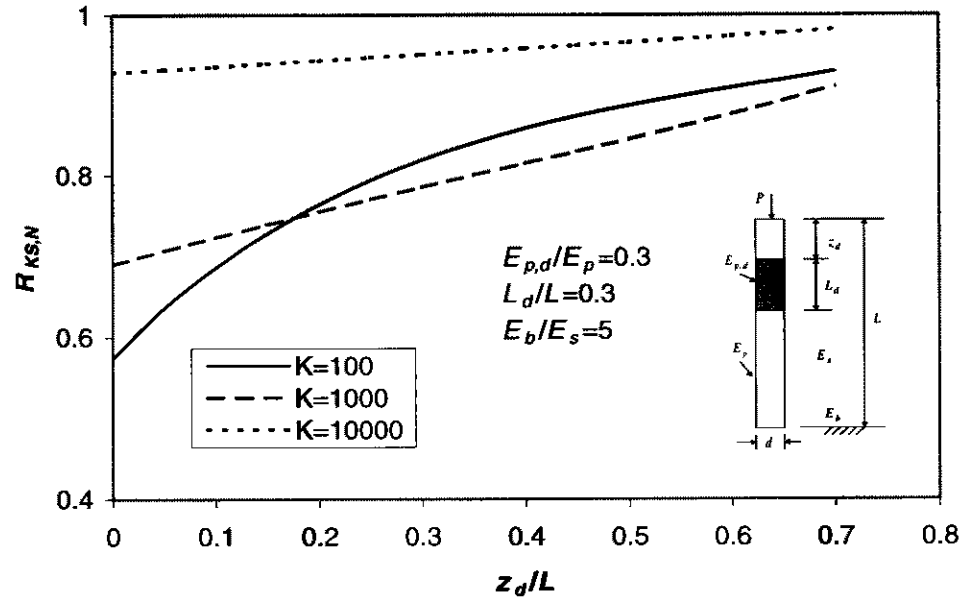

Fig. 6.18 $R_{KS,N}$ vs z_d/L of an end-bearing pile containing a honey-comb

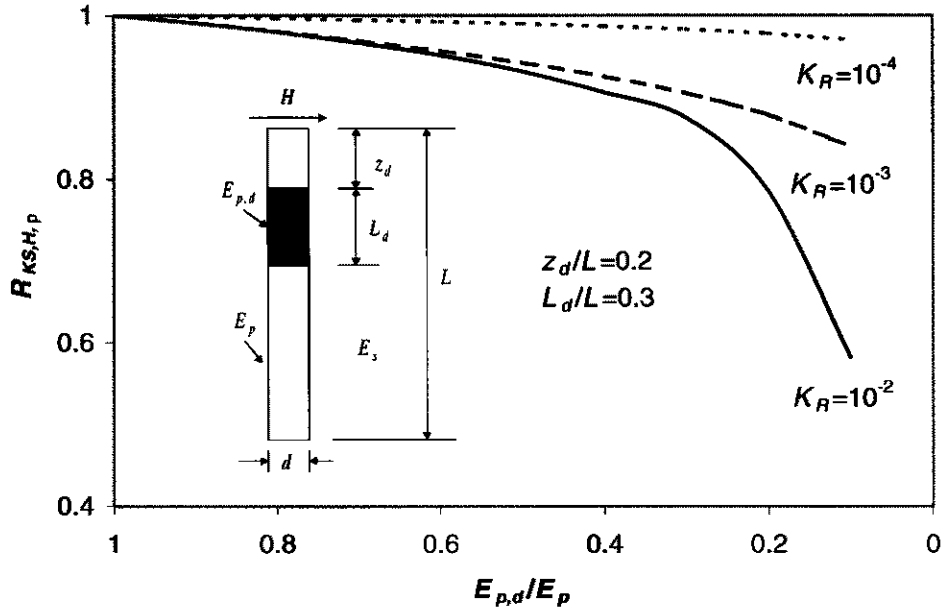

Fig. 6.19 $R_{KS,H,\rho}$ vs $E_{p,d}/E_p$ of a pile containging a honey-comb

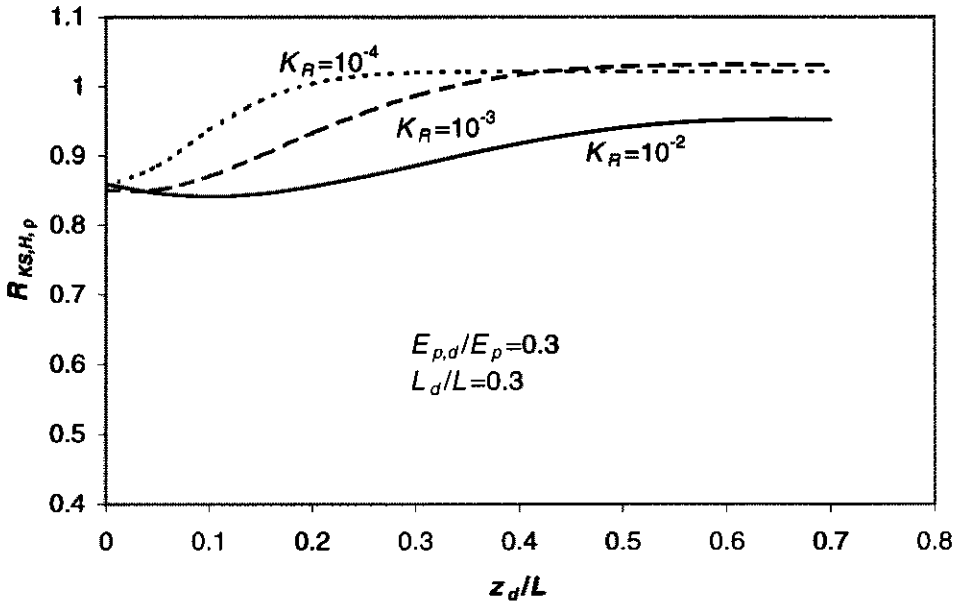

Fig. 6.20 $R_{KS,H,\rho}$ vs z_d/L of a pile containging a honey-comb

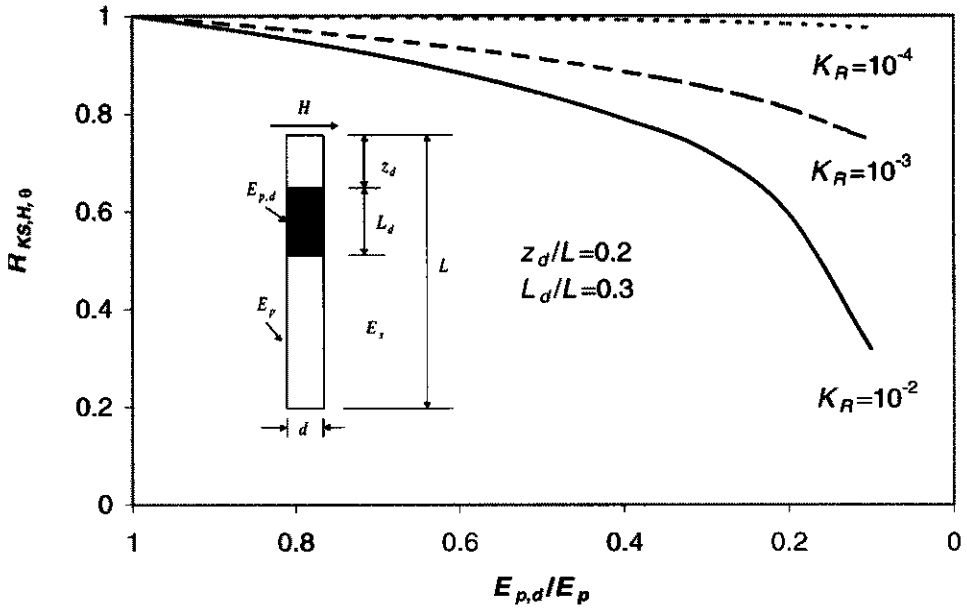

Fig. 6.21 $R_{KS,H,\theta}$ vs $E_{p,d}/E_p$ of a pile containging a honey-comb

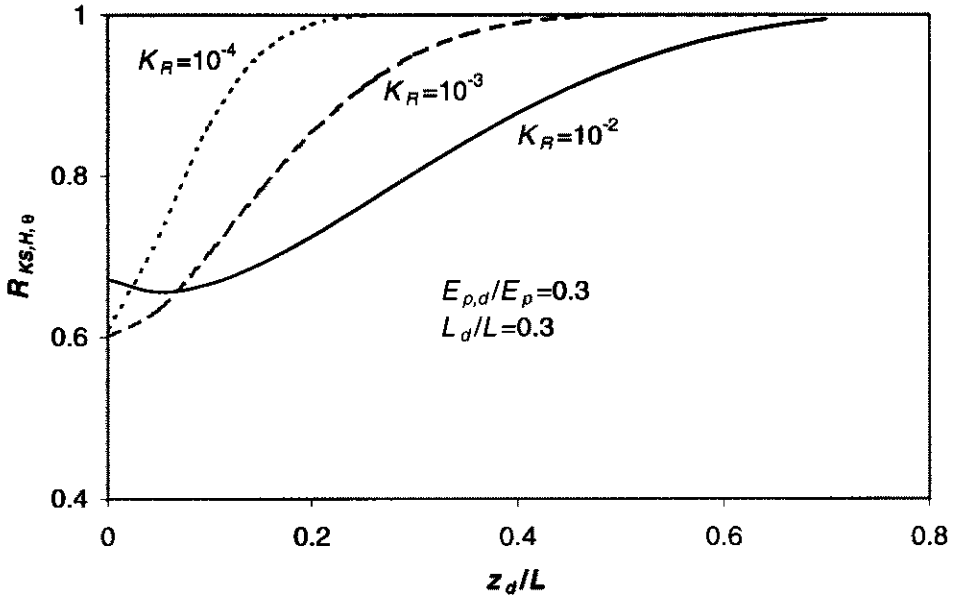

Fig. 6.22 $R_{KS,H,\theta}$ vs z_d/L of a pile containging a honey-comb

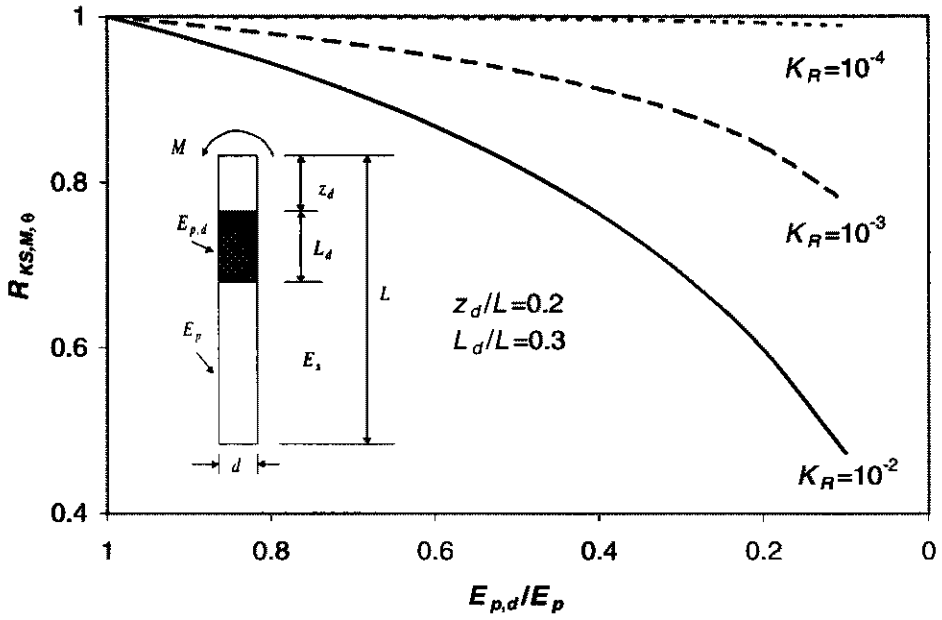

Fig. 6.23 $R_{KS,M,\theta}$ vs $E_{p,d}/E_p$ of a pile containging a honey-comb

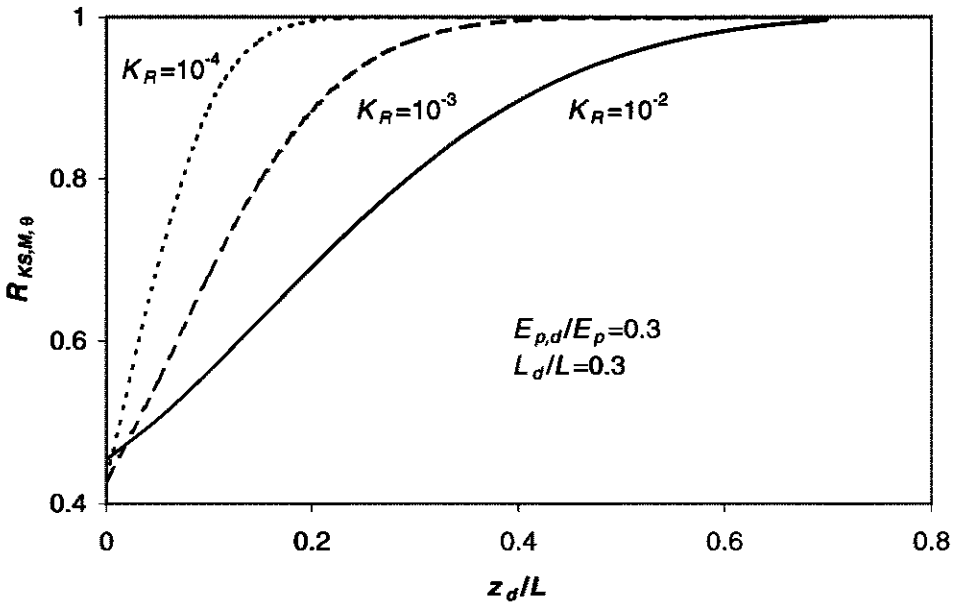

Fig. 6.24 $R_{KS,M,\theta}$ vs z_d/L of a pile containging a honey-comb

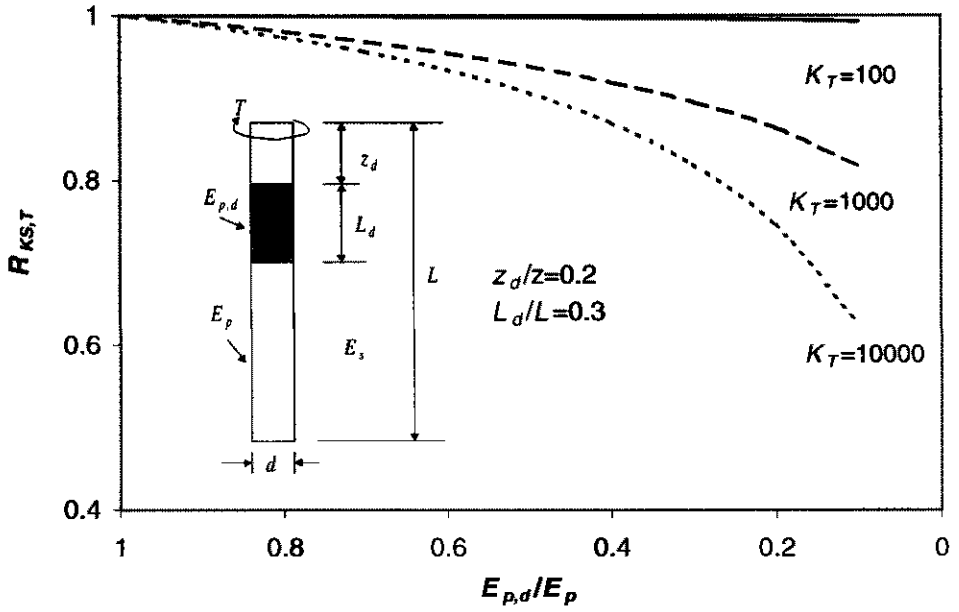

Fig. 6.25 $R_{KS,T}$ vs $E_{p,d}/E_p$ of a pile containging a honey-comb

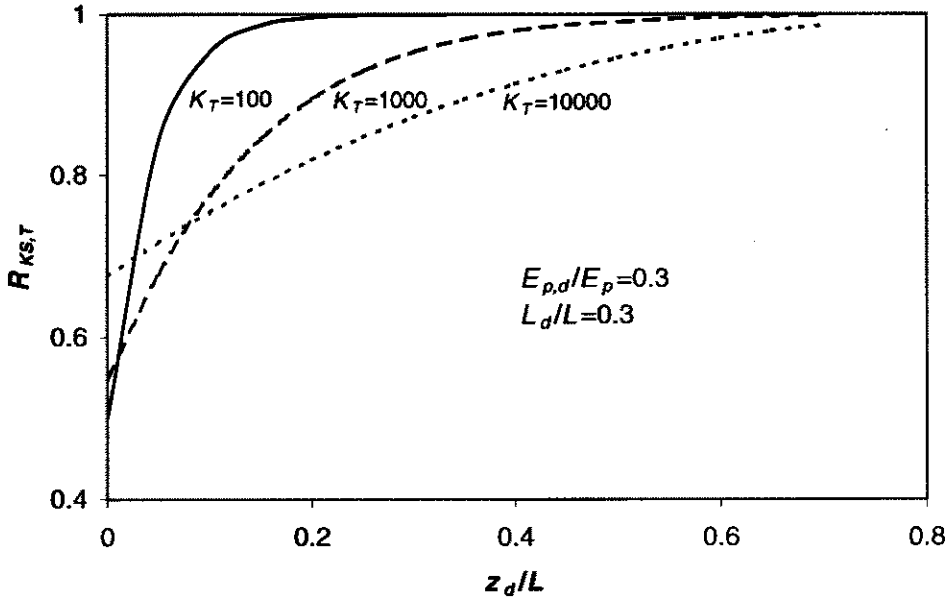

Fig. 6.26 $R_{KS,T}$ vs z_d/L of a pile containging a honey-comb

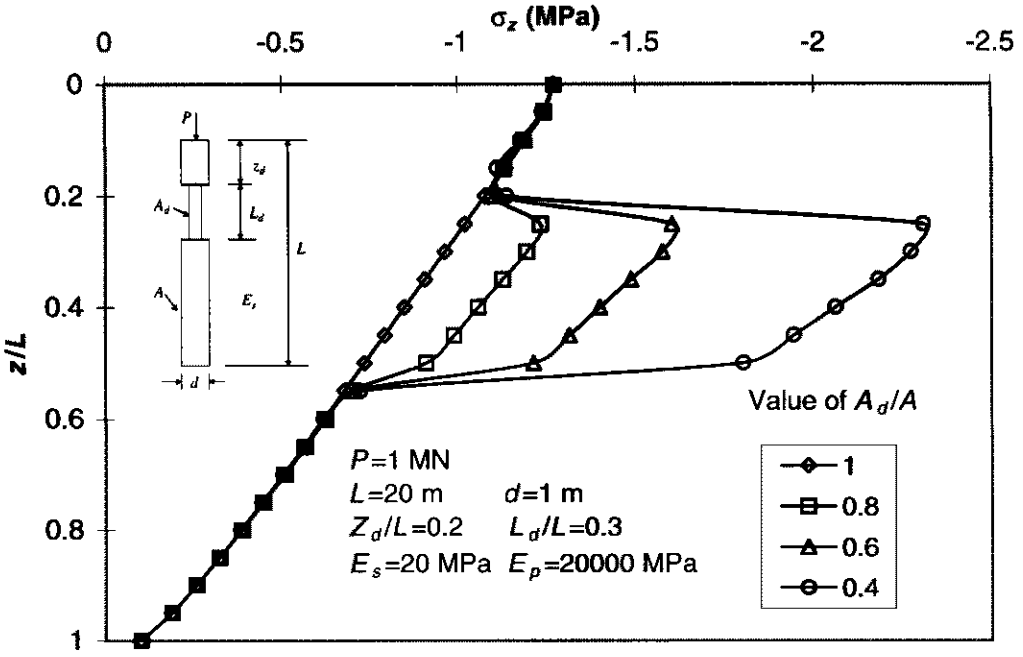

Fig. 6.27 Pile stress along necked pile

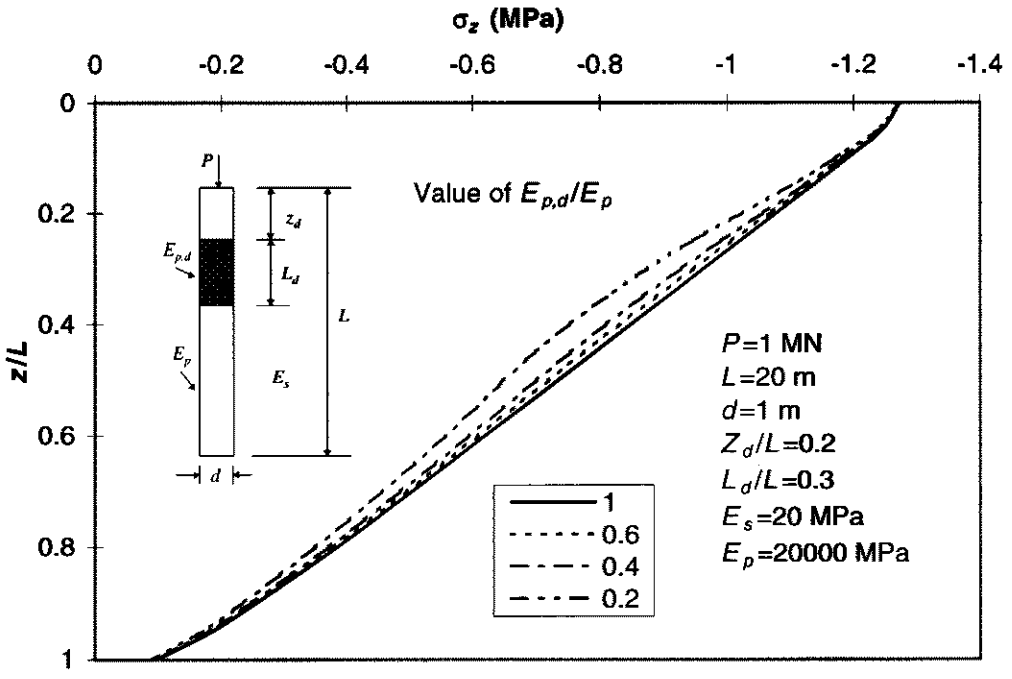

Fig. 6.28 Pile stress along honey-combed pile

Chapter 7

Interaction Analysis of Sound and Defective Piles

7.1 Introduction

The previous Chapter has presented the effects of pile defects on simple pile behaviour. However, it is also important to know how the defective piles affect other piles, *i.e.* to examine pile-soil-pile interaction problems. Elastic continuum-based approaches to the analysis of groups of piles allow for the interaction between piles to be modelled. Although the effects of non-linear soil behaviour are expected to alter the response, the elastic analysis remains a sound basis from which to study these phenomena. Interaction factors for two identical piles have been widely used to analyse pile group settlements (Poulos, 1968, Randolph and Wroth, 1979, Poulos and Davis, 1980). Interaction between two dissimilar piles was studied by Hewitt (1988) and Hull (1996). However these available solutions for interaction factors are confined to two-sound piles, and are based on a simplified definition of the interaction factors.

Based on introducing accurate definitions of interaction factors under general loadings, and using the general pile analysis, GEPAN (which is presented in Chapter 3 in detail), the interaction of two piles containing defects is analysed in this Chapter. A study is made of the interaction factors for different types of defects with different sizes and locations, under general loadings (axial, lateral, moment and torsional). The influence of a number of pile parameters (pile length, diameter, spacing, pile stiffness factor, pile flexibility factor, *etc.*), on the interaction between two piles containing defects is also presented. Some simple-but-important relationships between interaction factors for defective piles are developed from the analysis.

7.2 Definition of Interaction Factor

This part describes the general definition of interaction factors of two dissimilar piles under general loadings (such as axial, lateral, moment and torsional loading). The physical meanings of the interaction factors are presented by isolated and "interacting"

pile stiffnesses. The two kinds of interaction factors, a cross-interaction factor and an auto interaction factor, are catalogued and characterized. The effect of off-line response, which is presented in Chapter 3, is neglected in the following definitions.

7.2.1 Axial Loading

7.2.1.1 Isolated Pile 1 and Pile 2

It is assumed that an isolated pile i with an axial load-deformation stiffness K_i, develops a vertical pile head displacement $S_{s,i}$ under an axial pile head load P_i. The load-deformation behaviour of two isolated piles may be expressed as follows:

$$S_{s,1} = \frac{P_1}{K_1}$$
$$S_{s,2} = \frac{P_2}{K_2} \qquad \text{..... (7.1)}$$

where

$S_{s,i}$ = axial head displacement on pile i

P_i = axial head load on pile i

K_i = axial stiffness of pile i

7.2.1.2 Interacting Pile 1 and Pile 2

Unlike the isolated piles, the interaction of a group of two piles is now considered. Using the concept of interaction stiffness, the load-deformation behaviour of a group of two interacting piles is described as follows:

$$S_1 = \frac{P_1}{K_{11}} + \frac{P_2}{K_{12}}$$
$$S_2 = \frac{P_1}{K_{21}} + \frac{P_2}{K_{22}} \qquad \text{..... (7.2)}$$

where

S_i = axial head displacement on pile i

P_i = axial head load on pile i

K_{ij} = axial interaction stiffness of pile i due to load P_j on pile j

7.2.1.3 Axial Interaction Factors of Two Piles

Alternatively but more effectively, the load-deformation behaviour of these two interacting piles can be expressed by the stiffness of corresponding isolated piles and by interaction factors, *i.e.*

$$S_1 = \alpha_{11}\frac{P_1}{K_1} + \alpha_{12}\frac{P_2}{K_2}$$
$$S_2 = \alpha_{21}\frac{P_1}{K_1} + \alpha_{22}\frac{P_2}{K_2} \qquad \text{..... (7.3)}$$

where

α_{ij}= axial interaction factor of pile i on pile j

$$\alpha_{ij} = \frac{K_j}{K_{ij}} \qquad \text{..... (7.4)}$$

From above expression, the physical meaning of the axial interaction factor is the ratio of an isolated pile stiffness to an interacted pile stiffness.

7.2.2 Lateral Loading

Similar to the axial interaction factor defined above, the interaction behaviour of a group of two piles will be described in terms of lateral interaction factors. However, the coupling effect of a horizontal displacement and a rotation at the pile head needs to be considered.

7.2.2.1 Isolated Pile 1 and Pile 2

It is assumed that, an isolated pile 1 to be loaded a horizontal force H_1 and moment M_1 on the pile head, and isolated pile 2 with H_2 and M_2. The head horizontal displacement and rotation of these piles may be expressed as follows:

$$\rho_{s,1} = \frac{H_1}{K_{\rho H,1}} + \frac{M_1}{K_{\rho M,1}}$$
$$\rho_{s,2} = \frac{H_2}{K_{\rho H,2}} + \frac{M_2}{K_{\rho M,2}}$$
$$\theta_{s,1} = \frac{H_1}{K_{\theta H,1}} + \frac{M_1}{K_{\theta M,1}} \qquad \text{..... (7.5)}$$
$$\theta_{s,2} = \frac{H_2}{K_{\theta H,2}} + \frac{M_2}{K_{\theta M,2}}$$

where

$\rho_{s,i}$ = lateral head displacement on pile i

$\theta_{s,i}$ = head rotation on pile i

H_i = lateral head load on pile i

M_i = head bending moment on pile i

$K_{\omega F,i}$ = lateral (moment) stiffness of movement ω due to load F on pile i

7.2.2.2 Interacting Pile 1 and Pile 2

For a group of two interacting piles, in which pile1 is loaded by H_1 and M_1 and pile 2 is loaded by H_2 and M_2, the horizontal displacement and rotation of these interacting piles can be presented in terms of interacting pile stiffnesses as follows:

$$\rho_1 = \frac{H_1}{K_{\rho H,11}} + \frac{M_1}{K_{\rho M,11}} + \frac{H_2}{K_{\rho H,12}} + \frac{M_2}{K_{\rho M,12}}$$
$$\rho_2 = \frac{H_1}{K_{\rho H,21}} + \frac{M_1}{K_{\rho M,21}} + \frac{H_2}{K_{\rho H,22}} + \frac{M_2}{K_{\rho M,22}} \qquad \text{..... (7.6)}$$
$$\theta_1 = \frac{H_1}{K_{\theta H,11}} + \frac{M_1}{K_{\theta M,11}} + \frac{H_2}{K_{\theta H,12}} + \frac{M_2}{K_{\theta M,12}}$$
$$\theta_2 = \frac{H_1}{K_{\theta H,21}} + \frac{M_1}{K_{\theta M,21}} + \frac{H_2}{K_{\theta H,22}} + \frac{M_2}{K_{\theta M,22}}$$

where

ρ_i = horizontal pile head displacement on pile i

θ_i = pile head rotation on pile i

H_i = lateral head load on pile i

M_i = head bending moment on pile i

$K_{\omega F,ij}$ = lateral (moment) interaction stiffness of displacement ω on pile i due to load F on pile j

7.2.2.3 Lateral Interaction Factors of Two Piles

The lateral load-deformation behaviour of these two interacting piles can be expressed by the lateral stiffness of corresponding isolated piles and some lateral interaction factors, *i.e.*

$$\begin{aligned}
\rho_1 &= \alpha_{\rho H,11}\frac{H_1}{K_{\rho H,1}} + \alpha_{\rho M,11}\frac{M_1}{K_{\rho M,1}} + \alpha_{\rho H,12}\frac{H_2}{K_{\rho H,2}} + \alpha_{\rho M,12}\frac{M_2}{K_{\rho M,2}} \\
\rho_2 &= \alpha_{\rho H,21}\frac{H_1}{K_{\rho H,1}} + \alpha_{\rho M,21}\frac{M_1}{K_{\rho M,1}} + \alpha_{\rho H,22}\frac{H_2}{K_{\rho H,2}} + \alpha_{\rho M,22}\frac{M_2}{K_{\rho M,2}} \\
\theta_1 &= \alpha_{\theta H,11}\frac{H_1}{K_{\theta H,1}} + \alpha_{\theta M,11}\frac{M_1}{K_{\theta M,1}} + \alpha_{\theta H,12}\frac{H_2}{K_{\theta H,2}} + \alpha_{\theta M,12}\frac{M_2}{K_{\theta M,2}} \\
\theta_2 &= \alpha_{\theta H,21}\frac{H_1}{K_{\theta H,1}} + \alpha_{\theta M,21}\frac{M_1}{K_{\theta M,1}} + \alpha_{\theta H,22}\frac{H_2}{K_{\theta H,2}} + \alpha_{\theta M,22}\frac{M_2}{K_{\theta M,2}}
\end{aligned} \quad \text{..... (7.7)}$$

where

$\alpha_{\omega F,ij}$= lateral (moment) interaction factor of head movement ω of pile i due to pile head load F on pile j

$$\alpha_{\omega F,ij} = \frac{K_{\omega F,i}}{K_{\omega F,ij}} \quad \text{..... (7.8)}$$

By the reciprocal theorem, for the elastic case

$\alpha_{\rho M,12} = \alpha_{\theta H,21}$ ..... (7.9.1)

$\alpha_{\rho M,21} = \alpha_{\theta H,12}$ ..... (7.9.2)

The physical meaning of the lateral (moment) interaction factor is the stiffness ratio of an isolated pile and an interacting pile.

7.2.3 Torsional Loading

As with the definitions for axial loading, the torsional interaction factor can be defined in terms of torsional pile stiffness. The definitions of the torsional stiffness and interaction factors are as follows:

7.2.3.1 Isolated Pile 1 and Pile 2

$$\phi_{s,1} = \frac{T_1}{K_{\phi,1}}$$
$$\phi_{s,2} = \frac{T_2}{K_{\phi,2}} \qquad \text{..... (7.10)}$$

where

$\phi_{s,i}$ = pile head twist on single pile i

T_i = pile head torque on single pile i

$K_{\phi,i}$ = torsional stiffness of single pile i

7.2.3.2 Interacting Pile 1 and Pile 2

$$\phi_1 = \frac{T_1}{K_{\phi,11}} + \frac{T_2}{K_{\phi,12}}$$
$$\phi_2 = \frac{T_1}{K_{\phi,21}} + \frac{T_2}{K_{\phi,22}} \qquad \text{..... (7.11)}$$

where

ϕ_i = head twist on pile i

T_i = pile head torque on single pile i

$K_{\phi,ij}$ = torsional interaction stiffness of pile i due to load P_j on pile j

7.2.3.3 Torsional Interaction Factors for Two Piles

$$\phi_1 = \alpha_{\phi,11}\frac{T_1}{K_1} + \alpha_{\phi,12}\frac{T_2}{K_{\phi 2}}$$
$$\phi_2 = \alpha_{\phi,21}\frac{T_1}{K_1} + \alpha_{\phi,22}\frac{T_2}{K_2} \quad \text{..... (7.12)}$$

where

$\alpha_{\phi,ij}$ = torsional interaction factor of pile i on pile j

$$\alpha_{\phi,ij} = \frac{K_{\phi,i}}{K_{\phi,ij}} \quad \text{..... (7.13)}$$

7.2.4 Auto Interaction Factors and Cross Interaction Factors

The interaction factors influenced by the own pile loading are called "auto interaction factors", *e.g.*, α_{11}, α_{22}, $\alpha_{\rho H,11}$, $\alpha_{\rho H,22}$, $\alpha_{T,11}$, *etc.*. The interaction factors due to other pile loading are "called cross interaction factors", *e.g.*, α_{12}, α_{21}, $\alpha_{\rho H,12}$, $\alpha_{\rho H,21}$, $\alpha_{T,12}$ and so on.

7.3 Comparisons for Axial Loading

This section shows the comparisons of pile head settlements in a group of two piles containing defects, via the computer program GEPAN and DAMPA. The problem is illustrated in Table 7.1. There are two piles embedded in a layer of soil in which the Young's modulus is assumed as 20 *MPa*. Pile 1 is sound with length L = 20 *m*, diameter d = 1 *m* and base Young's modulus E_p=100 *MPa*, while pile 2 contains a neck and honey-

comb in which A_d/A=0.5 and $E_{p,d}/E_p$ = 0.5. Pile 1 is not loaded while pile 2 is loaded with P_2 = 1 *MN*. The number of depth divisions for the pile element is 20 for both programs, while there are 4 circumference divisions of each pile element for GEPAN and 1 for DAMPA (cylindrical element). It is found that the results of GEPAN and DAMPA agree well (to within 4%) over extensive ranges of spacing s (1.5 m to 20 m) and pile stiffness factor K (100 to 10000).

7.4 Interaction Behaviour of Two Piles under Axial Loading

The interaction of two piles, under axial loading, containing defects is analyzed in this section. The interaction factors for intact-intact piles, damaged-damaged piles and damaged-intact (intact-damaged) piles, are carried out for various dimensionless values of s/d, K, E_b/E_s *etc.*

7.4.1 Intact Pile to Intact Pile

The cross interaction factors α_{12} (= α_{21}, via the reciprocal theorem) for two floating intact piles, are shown in Fig. 7.1, as a function of dimensionless pile spacing s/d. As expected, the decreasing interaction with increasing spacing is clearly shown in the figure. But in contrast to the cross interaction factors, the auto interaction factors α_{11} (= α_{22}), shown in Fig. 7.2, increase when s/d increases. It is shown that the effect of auto interaction is much smaller than cross interaction. The auto interaction factors approach 1 when $s/d \geq 5$, but decrease significantly when $s/d<5$. It should be noted that the values of auto interaction factors are less than 1 due to the existence of the load-free pile.

Figs. 7.3 and 7.4 show the cross/auto interaction factors for two end-bearing intact piles. The general tendency of the interaction factors for the two end-bearing intact-intact piles is similar with for the two floating intact-intact piles. The cross interaction factors for the end-bearing piles are smaller than for the floating piles in particularly for a very compressible pile (K=100), but the auto interaction factors for the end-bearing piles are almost the same as for the floating piles.

7.4.2 Damaged Pile to Damaged Pile

The cross interaction factors α_{12} (= α_{21}) of a group of two floating identical necked piles is analyzed, as shown in Figs. 7.5, and show a tendency which is similar with the two floating identical intact piles. However, the interaction factor values are smaller than those for the two floating identical intact piles. The cross interaction factors for two end-bearing identically damaged piles are plotted in Fig. 7.7, and here, the values are smaller than those for the floating piles shown in Fig. 7.5. The auto interaction factors, α_{11} (= α_{22}), of the two floating/end-bearing identical necked piles, as shown in Figs. 7.6 and 7.8, are similar with those of the corresponding intact piles; the values are less, but approach 1.

Compared with the cases of two intact-intact piles (Figs. 7.1 to 7.4) and two damaged-damaged piles (Figs. 7.5 to 7.8), the cross interaction factors of two identically damaged-damaged piles are smaller than of two identical intact-intact piles, especially for very compressible piles (K=100), but the differences between auto interaction factors for two identical damaged-damaged and intact-intact piles are small.

7.4.3 Intact Pile to Damaged Pile

The interaction of two intact-damaged piles (assuming pile 1 intact and pile 2 damaged), is analyzed in this part. The cross interaction factors, α_{12} and α_{21}, of two floating intact-damaged piles are shown in Figs. 7.9 and the solution for the corresponding end-bearing piles are shown in Fig. 7.11. It is found that the value of the cross interaction factors α_{12} (interaction factor of intact pile 1 on damaged pile 2) is not reciprocal to the value of α_{21} (interaction factor of damaged pile 2 on intact pile 1). The value of α_{12} is larger than α_{21}, particularly for very compressible piles.

The auto interaction factors, α_{11} and α_{22}, of two floating intact-damaged piles are illustrated in Fig. 7.10 and in Fig. 7.12 for the corresponding end-bearing piles. The difference in the values of α_{11} and α_{22} is quite small, and all values of the auto interaction factors are less than but nearly equal to 1.

Compared with Figs. 7.9 to 7.12, the cross interaction factors for the two ending-bearing piles are less than those of the floating piles, while the auto interaction factors of the two end-bearing piles are slightly larger than those of the floating piles.

7.4.4 Approximate Expressions for the Interaction Factors of Two Piles

As mentioned above, if the pile spacing is not very close (*e.g.*, $s/d \geq 4$), the auto interaction factors are almost 1. In this case, from equation 7.3, the expression for the load-deformation of two interacting piles in terms of interaction factors, can then be simplified as follows:

$$S_1 \approx \frac{P_1}{K_1} + \alpha_{12}\frac{P_2}{K_2}$$
$$S_2 \approx \alpha_{21}\frac{P_1}{K_1} + \frac{P_2}{K_2} \qquad \text{..... (7.14)}$$

The simplified expressions for the interaction factors are the same as the definition by Poulos *et al* (1980).

7.4.5 Relationships for Cross Interaction Factors of Two Piles Containing Defects

From above analysis, it can be seen that the cross interaction factors are critical factors in the interaction analysis. The relationships for cross interaction factors of two piles containing defects will be developed in this section.

For convenience in the analysis of the interaction of defective piles, the following symbols for cross interaction factors are defined:

α_{ii} = cross interaction factor of two identical intact piles .....(7.15a)

α_{dd} = cross interaction factor of two identical damaged piles .....(7.15b)

α_{id} = cross interaction factor of the intact pile on the damaged pile ....(7.15c)

α_{di} = cross interaction factor of the damaged pile on the intact pile ...(7.15d)

Compared with the cross interaction factors defined in Section 7.2, the relationships of these definitions can be set up as follows:

α_{ii} = α_{12} or α_{21} for two identical intact piles .....(7.16a)

α_{dd} = α_{12} or α_{21} for two identical damaged piles .....(7.16b)

α_{id} = α_{12} (interaction factor of intact pile 1 on damaged pile 2) .....(7.16c)

α_{di} = α_{21} (interaction factor of damaged pile 2 on intact pile 1) .....(7.16d)

Fig. 7.13 shows the newly-introduced interaction factors for two floating piles containing a neck, as a function of dimensionless pile spacing *s/d*, and in Fig. 7.14 for two end-bearing piles. Furthermore, the interaction factors of two defective piles, for various values of ratio of neck length L_d/L, ratio of neck area A_d/A, pile stiffness factor K, ratio of base and soil Young's modulus E_b/E_s, are shown in Figs. 7.15 to 7.18.

From Figs. 7.13 to 7.18, the approximate relationships for the cross interaction factors for defective piles are found to be as follows:

$$\alpha_{di} = \alpha_{ii} \quad \text{.....} \quad (7.17)$$

$$\alpha_{id} = \alpha_{dd} \quad \text{.....} \quad (7.18)$$

In other words, the cross interaction factor of the damaged pile on the intact pile α_{di} is approximately equal to cross interaction factor of two identical intact-intact piles α_{ii}. The cross interaction factor of the intact pile on the damaged pile α_{id} is approximately equal to the cross interaction factor of two identical damaged-damaged piles α_{dd}.

Equations 7.17 and 7.18 have considerable significance in the interaction analysis of a group of defective piles. Firstly, the interaction factor α_{id} (or α_{12}) can be easily obtained from the cross interaction factor of two identical damaged-damaged piles. Secondly, programs based on interaction factors for sound piles, such as DEFPIG (Poulos, 1990a),

PIGLET (Randolph, 1989), DAMPIG (Poulos, 1997), can be extend to analyse defective piles, if the interaction factor α_{id} (α_{12}) is incorporated into these programs. Third, the above equations can be used to develop a general "conservation" equation for the interaction factors of two dissimilar piles:

$$\alpha_{di}\,\alpha_{id} = \alpha_{ii}\,\alpha_{dd} \quad \text{..... (7.19)}$$

7.4.6 Cross Interaction Factor α_{12} (α_{id}) for Defective Piles

As presented above, the cross interaction factor α_{12} (or α_{id}) is a key factor in the interaction analysis for two piles containing defects. This section will illustrate some parametric effects on interaction factors of the defective piles.

7.4.6.1 Effect of Length of Defect

The interaction factors, α_{12} (or α_{id}), of two piles for various values of ratios of necked length L_d/L and necked area A_d/A, are shown in Fig. 7.19. For severe necking (such as A_d/A=0.3, 0.1), the value of α_{12} decreases significantly as L_d/d increases for "short necking" (L_d/d <0.5), and α_{12} approximately becomes a constant for "long necking" (L_d/d =0.5). The effect of the length of defects becomes apparent if the piles are locally necked severely (*e.g.*, A_d/A= 0.1).

7.4.6.2 Effect of Position of Defect

Fig. 7.20 shows the effect of the location of a defect (neck) along the pile depth. The cross interaction factors, α_{12}, increase as the ratio of necked depth z_d/L increases, this effect being most pronounced for severe necking near the pile top. For necking near the pile tip, the effect of the defect position is small, and all values of α_{12} approach α_{ii}.

7.4.6.3 Effect of Pile Stiffness Factor

Fig. 7.21 shows the effect of the pile stiffness factor K on interaction factor α_{12} for a typical case of the interaction of intact-damaged piles. α_{12} increases as the value of K

increases. For very stiff pile (*e.g.*, $K>10^4$), the effect of the ratio of necked area A_d/A becomes small, and all values of α_{12} approach the value of α_{ii}.

7.4.6.4 End-Bearing Defective Pile on Rigid Stratum

An example of the influence of the stiffness of the bearing stratum on the interaction factors is shown in Fig. 7.22, in which interaction factors, α_{12}, are plotted against the ratio of the modulus E_b of the bearing stratum to the soil modulus E_s. α_{12} decreases significantly as E_b/E_s increases until the value of E_b/E_s is near100. When $E_b/E_s>100$, α_{12} approximately becomes a constant.

7.4.6.5 Piles Containing a Neck and a Honey-Comb

Interaction factors α_{12} for two piles, one of which contains a neck and a honey-comb, are shown in Fig. 7.23. Like the interaction of two identical intact piles, α_{12} decreases, as *s/d* increases. For defects, the more the necking and/or honey-combing, the less is the value of α_{12}.

7.4.6.6 Piles Containing a Soft-Base

Fig. 7.24 shows the effect of a soft-base on the interaction of two piles. As the ratio of soft-base Young's modulus $E_{b,s}$ to base Young's modulus E_b decreases, the interaction factor α_{12} increases. However, the interaction factor α_{12} due to soft-base decreases less than that due to a neck and/or honey-comb (which is shown in Fig. 7.23). This implies that the effect of soft-base on interaction factors is less than other defects such as a neck or honey-comb.

7.5 Interaction of Two Piles Under Non-Axial Loading

7.5.1 Lateral/Moment Loadings

Paralleling the interaction analysis of axially –loaded piles, two typical intact-damaged piles (pile 1 unloaded, intact; pile 2 loaded, necked) are examined. The intact pile is assumed to have a pile flexibility factor $K_R=10^{-3}$, and a ratio of pile length and diameter

L/d=20. The damaged pile is assumed to contain a neck and a honey-comb. The emphasis is put on studying the lateral/moment cross interaction factors of the intact pile on the damaged pile), for varying ranges of ratios of pile spacing to pile diameter s/d (0 to 20), necked area to intact area A_d/A (1 to 0.1) and honey-combed pile Young's modulus to intact pile Young's modulus $E_{p,d}/E_p$ (1 to 0.01).

As with axially-loaded piles, the auto lateral interaction factors increase as s/d increases, as shown in Fig. 7.25. Furthermore, the value of $\alpha_{\rho H,22}$ increases as defects develop. However, the value of auto lateral interaction factors $\alpha_{\rho H,22}$ is very close to 1, especially when s/d>5. Other auto lateral/moment interaction factors exhibit similar behaviour, Thus, Equation 7.7, the expression for the load-deformation of two interacted piles under lateral/moment loadings, can be simplified as follows:

$$\begin{aligned}
\rho_1 &\approx \frac{H_1}{K_{\rho H,1}} + \frac{M_1}{K_{\rho M,1}} + \alpha_{\rho H,12}\frac{H_2}{K_{\rho H,2}} + \alpha_{\rho M,12}\frac{M_2}{K_{\rho M,2}} \\
\rho_2 &\approx \alpha_{\rho H,21}\frac{H_1}{K_{\rho H,1}} + \alpha_{\rho M,21}\frac{M_1}{K_{\rho M,1}} + \frac{H_2}{K_{\rho H,2}} + \frac{M_2}{K_{\rho M,2}} \\
\theta_1 &\approx \frac{H_1}{K_{\theta H,1}} + \frac{M_1}{K_{\theta M,1}} + \alpha_{\theta H,12}\frac{H_2}{K_{\theta H,2}} + \alpha_{\theta M,12}\frac{M_2}{K_{\theta M,2}} \\
\theta_2 &\approx \alpha_{\theta H,21}\frac{H_1}{K_{\theta H,1}} + \alpha_{\theta M,21}\frac{M_1}{K_{\theta M,1}} + \frac{H_2}{K_{\theta H,2}} + \frac{M_2}{K_{\theta M,2}}
\end{aligned} \qquad \text{..... (7.20)}$$

and

$$\alpha_{\rho M,12} = \alpha_{\theta H,21}$$

$$\alpha_{\rho M,21} = \alpha_{\theta H,12}$$

This simplified expression is consistent with Poulos' definition in the interaction of two identical sound piles (1980).

Figs. 7.26 to 7.28 show lateral cross interaction factors, $\alpha_{\rho H,12}$, $\alpha_{\theta H,12}$ ($\alpha_{\rho M,12}$) and $\alpha_{\theta M,12}$ of the two piles containing a neck and honey-comb respectively. Clearly, these lateral

cross interaction factors decrease as *s/d* increases. Compared with the axial loading, the effect of neck and honey-comb on the interaction factors is substantial, and the lateral cross interaction factors decrease significantly as A_d/A and/or $E_{p,d}/E_p$ decrease. Compared with these lateral cross interaction factors under the same conditions, it is shown that the value of $\alpha_{\rho H,12}$ is the largest, $\alpha_{\theta H,12}$ ($\alpha_{\rho M,12}$) is in middle and $\alpha_{\theta M,12}$ is the smallest, This phenomenon has been confirmed by Poulos and Davis (1980) in the interaction analysis of two identical sound piles.

7.5.2 Torsional Loading

In a similar manner to the interaction analysis of laterally–loaded piles, two typically intact-damaged piles (pile 1 unloaded, intact; pile 2 loaded, necked plus honey-comb) are examined. The intact pile is assumed to have a pile torsional stiffness factor K_T = 1000, and a ratio of pile length to diameter L/d=20. The damaged pile is assumed to contain a neck and a honey-comb, for which the parameters of the defects are the same as in the lateral (moment) interaction analysis described in Section 7.5.1. The auto torsional interaction factors increase significantly as *s/d* increases, and the value of $\alpha_{T,22}$ approximately becomes 1 after s/d>3, as shown in Fig. 7.29. The value of $\alpha_{T,22}$ increases quickly as well when defects develop. Equation 7.12, the expression for the load-deformation behaviour of two interacted piles under torsional loading, can then be simplified as follows:

$$\begin{aligned} \phi_1 &\approx \frac{T_1}{K_1} + \alpha_{\phi,12}\frac{T_2}{K_{\phi 2}} \\ \phi_2 &\approx \alpha_{\phi,21}\frac{T_1}{K_1} + \frac{T_2}{K_2} \end{aligned} \qquad \text{..... (7.21)}$$

Figs. 7.30 shows torsional cross interaction factors, $\alpha_{T,12}$, decrease as *s/d* increases. The torsional cross interaction factor decreases significantly as A_d/A and/or $E_{p,d}/E_p$ decrease. Compared with those axial and lateral cross interaction factors under the same conditions, it is shown that the value of $\alpha_{T,12}$ is the smallest, which means that the torsional interaction factor is less important than the axial and lateral interaction factors.

7.6 Conclusions

By applying the program GEPAN, this Chapter analyses the interaction of two piles containing defects. The general interaction factors are defined, and the main conclusions drawn from this linear elastic analysis are as follows:

1) The "auto interaction factor" increases to 1 as *s/d* increases.
2) The "cross interaction factor" of the damaged pile on the intact pile is approximately equal to the cross interaction factor of two identical intact piles. The cross interaction factor of the intact pile on the damaged pile is approximately equal to cross interaction factor of two identical damaged piles.
3) Pile defects result in smaller cross interaction factors.
4) The influence of lateral (moment) loading on cross interaction factors of two pile containing shallow defects is larger than for axial loading.
5) The effect of a soft-base on interaction factors is less than the influence of other defects such as a neck or honey-comb.
6) The effect of torsion on interaction is less than the effects of axial and lateral loading on interaction.

It is anticipated that the nonlinearity effects will overshadow some of the linear conclusions. For example, the nonlinearity in the lateral loading mode is expected to alter the behaviour significantly, especially for piles with shallow defects. In this case, the pile behaviour will be dominated by the characteristics of the soil above the defect level. The pile discontinuity will result in stress concentration in the vicinity of the defect and the load transfer pattern will be altered.

Table 7.1 Comparison of Pile Head Settlements with GEPAN and DAMPA

Parameters:
P_1=0MN,P_2=1MN
v_s=0.3, v_p=0.3
E_s=20MPa, E_b=100MPa
L=20m, d=1m, H=100m
z_d/L=0.2, L_d/L=0.3
A_d/A=0.5, $E_{p,d}/E_p$=0.5
Element division:
depth divn. =20 (DAMPA)
depth divn. =20 (GEPAN)
circ. divn. =4 (GEPAN)

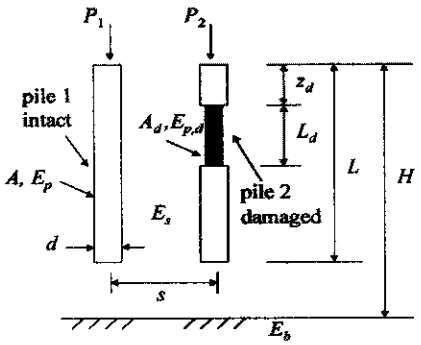

Pile Head Settlement S_z (mm) on pile 2

	K=100			K=1000			K=10000		
s (m)	GEPAN	DAMPA	RE(%)	GEPAN	DAMPA	RE(%)	GEPAN	DAMPA	RE(%)
1.5	8.7482	8.6308	1.36	4.7991	4.7982	0.02	3.9699	3.9918	-0.55
3	9.3451	9.0511	3.25	4.9301	4.8511	1.63	4.0513	4.0008	1.26
4.5	9.4817	9.1641	3.47	4.9641	4.8727	1.88	4.0717	4.0092	1.56
6	9.5301	9.2053	3.53	4.9795	4.8842	1.95	4.0816	4.0152	1.65
7.5	9.5507	9.2228	3.56	4.9879	4.8908	1.99	4.0873	4.0193	1.69
10	9.5641	9.2337	3.58	4.9947	4.8961	2.01	4.0925	4.0231	1.73
12.5	9.5684	9.2371	3.59	4.9975	4.8983	2.03	4.0949	4.0248	1.74
15	9.5701	9.2381	3.59	4.9988	4.8992	2.03	4.0961	4.0256	1.75
17.5	9.5706	9.2384	3.60	4.9994	4.8995	2.04	4.0965	4.0259	1.75
20	9.5709	9.2385	3.60	4.9996	4.8996	2.04	4.0968	4.0261	1.76

Pile Head Settlement S_z (mm) on pile 1

	K=100			K=1000			K=10000		
s (m)	GEPAN	DAMPA	R. E.	GEPAN	DAMPA	R.E.	GEPAN	DAMPA	R.E.
1.5	3.8771	3.8637	0.3	2.8794	2.8932	-0.5	2.8042	2.8172	-0.5
3	2.7301	2.7678	-1.4	2.1713	2.2032	-1.4	2.1184	2.1488	-1.4
4.5	2.1354	2.1682	-1.5	1.7769	1.8053	-1.6	1.7365	1.7639	-1.6
6	1.7464	1.7729	-1.5	1.5059	1.5303	-1.6	1.4748	1.4986	-1.6
7.5	1.4673	1.4886	-1.4	1.3021	1.3231	-1.6	1.2781	1.2988	-1.6
10	1.1408	1.1564	-1.3	1.0498	1.0666	-1.6	1.0345	1.0515	-1.6
12.5	0.9163	0.9282	-1.3	0.8655	0.8794	-1.6	0.8559	0.8701	-1.6
15	0.7529	0.7652	-1.6	0.7246	0.7364	-1.6	0.7187	0.7311	-1.7
17.5	0.6293	0.6374	-1.3	0.6139	0.6242	-1.7	0.6103	0.6211	-1.7
20	0.5332	0.5403	-1.3	0.5252	0.5344	-1.7	0.5231	0.5327	-1.8

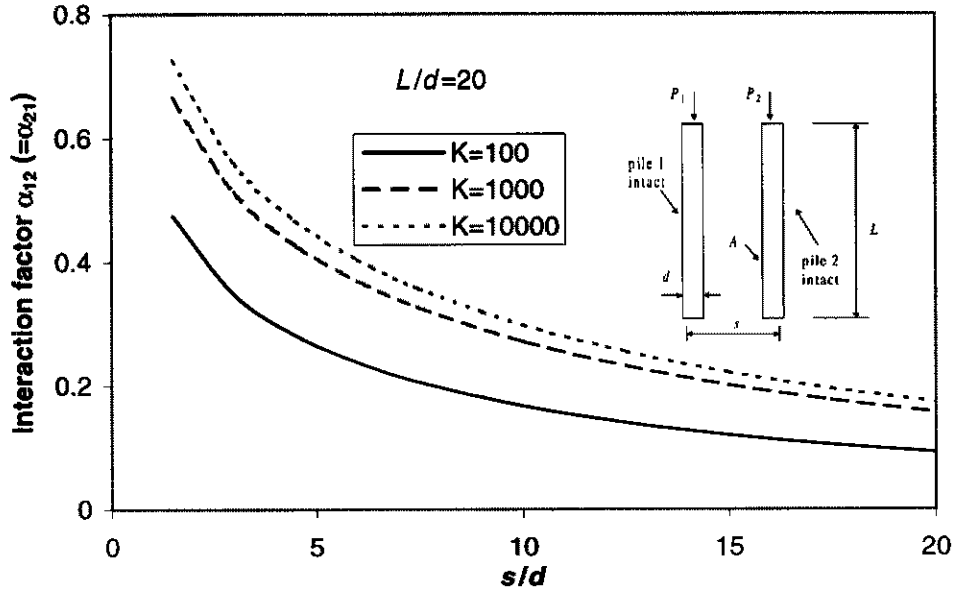

Fig. 7.1 Cross Interaction factor of two floating intact piles

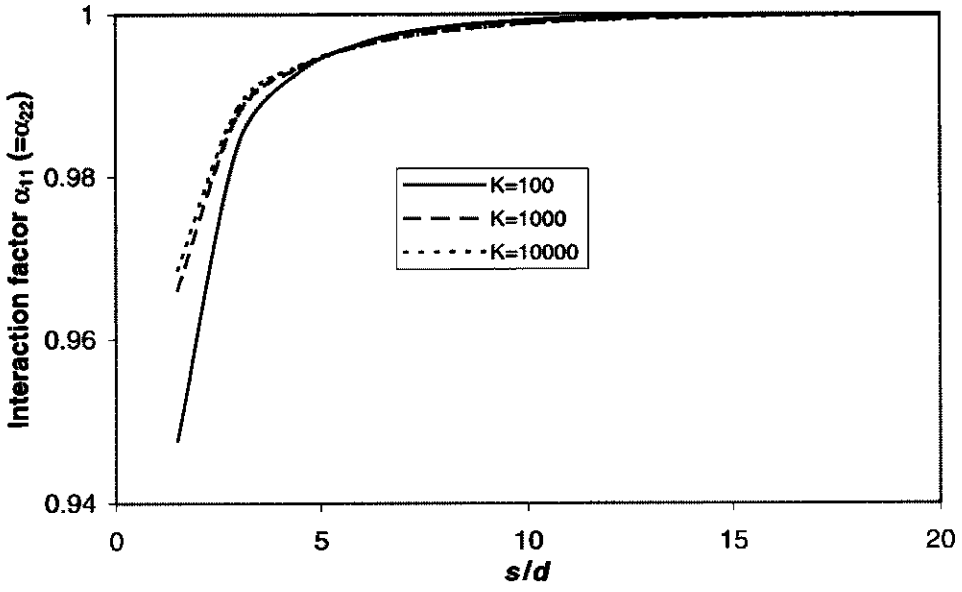

Fig. 7.2 Auto Interaction factor of two floating intact piles

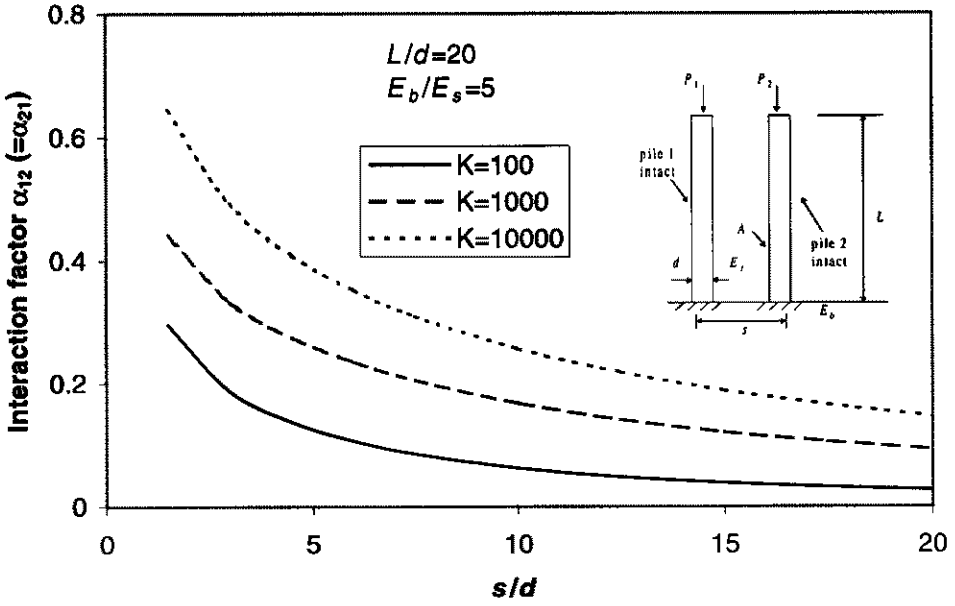

Fig. 7.3 Cross Interaction factor of two end-bearing intact piles

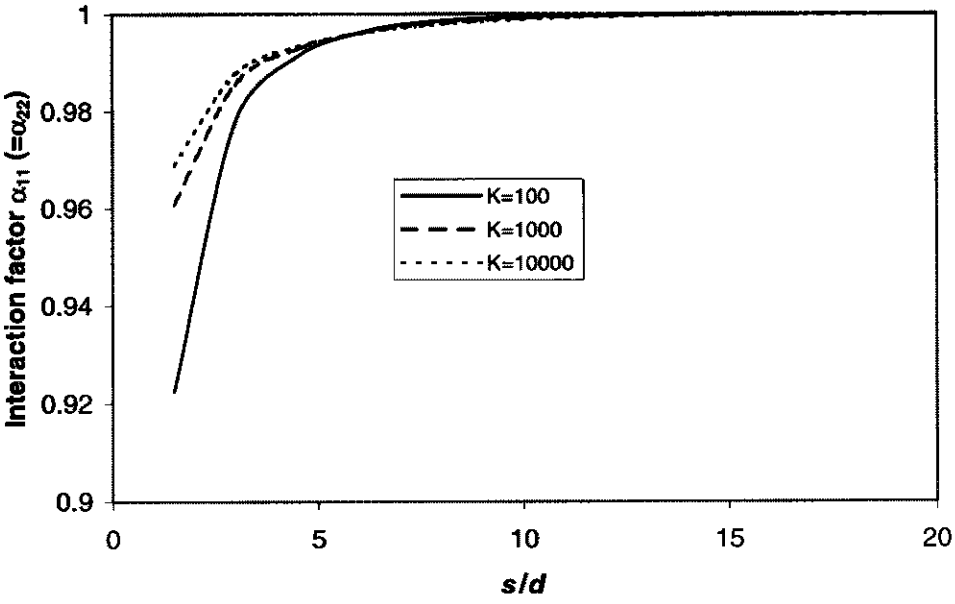

Fig. 7.4 Auto Interaction factor of two end-bearing intact piles

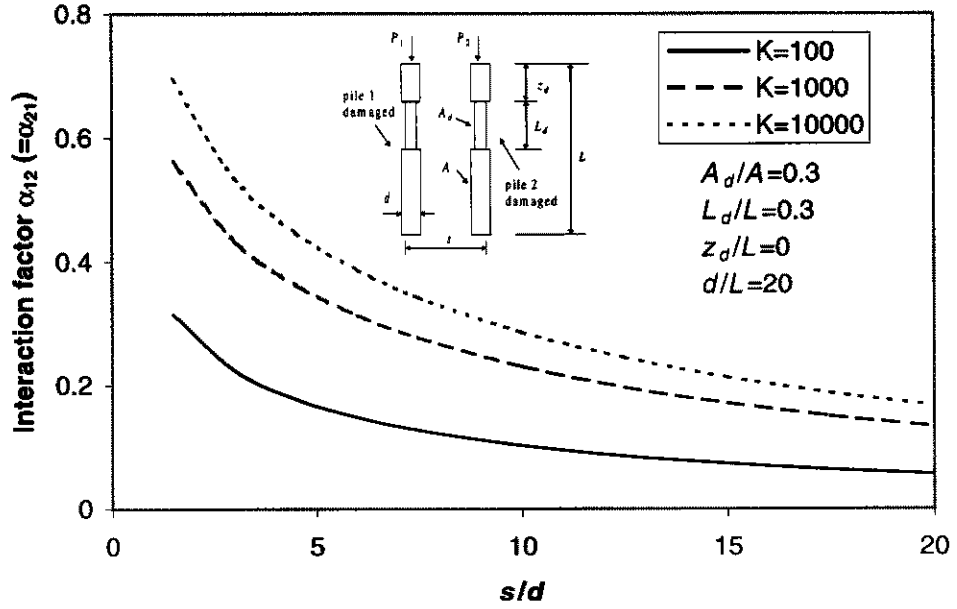

Fig. 7.5 Cross Interaction factor of two floating damaged piles

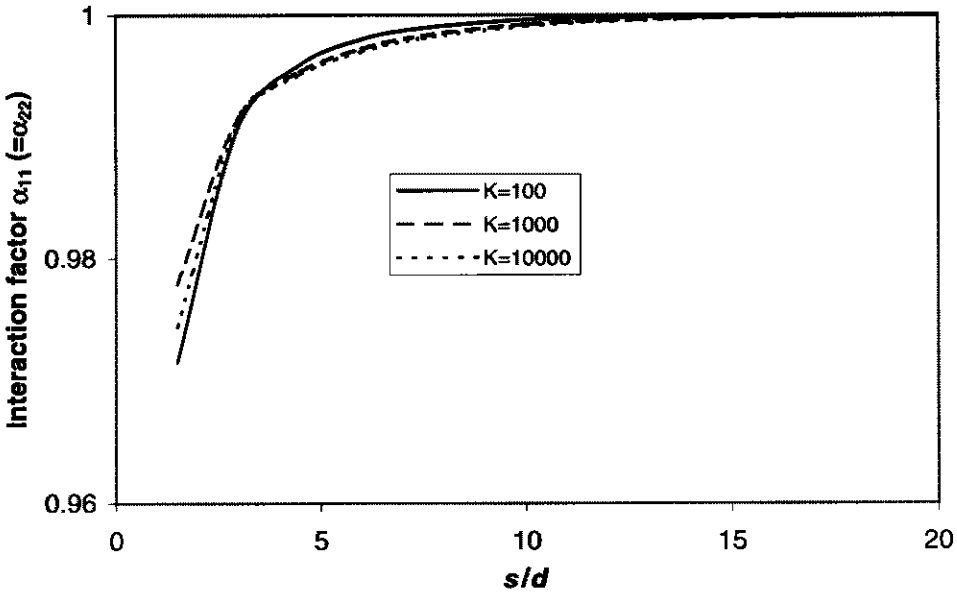

Fig. 7.6 Auto Interaction factor of two floating damaged piles

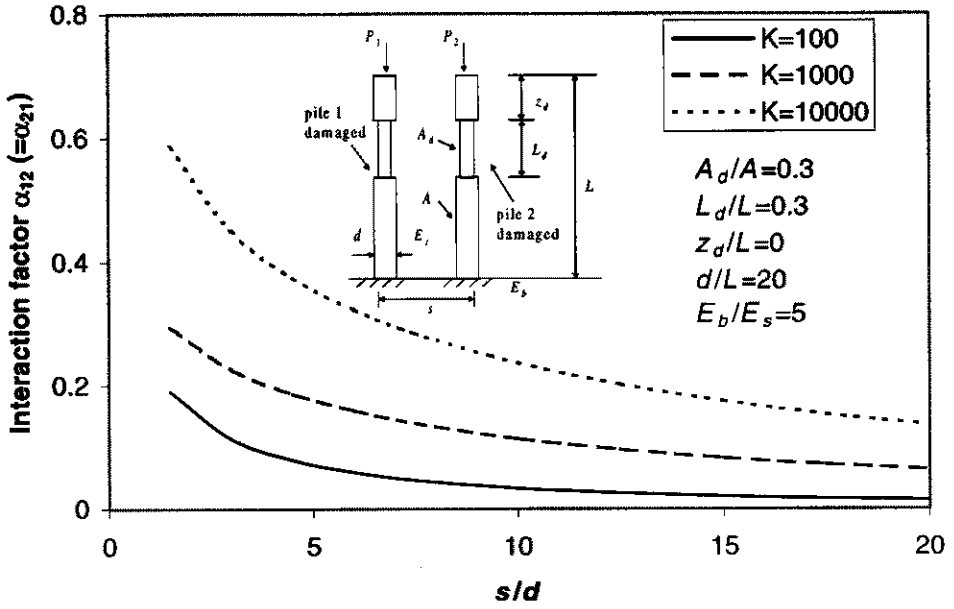

Fig. 7.7 Cross Interaction factor of two end-bearing damaged piles

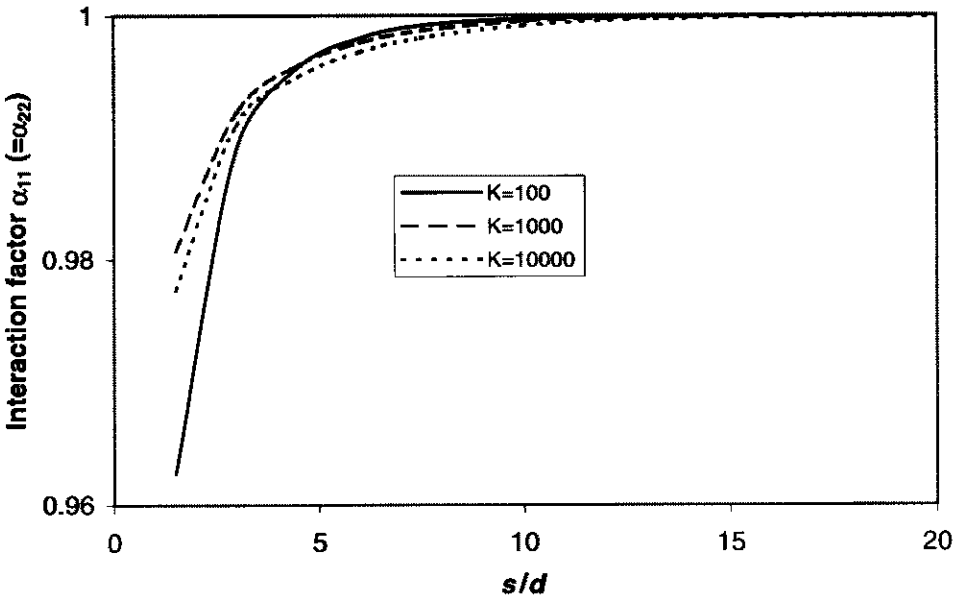

Fig. 7.8 Auto Interaction factor of two end-bearing damaged piles

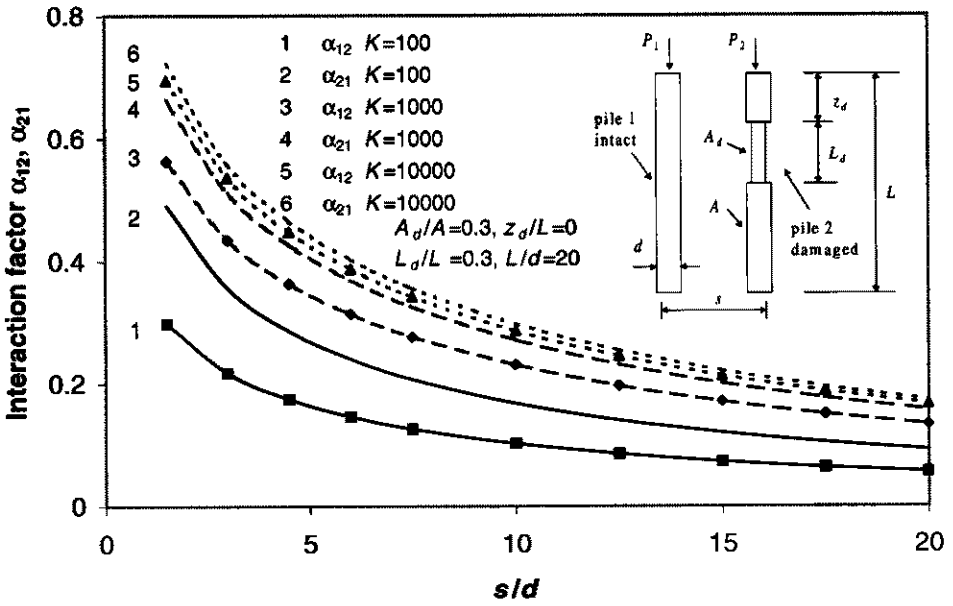

Fig. 7.9 Cross Interaction factor of two floating intact-damaged piles

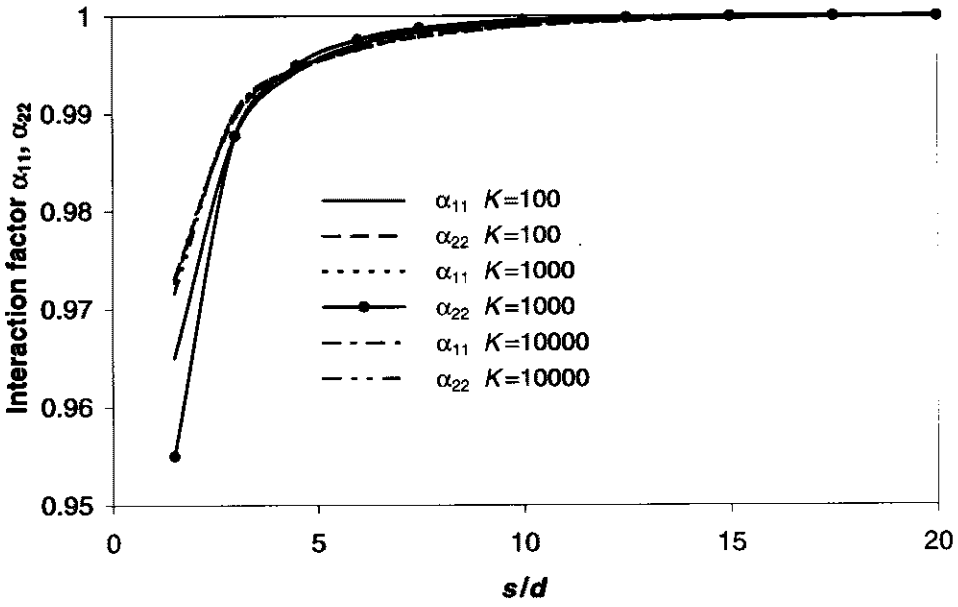

Fig. 7.10 Auto Interaction factor of two floating intact-damaged piles

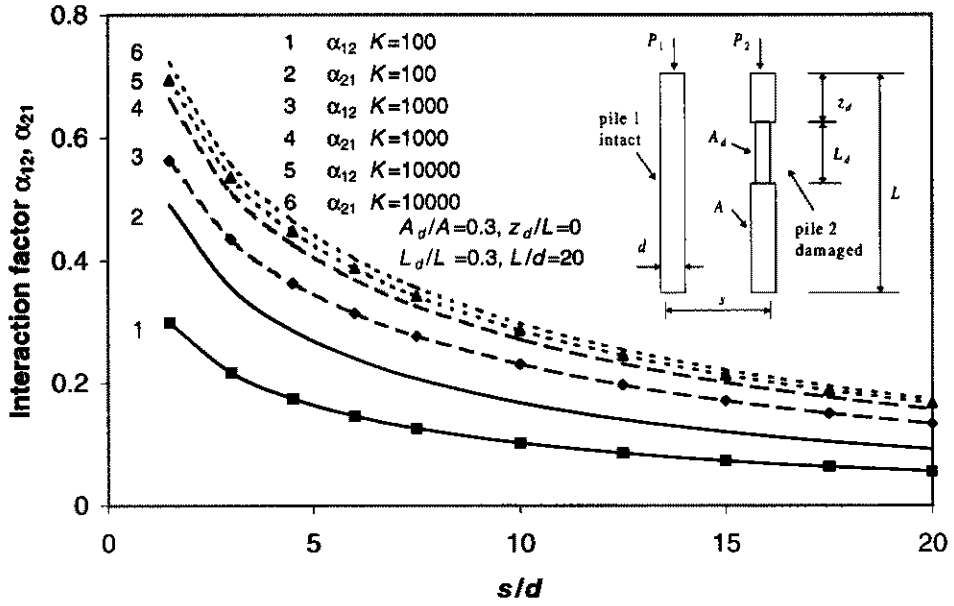

Fig. 7.9 Cross Interaction factor of two floating intact-damaged piles

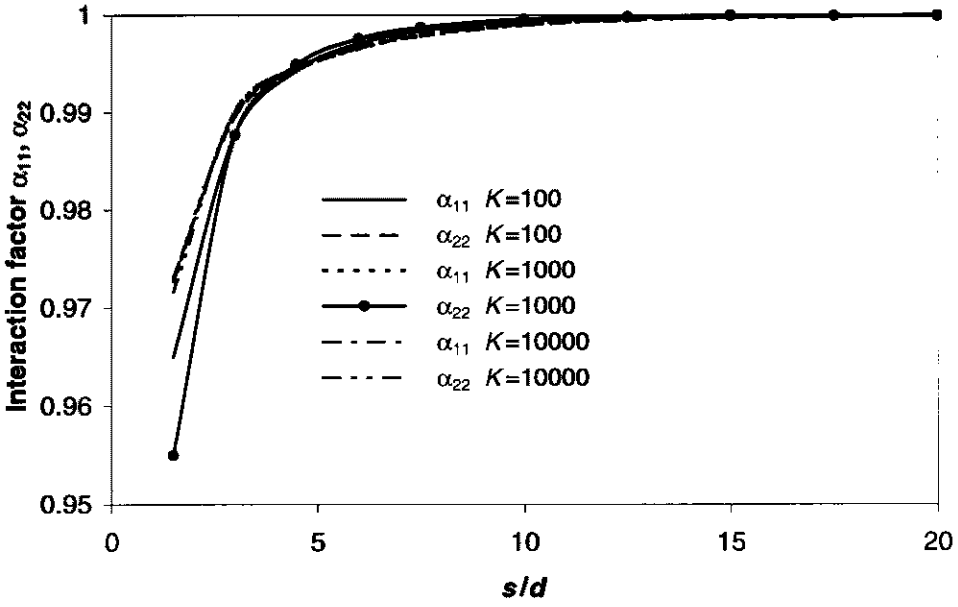

Fig. 7.10 Auto Interaction factor of two floating intact-damaged piles

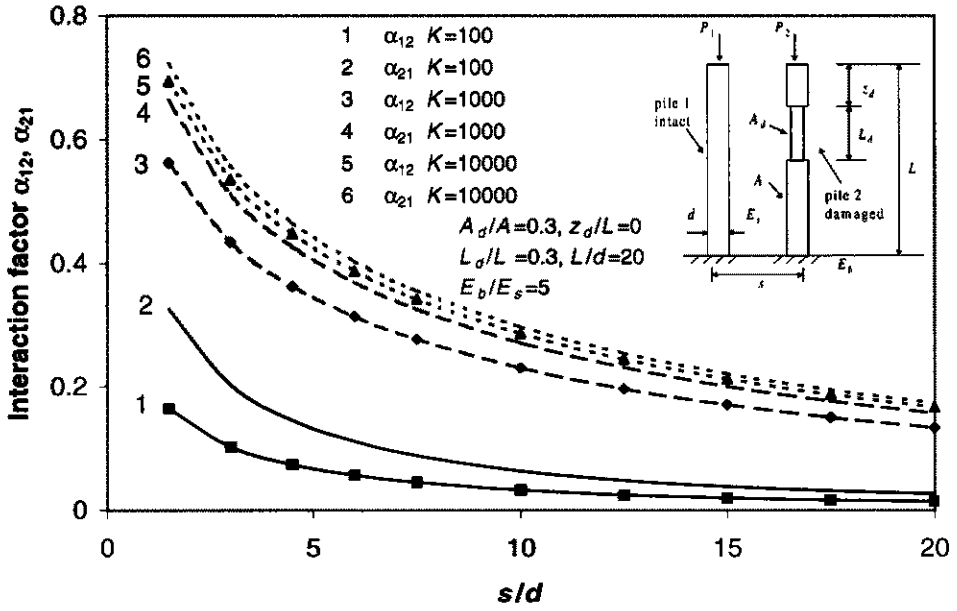

Fig. 7.11 Cross Interaction factor of two end-bearing intact-damaged piles

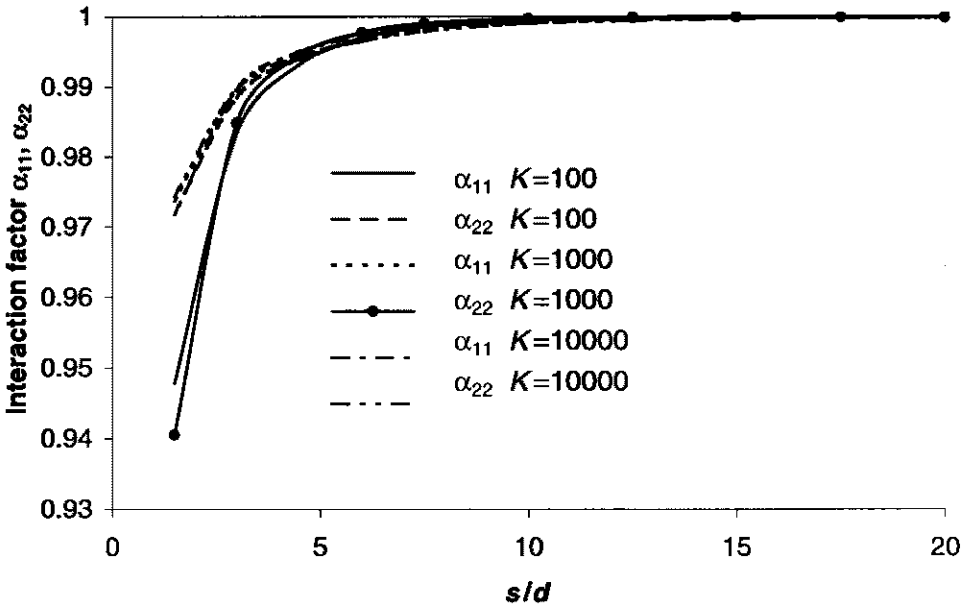

Fig. 7.12 Auto Interaction factor of two end-bearing intact-damaged piles

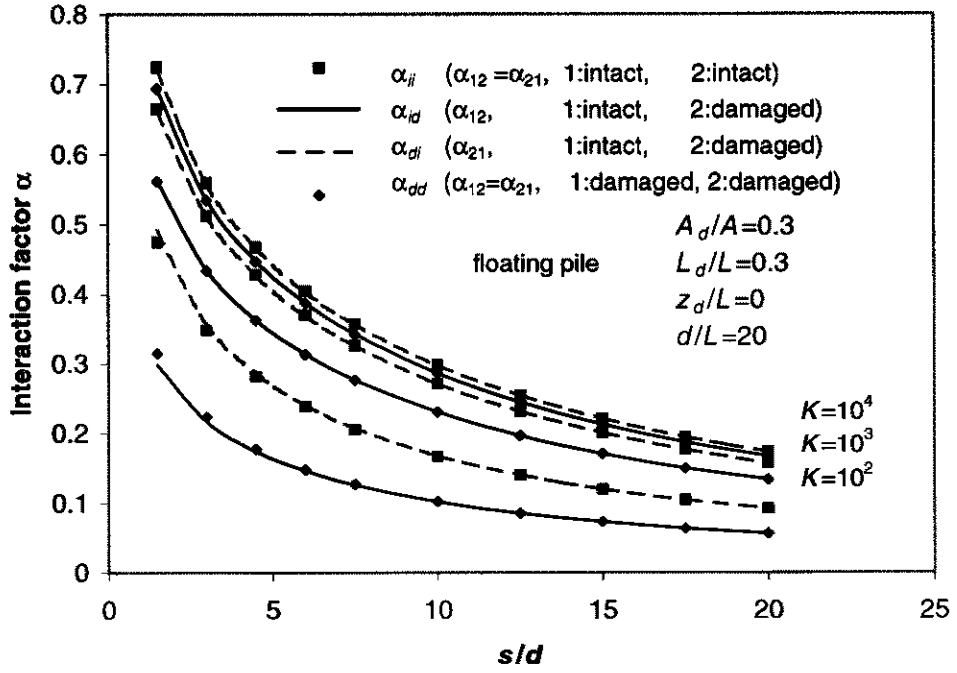

Fig. 7.13 Interaction factor of two floating piles

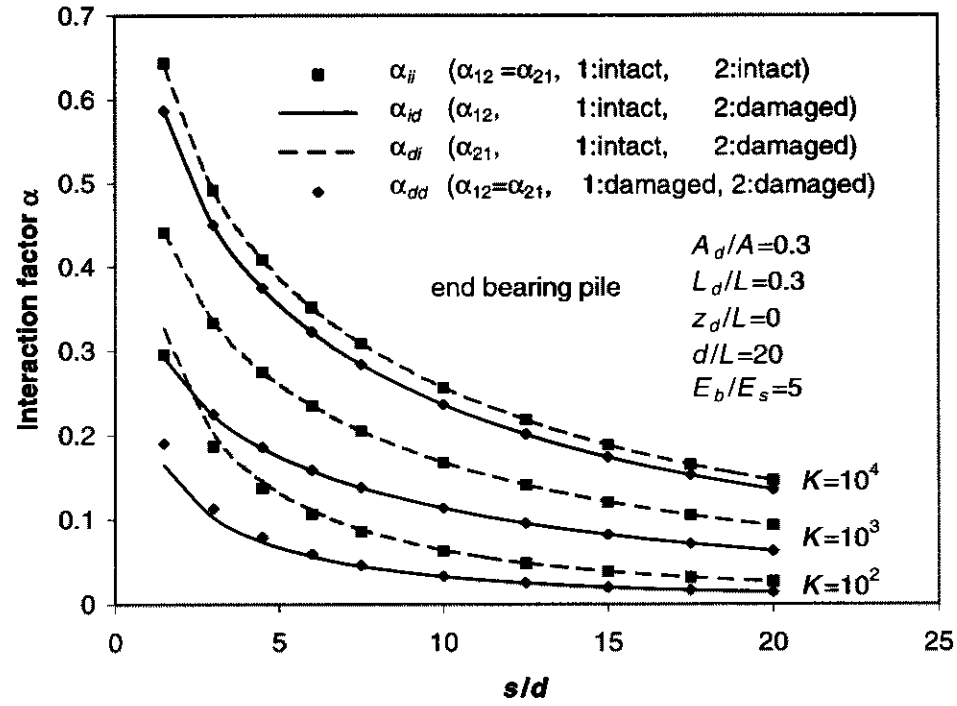

Fig. 7.14 Interaction factor of two end-bearing piles

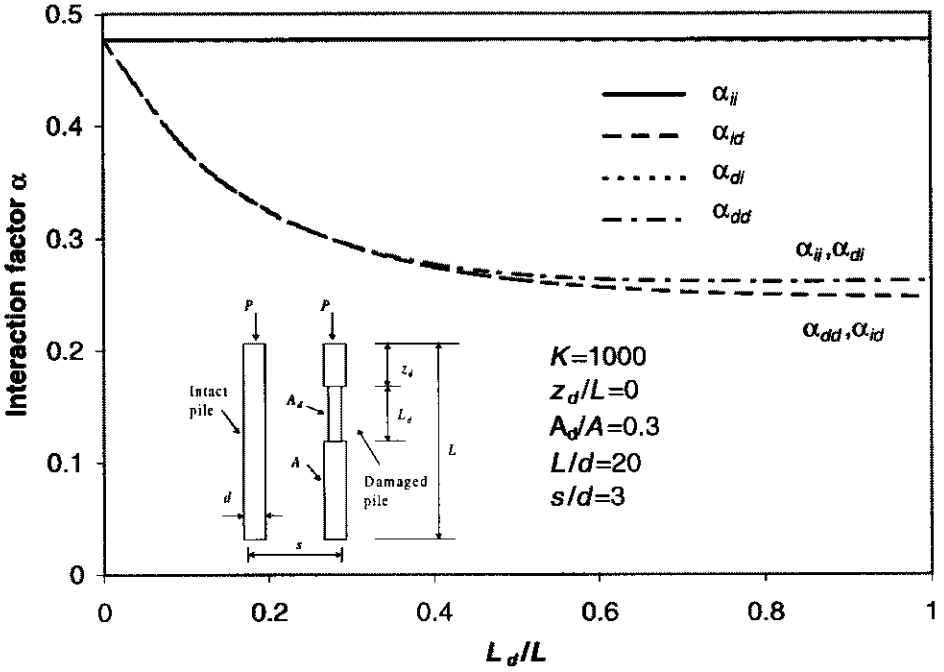

Fig. 7.15 Interaction factor α vs L_d/L of two piles containing neck

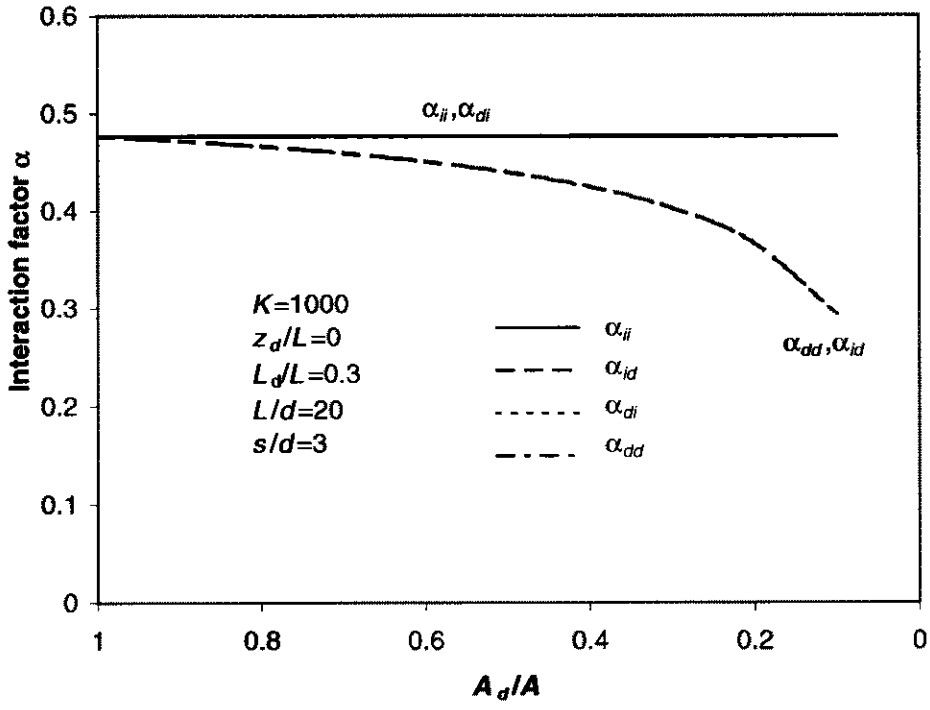

Fig. 7.16 Interaction factor α vs A_d/A of two piles containing neck

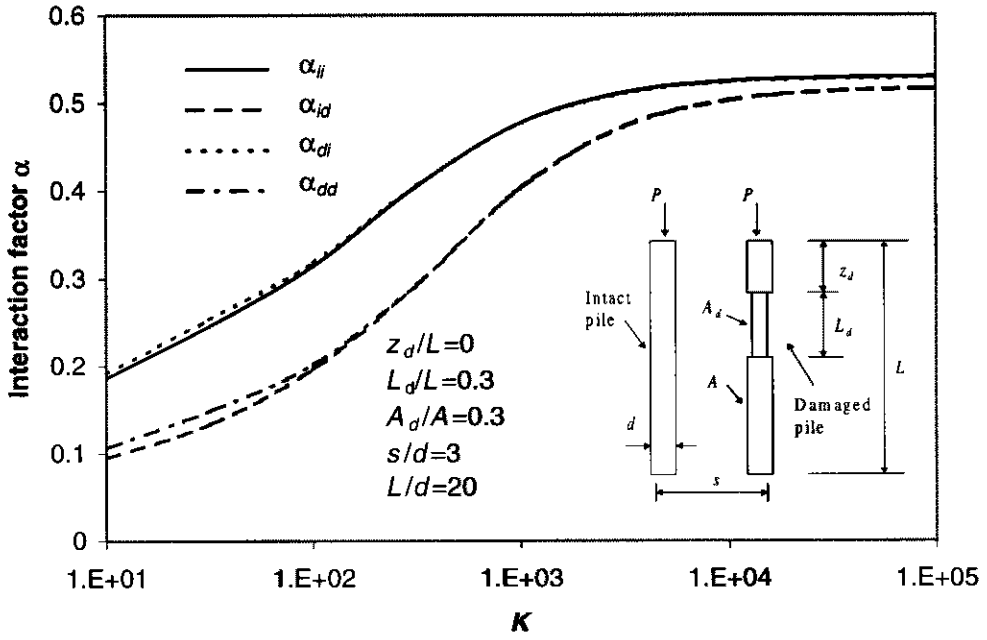

Fig. 7.17 Interaction factor α vs K of two piles containing neck

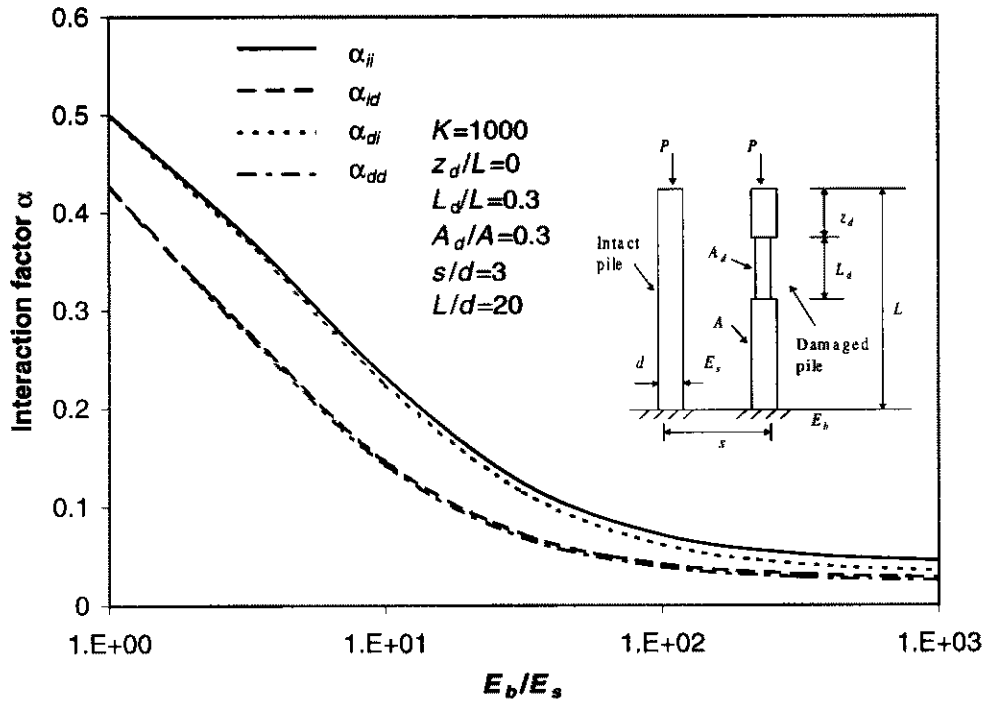

Fig. 7.18 Interaction factor α vs E_b/E_s of two end-bearing piles containing neck

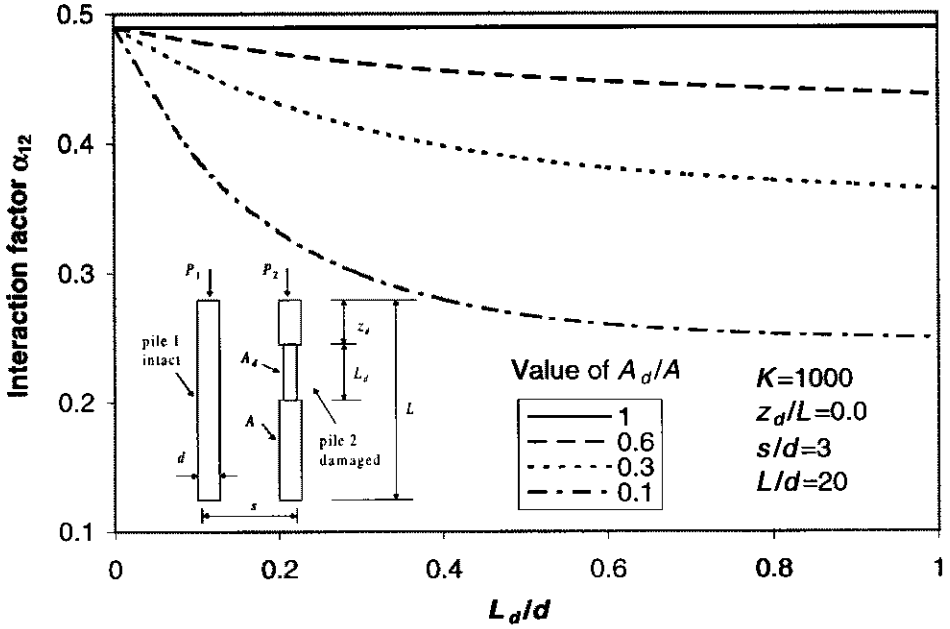

Fig. 7.19 Interaction factor α_{12} vs L_d/d of two intact-damaged piles

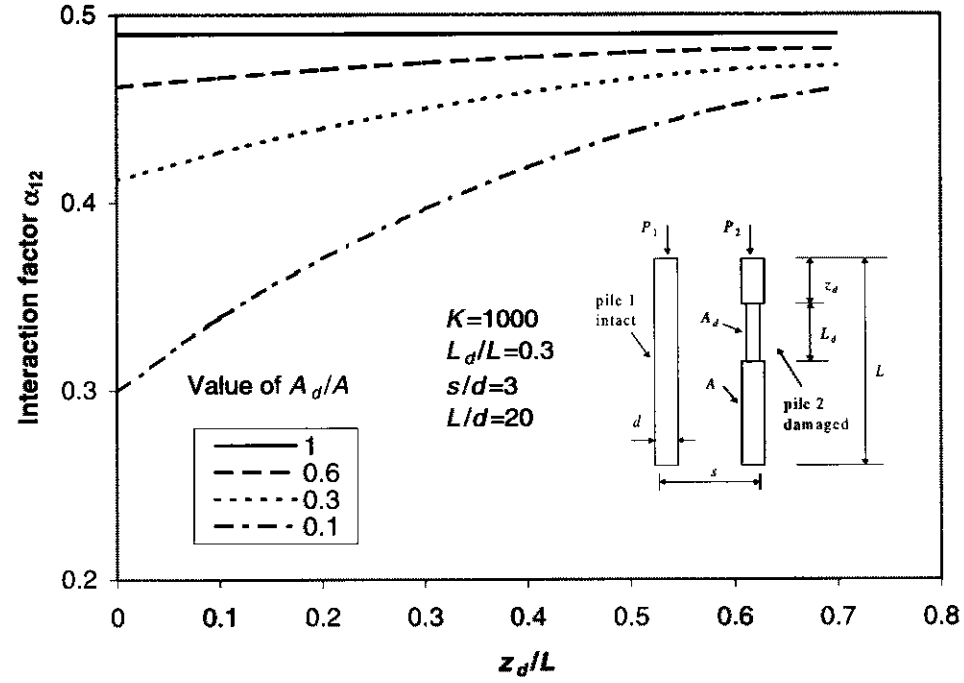

Fig. 7.20 Interaction factor α_{12} vs z_d/L of two intact-damaged piles

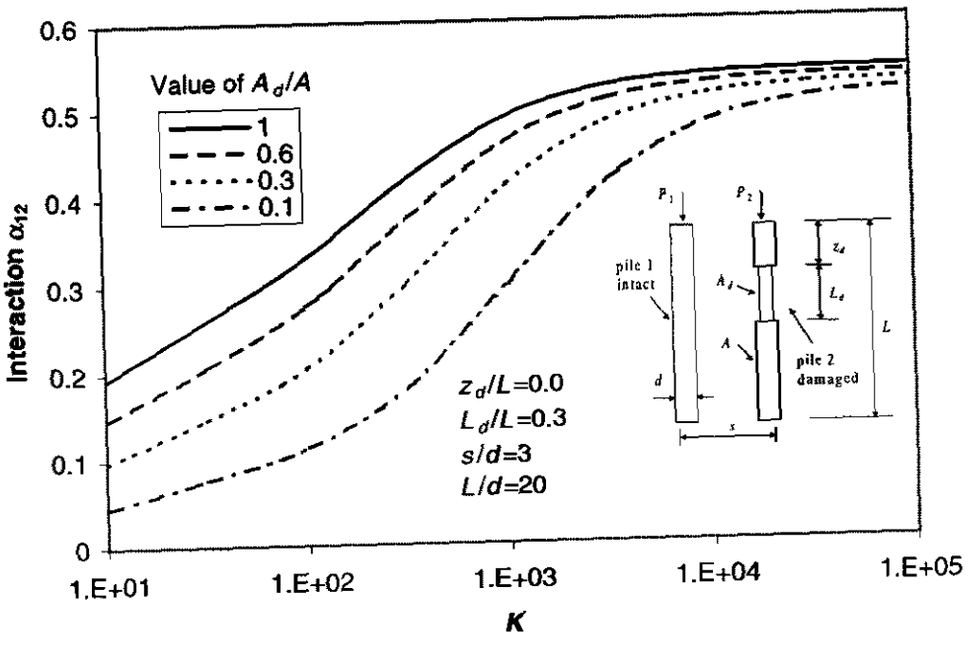

Fig. 7.21 Interaction factor α_{12} vs K of two intact-damaged piles

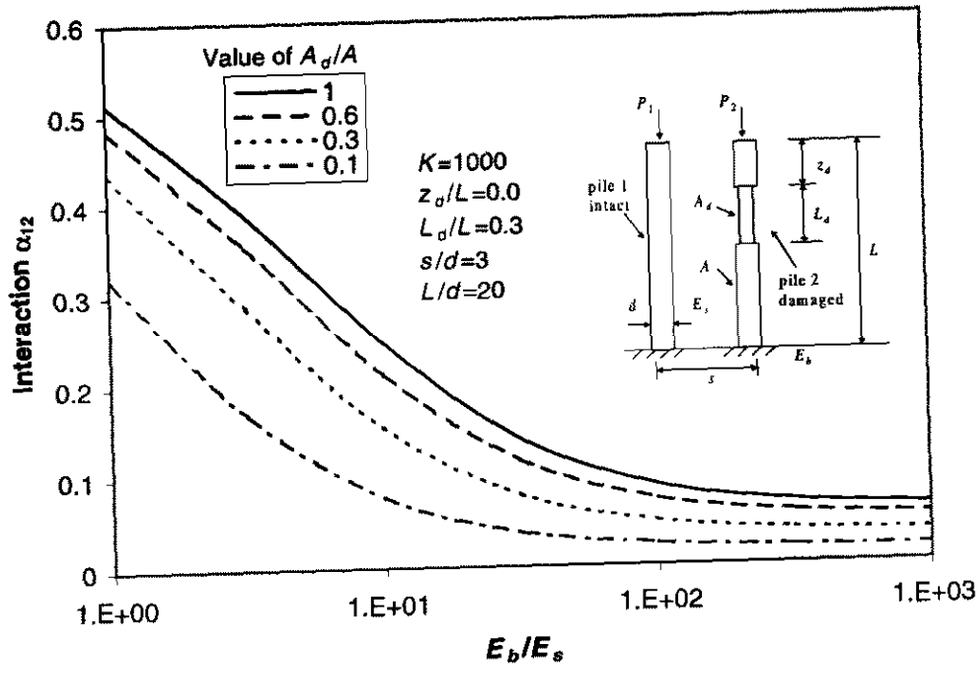

Fig. 7.22 Interaction factor α_{12} vs E_b/E_d of two intact-damaged piles

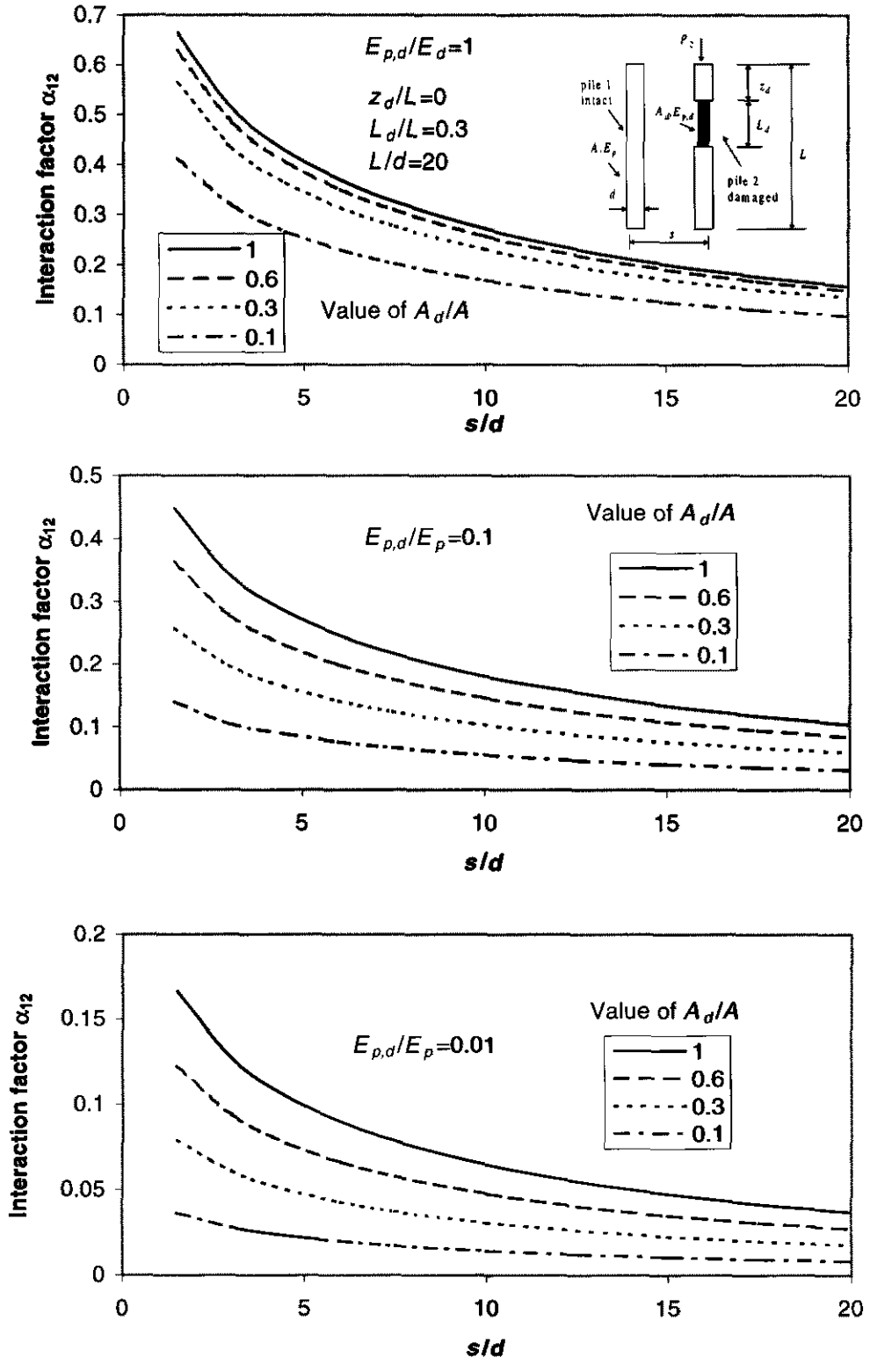

Fig. 7.23 Interaction factor α_{12} of two piles containing neck and honey-comb

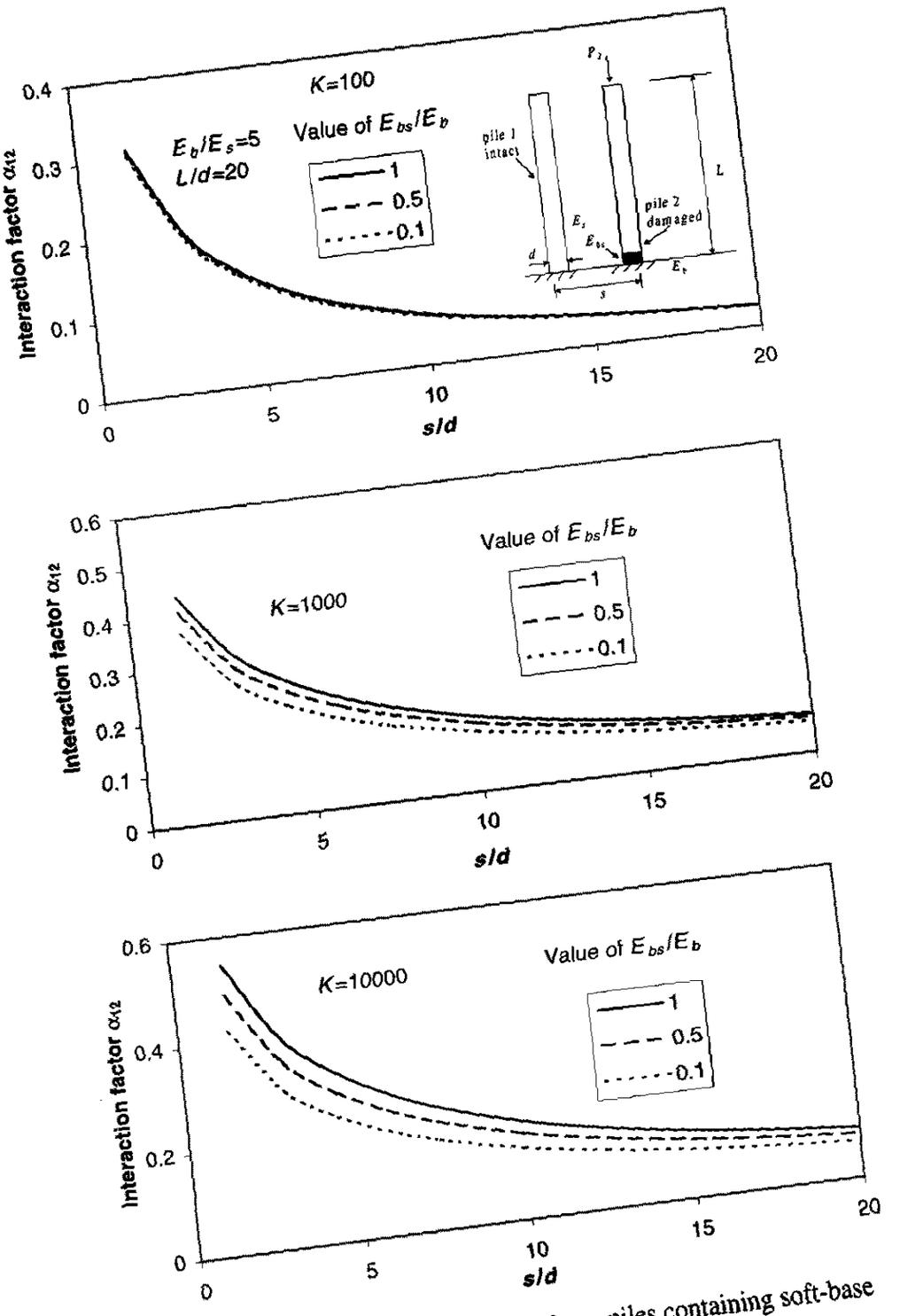

Fig. 7.24 Interaction factor α_{12} of two piles containing soft-base

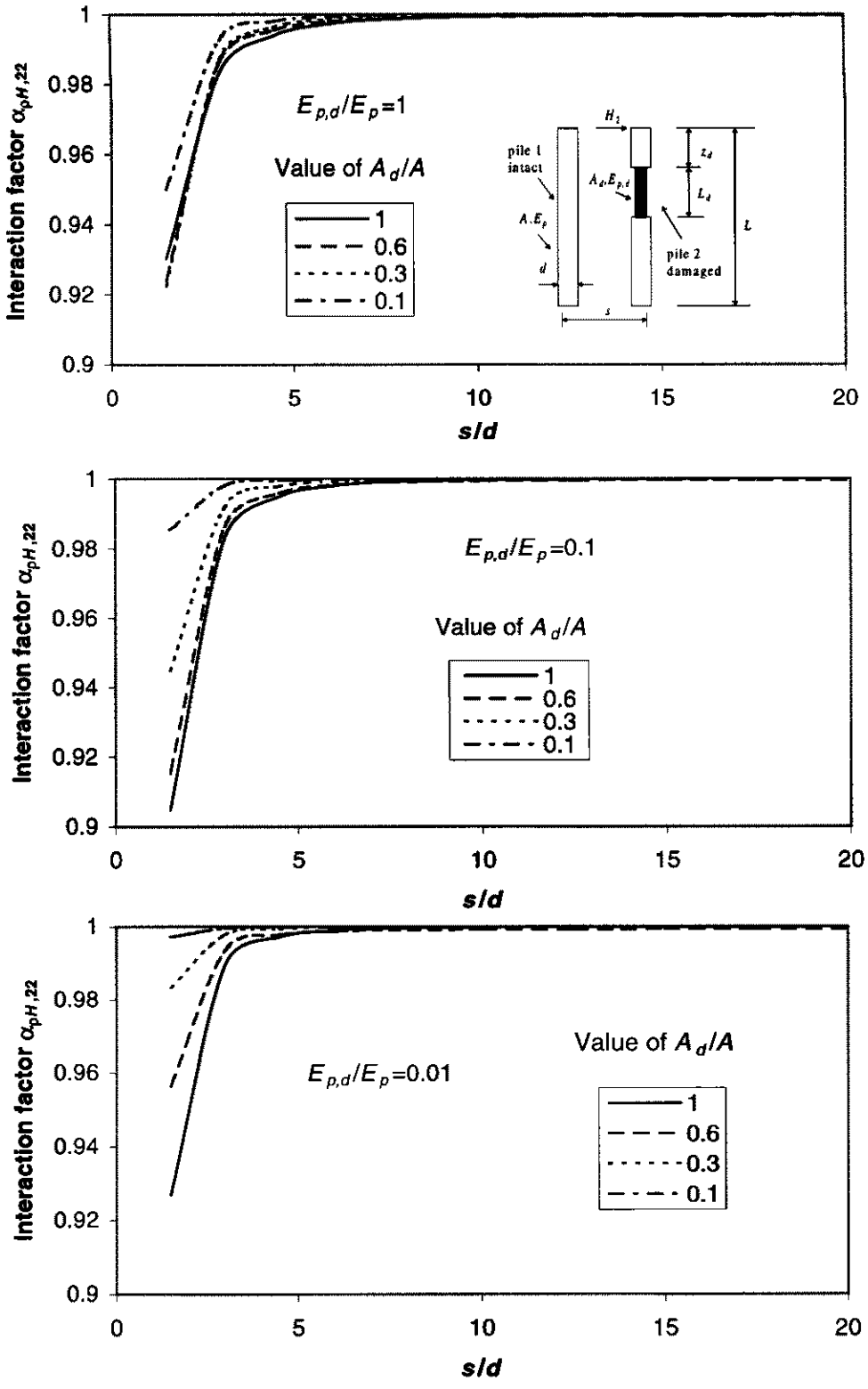

Fig. 7.25 Lateral $\alpha_{\rho H,22}$ of two piles containing neck and honey-comb

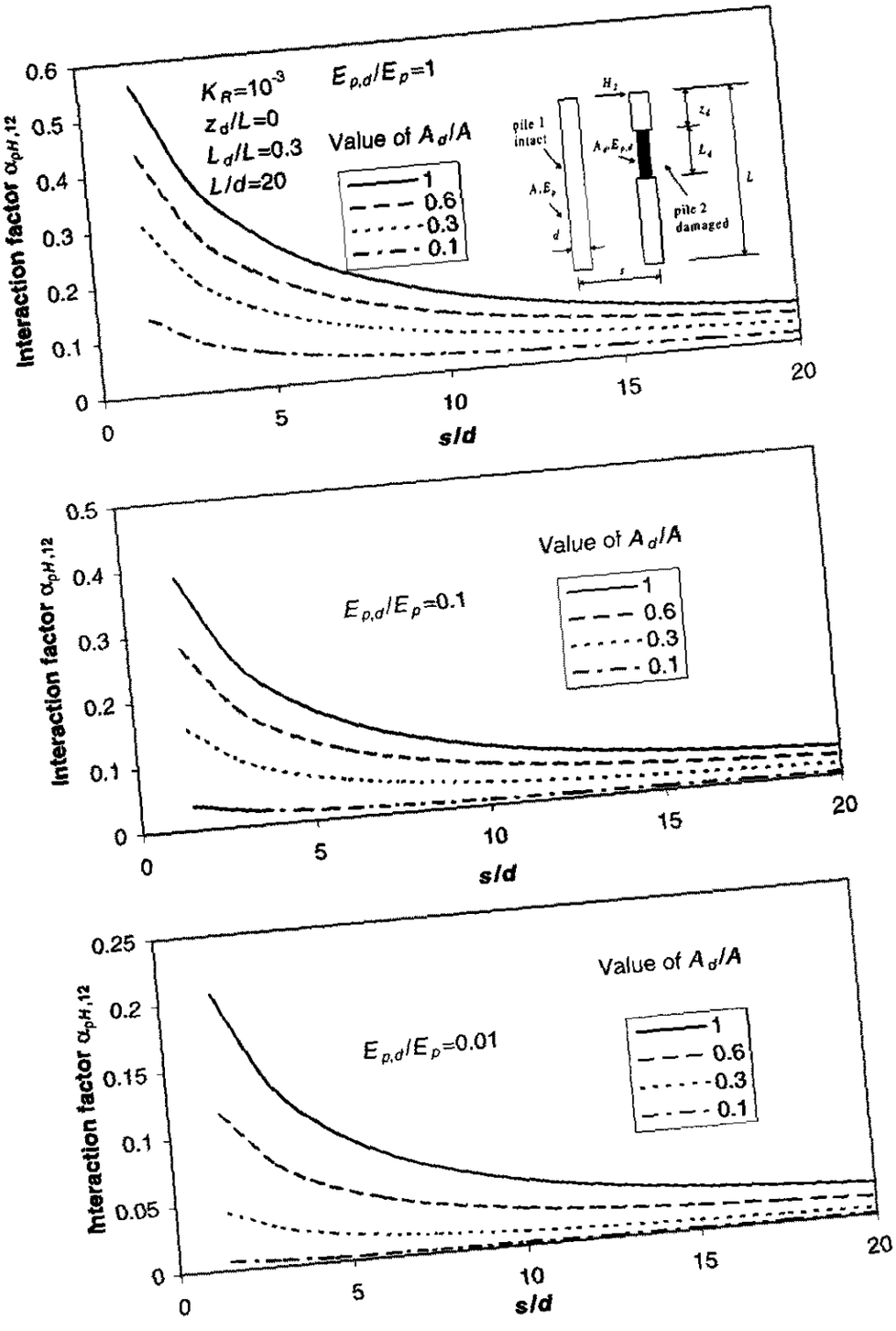

Fig. 7.26 Lateral $\alpha_{pH,12}$ of two piles containing neck and honey-comb

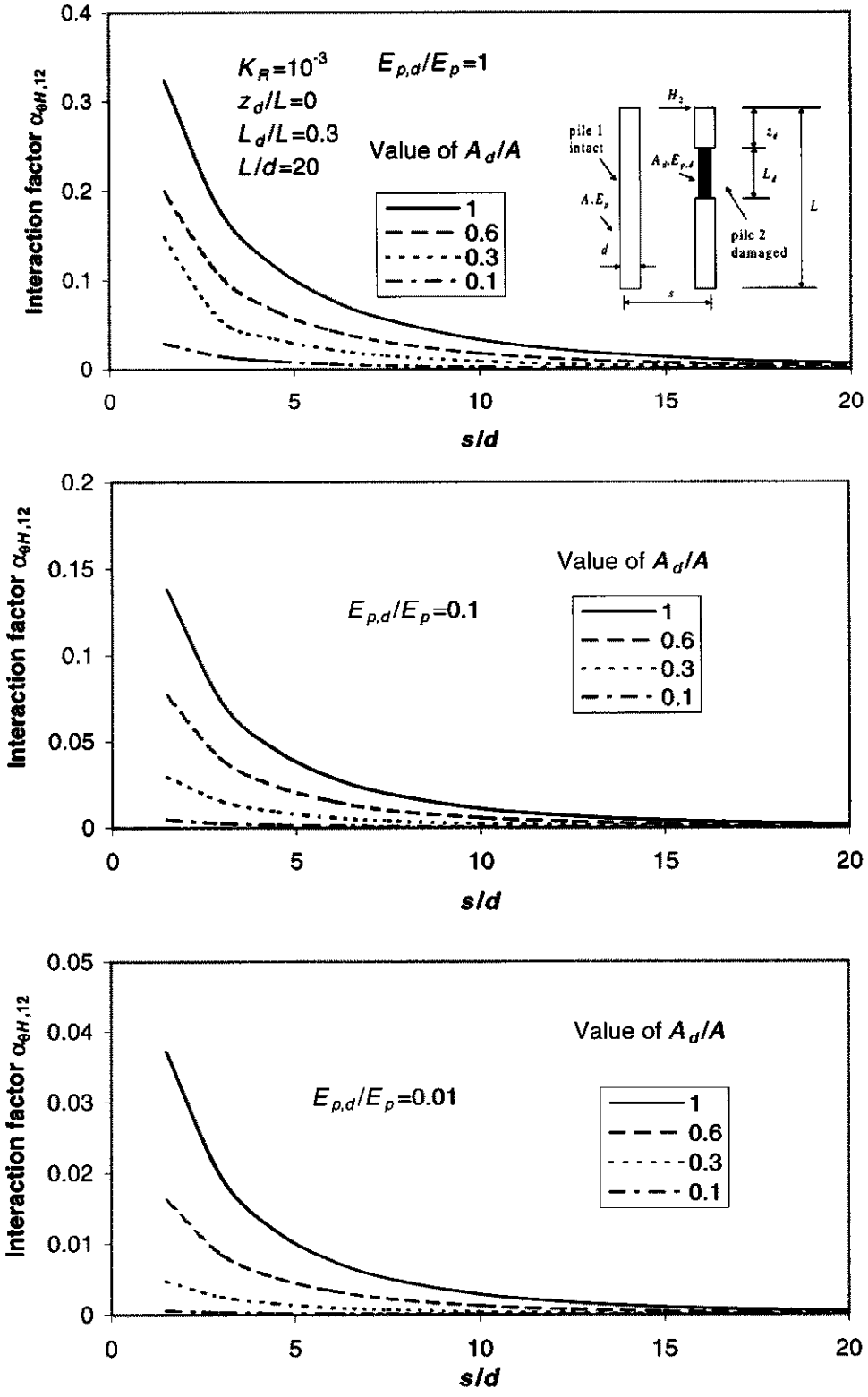

Fig. 7.27 Lateral $\alpha_{\theta H,12}$ of two piles containing neck and honey-comb

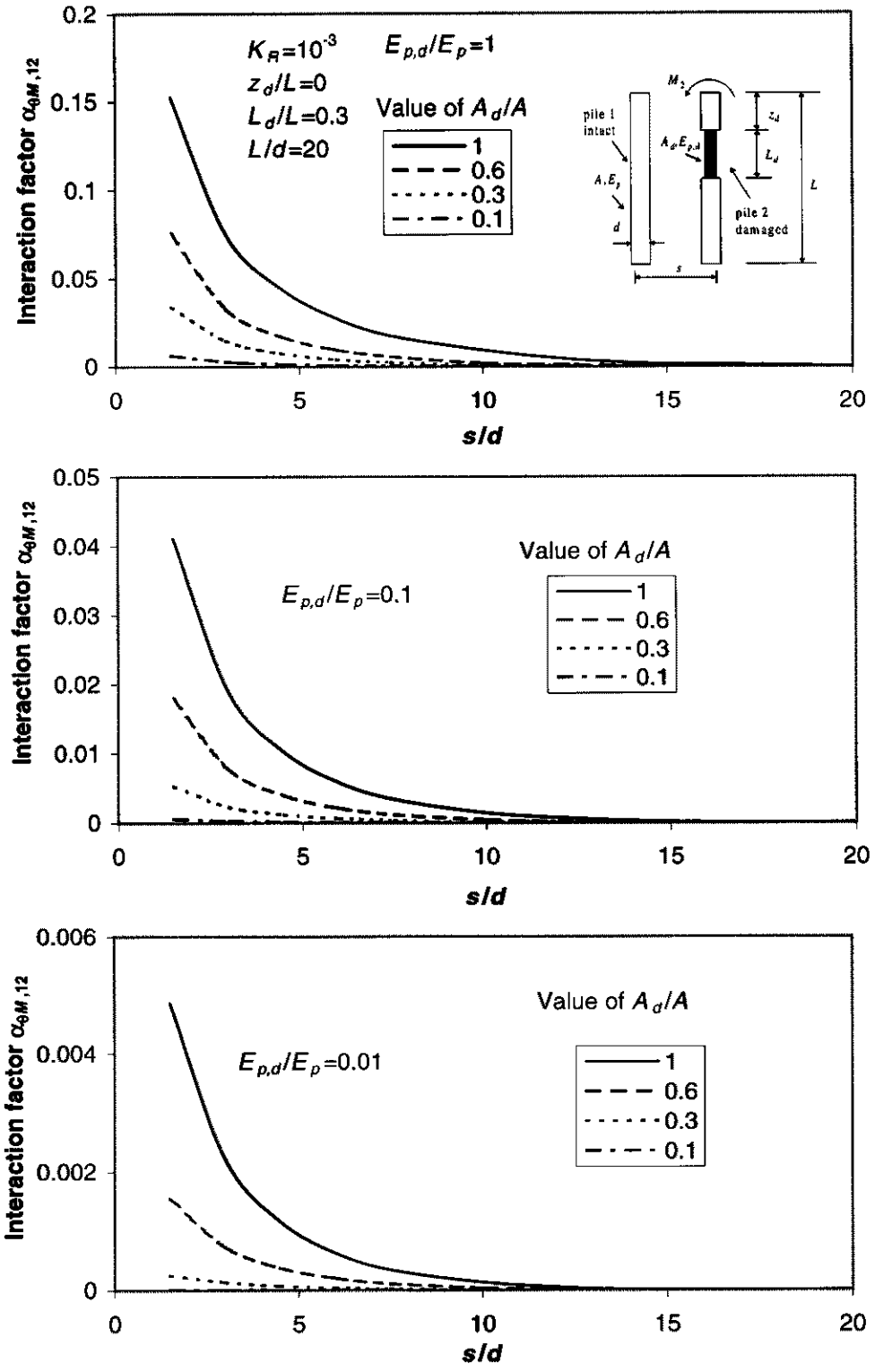

Fig. 7.28 Moment $\alpha_{\theta M,12}$ of two piles containing neck and honey-comb

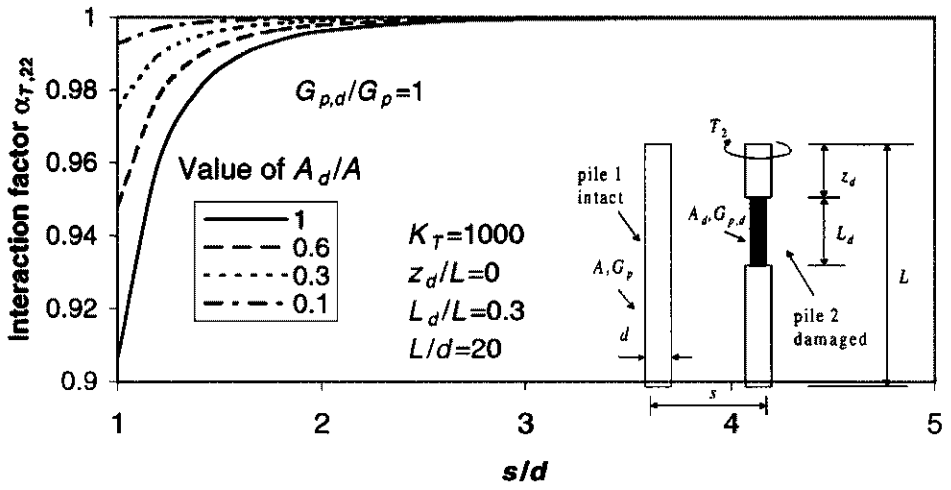

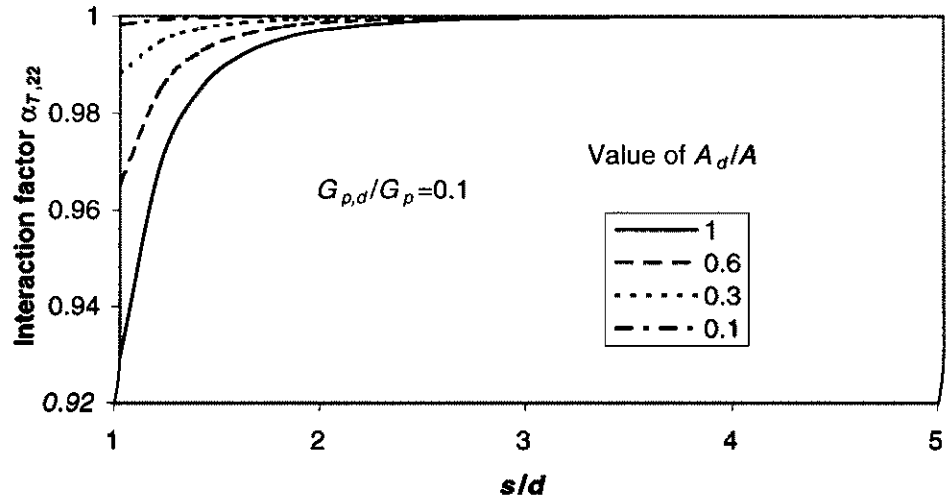

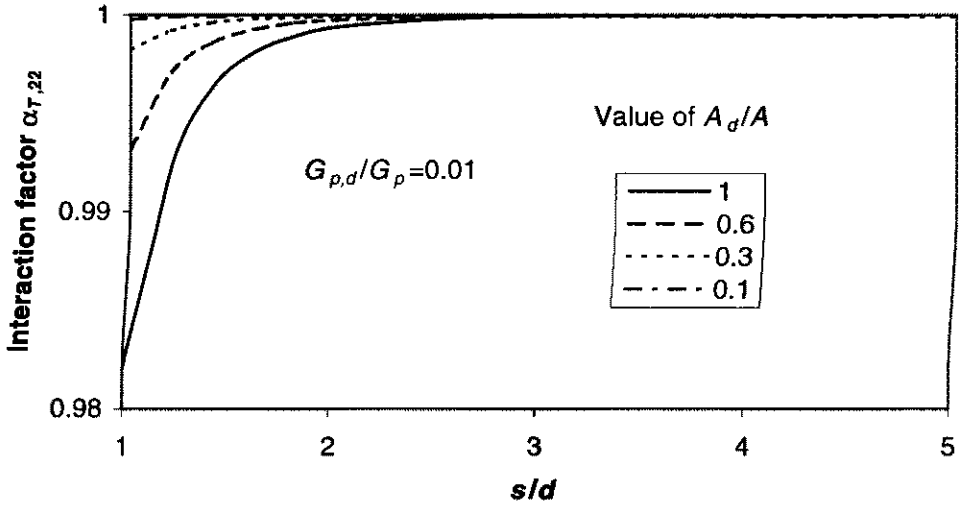

Fig. 7.29 Tortional $\alpha_{T,22}$ of two piles containing neck and honey-comb

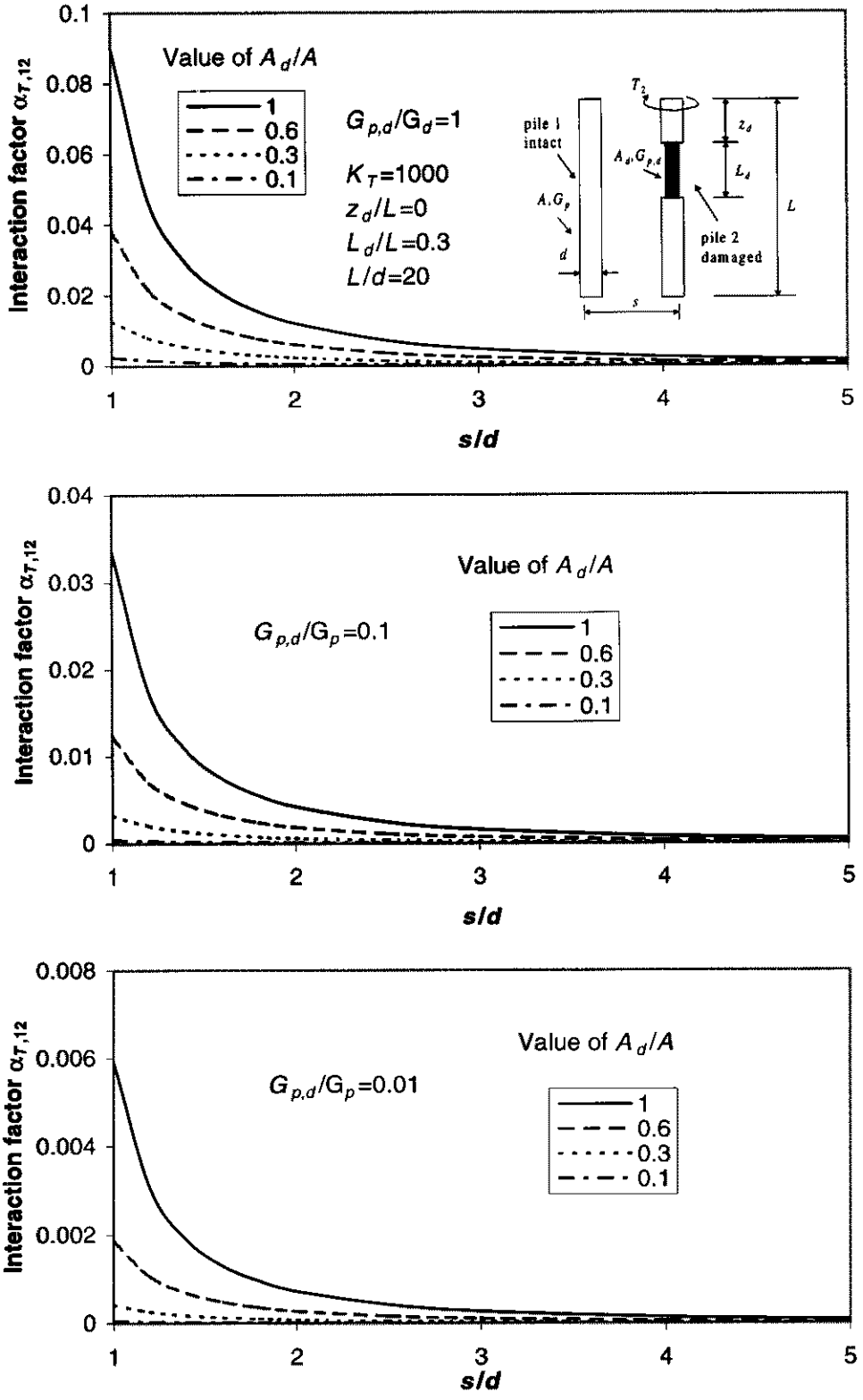

Fig. 7.30 Tortional $\alpha_{T,12}$ of two piles containing neck and honey-comb

Chapter 8

Behaviour of Pile Group Containing Defective Piles

8.1 Introduction

As reviewed in Chapter 2, it is a common experience to come across defects in concrete piles. Such defects have been discussed extensively in the literature. The behaviour of single defective piles has been examined via a parametric study in Chapter 6, and the interaction of two piles containing defects has been analysed in Chapter 7. However, there is little information on the behaviour of a pile group containing the defective piles. In many cases in the past, it has been assumed that the defective pile will not carry any load and an additional pile or piles have been installed within the group to compensate for the defective piles. Such a procedure can be both costly and time-consuming, and it is therefore of some interest to examine whether such remedial works are indeed justified, or whether the group containing the defective pile (or piles) can still function satisfactorily.

An interaction-factor-based group analysis and corresponding computer program, DAMPIG, were developed by Poulos (1997). For defective piles, reduction factors are input for axial and lateral stiffness, these being obtained from an independent analysis for a defective pile, using the program DAMPA (Poulos, 1997). Via DAMPA, a simple hypothetical 2×3 vertically loaded group containing defective piles has been studied. A more general elastic analysis of pile groups containing pile defects has been developed by Xu and Poulos (1999a, 1999c), which is presented in detail in Chapter 3. The analysis has been implemented via the program GEPAN. In defective pile analysis, GEPAN is more rigorous as well, because it is able to study defects in one-or-more piles rather than merely "defective piles in a group", like DAMPIG.

The objective of this Chapter is, via GEPAN, to study the load-displacement performance of groups containing defective piles. An attempt is made to relate the type of defects, pile spacing, pile stiffness/flexibility factors, to the load-displacement behaviour of the group.

The results may provide some guidance for assessing defect-induced factors, such as, group stiffness reduction factors, load redistribution and "off-line" movements.

8.2 Some Assumptions, Definitions and "Standard Cases"

8.2.1 Some Assumptions

The following assumptions are employed for the analysis:

1. all the assumptions of the theory of general pile analysis made in Chapter 3 apply in this case
2. all the assumptions of the numerical model of pile defects made in Chapter 6 apply in this case
3. the piles do not fail structurally or geotechnically.

8.2.2 Definitions

In parallel with the definition of the single pile stiffness reduction factor, $R_{KS,A,B}$, in Chapter 6, a pile group (cap) stiffness reduction factor, $R_{KG,A,B}$, can be expressed as follows:

$$R_{KG,A,B} = \frac{K_{GD,A,B}}{K_{GI,A,B}} \quad \text{..... (8.1)}$$

where

$K_{GD,A,B}$ =group (cap) stiffness of a defective group for cap displacement component B due to cap loading A

$K_{GI,A,B}$ = group (cap) stiffness of an intact group for cap displacement component B due to cap loading A

For example,

$R_{KG,N,S}$= $R_{KS,N}$ = vertical group (cap) stiffness reduction factor for vertical cap settlement component S due to a central vertical cap load N.

$R_{KG,H,\rho}$= horizontal group (cap) stiffness reduction factor for cap horizontal displacement component ρ, due to a central horizontal cap load H.

$R_{KG,H,\theta}$= horizontal group (cap) stiffness reduction factor for cap rotation component θ, due to a central horizontal cap load H.

The pile stiffness and flexibility factors (K, K_R) were defined by Poulos and Davis (1980), and these definitions, which are given in Chapter 6, will be employed for the solution described in this chapter.

8.2.3 "Standard" Case

In order to provided "benchmark" results, two kinds of "standard" groups are considered. One is a 2^2 pile group, to study the behaviour of group stiffness reduction factors, "off-line" effects and load redistribution. The other is a 3^2 pile group, which is used to study the effect of position of defective piles within a group. The main parameters within the "standard" groups are listed in Table 8.1.

Table 8.1 Main Parameters of Two "Standard" Groups

Dimensionless parameters	2^2 Pile Group		3^2 Pile Group	
	"Standard" Values	Parametric Range	"Standard" Values	Parametric Range
pile length/ diameter, L/d	20		20	
pile spacing/diameter, s/d	4	1~10		1~5
pile stiffness factor, K	10^3	10^1~10^5	10^3	
pile flexibility factor, K_R	10^{-3}	10^{-2}~10^{-4}	10^{-3}	
base modulus/soil modulus, E_b/E_s	5	1~1000		
defect depth/pile length, z_d/L	0.2		0.2	
defect length/pile length, L_d/L	0.3		0.4	
neck area/ intact area, A_d/A		1~0.1	0.1	
honey-comb modulus/intact pile modulus, $E_{p,d}/E_p$		1~0.01	0.01	
base-soft modulus/intact base modulus, $E_{p,d}/E_s$	5			
no. of defective pile	Pile 4			piles 1,2,5

8.3 Effects of Pile Defects in a Vertically-Loaded Pile Group

8.3.1 Necking in a Vertically-Loaded Pile Group

Analyses have been carried out to examine the effect of necking on a 2^2 pile group subjected a vertically loading, with various values of s/d, K and E_p/E_s.

8.3.1.1 Effect of Pile Spacing

Fig. 8.1 shows that, as expected, larger values of the ratio of cap settlement to pile diameter, S_z/d, occur as the ratio of neck and intact area, A_d/A, decreases. The vertical group stiffness reduction factor, $R_{KG,N}$, for the pile group containing the neck, under a vertical loading, is plotted against s/d in Fig. 8.2. It is seen that a decrease in the relative neck area, A_d/A, leads to a decrease in $R_{KG,N}$, especially for cases of severe necking (such as, A_d/A=0.1). The value of $R_{KG,N}$ becomes smaller as s/d increases.

8.3.1.2 Effect of "Off-line" Movement

An interesting feature of group response with defective piles is that the group will deflect laterally and suffer a rotation under purely axial applied loading, *e.g.*, "off-line" effects occur. As described in Chapter 3, the GEPAN analysis incorporates full coupling effects for 6 load components and 6 displacement components, so that "off-line" movements of a pile cap due to the defective pile, can be analysed. Figs. 8.3 and 8.4 show the "off-line" horizontal movement (toward the defective pile), S_x/d, and rotation (toward the defective pile), θ_y, respectively as a function of s/d. They increase as A_d/A increases. As expected, smaller values of the off-line movements occur for groups with a larger pile spacing, the difference induced by A_d/A becoming less as the pile spacing increases.

8.3.1.3 Effect of Load Distribution

For ranges of values of A_d/A and s/d, load distributions within a pile group with a rigid cap are shown in Fig. 8.5, the pile load being expressed as a fraction of the average load on a pile in the group. The load at pile 1 (diagonally opposite the defective pile 4) decreases, as the ratio of neck area in the defective pile 4, A_d/A, decreases. Increases of

load occurs at piles 2 and 3 (at side of defective pile 4) result from a decrease of A_d/A in the defective pile 4. The load on the defective pile 4 decreases, as the A_d/A of the pile itself decreases. The load distribution tends to become less uniform as the neck area decreases, and also as the pile spacing decreases.

As demonstrated above, "off-line" movements occur in a pile group containing defective piles. The "off-line" movements, of course, will produce extra internal forces in the piles. Fig. 8.6 shows that the resultant pile head moment M_r (square root of $M_x^2+M_y^2$) increases significantly as A_d/A decreases. The value of M_r decreases with increasing the ratio of pile spacing and diameter, *s/d*. Furthermore, Fig. 8.7 shows a ratio of resultant pile head moment of an intact pile group ($M_{r,i,intact}$) and a group containing a defective pile ($M_{r,i,damaged}$). It is shown that the ratio may be over 60 in the case of severe necking (e.g. Ad/A=0.1). Consequently, allowance should be made in the pile design for the larger pile head moments which may be induced by pile defects existing in the pile group.

8.3.1.4 Effect of Pile Compressibility

Pile compressibility can be expressed in term of a pile stiffness factor K, the effect of which is shown in Figs. 8.8 and 8.9. Pile cap settlements decease with increasing values of K, as shown in Fig. 8.8(a). The vertical group stiffness reduction factor, $R_{KG,N}$, as shown in Fig. 8.8(b), reaches a minimum around $K=10^2$, while it approaches 1 both for very soft piles or very stiff piles. Fig. 8.8(c) shows that the least uniform load distribution occurs for values of pile stiffness factor, K, between about 10^2 and 10^3. For the extremes (very soft piles or very stiff piles), the load distributions tend to be uniform. Furthermore, the effect of K on the load distributions at pile heads is shown in Fig. 8.9, for values of A_d/A of 1, 0.6, 0.3 and 0.1. It demonstrated again that the greatest changes in load re-distribution, induced by pile defects, occur in moderately compressible piles.

8.3.1.5 End-Bearing Piles on Compressible Stratum

For an end-bearing group containing a defective pile (pile 4), Fig. 8.10 shows the relationship between dimensionless cap settlement S_z/d and dimensionless base Young's modulus E_b/E_s. Like a group containing intact piles, as E_b/E_s increases, S_z/d decreases for

the group containing a defective pile. Fig. 8.11 shows the vertical group stiffness reduction factor, $R_{KG,N}$, plotted against E_b/E_s for various "neck" area ratios. $R_{KG,N}$ decreases as E_b/E_s increases, the difference due to necking becoming greater for the stiffer stratum at the pile tips. Fig. 8.12 shows the effect of a compressible stratum on pile load distributions within the pile group containing various pile necks. As E_b/E_s increase, loads on piles 1 and 4 decrease, while loads on piles 2 and 3 increase. Necking induces a less uniform load distribution within a group resting on a stiff stratum, in particular, for severe necking. Therefore, the effect of pile defects on group stiffness reduction of an end-bearing pile group is generally greater than for a floating pile group.

8.3.2 Honey-Combing in a Vertically-Loaded Pile Group

Figs. 8.13 and 8.14 show the effect of a "honey-comb" section on one pile (pile 4) in a pile group, in term of S_z/d or $R_{KG,N}$. As s/d decreases and/or $E_{p,d}/E_p$ decreases, the dimensionless cap settlement S_z/d increases, and the vertical group stiffness reduction factor $R_{KG,N}$ decreases, especially for severe homey-combing. The "off-line" horizontal cap displacement and rotation induced by honey-combing, are shown in Figs. 8.15 and 8.16 respectively. The more severe the honey-combing (as expressed by the ratio $E_{p,d}/E_p$), the greater are the "off-line" movements induced. Fig. 8.17 shows the influence of the defect on the pile redistribution. The load distribution becomes less uniform as the severity of the honey-combing increases.

In general, the effect of honey-combing on vertical group stiffness reduction and load redistribution, is similar to the effects of necking which have been analyzed previously.

8.3.3 Base-Softening in a Vertically-Loaded Pile Group

For a group containing a pile with a "soft base", the cap settlement, vertical stiffness reduction factor of pile group and load distribution, are plotted against dimensionless spacing in Figs. 8.18, 8.19 and 8.20 respectively. These figures show that:

1. the more severe the base-softening (as expressed by the ratio $E_{p,d}/E_p$), the smaller is the stiffness reduction factor $R_{KG,N}$ is induced
2. the load distribution becomes less uniform as the degree of base-softening increases
3. dimensionless spacing, *s/d*, has relatively little influence on $R_{KG,N}$ and $P_{z,i}/P_{z,av}$ induced by base-softening
4. for slight base-softening ($E_{p,d}/E_p$=1~0.1) or severe base-softening ($E_{p,d}/E_p$ =10^{-3}~10^{-4}), the ratio of $E_{p,d}/E_p$ causes little change in the pile response to base-softening.

8.4 Effects of Pile Defects in Horizontally-Loaded Pile Group

8.4.1 Effect of Necking

Figs. 8.21 and 8.22 show horizontal cap displacement s_x/d, and rotation θ_y, for a 2^2 pile group containing a neck (pile 4: A_d/A=0.3, z_d/d=0.2, L_d/L=0.3), subjected a central-applied horizontal load *H*. As *s/d* increases, S_x/d and θ_y decrease. The more severe the necking, the larger is the value of S_x/d produced.

The horizontal group stiffness reduction factors, $R_{KG,H,\rho}$ and $R_{KG,H,\theta}$, are plotted against *s/d* in Figs. 8.23 and 8.24 respectively. Generally as *s/d* increases, $R_{KG,H,\rho}$ and $R_{KG,H,\theta}$, increase, the differences for various K_R being greater as *s/d* increases.

The effect of load distribution induced by a pile defect (necking), is shown in Fig. 8.25. For the defect (necking) existing in pile 4, the loads in the four piles within the group are redistributed as follows:

1. the load of the defective pile 4 decreases
2. the load of pile 2 (the neighbor of the pile 4 and parallel to load *H*) increases
3. the values of the load fractions $P_{x,i}/P_{x,av}$ of piles 1 and 3 are close (the load in pile 3 is slightly larger than that in pile1), but significantly smaller than those of piles 2 and 4
4. after *s/d*>6 approximately, the effect of dimensionless spacing, *s/d*, can be neglected.

8.4.2 Effect of Honey-Combing

Figs. 8.26 and 8.27 show horizontal group stiffness reduction factors, $R_{KG,H,\rho}$ and $R_{KG,H,\theta}$, for a 2^2 pile group containing a "honey-comb" section (pile 4:, z_d/d=0.2, L_d/L=0.3, $E_{p,d}/E_p$=1(intact), 0.1, 0.01), subjected a central-applied horizontal load H. As $E_{p,d}/E_p$ decreases, $R_{KG,H,\rho}$ and $R_{KG,H,\theta}$, decrease.

Figs. 8.28 and 8.29 show the load distribution within the group induced by the honey-combing. The characteristics of the load redistribution are similar with that of necking which is presented in the previous section.

8.5 Comparison of Single Pile and Group Stiffness Reduction

The effect of single pile stiffness reduction has been studied in Chapter 6, and comparisons can be made between a single pile and a group in terms of stiffness reduction.

It is clearly shown that, the group stiffness reduction factors are significantly larger than those of single pile stiffness reduction factors, which is consistent with a similar finding by Poulos (1997) from a 2×3 vertically-loaded group. This is because of the ability of the stiffer intact piles in the group to compensate for the defective pile and carry a greater proportion of the load.

8.6 Effects of Position of Defective Piles in Pile Group

In order to analyse the effect of the position of defective piles in a pile group, a "standard" 3^2 cap-rigid floating group containing a defective pile has been considered as described in Section 8.2. The defects are assumed to be both a neck and a honey-comb.

Three of positions of a defective pile within the group are considered, as shown in Fig. 8.30, *i.e.*

1. at the corner (defective pile 1)
2. at the edge (defective pile 2)
3. at the centre (defective pile 5).

Firstly, a central vertical load is considered to be acting on the group containing a defective pile which is located at the different positions. A plot of the vertical group stiffness reduction factor, $R_{KG,N}$, as a function of the pile spacing is shown in Fig. 8.30. It is shown that the value of $R_{KG,N}$ is:

1. least if the defective pile is at the corner (pile 1)
2. greatest if the defective pile is at centre (pile 5)
3. in between these extremes if the defective pile is at the edge (pile 2).

As discussed previously, there is also the development of "off-line" movements of the group. The "off-line" rotation (toward the defective pile), θ_y, for example, of the group subjected to the vertical load, is shown in Fig. 8.31. The value of θ_y is least if the defective pile is located at the corner, and zero for the defective pile at the center.

Secondly, a centrally applied horizontal load is considered. Lateral group stiffness reduction factors, $R_{KG,H,\rho}$ and $R_{KG,H,\theta}$, for the different locations of the defective pile, are shown in Figs. 8.32 and 8.33 respectively. Like the centrally vertical loading, these lateral group stiffness reduction factors are least if the defective pile is at corner, and greatest when the defective pile is at the center.

Consequently, the more asymmetric the location of the defective piles, the greater is the effect of the pile defects on group response.

8.7 Conclusions

On linear elastic analysis, the main findings of the investigation on groups containing defective piles can be summarized as follows:

1. group stiffness reduction factors decrease as the severity of the pile defects increases.
2. "off-line" movements are induced by pile defects
3. extra larger pile head moments may be induced by pile defects existing in the pile group
4. group stiffness reduction factors are more sensitive for piles of moderate relative stiffness (K)
5. the more severe the pile defects, the less uniform is the load distribution within the group
6. when a defective pile exists within a group, the load on the defective pile decreases, while the loads on piles neighboring the defective pile may increase
7. the more asymmetric the location of the defective pile (or piles), the greater is the effect of the defects on the response of the group
8. the group stiffness reduction factors are less than corresponding single pile stiffness reduction factor.

It should be noted that the assumption of linear behaviour in this chapter is stretched very thin for "severe" necking cases as A_d/A=0.1. The results in Fig.8.5 show that for most practical situations (s/d>=3) the defective pile will fail either structurally or geotechnically at 80% of the design load and the load redistribution pattern will have to change to accommodate this failure.

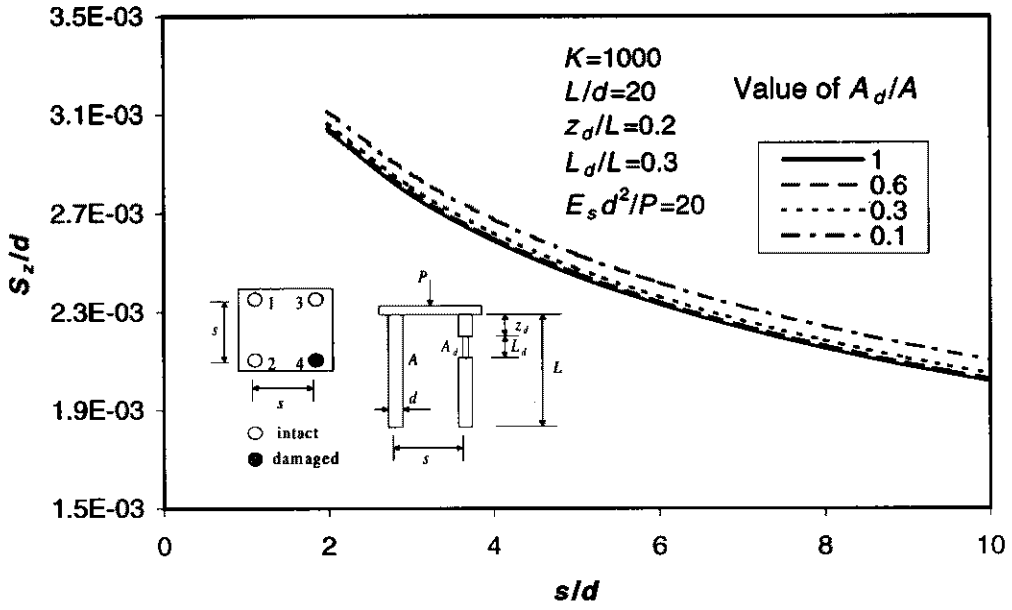

Fig. 8.1 S_z/d vs s/d of a pile group containing a ncek

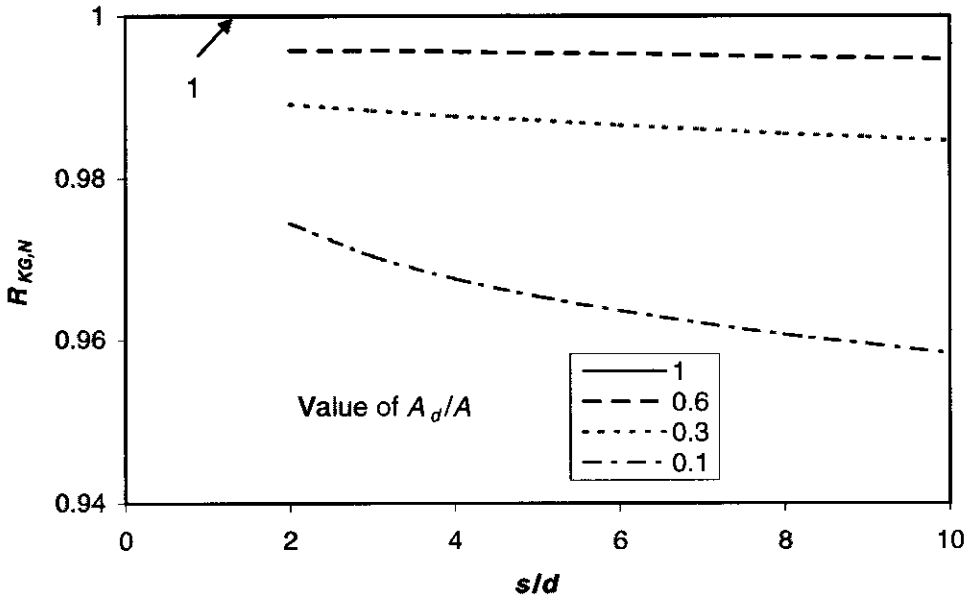

Fig. 8.2 $R_{KG,N}$ vs s/d of a pile group containing a ncek

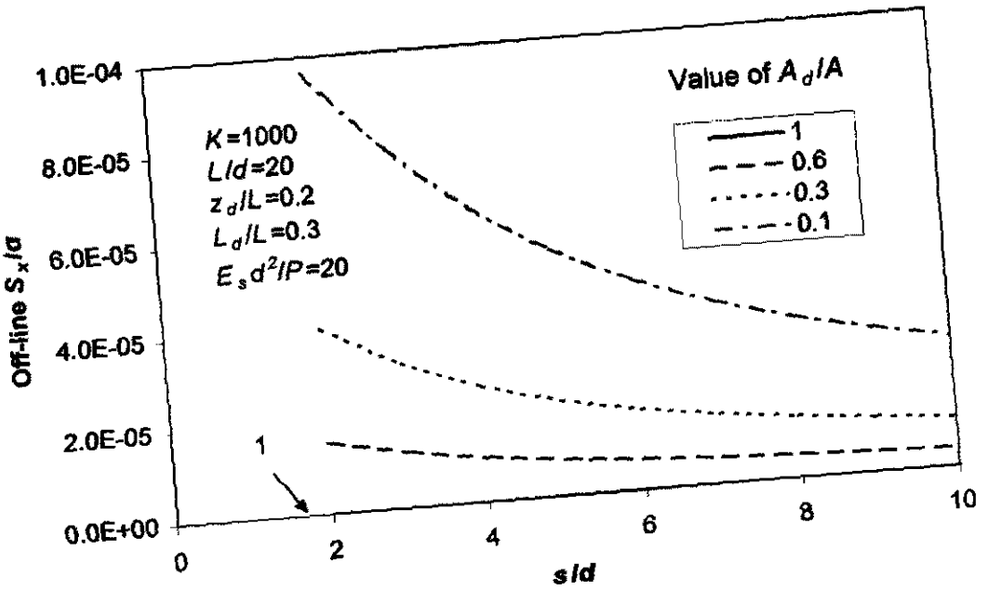

Fig. 8.3 Off-line S_x/d vs s/d of a pile group containing a neck

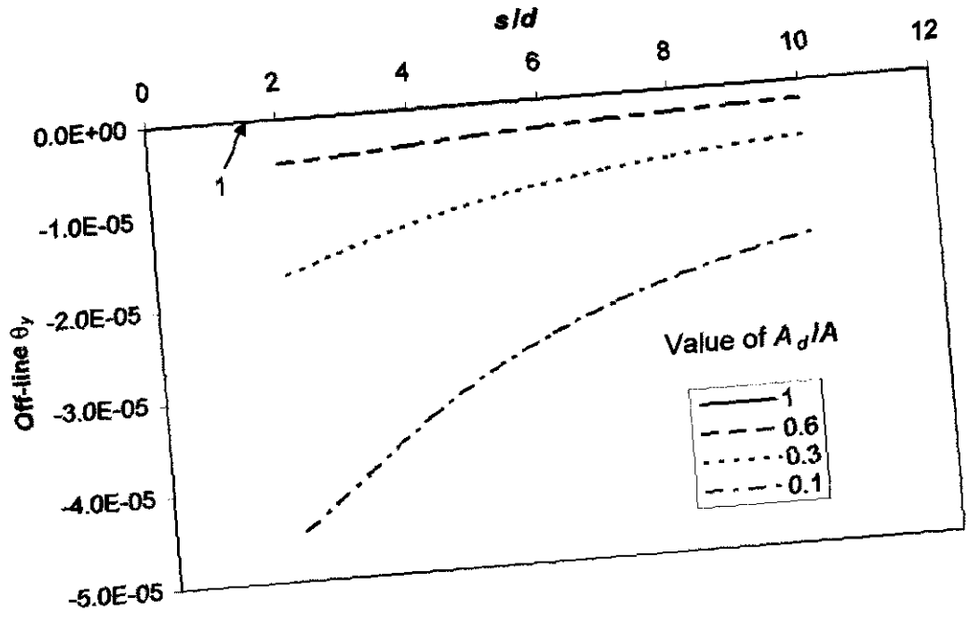

Fig. 8.4 Off-line θ_x vs s/d of a pile group containing a neck

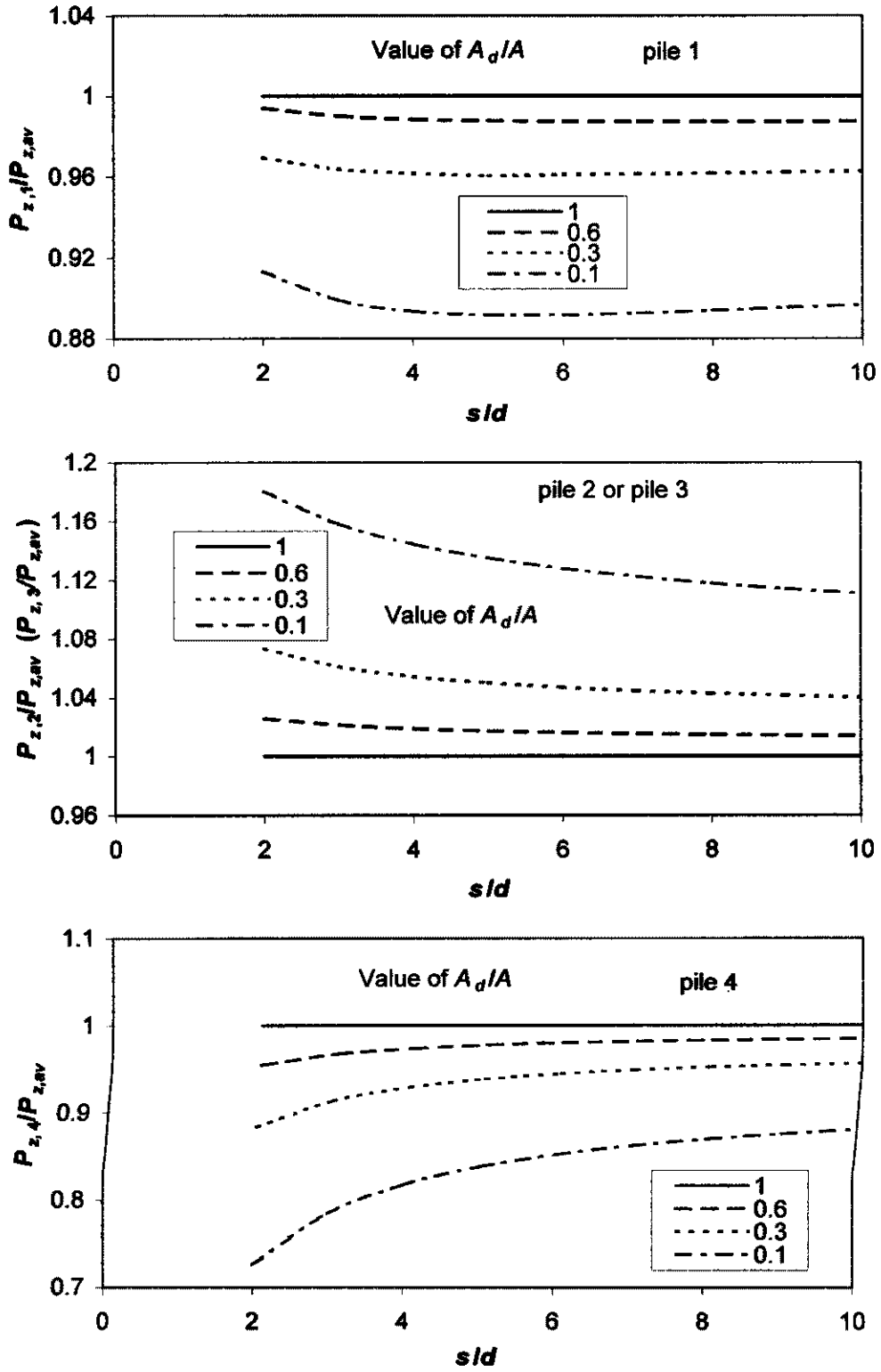

Fig. 8.5 $P_{z,i} / P_{z,av}$ vs s/d of a pile group containing a neck

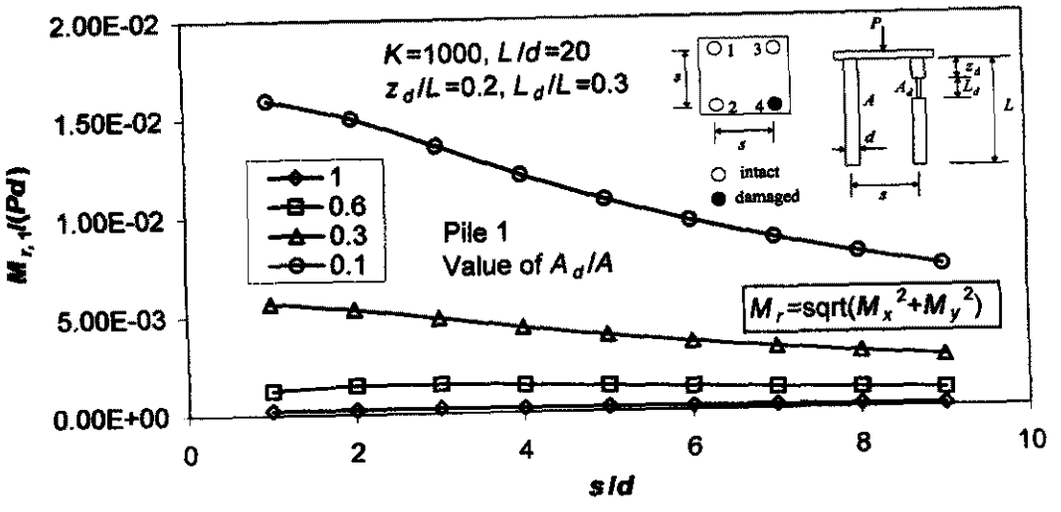

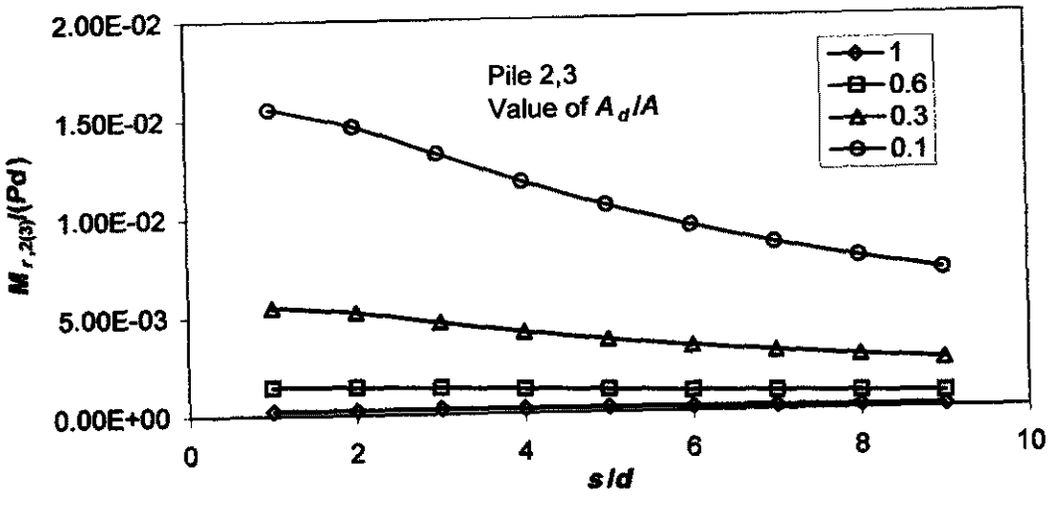

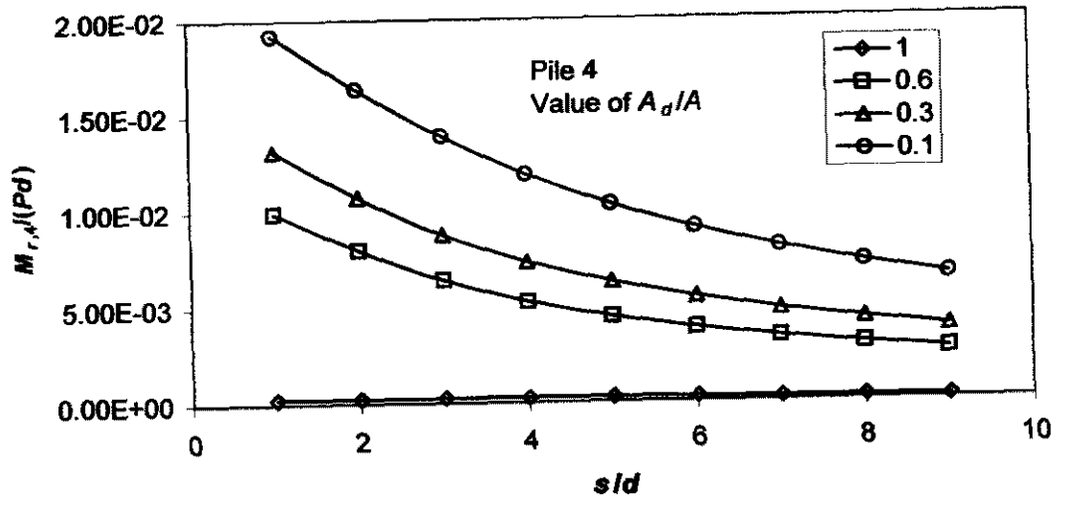

8.6 Normalized cap resultant moment of a pile group containing a neck

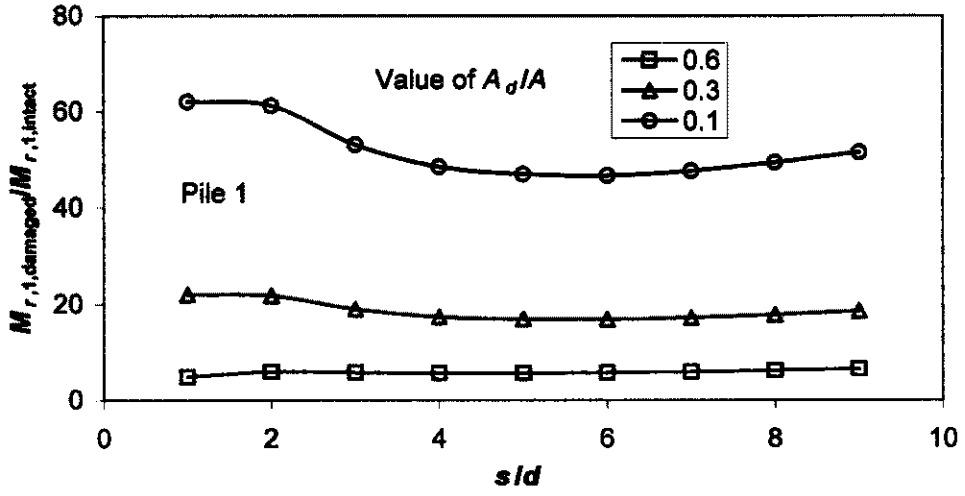

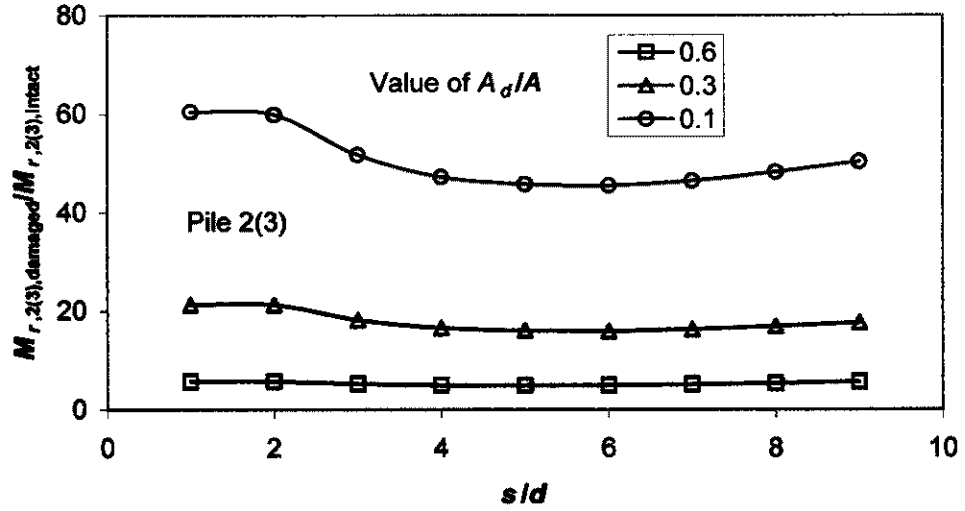

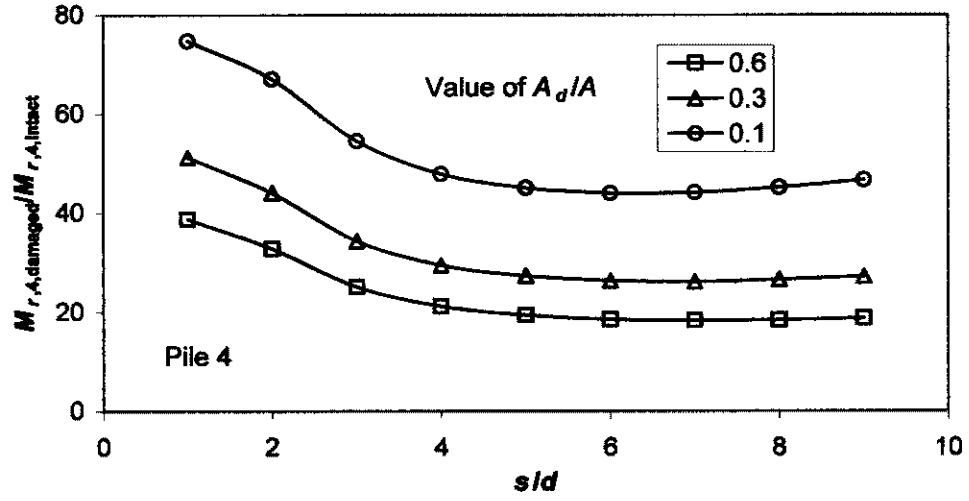

8.7 Ratio of cap resultant moment of a pile group containing a neck

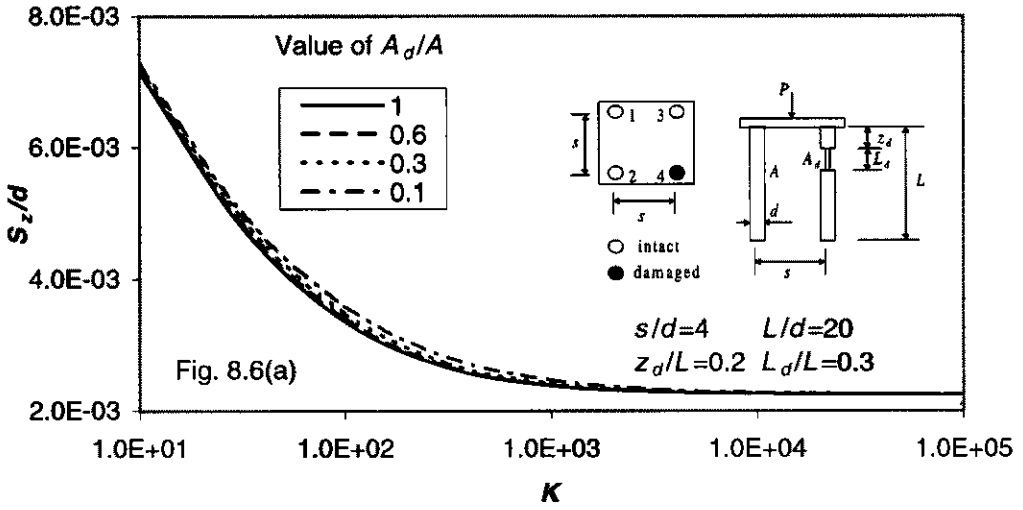

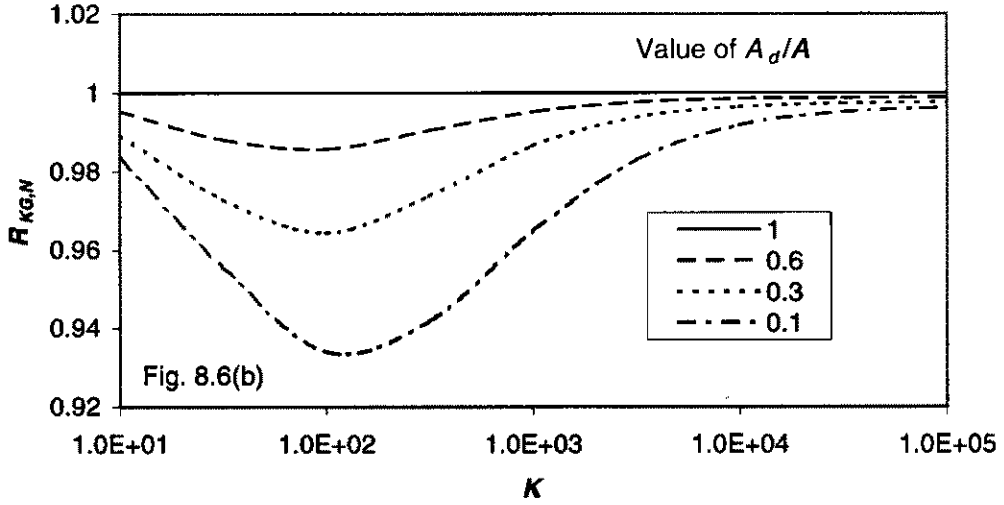

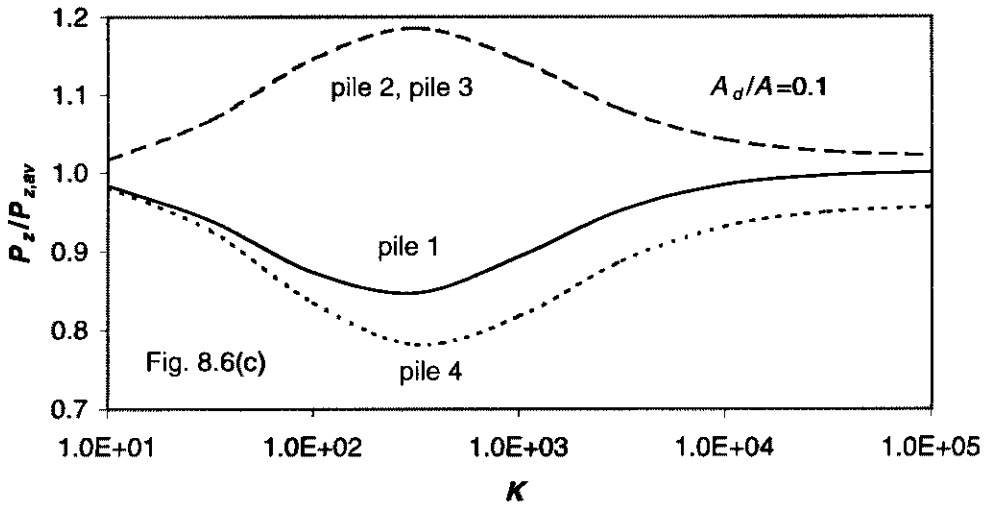

Fig. 8.8 Effect of K on a pile group containing a neck

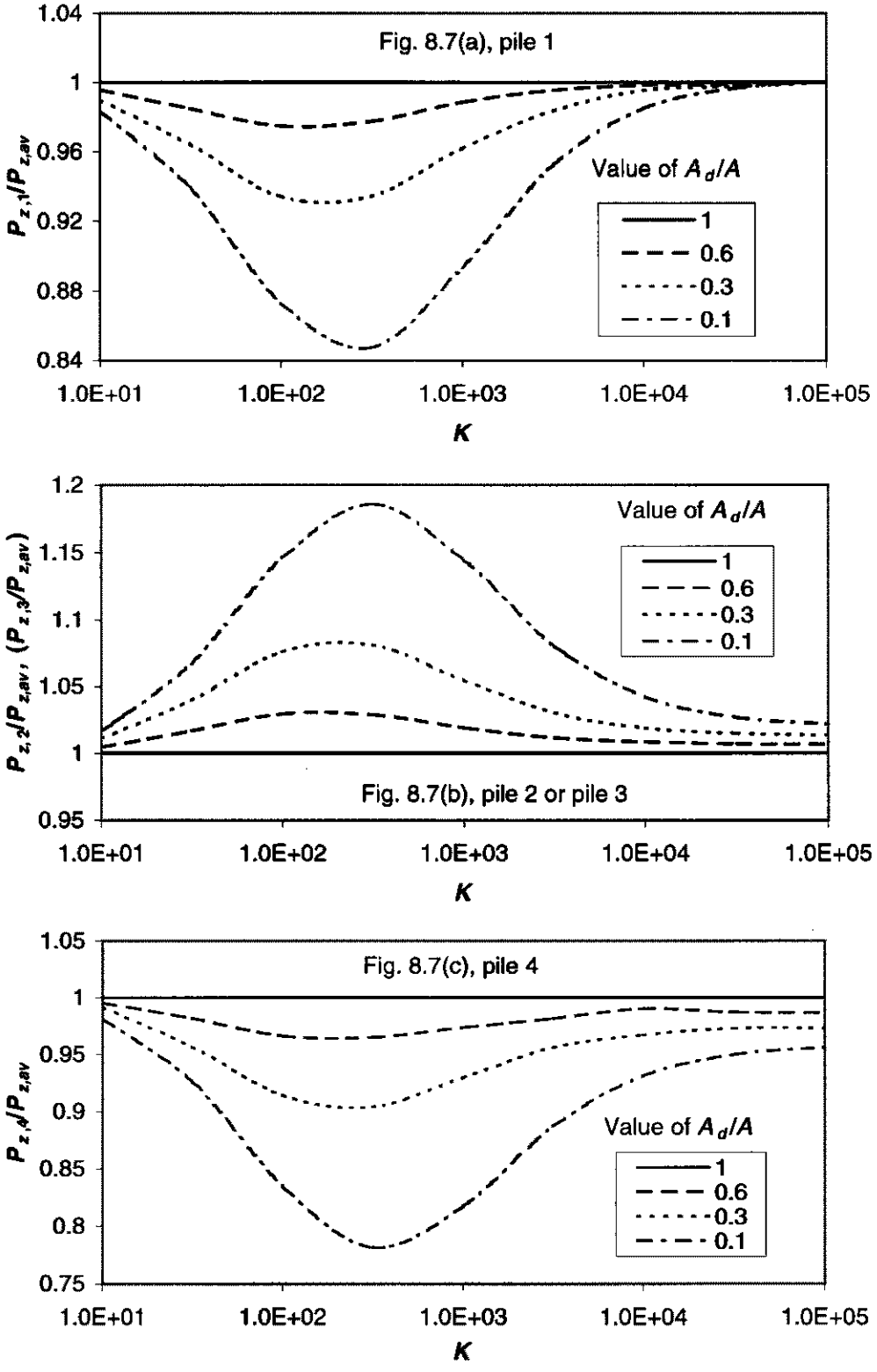

Fig. 8.9 Effect of K on pile head forces in a pile group containing a neck

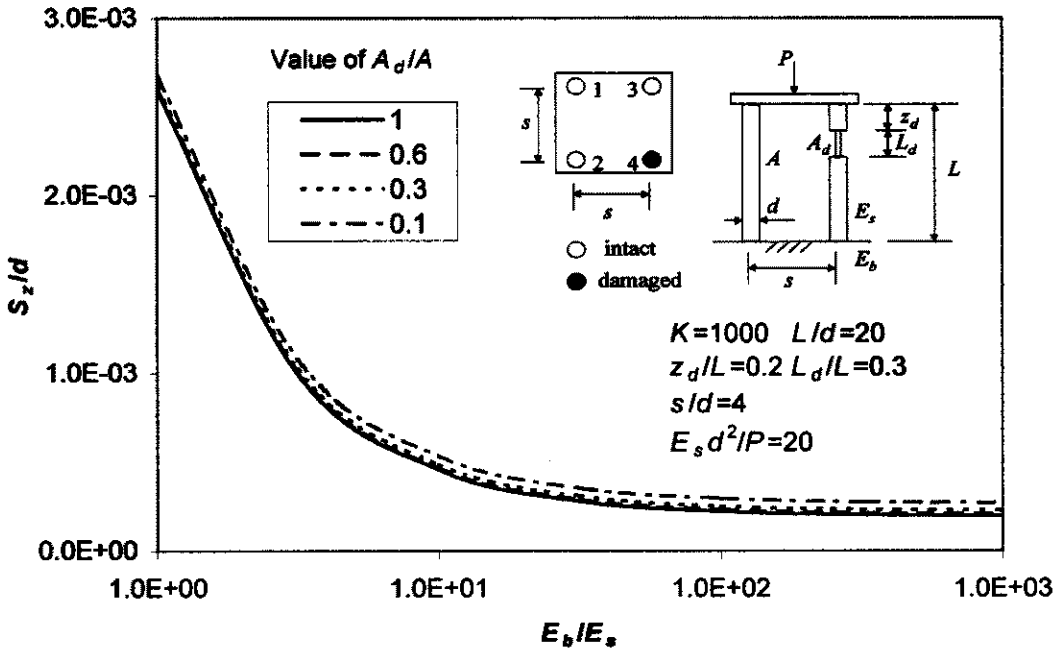

Fig. 8.10 S_z/d vs E_b/E_s of a pile group containg a necke pile

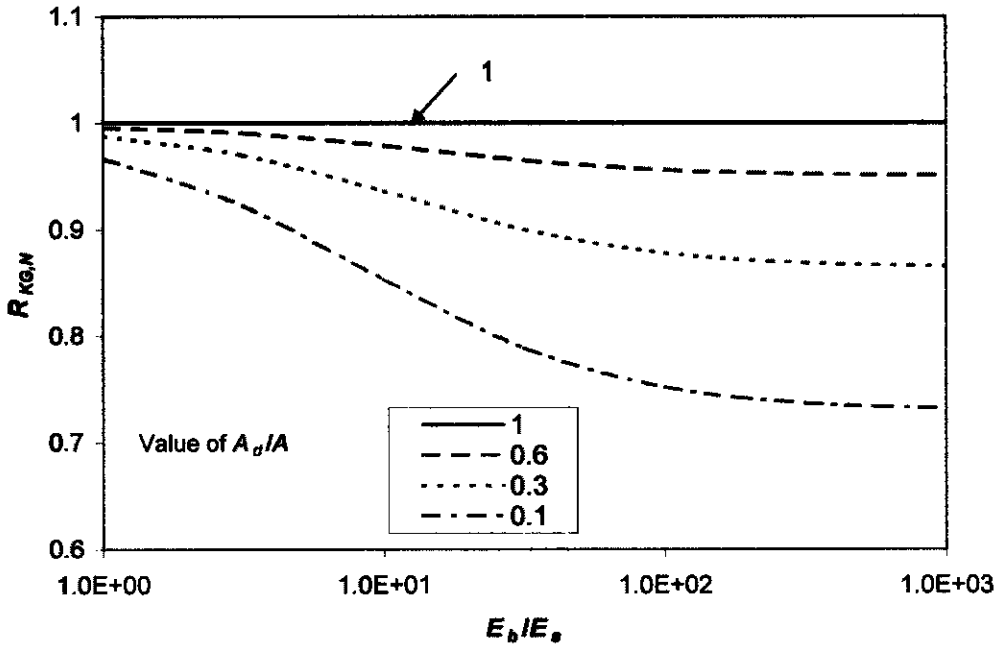

Fig. 8.11 $R_{KG,N}$ vs E_b/E_s of a pile group containg a necked pile

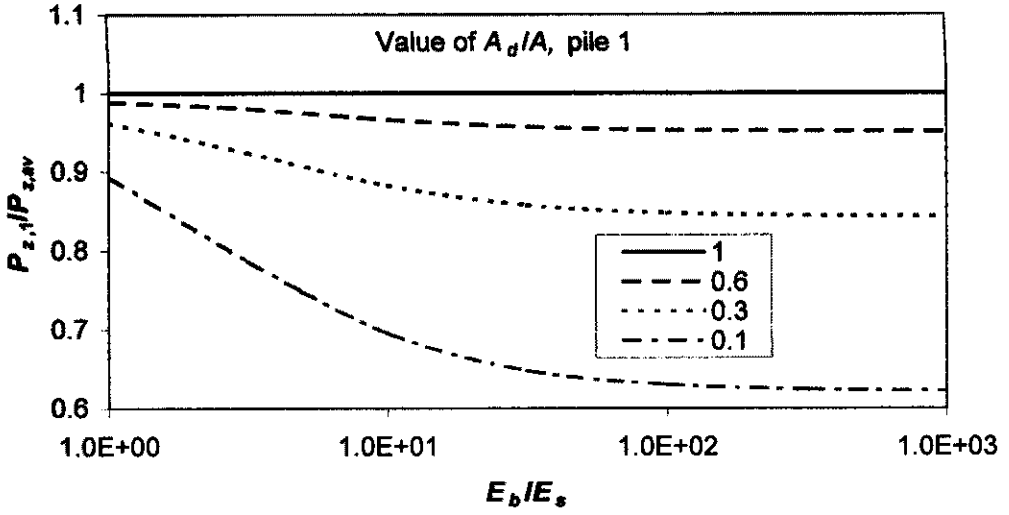

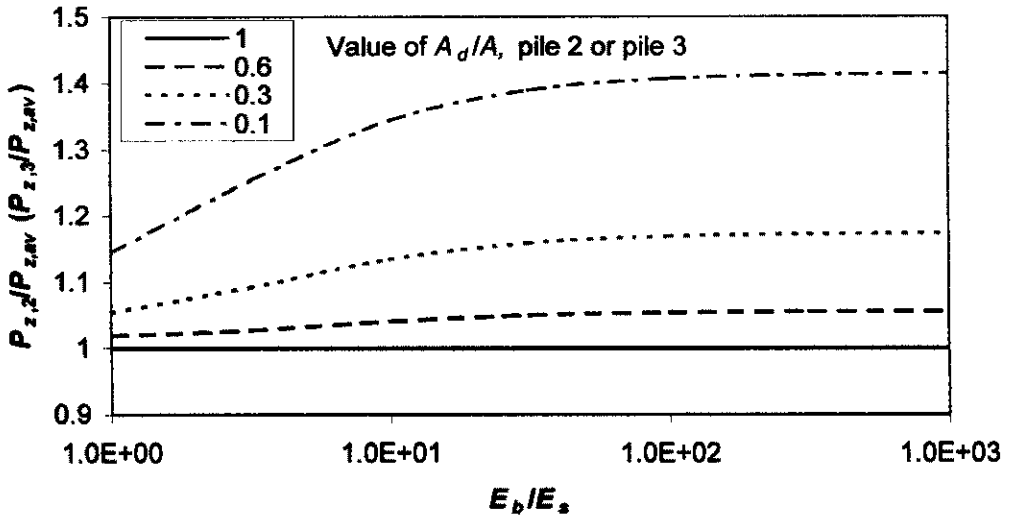

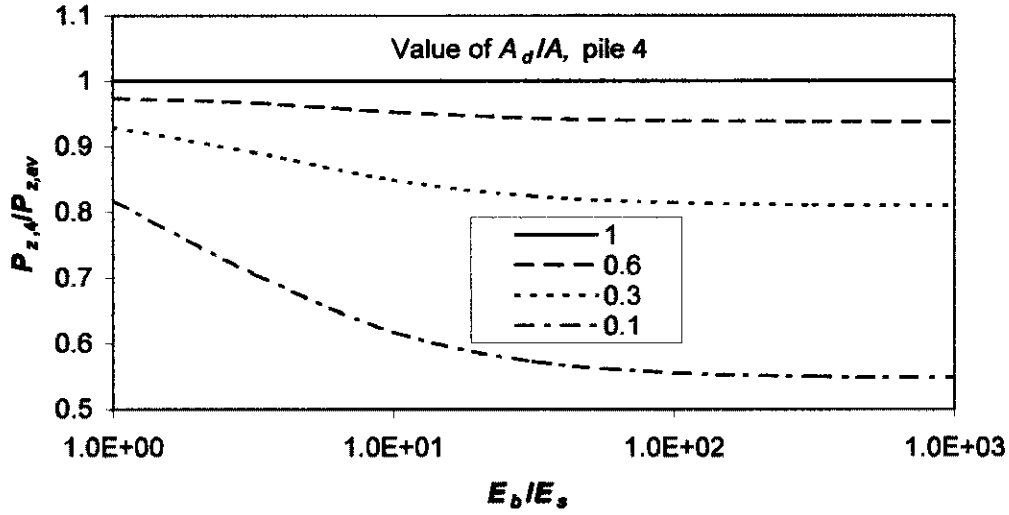

Fig. 8.12 $P_{z,i}/P_{z,av}$ vs E_b/E_s of a pile group containg a necked pile

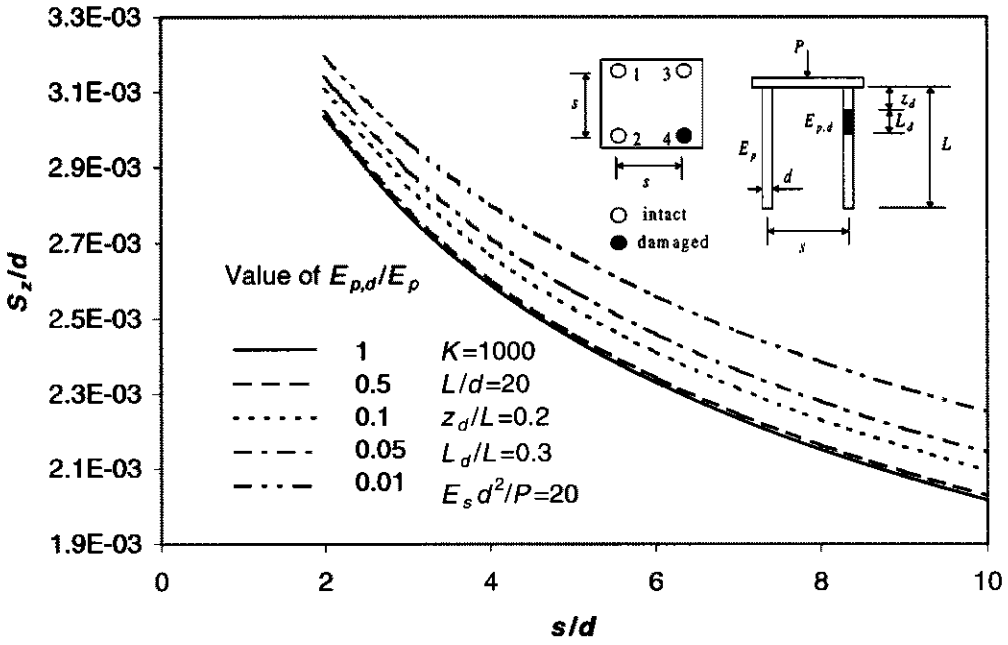

Fig. 8.13 S_z/d vs s/d of a pile group containing a honey-comb

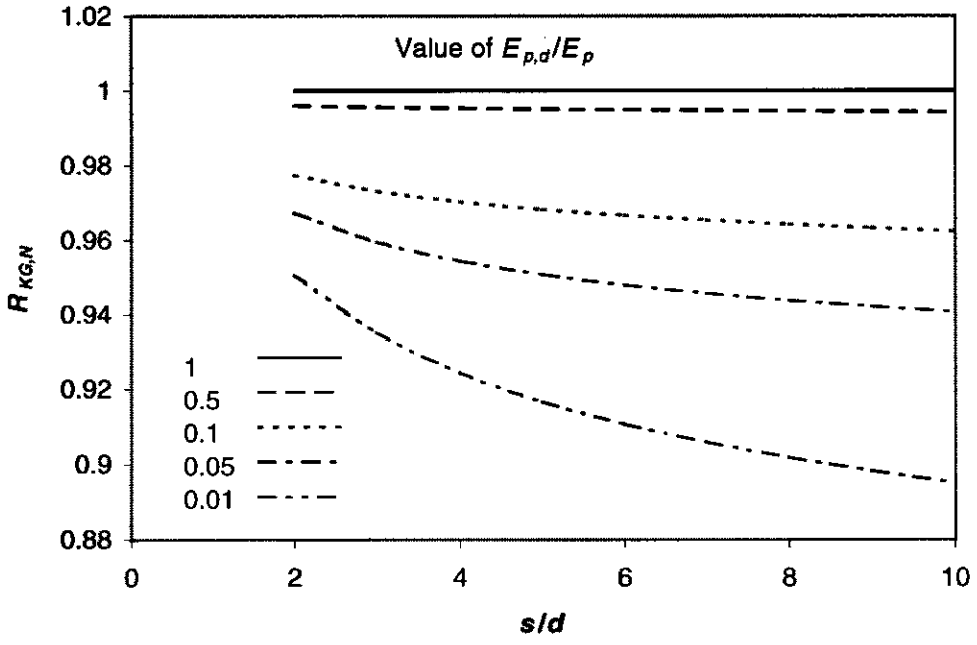

Fig. 8.14 $R_{KG,N}$ vs s/d of a pile group containing a honey-comb

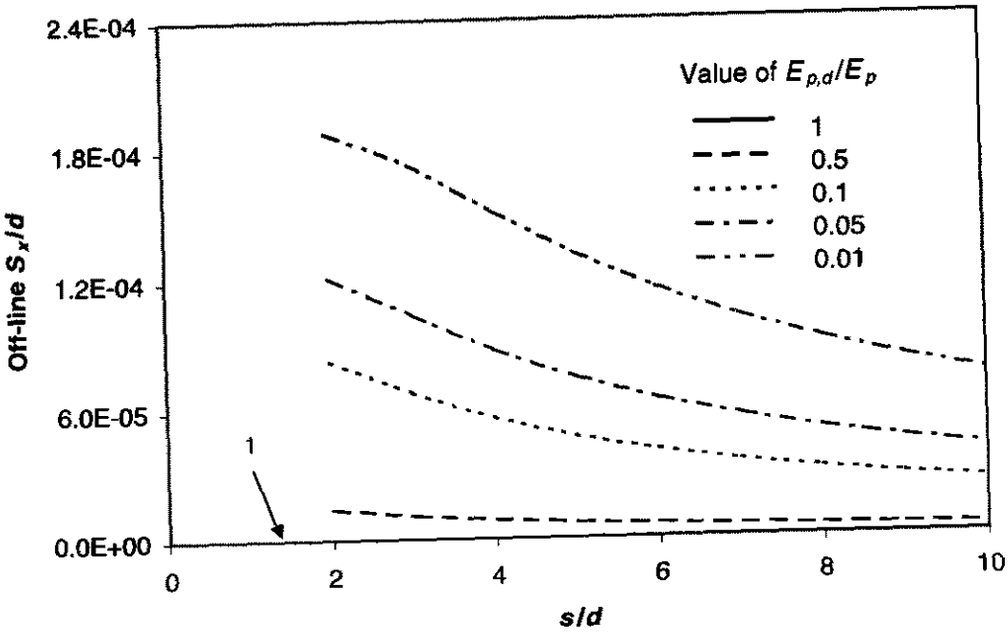

Fig. 8.15 Off-line S_x/d vs s/d of a pile group containing a honey-comb

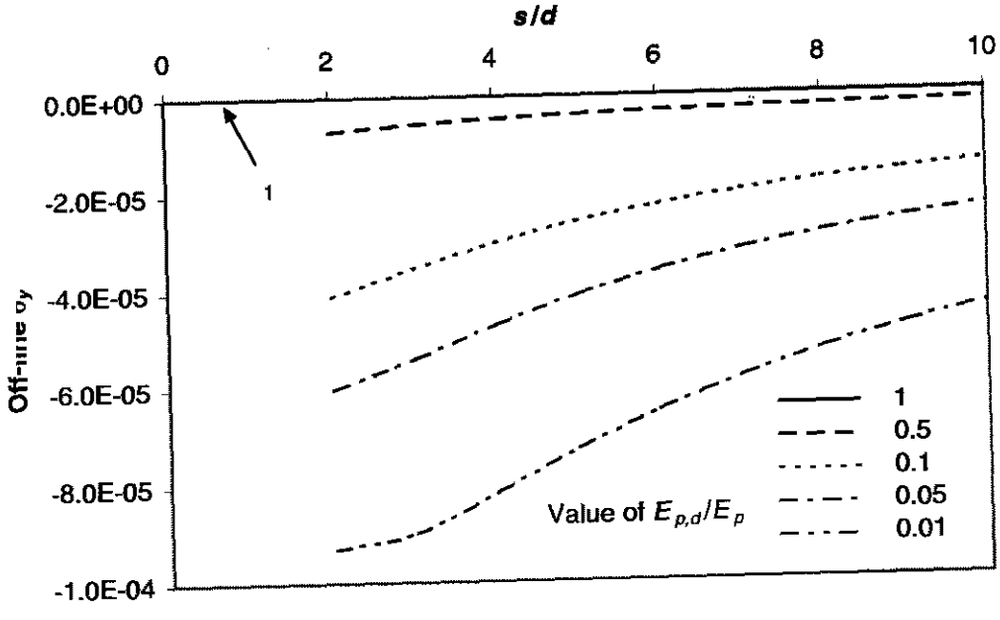

Fig. 8.16 Off-line θ_x vs s/d of a pile group containing a honey-comb

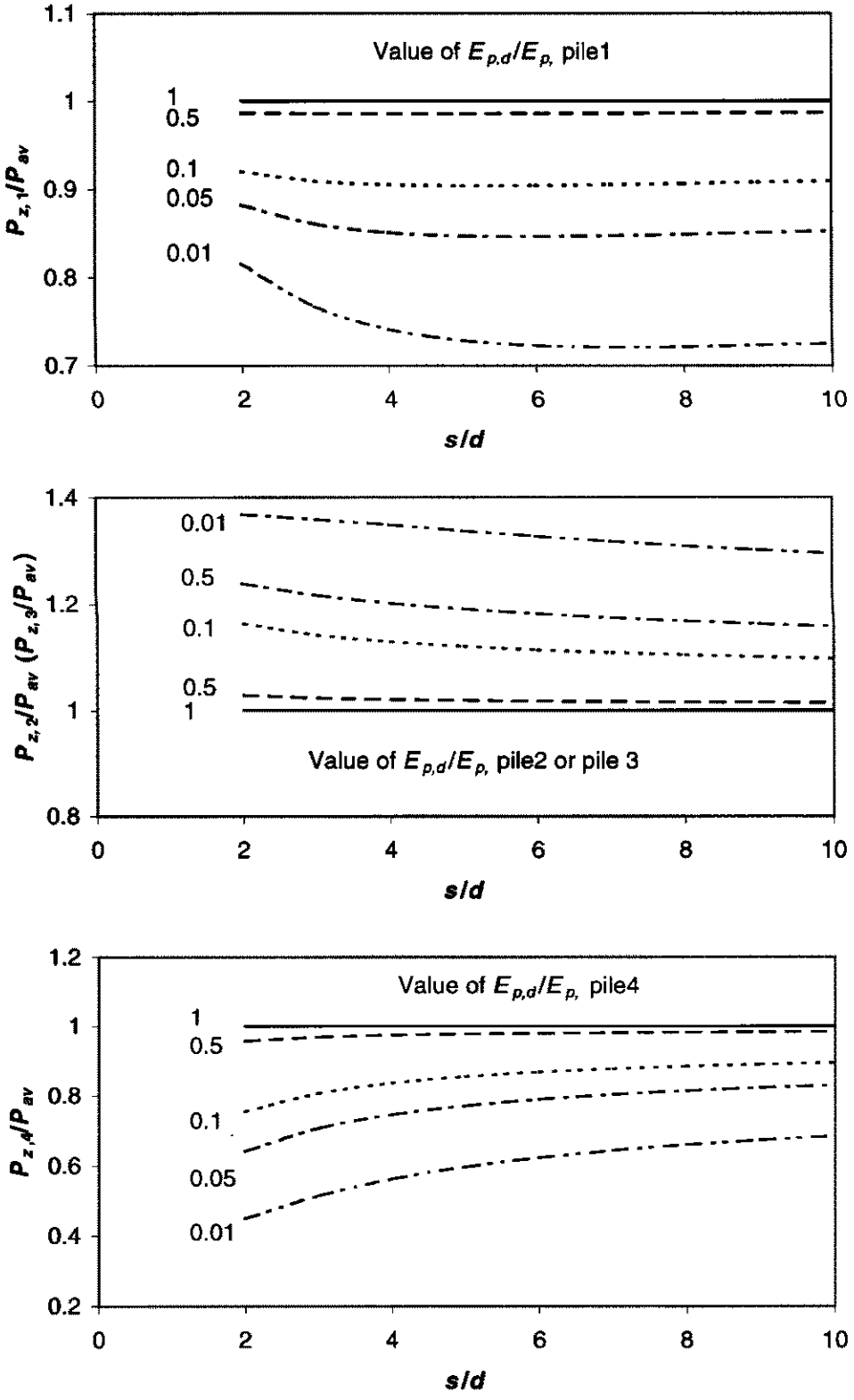

Fig. 8.17 Off-line S_x/d vs s/d of a pile group containing a honey-comb

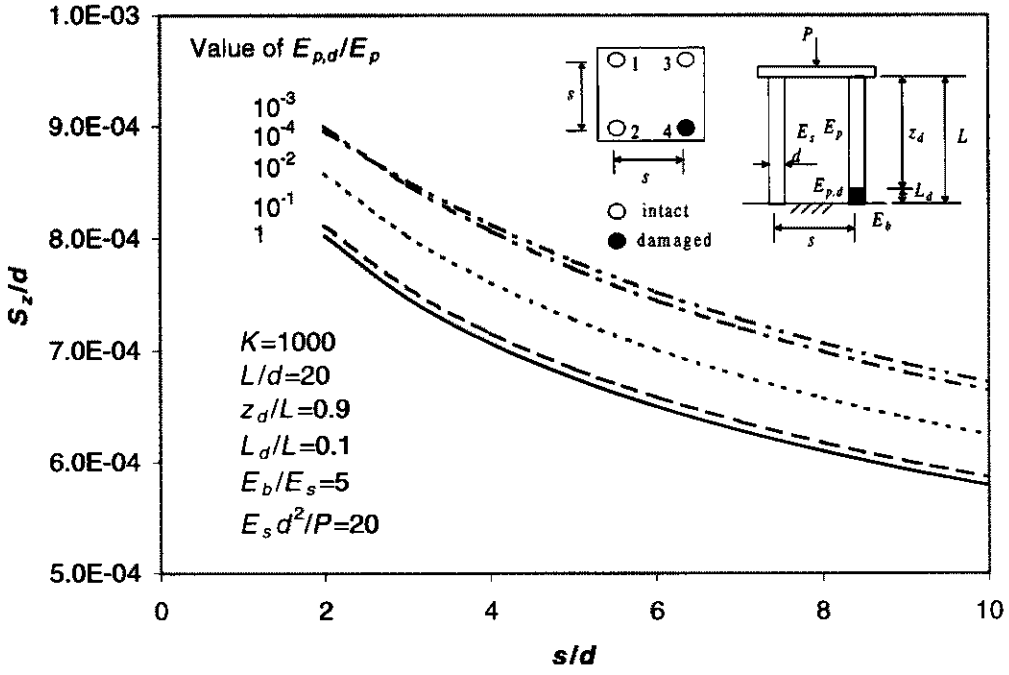

Fig. 8.18 S_z/d vs s/d of a pile group containing a soft-base

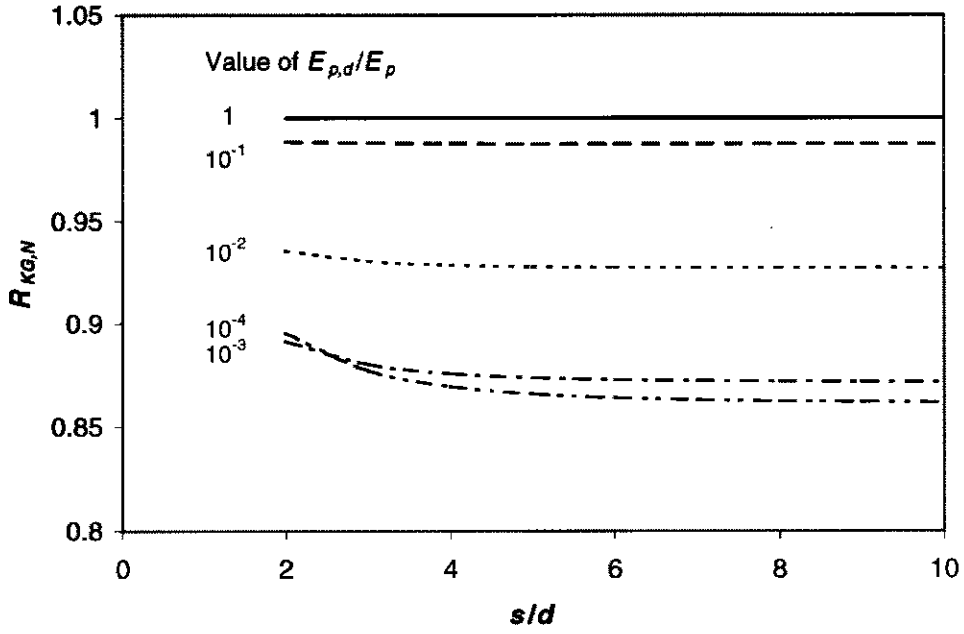

Fig. 8.19 $R_{KG,N}$ vs s/d of a pile group containing a soft-base

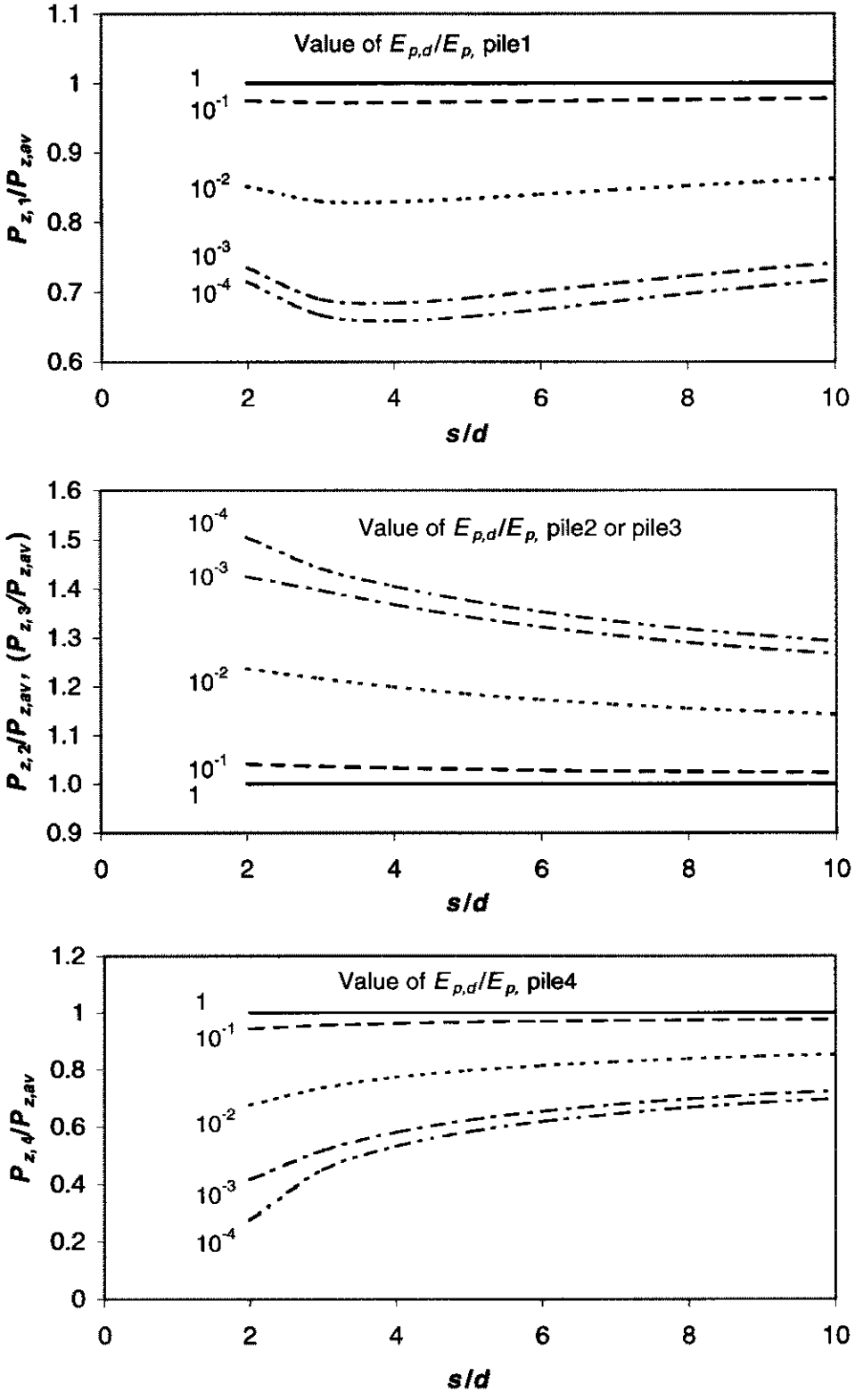

Fig. 8.20 $P_{z,i}/d$ vs s/d of a pile group containing a soft-base

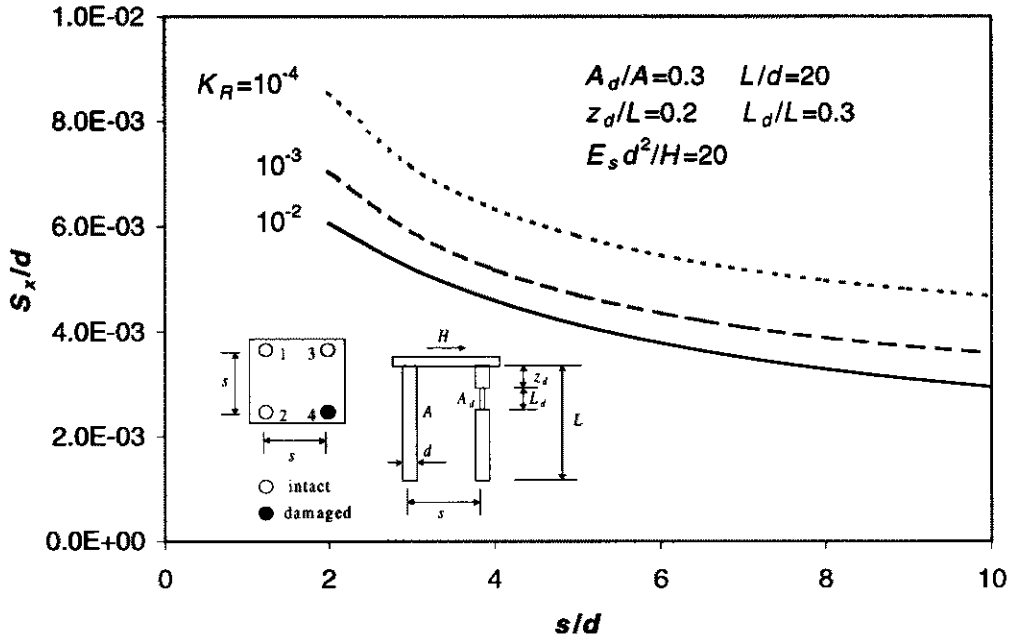

Fig. 8.21 S_x/d vs s/d of a pile group containing a neck

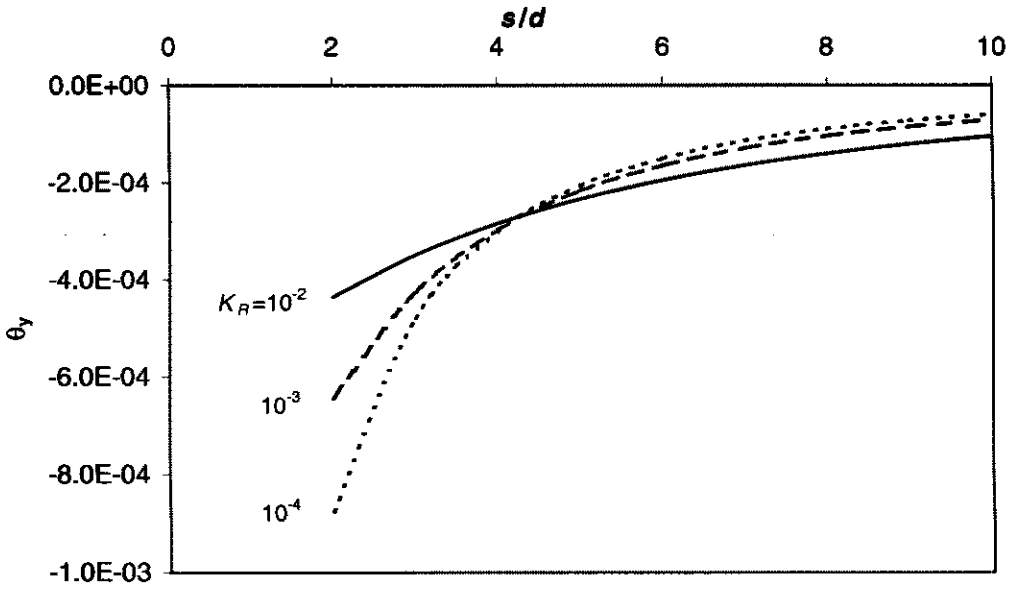

Fig. 8.22 θ_y vs s/d of a pile group containing a neck

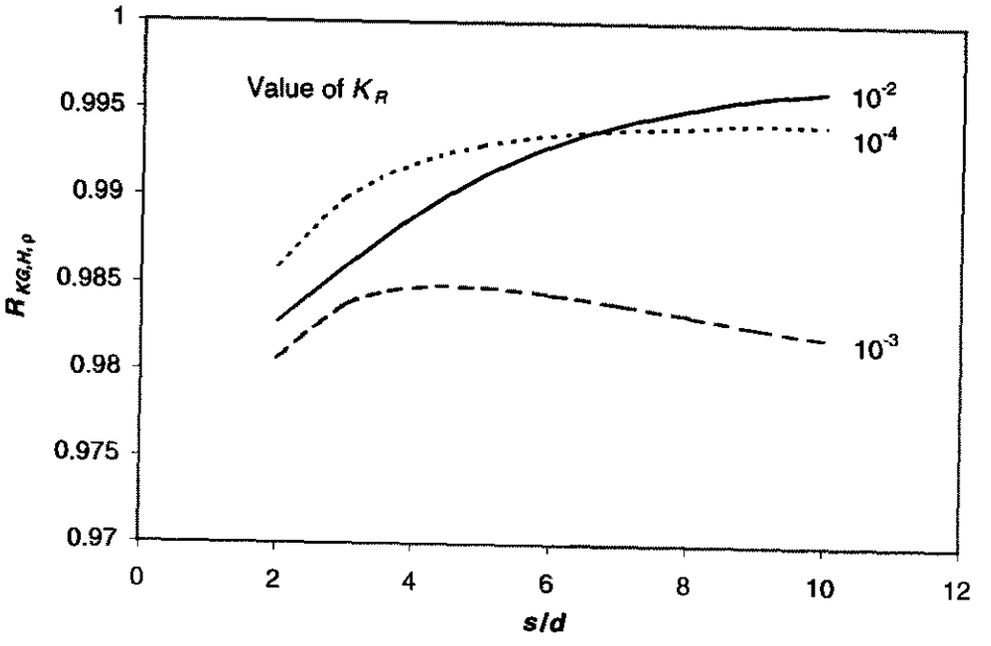

Fig. 8.23 $R_{KG,H,\rho}$ vs s/d of a pile group containing a neck

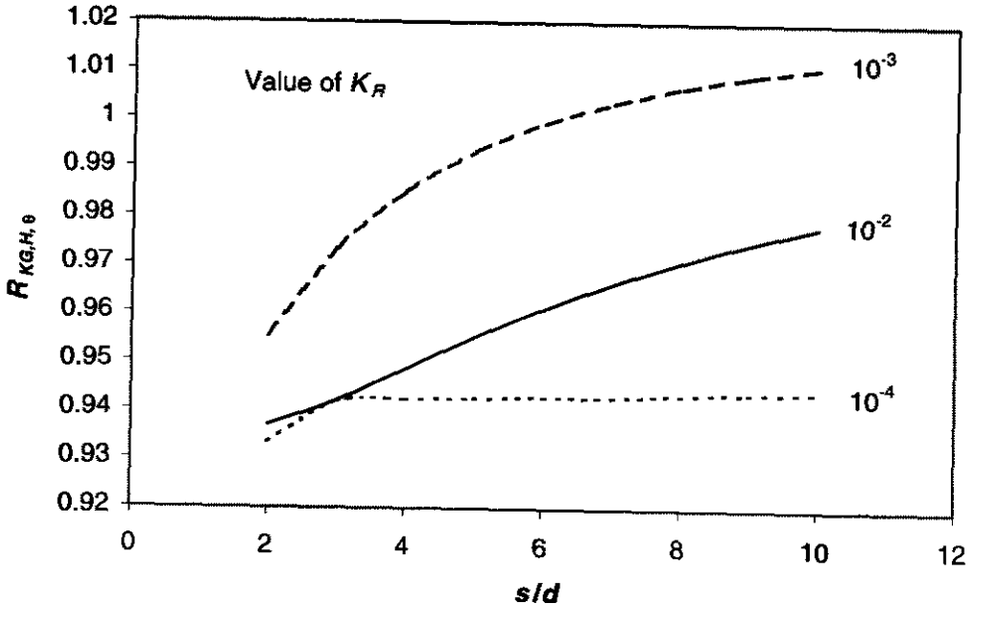

Fig. 8.24 $R_{KG,H,\theta}$ vs s/d of a pile group containing a neck

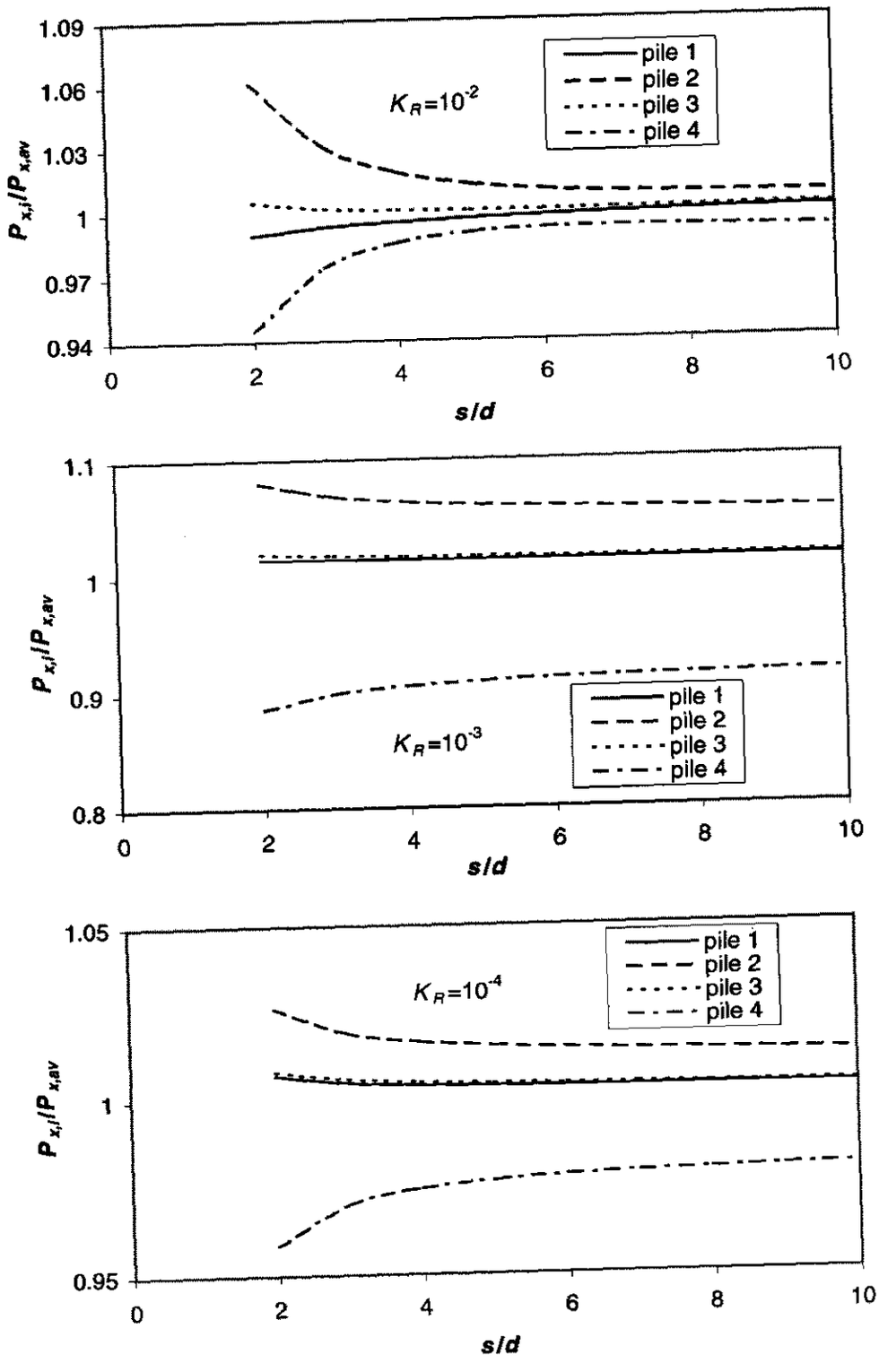

Fig. 8.25 $P_{x,i}/P_{x,av}$ vs s/d of a pile group containing a neck

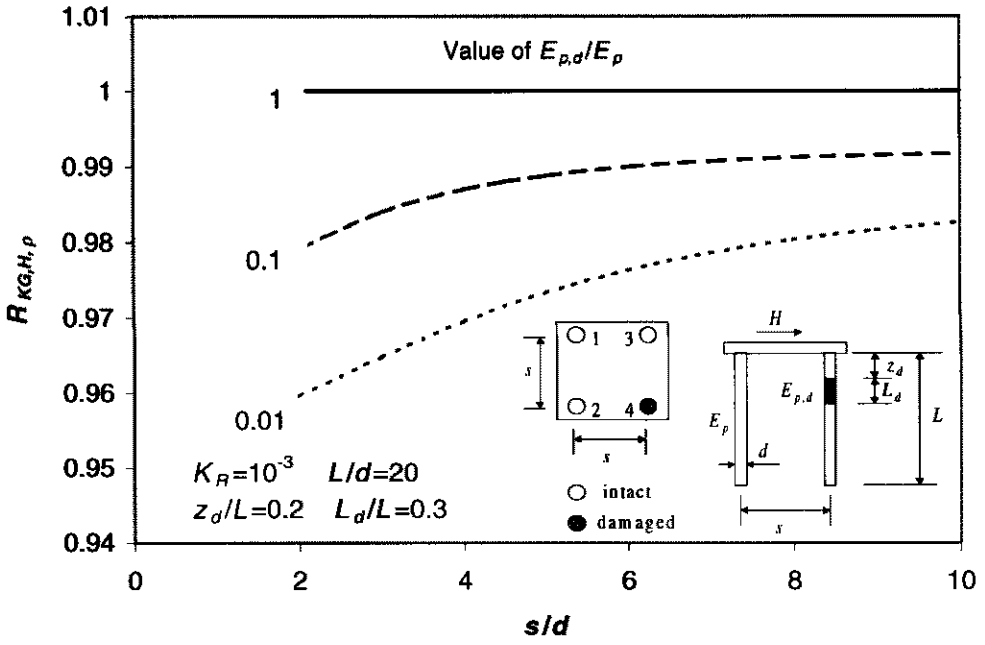

Fig. 8.26 $R_{KG,H,\rho}$ vs s/d of a pile group containing a honey-comb

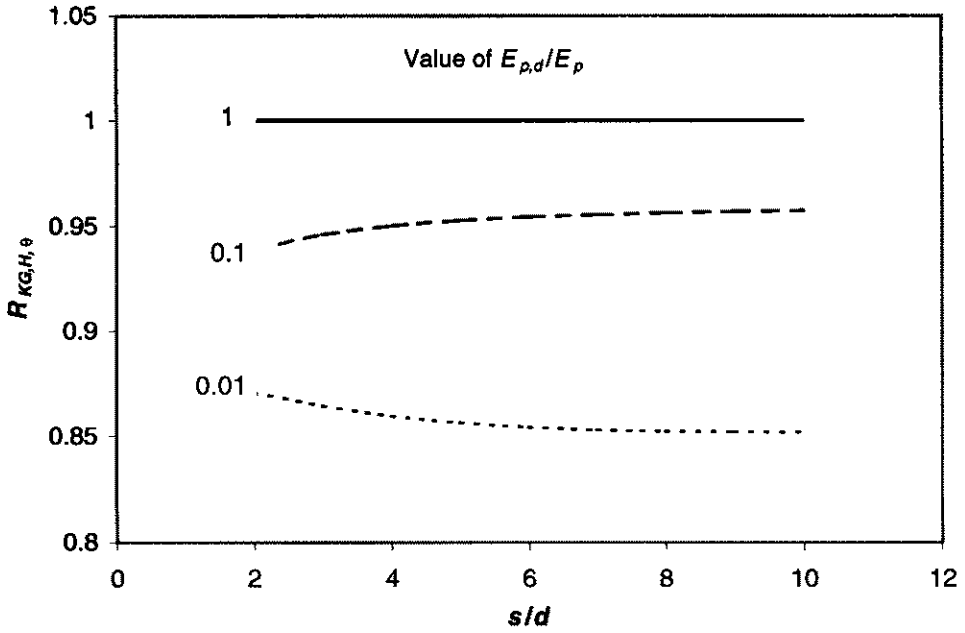

Fig. 8.27 $R_{KG,H,\theta}$ vs s/d of a pile group containing a honey-comb

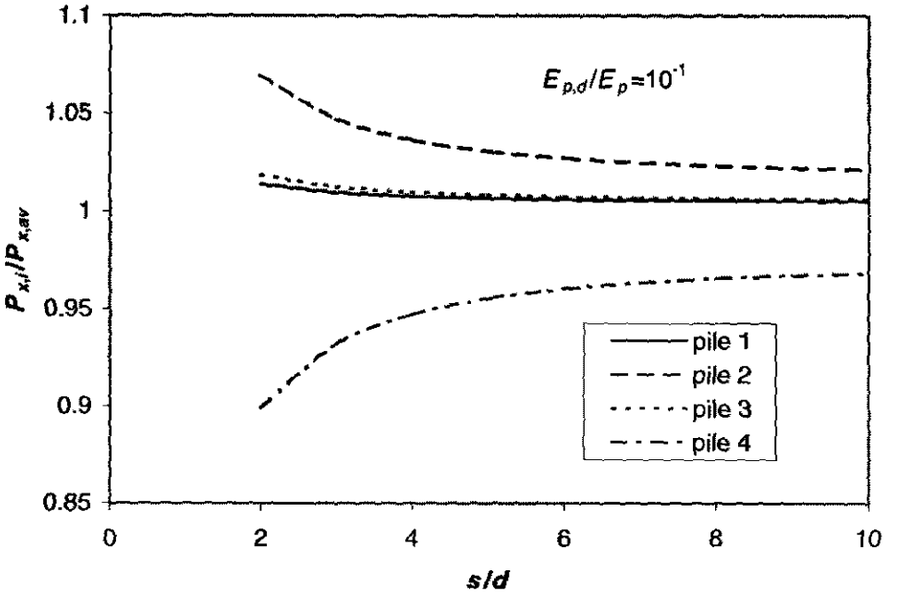

Fig. 8.28 $P_{x,i}/P_{x,av}$ vs s/d of a pile group containing a honey-comb

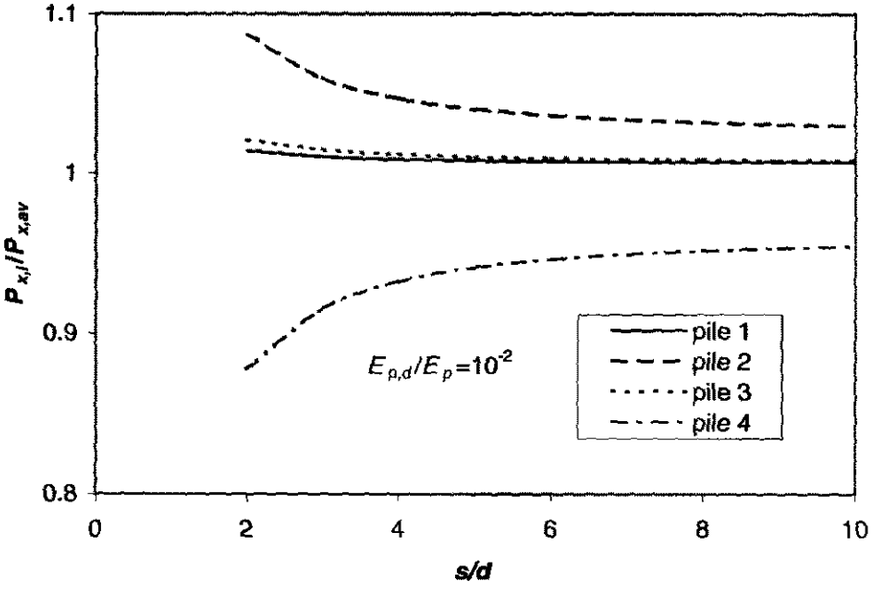

Fig. 8.29 $P_{x,i}/P_{x,av}$ vs s/d of a pile group containing a honey-comb

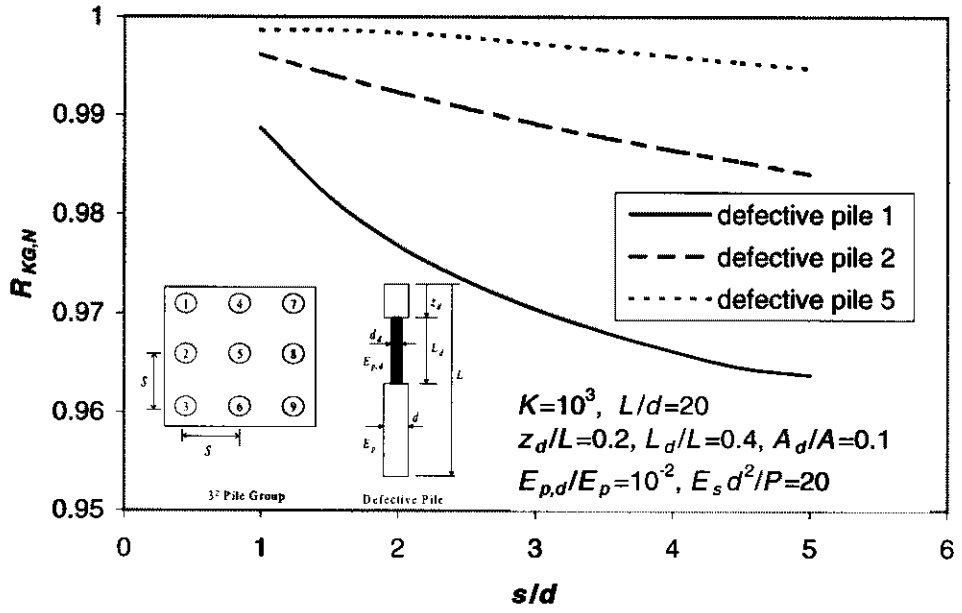

Fig. 8.30 $R_{KG,N}$ vs s/d of a group containing a defective pile

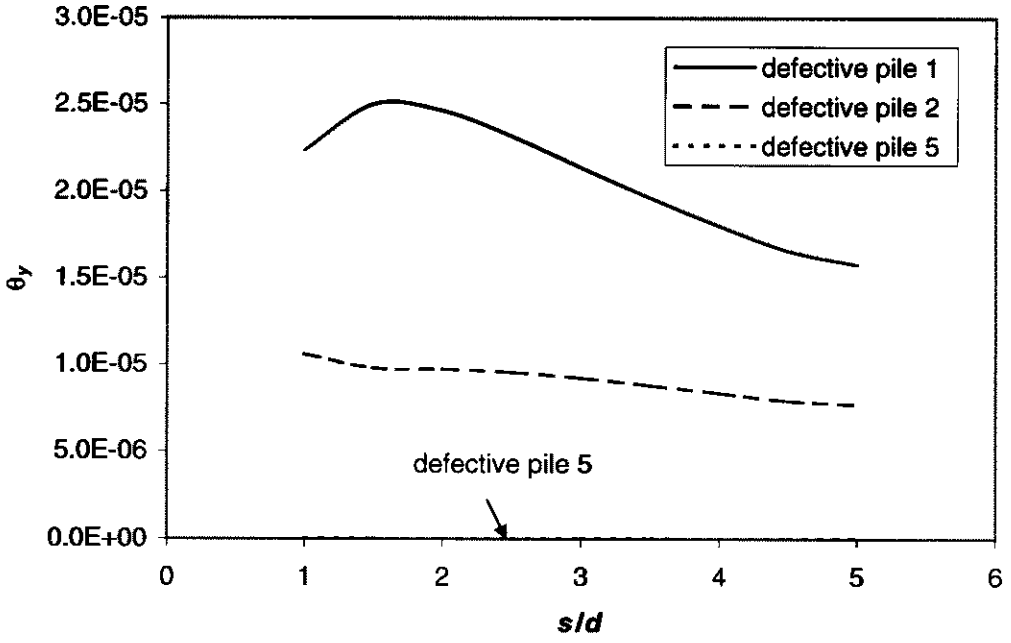

Fig. 8.31 θ_y vs s/d of a group containing a defective pile

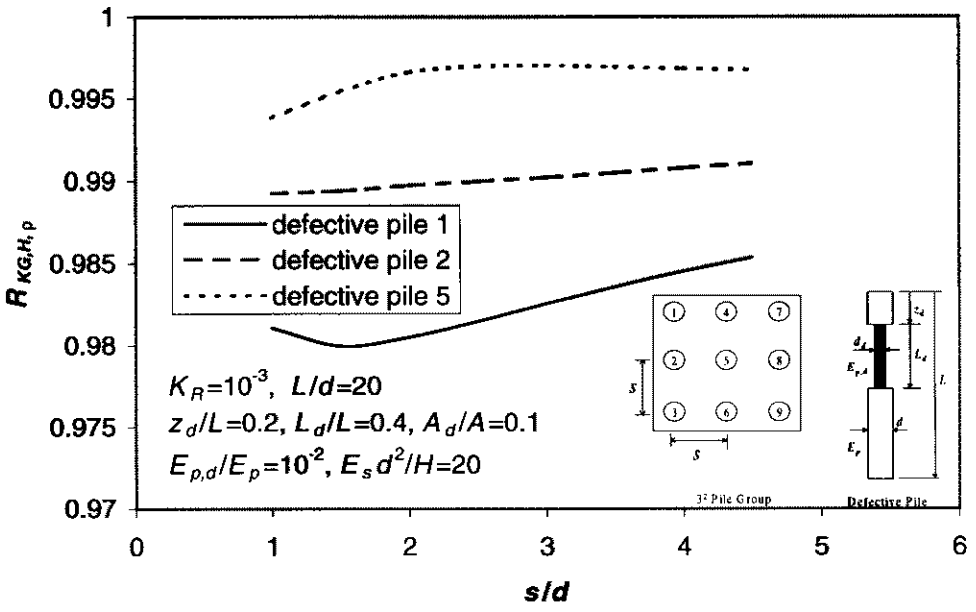

Fig. 8.32 $R_{KG,H,\rho}$ vs s/d of a group containing a defective pile

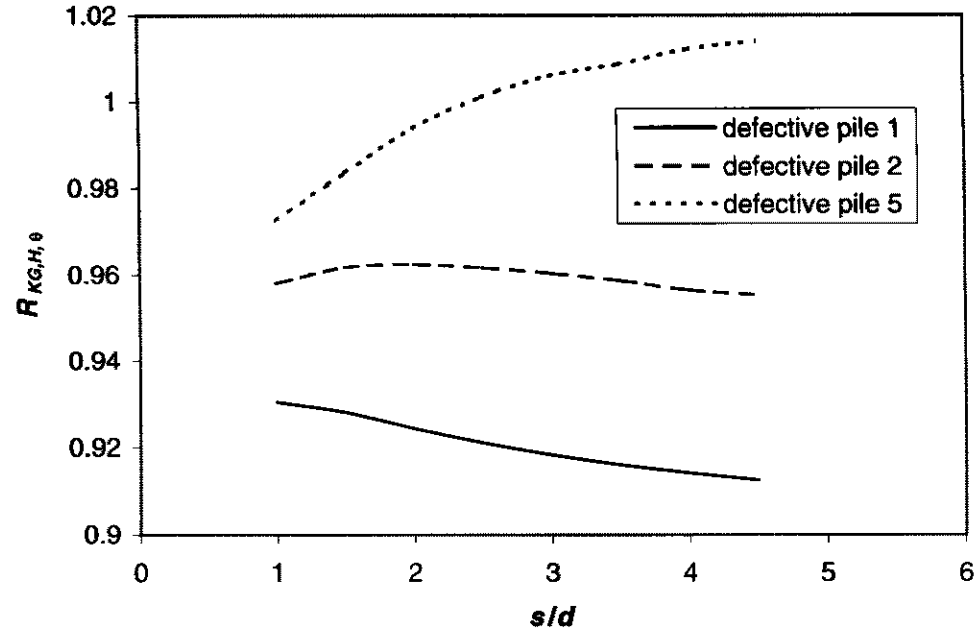

Fig. 8.33 $R_{KG,H,\theta}$ vs s/d of a group containing a defective pile

Chapter 9

Tests on Model Piles Containing Structural Defects

9.1 Introduction

As reviewed in Chapter 2, a considerable amount of literature has been published on investigations into the dynamical behaviour of defective piles via low-strain integrity testing and high-strain dynamic pile testing. Because it is difficult to experimentally model "defects" in a real pile which has been embedded in soil, there appears to be very little experimental data regarding the static behaviour of defective piles, such as the effects of stiffness reduction of defective piles compared to sound piles. Rao *et al* (1992) performed model tests on piles with various types of defects, and found (as would be expected) that significant increases in settlement could occur because of the presence of such defects. Before theories are applied to practical problems, the accuracy of the behaviour predicted needs to be established. This can best be achieved by carrying out model pile tests under controlled conditions.

In this chapter, the main objective has been to study the static behaviour load-settlement characteristics and stiffness reduction effects, of piles containing "necks" which are a common, form of structural defect. The results are believed to provide a better insight into the behaviour of structurally defective piles and, importantly, to provide experimental data against which to compare the theoretical analyses.

In the series of tests described herein the defective piles have been driven into a consolidated layer of clay. Attention has been directed towards the load settlement behaviour of defective piles for a range of length and diameter ratios of the defective part to the sound part. No attempt has been made to determine the strains or deformations within the soil mass.

9.2 Defective Pile Model Testing

9.2.1 Experimental Apparatus

The basic components of the apparatus were a steel pressure vessel, an applied load system, data acquisition system, a pore water system and a pressure supply. The layout of the apparatus is shown diagrammatically in Fig. 9.1.

The internal diameter of the large pressure vessel was 590mm, which provided sufficient area for the installation of eight relatively small-diameter defective piles, while the depth was 540mm. Drains were provided on the top and base vessel, and in the centre of base plate, the drain was protected with gauze and covered with filter paper to permit drainage of water from the clay under pressure. The vessel cover is also shown in Fig. 9.1 and consisted of an O ring (to provide the seal), a rubber membrane, a spacing ring, a domed lid and a stiffening ring. This top assembly was secured to the base of the vessel with twenty Allen screws. The design of the pressure vessel was similar to that described by Wiesner (1977) and Rowe (1978).

The applied load was measured by the deflection of a proving ring, which was recorded by a linear displacement transducer. The pile vertical displacement near the soil surface was recorded by two linear displacement transducers which were located on a hole-centred plate. The plate could be vertically slipped along a pile and fixed into a required position (slightly over soil surface). A microcomputer-based data acquisition system was used to convert voltage outputs from the displacement transducers at the pile head and in the proving ring into load and deflection values. The connections between the loading machine, proving ring and piles were all rigid. The nominal pile loading rate was 1.53 *mm/min.*

9.2.2 Defective Pile Details

For convenience of installation, the structural defect was designed to be located in the lower part of a pile. The model defective and sound piles are graphically shown in Fig. 9.2, where diameter D_1 and length L_1 are for the "intact part" and diameter D_2 and length L_2 are for the "defective (necked) part". The "intact part" of a pile was an aluminum tube of 25 mm diameter, except piles no. 1 and 8 which were solid with diameters of 12 *mm* and 6 *mm* respectively. The "defective part" was made of a solid rod with a diameter ranging from 5 to 12 *mm*. The tip of the piles was closed. The model piles were made from aluminum with a Young's Modulus of 7.0 x 10^4 *MPa*. The assembled parts of the model piles, pictured in Fig. 9.3, were manufactured separately and could be easily screwed together. Details of these model piles are shown in Table 9.1. It should be noted that these model piles used are not truly "defective" piles, which may be classified as "step-taper piles" (Bowles 1988). The main reasons to choose these step-taper piles as "defective" piles are for: 1. easily testing, 2. better pile-soil interface. 3. easily interpreting.

Table 9.1. Details of the parts of model defective piles

Pile No	Defective Part		Sound Part		
	Length (*mm*)	Diameter (*mm*)	Length (*mm*)	Outer Diameter (*mm*)	Wall Thickness (*mm*)
1	0		360	12	Solid
2	150	10	470	25	1.2
3	150	5	470	25	1.2
4	240	6	470	25	1.2
5	240	12	470	25	1.2
6	0		470	25	1.2
7	0		570	25	1.2
8	0		500	6	Solid

9.2.3 Properties of the Clay

The series of tests reported in this section were performed using a refined type C/10 Kaolin. This material was selected because it consolidates quickly and does not creep excessively. It has been used successfully in previous model foundation tests by Davis and Poulos (1968), Mattes and Poulos (1971), Brown (1972), Wiesner (1977) and Rowe (1978).

9.2.3.1 General Properties of the Clay

The typical chemical, physical and size properties of the clay, supplied by Commercial Minerals Limited, Australia, are listed below:

Typical physical properties are as follows:

Specific gravity	2.6
Bulk density	0.65 g/cm^3

Typical particle size characteristics are:

Retained on 150 micron sieve maximum 0.1 per cent
Retained on 75 micron sieve maximum 1.0 per cent
Retained on 53 micron sieve maximum 2.0 per cent

The grading curve obtained from a particle size analysis using the hydrometer method (Wiesner, loc cit), indicted that in terms of the M.I.T. grain size classification, the material contains 70% silt and 30% clay. Liquid and plastic limits for the C/10 Kaolin were 45 and 33 respectively, and hence by the unified system, it may be classified as a silty clay (Rowe, 1978).

9.2.3.2 Consolidation Characteristics of the Clay

In order to carry out the consolidation of the clay properly for model pile tests, the consolidation characteristics of the clay should be known. The permeability of the clay was obtained via a conventional oedometer consolidation test, and the results of these curves (void ratio e *v.s.* logarithmic effective vertical stress $\log\sigma'_v$ and coefficient of consolidation c_v against $\log\sigma'_v$) are shown in Figs. 9.4 and 9.5.

9.2.4 Clay Preparation

In eight galvanised steel containers, Kaolin clay was mixed mechanically, using a power drill fitted with a propeller until a reasonably uniform paste with 55% water content was formed. The containers were sealed and allowed to stand for 24 hours, after which the clay was again thoroughly mixed. It was then poured into the pressure vessel and vibrated to remove as much of the entrapped air as possible. When the vessel was full of clay, the top assembly (*i.e.* O-ring, rubber membrane, spacing ring, domed lid and stiffening ring) was screwed on. Water under pressure was injected between the domed lid and rubber membrane to consolidate the clay. The pressure was applied via an air-water exchange bottle using a controlled pressure. As the clay consolidated, water flowed out of the drains at the top and bottom of the vessel and the total volume of expelled water was continuously measured in a measuring cylinder.

Initial consolidation of the clay was carried out under a pressure of 100 *kPa*. After this initial consolidation, the applied pressure was relieved and the lid removed and the clay re-topped. Several increments of such consolidation, followed by re-topping of the clay in the pot, were required to finally achieve the required depth of normally consolidated clay. The top assembly was screwed onto the vessel and the clay was consolidated under a final consolidation pressure of 200 *kPa*. On completion of primary consolidation under this pressure the clay was left to age for 15 days in order to reduce the influence of the secondary compression on both the pore pressure and settlement behaviour in the test. After this time, the lid, sand and filter paper were removed and the model pile tests were performed. Soon after the pile tests had been completed, the clay was sampled at depth

intervals of every 200 *mm* and its moisture content was determined. At this stage, the average moisture content of the clay was about 36%.

9.2.5 Pile Testing

After the clay had been prepared inside the vessel, the steel loading handle attached to the loading device was lowered down, by hand winding the loading machine, to start installing the pile into the clay to the required depth. A rest period of 30 minute was allowed between pile installation and pile testing. Each pile was then loaded at a loading rate of 1.53 *mm/min* (see Fig. 9.6). The load-time and settlement-time data curve were synchronously recorded by the data acquisition system at intervals of 10.8 seconds. The model test program, using 8 model piles, involved a total of 36 tests in three categories:

A) 18 tests on defective floating piles

B) 16 tests on sound floating piles

C) 2 tests on end bearing piles, one sound, one defective.

Details of these tests are given in Table 9.2.

9.3 Experimental Results

9.3.1 Load-Settlement Behaviour of Model Piles

As is well known, a typical load-settlement curve for a sound pile can be characterised by three stages, *i.e.*, an early stage (small deformation, primarily elastic); an intermediate stage (larger deformations, progressively non-linear) and a final stage (very large deformations, yielding to failure). Very similar shapes were measured in defective pile tests as shown in Figs. 9.7 and 9.8 (Fig. 9.8 shown an enlarged view of the results in Fig. 9.7). These Figures indicate that the elastic deformation is very small compared with the deformation at yielding. In the unloading phase, the load decreases almost linearly, with a relatively small residual deformation. At yielding, the load capacity of the defective piles decreased compared to the intact piles, while the corresponding settlements are

approximately 0.2 *mm*, which implies that there is only a minor effect of the embedded length L_1.

Fig. 9.9 and 9.10 show the measured pile load and settlement versus time. Three approximately linearly phases exist in the load-time and settlement-time relationship, *i.e.*, rapid increase in the early and intermediate stages, a "flat-line" in the final stage, and a rapidly decrease in the unloading stage. It was found that all floating pile tests (34 tests) exhibited the load-time and settlement-time behaviours, regardless of whether the piles were defective or sound.

It was noticed that, in the curve for L_1=0 *mm*, in which the necking-induced annular or area underneath the sound section of the pile makes contact with the clay surface, the force increases significantly when the settlement reached about 4 *mm*, due to the bearing of the discontinuous cross-section onto the clay.

Figs. 9.11 and 9.12 show the influence of the embedded length on the load-settlement behaviour of defective and sound piles respectively. As would be expected, the load capacity is enhanced when the embedded length increases. Figs. 9.13 to 9.16 summarize the effect of embedded diameter change on the defective piles. The more severe the structural defect (neck), the less is the load capacity. The structural defects with the pile appear to have a strong impact on the load capacity, but a relatively minor effect on the settlement at yield. For most cases, the load-settlement relationship for a defective pile had a similar characteristic shape to a sound pile, but the pile load capacity was reduced.

9.3.2 Ultimate Capacity

Figs. 9.17 and 9.18 show that the ultimate capacity P_{ult} decreases when the embedded length ratio L_1/L_2 and/or diameter ratio D_2/D_1 decreases.

Figs. 9.19 and 9.20 show the ratio of settlement and load at the onset of failure, S_{ult}/P_{ult}, as a function of L_1/L_2 and D_1/D_2. The ratio S_{ult}/P_{ult}, generally decreases when the ratio

L_1/L_2.increases. Furthermore, while this ratio decreases monotonically for the intact piles, for severely necked piles, it may not (*e.g.* D_2/D_1= 5/25).

9.3.3 Pile Stiffness Reduction Factor

The effect of pile defects on the load-settlement behaviour of a pile can be expressed conveniently in terms of a pile head stiffness reduction factor R_{ks} , which is defined as:

$$R_{KS} = \frac{\text{stiffness of pile with defects}}{\text{stiffness of sound pile}}$$

The factor R_{ks} from the early to intermediate stage is of most interest in practical cases. Figs. 9.21 to 9.25 show the pile head stiffness reduction factor R_{ks} plotted against load for different embedded length ratios ranging between L_1/L_2 = 0.31 and 1.5 and diameter ratios D_1/D_2 of 2.1 to 5. This figure illustrates that the pile head stiffness is typically reduced by a factor of about 0.7 to 0.4 for the intermediate stage. For the severe necking cases, R_{ks} decreases significantly with increasing load as shown in Fig. 9.21 and Fig. 9.23. For cases of minor necking, R_{ks} remains at an approximately constant value, as shown in Fig. 9.22 and Fig. 9.24. Accurate values of R_{ks} could not be obtained at very small load levels ($P \leq 0.05$ *kN*), as measured settlements were very small, and therefore have not been reported.

Soon after yielding in the load-settlement behaviour, R_{ks} reduces very rapidly and then increases slightly as the load approaches ultimate. This is because the load yielding occurs at different deflections, with the defective pile yielding occurring prior to the sound pile.

9.3.4 Test on an End-Bearing Pile

Fig. 9.26 shows the load-settlement curves of model end bearing piles. A "curvature" point, at about 1.5 *kN*, exists in the load-settlement curve for the necked pile embedded in

the soft clay, indicating the continued development of end-bearing resistance after the shaft resistance is fully mobilized.

R_{ks} for the end-bearing pile is plotted in Fig. 9.27 as a function of applied load. R_{ks}, reaches a minimum at the "curvature" point. Figs. 9.28 and 9.29 plot measured load and settlement against time. The load still increases rapidly in the intermediate stage as shown in Fig. 9.26, instead of relatively slowly as in the floating pile case illustrated in Fig. 9.9.

9.4 Comparisons Between Model Pile Tests and Theory

9.4.1 Theoretical Analysis

One of the objectives of the experimental programme was to obtain data on defective pile behaviour which could be compared with theoretical predictions of the response of piles containing defects. Two theoretical analyses were used in this study as follows:

One is the general three dimensional load-deformation elastic analysis GEPAN, which is described in Chapter 3. In the version of GEPAN employed, only linear load-settlement response was computed.

The other theoretical analysis used was described by Poulos (1997), and employs a simplified boundary element approach. The analysis is implemented via the computer program DAMPA (DAMaged Pile Anaysis), which is described in Chapter 2 as well.

9.4.2 Assessment of Soil Parameters for Pile Deformation Analysis

Methods of estimating geotechnical parameters for pile settlement analyses have been discussed by Poulos (1989a). The most crucial soil parameter in estimating pile settlements via elastic-based methods is Young's modulus E_s of the soil and its distribution with depth. For nonlinear analysis, the limiting shaft resistance f_s and base

resistance f_b are also required. Assessment of these parameters was discussed by Poulos (1989a) and Fleming *et al* (1992). Poisson's ratio of the soil is not a very significant parameter for pile settlement prediction, and, a value of 0.3 can usually be adopted for predictions of final settlement.

Table 9.3 shows the values adopted for these parameters and the method by which they were assessed. For these driven model piles, the value of E_s was back-figured from pile load tests with five pile diameters (25,12,10,6,5 *mm*). The average of E_s for 25 *mm* diameter model piles, for example, was about 20 *MPa*. It was found that the value of E_s of the model test was approximately proportional to the pile diameter, *i.e.*, larger E_s values were obtained for the larger diameter piles driven into the clay. The average values of ultimate shaft friction, f_s, and ultimate end bearing, f_b, were calculated from the gradients of the measured ultimate capacities of pile with increasing embedded lengths. For the clay, the values of f_s so obtained varied between 13 and 18 *kPa*, and an average value of 15 *kPa* was adopted. The use of constant values of E_s, f_s and f_b was a simplifying approximation as all three parameters tended to decrease as the moisture content of the clay increased; however, there was insufficient data to define adequately the variation of these parameters with moisture content.

9.4.3 Discussion and Comparison with Theoretical Predictions

The predicted and measured results for four cases are shown in Figs. 9.30 to 9.33. It can be seen that both the predicted and measured load-settlement curves are quite similar, but some differences appear near the final stage of the load-deformation curve. The solution from DAMPA reproduced reasonably well the non-linear response and yielding progress on the load-deformation behaviour of model defective piles. In the early load-deformation stage, the elastic solution from GEPAN gave a reasonable estimate of the actual load-settlement behaviour.

Figs. 9.34 to 9.36 compare measured and theoretical distributions of the pile head stiffness reduction factor with load level. The DAMPA solution agrees well overall with

the experimental data, although it tends to predict a more severe pile head stiffness reduction than was actually observed. The elastic solution via GEPAN appeared comparable to the experimental data for load levels up to almost 50% of ultimate, although the predicted R_{ks} was significantly higher that the measured values for the more severely necked piles, as shown in Fig. 9.36.

Figs. 9.37 and 9.38 compare measured and theoretical values of pile head stiffness reduction factor against embedded sound/defective length ratio L_1/L_2. The measured R_{ks} values lie between the two theoretical predictions. However, GEPAN predicts a higher value of R_{ks} for the necked pile than either the measurements or DAMPA, (*e.g.* D_1/D_2=25/5), as shown in Fig. 9.37.

For DAMPA, the predictions of load-settlement progress and pile stiffness reduction factor near the ultimate load are generally not very satisfactory. The theory is more suitable for small deformation analysis, and the hyperbolic representation of the shaft and end-bearing responses used in the program is over-simplified. Fortunately, the load-settlement response at loads approaching ultimate is of less interest than at design load levels, and at such load levels, DAMPA shows better agreement with the measurements. In all cases, the general characteristics of load-deformation and stiffness reduction behaviour of defective piles are well-reproduced at early and intermediate stages of load-deformation development. The predictions by GEPAN are also reasonably satisfactory at the earlier load-deformation stages, but, the pile stiffness factor for defective piles may be considerably underestimated by GEPAN for piles containing "severe" structural defects.

9.5 Conclusions

Tests have been carried out on model piles in a consolidated clay to study the load-settlement relationship and pile stiffness reduction factor R_{ks} of piles containing structural defects. The main conclusions from the model tests may be summarized as follows:

1) The load-settlement relationship of the defective piles has a similar characteristic shape to those of sound piles (Figs. 9.7 to 9.16).
2) Structural defects in a pile can have a strong impact on the load capacity but only a relatively minor effect on the settlement at yield (Figs. 9.7 to 9.20).
3) The pile stiffness reduction factor R_{ks} for a defective pile decreases with decreasing embedded sound/defective length ratio L_1/L_2 and/or diameter ratio D_1/D_2 (Figs. 9.21 to 9.25).
4) The reduction of R_{ks} with load is relatively moderate for piles containing relatively small structural defects but can be significant for piles with severe structural defects (Figs. 9.21 to 9.24).
5) The load-settlement curve of a defective end bearing pile exhibits a "curvature" after the shaft friction is mobilized (Fig. 9.27).

Comparisons have been made between the measured behavior and that predicted from two theoretical approaches, the general elastic pile analysis GEPAN and the non-linear damaged pile analysis DAMPA. Both theoretical solutions agree reasonably well and are generally in fair agreement with the measured values, provided that appropriate values of soil parameters E_s, f_s and f_b are chosen. However, R_{ks} may be overestimated by GEPAN for the higher structurally defected piles with severe structural defects.

Considerable scope exists for modifications and improvements to the theoretical analysis to better model the load-settlement relationship and pile stiffness reduction factor of defective piles, especially in relation to the representation of the non-linear behaviour as the ultimate load is approached. In addition, more detailed and larger scale tests on defective piles, including instrumentation to measure load transfer would be desirable.

Table 9.2 Details of Pile Test Series

Test No	Pile No	L_2	D_2	L_1	D_1	Defect	Tip
1	1	0	0	100	12	S	F
2	1	0	0	200	12	S	F
3	1	0	0	300	12	S	F
4	2	150	10	0	25	D	F
5	2	150	10	75	25	D	F
6	2	150	10	150	25	D	F
7	2	150	10	225	25	D	F
8	2	150	10	300	25	D	F
9	3	150	5	0	25	D	F
10	3	150	5	75	25	D	F
11	3	150	5	150	25	D	F
12	3	150	5	225	25	D	F
13	3	150	5	300	25	D	F
14	4	240	6	0	25	D	F
15	4	240	6	75	25	D	F
16	4	240	6	150	25	D	F
17	4	240	6	225	25	D	F
18	4	240	6	300	25	D	(E)
19	5	240	12	0	25	D	F
20	5	240	12	75	25	D	F
21	5	240	12	150	25	D	F
22	5	240	12	225	25	D	F
23	6	0	0	75	25	S	F
24	6	0	0	150	25	S	F
25	6	0	0	225	25	S	F
26	6	0	0	300	25	S	F
27	6	0	0	375	25	S	F
28	7	240	25	0	25	S	F
29	7	240	25	75	25	S	F
30	7	240	25	150	25	S	F
31	7	240	25	225	25	S	F
32	7	240	25	300	25	S	(E)
33	8	0	0	75	6	S	F
34	8	0	0	150	6	S	F
35	8	0	0	225	6	S	F
36	8	0	0	300	6	S	F

L_1: necked length
D_1: necked diameter
L_2: sound length
D_2: sound diameter

S: sound
D: defective
F: floating
E: end-bearing

Table 9.3 Parameters Adopted for Theoretical Analysis

Parameter	Value adopted	Method of Estimation
Soil Young's Modulus, E_s	Proportional changes with the diameter of a driven model pile, 20 *MPa* for Φ25 model pile.	Back-figured from load-settlement curves of model tests and idealization
Limiting skin friction, f_s	15 *kPa*	Interpreted from measured ultimate capacity with a range of pile length and diameter
Limiting end bearing resistance, f_b	250 *kPa*	Interpreted from measured ultimate capacity with a range of pile length and diameter
Hyperbolic parameter for shaft elements, R_{fs}	0.5	Recommended by Poulos (1997)
Hyperbolic parameter for base elements, R_{fb}	0.75	Recommended by Poulos (1997)
Young's Modulus of pile, E_p	70 000 *MPa*	Typical value for aluminum
Yield stress of pile, $\sigma_{y,p}$	200 *MPa*	Typical value for aluminum
Depth of soil	540 *mm*	Height of the clay vessel

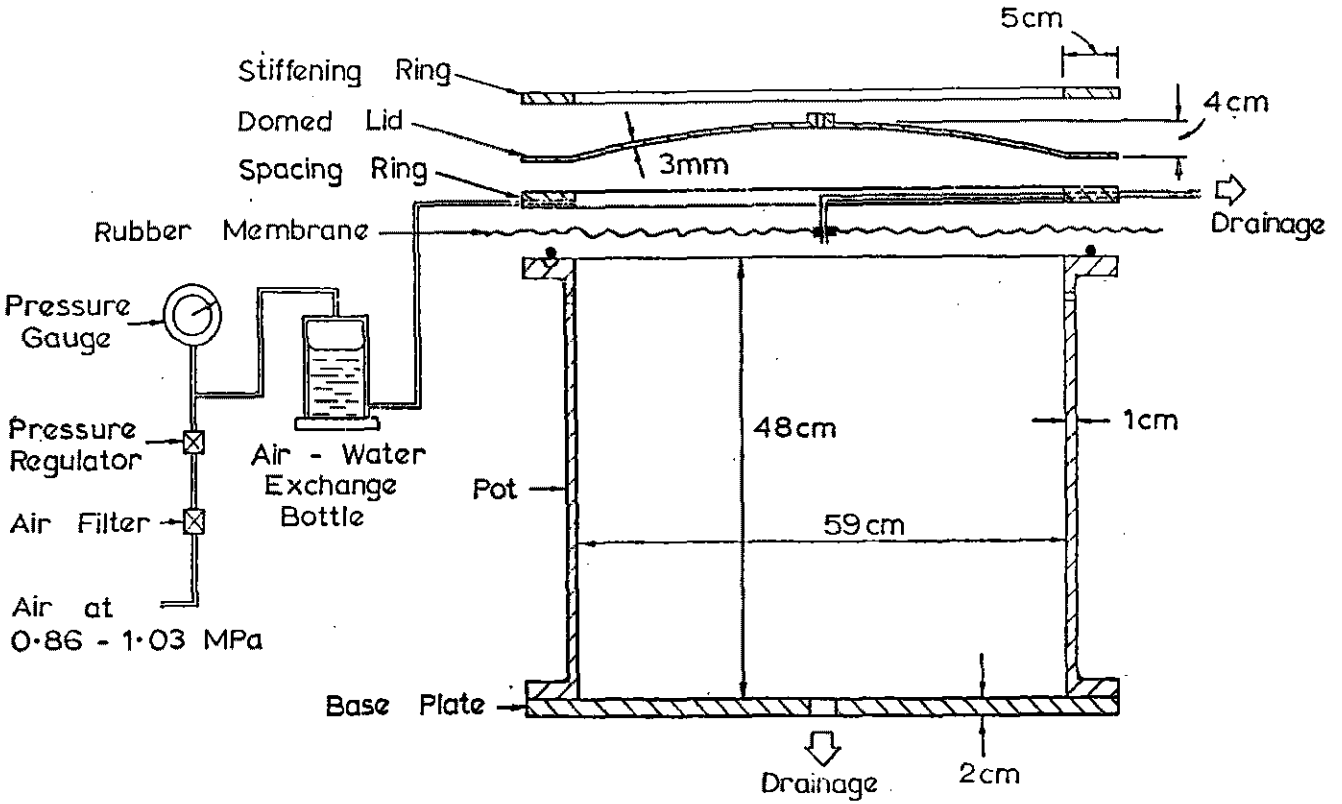

Fig. 9.1 Layout of apparatus for model pile tests

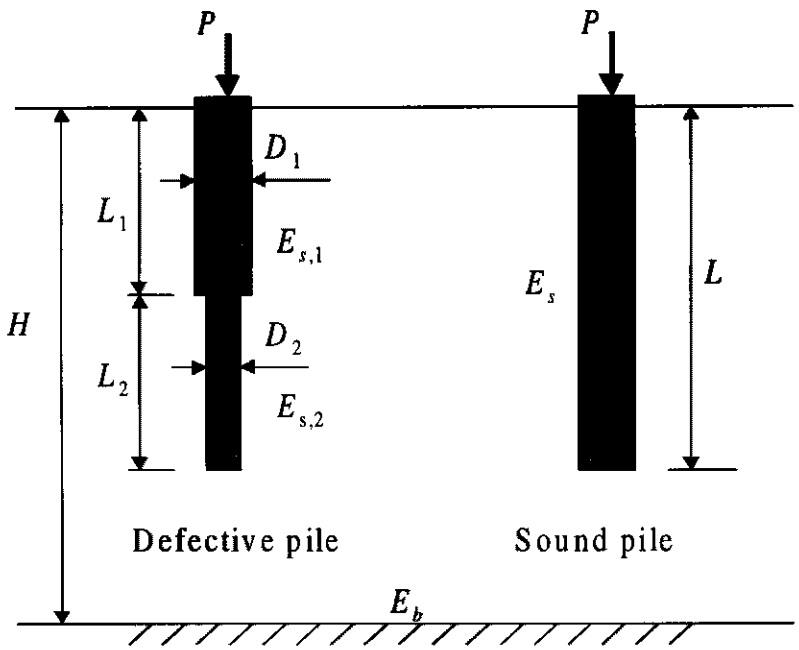

Fig. 9.2 Parameters of model pile

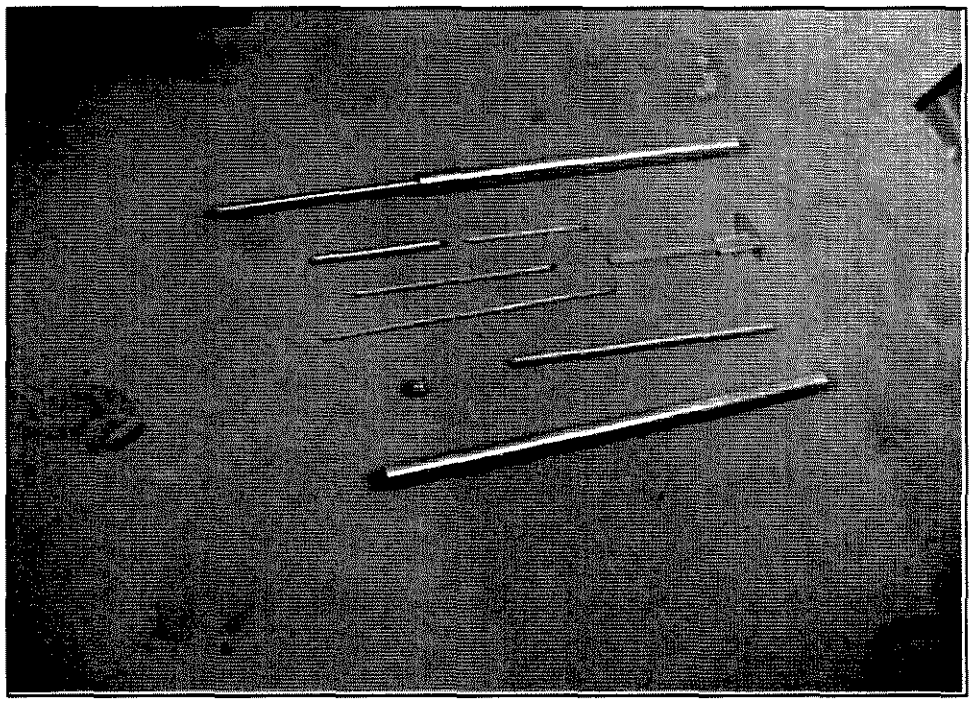

Fig. 9.3 Assembled parts of model piles

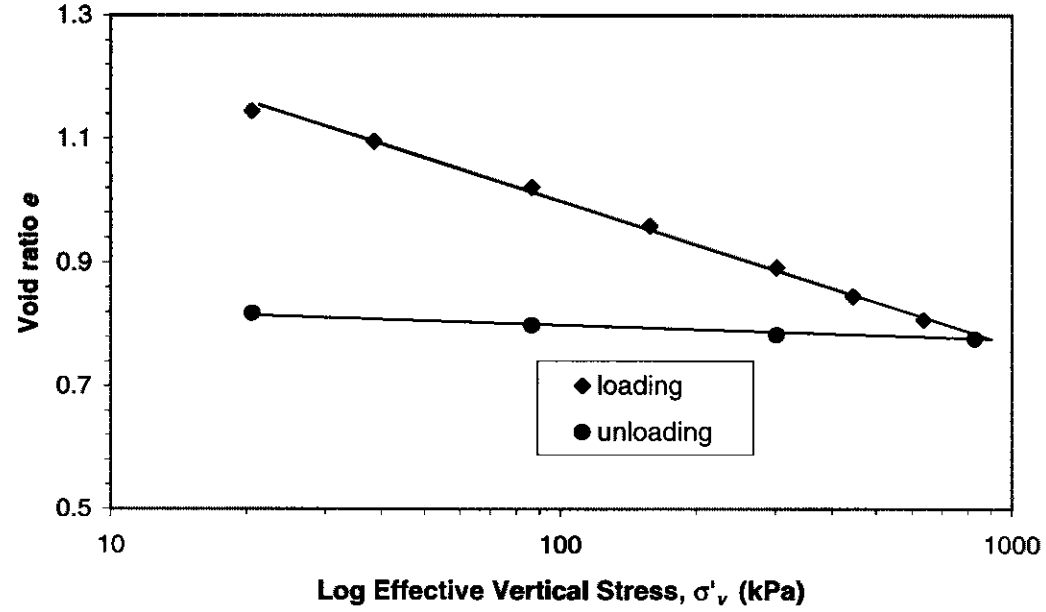

Fig. 7.4 Void ratio versus log effective vertical stress of Kaolin clay

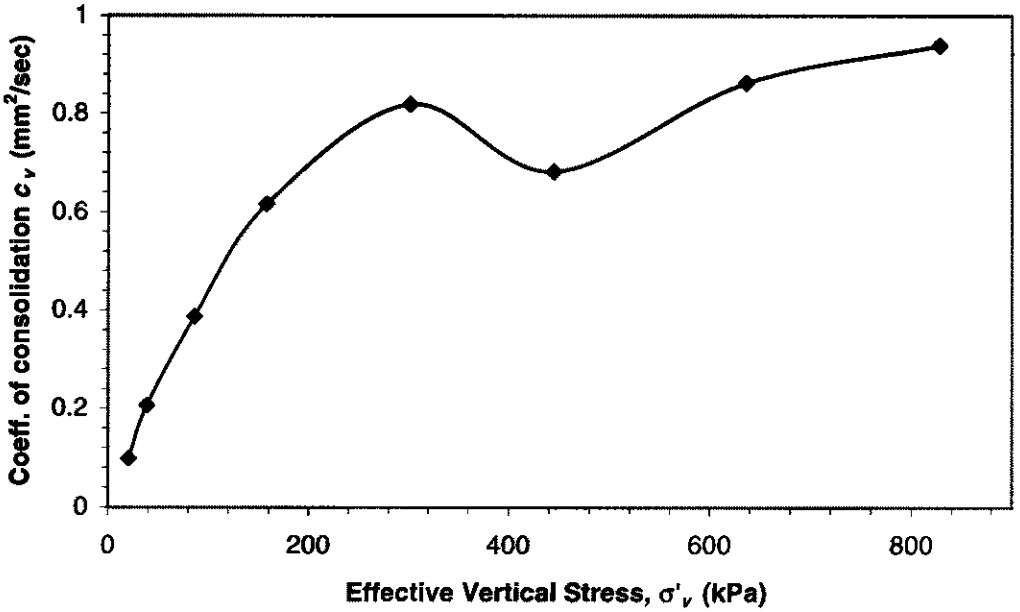

Fig. 7.5 Coefficient of consolidation versus effective vertical stress of Kaolin clay

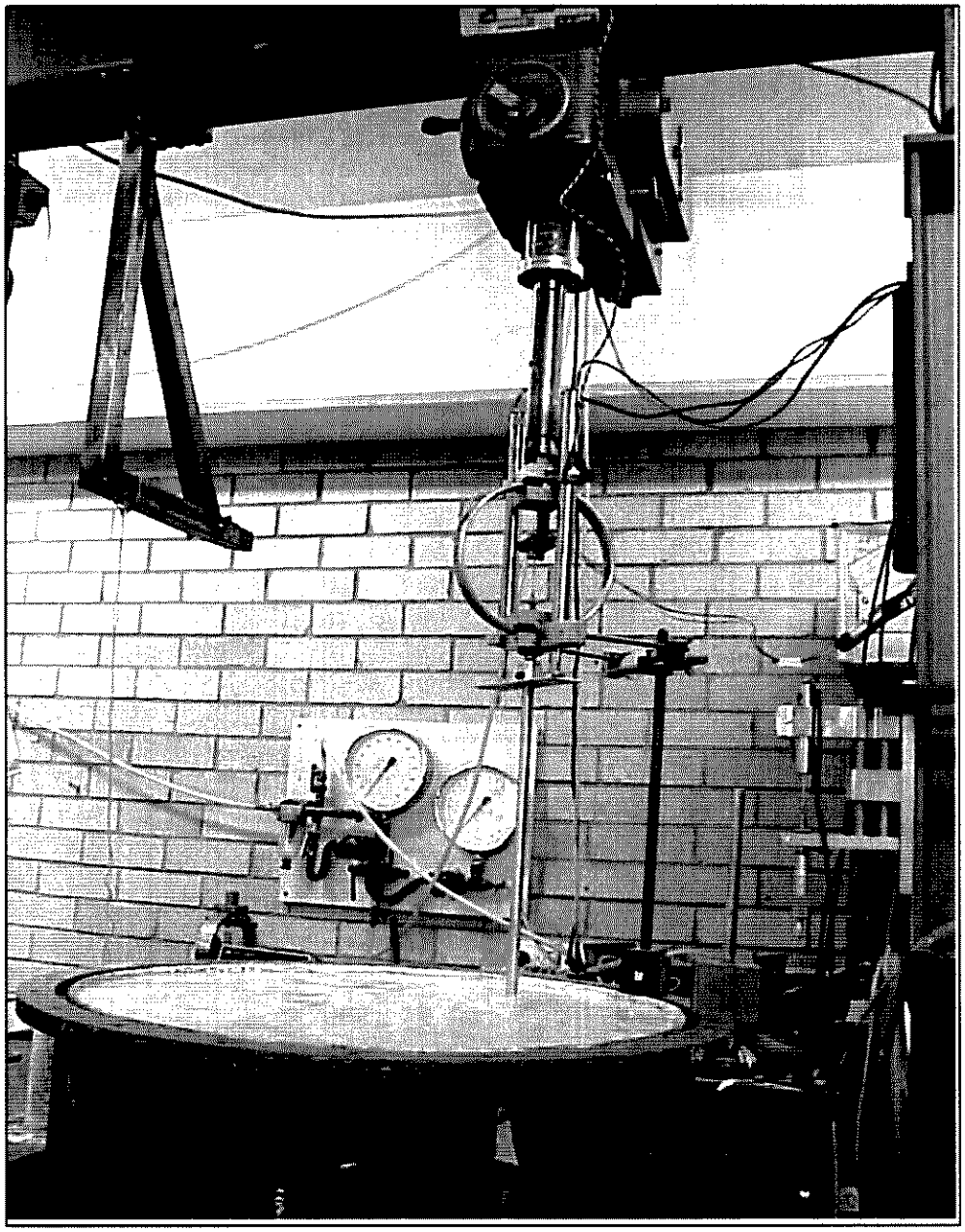

Fig. 9.6 View of model pile test

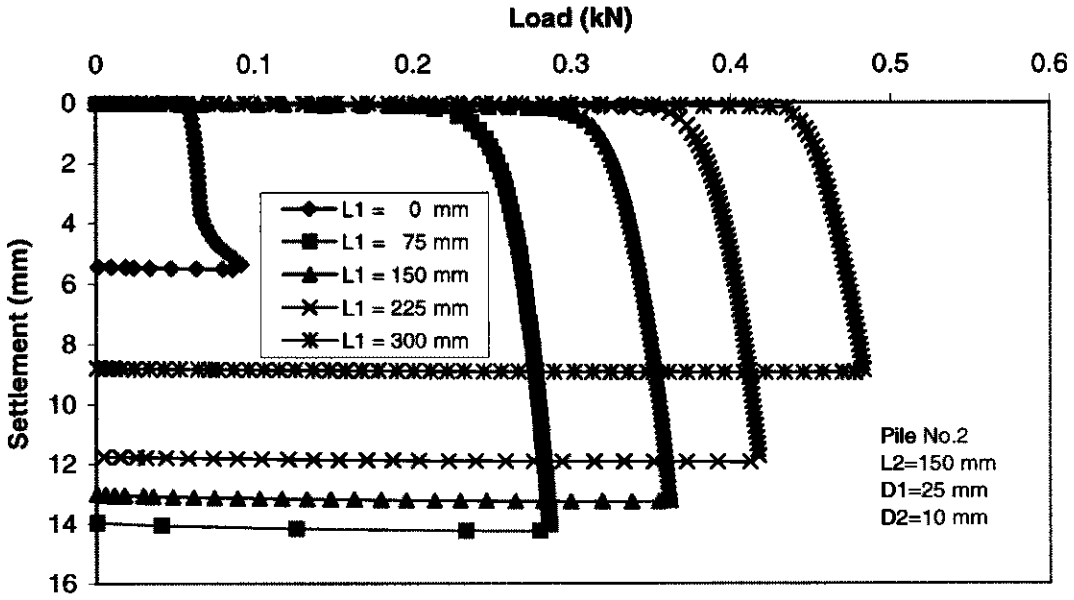

Fig. 7.7 Complete load-settlement curves of model pile no. 2

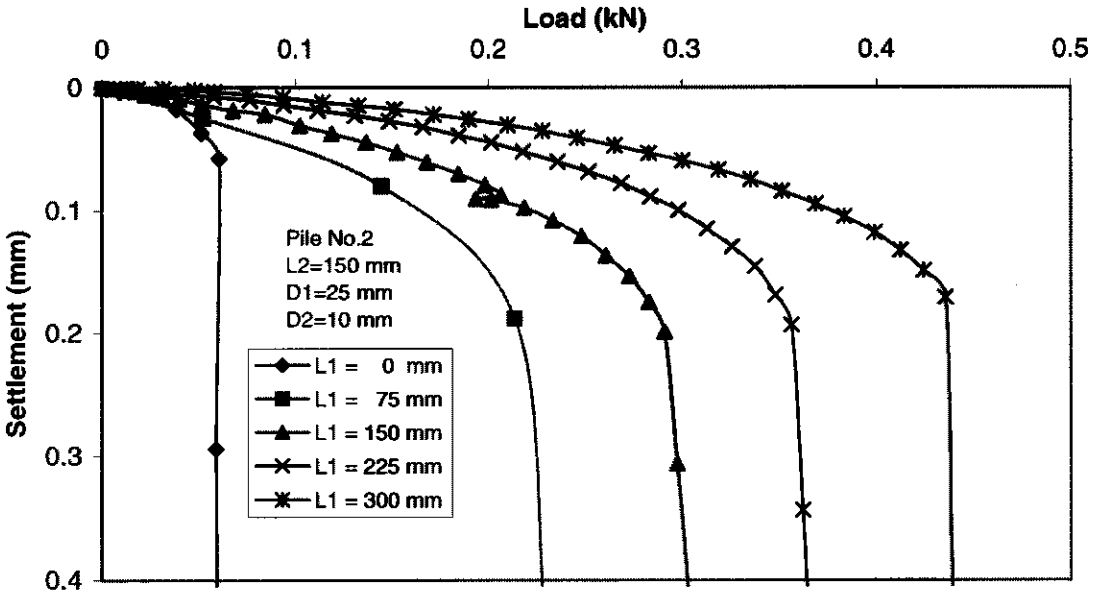

Fig. 7.8 Enlarged load-settlement curves of test pile no. 2

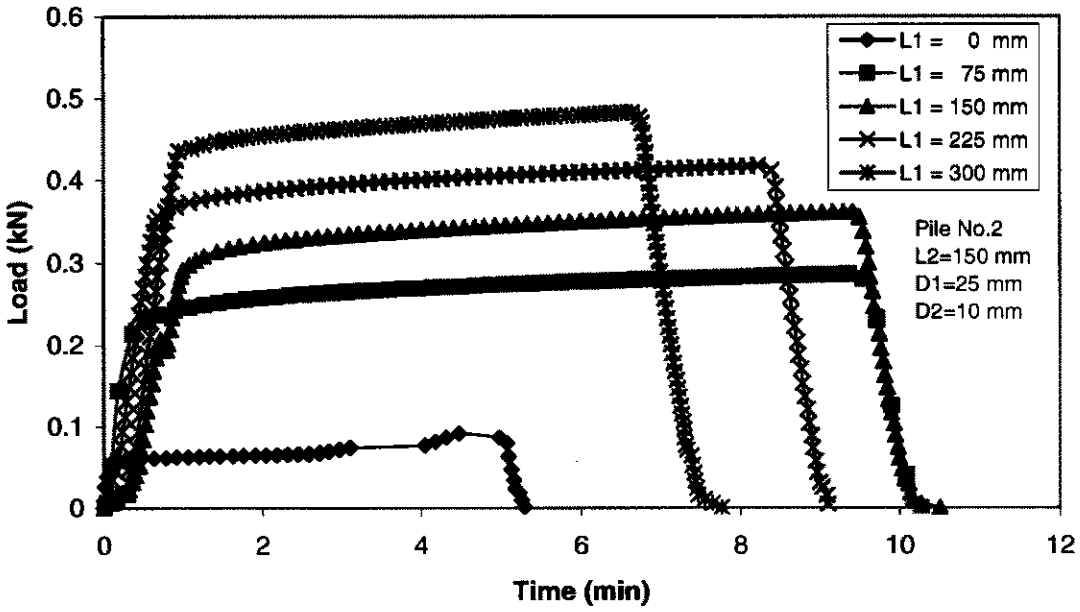

Fig. 8.9 Load-time behavior of test pile no. 2

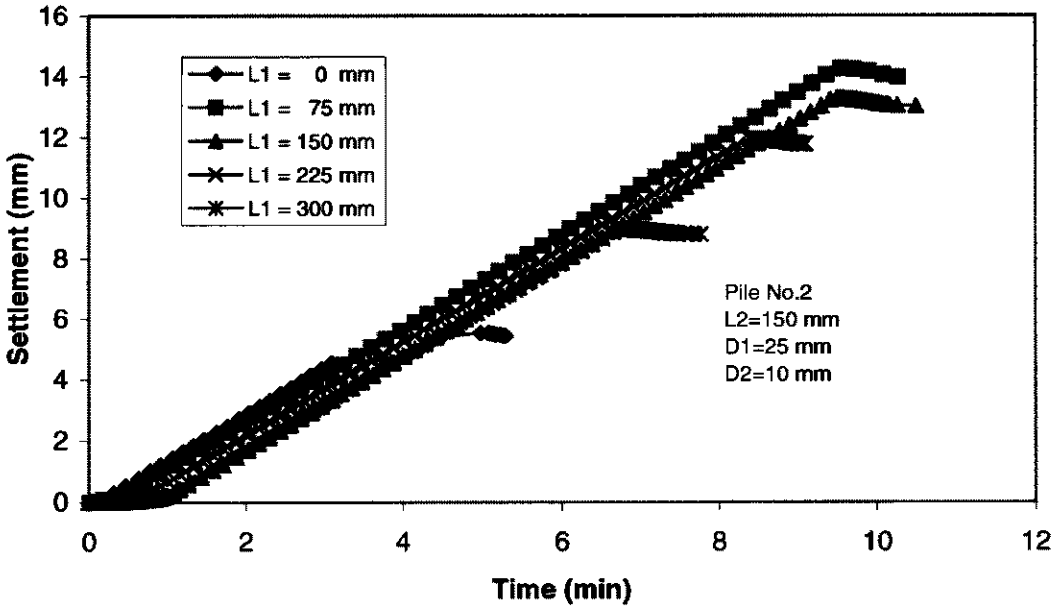

Fig. 8.10 Settlement-time behaviour of test pile no. 2

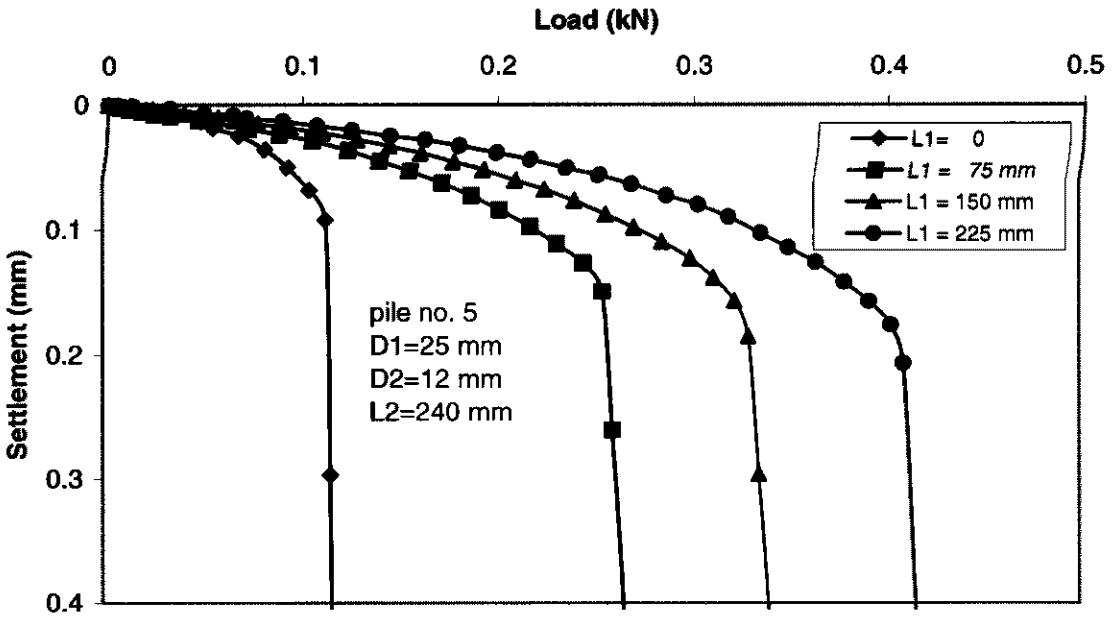

Fig. 9.11 Influence of length change on load-settlement behaviour of defective pile no. 5

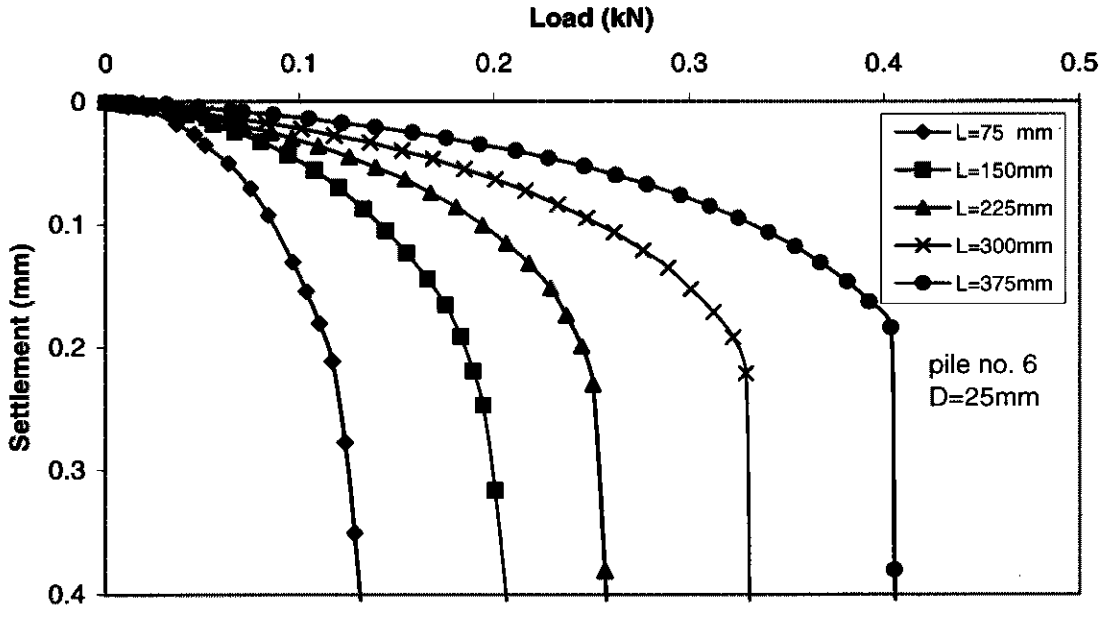

Fig. 9.12 Influence of length change on load-settlement behaviour of sound pile no. 5

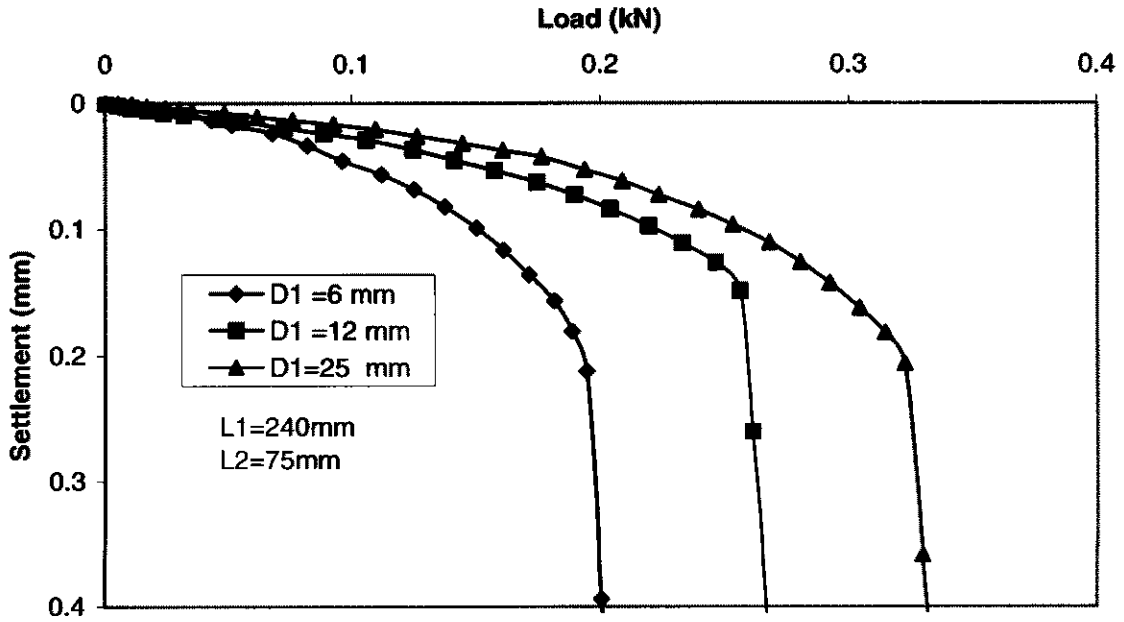

Fig. 7.13 Influence of diameter change on load-settlement behaviour for L_1/L_2=240/75

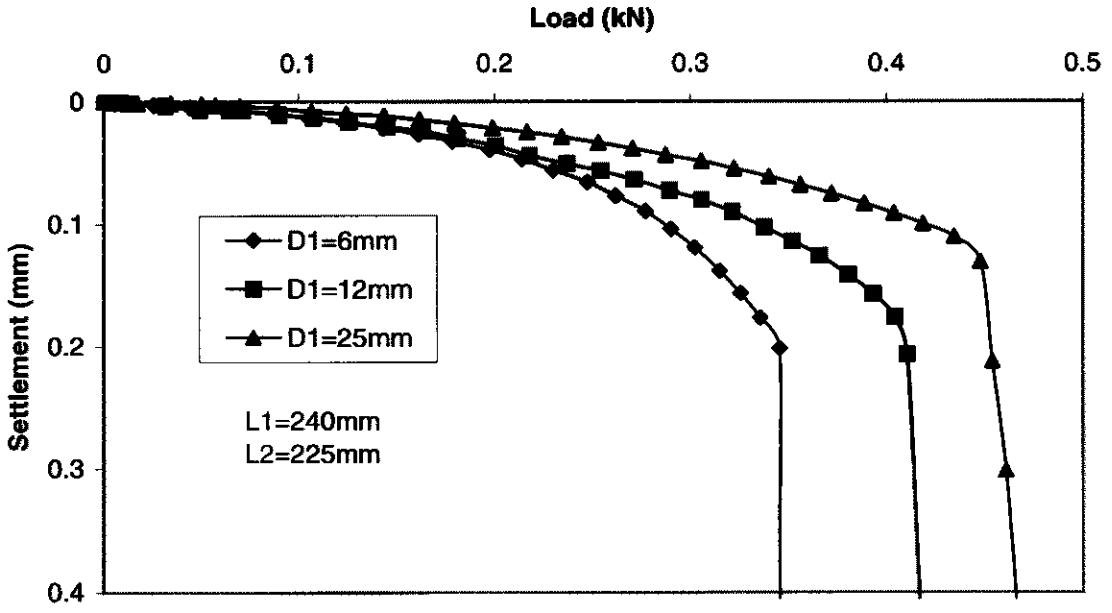

Fig. 7.14 Influence of diameter change on load-settlement behaviour for L_1/L_2=240/225

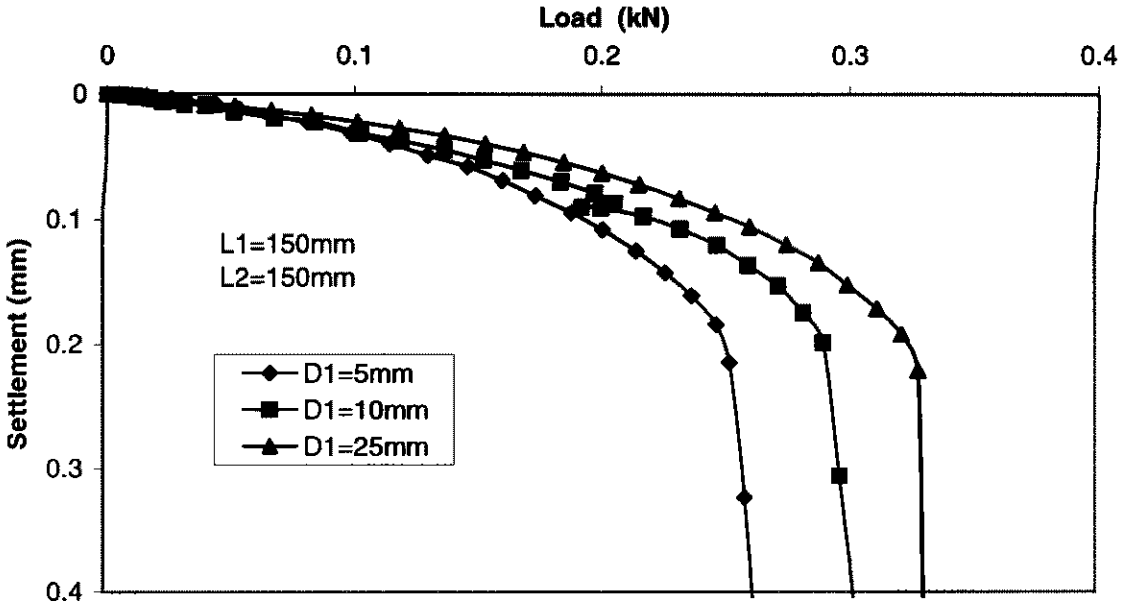

Fig. 7.15 Influence of diameter change on load-settlement behaviour for L_1/L_2=150/150

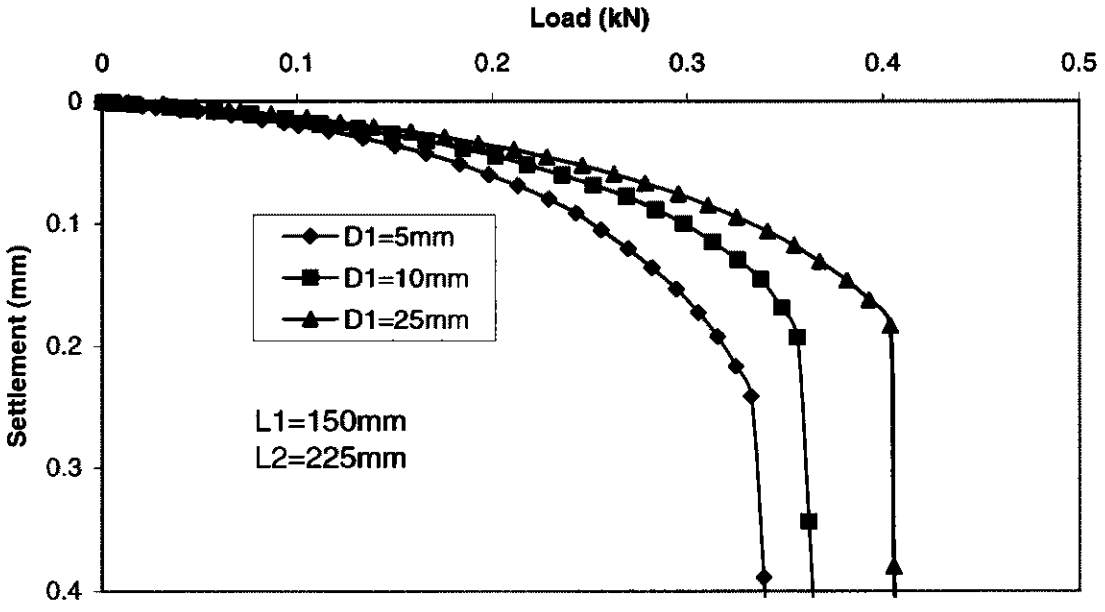

ig. 7.16 Influence of diameter change on load-settlement behaviour for L_1/L_2=150/225

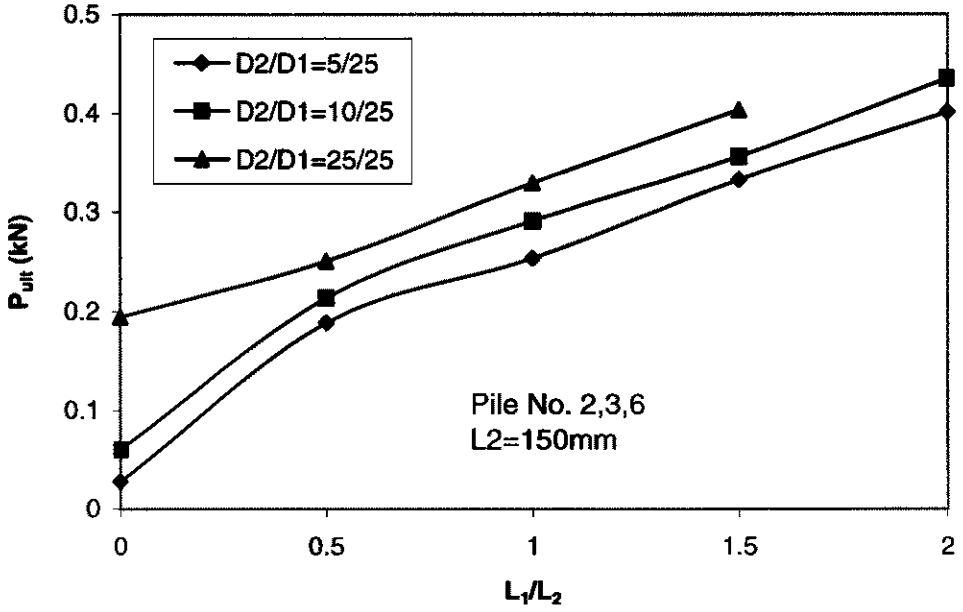

Fig. 7.17 Effect of structural defect on ultimate capacity of test piles L_2=150mm

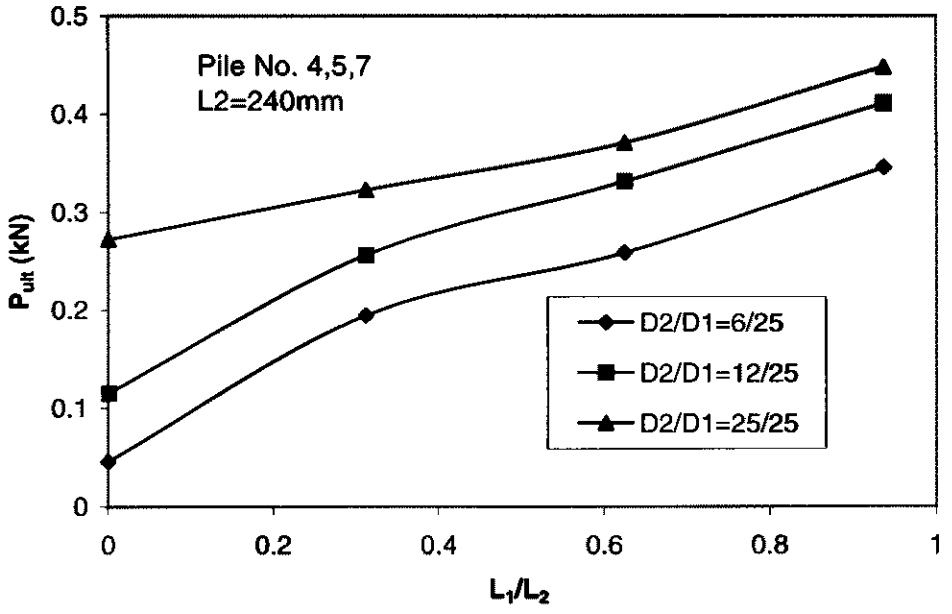

Fig. 7.18 Effect of structural defect on ultimate capacity of test piles L_2=240mm

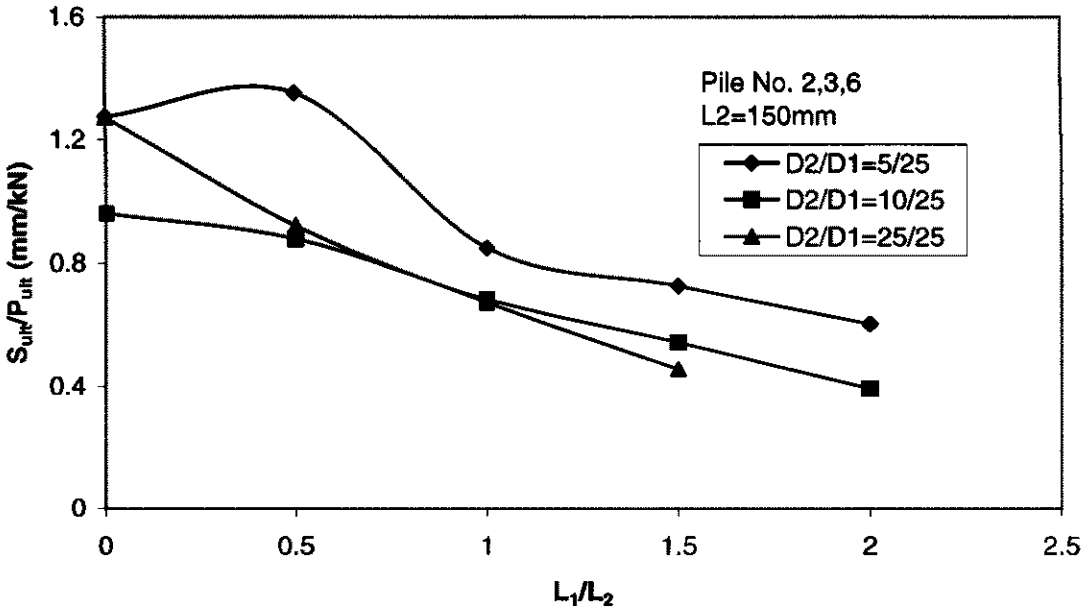

Fig. 7.19 Effect of structural defect on the ratio S_{ult}/P_{ult} of test piles L_2=150mm

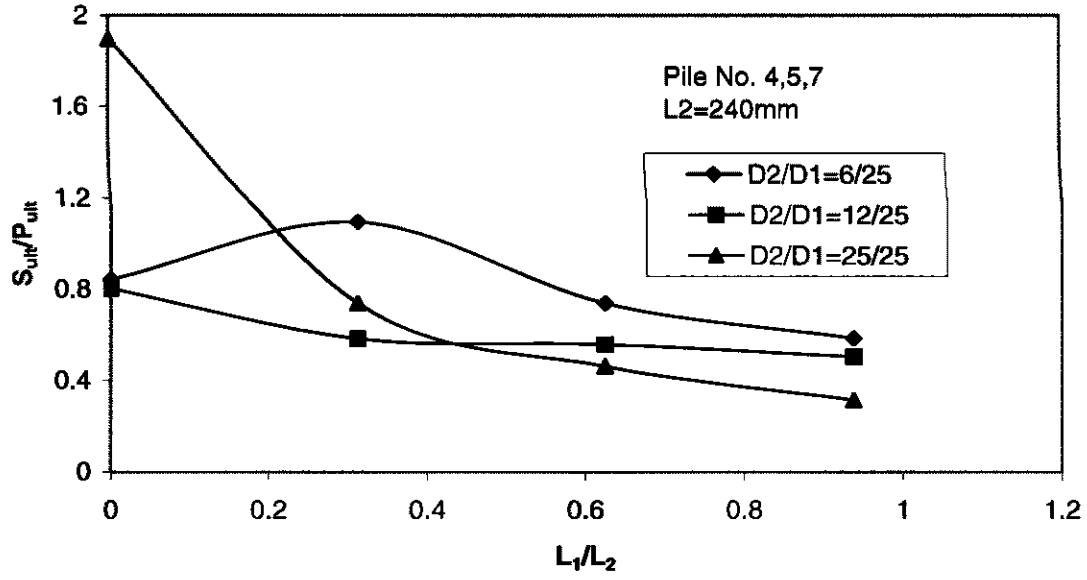

Fig. 7.20 Effect of structural defect on the ratio S_{ult}/P_{ult} of test piles L_2=240mm

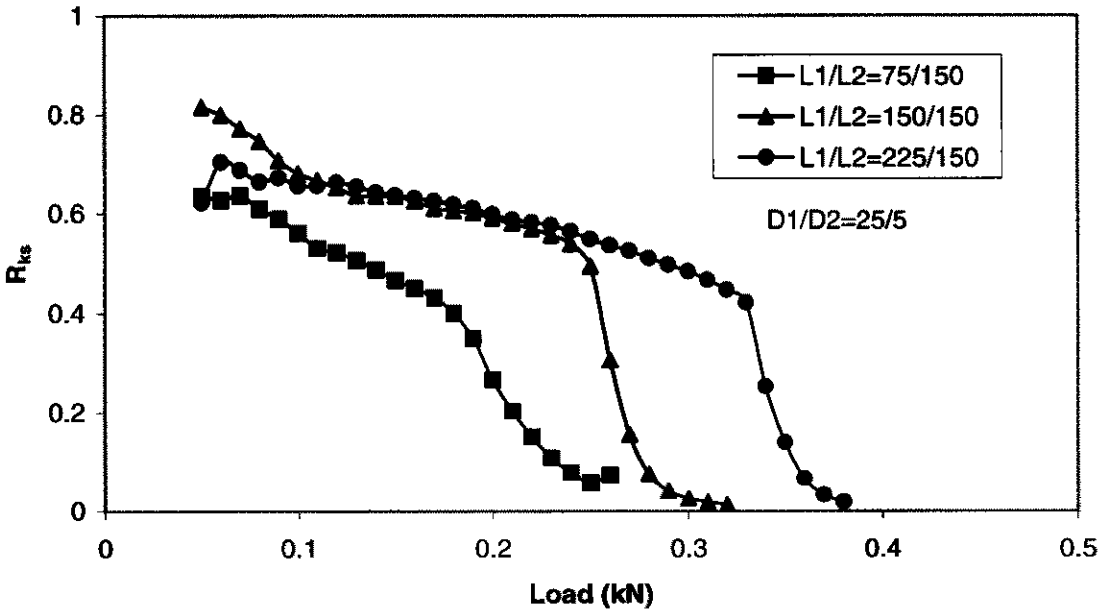

Fig. 7.21 Effect of structural defect on pile reduction stiffness, D_1/D_2=25/5

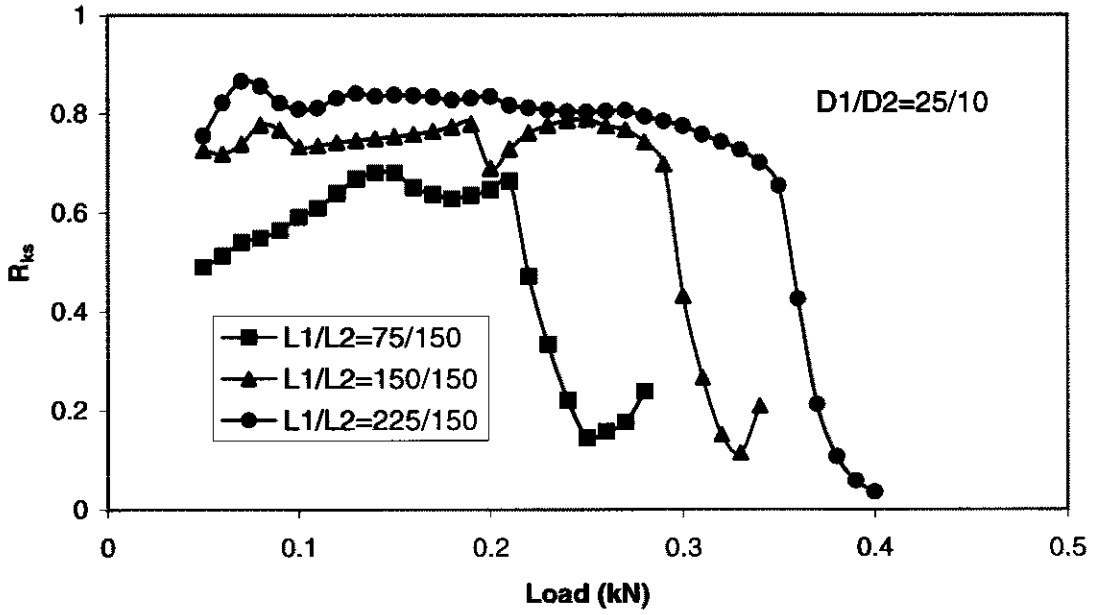

Fig. 7.22 Effect of structural defect on pile reduction stiffness, D_1/D_2=25/10

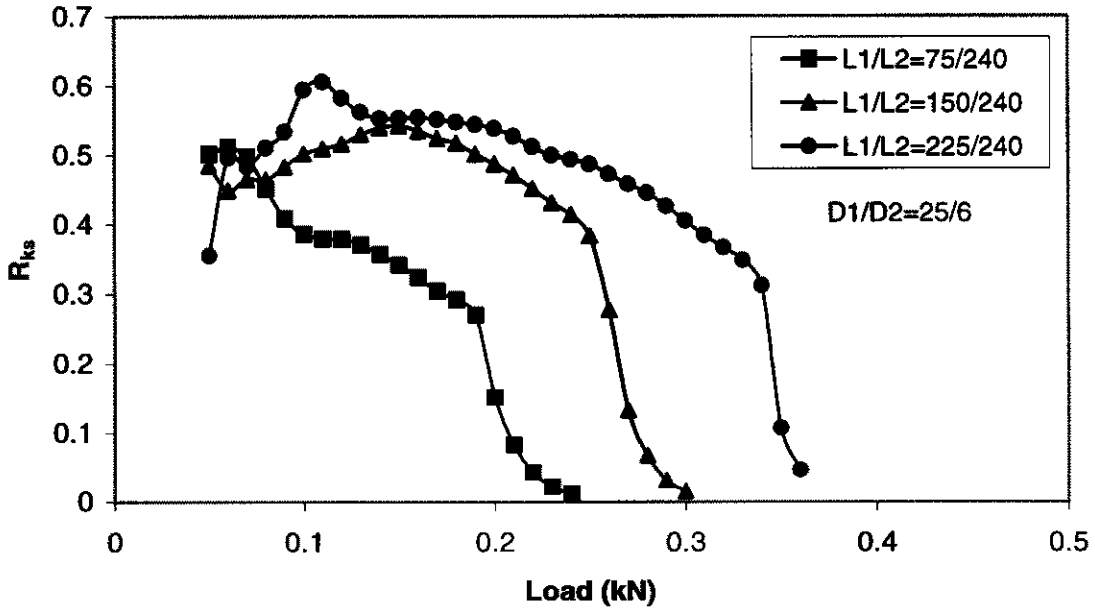

Fig. 7.23 Effect of structural defect on pile reduction stiffness, D_1/D_2=25/6

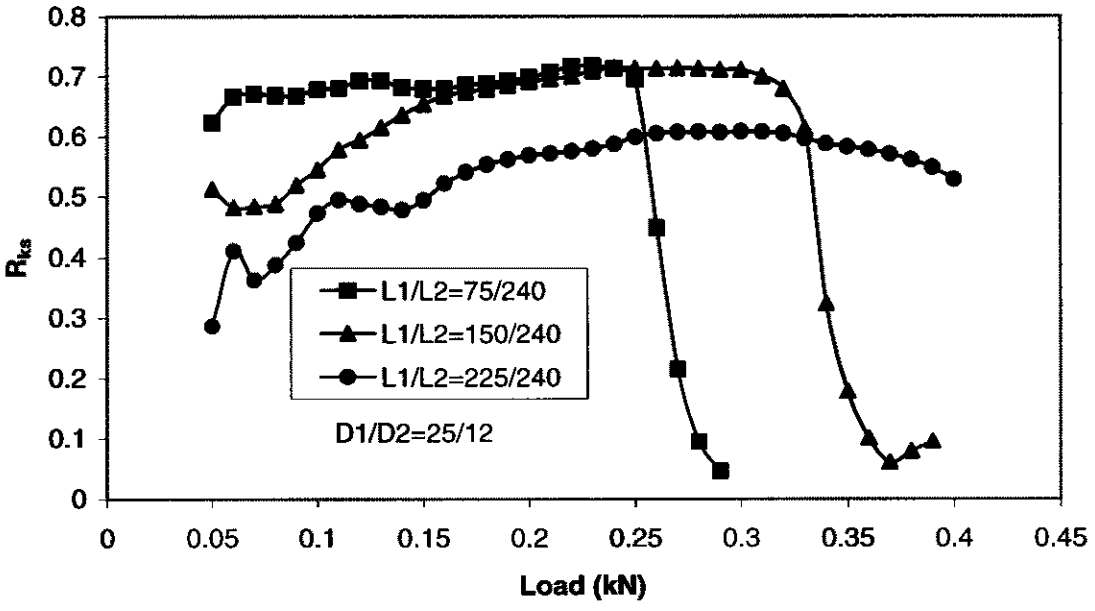

Fig. 7.24 Effect of structural defect on pile reduction stiffness, D_1/D_2=25/6

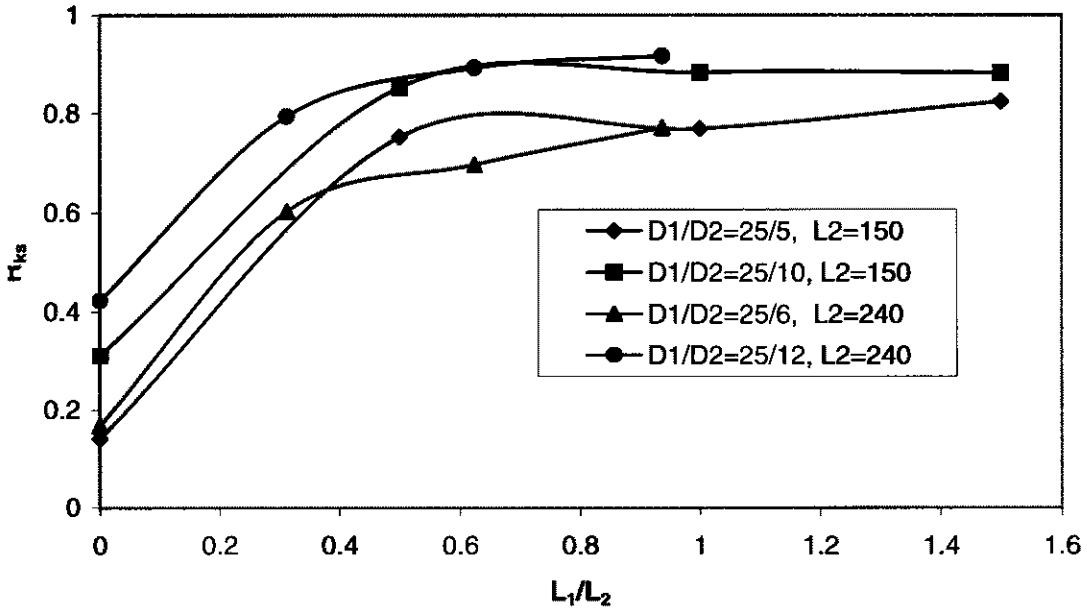

Fig. 7.25 Pile stiffness reduction factor at ultimate capacity

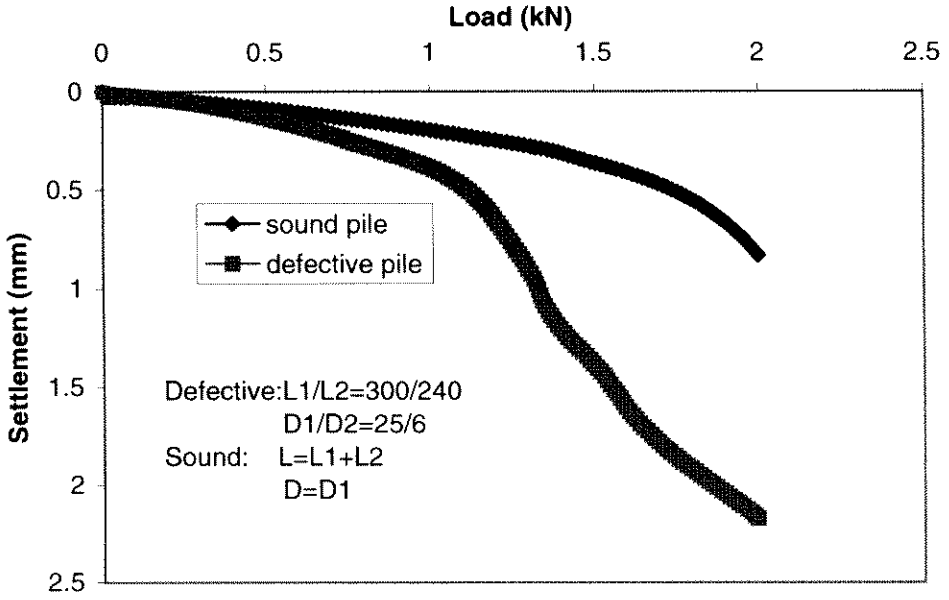

Fig. 7.26 Load-settlement behaviour of end-bearing piles

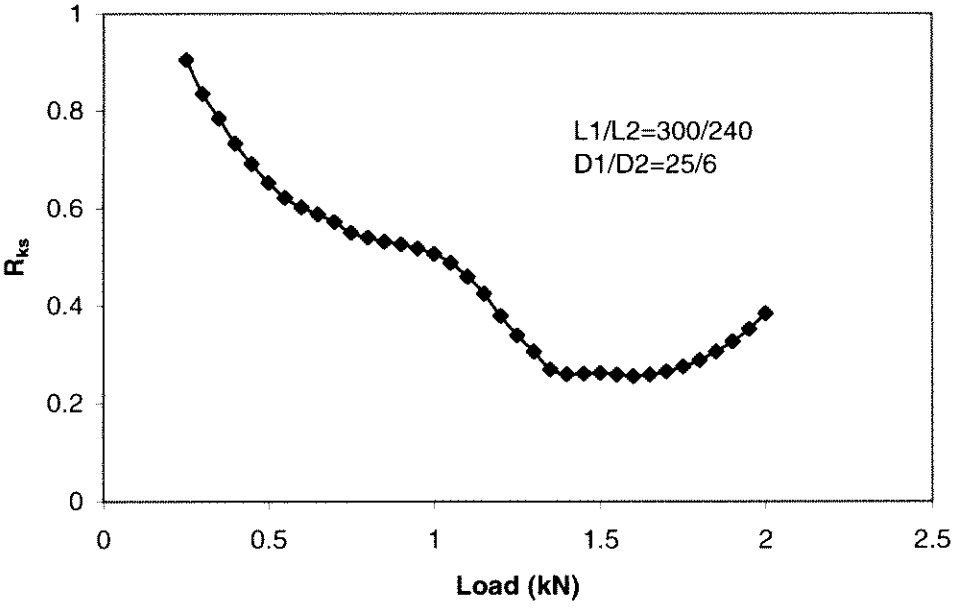

Fig. 7.27 Pile stiffness reduction factor of an end-bearing defective pile

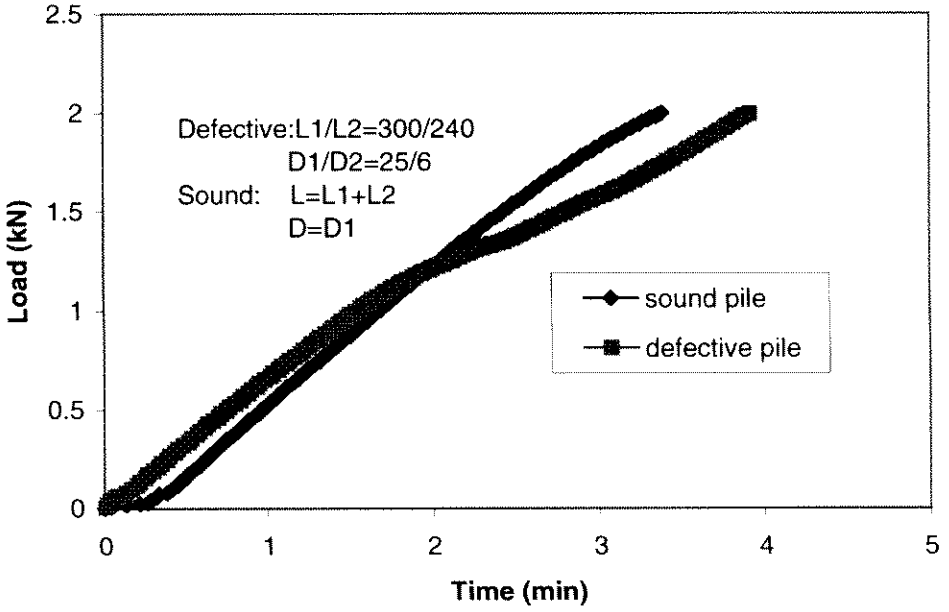

Fig. 7.28 Load-time behaviour of end-bearing piles

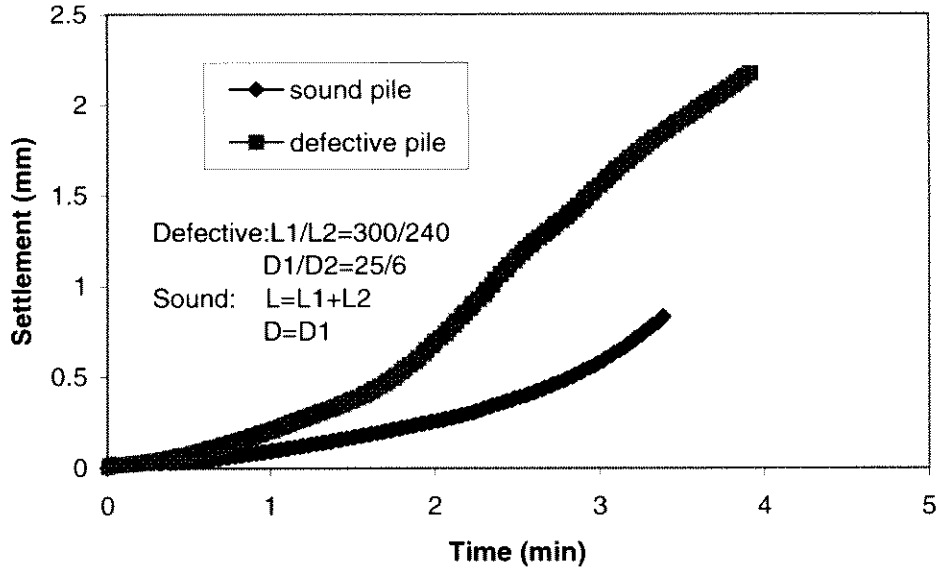

Fig. 7.29 Settlement-time behaviour of end-bearing piles

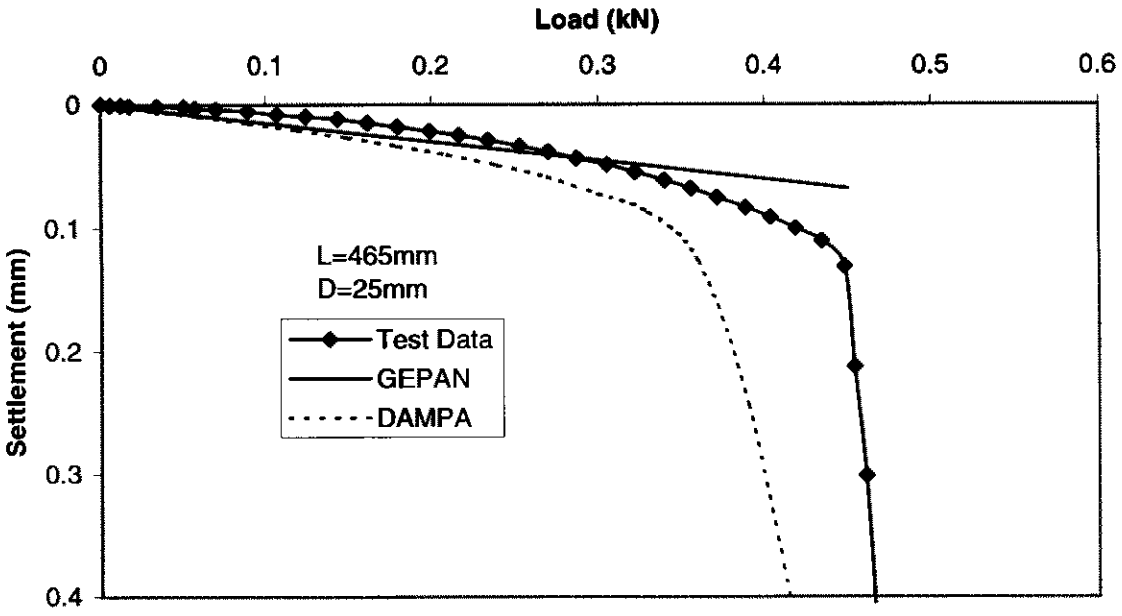

Fig. 9.30 Comparison of experimental and theoretical load-settlement curves for a sound pile (L=465, D=25)

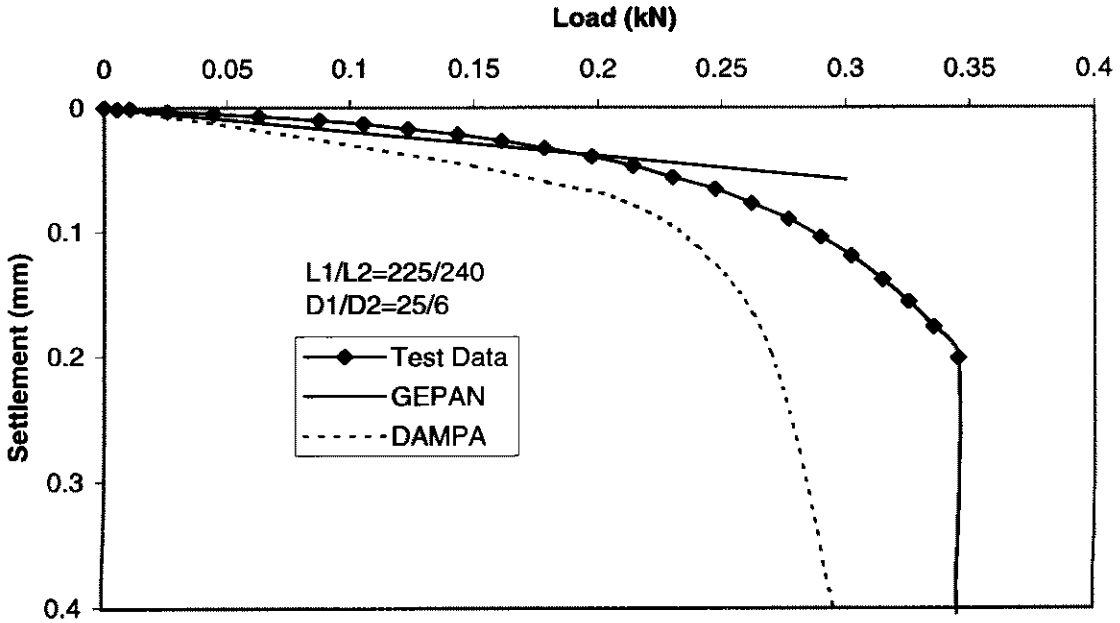

Fig. 9.31 Comparison of experimental and theoretical load-settlement curves for a defective pile (L_1/L_2=225/240, D_1/D_2=25/6)

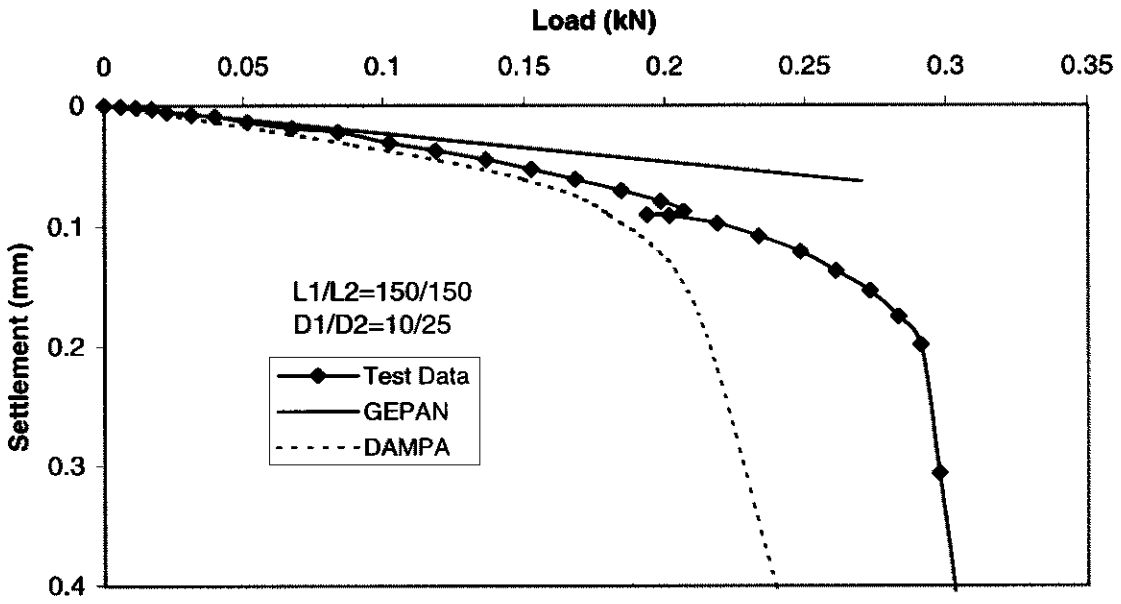

Fig. 9.32 Comparison of experimental and theoretical load-settlement curves for a defective pile (L_1/L_2=150/150, D_1/D_2=25/10)

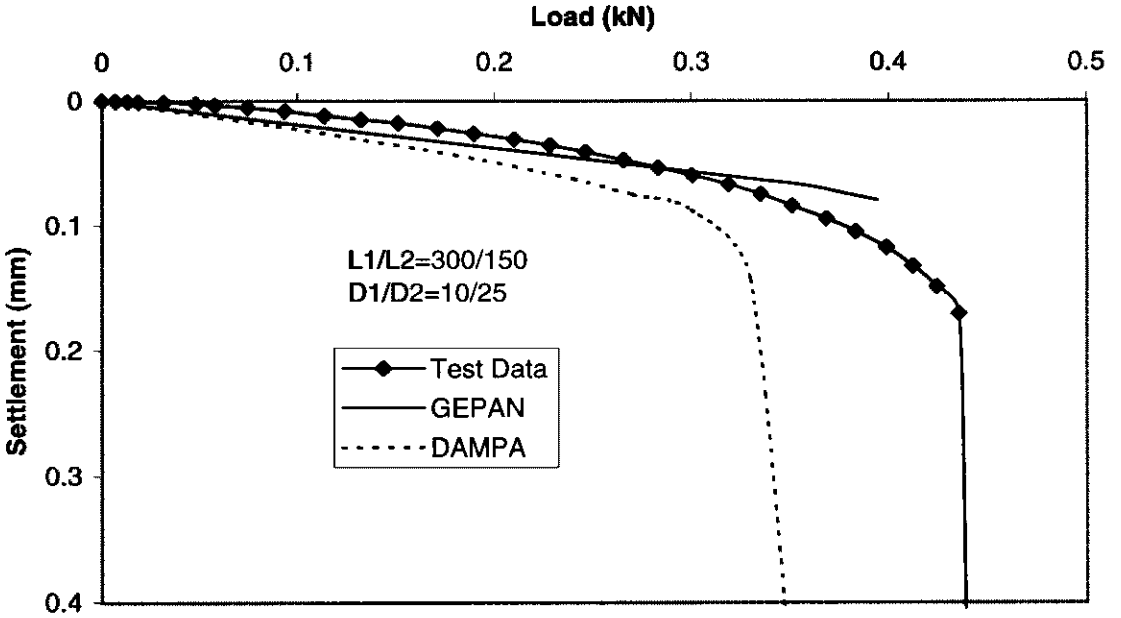

Fig. 9.33 Comparison of experimental and theoretical load-settlement curves for a defective pile (L_1/L_2=300/150, D_1/D_2=25/10)

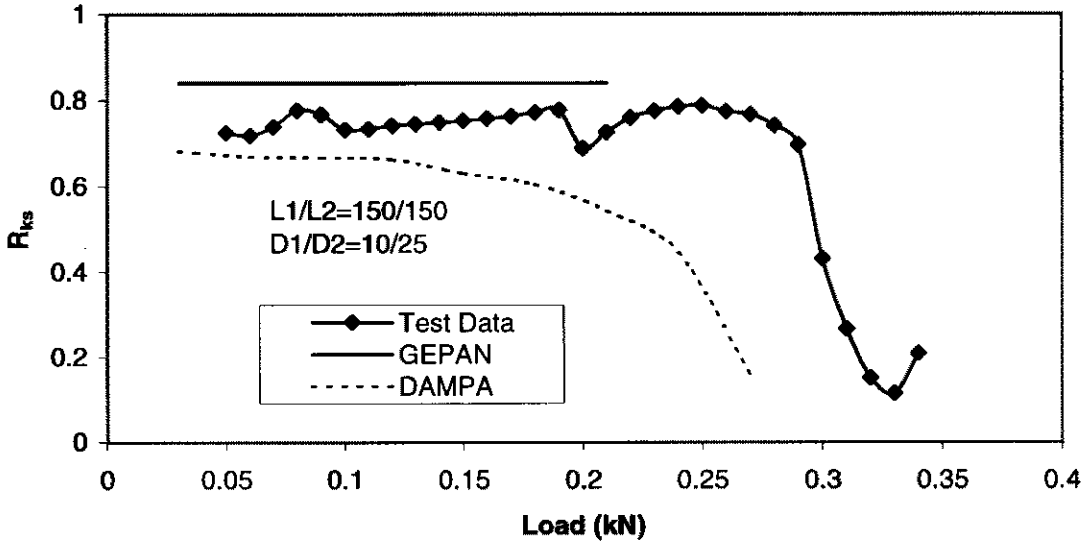

Fig. 7.34 Comparison of experimental and theoretical pile stiffness reduction fact for a defective pile (L_1/L_2=150/150, D_1/D_2=10/25)

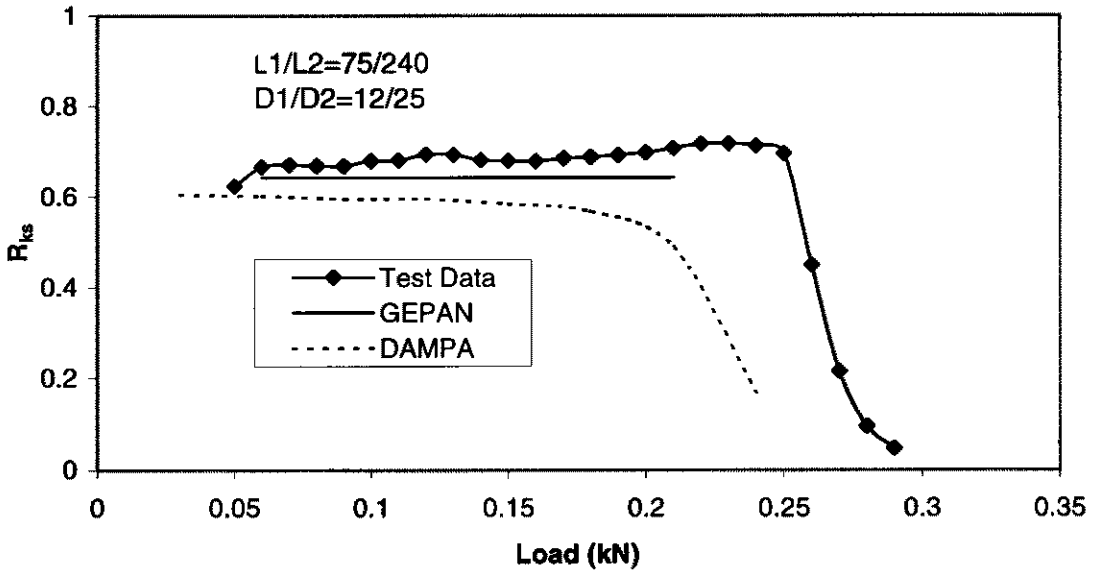

Fig. 7.35 Comparison of experimental and theoretical pile stiffness reduction fact for a defective pile (L_1/L_2=75/240, D_1/D_2=12/25)

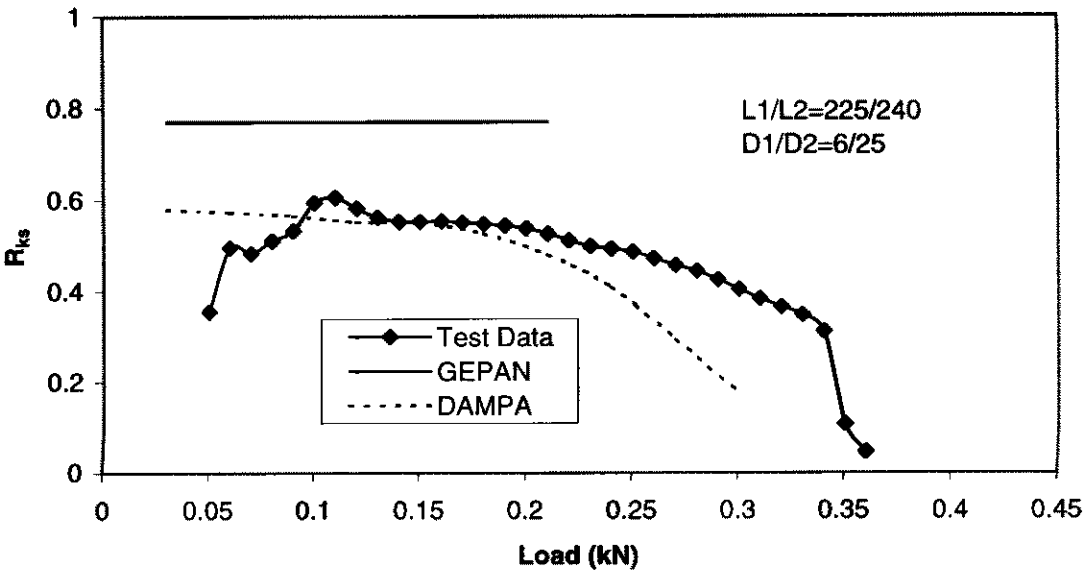

Fig. 7.36 Comparison of experimental and theoretical pile stiffness reduction factor for a defective pile (L_1/L_2=225/240, D_1/D_2=6/25)

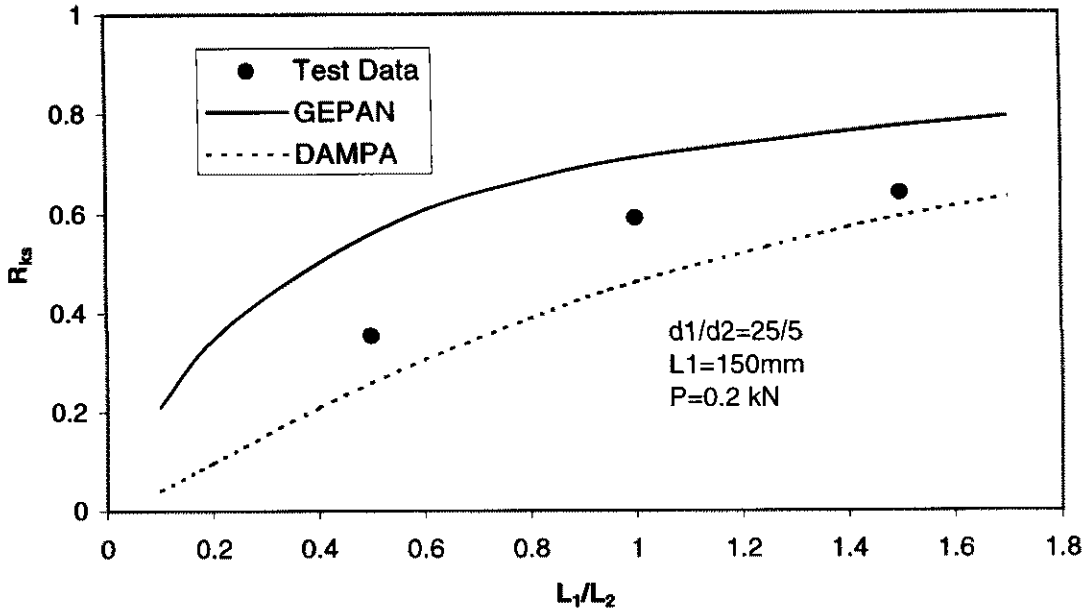

Fig. 7.37 Comparison of experimental and theoretical R_{ks}

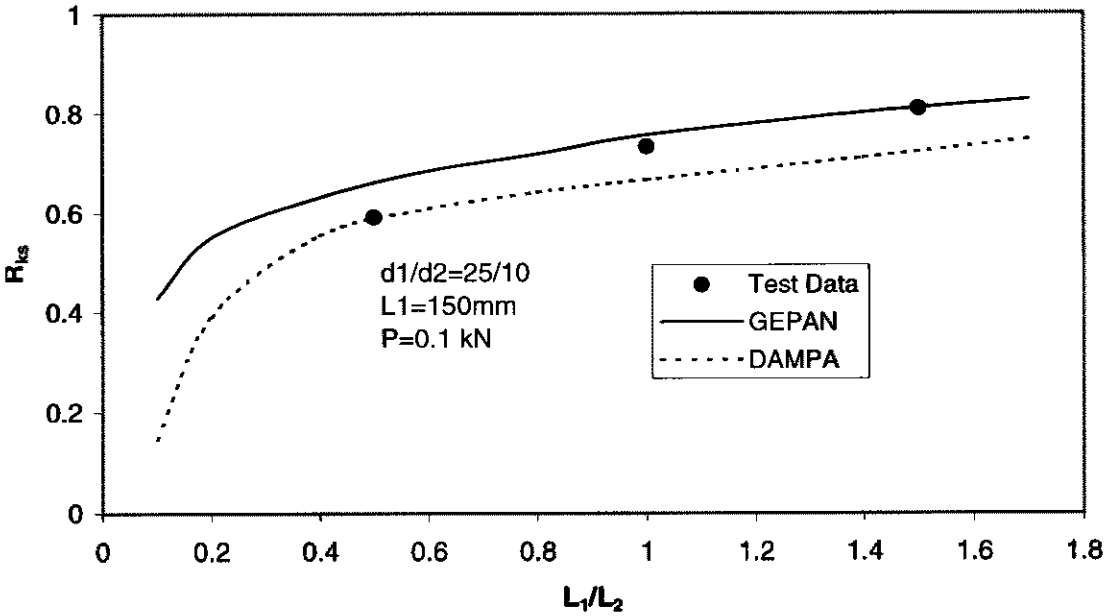

Fig. 7.38 Comparison of experimental and theoretical R_{ks}

Chapter 10

Further Development of Non-Linear Analysis in GEPAN

10.1 Introduction

From Chapter 2 to Chapter 9, it is shown that GEPAN has many applications in pile foundations, however, they are mainly focused on elastic analysis. As well known, non-linear analysis for pile foundation is also very important, especially for soils exhibiting strongly non-linear response or for studying the failure mechanism of a pile-soil system.

This Chapter describes the further development in GEPAN for non-linear analysis of pile foundation. The non-linear continuum analysis, load-transfer method and slip element are to be modelled into GEPAN. For the simplicity to the non-linear pile analysis, the following main assumptions are employed:

1. only monotonic loading is considered
2. no tensile gap failure occurs on the pile-soil interface
3. failure of pile-soil interface in one direction does not affect that in other directions.

10.2 Continuum Analysis

10.2.1 Failure Criterion

In the non-linear continuum analysis of piles, Poulos (1989b) set up failure criterion on the pile-soil interface. These concepts can be introduced, generalized into GEPAN for non-linear analysis in general 3-D conditions. The main principles are described below:

To allow for pile-soil or yield of an element, a check must be made on the total value of the interaction stress p at each element. When this is reached or exceeded at any element

i, the displacement compatibility equations at element *i* (described in Chapter 3), is replaced by the failure condition.

If an element *i* is in a compressive failure (FC) state, then one (or more) of following three FC criterion is (are) satisfied

$$\Delta p_{i,x} + p_{tot,i,x} \geq f_{c,i,x} \quad \text{.....(10.1)}$$

$$\Delta p_{i,y} + p_{tot,i,y} \geq f_{c,i,y} \quad \text{.....(10.2)}$$

$$\Delta p_{i,z} + p_{tot,i,z} \geq f_{c,i,z} \quad \text{.....(10.3)}$$

where

$f_{c,i,l}$ = limiting pile-soil stress in direction *l*, at element *i*, for compression loading

$p_{tot,i,l}$ = total pile-soil stress in direction *l*, at element *i*, at the previous load step

$\Delta p_{i,l}$ = increment pile-soil stress in direction *l*, at element *i*.

If Equation (10.1) is satisfied, the displacement compatibility relationship for element *i* is replaced by the condition:

$$\Delta p_{i,x} = f_{c,i,x} - p_{tot,i,x} \quad \text{..... (10.4)}$$

If Equation (10.2) is satisfied, the displacement compatibility relationship for element *i* is replaced by the condition

$$\Delta p_{i,y} = f_{c,i,y} - p_{tot,i,y} \quad \text{..... (10.5)}$$

If Equation (10.3) is satisfied, the displacement compatibility relationship for element *i* is replaced by the condition

$$\Delta p_{i,z} = f_{c,i,z} - p_{tot,i,z} \quad \text{..... (10.6)}$$

If an element i is in a tensile failure (FT) state, then satisfied one of following three FT criterion on more

$$\Delta p_{i,x} + p_{tot,i,x} \leq f_{t,i,x} \quad \text{.....(10.7)}$$

$$\Delta p_{i,y} + p_{tot,i,y} \leq f_{t,i,y} \quad \text{.....(10.8)}$$

$$\Delta p_{i,z} + p_{tot,i,z} \leq f_{t,i,z} \quad \text{.....(10.9)}$$

where

$f_{t,i,l}$ = limiting pile-soil stress in direction l, at element i, for tensile loading

If Equation (10.7) is satisfied, the displacement compatibility relationship for element i is replaced by the condition:

$$\Delta p_{i,x} = f_{t,i,x} - p_{tot,i,x} \quad \text{..... (10.10)}$$

If Equation (10.8) is satisfied, the displacement compatibility relationship for element i is replaced by the condition

$$\Delta p_{i,y} = f_{t,i,y} - p_{tot,i,y} \quad \text{..... (10.11)}$$

If Equation (10.9) is satisfied, the displacement compatibility relationship for element i is replaced by the condition

$$\Delta p_{i,z} = f_{t,i,z} - p_{tot,i,z} \quad \text{..... (10.12)}$$

The resulting set of equation for that load increment is then re-solved, and the check and re-solution procedure repeated until, at all elements, the total pile-soil stress does not exceed the limiting value ($f_{c,i,l}$ in compression, $f_{t,i,l}$ in tension).

10.2.2 Non-Linear Elastic Soil Behaviour

It is possible to incorporate non-linear behaviour of the soil, in an approximate manner, by assuming that the soil Young's modulus varies with either stress or strain level. Two models of non-linear-elastic response are proposed, which one is based on an empirical formula and other is on an explicit stress-strain equation for geo-material.

10.2.2.1 From an Empirical Formula

First, a hyperbolic response model, developed by Poulos (1989b), is incorporated into GEPAN in a 3-D loading. Allowing for non-linear soil behaviour by assuming a hyperbolic response at the pile-soil interfaces, the tangent Young's modulus of the soil $E_{s,i,l}$ at any element i is expressed as follows:

$$E_{s,i,l} = E_{o,i,l}(1 - R_{i,l}\frac{p_{i,l}}{p_{u,i,l}})^2 \quad \text{.....(10.13)}$$

where

$E_{s,i,l}$ = tangent Young's modulus of soil, in direction l, at element i

$E_{o,i,l}$ = initial tangent Young's modulus of soil, in direction l, at element i

R_{il} = hyperbolic factor in direction l, for element i

p_{il} = interaction stress in direction l, at element i

$p_{u,i,l}$ = limiting value of interaction stress in direction l, at element i.

l = direction x, y, z

Typical ranges for $R_{i,z}$ are 0 to 0.5 for shaft elements and 0.5 to 0.9 for base elements (Poulos, 1989b).

10.2.2.2 From an Explicit Stress-Strain Equation for Geo-Material

The second model to be used in GEPAN is based on an explicit stress-strain equations of geo-materials which is described in Chapter 11 (Xu *et al*, 1997). That stress-strain relationship can be explicitly expressed in terms of stress ratio and distortional strain. However, a number of findings are shown that the relationship of stress-displacment at pile-soil interface is quite similar to the above equation (Tabucanon, 1992, Kraft *et al*, 1981, O'Neil *et al*, 1982, 1977, Kezdi,1957). The explicit soil stress-displacement equations at pile-soil interface are assumed as follows:

$$p_{i,l} = p_{u,i,l}\left[1+\left(\frac{d_{i,l}}{d_{u,i,l}}-1\right)e^{-\frac{d_{i,l}}{d_{i,l,i}}}\right] \quad \text{.....(10.14)}$$

where

$p_{i,l}$ = interaction stress in direction l, at element i

$p_{u,,i,l}$ = limiting value of interaction stress in direction l, at element i

$d_{i,l}$ = displacement in direction l at element i

$d_{u,i,,l}$ = displacement at $p_{i,l} = p_{u,i,l}$ before the peck stress $p_{p,i,l}$ (the corresponding displacement $d_{p,i,l}$) reached, in direction l at element i

$d_{i,l} = d_{p,i,l}$-$d_{u,i,l}$, characteristic displacement in direction l at element i

l = direction x, y, z.

As shown in Fig. 10.1, the above equations can characterized by a basic material parameter $\alpha_{i,l}$ defined as follows:

$$\alpha_{i,l} = \frac{p_{i,i,l}}{p_{u,i,l}} \quad \text{.....(10.15)}$$

Mathematically transformed by equation 10.14, constitutive relationships of soil tangent Young's moduli are carried out in terms of soil stresses, as shown in Fig. 10.2. Furthermore, the approximate expression of soil tangent Young's moduli can be derived from equation 10.14 as follows:

$$E_{s,i,l} = E_{o,i,l}(1 - R_{i,l}\frac{p_{i,l}}{p_{u,i,l}}) \quad \text{.....(10.16)}$$

where

$$R_{i,l} = \frac{1}{1 + e^{\frac{1}{\alpha_{i,l}} - 1}} \quad \text{.....(10.17)}$$

10.3 Elastoplastic Response of Piles

In governing equation 3.1 in Chapter 3, the sub-matrixes *PIF*, *D*, *G*, *O*, *R* relating displacements due to stresses or loads on piles are to be modified when the elastoplastic response of piles is considered. The following modelling of pile elastoplatic response is proposed:

piles in compression:

$$E_{p,c,i} = \begin{cases} E_{p,i} & \sigma_i < \sigma_{y,c} \\ R_c E_{p,i} & \sigma_{y,c} \le \sigma_i < \sigma_{b,c} \\ 0 & \sigma_i \ge \sigma_{b,c} \end{cases} \quad \text{.....} \quad (10.18)$$

where

$E_{p,c,i}$ = pile Young's modulus in compression, at element i

$E_{p,i}$ = pile elastic Young's modulus, at element i

R_c = ratio of post-yield modulus to elastic Young's modulus in compression

σ_i = pile normal stress at element i

$\sigma_{y,c}$ = pile yield stress in compression

$\sigma_{b,c}$ = pile strength in compression

piles in tension:

$$E_{p,t,i} = \begin{cases} E_{p,i} & \sigma_i > \sigma_{y,t} \\ R_t E_{p,i} & \sigma_{b,t} \le \sigma_i < \sigma_{y,t} \\ 0 & \sigma_i \le \sigma_{b,t} \end{cases} \quad \text{..... (10.19)}$$

where

$E_{p,t,i}$ = pile Young's modulus in tension, at element i

R_t = ratio of post-yield modulus to elastic Young's modulus in tension

$\sigma_{y,t}$ = pile yield stress in tension

$\sigma_{b,t}$ = pile strength in tension

piles in torsion:

$$G_{p,s,i} = \begin{cases} G_{p,i} & |\tau_i| < |\tau_y| \\ R_s G_{p,i} & |\tau_y| \le |\tau_i| < |\tau_b| \\ 0 & |\tau_i| \ge |\tau_b| \end{cases} \quad \text{.....(10.20)}$$

where

$G_{p,s,i}$ = pile shear modulus at element i

R_s = ratio of post-yield share modulus to elastic shear modulus

τ_y = pile yield share stress

τ_b = pile shear strength

10.4 Slip at Pile-Soil Interface

In the governing equation, no slip at pile-soil interface is assumed. The assumption, however, may be unrealistic some times. For examples, slips may occur even in elastic if the pile-soil interface is very smooth and slips may not happen even in plastic if the interface is very rough. In fact, the slip behaviour is mainly determined by friction strength.

10.4.1 "Slip" Element

10.4.1 "Slip" Element

First, it is assumed that there exist zero thickness "slip" elements (or joint element) between pile and soil. In the slip elements on pile-soil interface, there are six unknowns at any element *i* (three stresses and three slips) rather than three unknowns (stresses) before. The style of constitution equations is proposed as follows:

$$[W]\{X_e\}+[Z]\{X_s\}=\{Y_s\} \qquad \text{..... (10.21)}$$

where

W = coefficient matrix of slip-friction

Z = coefficient matrix of slip

X_e = vector of pile-soil stresses

X_s = vector of slips in cylindrical coordinate system

Y_s = vector of constants

10.4.2 Global Slip-Involved Equation

Incorporated the constitution equation, the global equation can be extended into following form:

$$\begin{pmatrix} A & B & 0 & D & E \\ 0 & 0 & G & H & 0 \\ O & P & Q & R & 0 \\ S & 0 & 0 & V & 0 \\ W & 0 & 0 & 0 & Z \end{pmatrix} \begin{pmatrix} X_e \\ X_b \\ X_c \\ X_t \\ X_s \end{pmatrix} = \begin{pmatrix} Y_q \\ Y_c \\ 0 \\ Y_p \\ Y_s \end{pmatrix} \qquad \text{..... (10.22)}$$

E = projection matrix of slips

and

$$E = \begin{pmatrix} E_1 & & & \\ & E_2 & & \\ & & E_i & \\ & & & E_{ntot} \end{pmatrix}_{3\times ntot} \quad \text{..... (10.22)}$$

$$E_i = \begin{pmatrix} \cos\theta_i & -\sin\theta_i & 0 \\ \sin\theta_i & \cos\theta_i & 0 \\ 0 & 0 & 1 \end{pmatrix}_{3\times 3} \quad \text{..... (10.23)}$$

where

θ_i = normal angle of element i

10.5 General Load Transfer Method

10.5.1 General Load-Transfer Equations

In Load-transfer analysis, the soil resistance is modelled by a discrete spring at each element, which is characterized by load-transfer equations, *i.e.*, the "*t-z*" and/or "*p-y*" curves. Same as the equation 10.14, the general load-transfer equations can be expressed as follows:

$$p_{i,l} = p_{u,i,l}\left[1+\left(\frac{d_{i,l}}{d_{u,i,l}}-1\right)e^{\frac{d_{i,l}}{d_{i,i,l}}}\right] \quad \text{.....(10.24) (10.14bis)}$$

10.5.2 Modify Soil Behaviour Matrix *SIF*

For the continuum analysis and load-transfer analysis, the only differences arise in the soil behaviour matrix *SIF* described in Chapter 3. In load-transfer analysis, the off-diagonal components of *SIF* are zero as follows:

$$SIF = \begin{pmatrix} I_{1,1} & 0 & \dots & 0 \\ 0 & I_{2,2} & \dots & \dots \\ \dots & \dots & I_{i,j} & 0 \\ 0 & \dots & 0 & I_{ntot,ntot} \end{pmatrix}_{3*ntot \times 3*ntot} \quad \dots\dots\dots\dots (10.25)$$

$I_{i,j}$ is the 3×3 BIFM of displacements at soil element i due to unit stresses on soil element j which is expressed as follows:

$$I_{i,j} = \begin{pmatrix} I_{i,j,1,1} & 0 & 0 \\ 0 & I_{i,j,2,2} & 0 \\ 0 & 0 & I_{i,j,3,3} \end{pmatrix}_{3\times 3} \quad \dots\dots\dots\dots (10.26)$$

$I_{i,j,k,l}$ = soil displacement in direction k at element i due to a unit stress in direction l on element j.

Unlike the continuum analysis, in which the soil influence factor $I_{i,j,k,l}$ is carried out by integration of Mindlin's equations, the diagonal components of $I_{i,j,k,k}$ are determined by the load-transfer equation 10.24(10.14bis).

10.6 Some Evaluations

These non-linear analyses in GEPAN are being developed progressively. Some of them have been incorporated into GEPAN (like failure criterion in non-linear continuum analysis for vertical loading). The comparisons of effect of non-linearity of vertical loading via GEPAN and PIES (Poulos, 1989b) are shown in Fig. 10.3 (floating pile) and Fig. 10.4 (end-bearing pile). The parameters in these two cases are assumed: pile length

L=20 m, diameter d=10 m, soil Young's modulus E_s = 20 MPa, base Young's modulus E_b=100 MPa (for end-bearing pile), ultimate skin friction in compression f_s=50 kPa, ultimate base friction in compression f_b=100 kPa. It is shown the non-linear pile analysis via GEPAN and PIES are in relatively good agreement.

10.7 Conclusions

This Chapter describes the availability of the general non-linear analysis for pile foundations in GEPAN. The models of 3-D non-linear analysis in pile-soil system (such as, simple non-linear continuum analysis, general load-transfer method, elastic-plastic piles and slip development) are concisely set up. Via applying models and modifying the soil behaviour matrix and the pile behaviour matrix in the governing equation, a general 3-D non-linear analysis for pile foundation can be implemented.

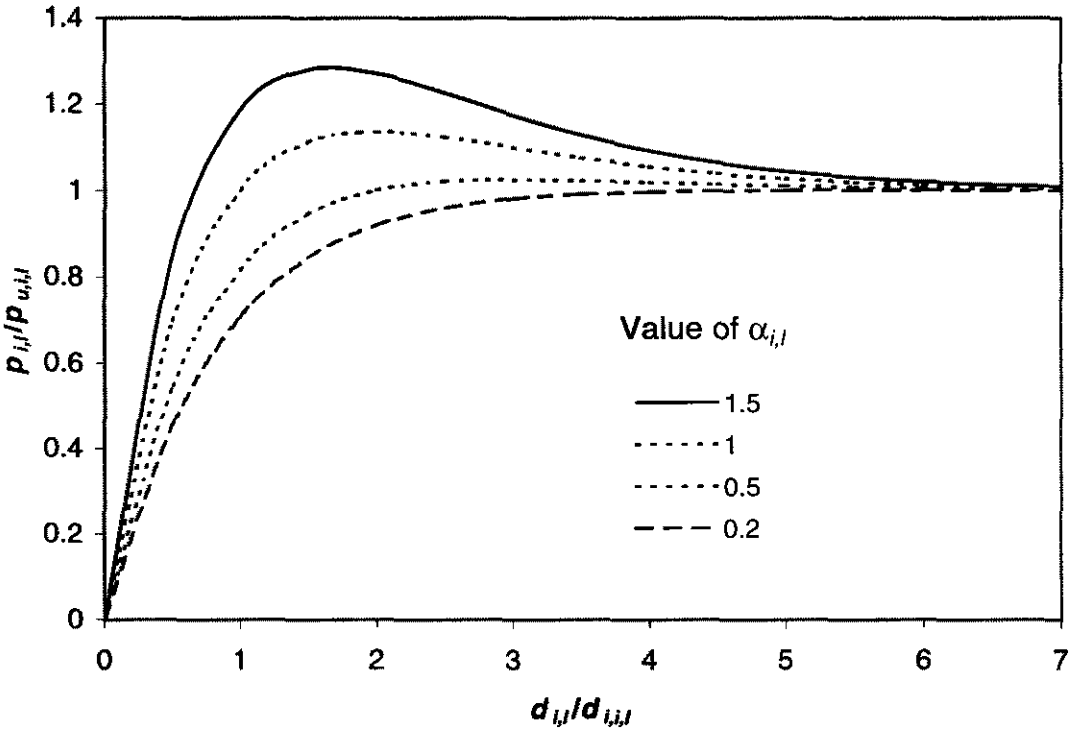

Fig. 10.1 Behaviour of stress-displacement at pile-soil interface

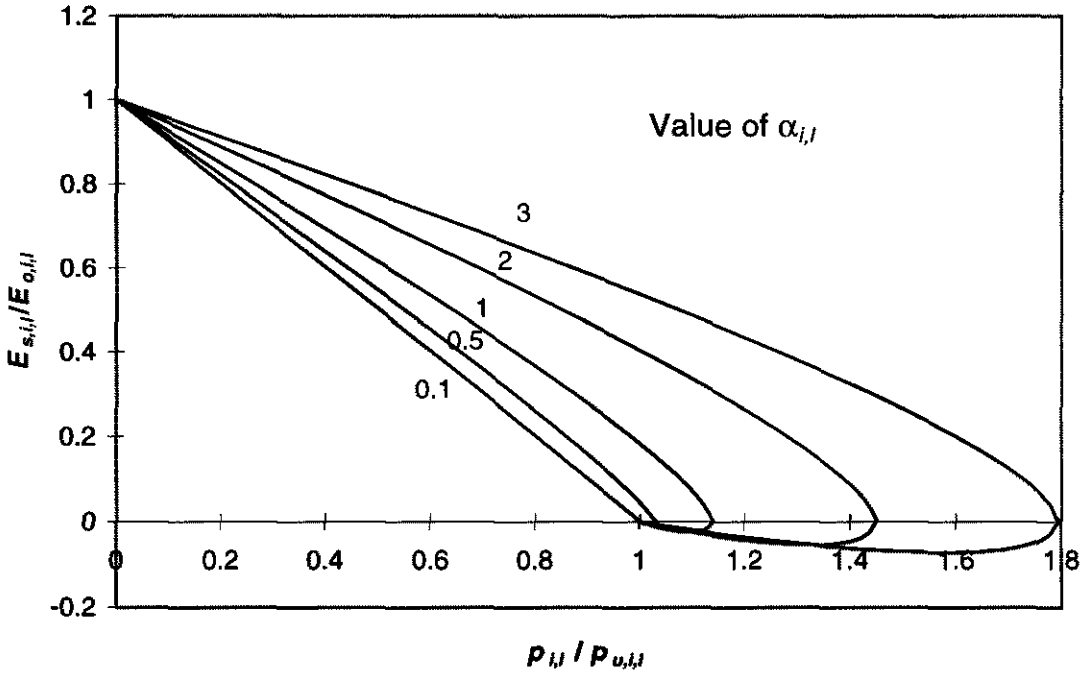

Fig. 10.2 Soil tangent Young's modulus vs soil stress at pile-soil interface

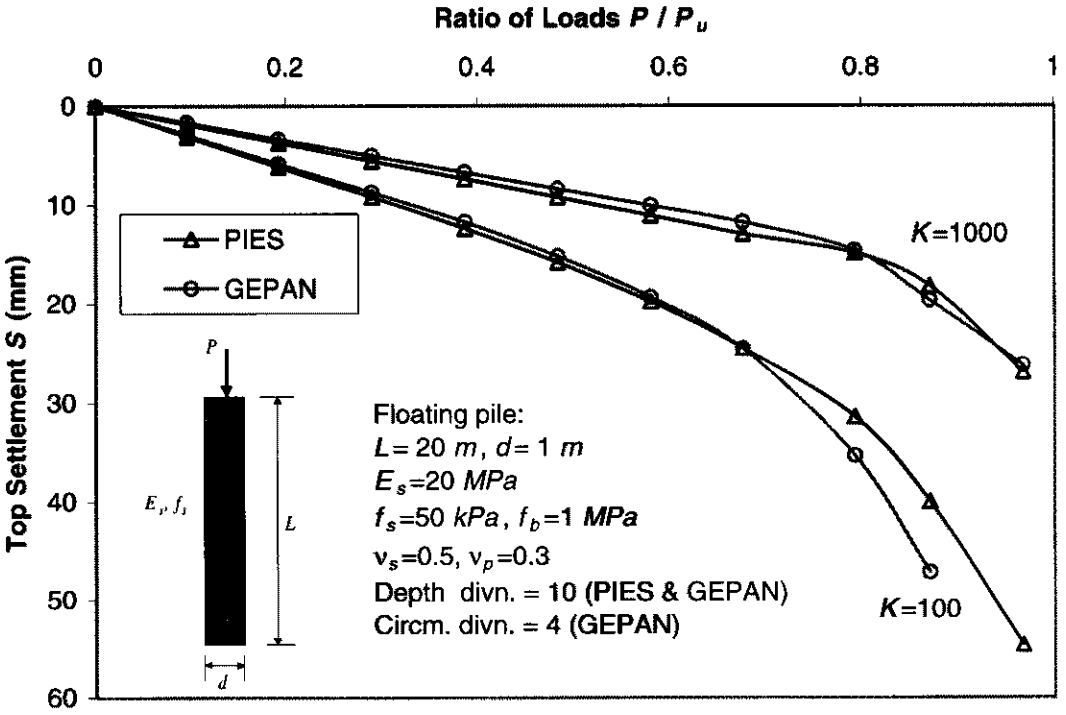

Fig. 10.3 Comparisons between GEPAN and PIES, Floating pile

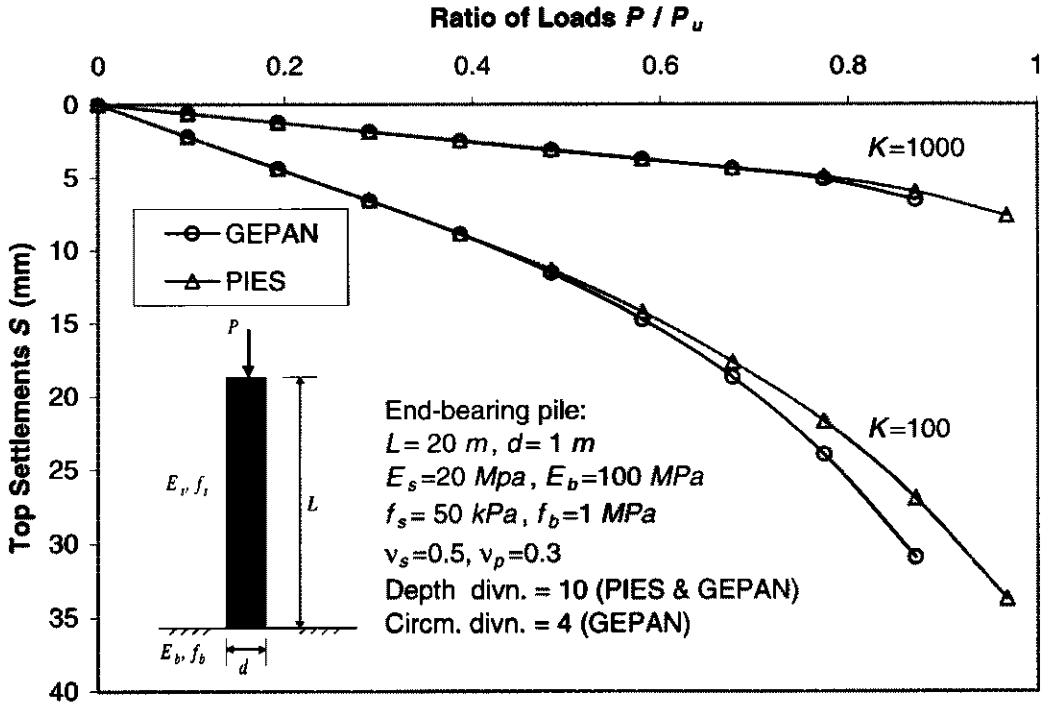

Fig. 10.4 Comparisons between GEPAN and PIES, End-bearing pile

Chapter 11

Simulating the Shearing Behaviour of Frictional Materials

11.1 Introduction

This chapter seems rather different in character to the remainder of the thesis, but has relevance for future research on general non-linear pile analysis. As described in Chapters 1 and 10, the critical aspect in general non-linear analysis for pile foundations is to model the shearing behaviour at the pile-soil interface. It is very hard to obtain good predictions of the shearing strength with making allowance for the volume changes that occur in the soil (Poulos, 1989), however, very little methods of pile analysis exist to consider the volume effect. On the other hand, the key problem in the boundary element method applied to pile foundations is to set up explicit equations for the load-deformation behaviour of soils. It is very necessary to develop a set of unified explicit equations describing the shearing (distortional and volumetric) behaviours of soil in the non-linear analysis of pile foundation using the boundary element method. Thus, one of main objectives of this chapter is to supply a more realistic nonlinear soil model to extend the non-linear pile analysis in future.

In this chapter, a set of two explicit equations, describing the relationship between the shear stress ratio and the distortional strain and that between the volumetric strain and the distortional strain, are formulated independently based on various assumptions. Features of the constitutive equations are demonstrated. It is shown that the proposed equations have the capacity to simulate the behaviour of many different types of frictional materials including geo-materials. The proposed model is used to simulate the behaviour of twenty-one different types of frictional materials for one hundred and nine tests. The proposed model is evaluated based on an extensive comparison between model simulations and experimental data. An extensive study of material parameters and an examination of the relationship between the distortional deformation equation and the volumetric deformation equation are performed.

11.2 Formulation of the Shear Stress-strain Equations

11.2.1 Method of Simulating the Shearing Behaviour of Frictional Materials

Xu *et al* (1997) present a study on the numerical simulation of the constitutive behaviour of various frictional materials under monotonic shearing, on the assumptions of the parameters

of distortional deformation and volumetric deformation being dependent and the flow rule being the same as in the Cam Clay model (Roscoe *et al*, 1958). It is found that, however, shearing model may be not accurate for describing the shearing behaviour of some frictional materials because the flow rule is not obeyed in those cases. In order to set up a unified shearing model, the distortional deformation and volumetric deformation in this chapter are firstly simulated independently and no hypothetical relationship is made between parameters from the two types of deformation. The relationship between the two types of deformation is examined later according to values of model parameters identified. The greatest advantage for this procedure is that pre-assumptions, and possibly artificial constraints on the relationship between the distortional deformation and the volumetric deformation imposed by classic research, are removed.

Two controlling factors in engineering design are the strength of a structure and the deformation of a structure. It appears rational in simulating the constitutive behaviour of materials to choose one set for parameters for material strength and another set for material deformation (or stiffness). Critical state soil mechanics is centred on the assumption of the existence of critical states of deformation (Schofield and Wroth, 1968). The critical state is a mathematical convergent point for stress states under monotonic shearing no matter what the initial state of the soil and the testing stress and strain paths are (Xu *et al* 1997). The critical state seems to provide a "perfect" state for choosing strength parameters. There needs to be also a mathematical convergent point for strain states. The strain convergent point is chosen to be the characteristic point at which the tangent distortional modulus is a material constant (For the definition of the modulus see equations (A8) and (A9) in the Notation Appendix at the end of this chapter). Based on the two convergent points and some assumptions, a constitutive equation between the shear stress ratio and the distortional strain is formulated. The explicit equation for the volumetric strain is derived from the known distortional strain based on a proposed relationship among the strain increment under monotonic shearing, or flow rule. However, the parameters for the distortional deformation and those for the volumetric deformation are completely independent.

11.2.2 Some Basic Ideas

Assumption 1: The response of frictional materials to shearing is dependent on shear stress ratio, not the shear stress.

Assumption 1 is a fundamental concept in this chapter on modelling the shearing behaviour of frictional materials. Consequently, material properties for shearing as well material response should be described in terms of shear stress ratio, not the conventional shear stress. A new modulus G, the distortional modulus, is suggested – see equation (A8) for secant distortional modulus and equation (A9) for tangent distortional modulus. These two moduli are related to the stress ratio directly.

Assumption 2: It is assumed that the mathematical format for shearing response of a frictional material can be expressed as an exponential function modified by a linear function as follows

$$\eta = f_1(\zeta, \varepsilon_d) * e^{f_2(\xi, \varepsilon_d)} + c \qquad \text{.....(11.1)}$$

where η and ε_d are the shear stress ratio and distortional strain respectively, ξ and ζ indicate material parameters, and f_1 and f_2 represent two linear functions, and c is a constant. The definitions of stress quantities p' and q and η, and strain quantities ε_v and ε_d are given in the notation appendix. Equation (11.1) is developed from the empirical expressions of shearing obtained by Prat *et al* (1991) and Xu *et al* (1997) via trial and error method.

Two types of distortional behaviour: There are two basic types of response of frictional materials to shearing in the distortional strain and shear stress ratio space (Fig. 11.1a). "Dry distortional behaviour" is defined as the response of frictional materials to monotonic shearing that reaches a peak strength firstly then drops to a final strength. "Wet distortional behaviour" is defined as the response of frictional materials to monotonic shearing that approaches a final strength as the distortional increases and there is no peak strength.

Two types of volumetric behaviour: There are also two basic types of response of frictional materials to shearing in the volumetric and distortional strain space (Fig. 11.1b). "Dry volumetric behaviour" is defined as the response of frictional materials to monotonic shearing that contracts at low stress ratio range and then expands at high stress ratio range. "Wet volumetric behaviour" is defined as the response of frictional materials to monotonic shearing that exhibits only volumetric compression.

11.2.3 Modelling the Distortional Behaviour

Assumption 3: The final state of the deformation of a frictional material under monotonic shearing is assumed to be that at which the distortional strain increases infinitely with the

stress state and voids ratio remaining constant.

The final state is a perfect plastic state at which a frictional material has no resistance to further increase of shear stress ratio. For sands and most clays, the final state is the critical state of deformation (Muir-Wood, 1990). For clay with enough platy particles, the final state may be the residual strength state if the platy particles have formed a smooth sliding plane along the failure surface. No special distinction is made for this simulation between the critical state of deformation and the residual of deformation, and the term "the final state" is thus suggested as the stress convergent point for the behaviour of frictional materials of a given mineralogy. The final state may be regarded as the point where soil is distorted continuously with no change or negligible change in stress state and voids ratio. A comprehensive study of the residual strength can be found from Skempton (1985), and a study on the modelling of the critical state strength and the residual strength and the transition of soil final strength as the clay fraction varies can be found from Liu and Carter (1998).

Mathematically, assumption (3) can be expressed as

$$\begin{cases} \eta \xrightarrow{\varepsilon_d \to \infty} M_f \\ \dfrac{d\varepsilon_v}{d\varepsilon_d} \xrightarrow{\varepsilon_d \to \infty} 0 \end{cases} \qquad \text{.....(11.2)}$$

where M_f is the stress ratio at the final state.

The relationship between the tangent distortional modulus and the distortional strain, for a frictional material with both "dry distortional behaviour" and "wet distortional behaviour", is shown in Fig. 11.2a. The two curves intersect twice on this plot, at points *I* and *C*. Point *C* corresponds to the final state of deformation. If the coordinates for point *I* are denoted as ($\varepsilon_{d,i}$, G_i), then the quantities $\varepsilon_{d,i}$ and G_i may be defined as the characteristic distortional strain and the characteristic distortional modulus.

Assumption 4: It is assumed that there exists a common point, the characteristic point, in the ε_d and G_t curves for all shearing tests on a frictional material of the same mineralogy.

The coordinates of the characteristic point, $\varepsilon_{d,i}$ and G_i, are therefore independent of the initial stress and strain states of the material. Point *I* in Fig. 11.2a is therefore the convergent point of frictional material behaviour in the ε_d and G_t space. Assumption (4) can be expressed as

$$\left.\frac{\partial \eta}{\partial \varepsilon_d}\right|_{\varepsilon_d=\varepsilon_{d,i}} = G_i \qquad \text{.....(11.3)}$$

It may be noticed that condition (11.3) is valid for any selected mathematical format of the η and ε_d relationship.

Assumption 5: The distortional strain is assigned to be zero for a material which has never experienced any shearing, ***i.e.***,

$$\varepsilon_d = 0 \text{ for } \eta = 0 \qquad \text{..... (11.4)}$$

It is found that the following equation, a special form of the mathematical expression (11.1), can satisfy all the conditions expressed by equations (11.2) and (11.3) and (11.4).

$$\eta = \mathrm{M}_f \left[1 + \left(\frac{\varepsilon_d}{\varepsilon_{d,u}} - 1 \right) e^{-\frac{\varepsilon_d}{\varepsilon_{d,i}}} \right] \qquad \text{..... (11.5)}$$

Strain $\varepsilon_{d,u}$ is defined in the Appendix and on Fig. 11.1a.

Under standard test procedures, a specimen of a frictional material may be expected to deform with highly uniform stress and strain for the entire process of "wet distortional behaviour" and for the hardening process of "dry distortional behaviour". It is normally expected that non-uniformity in stress and strain states will occur during softening. As a result, the deformation of the specimen in softening is affected by the factors such as bulge, fracture, and rupture. An effective way to describe the influence of this non-uniformity is to modify the constitutive equation through the introduction of a function representing the relative effects of the non-homogeneous behaviour. Equation (11.5) is modified by a relative non-uniformity function $D(\varepsilon_d)$ as follows

$$\eta = \mathrm{M}_f \left[1 + D(\varepsilon_d) \left(\frac{\varepsilon_d}{\varepsilon_{d,u}} - 1 \right) e^{-\frac{\varepsilon_d}{\varepsilon_{d,i}}} \right] \qquad \text{.....(11.6)}$$

where $D(\varepsilon_d)$ is expressed as

$$D(\varepsilon_d) = e^{-B\left(\frac{\varepsilon_d}{\varepsilon_{d,u}+\varepsilon_{d,i}}\right)} \qquad \text{.....(11.7)}$$

in which

$$B=\begin{cases}0 \text{ for } \varepsilon_d \le \varepsilon_{d,u}+\varepsilon_{d,i} \\ \beta \text{ for } \varepsilon_d > \varepsilon_{d,u}+\varepsilon_{d,i}\end{cases} \qquad \text{.....(11.8)}$$

β is a parameter to describe the non-homogeneous behaviour of the specimen. Comparing equation (11.6) with equation (11.5), it can be seen that only the behaviour during softening process, *i.e.*, for $\varepsilon_d > \varepsilon_{d,u}+\varepsilon_{d,i}$, is modified by parameter β, and equation (11.6) also satisfies conditions (11.2), (11.3), and (11.4), but does not obey the format of equation (11.1).

11.2.4 Modelling the Volumetric Behaviour

The plastic flow rule may be defined as the ratio of the plastic volumetric strain increment over the plastic distortional strain increment. With the flow rule known, the volumetric strain can be calculated from the distortional strain, and the vice versa. Some of the well known flow rule are proposed by Roscoe *et al* (1958), Rowe (1962), Roscoe and Burland (1968), Mroz *et al* (1981), and Houlsby *et al* (1982). In all these proposed rules, the plastic flow rule during monotonic shearing is dependent only on the critical state strength, and the current stress ratio. For an example, the flow in the Cam Clay model (Roscoe *et al*, 1958) is

$$\frac{d\varepsilon_v^p}{d\varepsilon_d^p}=\mathrm{M}_f-\eta \qquad \text{.....(11.9)}$$

where ε_d^p is plastic distortional strain, ε_v^p is plastic volumetric strain. The final state in shearing for soils is assumed to be the critical state.

The volumetric deformation of frictional materials is rather complicated and varies with a particular material and its micro-structure. In order to model the possible variation due to different geo-materials the following equations are suggested to calculate the volumetric strain increment

$$\frac{d\varepsilon_v}{d\varepsilon_d}=\mathrm{M}^v-\eta^v \qquad \text{.....(11.10)}$$

where

$$\eta^{v} = \mathrm{M}^{v}\left[1+\left(\frac{\varepsilon_d}{\varepsilon^{v}_{d,u}}-1\right)e^{\frac{\varepsilon_d}{\varepsilon^{v}_{d,i}}}\right] \qquad \text{.....(11.11)}$$

M^{v}, $\varepsilon^{v}_{d,i}$, and $\varepsilon^{v}_{d,u}$ are material parameters to describe the volumetric deformation of frictional materials. Parameter η^{v} is calculated from material parameters M^{v}, $\varepsilon^{v}_{d,i}$, and $\varepsilon^{v}_{d,u}$ and the current distortional strain ε_d. There are actually only three parameters for the flow rule. Definitions of M^{v} and $\varepsilon^{v}_{d,u}$ are shown in Fig. 11.1b. Combining equation (11.10) with equation (11.11), the proposed new flow rule for modelling the shearing behaviour of a frictional material is obtained as follows

$$\frac{d\varepsilon_v}{d\varepsilon_d} = \mathrm{M}^{v}\left(1-\frac{\varepsilon_d}{\varepsilon^{v}_{d,u}}\right)e^{\frac{\varepsilon_d}{\varepsilon^{v}_{d,i}}} \qquad \text{.....(11.12)}$$

The following condition can be obtained from equations (11.10) and (11.11)

$$\left.\frac{d^2\varepsilon_v}{d^2\varepsilon_d}\right|_{\varepsilon_d=\varepsilon^{v}_{d,i}} = -\left.\frac{d\eta^{v}}{d\varepsilon_d}\right|_{\varepsilon_d=\varepsilon^{v}_{d,i}} = \text{constant} \qquad \text{..... (11.13)}$$

Similar to characteristic point I in the ε_d and G_t space, point $J\left(\varepsilon^{v}_{d,i}, d^2\varepsilon_v/d^2\varepsilon_d\big|_{\varepsilon_d=\varepsilon^{v}_{d,i}}\right)$ is another assumed convergent point for the behaviour of a frictional material under monotonic shearing in the $\varepsilon_d \sim d^2\varepsilon_v/d^2\varepsilon_d$ space (see Fig. 11.2b).

As has been described by Xu *et al* (1997), if the following constraints are enforced for the three volumetric deformation parameters, *i.e.*,

$$\begin{cases} \mathrm{M}^{v} = \mathrm{M}_f \\ \varepsilon^{v}_{d,i} = \varepsilon_{d,i} \\ \varepsilon^{v}_{d,u} = \varepsilon_{d,u} \end{cases} \qquad \text{.....(11.14)}$$

then, the proposed flow law is the same as equation (11.9) because $\eta^{v} = \eta$. It may be seen that the proposed flow law has a form similar to that of the original Cam Clay Model; however, constraints (11.13) are released. The volumetric deformation thus formulated is independent of the distortional deformation because the set of material parameters for distortional deformation and the set of parameters for volumetric deformation are

independent.

The total volumetric strain can be computed as

$$\varepsilon_v = \int_0^{\varepsilon_d} \left(\mathrm{M}^v - \eta^v\right) d\varepsilon_d \qquad \text{.....(11.15)}$$

After some manipulation, the following explicit expression for the total volumetric strain is obtained

$$\varepsilon_v = \varepsilon_{d,i}^v \mathrm{M}^v \left[1 - \frac{\varepsilon_{d,i}^v}{\varepsilon_{d,u}^v} + \frac{\varepsilon_{d,i}^v}{\varepsilon_{d,u}^v}\left(1-m^2\right) e^{-\left(\frac{\varepsilon_{d,u}^v + \varepsilon_{d,i}^v}{\varepsilon_{d,i}}\right)} + \left(\frac{\varepsilon_d}{\varepsilon_{d,u}^v} + m^2 \frac{\varepsilon_{d,i}^v}{\varepsilon_{d,u}^v} - 1 \right) e^{B - \left(\frac{\varepsilon_d}{m\varepsilon_{d,i}^v}\right)} \right] \qquad \text{....(11.16)}$$

where

$$m = \frac{\varepsilon_{d,u}^v + \varepsilon_{d,i}^v}{\varepsilon_{d,u}^v + (1+B)\varepsilon_{d,i}^v} \qquad \text{.....(11.17)}$$

If $\beta = 0$, equation (11.16) can be simplified as

$$\varepsilon_v = \varepsilon_{d,i}^v \mathrm{M}^v \left[1 - \frac{\varepsilon_{d,i}^v}{\varepsilon_{d,u}^v} + \left(\frac{\varepsilon_{d,i}^v + \varepsilon_d}{\varepsilon_{d,u}^v} - 1 \right) e^{-\left(\frac{\varepsilon_d}{\varepsilon_{d,i}^v}\right)} \right] \qquad \text{.....(11.18)}$$

11.3 Features of the Proposed Model

11.3.1 Model Parameters and Their Physical Meanings

Seven parameters are needed to define the two constitutive equations. Three of the parameters are used for the distortional strain and shear stress ratio equation. They are M_f, $\varepsilon_{d,u}$, and $\varepsilon_{d,i}$. The three parameters required for the volumetric strain and the distortional strain equation are M^v, $\varepsilon^v_{d,u}$, and $\varepsilon^v_{d,i}$. Parameter β is introduced to represent the effect of the non-uniformity of the sample deformation during softening process, and it has influence on both the distortional and the volumetric deformation produced in the softening process.

M_f is the value of the final shear strength of a frictional material as the distortional strain increases (Fig. 11.1a). M_f is a material constant.

$\varepsilon_{d,i}$ is the value of the distortional strain at the characteristic point *I* in the ε_d~G_t coordinates (Fig. 11.2a). The characteristic point *I* is independent of the stress and strain state of the material, and is a convergent point of geo-material behaviour in the ε_d~G_t space.

The parameter $\varepsilon_{d,u}$ is the distortional strain at $\eta = M_f$ before the peak strength is reached, and consequently it reflects the relative shear stiffness for a given material (Fig. 11.1a). With a decrease in the value of $\varepsilon_{d,u}$, the material reaches the peak strength at a lower shear strain. The value of $\varepsilon_{d,u}$ can be measured directly from a shear stress-strain $\varepsilon_d \sim \eta$ curve.

According to equation (11.12), M^v is numerically equal to the rate of dilatancy, or $d\varepsilon_v / d\varepsilon_d$, at $\eta = 0$. Theoretically speaking, the dilatancy at $\eta = 0$ should be zero for an isotropic material, and the flow rules such as this and those in the Cam Clay Model (Schofield and Wroth, 1968) and Rowe's stress-dilatancy model (1962) are incorrect for this situation. However, it has been observed that those flow rules describe satisfactorily experimental data on the shearing behaviour of soils (Muir-Wood, 1990; Yu, 1998). Obviously such equations are not valid for isotropic compression, but the effect of this problem should be insignificant for a model concerning the effect of monotonic shearing. As far as identifying the value of M^v is concerned, M^v can still be measured from a volumetric and distortional curve based on its definition because a non-zero value for the initial dilatancy is clearly found in most shearing test data (Fig. 11.1b).

As is shown in Fig. 11.2b, $\varepsilon^v_{d,i}$ is the distortional strain at the convergent point for the curvature rate of the volumetric strain and the distortional strain relationship. $\varepsilon^v_{d,u}$ is the value of distortional strain at the peak volumetric strain (Fig. 11.1b). These parameters can be determined from a shearing test accordingly.

Parameter β describes the softening process only, and it reflects the influence of the non-uniformity of the sample deformation. Its value is determined by matching the softening curve simulated with that measured. β is the only parameter which needs to be decided by fitting.

All the seven parameters discussed above can be determined from a single test where the specimen is sheared to reach the final strength. It should be pointed out that difficulty may

arise in determining parameters $\varepsilon_{d,u}$ from "wet distortional behaviour" based on its definition. The distortional strain at the $\eta=M_f$ before peak state usually can not clearly defined. For "wet distortional behaviour", a practical method for determining $\varepsilon_{d,u}$ may be by the means of best fitting. A similar problem exists for $\varepsilon^{v}_{d,u}$ as well in the situation of "wet volumetric behaviour".

11.3.2 Peak Strength of a Frictional Material

The proposed stress-strain equation predicts a peak strength for frictional materials under monotonic shearing, irrespective of the initial stress and strain states. It can be shown mathematically that the stress ratio η_p and the distortional strain $\varepsilon_{d,p}$ at the peak are given by

$$\eta_p = \mathrm{M}_f\left[1+\frac{\varepsilon_{d,i}}{\varepsilon_{d,u}}e^{-\left(1+\frac{\varepsilon_{d,u}}{\varepsilon_{d,i}}\right)}\right] \qquad \text{.....(11.19)}$$

$$\varepsilon_{d,p} = \varepsilon_{d,i} + \varepsilon_{d,u} \qquad \text{.....(11.20)}$$

Furthermore, from equation (11.19) it can be shown that

$$\begin{cases} \eta_p < 1.025\mathrm{M}_f \text{ if } \dfrac{\varepsilon_{d,i}}{\varepsilon_{d,u}} < 0.5 \\ \eta_p < 1.0005\mathrm{M}_f \text{ if } \dfrac{\varepsilon_{d,i}}{\varepsilon_{d,u}} < 0.2 \end{cases} \qquad \text{.....(11.21)}$$

For frictional material with "wet distortional behaviour", values of $\varepsilon_{d,i}/\varepsilon_{d,u}$ less than 0.5 are normally expected. Therefore, the difference between the peak strength and the final strength is negligible.

11.3.3 Features of the Shear Stress Ratio and Distortional Strain Curve

In order to demonstrate the power of the proposed general distortional strain and shear stress ratio equation, *i.e.*, equation (11.6), nine cases of simulation have been made. The values of the material parameters for these cases are listed in Table 11.1. Non-uniformity of stress and strain state is not considered in this series of calculations, therefore, $\beta = 0$ is assigned. The variation of shear stress ratio η with the distortional strain ε_d is indicated in Fig. 11.3. The values of material parameters are selected to be consistent with the actual materials that the

equation has the capacity to represent. For curves 1 and 2, the values selected for M_f are different for all other cases, because the materials represented are very stiff and they have much higher final strength than most geo-materials.

Table 11.1 Values of material parameters

	Hard material		Geo-material					Soft material	
Case	1	2	3	4	5	6	7	8	9
M_f	2.8	2.5	1.2	1.2	1.2	1.2	1.2	1	1
$\varepsilon_{d,i}$	0.0005	0.005	0.025	0.025	0.025	0.04	0.05	0.3	0.8
$\varepsilon_{d,i}/\varepsilon_{d,u}$	0.1	0.8	3.5	2	1	0.3	0.1	0.5	0.5

As can be seen from the mathematical format of equation (11.6), the following general features of the curves are observed.

(1) The absolute magnitude of the shear stress is controlled by the value of the final strength M_f, meanwhile the absolute magnitude of the distortional strain is controlled by the value of the characteristic strain $\varepsilon_{d,i}$. Consequently, the shearing behaviour of a frictional material can be normalized. The final strength M_f is the quantity for normalizing the shear stress ratio and characteristic strain $\varepsilon_{d,i}$ for the distortional strain.

(2) The shape and curvature of the stress ratio and distortional strain relationship is controlled by the ratio of $\varepsilon_{d,i}$ over $\varepsilon_{d,u}$. The distortional behaviour of a material is "dry behaviour" if $\varepsilon_{d,i}/\varepsilon_{d,u} > 1$, and the behaviour is "wet behaviour" if $\varepsilon_{d,i}/\varepsilon_{d,u} < 0.5$. For $0.5 \le \varepsilon_{d,i}/\varepsilon_{d,u} \le 1$, the behaviour of a material falls into the transitional range, and there is a small peak strength at a large strain.

It is seen from the simulation that the proposed simple equation has the power to represent a wide range of behaviour of engineering materials. For the convenience of discussion, three categories of materials are considered: hard materials, geo-materials, and soft materials, depending on the value of characteristic strain $\varepsilon_{d,i}$.

The geo-materials considered have two typical patterns of behaviour, *viz.* the "wet distortional behaviour" and the "dry distortional behaviour". It is also observed that the "wet distortional behaviour" simulated can exhibit a wide range of different stiffness.

The so-called "hard" material has a basically linear shear stress-strain relationship prior to the peak, and reaches the peak strength at very small strain. If $\varepsilon_{d,i}/\varepsilon_{d,u} \leq 0.2$, there is virtually no softening, and the material behaves as would a perfectly plastic material after the strength is reached. If $\alpha > 0.75$, softening is clearly observed. Among the three types of materials, *i.e.*, "hard" materials and geo-materials and "soft" materials, the "hard" materials have the lowest value of $\varepsilon_{d,i}$.

If $\varepsilon_{d,i} \rightarrow 0$ the shear stress-strain equation (11.6) is simplified as

$$\eta = M_f \qquad \text{.....(11.22)}$$

In this case, the material is extremely hard and behaves in the same manner as the classical rigid perfectly plastic material which obeys the Mohr-Coulomb failure criterion (Carter and Balaam, 1995).

The so-called "soft" materials have the highest values of $\varepsilon_{d,i}$ among the three types of materials. The relationship between the shear stress ratio and the shear strain is basically linear when the value of the characteristic strain is very large.

11.3.4 Features of the Volumetric Strain and Distortional Strain Curve

In order to demonstrate characteristics of the proposed volumetric deformation equation (11.16), eight cases of simulation have been made. The values of the material parameters used are listed in Table 11.2. Non-uniformity of stress and strain state is not considered in this calculation, therefore, β is assigned to be zero. The variation of volumetric strain ε_v with distortional strain ε_d is indicated in Fig. 11.4.

Table 11.2 Values of material parameters

Case	1	2	3	4	5	6	7	8
M^v	0	1.5	1	1	1	1	-1	-1
$\varepsilon^v_{d,i}$	--	0.25	0.2	0.03	0.03	0.03	0.15	0.05
$\frac{\varepsilon^v_{d,i}}{\varepsilon^v_{d,u}}$	--	0.3	0.5	1	2	6	0.5	3

The following features of the volumetric deformation are seen from Fig. 11.4.

(1) As is the situation for curve 1, no volumetric strain will be produced by shearing if $M^v = 0$. This situation is commonly found in metal plasticity (*e.g.* Calladine, 1985).

(2) If $\varepsilon^v_{d,i}/\varepsilon^v_{d,u} < 0.5$, the material exhibits essentially monotonic volumetric compression during shearing. If $\varepsilon^v_{d,i}/\varepsilon^v_{d,u} > 1$, the material exhibits volumetric compression in the low stress ratio range, and exhibits volumetric expansion in the high stress ratio range. As the value of $\varepsilon^v_{d,i}/\varepsilon^v_{d,u}$ increases, the expansive volumetric deformation becomes the dominant feature of the volumetric deformation. For $0.5 \le \varepsilon^v_{d,i}/\varepsilon^v_{d,u} \le 1$, the behaviour of the material falls into the transition behaviour between the two types of typical behaviour.

(3) The situations with negative value of M^v are also modelled. The feature of the volumetric deformation is exactly opposite to that with the same value of M^v but positive and the same values of $\varepsilon^v_{d,i}$ and $\varepsilon^v_{d,i}/\varepsilon^v_{d,u}$. The possibility of material deformation with negative M^v will be examined in section 11.5.

11.3.5 Effect of β on Shearing Deformation Curves

The proposed constitutive equations (11.6) and (11.16) describe, through the parameter β, the effect of non-uniformity of stress and strain states on the softening behaviour of a frictional material. Five cases of calculation are made to give a quantitative illustration of the effect of β. The values of the material parameters are listed in Table 11.3, and β is the only variable among the six cases. In the calculation, it is assumed that $M^v = M_f$, $\varepsilon^v_{d,i} = \varepsilon_{d,i}$, and $\varepsilon^v_{d,u} = \varepsilon_{d,u}$. The effect of non-uniformity of stress and strain states on the softening behaviour simulated is indicated in Fig. 11.5a and 11.5b.

Table 11.3 Values of material parameters

Case	1	2	3	4	5
M_f	1	1	1	1	1
$\varepsilon_{d,i}$	0.03	0.03	0.03	0.03	0.03
$\varepsilon_{d,i}/\varepsilon_{d,u}$	3	3	3	3	3
β	0	0.3	1	3	6

The proposed constitutive equation (11.6) predicts the following features of the distortional behaviour of a frictional material under non-uniformity in stress and states in a specimen (Fig. 11.5a).

(1) The value of β is zero for a specimen with uniform distribution in stress and strain, and under this situation both η and $d\eta/d\varepsilon_d$ with respect to ε_d are continuous. If the stress and strain distribution within a specimen is no longer uniform, then $\beta \neq 0$. As a result, η with respect to ε_d maintains continuous; however, $d\eta/d\varepsilon_d$ with respect to ε_d is discontinuous at the point where non-uniformity in stress and strain is supposed to occur (such as the occurrence of bulge, rapture and fracture). In the current simulation, the uniform distribution in stress and strain is supposed to be maintained before the peak strength is reached; therefore, material deformation before peak strength is not affected by β.

(2) The higher the non-uniformity of the stress and strain distribution within the sample, the higher the value for β will be.

(3) Compared with the behaviour of an "ideal" uniform specimen, the stress ratio for a non-uniform specimen drops rapidly. The higher the value of β, the faster the strength is reduced. However, the final strength is not affected by the non-uniformity of the stress strain distribution within the sample.

The proposed constitutive equation (11.10) predicts the following features of the volumetric deformation of a frictional material under the influence of non-uniformity in stress and strain states (Fig. 11.5b).

(1) The final volumetric strain is dependent on the value of β. The higher the non-uniformity

of the stress and strain distribution within the sample, the higher the value for β is, and the lower the final expansive volumetric strain is.

(2) The volumetric strain and distortional strain curve for a non-uniform sample and that for an "ideal" uniform sample intersect at two points, namely point *A* and *B* (Fig. 11.5b). Therefore, this means that the volumetric strain for the non-uniform sample is initially higher than that of the "ideal" uniform sample, but is reduced less than that of the uniform sample finally.

The features of the distortional strain and stress ratio relationship predicted have been widely confirmed in laboratory tests on both soils and rocks (*e.g.*, Crouch, 1970; Read and Hegemier, 1984; Tatsuoka *et al*, 1993; Adachi and Oka, 1993; Burland *et al*, 1996; Kaiser and Tang, 1998). As far as the volumetric deformation is concerned, the features described in point (1) are observed directly in laboratory tests on both soils and rocks. An examination of experimental data suggest the features in point (2) is consistent with the experimental observation. Some of the experimental data can be found from work such as by Crouch (1970), Dendani *et al* (1988), Adachi and Oka (1993), and Burland *et al* (1996). It appears that the proposed modification to allow for the influence of the non-uniform distribution in stress and strain state within a specimen is reasonable.

There are various factors which result in non-uniformity of stress and strain in a specimen such as specimen geometry, material deficiency, bulge and fracture. The qualitative demonstration on effect of parameter β is made here; however, quantitative validation of the proposed constitutive equations on the simulation of the non-uniform behaviour is not presented herein.

11.4 Validation of the Proposed Equations

In this section, the proposed constitutive equations are employed to make simulations of the behaviour of a wide selection of frictional materials with the focus being on geo-materials. The experimental data are obtained from previous publications. The values of material parameters are determined according to their definitions introduced in Section 11.3.1. Then the theoretical stress and strain curves are computed via equation (11.6) and equation (11.16). The simulation of the effect of non-uniformity in stress and strain on material deformation is not verified herein, therefore for all the simulations $\beta = 0$ is assumed. The proposed

equations are employed to simulate the stress-strain behaviour for twenty-one different types of materials over one hundred and nine tests. All the tests were drained tests performed by means of a conventional triaxial apparatus. Only the simulation of seventy-two tests is described in detail, and the comparison between the simulation and experimental data are presented in figures in this chapter. A summary of these seventy-two tests is given in Table 11.4. However, the values of material parameters identified for all these one hundred and nine tests are presented in the parametric study in the next section. The references for the information of the experimental data of the seventy-two tests are given in this section when each group of tests are studied, and the references for the rest of tests are given in the next section.

The twenty-one types of frictional materials are reconstituted soft and stiff clays, sands, silts, clay-sand mixtures, compacted materials, filter material, volcanic soils, decomposed granite soils, gravel, rock masses, rocks, natural clays, aged sand, natural and reconstituted calcareous soils, cemented soils, partially saturated soils, reinforced geo-materials, wheat, sugar, rape, and type chips. The experimental data from one set of tests may be used to verify the applicability of the model for several types of materials. For example, the experimental data on unsaturated compacted silt may be used to verify the suitability of a model for silt, for compacted silt, and for unsaturated silt. This chapter focuses on the numerical simulation of the behaviour of frictional materials under monotonic shearing.

11.4.1 Simulating the Behaviour of Sands

Two sets of the simulations are presented here. The first group of test data is quoted from Tatsuoka (1972). There are three tests on Fuji sand. The voids ratios of the sand samples, being the only variable in the tests, vary from 0.52 to 0.85. The maximum and minimum voids ratio for Fuji sand are 1.08 and 0.53 respectively. The values of soil parameters used to generate the theoretical curves are listed in Table 11.5. The simulations and experimental data are shown in Fig. 11.6a for the relationship between the distortional strain and shear stress ratio, and in Fig. 11.6b for the relationship between the distortional strain and the volumetric strain. The second group of test data includes five tests on a dense Cambria sand quoted from Yamanuro *et al* (1996). They were high stress tests. The confining stress of the test samples, being the only variable in the tests, varies from 2.1 MPa to 11.5 MPa. The values of soil parameters identified are listed in Table 11.5. The simulations and experimental data are shown in Fig. 11.7.

Comparing the behaviour of the two sands between the simulations and the experimental data, it is seen that the simulations from the proposed constitutive equations are satisfactory over the large range of voids ratio and stress level considered.

11.4.2 Simulating the Behaviour of Clays

The simulation of four groups of clays is presented. The first set of tests includes two tests on Ancona clay (Canestrari and Scarpelli, 1993). One of the samples is reconstituted, and the other is natural intact clay. The confining pressuring for the two tests is the same with σ'_3 =196.2 kPa. Some difference in the clay mineralogy was observed between the intact soil and the reconstituted soil and the water content for the intact clay was slightly higher than that of the reconstituted clay; however, the difference in soil behaviour is principally caused by soil structure (Canestrari and Scarpelli, 1993). The second set of tests includes six tests on Corinth marl clay (Burland *et al*, 1996). Three of the samples are reconstituted, and the other three are natural stiff clay. The three samples of reconstituted clay were swelled isotropically from p'=700 kPa to p'=98 kPa, p'=294 kPa, and p'=500 kPa respectively. Then the samples were loaded axially to failure. The intact samples were obtained from a large block sample. The three intact samples were consolidated isotropically to p'=98 kPa, p'=294 kPa, and p'=500 kPa respectively, and then the samples were loaded axially to failure. There are two tests on natural Weald clay in the third set of tests (Henkel, 1956). Sample A is normally consolidated, and sample B is very heavily overconsolidated with OCR = 24. The fourth set of tests includes two tests on intact stiff Nanticoke clay (Lo, 1972). The two samples were consolidated isotropically to a stress state with σ'_3 = 552 kPa and σ'_3 = 345 kPa respectively. After that, the samples were loaded axially to failure.

The values of soil parameters identified for all the four types of clays are listed in Table 11.6. A comparison between the model simulations and experimental data are shown in Fig. 11.8 for Ancona clay, in Fig 11.9 for reconstituted Corinth marl, in Fig. 11.10 for natural intact Corinth marl, in Fig. 11.11 for natural Weal clays, and in Fig. 11.12 for natural Nanticoke clay. It is seen that a very good agreement is achieved between the experimental data and the theoretical simulations for all the four types of clay. The proposed model has successfully described the behaviour of both natural and reconstituted clays with different overconsolidation ratios and confining pressures.

11.4.3 Simulating the Behaviour of Clay-Sand Mixtures

This group of simulations includes drained triaxial tests on Kaolinite-silt mixtures. The tests have been described by Marachi *et al* (1969), and they include two different confining pressures. Test A has 10% Kaolinite with $\sigma'_3 = 1.275$ MPa, and Test B has 50% Kaolinite with $\sigma'_3 = 550$ kPa. The values of model parameters used to fit the data are listed in Table 11.7. Because the clay percentages for the two samples are not the same, they are considered as two different materials and therefore require two unique sets of model parameters.

The results are shown in Fig. 11.13, where it can be seen that the simulation of the distortional strain behaviour is almost perfect, and the predicted volumetric strains also satisfactorily match those measured.

11.4.4 Simulating the Behaviour of Filter Materials

This set of tests is quoted from Dendani *et al*, 1988. Two triaxial compression tests on Grand-Maison filter material are included. The confining pressures for the two tests are 400 kPa and 800 kPa respectively. The values of material parameters identified for Grand-Maison filter material are listed in Table 11.7. The simulations and the test data are shown together in Fig. 11.14. It is found that the theoretical equations represent the behaviour of the compacted fill material quite accurately.

11.4.5 Simulating the Behaviour of a Decomposed Granite Soils

The set of simulation includes two triaxial compression tests on a decomposed granite soil performed by Lee and Coop (1995). Sample A was air-dried for one week, and sample B was fully saturated. The confining pressure for both tests was 100 kPa and with the same voids ratio. The structures of the two samples thus prepared are very different. The values of material parameters adopted for the simulation are listed in Table 11.7. The simulations and the test data are shown together in Fig. 11.15. It is seen that a reasonably good agreement is achieved between the theoretical simulations and the experimental data for the behaviour of the decomposed granite soil.

11.4.6 Simulating the Behaviour of Aged Sand

It has long been recognized that sand improves its mechanical properties considerably through aging by both practical engineers and theoreticians (Schmertmann, 1991). The

proposed constitutive equations are used to model the behaviour of Ham river sand with different aging periods. There are four tests performed by Daramola (1980) with the aging periods being 0, 10 days, 30 days, and 152 days. The values of material parameters used to generate the theoretical curves are also listed in Table 11.5 so that all the values of sand parameters are summarized into one table. A comparison between the simulations and the test data is shown in Fig. 11.16. It is seen that a satisfactorily agreement is achieved between the theoretical simulations and the experimental data for the behaviour of Ham river sand with different aging histories.

11.4.7 Simulating the Behaviour of Cemented Volcanic Soil

A set of conventional triaxial tests on naturally moderately cemented volcanic soil performed by O'Rourke *et al* (1988) is quoted for simulation. There are four tests with different confining pressures. They are $\sigma'_3 = 60$ kPa, $\sigma'_3 = 120$ kPa, $\sigma'_3 = 200$ kPa, and $\sigma'_3 = 300$ kPa. The values of material parameters used to generate the theoretical curves are also listed in Table 11.7. A comparison between the simulations and the test data is shown together in Fig. 11.17. It is seen that the behaviour of cemented volcanic soil under different confining pressures has been simulated quite accurately by the proposed constitutive equations.

11.4.8 Simulating the Behaviour of Calcareous Soils

There are two sets of simulations for this section. The first set of experimental data is quoted from Huang (1993) where the influence of cementation on carbonate sand behaviour was studied. The sand was obtained from Australia's North West Shelf and has a calcium carbonate content of approximately 90% by dry weight. Gypsum plaster was used as the cementing agent. Cement percentage was measured as the weight of the cement over the total weight of the cemented soil. There are two group of tests considered with the cement contents being 0% and 20% respectively. There are four tests in each group. The variable for each group is the confining pressures. They are $\sigma'_3 = 100$ kPa, $\sigma'_3 = 300$ kPa, $\sigma'_3 = 600$ kPa, and $\sigma'_3 = 1200$ kPa.

The values of material parameters used to generate the theoretical curves are listed in Table 11.8. A comparison between the simulations and the test data is shown together in Fig. 11.18. It is seen that a satisfactory agreement is achieved between the theoretical simulations

and the experimental data for the behaviour of the artificially cemented soil despite the great difference in the cement amounts and the confining pressures.

The second set of tests includes two tests on undisturbed Bass strait carbonate sand from Poulos *et al* (1982). The soil is grey sand with some silt. The carbonate content for the sand is 88%. The sand is not significantly cemented. There are two tests with the confining pressures being 138 kPa and 897 kPa respectively. The values of material parameters identified are listed in Table 11.8. The simulations and the test data are shown together in Fig. 11.19. Comparing the simulations and the experimental data, it is seen that the proposed constitutive equations describe the behaviour of the intact natural carbonate sand very satisfactorily.

11.4.9 Rock Mass and Rock

There are two sets of simulation on the behaviour of granular rocks. The first set of experimental data include the results of three triaxial tests on large rock mass samples under high stress (Michelis, 1981). The confining pressures are $\sigma'_3 = 13.8$ MPa, $\sigma'_3 = 71.7$ MPa, and $\sigma'_3 = 193$ MPa. The second set of experimental data includes the results of two tests on uncompacted ballast via a large triaxial cell (Alva-Hurtado *et al*, 1981). The confining pressures for the two tests are $\sigma'_3 = 34.5$ kPa and $\sigma'_3 = 138$ kPa. The values of the model parameters for both the granular rock and the uncompacted ballast are listed in Table 11.9. The predicted behaviour for the granular rock is shown in Fig. 11.20, and in Fig. 11.21 for the uncompacted ballast. It is observed that the proposed model successfully represents the behaviour of granular rocks.

Three tests on Oolitic limestone from Elliott (1983) are quoted for simulation. They are high stress level tests on the limestone. The confining pressures for the three samples are 2 MPa, 5 MPa, and 10 MPa respectively. The values of rock parameters identified are listed in Table 11.9 and the corresponding simulations are shown in Fig. 11.22. It can be seen that the equations predict the behaviour of the limestone very well.

11.4.10 Simulating the Behaviour of Partially Saturated Soils

The experimental data on unsaturated compacted silt performed by Cui *et al* (1996) is considered. There are four tests at constant confining pressure with $\sigma'_3 = 400$ kPa but with different suctions. The magnitudes of the suctions for the four tests are 200 kPa, 400 kPa,

800 kPa, and 1500 kPa. The values of soil parameters used to generate the theoretical curves are listed in Table 11.10. The simulations and the test data are shown together in Fig. 11.23. It is seen that the theoretical equations represent the behaviour of the unsaturated compacted fill material with different suctions quite accurately.

11.4.11 Simulating the Behaviour of Reinforced Soils

Two sets of tests on reinforced soils are quoted for simulation. The first set of tests includes four triaxial tests on sand reinforced with steel fibers performed by Michalowski (1996). Four of the tests are presented. They are two tests with $\sigma'_3 = 100$ kPa, one being reinforced and the other being plain; and the other two tests are with $\sigma'_3 = 600$ kPa, one being reinforced and the other being plain. The second set of tests considered are triaxial compression tests on large scale specimens of gravel reinforced with geosynthetics performed by Cazzuffi *et al* (1994). There are four tests with different confining pressures. The confining pressures are $\sigma'_3 = 50$ kPa, $\sigma'_3 = 100$ kPa, $\sigma'_3 = 200$ kPa, and $\sigma'_3 = 400$ kPa.

The values of model parameters used to generate the theoretical curves are listed in Table 11.11 for both the reinforced sand and the reinforced gravel. The comparison between the theoretical curves and the experimental data is shown in Fig. 11.24 for the reinforced sand and in Fig. 11.25 for the reinforced gravel. A reasonably good agreement is achieved between the model simulations and the experimental data.

11.4.12 Simulating the Behaviour of Some Other Materials

The proposed constitutive equations are also employed to simulate the behaviour of some other frictional materials under conventional triaxial compression tests. They are wheat, sugar, rape, and tire chips. The first set of tests includes two tests on wheat (Kolymbas *et al*, 1990). Two different confining pressures are applied to two identical samples, and they are $\sigma'_3 = 100$ kPa and $\sigma'_3 = 400$ kPa. The second set of tests is three tests on sugar with different confining pressures (Kolymbas *et al*, 1990). The confining pressures are $\sigma'_3 = 50$ kPa, $\sigma'_3 = 200$ kPa, and $\sigma'_3 = 800$ kPa. The third set of tests includes three tests on rape with different confining pressures (Kolmbas *et al*, 1990). The confining pressures are $\sigma'_3 = 100$ kPa, $\sigma'_3 = 200$ kPa, and $\sigma'_3 = 400$ kPa. The fourth set of tests includes three tests on tire chips (Wu *et al*, 1997). The confining pressures for the three tests are 350 kPa, 450 kPa, and 550 kPa respectively.

The values of material parameters identified for wheat, sugar, rape, and tire chips are listed in Table 11.12. A comparison between the theoretical simulations and the experimental data are shown in Fig. 11.26 for wheat, in Fig. 11.27 for sugar, in Fig. 11.28 for rape, and in Fig. 11.29 for tire chips. Based on the comparison between the model simulation and the experimental data, it can be concluded that the proposed constitutive equations can also describe successfully the behaviour of frictional materials such as wheat, sugar, rape, and tire chips, besides that of the geo-materials.

11.5 Statistical Analyses of Material Parameters

11.5.1 Background

Three new parameters are introduced for studying the parameters for distortional deformation and those for volumetric equation. They are phase angle for the distortional deformation ω, phase angle for the volumetric straining ω^v, and the phase difference θ. The definitions are given below.

$$\omega = \tan^{-1}\left(\frac{\varepsilon_{d,i}}{\varepsilon_{d,u}}\right) \qquad \text{.....(11.23)}$$

$$\omega^v = \tan^{-1}\left(\frac{\varepsilon^v_{d,i}}{\varepsilon^v_{d,u}}\right) \qquad \text{..... (11.24)}$$

$$\theta = \omega^v - \omega \qquad \text{.....(11.25)}$$

Obviously, the proposed constitutive equations (11.6) and (11.16) can be expressed in terms of M_f, $\varepsilon_{d,i}$, ω, M^v, $\varepsilon^v_{d,i}$, θ, and β.

A study of the model parameters is made based on the simulation of one hundred and nine tests on twenty-one different types of frictional materials. Some basic information on seventy-two tests has been introduced in section 11.4. The values of materials parameters identified for the rest thirty-seven tests are listed in Table 11.13, The detailed information for these tests can be found from the relevant references which are also given in Table 11.13.

11.5.2 Some Statistical Information on Material Parameters

The final strength parameter M_f

The value of the final strength parameter M_f is found to vary from 0.5 to 2.75 for all the materials considered. However, for most of the materials, the final strength parameter varies between 0.5 and 2. The three materials with the highest strength are found to be Dogs Bay carbonate sand with $M_f = 2.72$, a rock with $M_f = 2.1$, and a rock mass with $M_f = 2$. The values of mean and standard deviation for M_f are about 1.5 and 0.4 respectively. The corresponding friction angle is 35.7°. The final strength for structured clays, measured from laboratory tests with the distortional strain being around 10%, can be significantly higher than that of the corresponding reconstituted type. The structures of clays are those formed naturally in situ or formed artificially by consolidation and cementation. It is highly likely that the actually final strength for clays of a given mineralogy with different structures is the same when the clay has reached the critical state of deformation at very large distortional deformation. However, the structures of clays affect significantly the behaviour of soil both before and after peak strength, and reliable description of soil strength with strain less than 10% is perhaps more important for practical engineering problems than the ideally final strength at the critical state where the structure of the soil is supposed to be removed completely.

Characteristic distortional strain $\varepsilon_{d,i}$

The value of characteristic distortional strain $\varepsilon_{d,i}$ varies from 0.004 to 0.12 for all the tests considered. The average value of $\varepsilon_{d,i}$ is 0.026 with standard deviation 0.02. It appears that the values of $\varepsilon_{d,i}$ is fairly narrowly distributed for geotechnical materials. The values of $\varepsilon_{d,i}$ falls into the range from 0.004 to 0.07 for 107 tests out of the total 109 tests. It is also observed that $\varepsilon_{d,i}$ is essentially a constant for soil of a given mineralogy under "dry distortional behaviour"; but its value clearly changes for a given soil with "wet distortional behaviour" especially for structured soft soils, (see values of material parameters listed from Table 11.5 to Table 11.13). It is thus indicated that the value of $\varepsilon_{d,i}$ is independent of the initial stress and strain states and testing stress path if $\varepsilon_{d,i}/\varepsilon_{d,u} \geq 1$, *i.e.*, $\omega \geq 45°$. Therefore, the assumption on the existence of the characteristic point *I* is valid for a frictional material only for "dry distortional behaviour". For wet distortional behaviour, $\varepsilon_{d,i}$ increases as the material becomes "soft" due to factors such as the increase of confining pressure or the variation of soil structure.

Parameter $\varepsilon_{d,u}$

The value of the range of $\varepsilon_{d,u}$ is found to vary from 0.003 to 0.4 for all the tests considered. Compared with $\varepsilon_{d,i}$, the range for $\varepsilon_{d,u}$ value is much greater. The average value and the standard deviation for $\varepsilon_{d,u}$ are about 0.094 and 0.093. It is clearly shown that $\varepsilon_{d,u}$ is dependent on the structure of the material, the stress history, and the initial voids ratio and the initial stress state. It is also observed that $\varepsilon_{d,u}$ appears to vary relatively little for various "wet distortional behaviour" for a given soil. Consequently, $\varepsilon_{d,i}$ may be assumed approximately as a constant if $\varepsilon_{d,i}/\varepsilon_{d,u} < 0.5$, *i.e.*, $\omega < 45°$. However, its value changes with "dry distortional behaviour". For a given material, the value of $\varepsilon_{d,u}$ increases as the material becomes stiffer to shearing.

Parameter M^v

The value of M^v, which is numerically equal to the rate of the volumetric strain increment over the distortional strain increment at $\eta = 0$, varies between –0.83 to 2.73. The average value and corresponding standard deviation for M^v, after the five cases with negative M^v being exempted, are about 0.95 and 0.6. Comparing the average value for M_f, *i.e.*, $M_f = 1.45$, it is seen that M^v is generally less than M_f.

The value of M^v is negative for five tests. They are three tests on tire chips, one test on reconstituted Corinth marl clay and one test on natural Nanticoke clay. Negative M^v indicates volumetric expansion during initial shearing at low stress ratio range. The expansive volumetric deformation for tire chips during shearing is expected for this material. Both the reconstituted Corinth marl clay and the Nanticoke clay are heavily "overconsolidated" and respond very stiffly to shearing. As far as the simulation of these test results is concerned, a negative value for M^v is appropriate. The actual behaviour of naturally structured stiff clay can be very complicated. There is a possibility that some natural clay may have an insignificant small compression range at the initial shearing and after that the volumetric deformation becomes expansive. However, compression may still occur at the final stage when the soil structure collapses. If the initial small compression behaviour is ignored, the response for this type of material to shearing would be expansive at low stress ratio ranges but would turn into compressive behaviour at high stress ratios. This type of behaviour is exactly opposite to the widely observed "dry volumetric behaviour".

Examining all the experimental data for over one hundred tests plotted in the $\varepsilon_d \sim \varepsilon_v$ plane, it is clearly demonstrated that the value of $\varepsilon_v/\varepsilon_d$ is not zero at $\eta = 0$ for all the tests considered. For soils, both reconstituted soils and structured soils are included. It is thus concluded that the deficiency which is found in the many widely used flow rules, including this proposed one, is not a serious problem for describing the shearing behaviour of a frictional material.

Parameter $\varepsilon^v_{d,i}$

The value of $\varepsilon^v_{d,i}$ varies from 0.004 to 0.5. The values of mean and standard deviation for $\varepsilon^v_{d,i}$ are 0.07 and 0.085. It is observed that $\varepsilon^v_{d,i}$ is very sensitive to the compressibility of the material, and therefore is dependent on the stress level of the test and the voids ratio of the material. For example, $\varepsilon^v_{d,i}$ for rock is much smaller than that for the compressible soils.

Parameter $\varepsilon^v_{d,u}$

The value of $\varepsilon^v_{d,u}$ varies from 0.002 to 0.5. The values of mean and standard deviation for $\varepsilon^v_{d,u}$ are 0.1 and 0.12 respectively. The value of $\varepsilon^v_{d,u}$ is dependent on the stress level and voids ratio as well as the structure of the material. The range of the value for the three parameter $\varepsilon_{d,u}$, $\varepsilon^v_{d,i}$ and $\varepsilon^v_{d,i}$ is roughly the same, from 0.002 to 0.5.

11.5.3 Correlation Between the Distortional Deformation Parameters and the Volumetric Deformation Parameters

It has been shown in Section 11.2.4 that the proposed flow rule has a mathematical form similar to that proposed in the original Cam clay model; however constraints on the volumetric deformation parameters imposed in the Cam clay model have been removed. The applicability of the constraints imposed by the Cam clay model is examined here.

M_f *and* M^v

The correlation between parameter M_f and M^v is shown in Fig. 11.30, with the data for five tests with negative M^v excluded. It is clearly demonstrated that for far the majority of tests, $M_f > M^v$, that is, the dilatancy rate at $\eta = 0$ is less than the final strength parameter of the soil.

The average value for a linear correlation of the two parameters is found as follows

$$M_f^v = \frac{2}{3} M_f \qquad \text{..... (11.26)}$$

$\varepsilon_{d,i}$ and $\varepsilon^v_{d,i}$

The correlation between parameters $\varepsilon_{d,i}$ and $\varepsilon^v_{d,i}$ is shown in Fig. 11.31. It is seen that for almost all the tests considered $\varepsilon^v_{d,i} \geq \varepsilon_{d,i}$. The average value for a linear correlation of the two parameters is found as follows

$$\varepsilon^v_{d,i} = 3\varepsilon_{d,i} \qquad \text{.....(11.27)}$$

$\varepsilon_{d,u}$ and $\varepsilon^v_{d,u}$

The correlation between parameters $\varepsilon_{d,u}$ and $\varepsilon^v_{d,u}$ is shown in Fig. 11.32. Unlike the correlation between parameters M_f and M^v or between parameters $\varepsilon_{d,i}$ and $\varepsilon^v_{d,i}$, there is no obvious correlation between $\varepsilon_{d,u}$ and $\varepsilon^v_{d,u}$. The average value for a linear correlation of the two parameters is found as follows

$$\varepsilon^v_{d,u} = \varepsilon_{d,u} \qquad \text{.....(11.28)}$$

Based on the statistical analysis of the correlation between the parameters for distortional deformation and those for volumetric deformation, the following two conclusions can be made:

(1) It is seen that the constraints on the volumetric deformation imposed by the flow rule proposed for the original Cam clay model expressed by equation (11.14) are artificially imposed. Indeed constraint $\varepsilon^v_{d,i} = \varepsilon_{d,i}$ is bound to underestimate the value of $\varepsilon^v_{d,i}$ greatly, and constraint $M_f = M^v$ frequently overestimates the value of M^v. Thus the flow rule with the constraints of equation (11.14) has a systematic error. Contrary to a random error, a systematic error is an inherent error. It also seems appropriate to study the volumetric deformation independently and then to examine the relationship between the parameters for the distortional deformation and those for the volumetric deformation.

(2) Since systematic errors are found in the flow rule in the original Cam clay model, a simple correction of the Cam clay flow rule can be made. Considering statistical results expressed by equations (11.26) and (11.27) and (11.28), the following modified flow rule

is proposed:

$$\frac{d\varepsilon_v}{d\varepsilon_d} = \frac{2M_f}{3}\left(1-\frac{\varepsilon_d}{\varepsilon_{d,u}}\right)e^{\frac{\varepsilon_d}{3\varepsilon_{d,i}}} \qquad \text{.....(11.29)}$$

If equation (11.29) is employed to model the volumetric deformation of frictional materials, the total number of equation parameters will be reduced to four.

11.5.4 Four Typical Patterns of Shearing Behaviour

As was stated in section 11.2.2, there are two types of distortional behaviour and two types of volumetric behaviour. Combining the two types of behaviour for distortional strain and volumetric strain, a total of four typical patterns of shearing behaviour for frictional materials will be obtained (listed in Table 11.14). A graphical sketch of the four patterns is shown in Fig. 11.33. All the features are defined in the strain and shear stress ratio η space, not the strain and shear stress q space.

Table 11.14 Patterns of shearing behaviour

Shearing Types	Distortional behaviour	Volumetric behaviour	Conditions
D-D	Dry	Dry	$\varepsilon_{d,i}/\varepsilon_{d,u} > 1$ and $\varepsilon_{d,i}{}^{v}/\varepsilon_{d,u}{}^{v} > 1$
D-W	Dry	Wet	$\varepsilon_{d,i}/\varepsilon_{d,u} > 1$ and $\varepsilon_{d,i}{}^{v}/\varepsilon_{d,u}{}^{v} \le 0.5$
W-D	Wet	Dry	$\varepsilon_{d,i}/\varepsilon_{d,u} \le 0.5$ and $\varepsilon_{d,i}{}^{v}/\varepsilon_{d,u}{}^{v} > 1$
W-W	Wet	Wet	$\varepsilon_{d,i}/\varepsilon_{d,u} \le 0.5$ and $\varepsilon_{d,i}{}^{v}/\varepsilon_{d,u}{}^{v} \le 0.5$

When the values of $\varepsilon_{d,i}/\varepsilon_{d,u}$ and $\varepsilon_{d,i}{}^{v}/\varepsilon_{d,u}{}^{v}$ fall into the range between 0.5 to 1, the behaviour described is in the transition between "dry behaviour" and "wet behaviour". It may be difficult to define absolutely which type of behaviour the soil exhibits. As defined in equations (11.23) and (11.24), the corresponding ω is 26° for $\varepsilon_{d,i}/\varepsilon_{d,u} = 0.5$ and is 45° for $\varepsilon_{d,i}/\varepsilon_{d,u} = 1$, and ω^{v} is 26° for $\varepsilon^{v}{}_{d,i}/\varepsilon^{v}{}_{d,u} = 0.5$ and 45° for $\varepsilon^{v}{}_{d,i}/\varepsilon^{v}{}_{d,u} = 1$. All these four typical patterns of shearing behaviour are encountered for engineering materials. It has also been observed that M^{v} may be negative for some soils. If this situation is considered, there should be eight patterns in total. Because negative M^{v} is not often encountered in geotechnical engineering practice, the other four patterns corresponding to negative M^{v} are not discussed here.

D-D behaviour and W-W behaviour

These two types of shearing are foremost and have been well recognized and modelled. In critical state soil mechanics, D-D is termed as "dry behaviour", and W-W behaviour is termed as "wet behaviour" (Schofield and Wroth, 1968). For materials the behaviour of which can be described by D-D and W-W patterns, the behaviour of the materials generally transfers from the D-D behaviour to that of the W-W behaviour with an increase in voids ratio or in the stress level. It has also been reported that the pattern of material behaviour may be identified by a single parameter (Wroth and Basset, 1965). Been and Jefferies (1985) defined it as the state parameter and carried out an extensive study of its influence on soil behaviour. The state parameter is defined as the voids ratio difference between the current stress state and the state at the critical state line with the same value of mean effective stress. For materials which exhibit three or more types of behaviour, it seems that the division of geo-material behaviour solely by the state parameter is not enough.

D-W behaviour

D-W behaviour occurs when the material resistance to shearing has a peak value and then softens to the final strength, but its volumetric strain increment is always non-expansive in the entire shearing process. The type of behaviour has been reported for some cemented soils and other structured soils (Lo, 1972; Lam and Tatsuoka, 1988; Huang, 1994)

W-D behaviour

W-D behaviour occurs when the material hardens steadily in the shear stress ratio and the distortional strain relationship, but its volumetric deformation is initially compressive and becomes expansive when the distortional strain is large enough. The type of behaviour has been widely reported, *e.g.*, soils (Dendani *et al*, 1988; Jefferies, 1993), carbonate sands (Poulos et al 1982, O'Rourke 1988), and granular rock (Michelis, 1981; Alva-Hurtado *et al* 1981).

11.5.5 Some Features of the Deformation of Frictional Materials

Two figures are presented which show the values of ω and M_f (Fig. 11.34) and the values of ω^v and M_f (Fig. 11.35) for all the individual tests considered. M_f is the final strength of a frictional material and may be considered as a material intrinsic property. Parameters ω and ω^v controls the pattern of the distortional behaviour and volumetric behaviour respectively. Statistically speaking, there is no correlation either between ω and M_f or between ω^v and M_f.

Therefore, the patterns of both the distortional behaviour and volumetric behaviour are independent of the final intrinsic strength of the material, or the mineralogy of a material. It is indicated that the pattern for the behaviour of a frictional material is essentially dependent on conditions such as the stress and strain state, the arrangement and bonding of the material constituents, or the structure of the material. This statistical result has been now accepted in geotechnical engineering as a basic fact.

The correlation between ω and ω^v is shown in Fig. 11.36. It is seen that ω^v is almost always greater than or equal to ω, *i.e.*, $\omega^v \geq \omega$ for by far the majority of tests. The correlation between θ and ω is shown in Fig. 11.37. It is seen that $\theta > 0$ for the majority of tests and the value of θ increases with a decrease in the value of ω. The upper boundary for the parameters is defined by the following relationship:

$$\theta = 90° - \omega$$

If $\theta = 0$, which is a constraint imposed by the flow rule for the original Cam Clay model, the pattern of the distortional behaviour is exact the same as that of the volumetric behaviour. Then, the material only has two types of behaviour, *i.e.*, D-D behaviour and W-W behaviour.

If $\theta > 0$, then $\omega^v > \omega$. D-W type of behaviour can not occur for this situation. The corresponding behaviour for dry distortional behaviour is always dry volumetric behaviour; and the corresponding behaviour for wet distortional behaviour can be wet or dry volumetric behaviour.

If $\theta < 0$, then $\omega^v < \omega$. W-D type of behaviour can not occur for this situation. The corresponding behaviour for wet distortional behaviour is always wet volumetric behaviour; and the corresponding behaviour for dry distortional behaviour can be dry or wet volumetric behaviour.

For the majority of the tests, $\theta > 0$, which indicats that most of the frictional materials are more likely to exhibit expansive volumetric deformation than that predicted by the flow rule in the original Cam Clay model.

The correlation between $\varepsilon_{d,u}$ and ω is shown in Fig. 11.38. A boundary for the data is drawn and shown by broken lines and two data points with high values of $\varepsilon_{d,u}$ are exempted. It is seen that statistically there exists a relationship between $\varepsilon_{d,u}$ and ω. The value of $\varepsilon_{d,u}$

decreases with an increase of parameter ω.

The correlation between $\varepsilon^{v}_{d,u}$ and ω^{v} is shown in Fig. 11.39. A boundary for the data is indicted by broken lines, and there also exists relationship between material parameter $\varepsilon^{v}_{d,u}$ and ω^{v}. Opposite to the tendency for the $\varepsilon_{d,u}$ and ω relationship, the value of $\varepsilon^{v}_{d,u}$ is likely to increase with an increase in ω^{v}.

11.6 Basic Material Parameters α and α^{v}

11.6.1 Definitions

In order to define the correlation between the parameters describing the distortional strain and those describing the volumetric strain, the following linear relations in term of correlation coefficients (K_M, K_i, K_u) are proposed,

$$K_M = \frac{M^{v}}{M_f} \quad \text{..... (11.30)}$$

$$K_i = \frac{\varepsilon^{v}_{d,i}}{\varepsilon_{d,i}} \quad \text{..... (11.31)}$$

$$K_u = \frac{\varepsilon^{v}_{d,u}}{\varepsilon_{d,u}} \quad \text{..... (11.32)}$$

ısed on the assumption as K_M=1, K_i=1, K_u=1, Xu *et al* (1997) first introduced a "basic ıterial parameter", α, the definition being as follows:

$$\alpha = \frac{\varepsilon_{d,i}}{\varepsilon_{d,u}} \quad \text{..... (11.33)}$$

Via the parameter α, they successfully described the D-D and W-W shearing behaviours of some geo-materials. However, as has been presented in Section 11.5, in general these parameters K_M, K_l and K_u are not equal for most shearing problems. The volumetric deformation may be independent of the distortional deformation. Thus α should be a distortional parameter, which is termed the "basic distortional material parameter". In parallel, the "basic volumetric material parameter", α^v, is defined below:

$$\alpha^v = \frac{\varepsilon^v{}_{d,i}}{\varepsilon^v{}_{d,u}} \qquad \text{..... (11.34)}$$

In this section 11.6, the non-uniformity factor is neglected (β=0), and in the comparisons described, the "test data" means from the documents listed in Table 11.4.

11.6.2 Basic Features of α and α^v

11.6.2.1 Distortional and Volumetric Procedures

It can been seen from Sections 11.3 and 11.4, for frictional material (especially goemeterials), the parameters α and α^v show degrees of "moisture" of distortional behaviour and volumetric behaviour respectively. That is, the higher the value of α, the drier the distortional behaviour presents, and the higher α^v, the drier in the volumetric behaviour.

In general, the value of α is larger than α^v, as shown in Fig. 11.40.

11.6.2.2 Peak Strength

Peak strength for frictional materials can be predicted from the basic distortional equation 11.6, as expressed in following equation (Xu *et al*, 1997):

When $\varepsilon_d = \varepsilon_{d,u} + \varepsilon_{d,i}$ (peak distortional strain),

$$\frac{\eta_p}{M_f} = 1 + \alpha e^{-\left(1+\frac{1}{\alpha}\right)} \quad \text{..... (11.35)}$$

An evaluation of the peak strength equation is shown in Fig.11.41, where a summary of test data is included. It may be seen from Fig. 11.41 that the theory predicts quite well the variation of peak strength with the parameter α.

11.6.2.3 Peak Volumetric Strain

Via the basic volumetric equation 11.16, when distortional strain reaches $\varepsilon^{v}_{d,u}$, the peak volume ($\varepsilon_{v,p}$) before the residual state is obtained from Equation 11.36:

When $\varepsilon_d = \varepsilon^{v}_{d,u}$,

$$\frac{\varepsilon_{v,p}}{\varepsilon^{v}_{d,i} M^{v}} = 1 - \alpha^{v} + \alpha^{v} e^{\frac{1}{\alpha^{v}}} \quad \text{..... (11.36)}$$

Fig. 11.42 shows that the predicted relationship is located near the average of the test data for a number of frictional materials.

11.6.2.4 Residual Volumetric Strain

The residual volumetric strain is found to be as follows:

When $\varepsilon_d \to \infty$,

$$\frac{\varepsilon_{v,r}}{\varepsilon^{v}_{d,i} M^{v}} = 1 - \alpha^{v} \quad \text{..... (11.37)}$$

As is well known, there are two states at residural volumetric state, *i.e.*, dilation or compression. From equation 11.37, a simple criterion of state of residual volumetric strain is given in Table 11.14.

Table 11.14 Criterion of residual volumetric strain

M^v	α^v	$\varepsilon_{v,r}$
>0	>1	Dilation
>0	<1	Compression
<0	<1	Dilation
<0	>1	Compression

Fig. 11.43 shows the comparisons of the theoretical curve and the test data for frictional materials. It is found that the patterns of $\varepsilon_{v,r}$ vs α^v are fairly similar, however, the theoretical curve tends to underestimate residual volumetric strain.

11.6.2.5 Initial Distortional Modulus

Xu *et al* (1997) described the relations of initial distortional modulus G_o with the basic distortional material parameter α, as given in Equation 11.38, where G_o is defined as a slope of the η~ε_d curve at ε_d=0.

$$\frac{G_o}{G_{s,u}} = 1 + \frac{1}{\alpha} \quad \text{..... (11.38)}$$

where $G_{s,u} = \dfrac{M_f}{\varepsilon_{d,i}}$ (secant distortional modulus at $\varepsilon_d = \varepsilon_{d,u}$)

A comparison between the theoretical relation and the experimental data is given by Xu *et al* (1997) and is shown in Fig. 11.44; the agreement is satisfactory.

11.6.3 Relation of Distortional Energy and the Parameter α

With different stress history the deformation energy of geo-materials will increase or decrease. Suppose the change moves the η~ε_d curves from 1 to 2 as shown in Fig. 11.45. The shadowed area between curve 1 and curve 2 is defined as incremental distortional energy in term of ΔU, *i.e.*,

$$\Delta U = \int_0^{\infty} (\eta_2 - \eta_1) d\varepsilon_d \quad \text{..... (11.39)}$$

Based on the concept of characteristic points (Fig. 11.2), $\varepsilon_{d,i}$ is approximately assumed to be a constant, *i.e*, independent of stress history. Then, the explicit expression of incremental distortional energy can be given from Equations 11.39 and 11.6 as follows:

$$\Delta U = \mathrm{M}_f \varepsilon_{d,i} \left(\frac{\varepsilon_{d,i}}{\varepsilon_{d,u,2}} - \frac{\varepsilon_{d,i}}{\varepsilon_{d,u,1}} \right) = \mathrm{M}_f \varepsilon_{d,i} (\alpha_2 - \alpha_1) = \mathrm{M}_f \varepsilon_{d,i} \Delta\alpha \quad \text{.....(11.40)}$$

If $\Delta \to 0$, a compact energy differential distortional equation for friction materials is set up:

$$\frac{dU}{d\alpha} = \mathrm{M}_f \varepsilon_{d,i} \quad \text{..... (11.41)}$$

Because the product of M_f and $\varepsilon_{d,i}$ is a value of "distortional energy" as well, an incremental density of distortional energy is defined as follows:

$$dD = \frac{dU}{\mathrm{M}_f \varepsilon_{d,i}} \quad \text{..... (11.42)}$$

Thus the equation 11.41 can be presented in a more compact form as follows:

$$dD = d\alpha \quad \text{..... (11.43)}$$

The incremental basic distortional material parameter α is equal to the incremental density of distortional energy. Some shearing phenomena can be interpreted by above the equation. In most cases, from loose sand to dense sand, for example, the "moisture" of shearing behaviour will be from "wet" to "dry", *i.e.* parameters α or α^{v} are increased. This is because the density of distortional energy is increased.

11.6.4 Significance of the Basic Material Parameters, α and α^{v}, in Soil Mechanics

In soil mechanics, there are many material parameters, but most of them are state parameters rather than "procedure" parameters (for example, initial shear modulus for initial state, critical state stress ratio for critical state). In this section, we have discussed the normalized shearing behaviour, and the particular behaviours at initial state (initial modulus), "middle" state (peak strength and peak volumetric strain) and final state (residual volumetric strain). It is found that all these behaviours can be described by basic material parameters α or α^{v}, so that, these basic material parameters α, α^{v} can be taken as two procedure parameters in the shearing behaviour of frictional materials, *i.e.*, α can describe the distortional procedure, while α^{v} can describe the volumetric procedure. The basic distortional material parameter α is also a parameter of "distortional energy", and α is again supported as a procedure parameter (because energy is an accumulative procedure).

11.7 Some Expressions of Distortional Modulus

11.7.1 Definitions

The main purpose of the section is to set up some relationships for the stiffness of frictional materials, characterized by distortional shear moduli. It has been assumed that the response of frictional materials to shearing is dependent on stress ratio, and hence it is convenient to express both tangent and secant distortional moduli in terms of the variation of distortional strain with respect stress ratio. The tangent distortional shear modulus G_t is defined by:

$$G_t = \frac{d\eta}{d\varepsilon_d} \quad \text{..... (11.44)}$$

and secant distortional shear modulus G_s:

$$G_s = \frac{\eta}{\varepsilon_d} \quad \text{..... (11.45)}$$

Via equation 11.6, the expression for tangent distortional shear modulus G_t can be expressed by the following equation:

$$G_t = \mathrm{M}\left[\frac{1}{\varepsilon_{d,u}} - \frac{1}{m\varepsilon_{d,i}}\left(\frac{\varepsilon_d}{\varepsilon_{d,u}} - 1\right)\right] D(\varepsilon_d) e^{-\frac{\varepsilon_d}{\varepsilon_{d,i}}} \quad \text{..... (11.46)}$$

and expression for secant distortional shear modulus G_s is:

$$G_s = \mathrm{M}\frac{1}{\varepsilon_d}\left[1 + D(\varepsilon_d)\left(\frac{\varepsilon_d}{\varepsilon_{d,u}} - 1\right) e^{-\frac{\varepsilon_d}{\varepsilon_{d,i}}}\right] \quad \text{..... (11.47)}$$

If $\varepsilon_d = 0$ in Eq. 11.46, the initial tangent distortional modulus G_o is given by

$$G_o = \mathrm{M}_r\left(\frac{1}{\varepsilon_{d,u}} + \frac{1}{\varepsilon_{d,i}}\right) \quad \text{..... (11.48)}$$

In this section 11.7, the non-uniformity factor is assumed to be neglected, *i.e.*, β=0.

11.7.2 Variation of Distortional Moduli G_t and G_s with Stress Ratio η

The relations between shear modulus and stress are often used in the analysis of pile foundations, (Kraft, 1981; Poulos, 1990). Via a mathematical process, the variations of distortional moduli G_t and G_s with stress ratio η can be easily derived from Eqs. 11.46 to

11.48. Fig. 11.46 shows the constitutive relationship of normalized secant distortional shear modulus G_s/G_o with normalized stress ratio η/M_f. The relationship of nornalized tangent distortional shear modulus G_t/G_o with normalized stress ratio η/M_f is plotted in Fig. 11.47. The relation of ratio G_t/G_s with η/M is shown in Fig. 11.48.

For Fig. 11.46, the curves of G_t/G_o versus η / M_f can be approximately simplified to a family of straight lines before a peak strength is reached:

if $\eta \le \eta_p$

$$\frac{G_t}{G_o} = 1 - R_t \frac{\eta}{M} \qquad \text{.....(11.49)}$$

where

$$R_t = \frac{1}{1 + e^{-\frac{1}{\alpha}-1}} \qquad \text{.....(11.50)}$$

11.7.3 Variation of G_t with G_s

The secant shear modulus is more easily tested than the tangent shear modulus, and is widely used in geotechnical practice. However, the tangent shear modulus is sometimes needed, especially for numerical analysis of geotechnical problems. The relation of normalized tangent distortional modulus, G_t / G_o, and normalized secant distortional modulus G_s / G_o is shown in Fig. 11.59. It is found that the effect of the parameter α is small when G_s / G_o >=0.5, and an approximate relation of tangent and secant distortional strain can be obtained as follows:

When $\frac{G_s}{G_o} \ge 0.5$

$$\frac{G_t}{G_o} = 0.8(\frac{G_s}{G_o})^2 + 0.45(\frac{G_s}{G_o}) - 0.25 \qquad \text{..... (11.51)}$$

The above approximate correlation may be also used for the conversion between secant shear modulus and tangent shear modulus. Using the accurate mean of linear variable differential transformers (LVDTs) in triaxial undrained tests, Cuccovillo *et al* (1997) measured the tangent shear modulus and secant shear modulus against axial strain on Kaolin. As shown in Fig. 11.50, the comparison between the theory and test data is quite reasonable.

11.7.4 Approximate Expression of "Percentaged" Secant Shear Modulus $G_{s,n}$

The "percentaged" secant distortional modulus $G_{s,n}$ is defined as the secant distortional modulus G_s at $\eta = n\eta_p$, where n is a percentage value. The percentaged secant distortional modulus $G_{s,n}$ is expressed as:

$$G_{s,n} = c(\alpha,n)\, G_o \qquad \text{.....(11.52)}$$

It is found that the effect of α in the coefficient function $c(\alpha,n)$ is small when n<40% and α=0~3, and the average of value of $c(\alpha,n)$ can be approximately expressed as below:

$$c(\alpha,n) \approx 1-\frac{n}{2} \qquad \text{..... (11.53)}$$

Thus, the percentaged secant distortional modulus can be approximately expressed as follows:

$$G_{s,n} = [(1-\frac{n}{2}) \pm \frac{n}{2}]G_o \qquad \text{..... (11.54)}$$

The two secant distortional moduli $G_{s,10\%}$ and $G_{s,33\%}$ can be approximately predicted below.

$$G_{s,10\%} = (0.95 \pm 0.05)G_o \qquad \text{..... (11.55)}$$

$$G_{s,33\%} = (0.835 \pm 0.165) G_o \qquad \text{.....(11.56)}$$

In geo-engineering, especially for retaining wall, piles and footing *etc.*, conventional "percentaged" secant shear modulus value, such as $G_{s,10\%}$, $G_{s,33\%}$ and $G_{s,50\%}$ are widely used. Furthermore, by using Equations 11.51 and 11.54 in the pile analysis, it is possible to incorporate non-linear behaviour of the soil into the incremental non-linear analysis in GEPAN, if n is taken as the ratio of current pile-soil stress to corresponding peak stress.

11.8 Conclusions

This chapter presents a comprehensive study on the simulation of the shearing behaviour of frictional materials. A basic concept of this research is that the response of frictional materials to shearing is dependent on shear stress ratio, and not on the shear stress. This idea is termed Assumption 1. Consequently, it is proposed that material properties for shearing should be described in terms of shear stress ratio. Another basic assumption is that there is a characteristic distortional strain at which the tangent distortional modulus is independent of the initial stress and strain states of the material. This is Assumption 4. Based on these two ideas and certain other assumptions, a general explicit equation for the distortional strain and the shear stress ratio has been formulated. Modifications are made to include the effect of non-uniformity of stress and strain distribution within a testing specimen on the deformation. An explicit equation for the volumetric strain is also obtained, based on a proposed flow rule for the total strain increment. The proposed flow rule has a mathematical format similar to that proposed in the original Cam Clay model. However, the constraints on the material parameters for volumetric deformation imposed by the original flow rule are removed.

Seven parameters are introduced in the constitutive equations. M_f is the final strength of a frictional material. $\varepsilon_{d,i}$ is the characteristic distortional strain, *i.e.*, the value of the distortional strain at the characteristic point. $\varepsilon_{d,u}$ is the value of the distortional strain at $\eta = M$ before the peak strength. M^v is the value of strain increment rate $d\varepsilon_v / d\varepsilon_d$, at $\eta = 0$. $\varepsilon^v_{d,i}$ is the distortional strain at the convergent point of the curvature rate for the volumetric strain and the distortional strain relationship. $\varepsilon^v_{d,u}$ is the value of distortional strain at the peak volumetric strain. β is a parameter to reflect the influence of non-uniform deformation of a

sample during the softening process. All the seven parameters can be determined from a single shearing test accordingly. Ideally, the parameters M_f, $\varepsilon_{d,i}$, $\varepsilon_{d,u}$, M^v, $\varepsilon^v_{d,i}$, and $\varepsilon^v_{d,u}$ can be determined according to the physical meanings of the six parameters. Parameter β is determined by matching the simulated softening curve with that measured. However, difficulty may arise in determining $\varepsilon_{d,i}$ for wet distortional behaviour and in determining $\varepsilon^v_{d,i}$ for wet volumetric behaviour. An alternative way is to determine these two parameters also by fitting. Because any one of the seven parameters controls a distinctive feature of the mathematical curve, the determination of equation parameters is relatively simple and straightforward.

The proposed constitutive equations are employed to make simulations of the behaviour of a wide selection of frictional materials, with the focus being on geo-materials. There are in total twenty-one different types of materials with one hundred and nine tests considered. The twenty-one types of frictional materials are reconstituted soft and stiff clays, sands, silts, clay-sand mixtures, compacted materials, filter material, volcanic soils, decomposed granite soils, gravel, rock masses, rocks, natural clays, aged sand, natural and reconstituted calcareous soils, cemented soils, partially saturated soils, reinforced geo-materials, wheat, sugar, rape, and type chips. Despite the vast diversities in materials and test conditions and the simplicity of the equations, the overall agreement between the theoretical simulations and the experimental data is very good.

The following conclusions are drawn on the behaviour of frictional materials:

(1) From the good performance of the proposed constitutive equations, it is seen that Assumption 1 is reasonable. It is appropriate to define the shearing behaviour and material properties for shearing in terms of shear stress ratio rather than the shear stress as is currently widely used.

(2) Assumption 4, the existence of the convergent point in the $\varepsilon_d \sim G_t$ space, is an approximation. This assumption is applicable only for soil with "dry distortional behaviour"; however, it is obvious that $\varepsilon_{d,i}$ changes when the soil exhibits "wet distortional behaviour".

(3) Four typical patterns of shearing behaviour have been proposed for materials with positive initial slope on ε_v-ε_d curve, M^v. They are D-D behaviour, W-W behaviour, D-W

behaviour, and W-D behaviour. All four types of shearing behaviour have been found in geo-materials.

(4) It has been demonstrated clearly that the constraints imposed on the parameters for the volumetric deformation of frictional materials such as that in the original Cam Clay model are not supported by experimental data. Indeed there are some systematic errors associated with the flow rule proposed by the Cam Clay model. Describing the strain increment $d\varepsilon_v / d\varepsilon_d$ in terms of strain quantities, which was introduced in this chapter, appears more appropriate than describing the rate in terms of the final strength and the current stress ratio, which is currently a widely adopted method.

(5) Based on the study of a large body of experimental data, a modification of the flow rule of the original Cam Clay model is made based on the statistical study of the results for over one hundred tests.

It is found that there exist two basic material procedural parameters, one (α) for distortional procedure, the other (α^v) for volumetric procedure.

Finally, some approximate expressions of distortional moduli are presented, including secant, tangent, and "percentaged" distortional modulus. These expressions of soil stiffness can be applied into the non-linear pile analysis.

APPENDIX NOTATION

Some of the terms and symbols used in the chapter are defined by the following equations.

σ: vector of Cartesian stress components

$$= (\sigma_{11}, \sigma_{22}, \sigma_{33}, \sigma_{12}, \sigma_{23}, \sigma_{31})^T \tag{A1}$$

ε: vector of Cartesian strain components

$$= (\varepsilon_{11}, \varepsilon_{22}, \varepsilon_{33}, \varepsilon_{12}, \varepsilon_{23}, \varepsilon_{31})^T \tag{A2}$$

p': mean effective stress

$$= \frac{1}{3}(\sigma'_{11} + \sigma'_{22} + \sigma'_{33}) \tag{A3}$$

q : distortional stress

$$=\frac{1}{\sqrt{2}}\sqrt{\left[\left(\sigma'_{11}-\sigma'_{22}\right)^2+\left(\sigma'_{22}-\sigma'_{33}\right)^2+\left(\sigma'_{33}-\sigma'_{11}\right)^2+6\left(\sigma'^{\,2}_{12}+\sigma'^{\,2}_{23}+\sigma'^{\,2}_{31}\right)\right]} \tag{A4}$$

η : shear stress ratio

$$= q/p' \tag{A5}$$

ε_v : volumetric strain

$$=\varepsilon_{11}+\varepsilon_{22}+\varepsilon_{33} \tag{A6}$$

ε_d : distortional strain

$$=\frac{\sqrt{2}}{3}\sqrt{\left[\left(\varepsilon_{11}-\varepsilon_{22}\right)^2+\left(\varepsilon_{22}-\varepsilon_{33}\right)^2+\left(\varepsilon_{33}-\varepsilon_{11}\right)^2+6\left(\varepsilon_{12}^{\,2}+\varepsilon_{23}^{\,2}+\varepsilon_{31}^{\,2}\right)\right]} \tag{A7}$$

G_s : secant distortional modulus

$$=\frac{\eta}{\varepsilon_d} \tag{A8}$$

G_t : tangent distortional modulus

$$=\frac{d\eta}{d\varepsilon_d} \tag{A9}$$

M_f : final strength in term of shear stress ratio (Fig. 11.1(a))

$\varepsilon_{v,r}$: residual volumetric strain

η_p : peak strength in term of shear stress ratio

$\varepsilon_{v,p}$: peak volumetric strain

$\varepsilon_{d,u}$: distortional strain at $\eta = M_f$ before the peak strength η_p is reached (Fig. 11.1(a))

$\varepsilon_{d,i}$: characteristic distortional strain (Fig. 11.1(a) and Fig. 11.2(a))

M^v : initial slope on ε_v-ε_d curve (Fig. 11.1(b))

$\varepsilon^v_{d,u}$: volumetric strain at $\varepsilon_v = \varepsilon_{v,p}$ before the $\varepsilon_{v,r}$ is reached (Fig. 11.1(b))

$\varepsilon^v_{d,i}$: characteristic volumetric strain (Fig. 11.1(b) and Fig.11.2(b))

β : a non-homogeneous parameter of distortional-volumetric behaviour

α: basic distortional material parameter (Eq. 11.33)

α^v: basic volumetric material parameter (Eq.11.34)

K_M: a correlation coefficient of distortional and volumetric deformation (Eq. 11.30)

K_i : a correlation coefficient of distortional and volumetric deformation (Eq. 11.31)

K_u : a correlation coefficient of distortional and volumetric deformation (Eq. 11.32)

ω : phase angle for the distortional deformation (Eq. 11.23)

ω^v : phase angle for volumetric deformation (Eq. 11.24)

θ : phase difference between distortional and volumetric deformation (Eq. 11.25)

e: natural exponent and e= 2.7182818.

Table 11.4 Lists of frictional materials and No. of tests and references

Types of materials	Name of the materials	Reference	No. of tests & Fig. No.
Sands	Fuji sand	Tatsuoka, 1972	3 Fig. 11.6
	Dense Cambria sand	Yamanuro et al, 1996	5 Fig. 11.7
	Ham River sand	Daramola, 1980	4 Fig. 11.16
Reconstituted clays	Soft Ancona clay	Canestrari *et al*,1993	1 Fig. 11.8
	Soft and stiff Corinth marl	Burland *et al*, 1996	3 Fig. 11.9
Silts	Unsaturated & compacted Silt	Cui *et al*, 1996	4 Fig. 11.23
Clay-sand mixtures	Kaolinite-silt	Stark *et al*, 1969	2 Fig.11.13
Compacted materials	Unsaturated & compacted silt	Cui *et al*, 1996	4 Fig. 11.23
Filters	Grand-Maison filter	Dendani *et al*, 1988	2 Fig. 11.14
Decomposed rock soils	Decomposed granite soil	Lee *et al*, 1995	2 Fig. 11.15
Volcanic soils	Cemented volcanic soils	O'Rouke, 1988	4 Fig. 11.17
Natural clays	Ancona clay	Canestrari *et al*,1993	1 Fig. 11.8
	Soft and stiff Weald clay	Henkel, 1956	2 Fig. 11.11
	Soft & stiff Corinth marl	Burland *et al*, 1996	3 Fig. 11.10
	Nanticoke clay	Scott *et al*, 1972	2 Fig. 11.12
Cemented soils	Artificially cemented carbonate sand	Hunag, 1994	4 Fig. 11.18
	Naturally cemented volcanic soil	O'Rouke, 1988	4 Fig. 11.17
Aged sands	Aged Ham river sand	Daramola, 1980	4 Fig. 11.16
Calcareous soils	Reconstituted and artificially cemented soil	Huang, 1994	8 Fig. 11.18
	Intact Bass strait carbonate sand	Poulos *et al*, 1982	2 Fig. 11.19
Gravel	Reinforced gravel	Cazzuffi *et al*, 1994	4 Fig. 11.25
Granular rocks	Granular rock	Michelic *et al*, 1981	3 Fig. 11.20
	Uncompacted ballast	Alva-Hurtado *et al*, 1981	2 Fig. 11.21
Rock	Oolitic limestone	Elliott, 1983	3 Fig.11.22
Unsaturated soil	Unsaturated & compacted Silt	Cui *et al*, 1996	4 Fig. 11.23
Reinforced geo-materials	Reinforced soil	Michalowski *et al*, 1996	4 Fig.11.24
	Reinforced gravel	Cazzuffi *et al*, 1994	4 Fig. 11.25

Types of materials	Name of the materials	Reference	No. of tests & Fig. No.
Wheat	Wheat	Kolymbas *et al*, 1990	2 Fig. 11.26
Sugar	Sugar	Kolymbas *et al*, 1990	3 Fig. 11.27
Rape	Rape	Kolymbas *et al*, 1990	3 Fig. 11.28
Tire chips	Wu *et al*, 1997	Wu *et al*, 1997	3 Fig. 11.29

Table 11.5 Values of model parameters for sands

Material	Tests	M_f	$\varepsilon_{d,u}$	$\varepsilon_{d,i}$	M^v	$\varepsilon^v_{d,u}$	$\varepsilon^v_{d,i}$
Fuji sand	A: $e_v = 0.52$	1.5	0.01	0.037	1.0	0.01	0.037
	B: $e_v = 0.78$	1.5	0.04	0.037	0.7	0.04	0.060
	C: $e_v = 0.85$	1.4	0.20	0.037	1.0	0.20	0.037
Dense Cambria sand	A: $\sigma'_3 = 11.5$ MPa	1.33	0.3	0.1	1	0.40	0.50
	B: $\sigma'_3 = 8$ MPa	1.33	0.25	0.07	0.9	0.40	0.35
	C: $\sigma'_3 = 5.8$ MPa	1.33	0.25	0.05	0.8	0.50	0.20
	D: $\sigma'_3 = 4$ MPa	1.33	0.10	0.035	0.5	0.50	0.18
	E: $\sigma'_3 = 2.1$ MPa	1.33	0.04	0.03	1	0.2	0.03
Ham river sand with aging effect	A: 0 day	1.54	0.04	0.025	0.31	0.013	0.091
	B: 10 days	1.54	0.04	0.03	0.46	0.009	0.031
	C: 30 days	1.54	0.03	0.02	0.25	0.011	0.083
	D: 152 days	1.54	0.02	0.01	0.18	0.007	0.074

Table 11.6 Values of model parameters for clays

Material	Tests	M_f	$\varepsilon_{d,u}$	$\varepsilon_{d,i}$	M^v	$\varepsilon^v_{d,u}$	$\varepsilon^v_{d,i}$
Ancona clay	A: reconstituted	0.94	0.20	0.04	0.94	0.2	0.15
	B: natural	1.16	0.008	0.02	1.16	0.025	0.04
Corinth marl	Reconstituted: OCR = 7	1.6	0.015	0.015	-0.37	0.008	0.02
	Reconstituted: OCR = 2.4	1.6	0.035	0.025	0.5	0.037	0.04
	Reconstituted: OCR = 1.4	1.6	0.04	0.27	0.85	0.04	0.03
	Natural: OCR = 7	1.88	0.004	0.005	1.88	0.002	0.005
	Natural: OCR = 2.4	1.88	0.008	0.005	1.00	0.006	0.009
	Natural: OCR = 1.4	1.24	0.003	0.004	1.24	0.003	0.004
Weald clay	Natural: OCR = 1	0.6	0.028	0.05	0.6	0.028	0.06
	Natural: OCR = 24	0.6	0.24	0.05	0.6	0.24	0.16
Nanticoke clay	Natural: $\sigma'_3 = 552$ kPa	0.66	0.015	0.021	0.65	0.09	0.04
	Natural: $\sigma'_3 = 345$ kPa	0.7	0.005	0.01	-0.7	0.012	0.01

Table 11.7 Values of model parameters for some soils

Material	Tests	M_f	$\varepsilon_{d,u}$	$\varepsilon_{d,i}$	M^v	$\varepsilon^v_{d,u}$	$\varepsilon^v_{d,i}$
Koalinite sand mixture	A: 10% Koalinite	1.4	0.04	0.03	0.5	0.04	0.06
	B: 50% Koalinite	1.1	0.18	0.055	1.1	0.18	0.055
Filter material	A: σ'_3 = 400 kPa	1.78	0.045	0.03	0.60	0.03	0.07
	B: σ'_3 = 800 kPa	1.78	0.075	0.03	0.90	0.01	0.05
Decomposed granite soil	A: air-dried	1.77	0.01	0.014	1.77	0.01	0.02
	B: saturated	1.6	0.03	0.014	1.60	0.04	0.02
Cemented volcanic soil	A: σ'_3 = 60 kPa	1.85	0.010	0.015	0.50	0.021	0.098
	B: σ'_3 = 120 kPa	1.85	0.018	0.015	0.42	0.027	0.096
	C: σ'_3 = 200 kPa	1.85	0.045	0.015	0.42	0.037	0.07
	D: σ'_3 = 300 kPa	1.67	0.060	0.020	0.51	0.039	0.035

Table 11.8 Values of model parameters for calcareous sols

Material	Tests	M_f	$\varepsilon_{d,u}$	$\varepsilon_{d,i}$	M^v	$\varepsilon^v_{d,u}$	$\varepsilon^v_{d,i}$
Reconstituted & artificially cemented carbonate sand	0% cement, σ'_3 = 100 kPa	1.58	0.015	0.015	1.58	0.015	0.015
	0% cement, σ'_3 = 300 kPa	1.47	0.1	0.017	1.47	0.1	0.03
	0% cement, σ'_3 = 600 kPa	1.35	0.22	0.02	1.35	0.22	0.1
	0% cement, σ'_3 = 1200 kPa	1.28	0.32	0.04	1.28	0.32	0.25
	20% cement, σ'_3 = 100 kPa	1.9	0.005	0.008	1.9	0.005	0.008
	20% cement, σ'_3 = 300 kPa	1.65	0.01	0.001	1.65	0.03	0.015
	20% cement, σ'_3 = 600 kPa	1.5	0.02	0.015	1.45	0.1	0.03
	20% cement, σ'_3 = 1200 kPa	1.35	0.07	0.02	1.35	0.22	0.2
Bass strait carbonate sand	A: σ'_3 = 897 kPa	1.65	0.1	0.014	0.9	0.05	0.05
	B: σ'_3 = 138 kPa	1.8	0.05	0.014	0.7	0.02	0.036

Table 11.9 Values of model parameters for gravel and rocks

Material	Tests	M_f	$\varepsilon_{d,u}$	$\varepsilon_{d,i}$	M^v	$\varepsilon^v_{d,u}$	$\varepsilon^v_{d,i}$
Granular rock	A: σ'_3 = 13.8 MPa	1.94	0.01	0.01	0.388	0.005	0.035
	B: σ'_3 = 71.1 MPa	1.26	0.02	0.01	0.378	0.009	0.050
	C: σ'_3 = 193 MPa	0.96	0.03	0.01	0.500	0.020	0.055
Uncompacted ballast	A: σ'_3 = 138 kPa	1.75	0.1	0.01	1.3	0.04	0.01
	B: σ'_3 = 34.5 kPa	2	0.05	0.01	0.7	0.015	0.035
Oolitic limestone	A: σ'_3 = 2 MPa	1.53	0.01	0.025	0.08	0.15	0.1
	B: σ'_3 = 5 MPa	1.97	0.02	0.01	0.05	0.035	0.09
	C: σ'_3 = 10 MPa	1.8	0.1	0.015	0.05	0.02	0.05

Table 11.10 Values of model parameters for an unsaturated soil

Material	Tests	M_f	$\varepsilon_{d,u}$	$\varepsilon_{d,i}$	M^v	$\varepsilon^v_{d,u}$	$\varepsilon^v_{d,i}$
Unsaturated & compacted silt	A: suction = 200 kPa	1.76	0.2	0.014	0.93	0.2	0.14
	B: suction = 400 kPa	1.37	0.2	0.016	0.69	0.2	0.16
	C: suction = 800 kPa	0.94	0.2	0.018	0.64	0.2	0.18
	D: suction = 1500 kPa	0.66	0.2	0.02	0.5	0.2	0.2

Table 11.11 Values of model parameters for reinforced geo-materials

Material	Tests	M_f	$\varepsilon_{d,u}$	$\varepsilon_{d,i}$	M^v	$\varepsilon^v_{d,u}$	$\varepsilon^v_{d,i}$
Reinforced soil	A: σ'_3 = 600 kPa, reinforced	1.59	0.1	0.009	0.45	0.017	0.045
	B: σ'_3 = 600 kPa, plain	1.44	0.1	0.008	0.50	0.014	0.04
	C: σ'_3 = 100 kPa, reinforced	1.72	0.1	0.006	0.17	0.004	0.04
	D: σ'_3 = 100 kPa, plain	1.52	0.1	0.007	0.20	0.005	0.05
Oolitic Limestone	A: σ'_3 = 2 MPa	1.53	0.01	0.025	0.08	0.15	0.10
	B: σ'_3 = 5 MPa	1.97	0.02	0.010	0.05	0.035	0.09
	C: σ'_3 = 10 MPa	1.80	0.10	0.015	0.05	0.02	0.05

Table 11.12 Values of model parameters for some other materials

Material	Tests	M_f	$\varepsilon_{d,u}$	$\varepsilon_{d,i}$	M^v	$\varepsilon^v_{d,u}$	$\varepsilon^v_{d,i}$
Wheat	A: σ'_3 = 100 kPa	1.2	0.2	0.02	0.75	0.2	0.05
	B: σ'_3 = 400 kPa	1	0.1	0.02	0.95	0.2	0.05
Sugar	A: σ'_3 = 50 kPa	1.5	0.186	0.0183	0.8	0.186	0.03
	B: σ'_3 = 200 kPa	1.36	0.25	0.0183	0.8	0.25	0.06
	C: σ'_3 = 800 kPa	1.16	0.25	0.0183	1.16	0.25	0.15
Rape	A: σ'_3 = 100 kPa	1.10	0.1	0.02	1.2	0.1	0.07
	B: σ'_3 = 200 kPa	1.04	0.1	0.03	1.3	0.1	0.15
	C: σ'_3 = 400 kPa	0.97	0.1	0.07	1.5	0.1	0.20
Tire chips	A: σ'_3 =350 kPa	0.66	0.1	0.06	-0.125	0.25	0.3
	B: σ'_3 = 450 kPa	0.66	0.11	0.06	-0.125	0.35	0.3
	C: σ'_3 = 550 kPa	0.66	0.12	0.06	-0.125	0.5	0.3

Table 11.13 Lists of geo-materials and references and parameter values

Materials & references	Tests	M_f	$\varepsilon_{d,u}$	$\varepsilon_{d,i}$	M^v	$\varepsilon^v_{d,u}$	$\varepsilon^v_{d,i}$
Siliceous sand Colliat-Dangus *et al*, 1988	σ'_3 = 50 kPa	1.27	0.02	0.05	1.27	0.02	0.05
	σ'_3 = 1000 kPa	1.27	0.035	0.05	1.27	0.035	0.05
	σ'_3 = 5000 kPa	1.27	0.25	0.05	1.27	0.25	0.05
	σ'_3 = 15000 kPa	1.27	0.5	0.01	1.27	0.5	0.01
Soma sand Oda, 1972	Tapping, σ'_3 = 50 kPa	1.45	0.01	0.007	0.4	0.004	0.01
	Plunging, σ'_3 = 50 kPa	1.45	0.07	0.001	0.3	0.01	0.02
Silt-fly admixture Sharma *et al*, 1984	σ'_3 = 324 kPa	1.51	0.028	0.015	1.51	0.05	0.2
	σ'_3 = 485 kPa	1.22	0.056	0.01	1.22	0.056	0.05
Compacted fill material Bishop *et al*, 1957	Test	1.44	0.017	0.024	1.22	0.017	0.024
Rock Mass Marachi *et al*,1969	σ'_3 = 210 kPa	1.55	0.02	0.035	1.55	0.02	0.035
	σ'_3 = 2900 kPa	1.55	0.03	0.035	1.55	0.03	0.035
Sandstone Moretto *et al*, 1970	σ'_3 = 1800 kPa	2.1	0.004	0.005	1.89	0.004	0.005
Reinforced soil Michalowski *et al*, 1996	Reinforced	1.67	0.1	0.008	0.47	0.01	0.04
	Plain	1.54	0.1	0.006	0.48	0.015	0.052
NR carbonate sand Kaggawa, 1988	σ'_3 = 50 kPa	1.74	0.026	0.03	1	0.02	0.04
	σ'_3 = 100 kPa	1.74	0.05	0.05	1	0.05	0.07
	σ'_3 = 200 kPa	1.7	0.06	0.03	1.7	0.06	0.03
	σ'_3 = 400 kPa	1.7	0.18	0.03	1.3	0.18	0.08
Cemented carbonate sand, 5% cement Hung, 1994	σ'_3 = 100 kPa	1.7	0.007	0.07	1.7	0.007	0.01
	σ'_3 = 300 kPa	1.47	0.08	0.009	1.47	0.08	0.02
	σ'_3 = 600 kPa	1.35	0.18	0.015	1.35	0.18	0.1
	σ'_3 = 1200 kPa	1.4	0.25	0.035	1.4	0.25	0.16
Ballyconneely carbonate sand Golightly, *et al*, 1988	σ'_3 = 50 kPa	1.65	0.015	0.023	1.65	0.01	0.032
	σ'_3 = 150 kPa	1.67	0.026	0.025	1	0.022	0.052
	σ'_3 = 300 kPa	1.63	0.05	0.03	1	0.05	0.02
	σ'_3 = 500 kPa	1.56	0.09	0.04	0.7	0.2	0.15
	σ'_3 = 1000 kPa	1.5	0.2	0.07	0.75	0.3	0.3
Dogs bay carbonate sand Golightly, *et al*, 1988	σ'_3 = 5 kPa	2.73	0.02	0.01	2.73	0.003	0.01
	σ'_3 = 25 kPa	2.46	0.04	0.01	1	0.01	0.06
	σ'_3 = 100 kPa	2.1	0.08	0.02	0.6	0.03	0.06
	σ'_3 = 300 kPa	1.8	0.15	0.035	0.8	0.15	0.09
	σ'_3 = 500 kPa	1.7	0.2	0.05	1	0.2	0.12
	σ'_3 = 1000 kPa	1.45	0.3	0.12	1	0.3	0.3

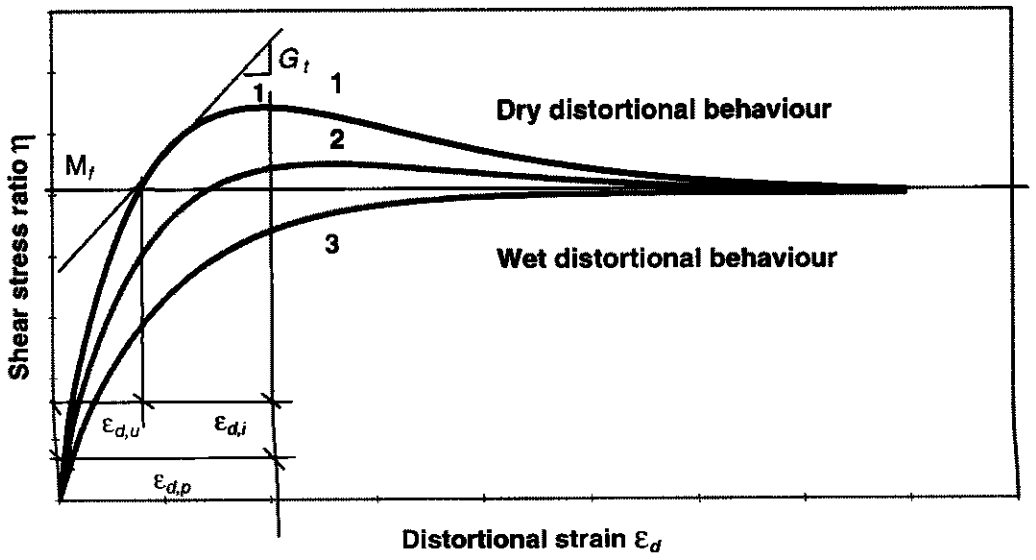

(a) Typical shearing behaviour of frictional materials

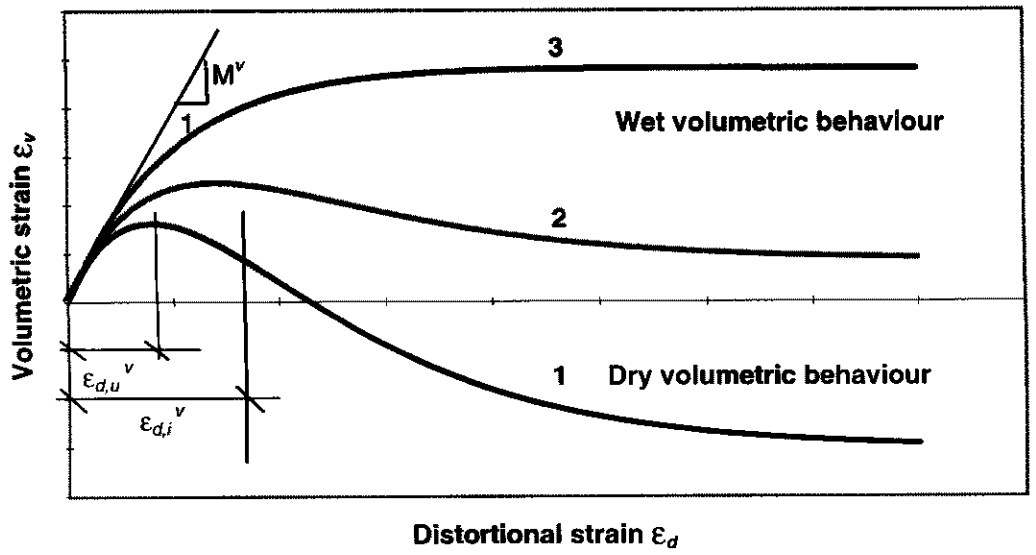

(b) Typical volumetric behaviour of frictional materials

Fig. 11.1 Stress-strain relationship of frictional materials during shearing

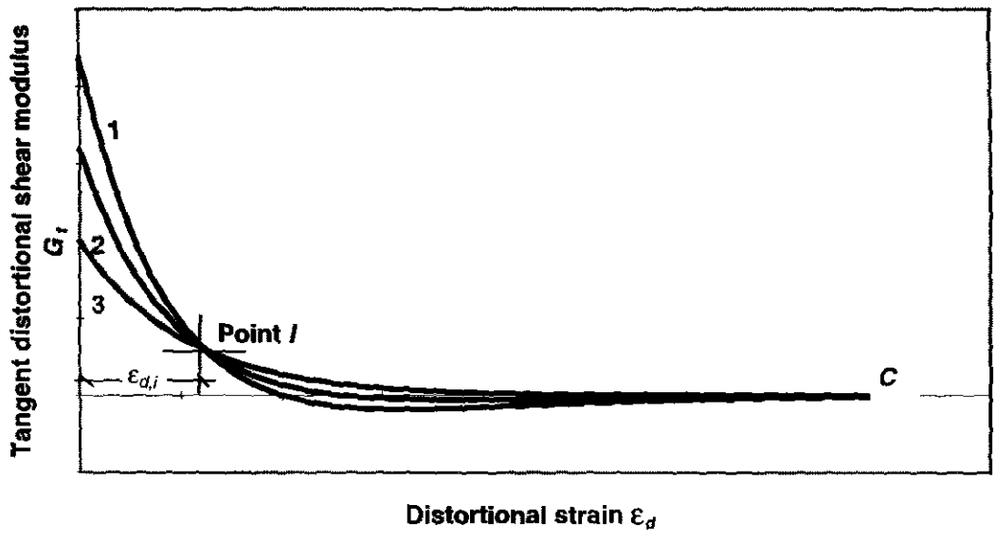

(a) Characteristic point of distortional behaviour

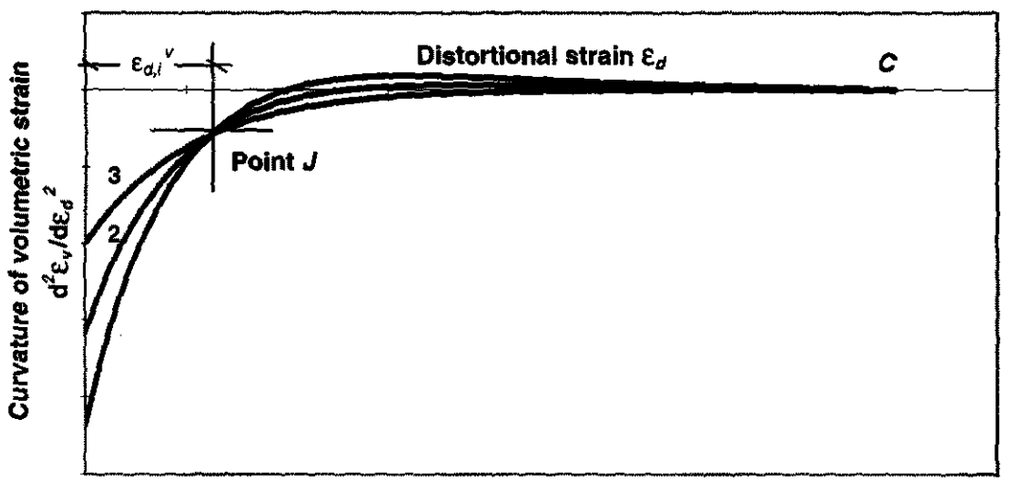

(b) Characteristic point of volumetric behaviour

Fig.11.2 *Characteristic points* of shearing behaviour of frictional materials

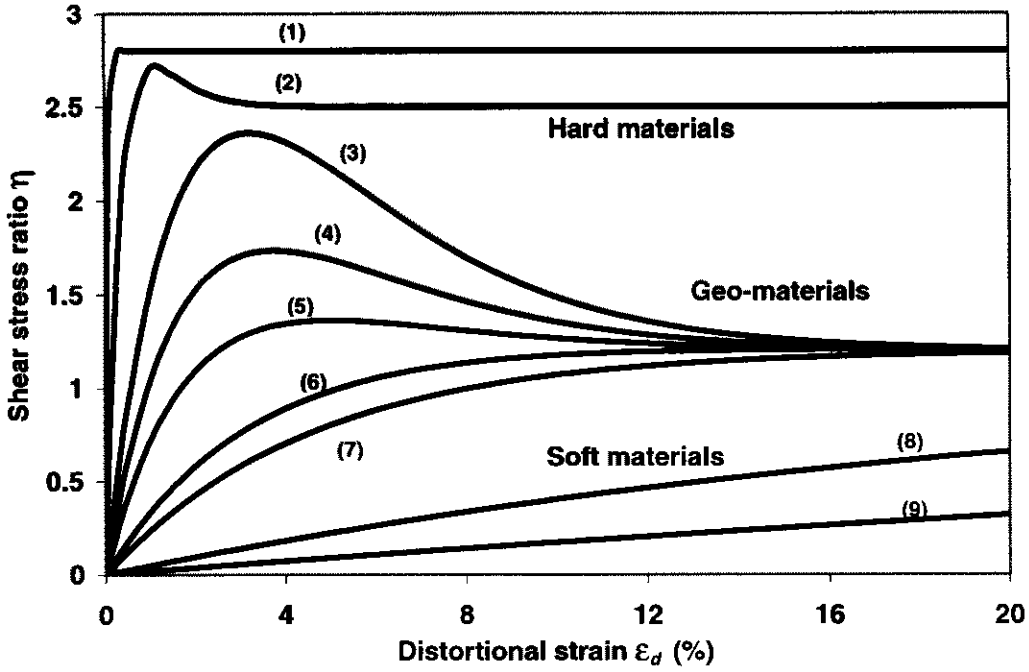

Fig. 11.3 Features of the proposed distortional strain and shear stress ratio equation

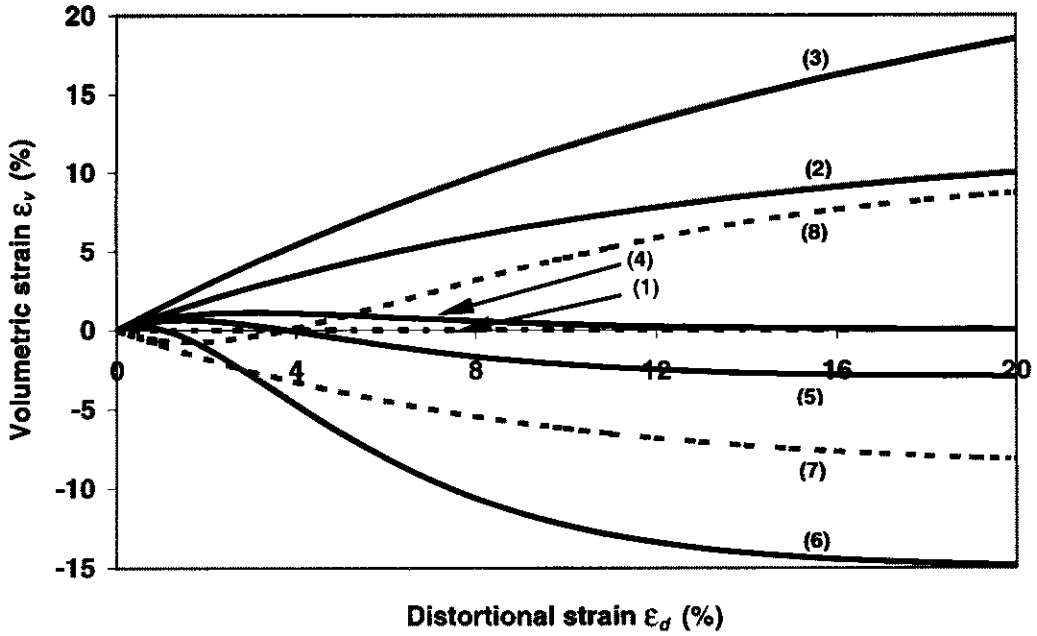

Fig. 11.4 Features of the proposed distortional strain and volumetric strain equation

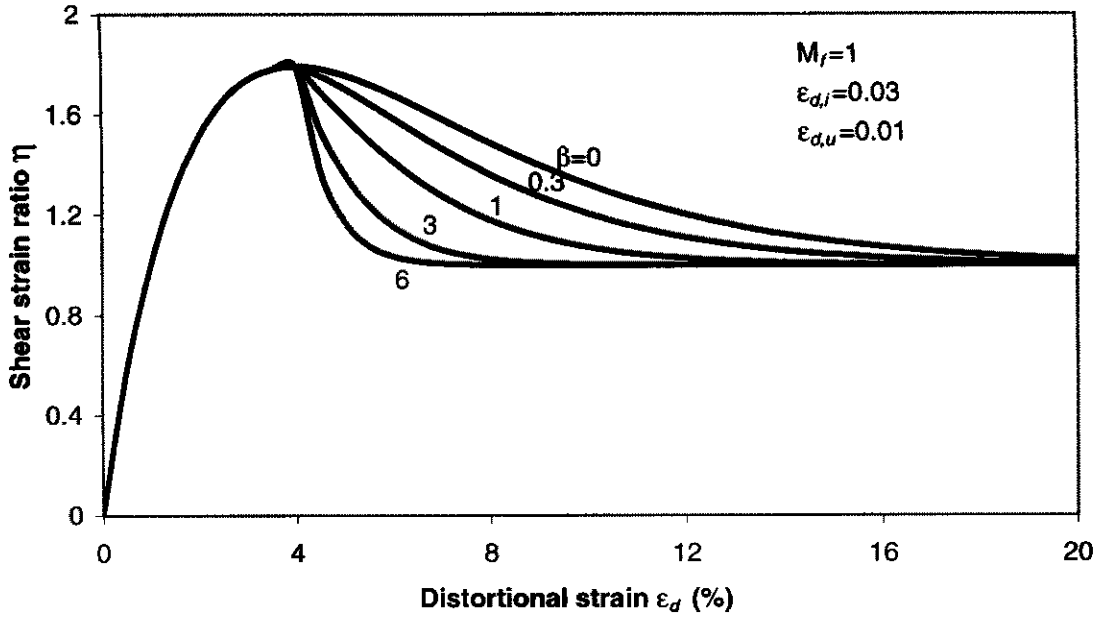

(a) Effect of β on distortional deformation

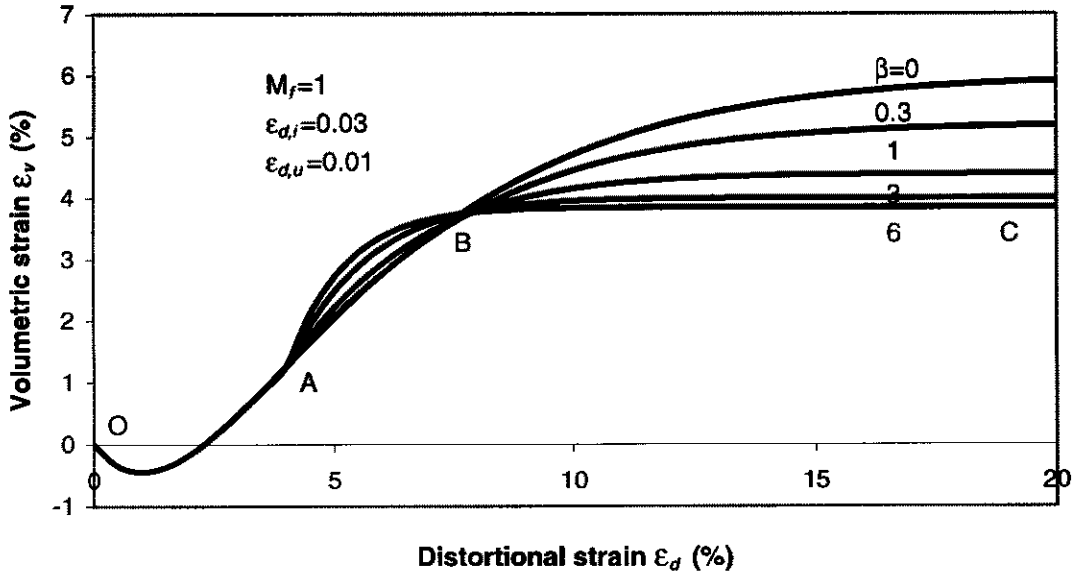

(b) Effect of β on volumetric deformation

Fig. 11.5 Effect on β on shearing behaviour of friction material

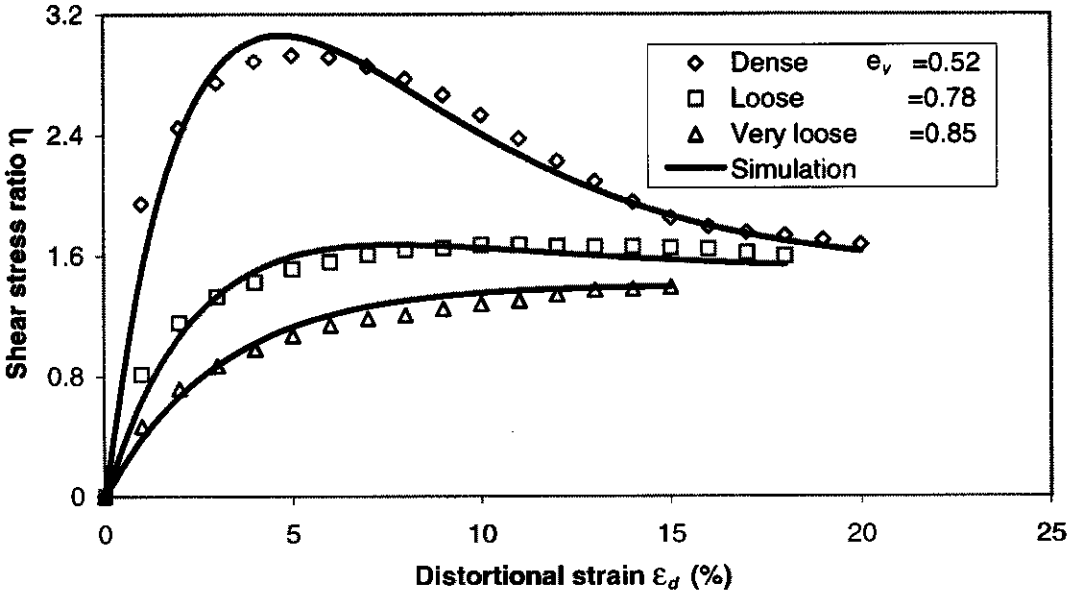

(a) Distortional behaviour of Fuji sand

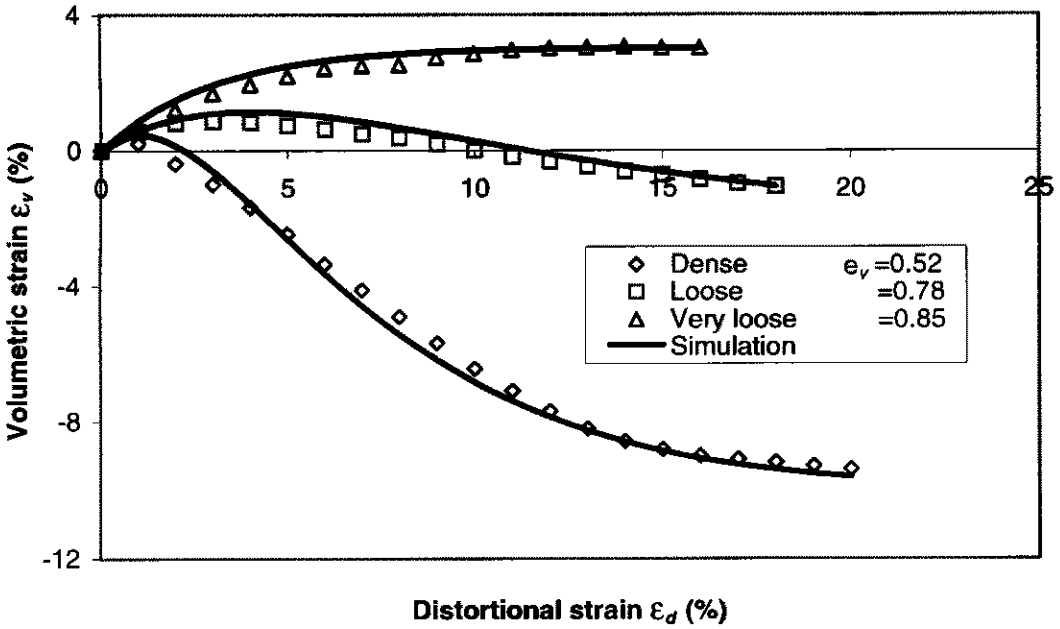

(b) Volumetric behaviour of Fuji sand

Fig. 11.6 Behaviour of Fuji sand during a shearing test (test data after Tatsuoka, 1972)

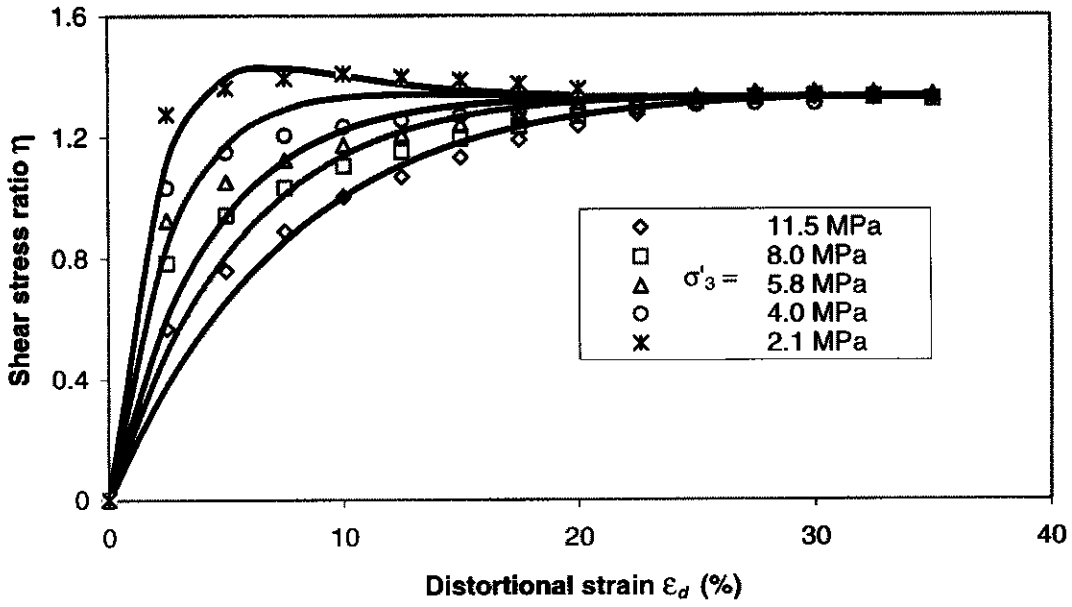

(a) Distortional behaviour of dense Cambria sand

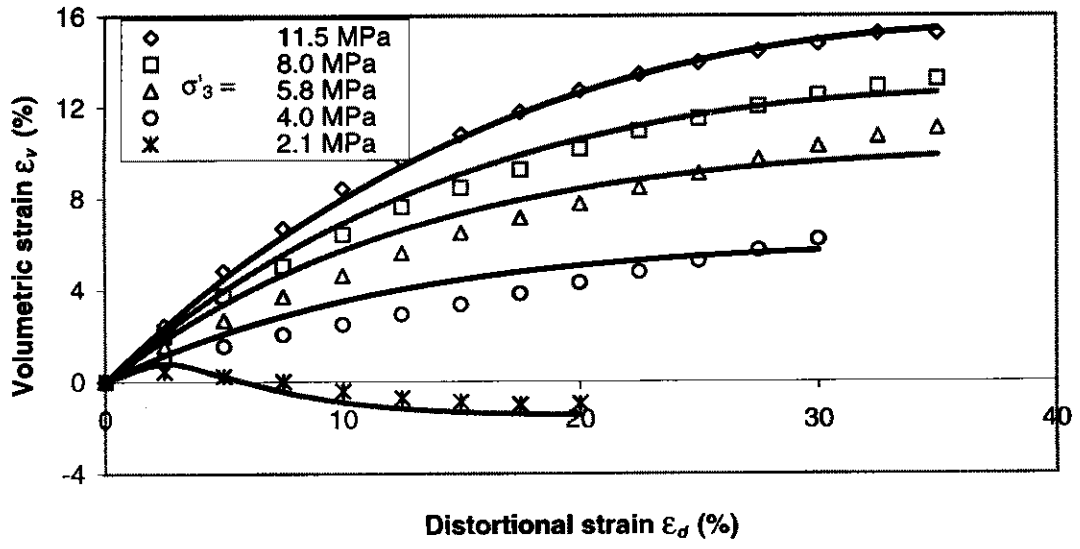

(b) Volumetric behaviour of dense Cambria sand

Fig. 11.7 Stress-strain behaviour of dense Cambrai sand during a shearing test (test data after Yamanuro *et al*,1996)

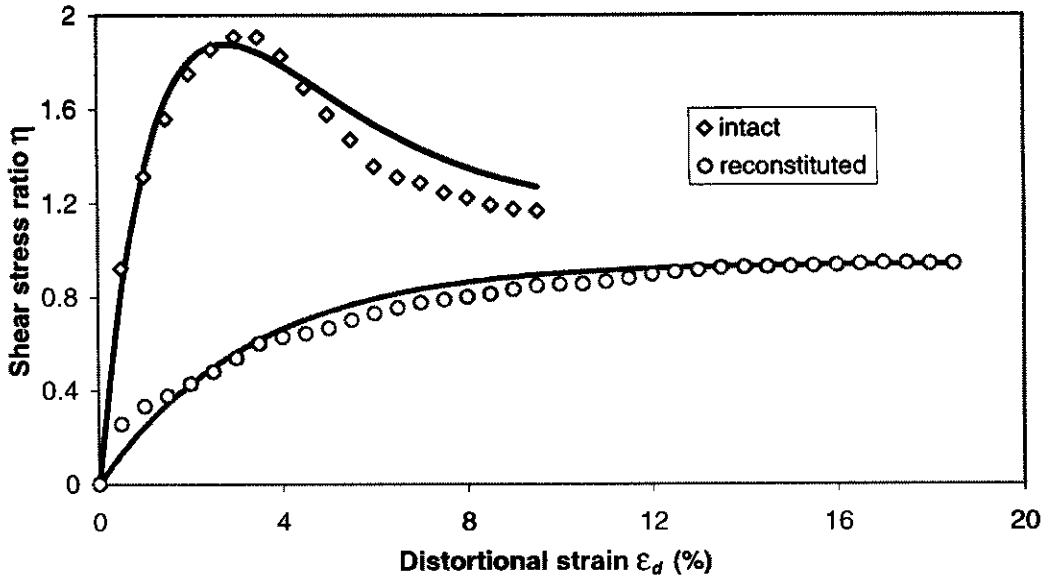

(a) Distortional behaviour of Ancona caly

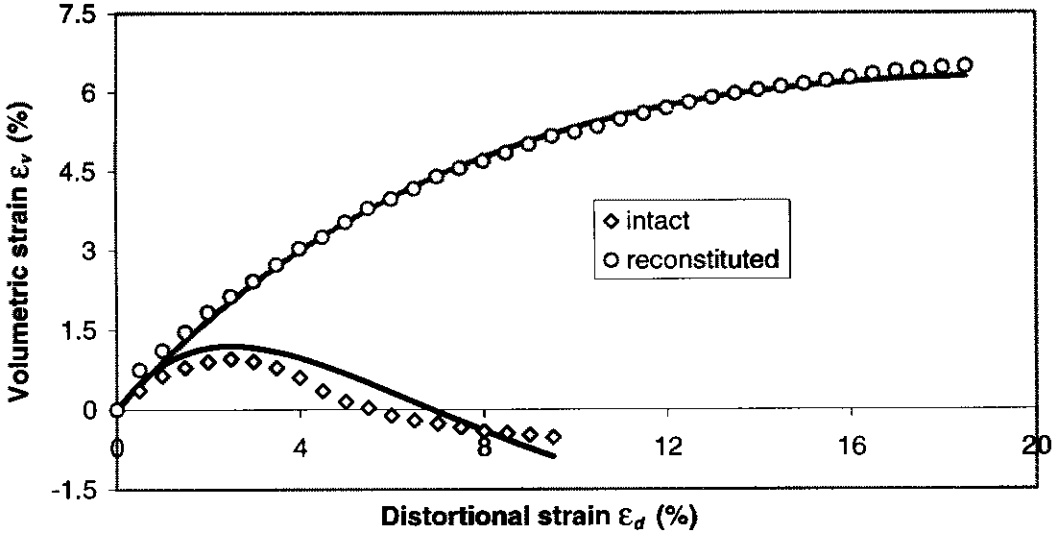

(b) Volumetric behaviour of Ancona clay

Fig. 11.8 Stress-strain behaviour of Ancona clay (test data after Canestrari *et al*, 1993)

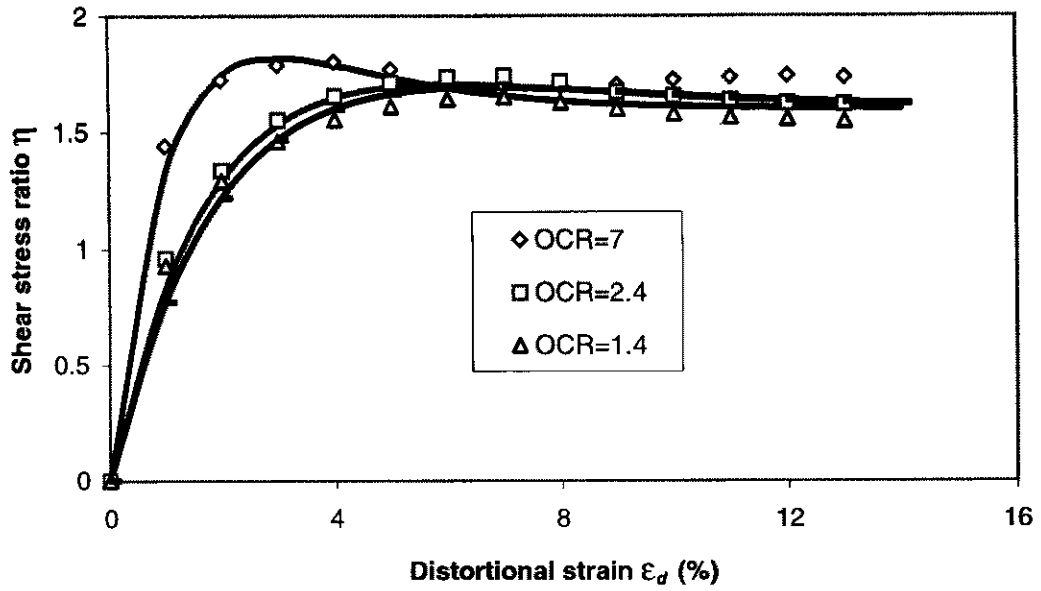

(a) Distortional behaviour of reconstituted Corinth marl

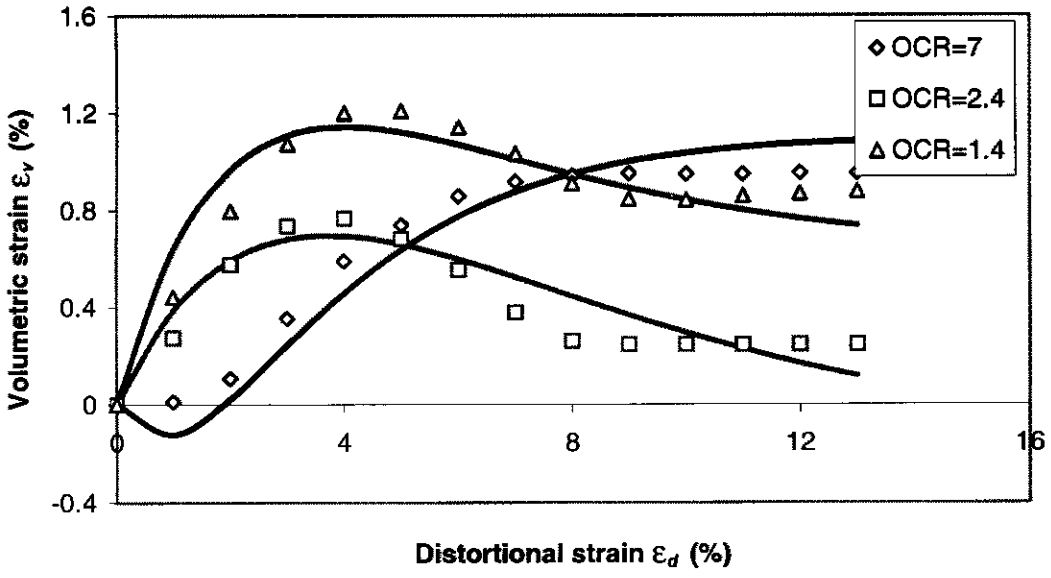

(b) Volumetric behaviour of reconstituted Corinth marl

Fig. 11.9 Stress-strain behaviour of reconstituted Corinth marl (test data after Burland *et al*, 1996)

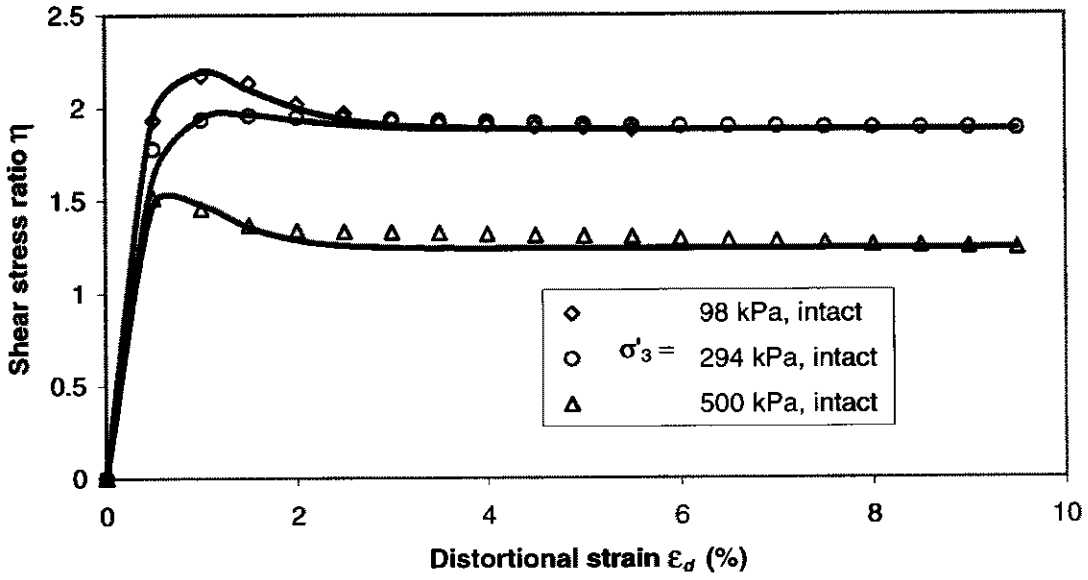

(a) Distortional behaviour of intact Corinth marl

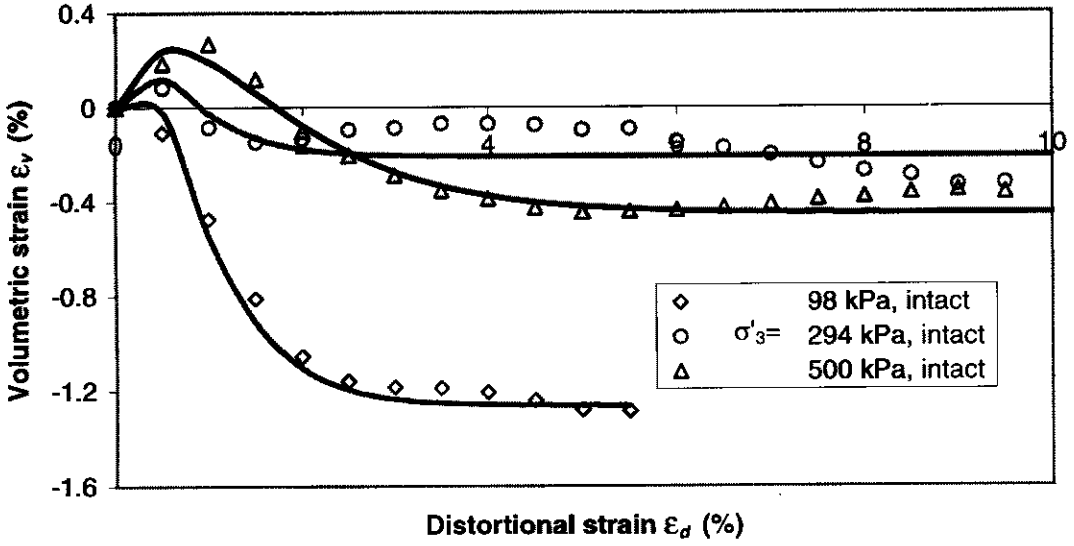

(b) Volumetric behaviour of intact Corinth marl

Fig. 11.10 Stress-strian behaviour of intact Corinth marl (test data after Burland *et al*, 1996)

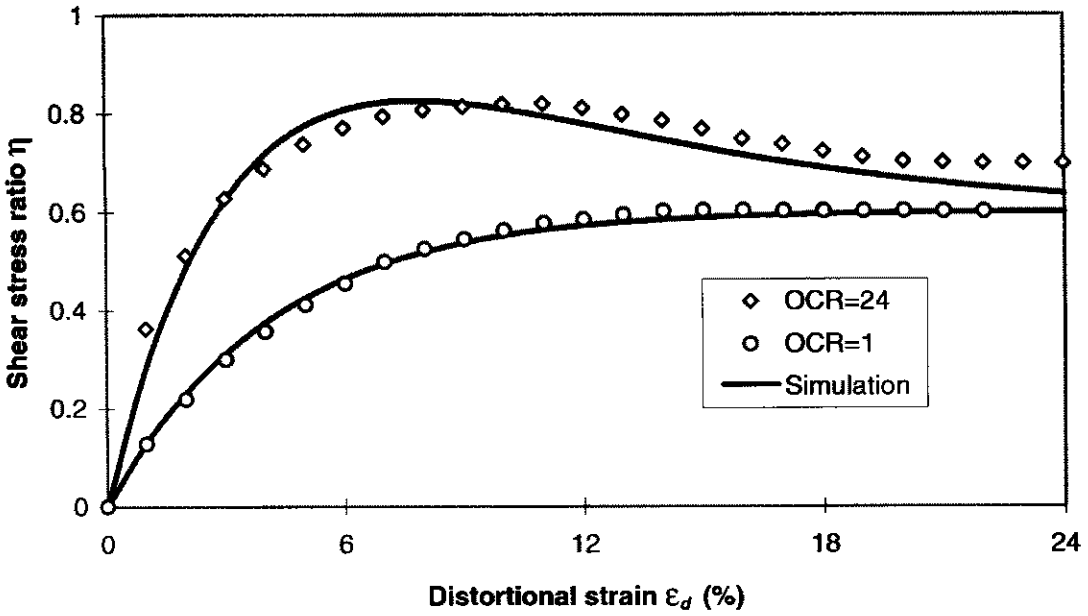

(a) Distortional behaviour of Weald clay

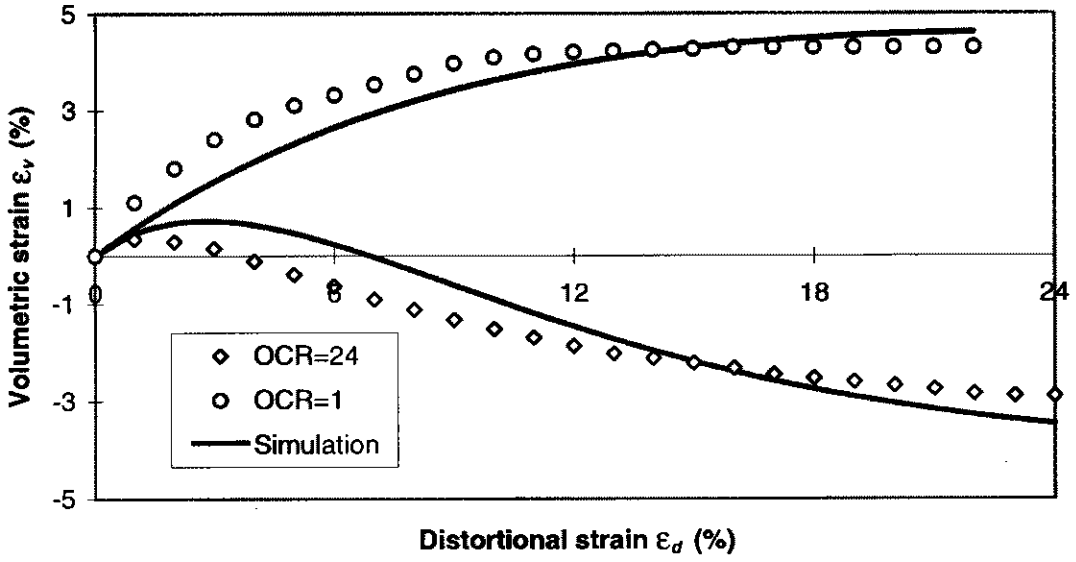

(b) Volumetric behaviour of Weald clay

Fig. 11.11 Stress-strain behaviour of intact Weald clay (test data after Henkel *et al*, 1956)

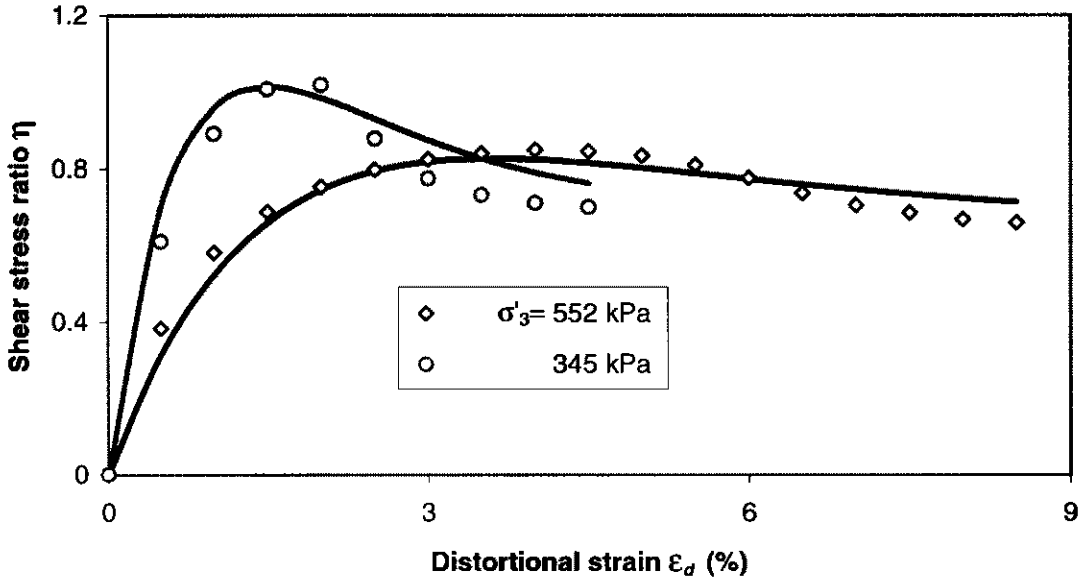

(a) Distortional behaviour of Nanticoke clay

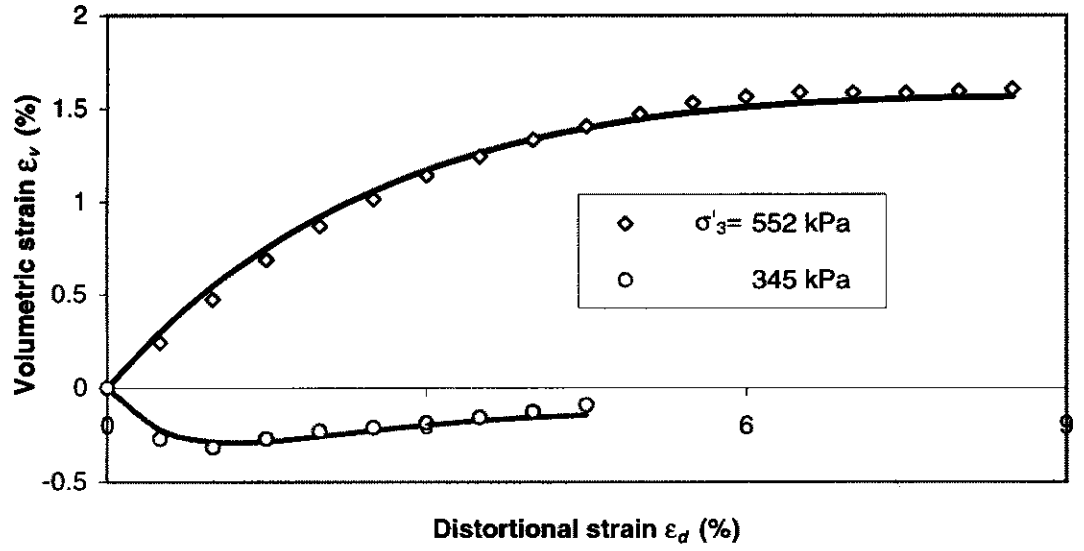

(b) Volumetric behaviour of Nanticoke clay

Fig. 11.12 Stress-strain behaviour of natural Nanticoke clay (test data after Lo, 1972)

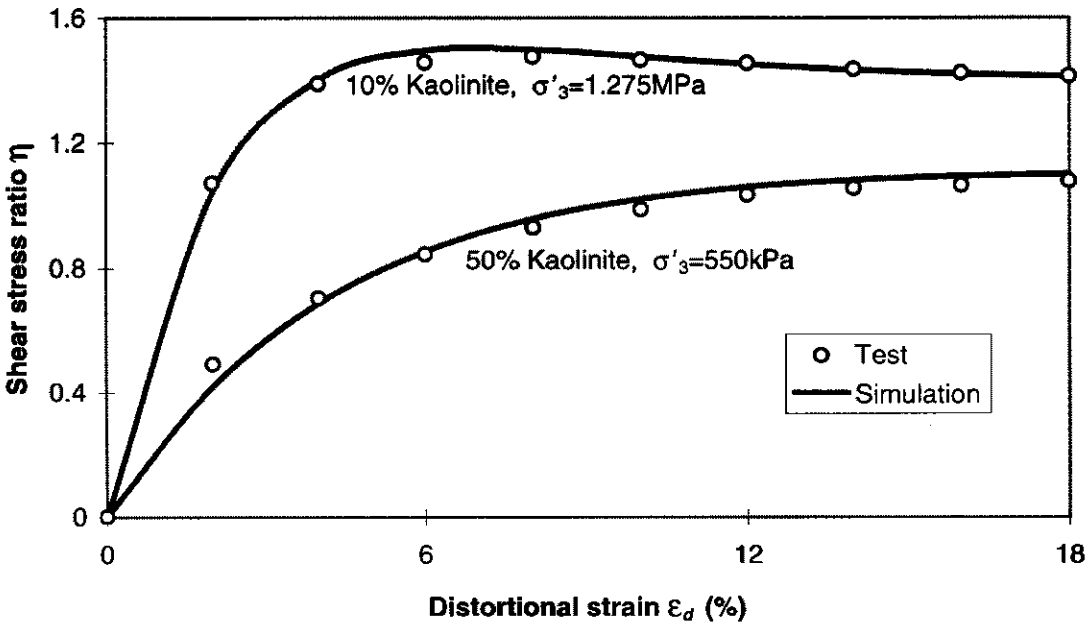

(a) Distortional behaviour of Kaolinite-silt mixture

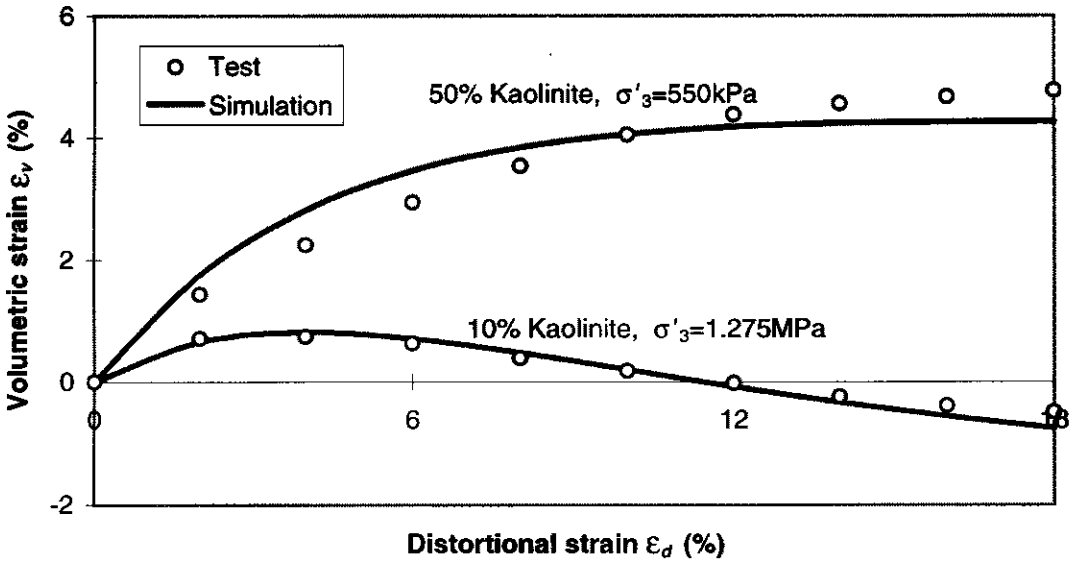

(b) Volumetric behaviour of Kaolinite-silt mixture

Fig. 11.13 Stress-strain behaviour of Kaolinite-silt mixture (test data after Marachi *et al*, 1969)

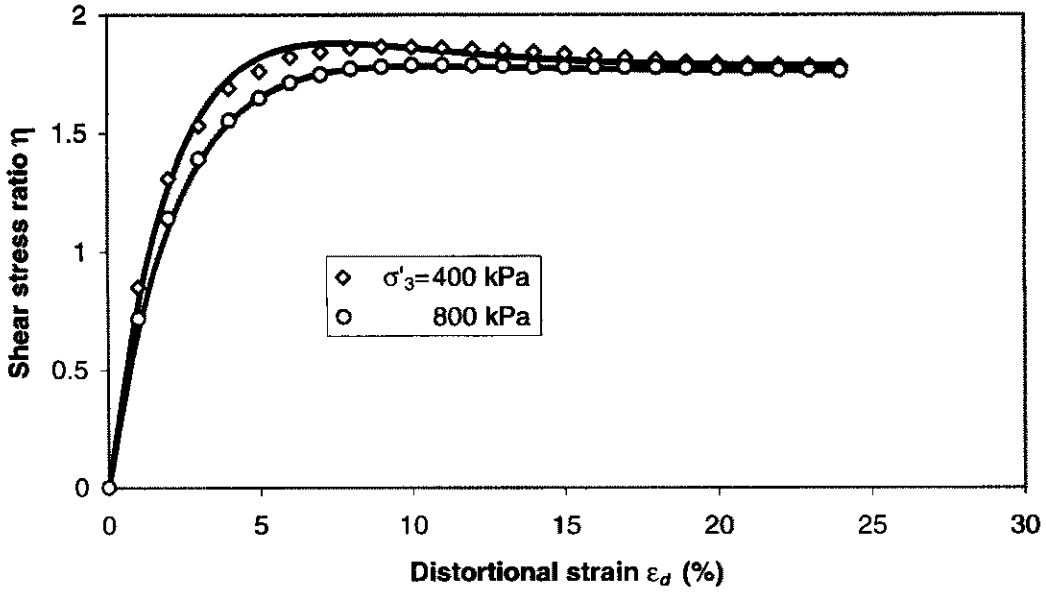

(a) Distortional behaviour of Grand-Maison filter material

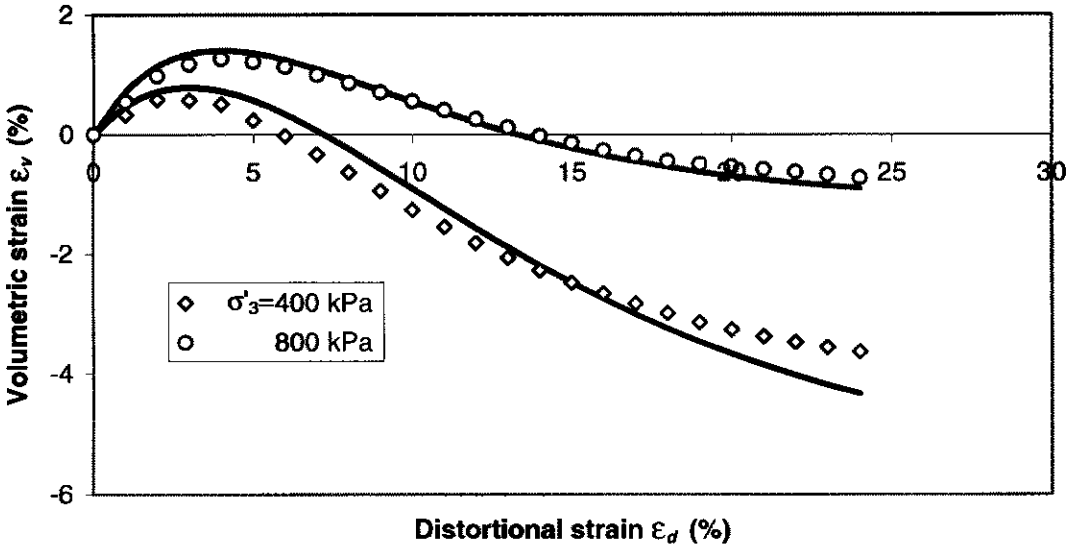

(b) Volumetric behaviour of Grand-Maison filter material

Fig. 11.14 Stress and strain behaviour of Grand-Maison filter material (test data after Dendani *et al*, 1988)

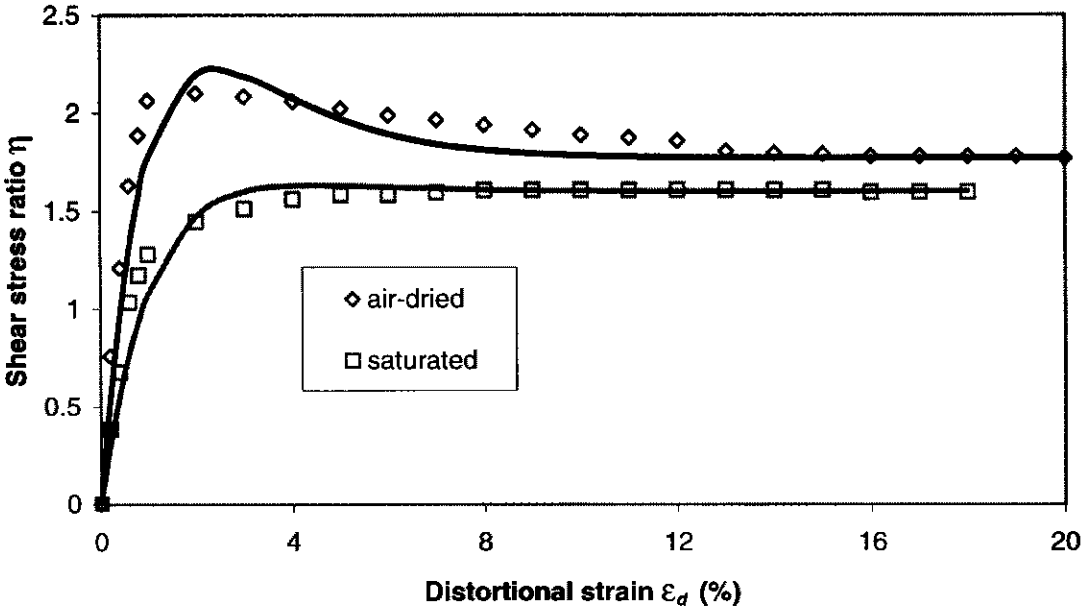

(a) Distortional behaviour of a decomposed granite soil

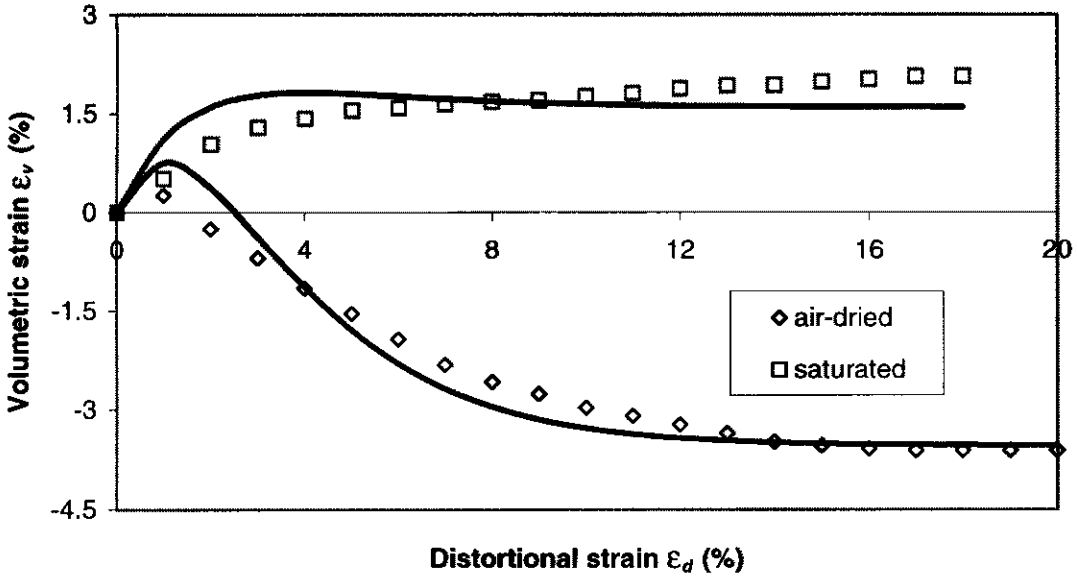

(b) Volumetric behaviour of a decomposed granite soil

Fig. 11.15 Stress and strain behaviour of a decomposed granite soil (test data after Lee *et al*, 1995)

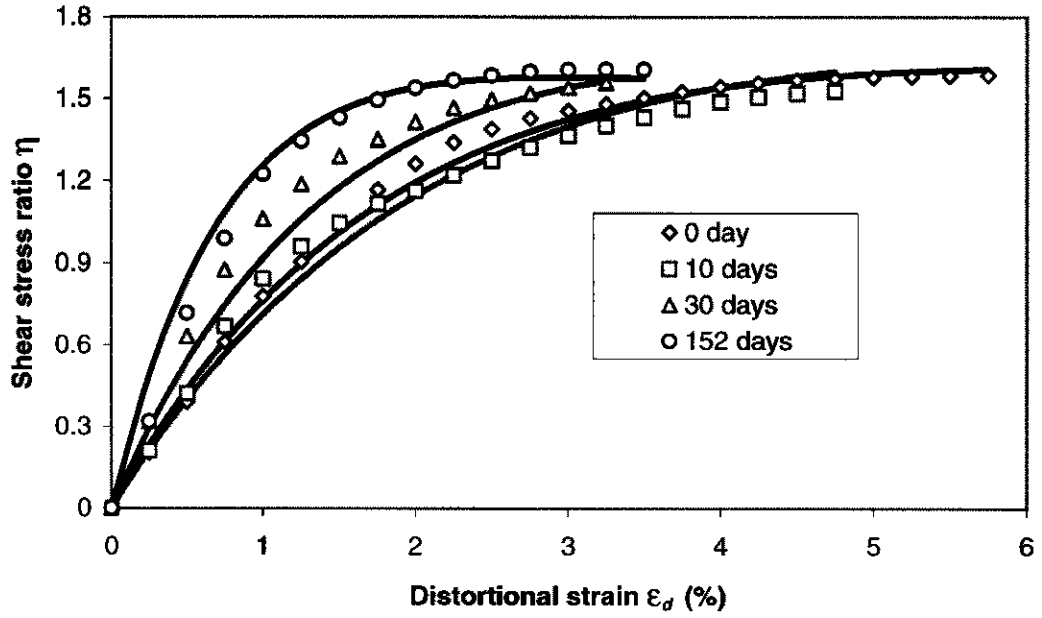

(a) Distortional behaviour of aged Ham River sand

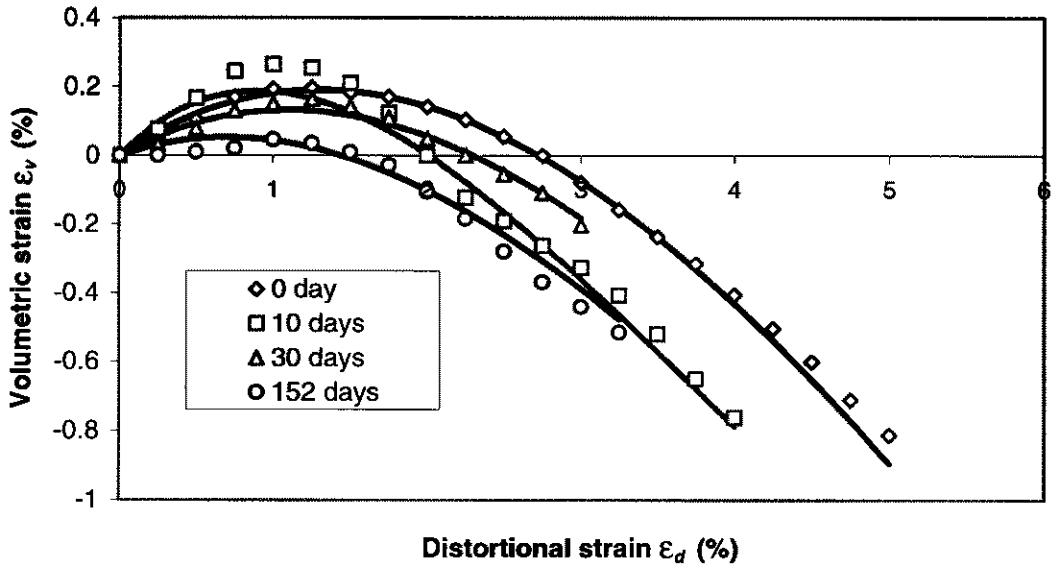

(b) Volumetric behaviour of aged Ham River sand

Fig. 11.16 The effect of consolidation age on stress-strain behaviour of Ham River sand (test data after Daramola,1980)

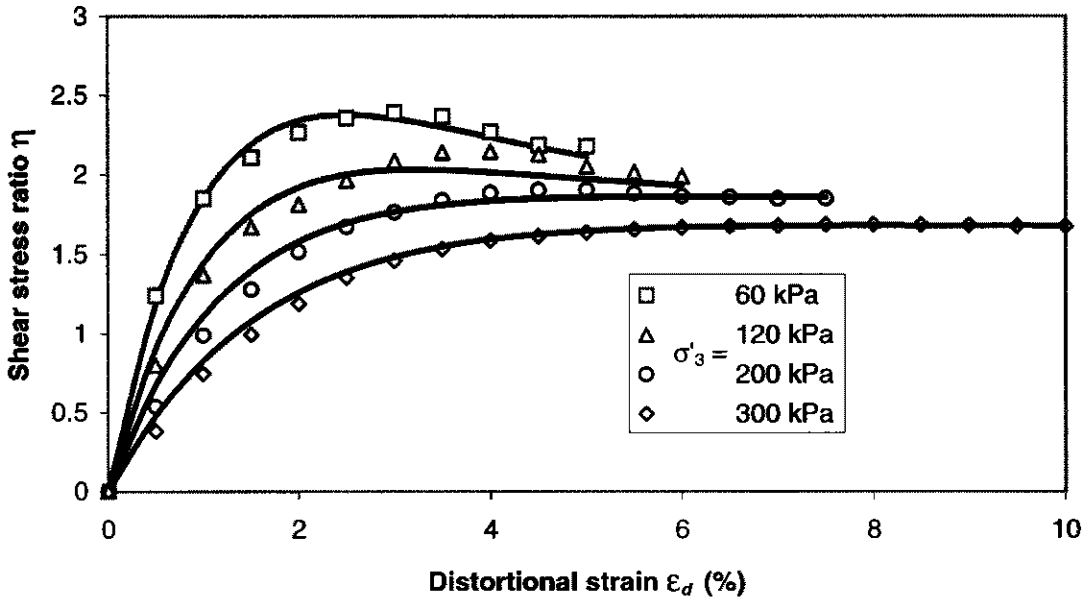

(a) Distortional behaviour of cemented volcanic soil

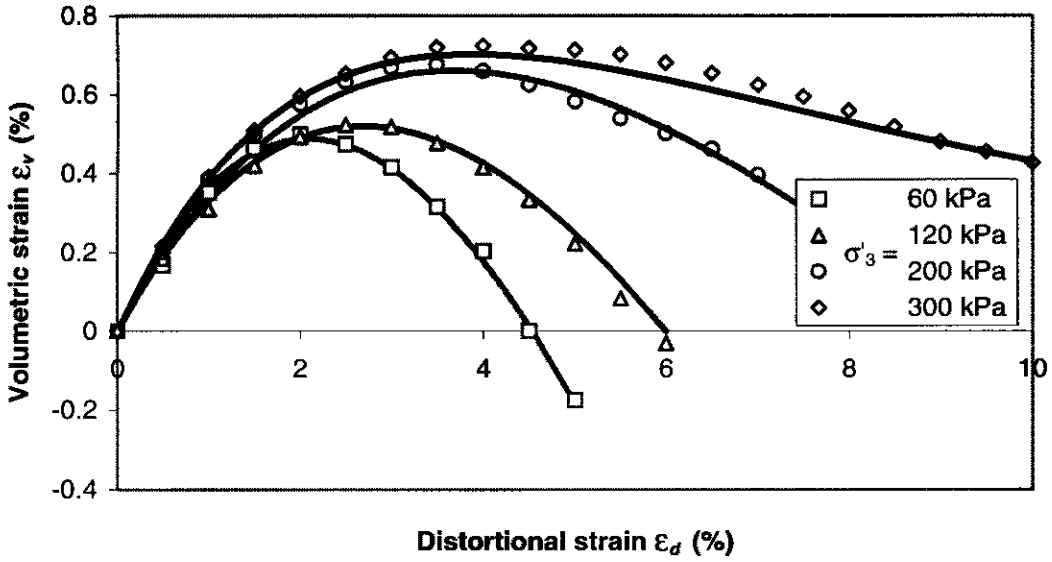

(b) Volumetric behaviour of cemented volcanic soil

Fig. 11.17 Stress-strain behaviour of cemented volcanic soil (test data after O'Rourke *et al*,1988)

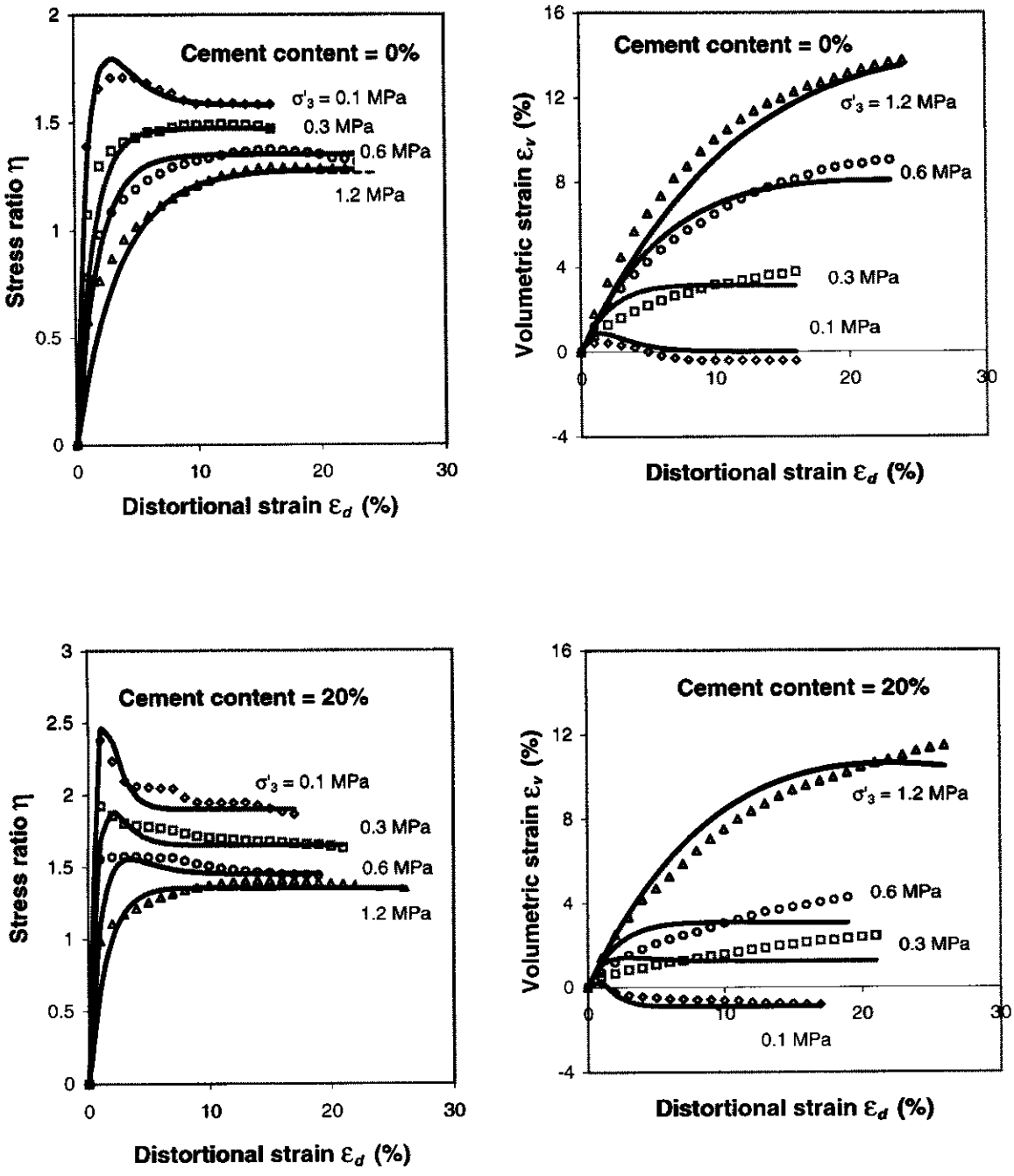

Fig. 11.18 Stress-strain behaviour of an artificially cemented carbonate sand (test data after Huang, 1994)

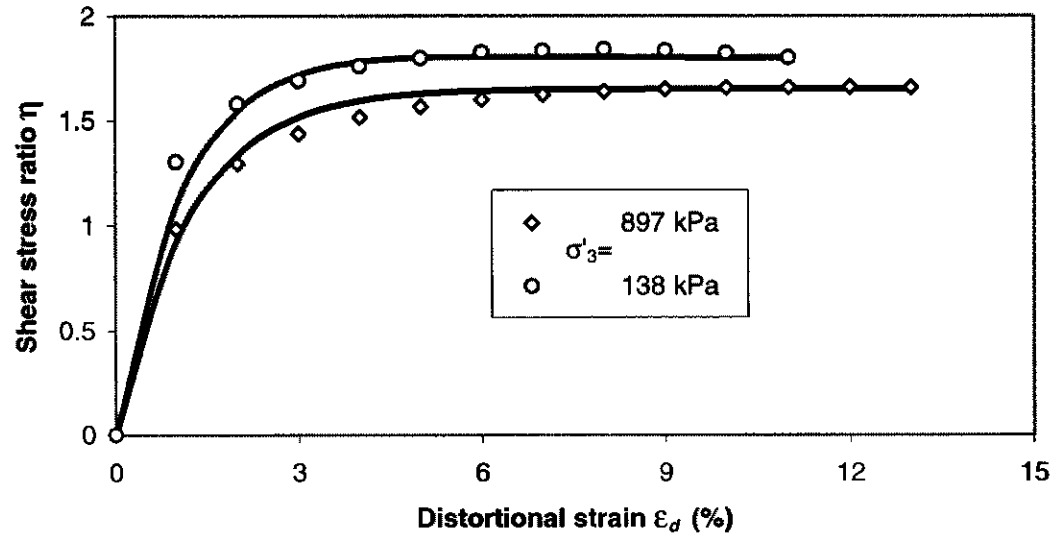

(a) Distortional behaviour of Bass strait carbonate sand

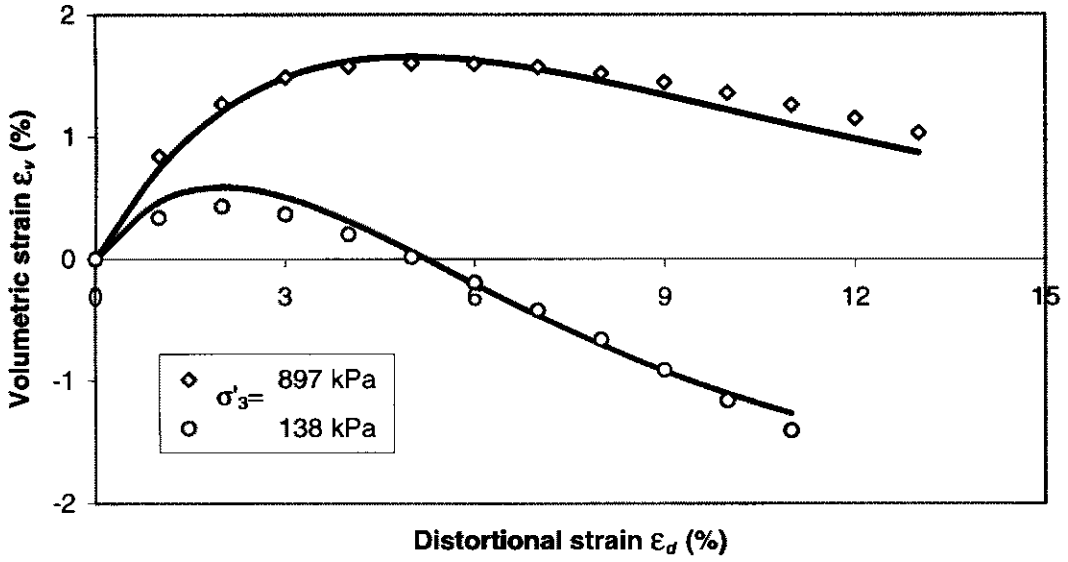

(b) Volumetric behaviour of Bass strait carbonate sand

Fig. 11.19 Stress-strain behaviour of Bass strait carbonate sand (test data after Poulos *et al*, 1982)

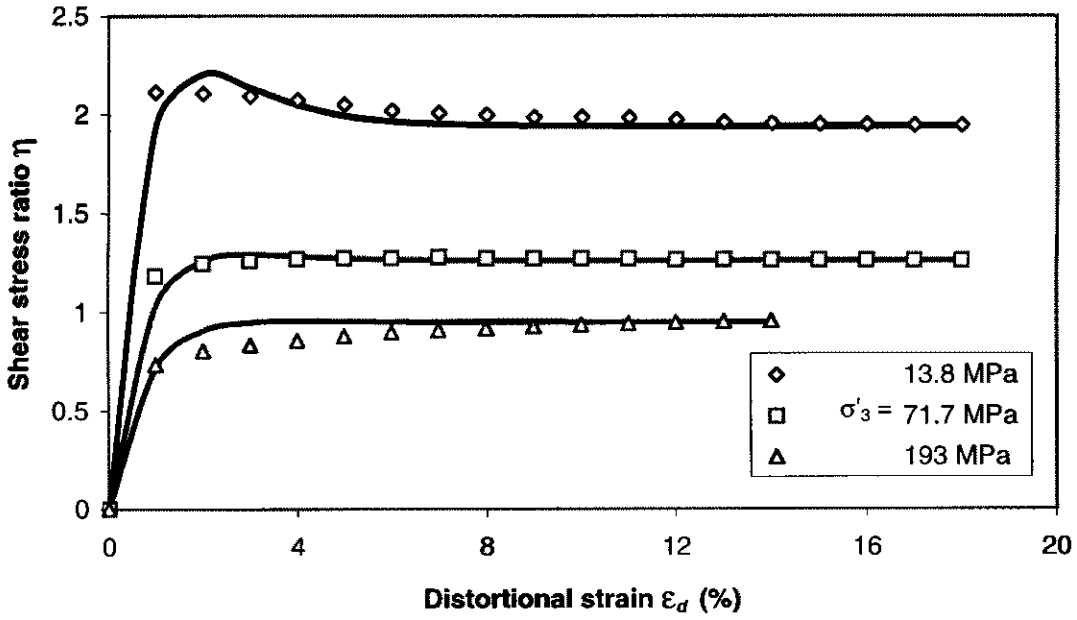

(a) Distortional behaviour of a granular rock

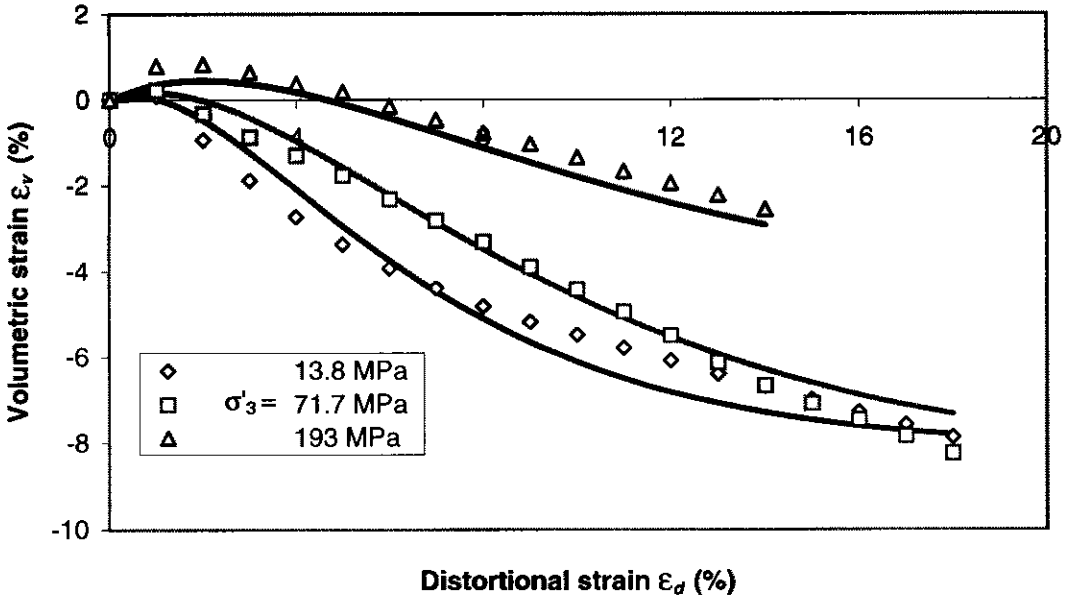

(b) Volumetric behaviour of a granular rock

Fig. 11.20 Stress-strain behaviour of a granular rock (test data after Michelis *et al*, 1981)

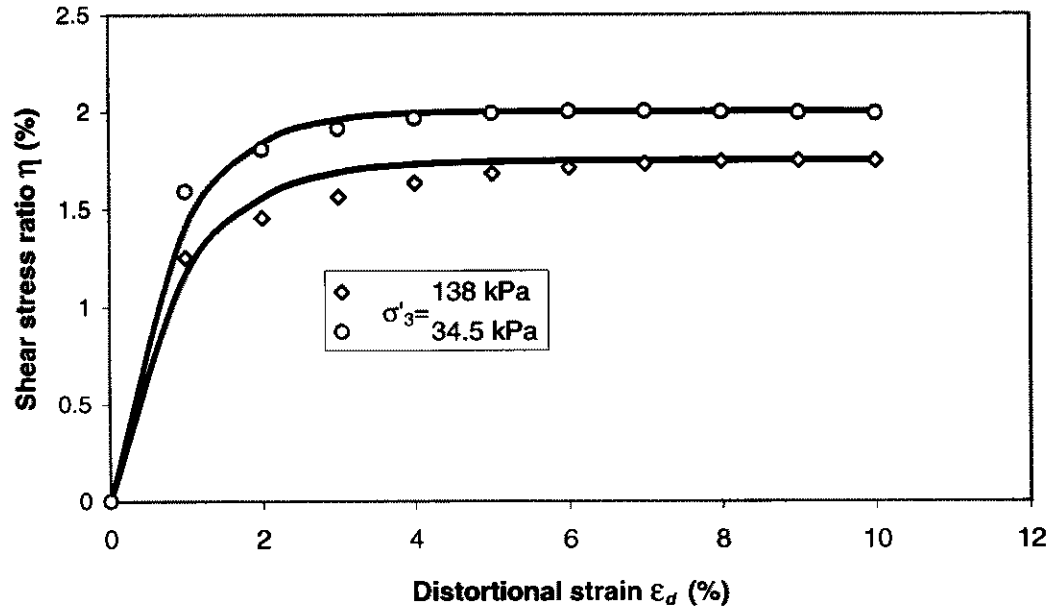

(a) Distortional behaviour of uncompacted ballast

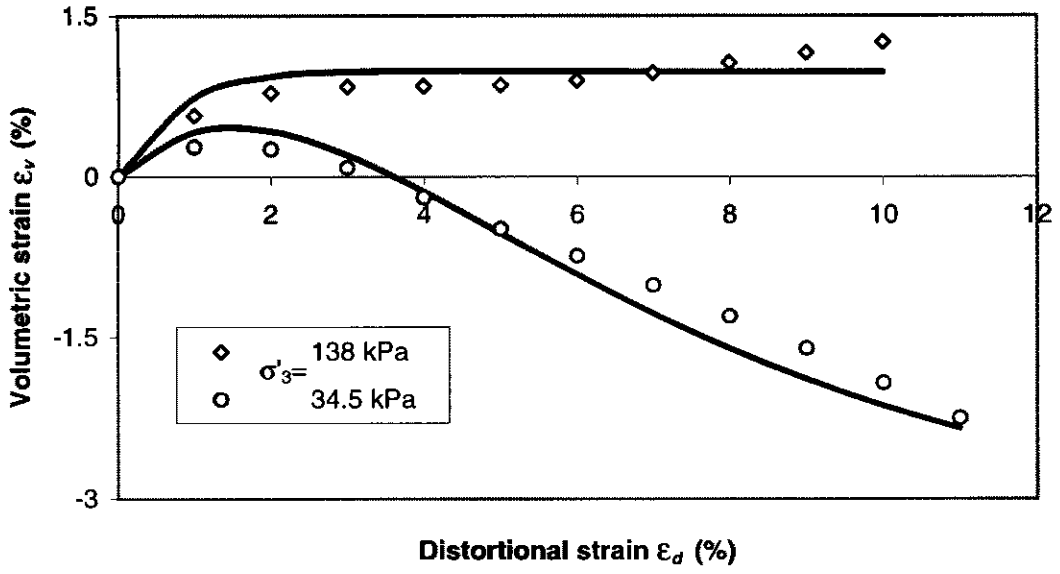

(b) Volumetric behaviour of uncompacted ballast

Fig. 11.21 Stress-strain behaviour of uncompacted ballast (test data after Alva-Hurtado *et al*, 1981)

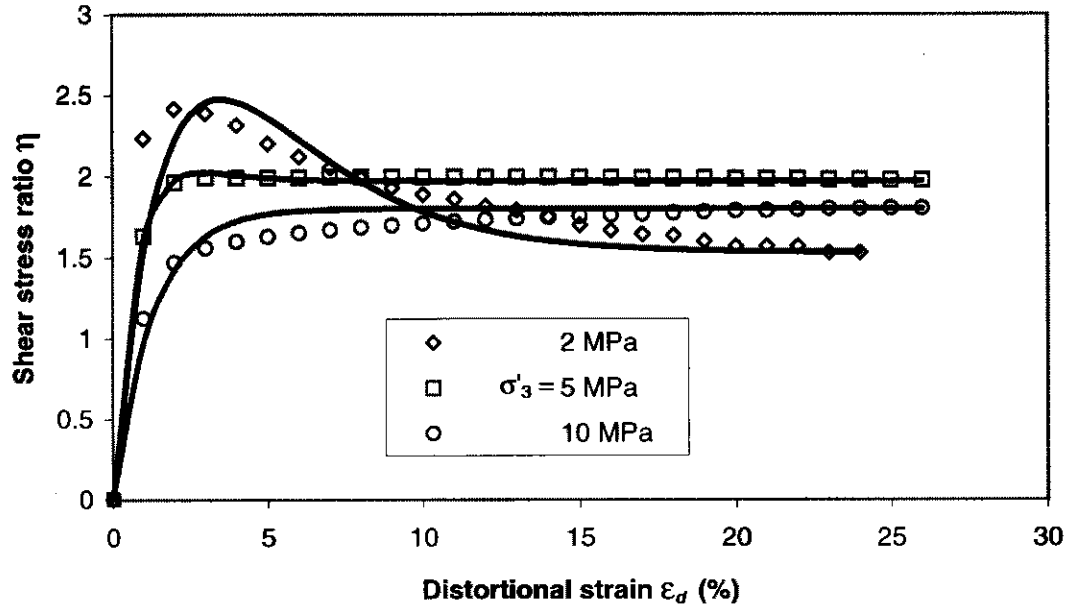

(a) Distortional behaviour of Oolitic limestone

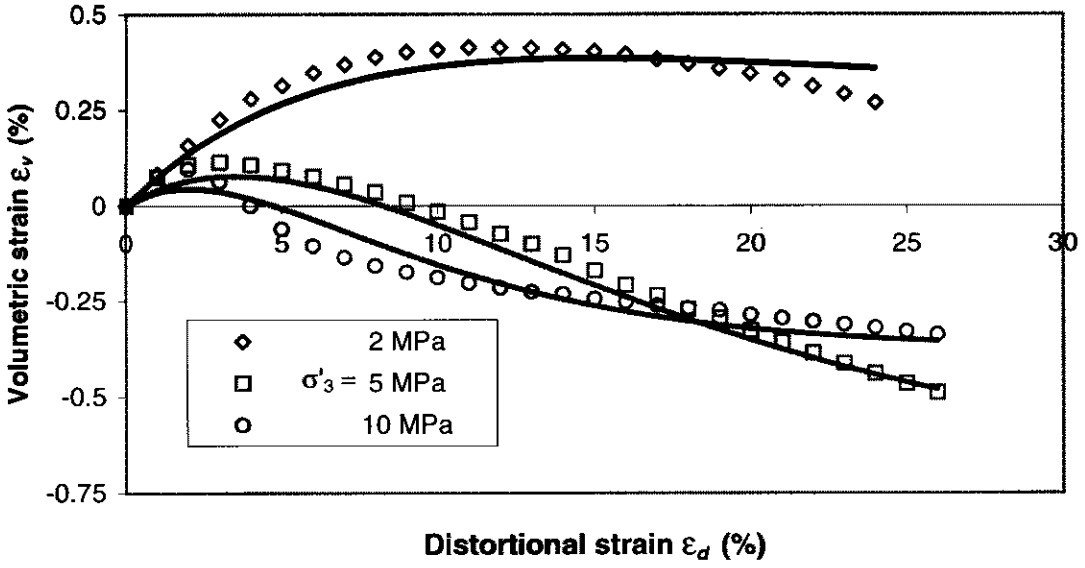

(b) Volumetric behaviour of Oolitic limestone

Fig. 11.22 Stress-strain behaviour of oolitic limestone (test data after Elliott, 1983)

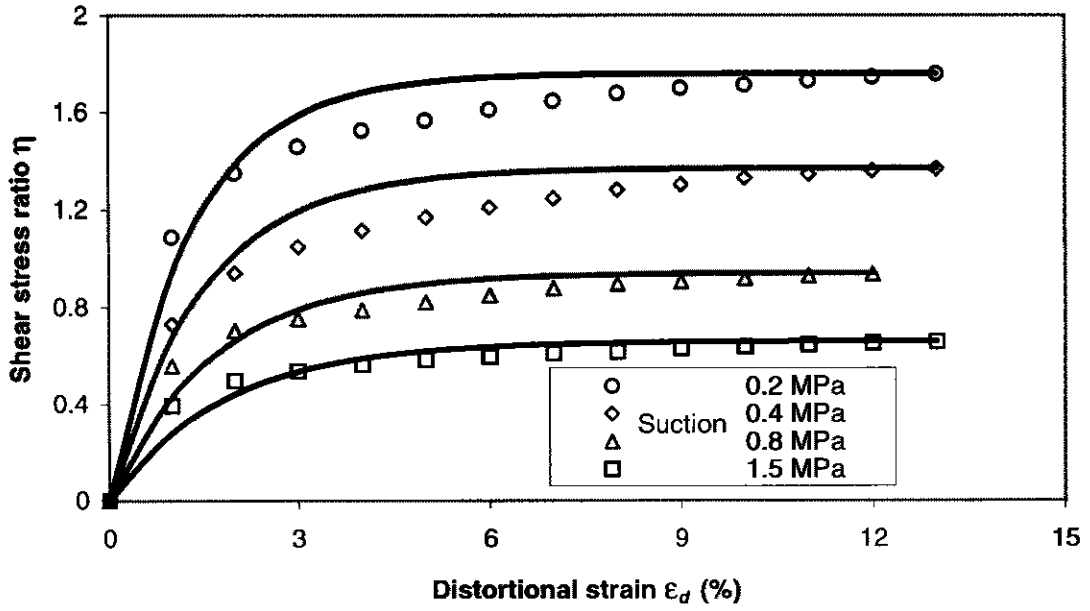

(a) Distortional behaviour of unsaturated compacted silt

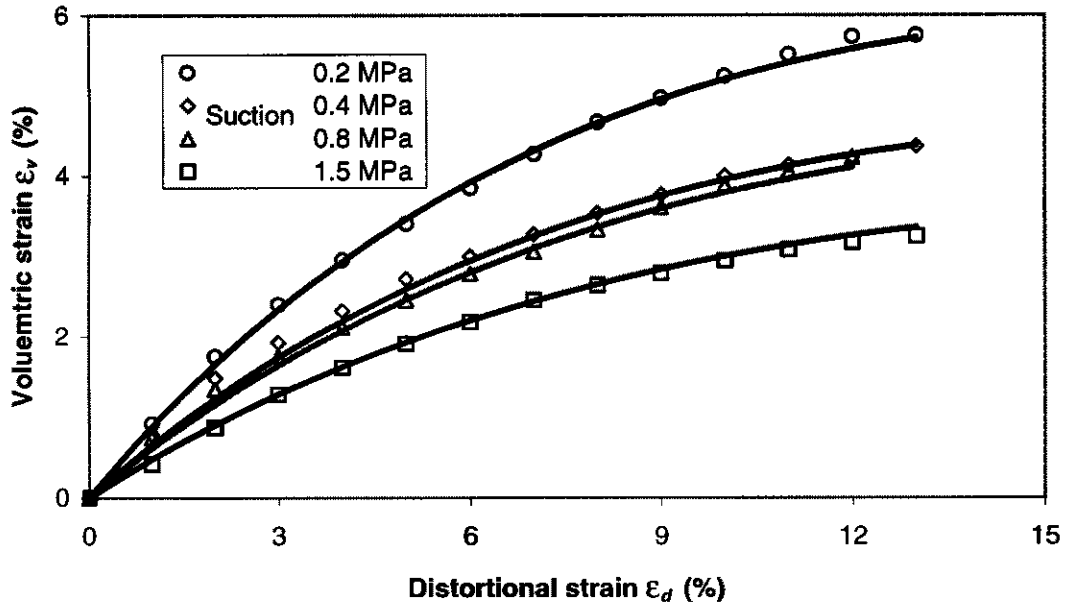

(b) Volumetric behaviour of unsaturated compacted silt

Fig. 11.23 Stress-strain behaviour of unsaturated compacted silt (test data after Cui *et al*, 1996)

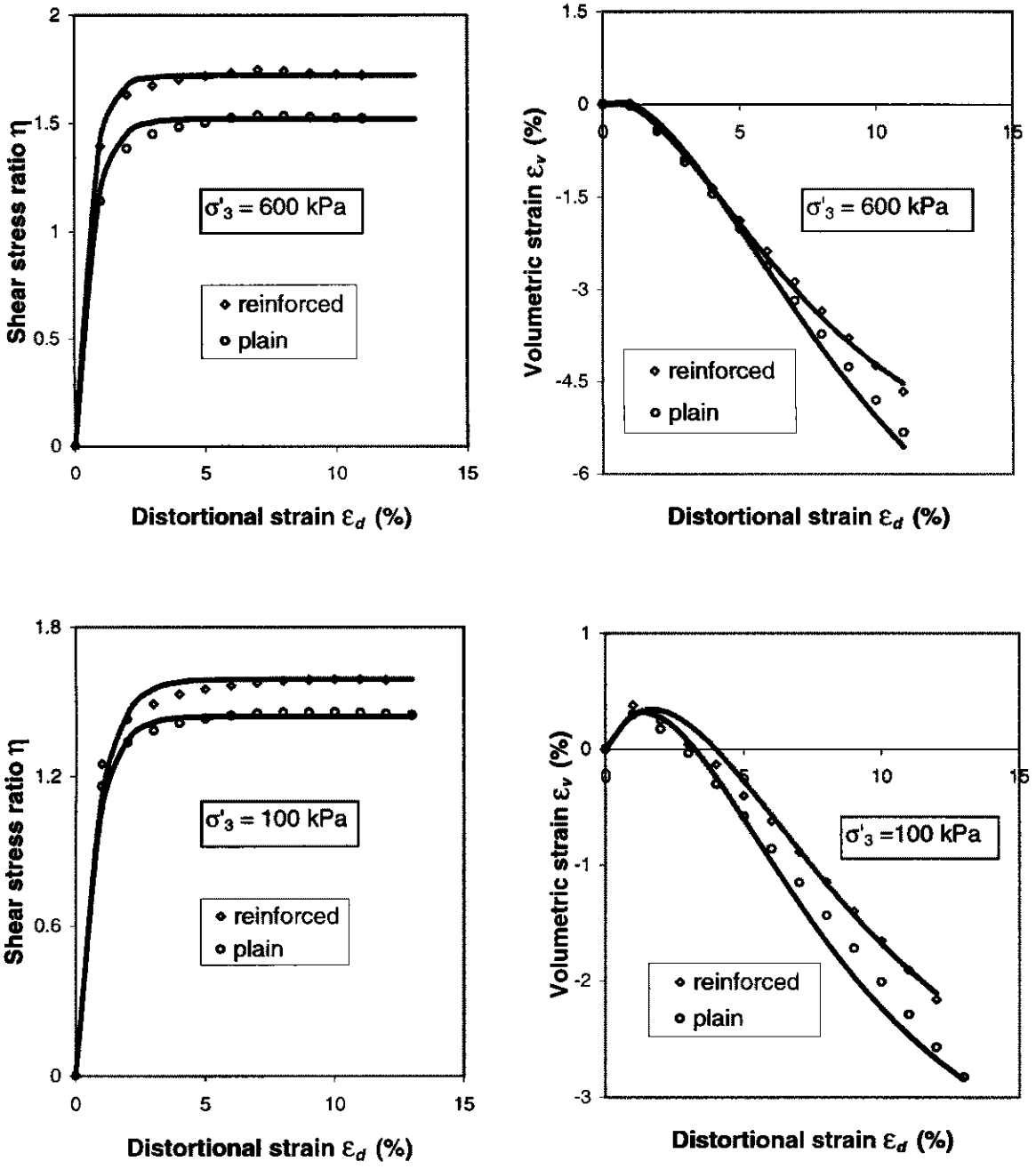

Fig. 11.24 Stress and strain behaviour of sand reinforced with steel fibers (test data after Michalowski *et al*, 1996)

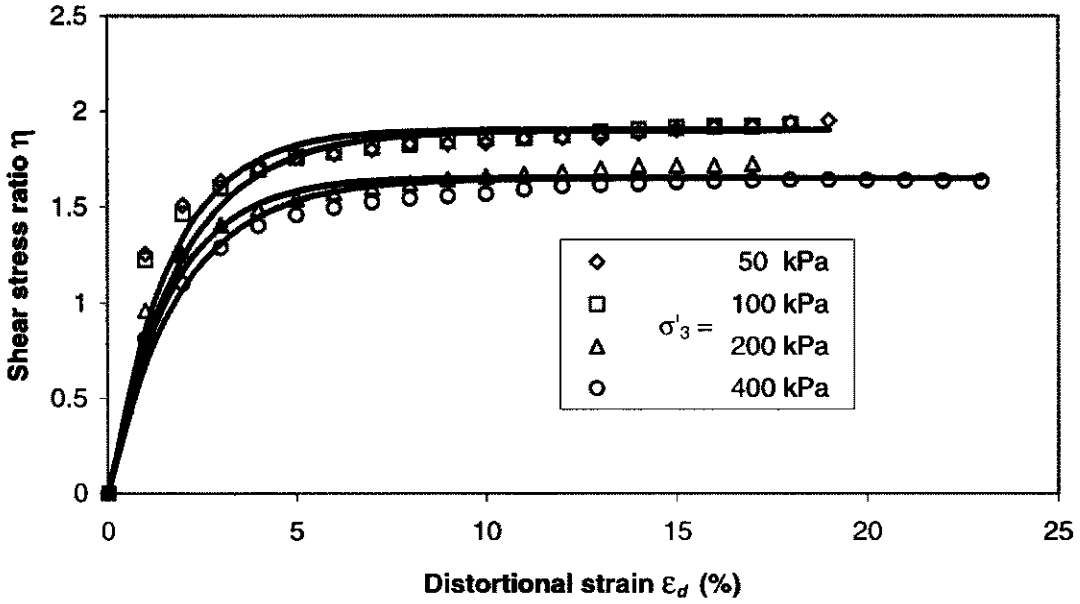

(a) Distortional behaviour of reinforced gravel

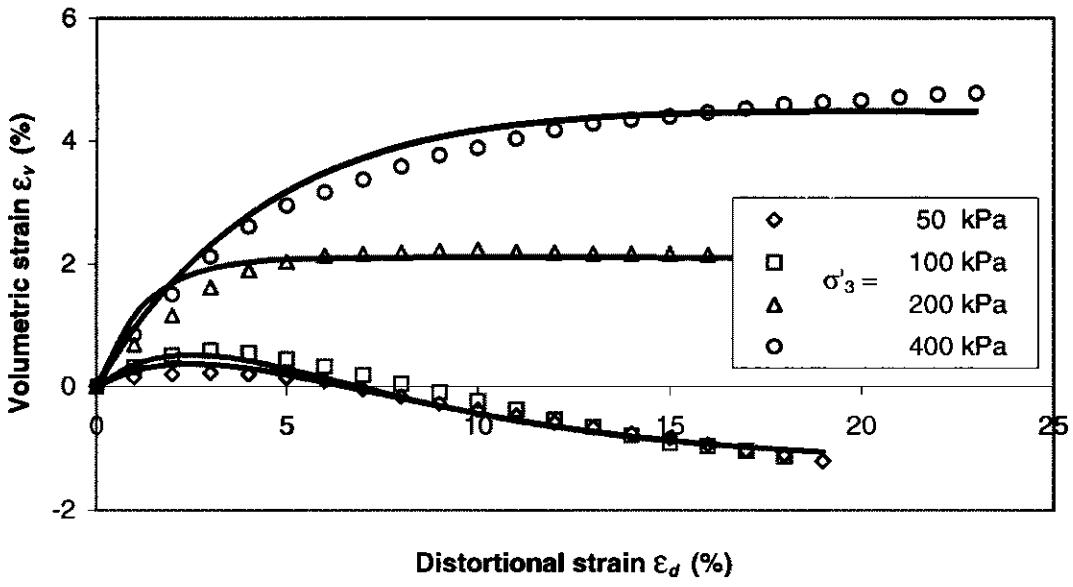

(b) Volumetric behaviour of reinforced gravel

Fig. 11.25 Stress and strain behaviour of reinforced gravel (test data after Cazzuffi *et al*, 1994)

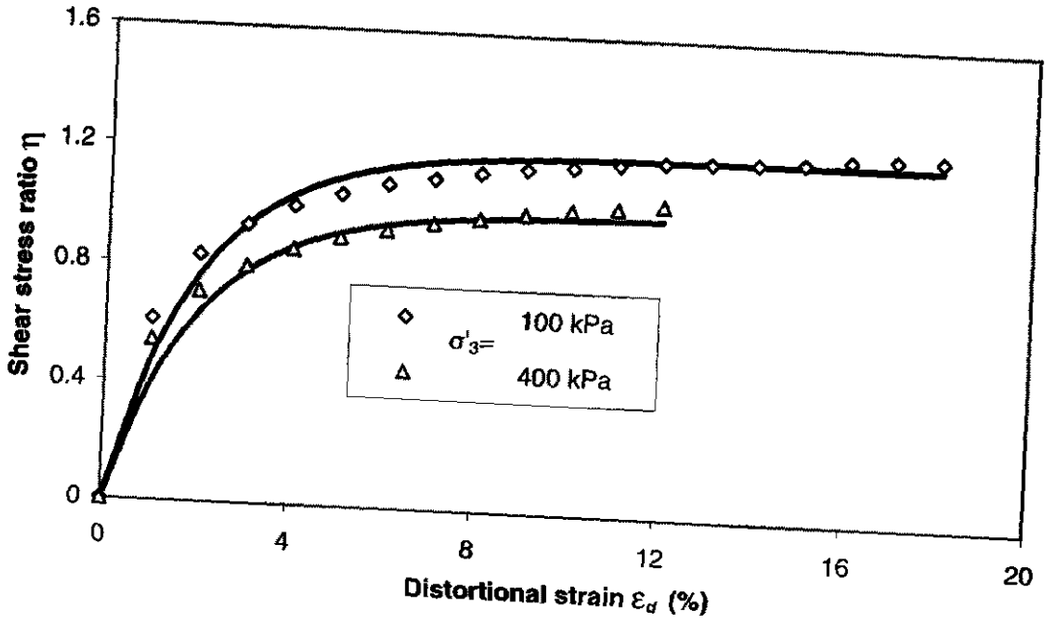

(a) Distortional behaviour of wheat

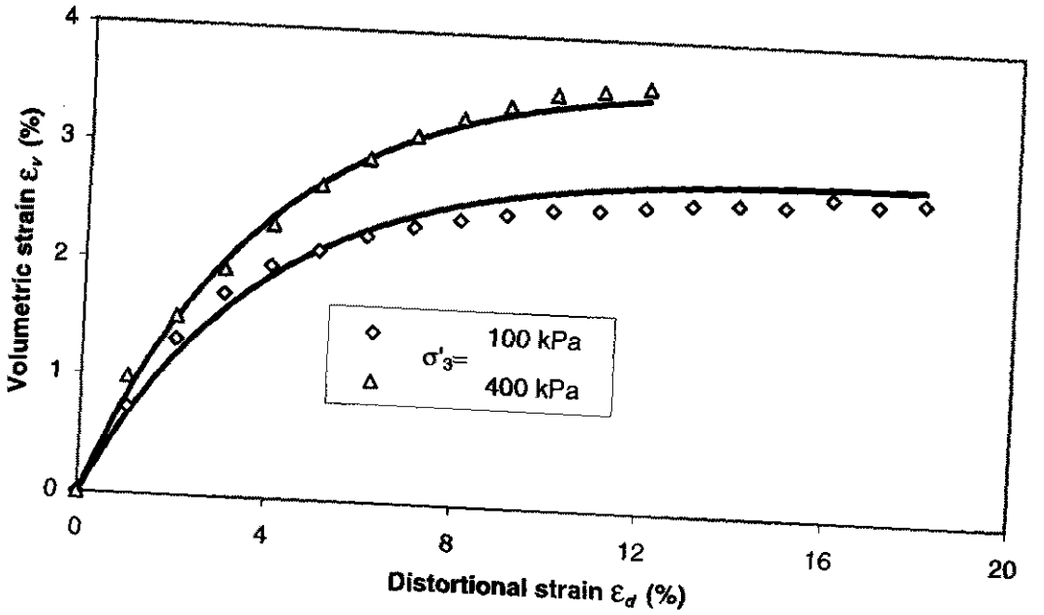

(b) Volumetric behaviour of wheat

Fig. 11.26 Stress-strain behaviour of wheat (test data after Kolymbas *et al*,1990)

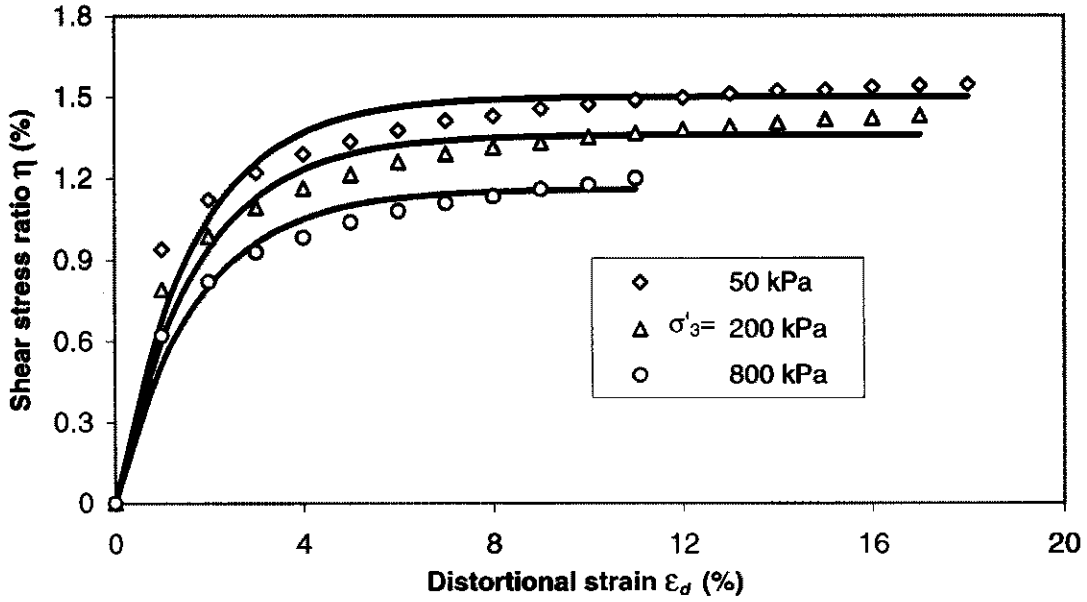

(a) Distortional behaviour of sugar

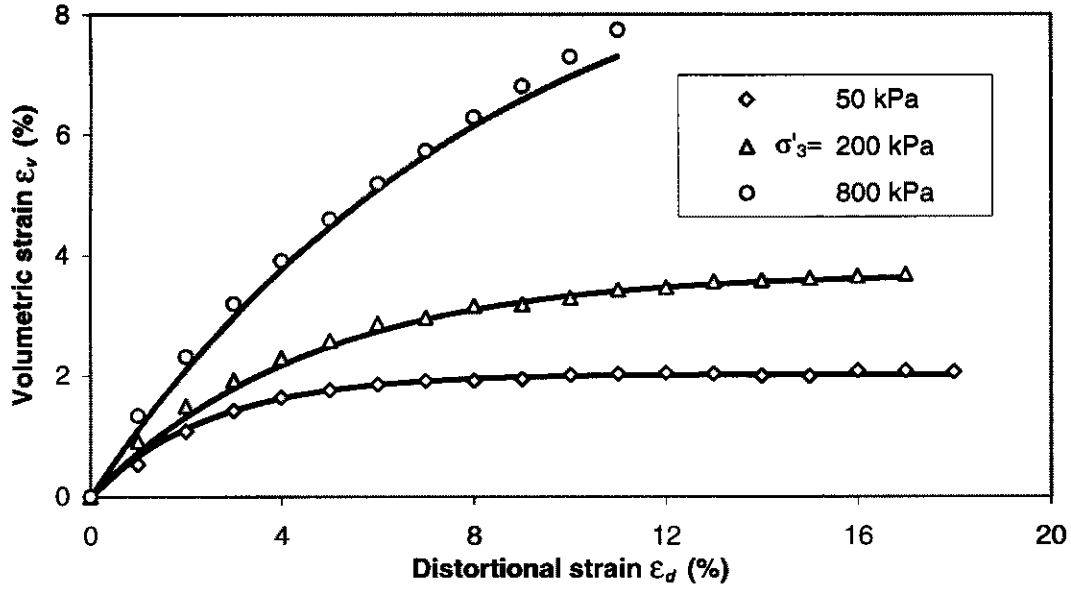

(b) Volumetric behaviour of sugar

Fig. 11.27 Stress-strain behaviour of sugar
(test data after Kolymbas *et al*,1990)

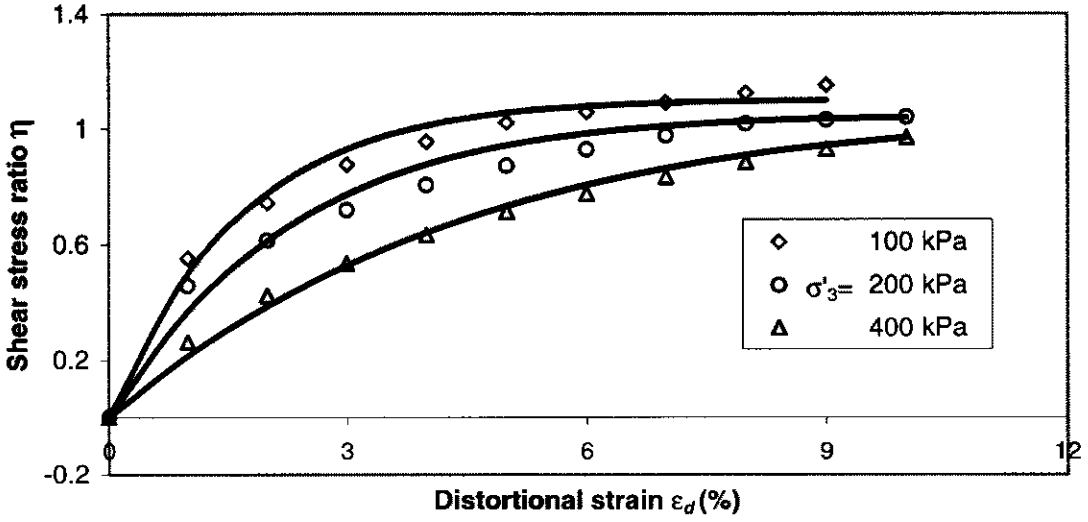

(a) Distortional behaviour of rape

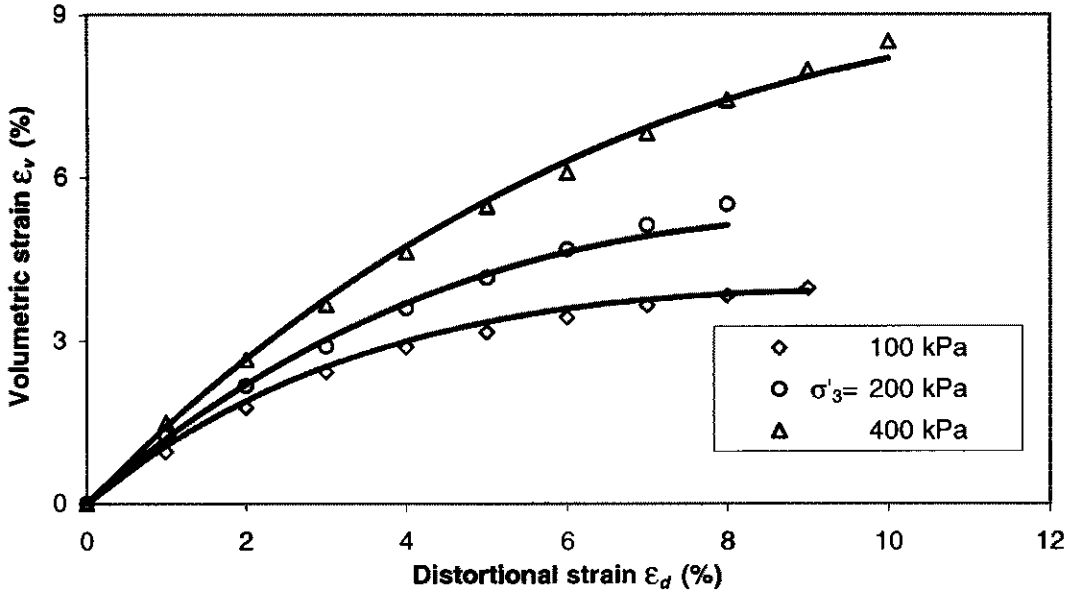

(b) Volumetric behaviour of rape

Fig. 11.28 Stress-strain behaviour of rape (test data after Kolymbal *et al*, 1990)

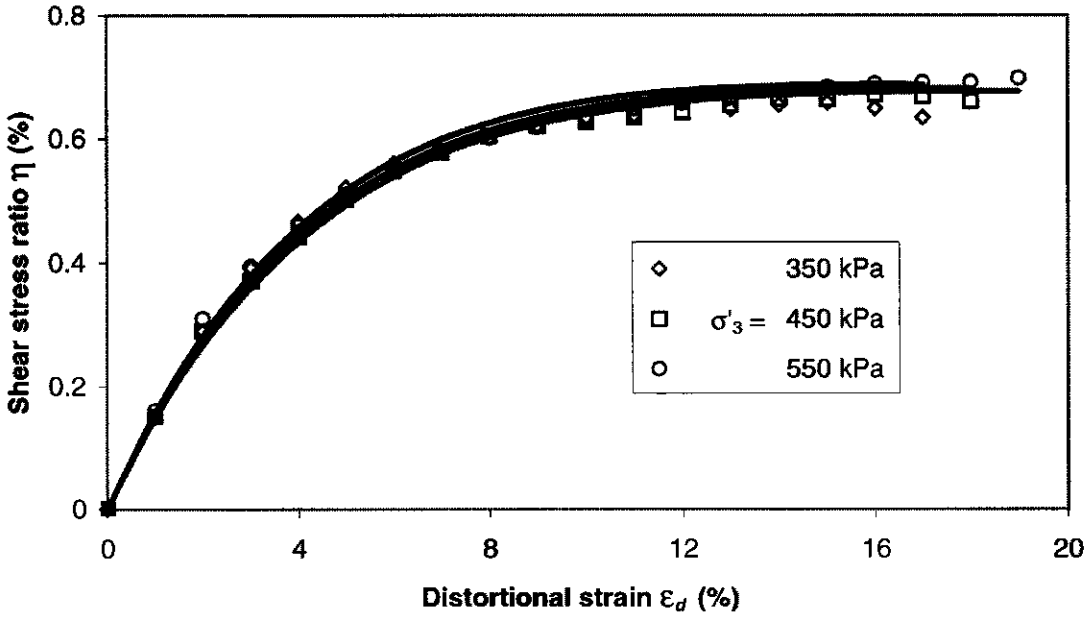

(a) Distortional behaviour of tire chips

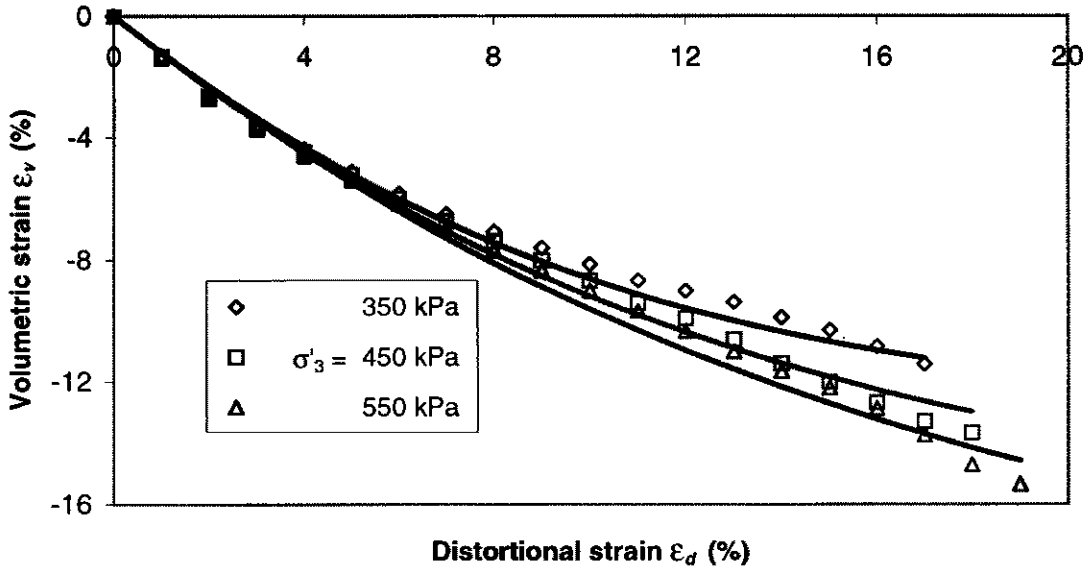

(b) Volumetric behaviour of tire chips

Fig. 11.29 Stress-strain behaviour of tire chips (test data after Wu *et al*, 1997)

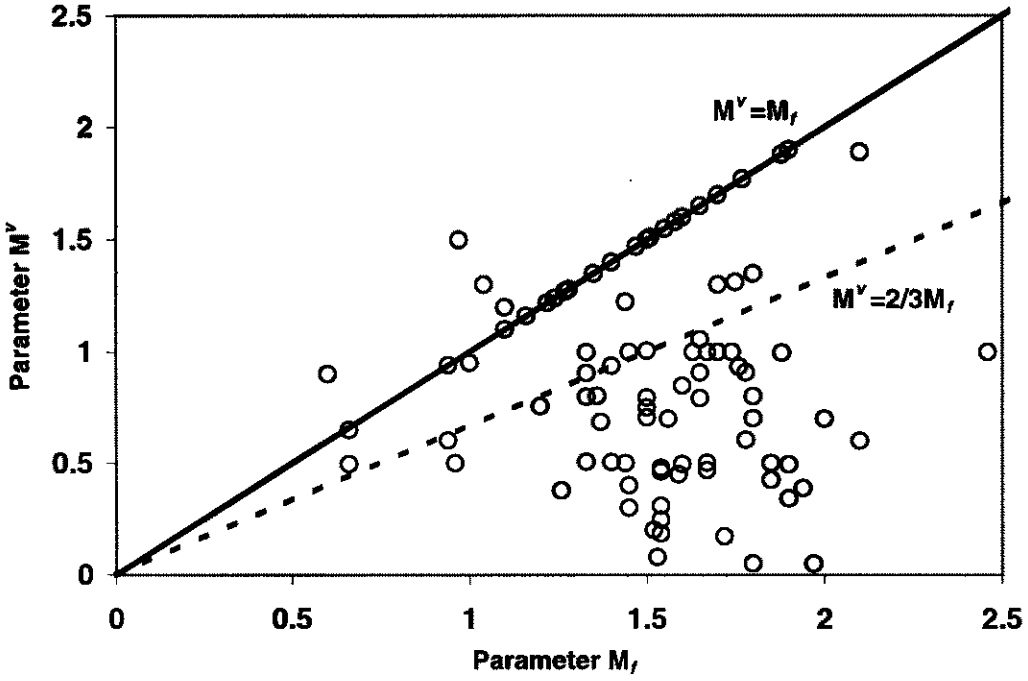

Fig. 11.30 Correlation between parameters M_f and M^v

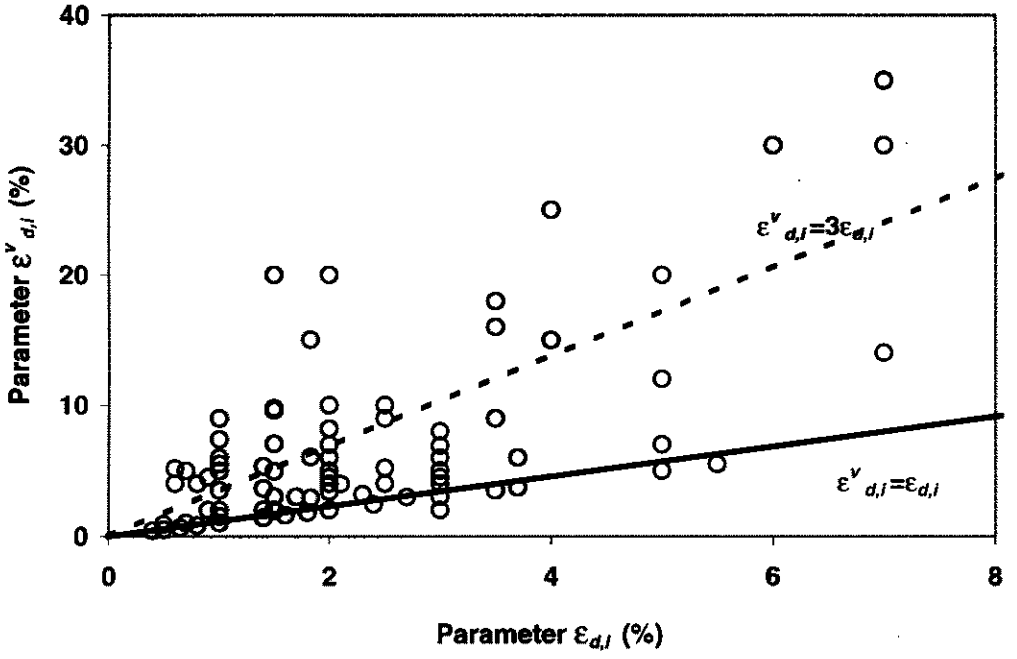

Fig. 11.31 Correlation between parameters $\varepsilon_{d,i}$ and $\varepsilon^v{}_{d,i}$

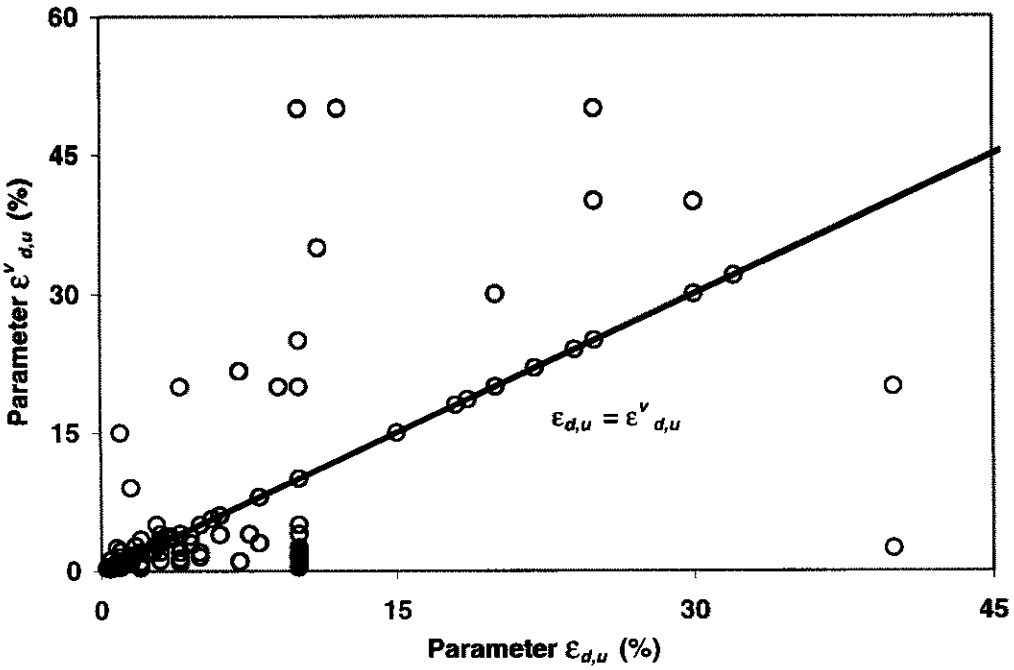

Fig. 11.32 Correlation between parameters $\varepsilon_{d,u}$ and $\varepsilon^{v}_{d,u}$

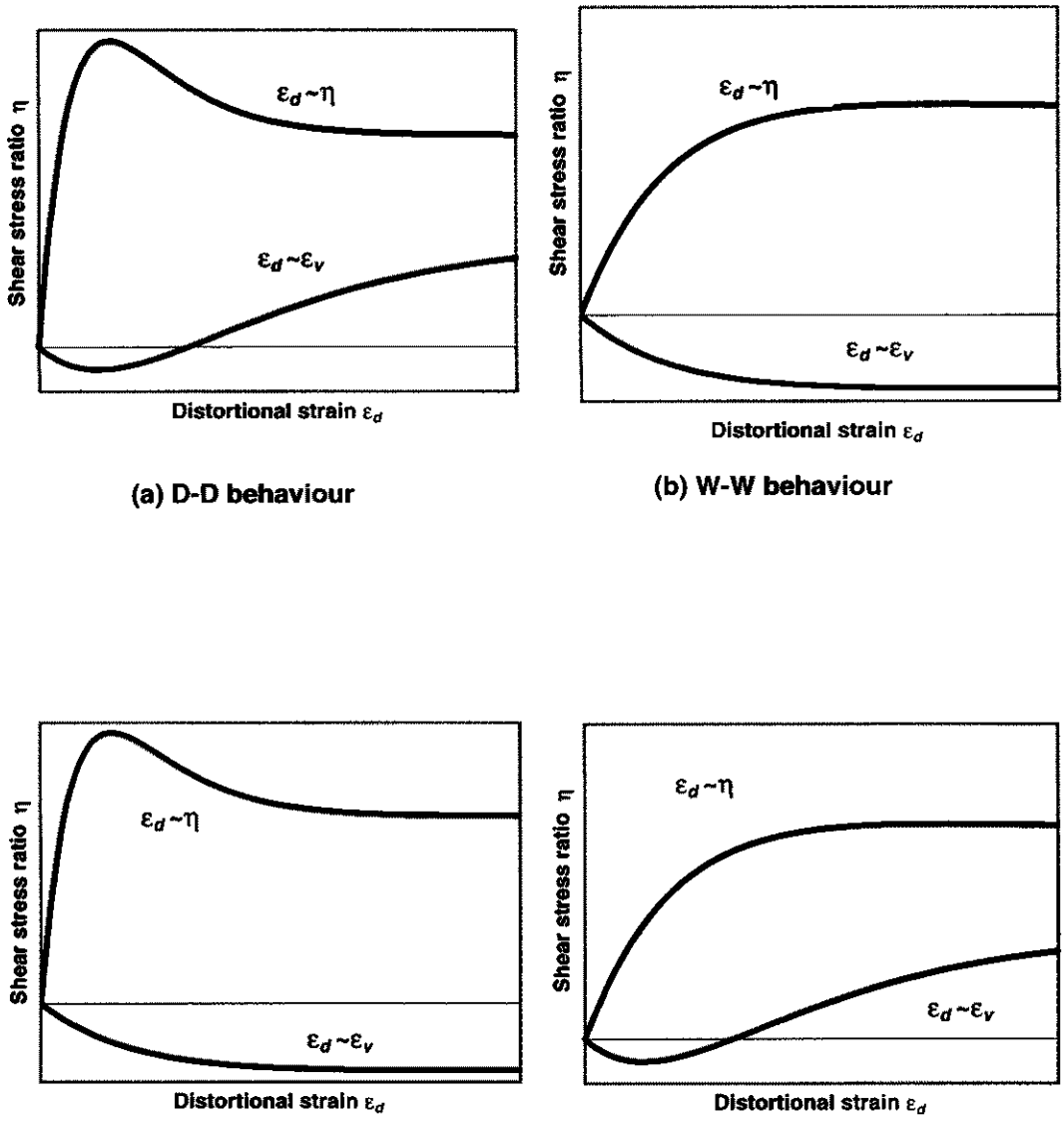

Fig. 11.33 Four typical patterns of behaviour for frcitonal materials

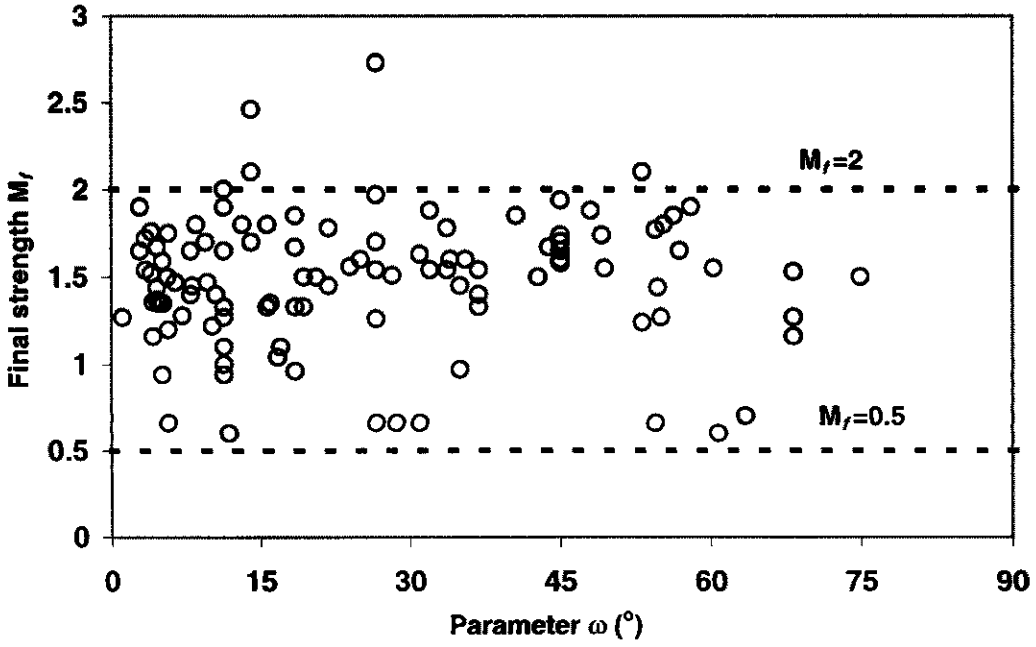

Fig. 11.34 Variation of parameters ω

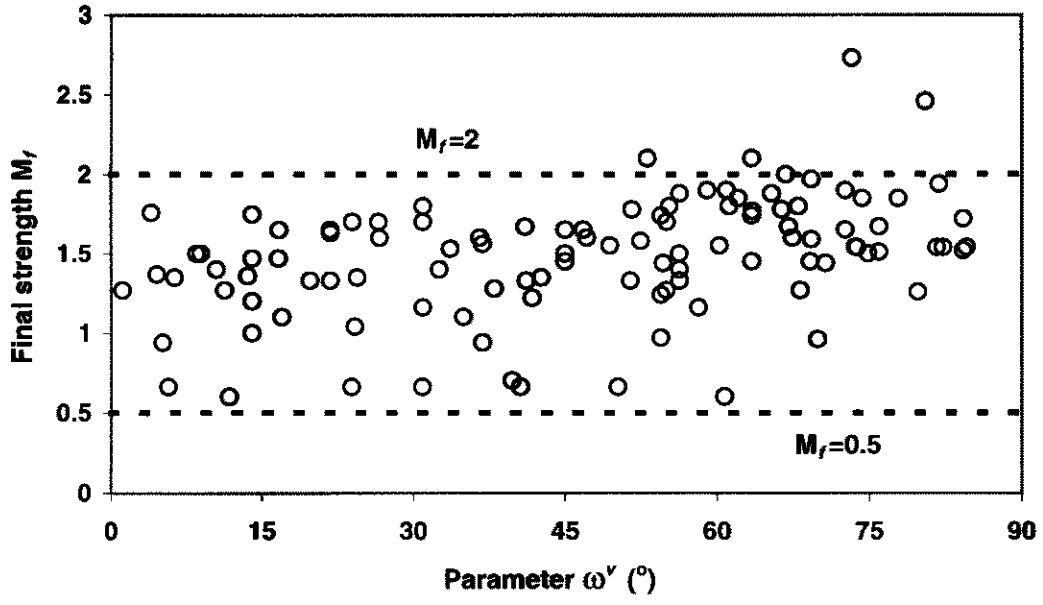

Fig. 11.35 Variation of parameters ω^v

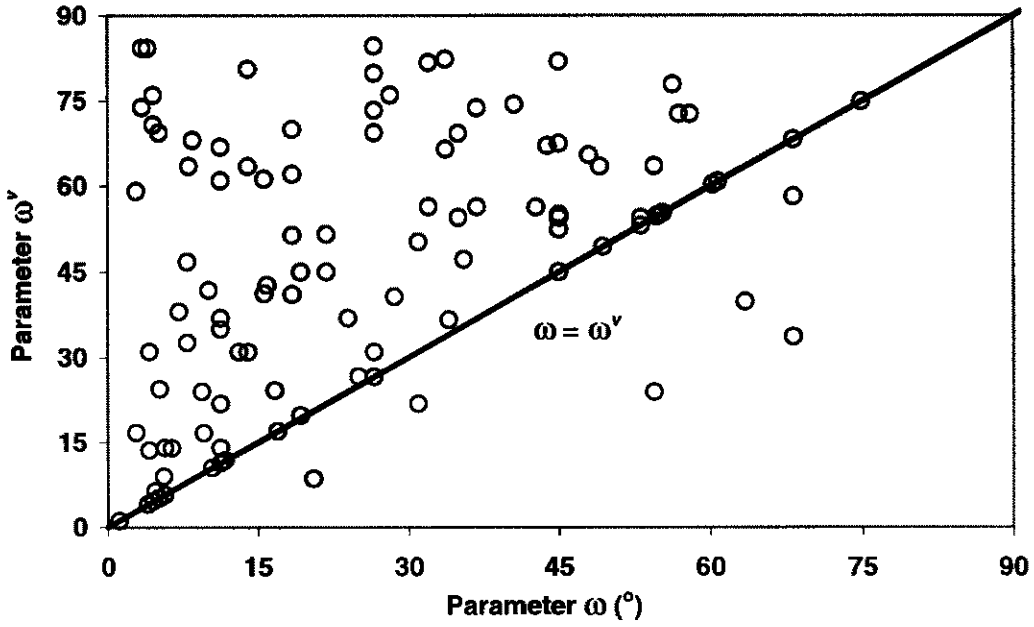

Fig. 11.36 Correlation between parameters ω and ω^v

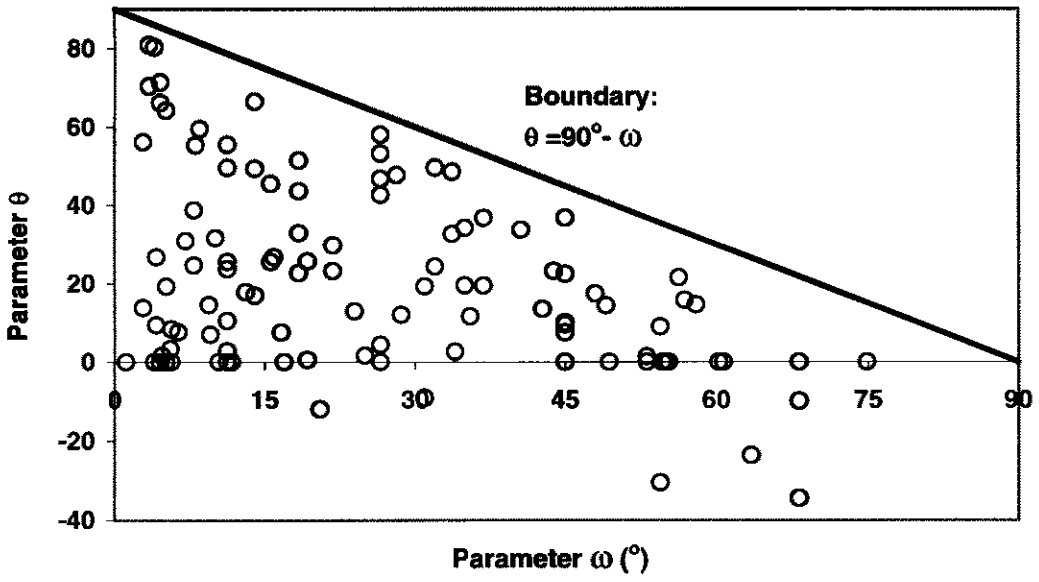

Fig. 11.37 Correlation between parameters θ and ω

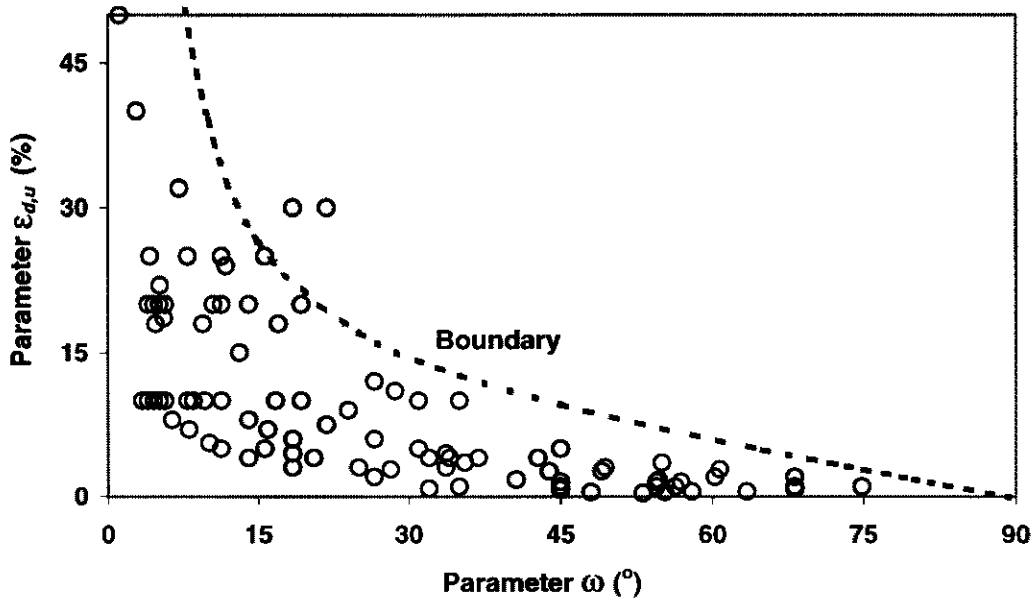

Fig. 11.38 Correlation between parameters ω and $\varepsilon_{d,u}$

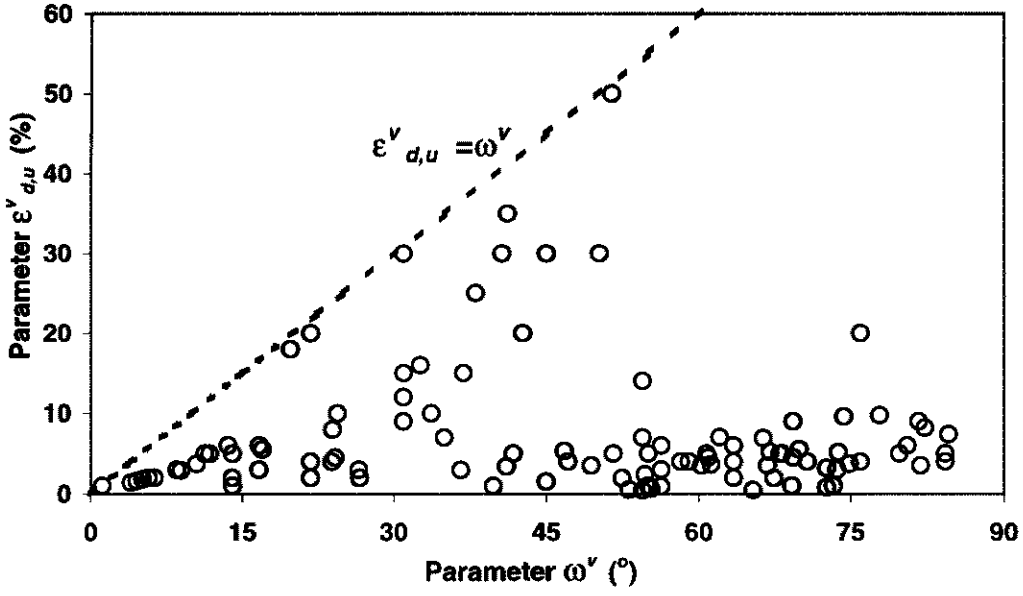

Fig. 11.39 Correlation between parameter ω^{v} and $\varepsilon^{v}_{d,u}$

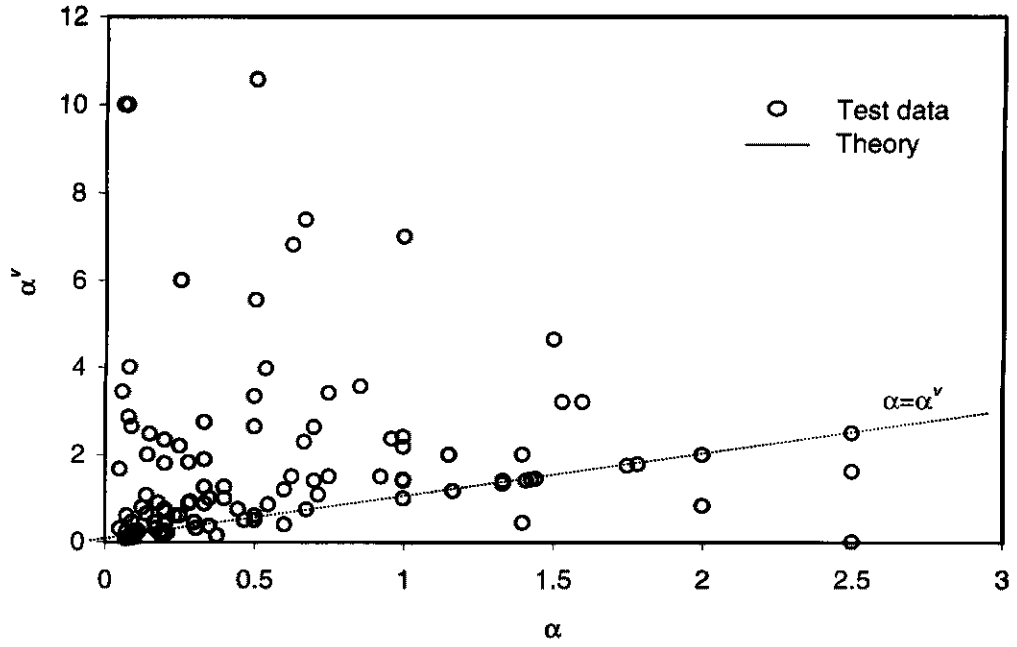

Fig. 11.40 Relationship between two basic material parameters

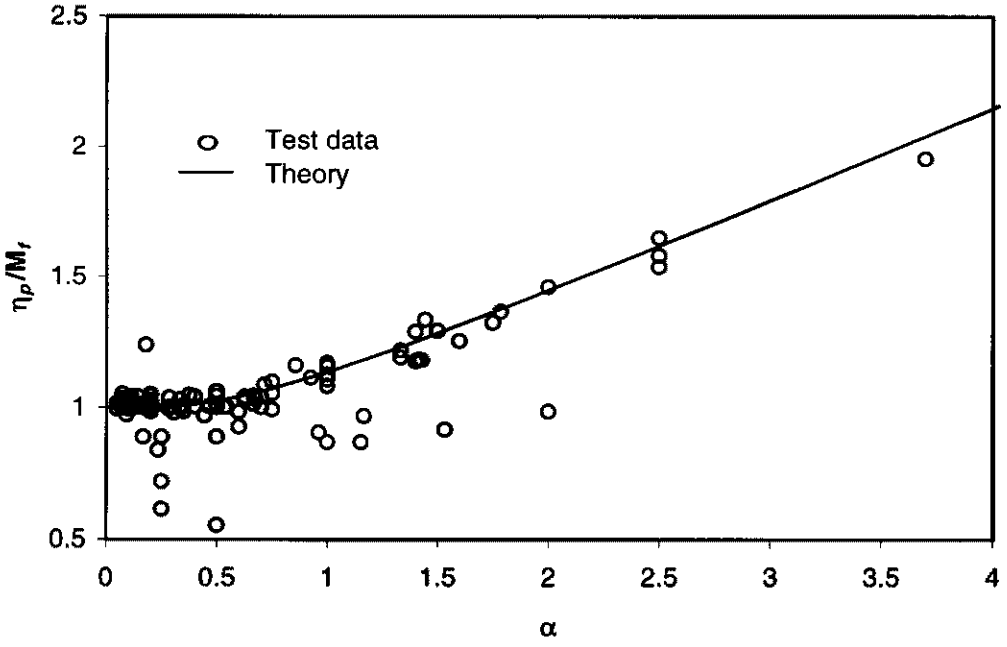

Fig. 11.41 Predicted and measured peak strengths for various geo-materials

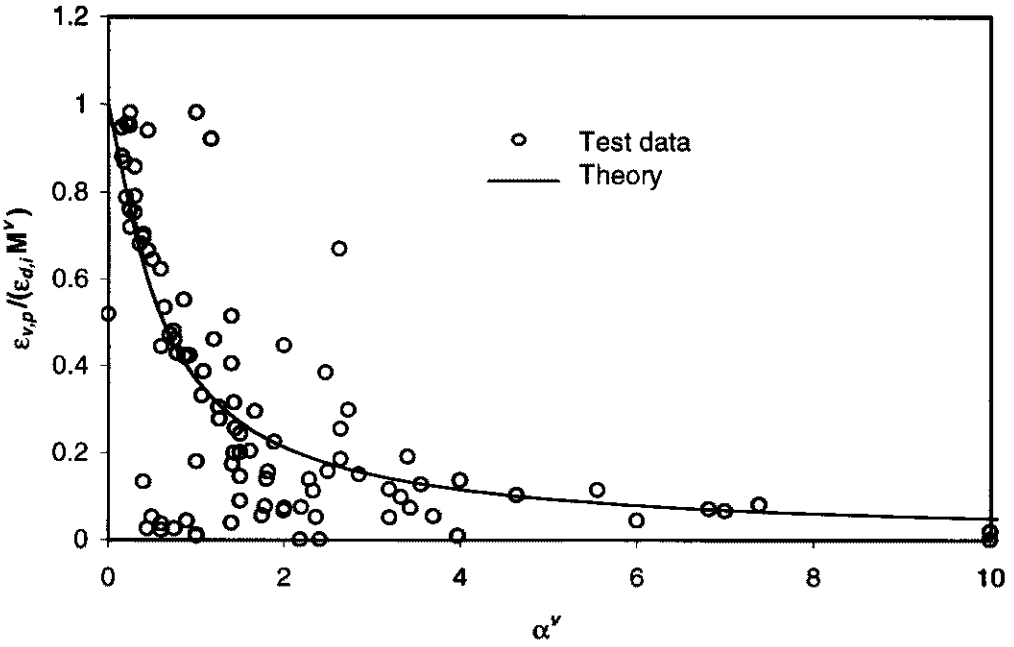

Fig. 11.42 Predicted and measured peak vlumetric strain for various geo-materials

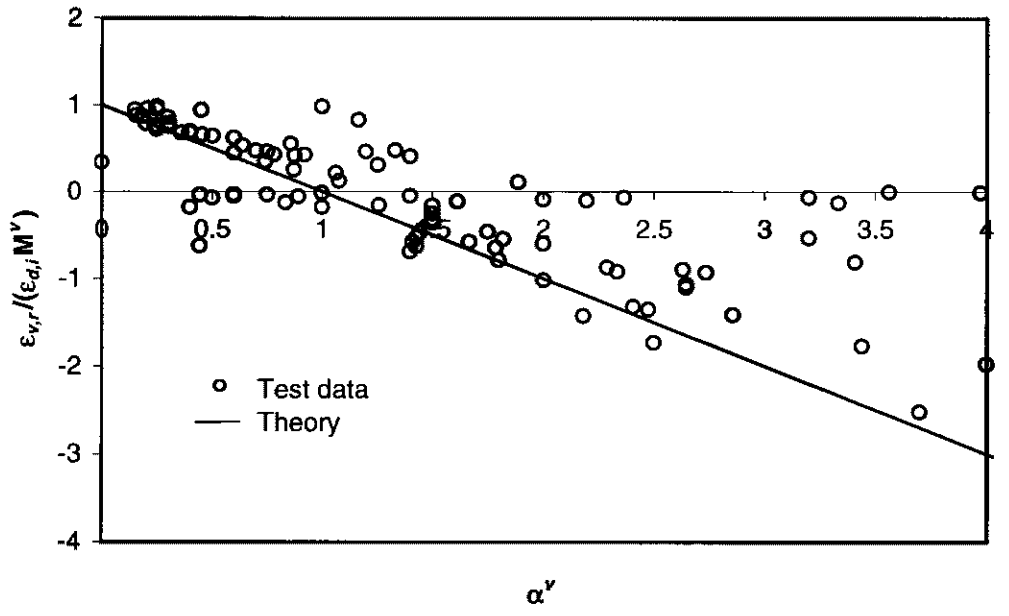

Fig. 11.43 Predicted and measured residual vlumetric strain for various geo-materials

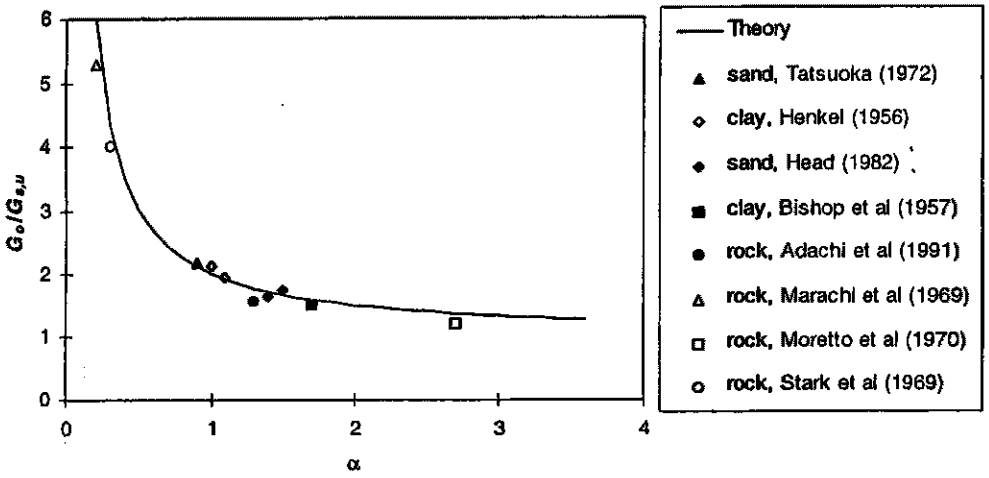

Fig. 11.44 Comparison of predicted and measured peak strengths (After Xu *et al*, 1997)

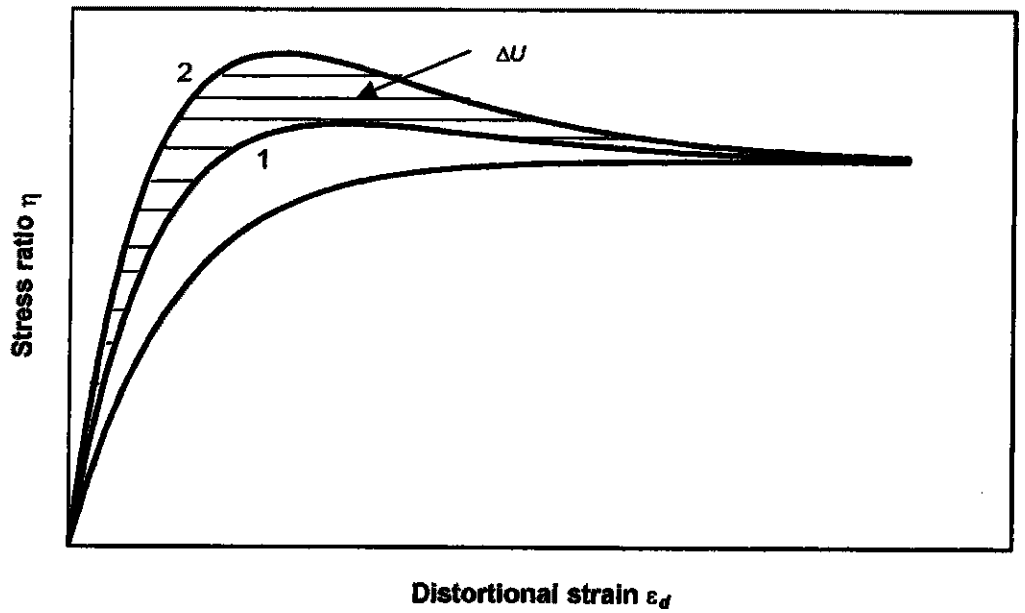

Fig. 11.45 Definition of incremental distortional energy

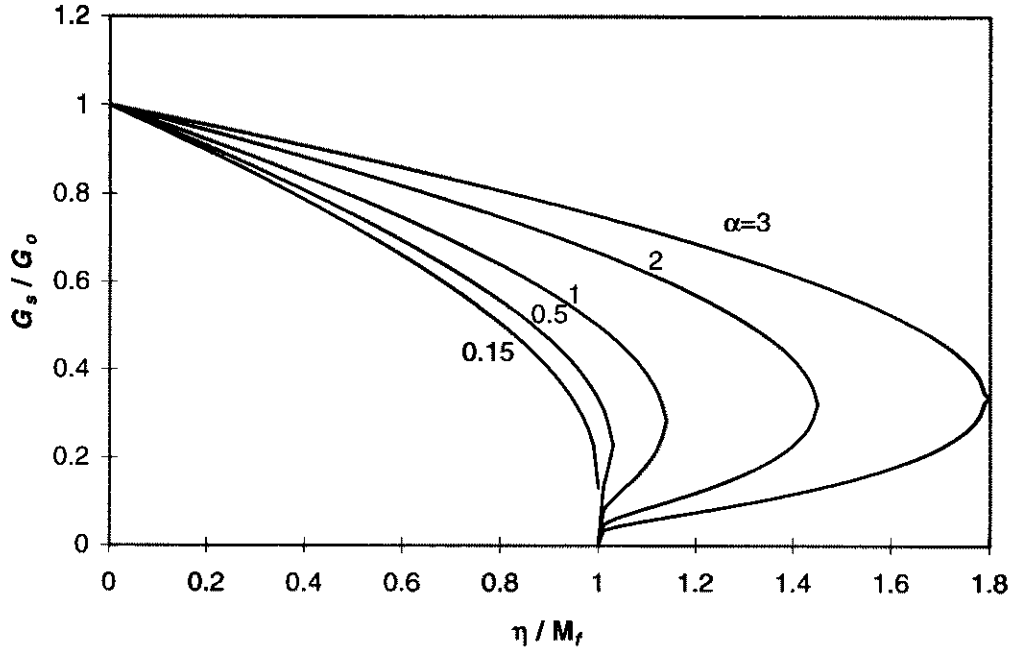

Fig. 11.46 Relationships of G_S/G_o with η/M

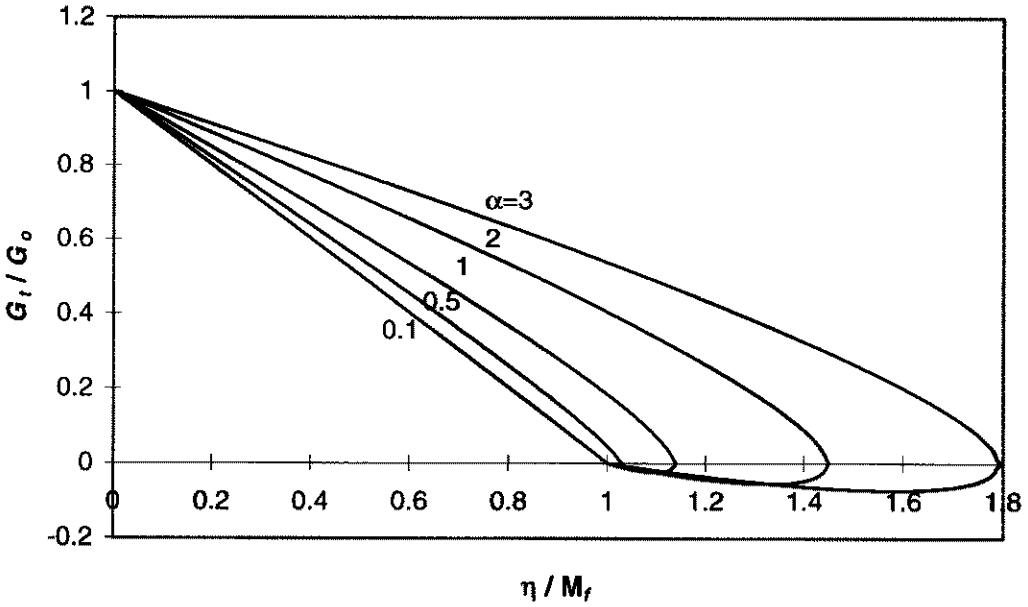

Fig. 11.47 Relationships of G_t/G_o with η/M

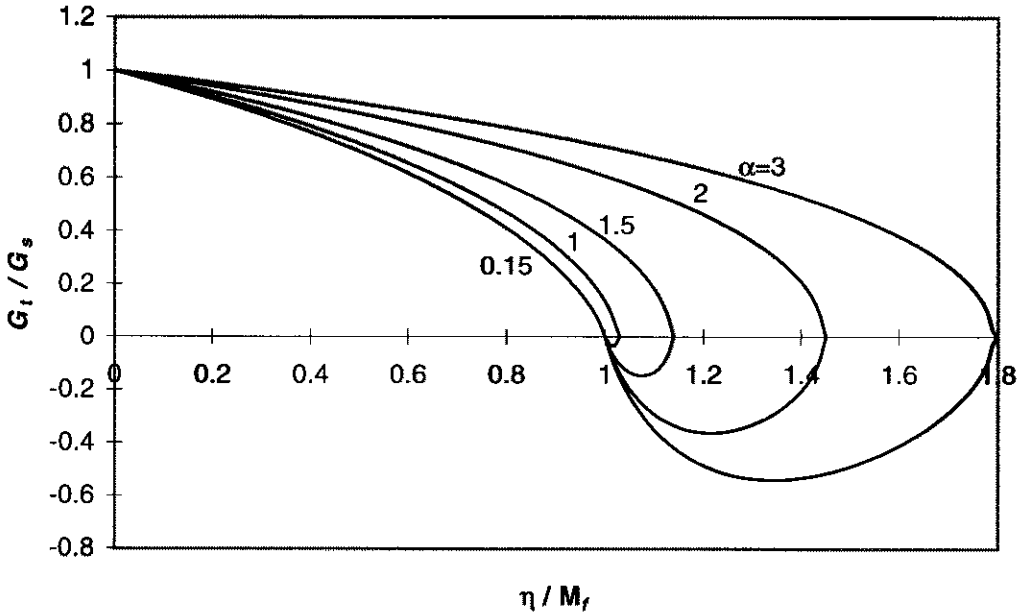

Fig. 11.48 Relationships of G_t/G_s with η/M

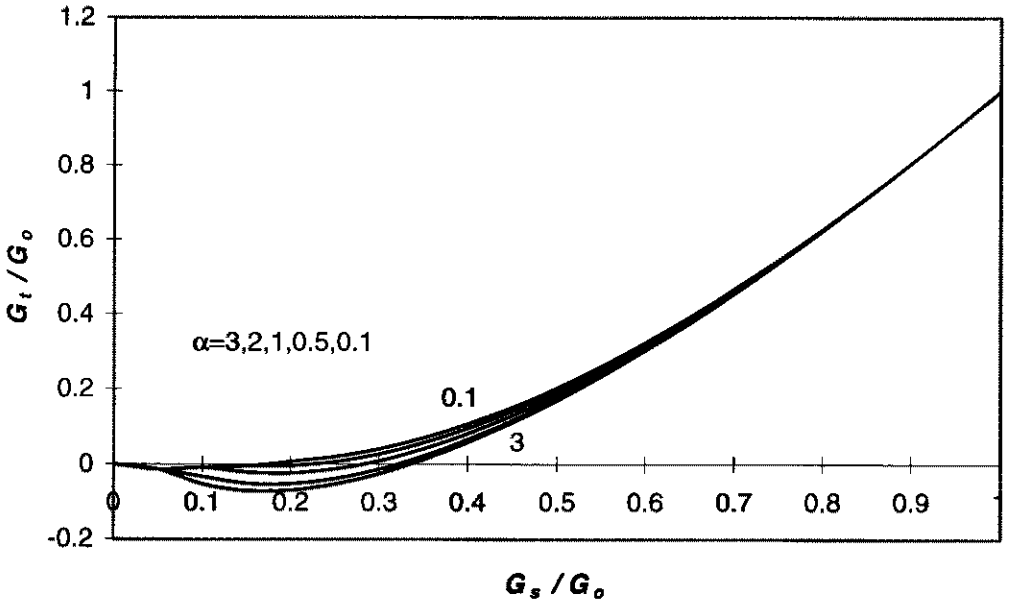

Fig. 11.49 Relationships of G_t/G_o with G_s/G_o

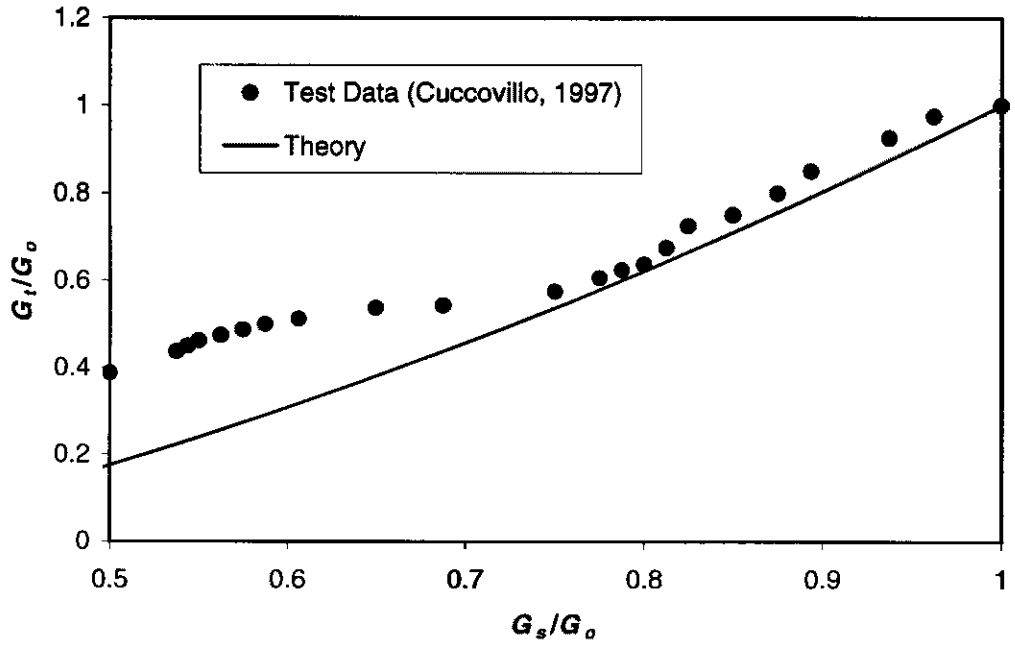

Fig. 11.50 Dependency of G_t/S_o and G_s/G_o

Chapter 12

Summary and Conclusions

12.1 Introduction

In this thesis, a general rigorous 3-D analysis of pile foundations has been developed, which is successfully applied to investigate the load-deformation behaviour of piles and pile groups subjected to "active" or "passive" loadings, and containing defective piles. This general analysis falls naturally into four main topics:

1. the theory and its application of general elastic analysis of piles and pile groups subjected to "active" loadings, as presented in chapter 3
2. the theory and its application of general elastic analysis of piles and pile groups subjected to "passive" loadings, as described in chapters 4 and 5
3. investigating the behaviour of pile foundations containing pile defects within a single pile, interaction between two defective piles, the behaviour of a pile group, and model pile testing, as described in chapters 6, 7, 8, 9 respectively
4. further development of non-linear pile foundation analysis, and investigating the shearing behaviour of friction materials, as set out in chapters 10 and 11.

12.2 Chapter Summaries

The summary and main conclusions of each chapter are summarized below:

Chapter 2

This chapter reviews some of the theoretical and engineering backgrounds of general boundary element analysis, as applied to pile foundations, and then discusses problems related to defective piles and pile testing. The principles and features of some current widely-used programs of general pile analysis are reviewed. It is shown that previous investigators have also paid considerable attention to the analysis of the behaviour of piles subjected to "passive" loadings. It is a common experience to encounter defects in piles (especially concrete piles), and progress in studying the behaviour of piles containing defects is summarized. Some methods of pile testing, and procedures for identifying defects in piles, are presented.

Chapter 3

This chapter describes the development of a boundary element analysis for the behaviour of single piles and pile groups subjected to general three-dimensional loading and to vertical and lateral ground movements. Each pile is discretised into a series of cylindrical elements, each of which is divided into several sub-elements. Compatibility of vertical, lateral and rotational movements is imposed in order to obtain the necessary equations for the pile response. Via hierarchical structures, twelve non-zero sub-matrices in a global matrix are derived for the basic influence factors. A computer program, GEPAN, has been developed to evaluate the analysis.

Solutions are presented for a series of cases involving single piles and pile groups. In each case, the solutions are compared with those from more simplified existing pile analyses such as those developed by Randolph and by Poulos. It is shown that for direct loading effects (*e.g.* the settlement of piles due to vertical loading), the simplified analyses work well. However, for "off-line" response (such as the lateral movement due to vertical loading) the differences are greater, and it is believed that the present analysis gives more reliable estimates.

Chapter 4

There are many cases where piles are subjected to "passive" loadings by soil movement past the piles. This chapter employs a general 3-D coupled boundary element approach to analyze the response of piles subjected to passive loadings. A number of theoretical expressions for soil movements are developed and presented. These expressions have been incorporated into the pile-soil governing equation previously developed in chapter 3. It has been shown that the program GEPAN is capable of giving realistic estimates of passive pile behaviour under a variety of situations, including soil shrink/swelling, soil surface surcharge, tunnelling, soil movements arising from driving piles and cavity formation in soil. Reasonable agreement is found between some existing published solutions and those developed herein. Using these analyses, it is possible to identify

situations in which the risk of pile damage is most severe, thus enabling mitigation strategies to be developed.

Chapter 5

This chapter presents an analytical methodology, using the boundary element method to study "passive" pile behaviour induced by a soil-cut, such as an excavation or retaining wall construction near the piles. This analysis involves two stages. First, based on a source-sink imaging technique, a general explicit equation is derived for cut-induced soil movements. Second, these estimated ground deformations are imposed on the passive pile through a general 3-D coupled pile boundary element analysis developed previously. Only some simple boundary parameters along the pile and the cut are required in the analysis. The results of published observations and/or analyses confirm reasonable agreement with the present theory. For convenience of characterization, the lateral wall deflection distribution with depth due to the cut is classified into three patterns, which are used to conduct an extensive parametric study of passive pile performance. The influences of various factors such as pile length, pile flexibility, distance between pile and cut, group effects, and the cut deflection patterns, are studied.

The important conclusions of this study are: 1) The pile length to diameter ratio L/d affects mainly the vertical pile head movement and pile head rotation of relatively short piles; 2) If a pile is at some distance from a cut or wall, the passive pile response are similar, regardless of the cut deflection pattern; 3) The horizontal pile head displacement is almost independent of pile flexibility factor, K_R, for flexible piles, while the vertical pile head displacement is insensitive to K_R for less-flexible piles; 4) The passive pile head displacements of a single pile and a pile group are similar except very close to the cut, where the group cap rotation is smaller than the single pile head rotation.

Chapter 6

Via the program GEPAN, this chapter presents analyses for response of single piles with three typical types of defect (necking, honey-combing and soft-base). For each type of defect, typical relationships for pile stiffness reduction have been developed, under

general loadings (axial, lateral, moment and torsional). Among the factors affecting the stiffness reduction are the extent of the defect, and the pile-soil stiffness/flexibility factors.

It is found that the presence of defects results in reduced stiffness of all components of pile response; Severe and/or shallow defects result in significantly lower stiffness reduction factors than defects at greater depth along the pile.

Chapter 7

Very little attention has been paid to the problem of interaction of defective piles under general loading. In this Chapter, based on introducing accurate definitions of interaction factors, the interaction between two piles containing defects is analyzed with different types of defects of different sizes and locations, and with varying pile parameters, (such as pile length, diameter, spacing, pile stiffness factor, pile flexibility factor, *etc.*). Some simple-but-important relationships between interaction factors for defective piles have been developed.

It is found that the cross interaction factor of the damaged pile on the intact pile is approximately equal to the cross interaction factor of two identical intact piles, while the cross interaction factor of the intact pile on the damaged pile is approximately equal to cross interaction factor of two identical damaged piles;

Chapter 8

The objective of the Chapter is, via GEPAN, to assess the load-displacement performance of groups containing defective piles. An attempt is made to relate the type of defects, pile spacing, pile stiffness/flexibility factors, to the behaviour of group, as represented by the group stiffness reduction factors, load redistribution, and "off-line" movements.

It is shown that the group stiffness reduction factors decrease as the severity of the pile defects increases, and that the response is more sensitive to defects for piles of moderate relative stiffness. The more severe the pile defects, the less uniform is the load distribution within the group.

Chapter 9

This chapter describes the results of tests on model single piles containing structural "defects", and driven into clay. The static load-settlement behaviour of the defective piles is investigated for various values of the length and diameter of the defects.

It is found that the structural defects of pile have a strong impact on the load capacity. The pile stiffness reduction factor significantly decreases with increasing degree of the structural defect in the piles.

Comparisons are made between the observed behaviour and that predicted from two theoretical defective pile analyses, the GEPAN analysis and a previously published approximate analysis. The general trends of behaviour are adequately reproduced by the theories.

Chapter 10

This chapter presents the further development of non-linear analysis for pile foundations in the program GEPAN. The models of 3-D non-linear analysis in a pile-soil system (such as, non-linear continuum analysis, load-transfer method, elastic-plastic behaviour of piles, slip development at interface) have been set up for incorporation into GEPAN. Preliminary results for axial loading give some confidence that future developments of GEPAN using these approaches will give satisfactory results for non-linear pile and pile group response.

Chapter 11

In this chapter, a comprehensive study on simulating the shearing behaviour of frictional materials is carried out. A set of two unified explicit equations, describing the relationship among the shear stress ratio and the distortional strain and the volumetric strain, are formulated independently. The proposed model contains six parameters for material properties and one parameter representing the effect of the non-uniformity in stress and strain within a sample on deformation during softening. All the parameters

have clear physical meanings and can be determined uniquely by a shearing test. It is also demonstrated that the proposed equations have the capacity of simulating the shearing behaviour of many types of frictional materials including geo-materials.

The proposed equations are employed to simulate the stress-strain behaviour for twenty-one different types of materials for over one hundred tests; Comparisons are presented between the simulations and experimental data for seventy-two of these tests. It is found that the proposed equations describe quite accurately the behaviour of all these materials under all the tests. A statistical study of material parameters has been performed. For types of distortional-volumetric behaviour (D-D, D-W, W-D, W-W) of frictional materials are characterized. It is found that there exist two basic material procedure parameters, one for distortional procedure, the other for volumetric procedure.

12.3 Topics for Future Research

Some topics related to the thesis for future research are suggested as follows:

1) Incorporation of the unified shearing model presented in Chapter 11 into the nonlinear GEPAN analysis.
2) Detailed study of single pile and group behaviour for non-linear soil behaviour.
3) A series of carefully controlled model tests on single piles and pile groups. Extend the number of the limited testing program in this thesis to include:
   i) lateral loading
   ii) geotechnical as well as structural defects
   iii) pile groups as well as single pile

   Measured both load-deflection behaviour and load-moment distribution in pile. Comparison between theory and experimental result.
4) Modifying GEPAN to be capable of analysing more general problems, such as, group with raked piles; raft-pile foundation, interaction of a structure-soil-pile system and cyclic response of offshore pile groups.

References in Chapters 1 to 10

Banerjee, P.K. and Driscoll, R.M.C., (1976). "Three-dimensional analysis of raked groups", *Proceedings, Institution of Civil Engineers*, Vol. 61, pp.653-671.

Bake, C.N. and Khan, F. (1971). "Caisson construction problems and correction in Chicago", J. Soil Mech. and Fndn. Div., ASCE, Vol. 97, No. SM2, pp.417-440.

Bobrowski, J., Bardhan Roy, B.K., Magiera, R.H. and Lowe, R.H. (1970). "The structural Integrity of Large Diameter Bored Piles", Proceedings of the Conference on Behaviour of Piles, London, Sept., pp.179-184.

Bowles, J.E. (1988). *Foundation Analysis and Design*, McGraw Hill

Broms, B.B. (1995). "Damage of piles during driving", Developments in Deep Foundations and Ground Improvement Schemes, Balasubramaniam *et al.* (eds), Belkema, Rotterdam.

Brown, P.T. (1972). "The analysis of rafts on clay", Ph.D. Thesis, University of Sydney, Australia.

Carter, J.P. (1982). "A numerical method for pile deformations due to nearby surface loadings", Proceedings of the fourth international conference on numerical methods in geomechanics, Edmonton, pp.811-817.

Carter, J.P., Randolph, M.F. and Wroth, C.P. (1979). "Some aspects of the performance of open and close-ended piles", Proceedings of the International Conference on Numerical Methods in Offshore Piling, ICE London, pp.165-170.

Challa, P.K. and Poulos, H.G. (1991). "Behaviour of Single Pile in Expansive Clay", Geot. Eng., Vol.22, No.2, pp.189-216.

Chen, F.K. (1978). "Diagnosis of pile condition", Geotechnical Engineering, Vol.9, No.2, pp.85-104.

Chen, L.T, Poulos, H.G. and Loganathan N., (1999). "Pile responses caused by tunneling", ASCE Journal of Geotechnical and Geoenvironmental Engineering, Vol.125, No.3, pp.802-811.

Chen, L.T. and Poulos, H.G. (1997). "Piles subjected to lateral soil movements", ASCE Journal of Geotechnical and Geoenvironmental Engineering,Vol.123, No.9, pp.802-811.

Cheung, Y.K., Tham, L. G. and Guo, D. J. (1988). "Analysis of pile group by infinite layer method", *Géotechnique*, Vol.38, No.3, pp.415-431.

Chow, Y.K. (1986). "Analysis of vertically loaded pile groups", *Int J Num Anal Methods Geomech*, Vol.10, No.1, pp.59-72.

Chow, Y.K., Teh, C. I. (1990). "A theoretical study of pile heave", Geotechnique, Vol.40, No.1, pp.1-14.

Chu, Y.K. (1994), "A failure case study of island method excavation in soft clay", Proc. Int. Conf. On Design and Construction of Deep Foundations, Vol. III, pp.1216-1230.

Clough, G.W., Smith, E. M. and Sweeney, B. P. (1989). "Movement control of excavation support system by iterative design", Foundation Eng., Current Principle and Practices, ed. F. H. Kulhawy, 2: pp.869-884.

Davis, A.G. and Hertlein, B.H. (1991). "Development of non-destructive small strain methods for testing deep foundations: A review", Trans. Research Record, 1331, pp.15-20.

Davis, E.H. and Poulos, H.G. (1968). "The use of elastic theory for settlement prediction under three-dimensional conditions", Geotechnique, Vol. 18, pp. 67-91.

Desai, C.S. (1974). "Numerical design --- analysis for piles in sands", *Jnl. Geot. Eng. Divn., ASCE*, No.100(GT6), pp.613-635.

Finno, R.J. and Lawrence, S.A. (1991). "Analysis of performance of pile groups adjacent to deep excavation", ASCE Journal of Geotechnical Engineering, Vol.117, No.6, pp.934-955.

Fleming, W.G.K., Weltman, A.J., Randolph, M.F. and Elson, W.K. (1992). *Piling Engineering*, Blackie Academic & Professional.

Focht J.A. and Koch, K.J. (1973). "Rational analysis of the lateral performance of offshore pile groups", *Proc. 5th Offshore Tech. Conf.*, Houstom, 2, pp.701-708.

Goble, G.G. and Rausche, F. (1979). "Pile drivability predictions by CAPWAP", in Proc. Int. Conf. on Num. Method in Offshore Piling, ICE, London, pp.29-36.

Goble, G.G., Rausche, F. and Likins, G.E., Jr. (1980). "The analysis of pile driving. A state of the art", Proceedings of the Int. Seminar on the Application of Stress-Wave Theory on Piles. Stockholm, June.

Goh, A.T.C., Teh, C.I. and Wong, K.S. (1997). "Analysis of piles subjected to embankment induced lateral soil movements", ASCE Journal of Geotechnical and Geoenviornmental Engineering, Vol.123, No.9, pp.792-801.

Goodman, R.E. (1976). *Methods of geological engineering*, West Publishing Company.

Gray, H. (1936). "Stress distribution in elastic solids", Proc. 1st Int. Conf. Soil Mechs. Fndn. Eng., 2, pp.157

Gray, H. (1936). "Stress distribution in elastic solids", Proc. 1st Int. Conf. Soil Mechs. Fndn. Eng., Vol. 2, pp.157

Hammond, A.J., Mitchel, J.M. and Lord, J.A. (1980). "Design and construction of driven cast in situ piles in stiff fissured clays", Recent Developments in the Design and Construction of Piles. Institution of Civil Engineers, London, pp.157-168.

Hara, M., Tani, M., Tsuda, K., and Taguchi, Y. (1991). "Great depth excavation-behaviour stimulation of steel pile", Geo-Coast' 91, 2, pp.187-192.

Hearne, T.M., Stokoe, K.H. and Reese, L.C. (1981). "Drilled shaft integrity by wave propagation method", Journal of the Geotechnical Engineering Division, ASCE, Vol. 107, No. GT10, October, 1981, pp.1327-1344.

Hewitt, C.M. (1988). "Cyclic Response of Offshore Pile Groups", PhD Thesis, Univ. of Sydney, Australia.

Hewlett, W.J. and Randolph, M.F. (1988). "Analysis of piled embankment", Ground Engineering, Vol.22, No.3, pp.12-18.

Hobbs, N.B. (1957). "Unusual necking of cast in-situ concrete piles", Proceedings of 4th International Conference on Soil Mechanics and Foundation Engineering, London, 1957, Vol.3, pp.40-42.

Hrennikoff, A. (1950). "Analysis of pile foundations with batter piles", *Trans. ASCE*,115, pp.351-374.

Hull, T.S. (1987). "The static behaviour of laterally loaded piles", *Ph.D. Dissertation*, University of Sydney, Australia.

Hull, T.S. (1996). "Analysis of Laterally Loaded Pile Groups with Unequal Dimensions", 7th Australia New Zealand Conference on Geomechanics, Adelaide, Australia, pp.521-525.

Jeong, S. and Kim, S. (1998). "Interaction factors for pile groups due to downdrag", Soils and Foundations, Vol. 38, No. 2, pp.49-61.

Jurgenson, L. (1934). "The application of theories of elasticity and plasticity to foundation problem", Contributions to soil Mechanics. Boston Society of Civil Engineers, pp.1925-1940.

Kao, J. (1985), "Application of pile retaining wall to building protection and slope stabilization", Canadian Geotechnical Conference, 38, Edmonton, Alberta.

Kezdi, A. (1957). "The bearing capacity of pile and pile groups", Proc, 4th ICSMFE, London, Vol.2, pp.46-51.

Kido, K., Gao, X., Kanako, Y., Kanai, H., Abe, M. Makino, S., Tsukada, Y., Sakai, T. and Chida, S. (1988). "Shape Estimation of Concrete Piles by Analysis Reactions of Pile Head to a Hammer Blow", Proc. 3rd Int. Conf. on App. Of Stress Wave Theory to Piles, Ottawa, pp.107-114.

Kocsis, P. (1968). *Lateral loads on piles*, Chicage: Bureau of Eng.

Kraft, L.M., Ray, R.P. and Kagawa, T (1981). "Theoretical *t-z* curves", J. Geotech. Engng, Vol.107, No.GT11, pp.1543-1561.

Lee, C.Y. (1993). "Settlement of pile group-practical approach", *J. of Geotech. Engrg. Div., ASCE*, Vol.199, No.9, pp.1449-1461.

Lee, C.Y., Poulos, H.G. and Hull, T.S. (1991). "Effect of Seafloor Instability on Offshore Pile Foundations", Canadian Geotechnical Journal, Vol.28, No.5, pp.729-737.

Leonards, G.A. (1982). "Investigation of failures", Journal of the Geotechnical Engineering Division, ASCE, Vol. 108, No. GT2, pp.187-246.

Likins, G., Rausche, F., Miner, R. and Hussein, M. (1993). "Verification of Deep Foundations by NDT Method", Design and Perf. of Deep Foundns. Geot. Spec. Pub. 38, ASCE, pp.76-90.

Loganathan, N. and Poulos, H.G. (1998). "Analytical Prediction for Tunnelling-induced Ground Movements in Clays", ASCE Journal of Geotechnical and Geoenvironmental Engineering, Vol.124, No.9, pp.846-856.

Loganathan, N. and Poulos, H.G. (1999a). "Tunnelling induced ground deformations and their effects on adjacent piles", Tenth Australian Tunnelling Conference, Melbourne, Austria, pp.241-249.

Loganathan, N., Poulos, H.G. and Xu, K.J. (1999b). "Ground Deformations and Pile-Ground Responses Due to Tunneling", Accepted for publication to Soils and Foundations.

Low, B.K., Tang, S.K. and Choa, V. (1994). "Arching in piled embankments", ASCE Journal of Geotechnical Engineering, Vol.120, No.11, pp.1917-1938.

Madhav, M.R. and Babu, M.S. (1997). "Effect of field displacments on passive piles to control lateral soil movements", In: Yuan editor. Computer Methods and Advances in Geomechanics, Balkema, Rotterdam, pp.2129-2134.

Mattes, N.S. and Poulos, H.G. (1969). "Settlement of single compressible pile", Journal of the Soil Mechanics and Foundation Division, ASCE, Vol. 95, No. SMI, pp.189-207.

Mattes, N.S. and Poulos, H.G. (1971). "Model Tests on Pile in Clay", Proceedings of First Aust.-N.Z. Conference on Geomechanics, Vol. 1, pp.254-260.

Middendorp, P. and Reiding, F.J. (1988). "Determination of discontinuities in piles by NTO testing and signal matching techniques", Proc. 3rd Int. Conf. on App. of Stress-Wave Theory to Piles", Ottawa, pp.33-43.

Mindlin, R.D. (1936). "Force at a point in the interior of a semi-infinite solid", Jnl. Appl. Phys., Vol. 7, No. 5, pp.195-202.

Mylonakis, G. and Gazetas, G. (1998). "Settlement and additional internal forces of grouped piles in layered", *Géotechnique*, Vol.48, No.1, pp.55-72.

Nair, K., Gray, J., and Donovan, N. (1969). "Analysis of pile group behavior", *ASTM, STP* 444, pp.118-159.

O'Neil, M.W., Hawkins, R.S. and Mahar, L.J. (1982). "Load transfer mechanisms in pile and pile groups", J. Geotech. Engng, ASCE, Vol.108, No.GT12, pp.1605-1623.

O'Neill, M.W., Ghazzaly, O.I. and Ha, H.B. (1977). "Analysis of there-dimensional pile groups with non-linear soil response and pile-soil-pile interaction", *Proc 9th Annual OTC*, Houston, Paper OTC 2838, pp.245-256.

Olson, L.D. and Thompson, R.W. (1985). "Case histories – Evaluation of drilled pier integrity by the stress wave propagation method", Proceedings of a session on drilled piers and caisson-2, Geotechnical Engineering Division, ASCE, May, pp.28-42.

Ottaviani, M. (1975). "Three-dimensional finite element analysis of vertically loaded pile groups", *Géotechnique*, Vol.25, No.2, pp.159-174.

Peck, R.B. (1965). " Pile and Pier Foundations", journal of the Soil Mechanics and Foundation Division, ASCE, Vol. 91, No. SM2, March, 1965, pp33-38.

Pennington, D.S. (1995). "Cracked? Exploring post-construction evidence in the interpretation of trial pile data", Proc. Instn. Civ. Engrs. Geotech. Engng, 113, July, pp.132-143.

Poulos, H.G. (1968). "Analysis of the settlement of pile groups", Geotechnique, Vol. 18, pp.449-471.

Poulos, H.G. (1971a). "The behaviour of laterally loaded piles: I. Single piles", Journal of the Soil Mechanics and Foundations Division, ASCE, Vol. 97, No. SM5, pp.711-731.

Poulos, H.G. (1971b). "The behaviour of laterally loaded piles: II. Pile group", Journal of the Soil Mechanics and Foundations Division, ASCE, Vol. 97, No. SM5, pp.733-751.

Poulos, H.G. (1973). "Analysis of piles in soil undergoing lateral movement", Jnl. Soil Mechs. And Fndns. Divn. ASCE, Vol. 99, No. SM5, pp.391-406.

Poulos, H.G. (1976). "Behaviour of laterally loaded piles near a cut or slope", Australian Geomechanics Journal, Vol.6, No.1, pp.6-12.

Poulos, H.G. (1979). "An approach for the analysis of offshore pile groups", *Proceedings, Conference on Numerical Methods in Offshore Piling*, Institution of Civil Engineers, London, England, pp.119-126.

Poulos, H.G. (1989a). "Pile behaviour – theory and application", 29th Rankine Lecture, *Géotechnique*, Vol.39, No.3, pp.365-415.

Poulos, H.G. (1989b). *PIES user's guide*, Centre for Geot. Res. Univ. of Sydney, Australia.

Poulos, H.G. (1990a). "DEFPIG-deformation analysis of pile groups. User's Guide", Centre for Geot Res, Unive of Sydney, Australia.

Poulos, H.G. (1990b). "Design of Piles for Negative Friction", Piletalk International '90, Jakarta, pp.123-129.

Poulos, H.G. (1994a). "Piles subjected to extremely–imposed soil movements", Research Report No. R689, The University of Sydney.

Poulos, H.G. (1994b). "Analysis and Design of Pile through Embankments", International conference on design and construction of deep foundations, Orlando, FL,3, pp.1403-1421.

Poulos, H.G. (1994c). "Effect of pile driving on adjacent piles in clay", Canadian Geotechnical Journal, Vol.31, No.6, pp.856-867.

Poulos, H.G. (1996). "Comparison of some methods for the design of piles through embankments", Proc. 12th SE. Asian Geot. Conf, Kuala Lumpur, 2, pp.157-167.

Poulos, H.G. (1997). "Behaviour of pile groups containing defective piles", Proc. 14th Int. Conf. Soil Mech. and Fondn. Eng., Hamburg, Vol. 2, pp.871-876.

Poulos, H.G. and Chen, L.T. (1996). "Pile response due to unsupported excavation – induced lateral soil movement", Canadian Geotechnical Journal, Vol.33, pp.670-677.

Poulos, H.G. and Chen, L.T. (1997). "Pile response due to excavation – induced lateral soil movement", Journal of Geotechnical and Geoenvironmental Engineering, ASCE, Vol.123, No.2, pp. 94-99.

Poulos, H.G. and Davis, E.H. (1968). "The settlement behaviour of sing axially-loaded incompressible piles and piers", Geotechnique, Vol. 18, pp.351-371.

Poulos, H.G. and Davis, E.H. (1974). *Elastic Solutions for Soil and Rock Mechanics*, John Wiley & Sons, Inc.

Poulos, H.G. and Davis, E.H. (1980). *Pile foundation analysis and design*, New York, John Wiley and Sons.

Poulos, H.G. and Madhav, M.R. (1971). "Analysis of the movement of battered piles", Proceedings, 1st Australian-New Zealand Conderence on Geomechanics, Vol.1, pp.28-275.

Poulos, H.G. and Mattes, N.S. (1971). "Settlement and load distribution analysis of pile groups", Australian Geomechanics Journal, Vol.G1, No.1, pp.10-28.

Poulos, H.G. and Randolph, M.F. (1983). "A study of two methods for pile group analysis", Jnl. Geot. Eng. Divn., ASCE, Vol. 109, No. GT3, pp.355-372.

Pressley, J.G. and Poulos, H.G. (1986). "Finite element analysis of mechanisms of pile group behavior", *Int Jnl Num Anal Meth Geomechs*, No.10, pp.213-221.

Randolph, M.F. (1980). "PIGLET: A computer program for the analysis and design of pile groups under general loading conditions", Soil Report TR91, CUED/D, Cambridge University, Cambridge England.

Randolph, M.F. (1989). *PIGLET: Analysis and design of pile groups*, Univ. of Western Australia, Australia.

Randolph, M.F. (1981a). "Analysis of the behaviour of piles subjected to torstion", J. of Geot. Engng. Div., ASCE, Vol. 107, No. GT8, pp.1095-1111.

Randolph, M.F. (1981b). "The response of flexible piles to lateral loading", Geotechnique, Vol. 31, No. 2, pp.247-259.

Randolph, M.F. (1992). "Piles as settlement reducers: pile group analysis", Lecture 3, Seminar on Modern Methods in the Design of Pile Foundations, Aust. Geomechanics Society/ACADS, Melbourne, Victoria.

Randolph, M.F. and Wroth, C.P. (1978a). "Analysis of deformation of vertically loaded piles", J. of the Geot. Eng. Div., ASCE, Vol. 104, No. GT12, pp.1465-1488.

Randolph, M.F. and Wroth, C.P. (1978b). "A simple approach to pile design and the analysis of pile tests", Proc. Symp. On Behaviour of Deep Foundations, ASTM STP 470, pp.484-599.

Randolph, M.F. and Wroth, C.P. (1979). "An analysis of the vertical deformation of pile groups", Geotechnique, Vol.29, No.4, pp.423-439.

Rao, S.N, Raddy, B.V.P., and Sakr, M.A.M. (1992). "Behaviour of defective piles in clay", Indian Geotechnical Journal, V22:2, Apr., Indian Geotechnical Journal, Indian Geotechnical Society, India, pp.69-84.

Rao, S.N. (1996). "Defective piles in clay", Proc. 6th Int. Conf. Deep Foundations, Bombay, 4.4.1-4.4.8.

Rausche, F., Likins, G.E. and Shen, R.K. (1992), "Pile Integrity Testing and Analysis", Proc. 4th Int. Conf. on App. of Stress Wave Theory to Piles, the Hague, pp.613-618.

Redman, P.G. (1980). "Analysis of undrained creep of foundations and embankment on clays", PhD thesis, Univ. of Sydney.

Reese, L.C. (1978). "Design and construction of drilled shafts", Jnl. Geot. Eng. Divn. ASCE, Vol.104, No. GT1, pp.91-166.

Rowe, R.K. (1978). "Soil structure interaction analysis and its application to the prediction of anchor plate behaviour", PhD thesis, Univ. of Sydney.

Sagaseta, C. (1987). "Analysis of undrained soil deformation due to ground loss", Geotechnique, Vol.37, No,.3, pp.301-320.

Scott, R.F. (1963). *Principles of Soil Mechanics*, Addison-Wesley.

Smith, E.A.L. (1960). "Pile driving analysis by the wave equation", J. Soil Medh. And Found. Div., ASCE, Vol.86, No.SM4, pp.35-61.

Stain, R.T. (1982). *Integrity testing*, Civil Engineering, April/May

Tabucanon, J.T. and Airey, D.W. (1992). "Interface Tests to Investingate Pile Skin Friction in Sands", Research Report No. R662, The University of Sydney.

Teh, C.I. and Wong, K.S. (1995). "Analysis of downdrag on pile groups", *Geotechnique*, Vol.45, No.2, pp.191-207.

Thorburn S. and Thorburn, J.Q. (1977). "Review of problems associated with the construction of cast-in-place concrete piles", DOE and CIRIA Piling Development Group, Rep. PG2, CIRIA, London.

Timoshenko, S. and Goodier, J. N. (1970). *Theory of elasticity*, Third edition, McGrow-Hill Book Company.

Tomlinson, M.J. (1987). *Pile Design and Construction Practice* (3rd edn.), A Viewpoint Publication.

Turner, M.J. (1997). *Integrity testing in Piling Practice*, Construction Industry Research and Information Association, CIRIA Report 144, ISBN: 0860174735.

Verruijt, A. and Booker, J.R. (1996). "Surface settlements due to deformation of a tunnel in an elastic half plane", Geotechnique, Vol.46, No.4, pp.753-756.

Watson, G.V.R. and Carder, D.R. (1994). "Comparison of the measured and computed performance of a propped bored pile retaining wall at Walthamstow", Geotechnical Engineering, Institution of Civil Engineers, Proceedings, Vol. 107, No. 3, pp.127-133.

Whitaker, T. (1975). *The Design of Piled Foundations* (2nd edn.), Pergamon, Oxford.

Wiesner, T.J. (1977). "The Behaviour of Piled Raft Foundation", Ph.D. thesis, Uni. of Sydney, Aust.

Xu, K.J. and Poulos, H.G. (1999a). "General Elastic Analysis of Piles and Pile Group", Int. Jour. for Numerical and Analytical Methods in Geomechanics, (in press).

Xu, K.J. and Poulos, H.G. (1999b). "General 3-D Elastic Analysis of Piles Subjected to Passive Loadings", Submitted for publication to Computers and Geotechnics, (under review).

Xu, K.J. and Poulos, H.G. (1999c). "Principles of Program GEPAN for General Pile Elastic Analysis", Research Report No. R782, The University of Sydney.

Xu, K.J. and Poulos, H.G. (1999d). *User's Manual for Program GEPAN Version 2.0*, The University of Sydney.

Xu, K.J., Liu, M.D, Carter, J.P., and Poulos, H.G. (1997), "Explicit stress-strain equations for geo-materials", Research Report No. R751, The University of Sydney.

References in Chapter 11

Adachi T. and Oka F. (1993), "An elasto-viscoplastic constitutive model for soft rock with strain softening", *Proc.* Int. Symposium on Geotechnical Engineering on hard Soils and Soft Rocks, pp.327-333.

Alva-Hurtado J. E., McMahon D. R. and Steward H. E. (1981), "Apparatus and Techniques for static triaxial testing of ballast", *Laboratory Shear Strength of Soil*, ASTM STP 740, R. N. Young and F. C. Townsend, Eds., American Society for Testing and Materials, 1981, pp. 94-113.

Been K. and Jefferies M. G. (1985), "A state parameter for sands", *Géotechnique*, Vol. 35(1), pp.99-112.

Bishop A. W. and Henkel D. J. (1957), *The Measurement of Soil Properties in the Triaxial Test*, Edward Arnold, London.

Bolton M. (1986), "The strength and dilatancy of sands", *Géotechnique*, Vol. 36(1), pp.65-78.

Burland J. .B., Rampell S., Georgiammou, V. N. and Calabresi G. (1996), "A laboratory study of the strength of four stiff clays", *Géotechnique*, Vol. 46(3), pp. 491-514.

Calladine C. R. (1985), *Plasticity For Engineers*, Chichester: Ellis Horwood Ltd..

Canestrari F. and Scarpelli G. (1993), "Stress-dilatancy and strength of Ancona clay", *Proc.* Int. Symposium on Geotechnical Engineering on Hard Soils and Soft Rocks, pp.417-424.

Carter J. P. and Airey D. W. (1994), "The engineering behaviour of cemented marine carbonate soils", *Geotechnical Engineering: Emerging Trends in Designs and Practice*, Saxena (*ed*), pp.65-101.

Carter J. P. and Balaam N. P. (1995), *AFENA, Users' Manual*, version 5.0.

Cazzuffi D., Picarelli L., Ricciuti A. and Rimold P. (1994), "behaviour of geogrid reinforced gravel in large scale triaxial tests", XIII ICSMFE, New Delhi, India, pp. 271-274.

Chu J. (1995), "An experimental examination of the critical state and other similar concepts for granular soils", *Canadian Geotechnical J.*, Vol. 32(5), pp.1065-1075.

Colliat-Dangus J. L., Desrues J. and Foray P. (1988), "Triaxial testing of granular soil under elevated cell pressures", *Advanced Triaxial Testing of Soil & Rock*, ASTM, STP, 977, Robert *et al* (*ed*), pp.290-310.

Crouch S. L. (1970), "Experimental determination of volumetric strains in failed rock", *Int. J. Rock Mechanics and Mining Science and Geomechanics*, Vol. 7(26), pp.589-603.

Cuccovillo, T. and Coop, M.R. (1997). "The measurement of local axial strains in triaxial tests using LVDTs", Geotechnique 47, No. 1, pp.167-171.

Cui Y. J. and Delage P. (1996), "Yielding and plastic behaviour of an unsaturated compacted silt", *Géotechnique*, Vol. 46(2), pp.291-311.

Daramola O. (1980), "Effect of consolidation age on stiffness of sand", *Géotechnique*, Vol. 30(2), pp.213-216.

Dendani H., Flavigny E., and Fry J. J. (1988), "Triaxial test for embankment dams: interpretation and validity", *Advanced Triaxial Testing of Soil and Rock*, Donaghe, Chaney, and Silver (*ed*), pp.486-500.

Duncan J. M. and Chang C. Y. (1970), "Nonlinear analysis of stress and strain in soils", *J. Soil Mechanics & Foundations*, ASCE, Vol. 96(5), pp.1629-1653.

Elliott G. M. (1983), *An Investigation of a Yield Criterion for Rock*, Ph.D. thesis, University of London.

Golightly C. R. and Hyde A. F. L. (1988), "Some fundamental properties of carbonate sands", *Engineering for Calcareous Sediments*, Jewell *et al* (ed), pp.69-78.

Head K. H. (1985), *Manual of Soil Laboratory Testing*, Pentech Press.

Henkel D. J. (1956), "The effect of overconsolidation on the behaviour of clays during shear", *Géotechnique*, Vol. 6(2), pp.139-150.

Houlsby G. T., Wroth C. P., and Wood D. M. (1982), "Prediction of the results of laboratory tests on a clay using a critical state model", *Proc.* Int. Workshop on Constitutive Behaviour of Soils, Grenoble, Gudehus *et al* (*ed*), pp.99-121.

Huang, J. T., (1994), *The Effects of Density and Cementation of Soils*, Ph.D. Thesis, Sydney University

Jefferies M. G. (1993), "Nor-sand: a simple critical state model for sand", *Géotechnique*, Vol. 43(1), pp.91-103.

Kaggwa W. S. (1988), "Cyclic Behaviour of carbonate sands", Ph.D. Thesis, The University of Sydney.

Kaiser P. K. and Tang C. A. (1998), "Numerical simulation of damage accumulation and seismic energy release during brittle rock failure: Part II: rib pillar collapse", *Int. Journal of Rock Mechanics and Mining Science*. Vol. 35(2), pp.123-134.

Kraft, L.M., Ray, R.P. and Kagawa, T. (1981), "Theoretical t-z curves", J. Geotech. Engng, Vol.107, No.GT11, pp.1543-1561.

Kolymbas D. and Wu W. (1990), "Recent results of triaxial tests with granular materials", *Powder Technology*, Vol. 60, pp.99-119.

Lade P. V. (1977), "Elastoplastic stress-strain theory for cohesionless soil with curved yield surfaces", *International J. Solids and Structure*, Vol. 13(1), pp.63-76.

Lambe T. W. (1973), "Predictions in soil engineering", *Géotechnique*, Vol. 23(2), pp.149-202.

Lam W. K. and Tatsuoka F. (1988), "effects of initial anisotropic fabric and σ'_2 on strength and deformation characteristics of sand", *Soils and Foundations*, Vol. 28(1), pp.89-106.

Lee I. K. and Coop M. R. (1995), "The intrinsic behaviour of a decomposed granite soil", *Géotechnique*, Vol. 45(1), pp.117-130.

Liu M. D. (1991), *A Constitutive Theory for Sand and Its Application*, Ph.D. thesis, Glasgow University.

Liu M. D. and Carter J. P. (1998), "An isotropic strength criterion for geo-materials including peak, critical state, and residual strengths", Research Report, Sydney University.

Lo K. Y. (1972), "An approach to the problem of progressive failure", *Canadian Geotechnical. J.*, Vol. 9(4), pp.407-429.

Marachi N. D., Chan C. K., Seed H. B., and Duncan J. M. (1969), "Strength and deformation characteristics of rockfill materials", Report No. TE-69-5, University of California, Berkeley.

Matsuoka H. and Sun D. (1995), "Extension of spatially mobilized plane (SMP) to frictional and cohesive materials and its application to cemented sands", *Soils and Foundations*, Vol. 35(4), pp.63-72.

Michalowski R. L. and Zhao A. (1996), "Failure of fiber-reinforced granular soils", *J. Geotechnical Engineering*, ASCE, Vol. 112(3), pp.226-234.

Michelis P. N. (1981), "Work-softening and hardening behaviour of granular rocks", *Rock Mechanics*, Vol. 14(4), pp.187-200.

Moretto O. and Bolognesi A. J. L. (1970), "Shear strength of soft intact clay and silty stones", *Proc. 2nd Conf. International Society for Rock Mechanics*, Beograd, pp.39-48.

Mroz Z., Norris V. A., and Zienkiewicz O. C. (1981), "An anisotropic, critical state model for soils subject to cyclic loading", *Géotechnique*, Vol. 31(4), pp.451-469.

Muir-Wood D. (1990), *Soil Behaviour and Critical State Soil Mechanics*, Cambridge University Press.

Nakai T (1987), "Elastoplastic model considering the stress path dependency of soil behaviour in three dimensional stresses", *Constitutive Laws for Engineering Materials: Theory and Application*, Desai *et al* (*ed*), pp.429-436.

Novello E. and Johnston I. W. (1995), "Geotechnical materials and the critical state", *Géotechnique*, Vol. 45(2), pp.223-235.

Oda M. (1972), "The mechanism of fabric changes during compression deformation of sand", *Soils and Foundations*, Vol. 12(2), pp.1-18.

O'Rourke T. D. and Crespo E. (1988), "Geotechnical properties of cemented volcanic soil", *J. Geotechnical Engineering*, ASCE, Vol. 114(10), pp.1126-1147.

Poulos H. G., Uesugi M., and Young G. S. (1982), "Strength and deformation properties of Bass strait carbonate sands", Geotechnical Engineering, Vol. 15, pp.189-211.

Poulos H. G. (1989), "Cyclic axial loading analysis of piles in sand", J. Geotechnical Eng. ASCE, Vol. 115, No. 6, pp.836-852.

Prat P. C. and Bazant Z. P. (1991), "Microplane constitutive model for inelastic behaviour of soils", *Computer Methods & Advances in Geomech*anics, Beer *et al*, (*ed*), pp.669-674.

Proceedings of 14th International Conference on Soil Mechanics and Foundation Engineering, 1997, Vol. 1, A A. Balkema.

Read H. E. and Hegemier G. A. (1984), "Strain softening of rock, soil, and concrete: a review article", Mechanics of Material, Vol. 3(2), pp.271-294.

Roscoe K. H., Schofield A. N., and Wroth C. P. (1958), "On the yielding of soil", *Géotechnique*, Vol. 8(1), pp.22-53.

Roscoe K. H. and Burland J. B. (1968), "On the generalized stress-strain behaviour of "wet clay", *Engineering Plasticity*, Heyman and Leckie (*ed*), pp.535-609.

Rowe P. W. (1962), "The stress-dilatancy relation for static equilibrium of an assembly of particles in contact". *Proc. Roy. Soc. A.* 269, pp. 500-537.

Salgado F. M. and Byme P. M. (1991), "A three dimensional constitutive elasto-plastic model for sands following the 'Spatial Mobilized Plane' concept", *Computer Methods & Advances in Geomech*anics, Beer *et al*, (*ed*), pp.675-682.

Schofield A. N. and Wroth C. P. (1968), *Critical State Soil Mechanics*, MacGraw-Hill, London.

Schmertmann J. H. (1991) "The mechanical aging of soils", *J. Geotechnical Engineering*, ASCE, Vol. 117(9), pp.1288-1330.

Scott R. F. (1985), "Plasticity and constitutive relations in soil mechanics", *J. Geotechnical Engineering*, ASCE, Vol. 111(5), pp.563-605.

Sharma K. G., Rao G. V., and Sharma J. C. (1984), "Elasto-plastic constitutive model for compacted silt-fly ash admixture", *Indian Geotechnical Journal*, Vol. 14(1), pp.67-80.

Stark T. D., Ebeling R. M., and Vettel J. J. (1994), "Hyperbolic stress-strain parameters for silts", *J. of Geotechnical Engineering*, ASCE, Vol. 120(3), pp.420-441.

Skempton A. W. (1985), "Residual strength of clays in landslides, folded strata and the laboratory", *Géotechnique*, Vol. 35(1), pp.1-18.

Tatsuoka F. (1972), *Shear Tests in a Triaxial Apparatus - A Fundamental Study of the Deformation of Sand*, Ph.D. thesis, Tokyo University.

Tatsuoka F., Siddiquee M. S. A., Park C. S., Sakamoto M., and Abe F. (1993), "Modelling stress-strain relationships of sand", *Soils and Foundations*, Vol. 33(2), pp.60-81.

Vermeer P. A. (1978), "A double hardening model for sand", *Géotechnique*, Vol. 28(4), pp.413-431.

Wroth C. P. and Bassett R. H. (1965), "A stress-strain relationship for the shearing behaviour of a sand", *Géotechnique*, 15 (1), pp.32-56.

Wu W. Y., Christopher C. B., and Robert F. C. (1997), "Triaxial determination of shear strength of tire chips", *Journal of Geotechnical and Geoenvironmental Engineering*, ASCE, Vol. 123(5), pp. 479-482.

Xu K.J., Liu M.D, Carter J.P., and Poulos H.G. (1997), "Explicit stress-strain equations for geo-materials", Research Report No. R751, The University of Sydney.

Yamamuro J. A. and Lade P. V. (1996), "Drained sand behavior in axisymmetric tests at high pressures", *Journal of Geotechnical and Geoenvironmental Engineering*, ASCE, Vol. 122(2), pp.109-115.

Yu H. S. (1998), "CASM: a unified state parameter model for clay and sand", accepted for publication in *Int. J. Numerical Analytical Method in Geomechanics*.

This thesis has been accepted for the award of the degree in the Faculty of Engineering